

Selected Abstracts from Pharmacology 2019

Posters, Sunday 15th December, 14:00

Poster Session: Cardiovascular and Respiratory Pharmacology 1

P027 | Involvement of Ca²⁺-sensing receptor–G_{q/11} protein signalling pathway in NO release from human vascular endothelial cells

Takahiro Horinouchi¹; Yuichi Mazaki¹; Koji Terada²; Soichi Miwa¹

¹Graduate School of Medicine, Hokkaido University; ²Shiga University of Medical Science

Background and Purpose: Ca²⁺-sensing receptor (CaSR) belongs to family C of GPCRs and is activated by the endogenous agonists such as Ca²⁺. Stimulation of CaSR expressed in vascular endothelial cells through the increase in extracellular Ca²⁺ concentration ([Ca²⁺]_o) is reported to induce vasorelaxation via the production of NO and the activation of intermediate conductance Ca²⁺-activated K⁺ channels. The purpose of the present study is to characterize the CaSR-mediated NO production in human vascular endothelial cells.

Experimental Approach: The human endothelial cell line EA.hy926 was used in the present study. Intracellular Ca²⁺ concentration ([Ca²⁺]_i) was measured using a fluorescent Ca²⁺ indicator, Fura-2/acetoxymethyl ester, at 30°C using a dual-wavelength spectrofluorometer (CAF-110) at excitation wavelengths of 340 and 380 nm and an emission wavelength of 500 nm. The activation of endothelial NOS (eNOS) was estimated by Western blot analysis using anti-phospho-eNOS (Ser¹¹⁷⁷) antibody. NO released from EA.hy926 cells was measured using 4,5-diaminofluorescein (DAF-2), a fluorescent NO indicator that reacts with NO to produce the fluorescent triazole adduct, triazolofluorescein (DAF-2T). The fluorescence intensity of the resultant DAF-2T was measured using a multi-mode spectroscopic reader (Varioskan Flash) using an excitation wavelength of 488 nm and an emission wavelength of 515 nm. Statistical significance was determined using Student's unpaired *t* test or ANOVA followed by Tukey's multiple comparisons test.

Key Results: Increase in the [Ca²⁺]_o from 0.2 to 2 mM induced a concentration-dependent increase in [Ca²⁺]_i, which was significantly inhibited by NPS 2143 (a CaSR antagonist) and YM-254890 (a G_{q/11} protein inhibitor). The maximum increase in [Ca²⁺]_i by 2-mM Ca²⁺ was 390.1 ± 9.9 nM (*n* = 5). Stimulation with 2-mM Ca²⁺ for 4 hr elicited an increase in the phosphorylation level of eNOS at Ser¹¹⁷⁷, which

was significantly depressed by NPS 2143, YM-254890, and removal of Ca²⁺ from the medium. Ca²⁺ (2 mM) induced an increase in DAF-2T fluorescence intensity, which was inhibited by NPS 2143, YM-254890, removal of Ca²⁺ from the medium, and L-NAME (a competitive eNOS inhibitor).

Conclusion and Implications: Results of the present study provide evidence that activation of CaSR with extracellular Ca²⁺ facilitates NO release from human vascular endothelial cells via a G_{q/11} protein-eNOS-dependent pathway.

P028 | Investigating the expression of purinergic receptors in arteries and associate autonomic ganglia

Mohamed Eldaly; Samuel Fountain

University of East Anglia

Background and Purpose: Purinergic receptors are implicated in cardiovascular disease, and P2X and P2Y are abundantly expressed by blood vessels. In humans, local neurogenic responses mediated by perivascular nerves (PVNs) contribute to normal blood flow and hypertension. Perivascular neurons located within the adventitia of arteries release neurotransmitters (including ATP) that influence arterial tone and alter BP. ATP released by PVNs are hypothesised to modulate release of other neurotransmitters by activating pre-junctional purinergic receptors, though the expression of such receptors is unclear. We investigate the expression and the function of pre-junctional P2 receptors in mouse superior mesenteric arteries (SMAs), carotid arteries (CAs), and superior cervical ganglion (SCG), aiming to understand the role that P2X and P2Y receptors possess in perivascular nerve control function.

Experimental Approach: RT-PCR was performed using 500 ng of total RNA to investigate the expression patterns of all P2X and P2Y receptors in different vascular beds, SCG, and brain in mouse. To investigate the distribution of perivascular nerves and detect any identified candidate P2 autoreceptors in tissue sections of SMA and CA and then determine the percentage of neurons expressing of each receptor (colocalization studies with primary antibodies against P2 receptors), confocal/apotome microscopy and immunocytochemistry were performed using antibody against the general neuronal marker PGP9.5.

Key Results: We demonstrated that many of P2X and P2Y receptors are expressed on the tissues, and this can lead us to further investigate the role of the expressed receptors in autonomic and sensory-motor nerve function. PGP immunoreactivity was present in all

neuronal parts of the extrinsic and intrinsic arteries innervation, including different subpopulations of nerves. The results can expand our understanding of purinergic receptor expression on the sympathetic efferent neurons which could be used in the development of a novel therapeutic target for the modulation of vascular tone, thus having implications for the treatment of hypertension.

Conclusion and Implications: P2 receptor expression in mouse SMA, CA, SCG, and brain was investigated using RT-PCR. Showing the expression of P2X and P2Y could further be studied in autonomic and sensory-motor nerve function. Further examination of purinergic receptor expression on the sympathetic efferent neurons could be potential novel BP targets.

REFERENCES

1. Ralevic, V. (2012). P2X receptors in the cardiovascular system. *Wiley Interdisciplinary Reviews: Membrane Transport and Signaling*, 1(5), 663–674.
2. Sperlágh, B., Heinrich, A., & Csölle, C. (2007). P2 receptor-mediated modulation of neurotransmitter release—An update. *Purinergic Signaling*, 3(4), 269–284.

P029 | Sex-dependent differences of vascular K_v7 channels

Samuel Baldwin; Vincenzo Barrese; Jennifer Stott; Iain Greenwood
St George's, University of London

Background and Purpose: Vascular smooth muscle cells (VSMCs) dictate arterial diameter. As VSMCs contract, blood vessels narrow, reducing blood flow and increasing total peripheral resistance. VSMC contraction is achieved by an increase in intracellular calcium. $[Ca^{2+}]_i$ is dictated by VSMC membrane potential and the opening of voltage-gated calcium channels (VGCC). KCNQ-encoded K_v7 channels are shown to regulate VSMC membrane potential at rest, their activity mediates VSMC hyperpolarization deterring VGCC opening and vasoconstriction. K_v7 channels also contribute to an array of receptor-mediated responses, and in conjunction, K_v7 channels are degraded in hypertension, contributing to a hypertensive phenotype (Jepps et al., 2011). Despite the known contribution of K_v7 channels to VSMC physiology and pathophysiology, the wealth of current literature focuses predominantly on males.

Experimental Approach: We have compared KCNQ expression and function in coronary, cerebral, and renal arteries from male and female Wistar rats. We have characterized the expression patterns of all subtypes of α -subunit KCNQ and B-auxiliary subunit KCNE transcripts via qPCR, demonstrated the effect of the efficacy of K_v7 activators S-1 and ML277 to relax pre-constricted vessels as well as the contribution of K_v7 channels to Tx A2 receptor-mediated vasoconstriction via pan K_v7 channel blocker linopirdine.

Key Results: Arteries from female Wistar rats in dioestrus and metoestrus are less contractile to U46619 in a $K_v7.2-5$ sensitive manner and are more sensitive to S-1 when compared to arteries from

male and female pro-oestrus and oestrus Wistar rats. All vessels are insensitive to $K_v7.1$ channel activator ML277. There were no differences observed in the KCNQ/KCNE transcript expression profiles in arteries from male or female pro-oestrus and oestrus or female dioestrus and metoestrus Wistar rats.

Conclusion and Implications: Our data indicate a sex-dependent post-transcriptional difference in KCNQ regulation resulting in differential functional responses, showing a cycle-dependent shift in the potency of $K_v7.2-5$ activator to mediate vasorelaxation, sensitivity to U46619-mediated vasoconstriction, and $K_v7.2-5$ channel modulation of vasoconstriction. ML277 was shown to be incapable of relaxing pre-contracted arterial tone, indicating no functional role for $K_v7.1$.

REFERENCE

1. Jepps, T. A., et al. (2011). Downregulation of $K_v7.4$ channel activity in primary and secondary hypertension. *Circulation*. <https://doi.org/10.1161/CIRCULATIONAHA.111.032136>

P030 | α -CGRP mediates calcium-sensing receptor-induced vasorelaxation in rat mesenteric arteries

Simonette Carlton-Carew; Iain Greenwood; Anthony Albert
St George's, University of London

Background and Purpose: Stimulation of calcium-sensing receptors (CaSRs) expressed in the vasculature is reported to regulate vascular tone and is a potential novel therapeutic target for cardiovascular diseases, such as hypertension (Schepelmann et al., 2016). Therefore, our work investigates the functional and cellular mechanisms induced by activation of vascular CaSRs.

Experimental Approach: Wistar male rats (200–250 g) were culled in accordance with Animals (Scientific Procedures) Act 1986, and superior mesenteric artery branches were dissected.

Transverse arterial sections (10 μ m) were fixed on microscope slides and incubated with anti-CaSR primary antibodies. Immunohistochemical distribution was detected using a confocal microscope.

Artery branches were mounted on a wire myograph in 1-mM $CaCl_2$ ($[Ca^{2+}]_o$) physiological salt solution (95% O_2 /5% CO_2 ; 37°C). Arteries were pre-contracted with the bath application of 300-nM U46619 (Tx receptor agonist), and CaSRs were stimulated with cumulative increases of $[Ca^{2+}]_o$ (1–10 mM) in the presence and absence of inhibitors and a functional endothelium. Percentage changes in isometric tension were analysed using a sigmoidal concentration-effect curve to determine EC_{50} and maximal effect (E_{max}).

Statistical significance was determined using an ANOVA with Bonferroni's multiple comparisons test, and n represents number of animals.

Key Results: CaSRs were expressed in the endothelium, vascular smooth muscle, and adventitial (perivascular neurone-containing) layers.

Increasing $[Ca^{2+}]_o$ induced relaxations of U46619-mediated pre-contracted tone (EC_{50} 5.8 ± 0.8 mM, E_{max} $95.5 \pm 1.7\%$; $n = 6$). $[Ca^{2+}]_o$ -mediated relaxations were significantly impaired in the presence of the CaSR negative allosteric modulator, Calhex-231 (3 μ M; EC_{50} 6.5 ± 0.2 mM, E_{max} $88.5 \pm 2.1\%$; $n = 12$), removal of a functional endothelium (EC_{50} 6.6 ± 0.4 mM, E_{max} $52.5 \pm 8.9\%$; $n = 7$), and the functional desensitization of perivascular neurones with chronic incubation of capsaicin (10 μ M; EC_{50} 7.3 ± 0.4 mM, E_{max} $45.1 \pm 6.9\%$; $n = 5$). Additionally, $[Ca^{2+}]_o$ -mediated relaxations were hindered by blockers of NOS (300- μ M L-NAME; EC_{50} 8.0 ± 0.4 mM, E_{max} $63.2 \pm 6.1\%$; $n = 7$), large-conductance Ca^{2+} -activated potassium channels (BK_{Ca}) (200-nM iberiotoxin; EC_{50} 6.6 ± 0.3 mM, E_{max} $88.8 \pm 4.3\%$; $n = 7$), and the potent vasorelaxant, α -CGRP (1- μ M CGRP₈₋₃₇; EC_{50} 5.8 ± 0.2 mM, E_{max} $44.2\% \pm 4.8\%$; $n = 5$).

Endothelium removal and chronic capsaicin incubation together did not produce an additive inhibitory effect on $[Ca^{2+}]_o$ -mediated relaxations.

Conclusion and Implications: These data propose that stimulation of CaSRs on perivascular neurones causes α -CGRP release which acts on endothelial CGRP₁ receptors to induce vasorelaxation through endothelium-dependent NO production and vascular smooth muscle BK_{Ca} channel activation.

REFERENCE

1. Schepelmann, M., Yarova, P. L., Lopez-Fernandez, I., et al. (2016). The vascular Ca^{2+} -sensing receptor regulates blood vessel tone and blood pressure. *American Journal of Physiology. Cell Physiology*, 310(3), C193–C204.

P032 | Treprostinil has opposing effects on eNOS and AMPK activities in human pulmonary artery smooth muscle cells

Heba Abdelazeem¹; Yasmine Amgoud¹; Salma Mani¹; Adam Silverstein²; Yves Castier³; Xavier Norel¹

¹INSERM U1148, Paris 13 University; ²United Therapeutics Corporation; ³Hôpital Bichat-Claude Bernard, AP-HP, Paris Diderot University, Université de Paris

Background and Purpose: Pulmonary hypertension (PH) is a fatal disease characterized by an elevation in the mean pulmonary artery

pressure (above 20 mmHg) and loss of endothelial function. Although their mechanism of action is not fully elucidated, prostacyclin analogues (including treprostinil) are, up to date, among the most efficient treatments for this disease (Clapp & Gurung, 2015). AMP-activated protein kinase (AMPK) has been highlighted as a potential target for the management of PH (Liu et al, 2019) and has been shown to activate endothelial NOS (eNOS) in rat pulmonary artery (Agard et al, 2009). In this study, we investigated the effect of treprostinil on AMPK and eNOS activities in human pulmonary artery smooth muscle cells (hPASCs).

Experimental Approach: hPASCs were isolated from pulmonary arteries of six patients undergoing surgery in Bichat Hospital, Paris, France. hPASCs were grown in medium containing 10% fetal calf serum until reaching 70–80% confluence. Cells were then incubated with treprostinil (10^{-8} – 10^{-6} M) or metformin (3 mM) for 2 hr. Subsequently, cells were lysed and used for Western blot analysis of phosphorylated AMPK (T172) (pAMPK), total AMPK (tAMPK), phosphorylated eNOS (S1177) (peNOS), and phosphorylated Akt (S473) (pAkt). Paired t test was used for statistical analysis.

Key Results: Treprostinil (10^{-8} – 10^{-6} M) significantly decreased the phosphorylation of AMPK in a concentration-dependent manner. On the other hand, the same concentrations significantly increased the phosphorylation of eNOS. Incubation with metformin (3 mM) (AMPK activator) significantly augmented the phosphorylation of eNOS, although the metformin-induced increase in pAMPK level did not reach significance. In addition, the expression level of pAkt (a recognized stimulator of eNOS) was significantly enhanced by treprostinil (10^{-7} M).

Conclusion and Implications: In vitro, treprostinil decreases the activity of AMPK and increases the activity of eNOS in hPASCs as measured by the expression of the phosphorylated forms of these enzymes. The two effects seem to be independent of each other as metformin was able to increase the eNOS activity. Moreover, the stimulating effect of treprostinil on eNOS may be mediated through Akt pathway. Importantly, the increase in eNOS activity induced by treprostinil and metformin might play a beneficial role in the treatment of PH since NO is a major vasodilator of pulmonary vessels. Further experiments are needed to explore the physiological significance of these observations and to investigate the underlying mechanisms.

REFERENCES

1. Agard, et al. (2009). *British Journal of Pharmacology*.

TABLE 1 Effect of treprostinil and metformin on the phosphorylated form of different enzymes

Treatment	pAMPK/ β -actin (fold change) (n = 6)	pAMPK/tAMPK (fold change) (n = 6)	peNOS/ β -actin (fold change) (n = 6)	pAkt/ β -actin (fold change) (n = 5)
Control (untreated)	1 \pm 0	1 \pm 0	1 \pm 0	1 \pm 0
Treprostinil (10^{-8} M)	0.88 \pm 0.06	0.77 \pm 0.05*	1.34 \pm 0.13*	1.16 \pm 0.09
Treprostinil (10^{-7} M)	0.76 \pm 0.08*	0.74 \pm 0.08*	1.58 \pm 0.09*	1.24 \pm 0.08*
Treprostinil (10^{-6} M)	0.62 \pm 0.07*	0.62 \pm 0.07*	1.61 \pm 0.22*	1.21 \pm 0.15
Metformin (3 mM)	1.1 \pm 0.05	1.22 \pm 0.1	1.51 \pm 0.06*	1.12 \pm 0.14

*P < .05 versus control (untreated).

2. Clapp & Gurung (2015). *Prostaglandins & Other Lipid Mediators*.
3. Liu, et al. (2019). *Journal of Vascular Research*.

P033 | Pharmacological evaluation of novel FFA4 compounds

Eloise Euston; Abdulrahman G. Alharbi; Zhaoyang Dong;
Rudi Prihandoko; Andrew Tobin; Graeme Milligan

University of Glasgow

Background and Purpose: Free fatty acid receptor 4 (FFA4) is a GPCR responding to medium- and long-chain fatty acids. FFA4 is present in many tissues, including the gut and lung, and may play vital roles in metabolic diseases, such as diabetes, and respiratory diseases (Milligan, Alvarez-Curto, Hudson, Prihandoko, & Tobin, 2017). FFA4 is a potential drug target for inflammatory and metabolic diseases, and there is a need for novel ligands with better selectivity and potency than existing drugs. Here, we aim to evaluate novel FFA4 compounds using biochemical and pharmacological assays to assess whether FFA4 agonists are possible therapeutic strategies for such metabolic and immunological diseases.

Experimental Approach: CHO cells were stably transfected with mFFA4, and expression of FFA4 was confirmed by Western blot, probed with mFFA4 antibody, and immunohistochemistry. Using this stably transfected cell line, we tested a range of FFA4 compounds. Prior to functionality assays, samples were screened by Western blot probed with pERK and pFFA4 antibodies to determine ability of the agonist to activate FFA4 via the pERK pathway and induce receptor phosphorylation. FFA4 signalling to pERK after agonist stimulation was also tested by pERK HTRF Cisbio kit, to compare the potency and efficacy of the drugs.

Key Results: Here, we confirm presence of mFFA4 in stably transfected cell lines by Western blot and immunohistochemistry. Following this, we found that numerous FFA4 agonists were able to elicit a response in stably transfected CHO cells. From Western blot analysis, we see that agonists activate FFA4 and substantially up-regulate pERK signalling. It is also evident that agonists stimulate robust phosphorylation of mFFA4 receptor at residues Thr³⁴⁷/Ser³⁵⁰. Results indicate that mFFA4 agonist, Agonist 2, is the most promising compound in comparison to a commonly used synthetic ligand, TUG-891. Agonist 2 had a potency nearly equivalent to TUG-891 (7 [±0.080] and 7.1 [±0.086], respectively) but had a greater % max response (108.7% [±4.7] and 186.1% [±8.4], respectively) using TUG-891 as a reference ligand.

Conclusion and Implications: We have identified in a stably transfected cell line that FFA4 agonists activate FFA4 and elicit pERK signalling and receptor phosphorylation. From a range of compounds, Agonist 2 had a greater efficacy than TUG-891. As agonists show promising effects, they may be taken forward to cells endogenously expressing FFA4 and mouse models, to understand whether FFA4 agonists may be a therapy in FFA4-related inflammatory and metabolic diseases.

REFERENCE

1. Milligan, G., Alvarez-Curto, E., Hudson, B., Prihandoko, R., & Tobin, A. (2017). FFA4/GPR120: Pharmacology and therapeutic opportunities. *Trends in Pharmacological Sciences*, 38(9), 809–821.

P034 | The vasoregulatory role of hydrogen sulfide in thoracic aorta of normotensive and spontaneously hypertensive rats

Andrea Berenyiova¹; Samuel Golas¹; Marian Grman²;
Martina Cebova¹; Sona Cacanyiova¹

¹Centre of Experimental Medicine SAS, Institute of Normal and Pathological Physiology; ²SAS, Institute of Clinical and Translational Research BMC

Background and Purpose: Cardiovascular studies have confirmed that hydrogen sulphide (H₂S) is involved in different signalling pathways in both physiological and pathological conditions, including the aetiopathogenesis of hypertension. In the vessels, H₂S is produced mainly by cystathionine γ -lyase (CSE), which converts L-cysteine to H₂S. The aim of study was to describe the impact endogenously produced (after a CSE inhibition) and exogenously applied H₂S on the vasoactive responses of thoracic aorta (TA) in normotensive (Wistar) and spontaneously hypertensive rats (SHR).

Experimental Approach: In the experiments, 17- to 20-week-old Wistar rats and SHR were included. Systolic BP (sBP) was measured by plethysmographic method, and vasoactivity of TA was recorded by sensors of changes of isometric tension. CSE inhibition was performed by DL-propargylglycine (PPG) incubation for 20 min. The expression of CSE was determined by Western blotting. Statistical significance was determined using an ANOVA followed by Bonferroni's post hoc test.

Key Results: We observed an increased sBP (SHR: 173.29 ± 2.6 mmHg vs. Wistar: 123.3 ± 2.4 mmHg, $n = 8$, $P < .001$) and hypertrophy of myocardium in SHR (heart weight/body weight; SHR: 3.7 ± 0.07 mg·g⁻¹ vs. Wistar: 2.7 ± 0.06 mg·g⁻¹, $n = 8$, $P < .001$). While in Wistar an acute inhibition of CSE had no effect on endothelium-dependent relaxation, in SHR inhibited the relaxant response of smooth muscle cells to endogenous NO. However, CSE inhibition induced a moderate increase in the basal arterial tone of both strains; in SHR, this increasing was higher than in Wistar (SHR: 0.23 ± 0.08 g vs. Wistar: 0.06 ± 0.05 g, $n = 8$, $P < .05$). On the other hand, in Wistar, in contrast to SHR, an increased force of the noradrenaline-induced contraction (PPG– 0.145 ± 0.05 g vs. PPG+ 0.345 ± 0.09 g, $n = 8$, $P < .05$) and an increased sensitivity of adrenergic receptors to noradrenaline (EC₅₀: PPG– 7.7 ± 0.09 mol·L⁻¹ vs. PPG+ 7.11 ± 0.11 mol·L⁻¹, $n = 8$, $P < .001$) was confirmed after CSE inhibition. Dual vasoactive effect of H₂S donor (Na₂S) was showed in both strains; however, an increased maximal vasorelaxation was proved in SHR (SHR: 71.24 ± 3.09% vs. Wistar: 37.41 ± 4.39%, $n = 8$, $P < .001$). There was no difference in the expression of CSE in Wistar and SHR (SHR: 1.4 ± 0.21 A.U. vs. Wistar: 1.3 ± 0.21 A.U., $n = 6$).

Conclusion and Implications: The data confirmed that endogenous H₂S system contributes in the maintenance of the endothelial functions and it is probably involved into the reserved mechanisms able to compensate the increased sBP in SHR. Moreover, the exogenously applied H₂S behaves as an effective vasorelaxant agent in essential hypertension. Therefore, H₂S could be considered as a high perspective tool in the hypertension treatment.

ACKNOWLEDGEMENTS: This study was supported by VEGA 2/0111/19, VEGA 2/0103/18, and APVV-15-0565.

P036 | Hypertensive stimuli promote brain inflammation and cognitive impairment in a pressure-dependent manner

Chris Sobey; Quynh Nhu Dinh; T. Michael De Silva;
Grant Drummond

La Trobe University

Background and Purpose: Hypertension increases the risk for stroke and cognitive impairment and is strongly associated with inflammation of the vasculature and kidneys, as well as cerebrovascular dysfunction and oxidative stress. However, it is unclear to what extent there is inflammation and immune cell infiltration in the brain during hypertension. We aimed to test whether chronic administration of angiotensin II or aldosterone/salt causes brain inflammation and whether this is BP dependent.

Experimental Approach: Male C57Bl/6 mice were administered with vehicle (saline; $n = 22$) or angiotensin II (Ang II, 0.7 mg·kg⁻¹·day⁻¹ s.c.; $n = 23$) for 14 days via osmotic minipumps. A subset of mice also received hydralazine hydrochloride (50 mg·kg⁻¹; $n = 15$) in their drinking water for 14 days after minipump implantation. Another cohort of mice were treated with vehicle (87% propylene glycol, 9% ethanol, and 4% water; $n = 7$) or aldosterone (0.72 mg·kg⁻¹·day⁻¹ s.c. plus 0.9% NaCl for drinking; $n = 8$) for 14 days using osmotic minipumps. Systolic BP was measured using tail-cuff plethysmography, immune cell numbers using flow cytometry, and inflammatory markers using real-time PCR. Cognitive function was assessed using the novel object recognition test.

Key Results: Ang II infusion caused an increase in BP and promoted accumulation of leukocytes in the brain, including neutrophils, monocytes, T cells, and B cells, all of which were elevated by ~2.5-fold compared to vehicle-treated mice ($P < .05$). Similarly, aldosterone/salt-induced hypertension was associated with increases in brain myeloid cells (~3.5-fold) and T cells (~2-fold) ($n = 7-8$, $P < .05$). Co-administration of hydralazine prevented the pressor response to Ang II (163 ± 5 mmHg vs. Ang II + hydralazine, 121 ± 4 mmHg; $n = 7-8$, $P < .05$). Ang II-induced increases in brain neutrophils and monocytes were blunted by co-administration of hydralazine ($n = 7-8$, $P < .05$). Ang II-induced increases in brain mRNA expression of chemokine (C-C motif) receptor 2 (CCR2) and chemokine (C-C motif) ligand 2 (CCL2) and CCL8 were also blunted by co-administration of hydralazine ($n = 7-8$, $P < .05$). Finally, Ang II resulted in mice having no

preference for interaction with the novel object, indicating impaired working memory, but this deficit was normalized by co-administration with hydralazine.

Conclusion and Implications: Our data indicate that immune cell infiltration and inflammation occur in the brain in association with cognitive impairment during hypertension. Hypertension-induced cognitive impairment and brain infiltration of myeloid cells appears to be pressure dependent. Chronic brain inflammation may be a contributing factor to the increased stroke risk and cognitive impairment during hypertension and may be mitigated by BP reduction.

P037 | Novel arginine formulations of celecoxib fully retain COX-2 inhibitory and anti-cancer activity and reverse L-NAME-induced endothelial dysfunction

Nicholas Kirkby; Hime Gashaw; Andreas Perikleous; Plinio Ferreira;
Blerina Ahmetaj-Shala; Jane Mitchell

Imperial College London

Background and Purpose: Celecoxib and other nonsteroidal anti-inflammatory drugs (NSAIDs) work by blocking COX-2. They have proven anti-inflammatory, analgesic, and anti-cancer effects, but their use is associated with increased risk of heart attacks and strokes. We have previously identified increased levels of the endogenous eNOS inhibitor asymmetric dimethylarginine (ADMA) as a potential explanation for NSAID-induced cardiovascular risk. As the effects of ADMA can be reversed by the eNOS substrate L-arginine, L-arginine-containing formulations of celecoxib could have the potential for improved cardiovascular safety. Here, we have tested whether a novel formulation (1:20 by mass) of celecoxib and L-arginine retains both efficacy as a COX-2 inhibitory and anti-cancer drug and can reverse endothelial dysfunction induced by eNOS inhibition.

Experimental Approach: In all assays, celecoxib, arginine, and celecoxib + arginine (in 0.1% DMSO) were tested in a 1:20 mass ratio, such that at a standard dose of celecoxib (200 mg·day⁻¹), a therapeutic dose of L-arginine might be delivered (4 g·day⁻¹). COX-2 activity was measured in LPS-induced J774 murine macrophage cells as PGE₂ release by immunoassay. Anti-cancer activity was measured in Caco2 human colon cancer cells by cell counting. Endothelial function was measured by wire myography in aortae from Lister Hooded rats pre-contracted with phenylephrine (1 μM in PBS), stimulated with ACh (10 μM in PBS), and with NOS dysfunction induced by L-NAME (100 μM in PBS).

Key Results: Celecoxib produced concentration-dependent inhibition of PGE₂ formation in LPS-induced J774 cells (Figure 1a) and killed Caco2 colon cancer cells (Figure 1b). Arginine had no effect alone in either assay and did not alter the activity of celecoxib when added together in a 1:20 mass ratio. Arginine produced a concentration-dependent reversal of L-NAME-induced endothelial dysfunction in rat aortae, and this was not altered in the presence of celecoxib (Figure 1c).

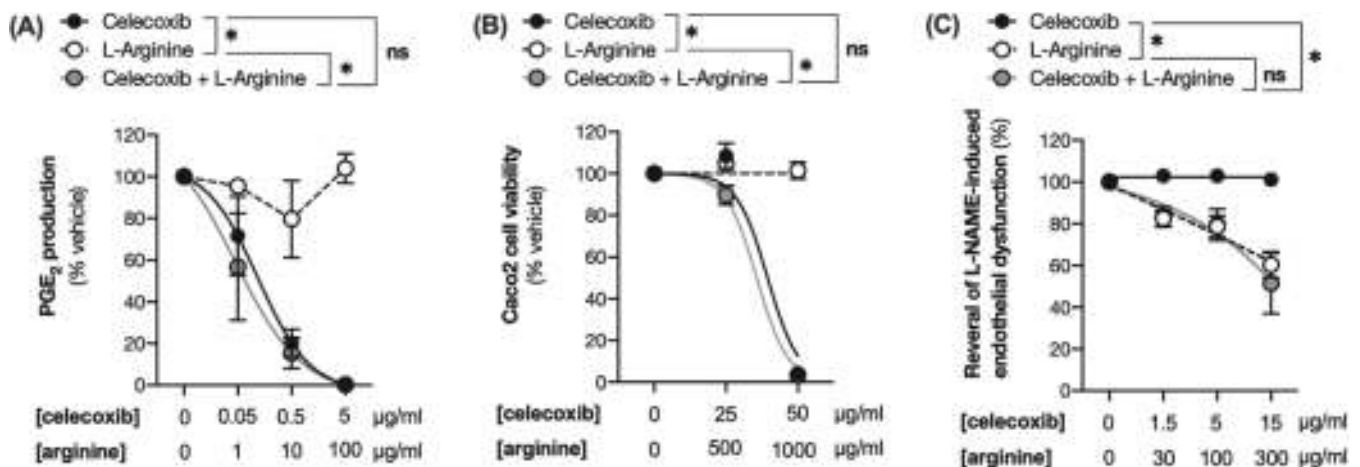


FIGURE 1. Effect of celecoxib and arginine, alone and in combination on (a) PGE₂ production by LPS-induced J774 cells ($n = 3$), (b) Caco2 colon cancer cell viability after 96 hr ($n = 3$), and (c) L-NAME-induced endothelial dysfunction in rat aortae ($n = 4$). * $P < .05$ by two-way ANOVA with Tukey's posttest

Conclusion and Implications: Combining celecoxib and arginine in this novel formulation does not compromise the COX-2 inhibitor and anti-cancer activity of celecoxib or the ability of arginine to reverse endothelial dysfunction induced by eNOS inhibition. As such, we suggest that arginine-containing formulations of celecoxib could be developed that fully retain therapeutic efficacy for the treatment of inflammation and cancer but can negate cardiovascular injury associated with celecoxib-triggered accumulation of ADMA and other endogenous eNOS inhibitors.

REFERENCE

- Ahmetaj-Shala, B., Kirkby, N. S., Knowles, R., Al-Yamani, M., Mazi, S., Wang, Z., ... Mitchell, J. A. (2014). Evidence that links loss of cyclooxygenase-2 with increased asymmetric dimethylarginine: Novel explanation of cardiovascular side effects associated with anti-inflammatory drugs. *Circulation*, 131(7), 633–642.

P038 | Unravelling β -phenylethylamine-induced vasodilation: A role for trace amine-associated receptors?

Alex Voisey; Kenneth Broadley; William Ford

Cardiff University

Background and Purpose: β -Phenylethylamine (β -PEA) is a trace amine that induces vasoconstriction at high concentrations. β -PEA also induces the release of NO from the endothelium that opposes this vasoconstrictor response. This study investigates the dual role of β -PEA as both a vasoconstrictor and a vasodilator.

Experimental Approach: Aortic rings (5 mm) from male Sprague Dawley rats were immersed in Krebs bicarbonate solution gassed CO₂/O₂ (5%/95%) at 37°C under 1.5 g of resting tension. Absence of endothelium was confirmed by a lack of relaxation to 100- μ M carbachol of rings pre-constricted with 60-mM KCl. Aortic rings were pre-

constricted with phenylephrine (30 nM) prior to construction of cumulative concentration–response curves (CRCs) to β -PEA. CRCs were generated in the presence or absence of endothelium, L-NAME (100 μ M), the β_2 -adrenoceptor antagonist, ICI,118,551 (1 μ M), atropine (100 nM), the trace amine-associated receptor (TAAR1) antagonist, EPPTB (5 μ M), or 5-HT receptor desensitisation (10 μ M). Vasodilator responses reported as a percentage of the contraction obtained with 60-mM KCl were measured using PowerLab, Chart 5 software (ADInstruments). Means were compared using Student's unpaired t test. Statistical significance was accepted for $P \leq .05$.

Key Results: β -PEA induced concentration-dependent vasodilation of rat aorta. Endothelium removal or inhibition of NO significantly, but not completely, suppressed vasodilator responses. Endothelium removal and inhibition of NO significantly reduced the maximum vasodilator response from $-37.8 \pm 5.6\%$ ($n = 17$) to $-16.2 \pm 2.1\%$ ($n = 11$) and $-17.8 \pm 4\%$ ($n = 7$), respectively. Atropine did not reduce β -PEA vasodilator responses in endothelium-intact aortic rings. In both endothelium intact and denuded aortic rings, ICI,118,551 and EPPTB did not significantly reduce vasodilator responses to β -PEA. Desensitisation of 5-HT receptors did not significantly reduce vasodilator responses to β -PEA in either endothelium intact or denuded aortic rings.

Conclusion and Implications: The vasodilatation of rat aorta by β -PEA is not mediated by muscarinic or 5-HT receptors or β_2 -adrenoceptors. The failure of EPPTB to inhibit the response suggests that TAAR1 is not involved, although its selectivity for rat TAAR1 is unknown.

P039 | Exploring the mechanism of hypotonic-induced ATP release

Samantha Atkinson; Alyn Morrice; Laura Sadofsky

University of Hull

Background and Purpose: Cough remains a poorly treatable, unmet clinical need. The complete pathway involved in the activation of afferent nerve fibres evoking the cough reflex remains unclear. Recent advances suggest that release of ATP in the airways leads to activation of the purinergic receptor, P2X3, evoking cough, which can be inhibited using Merck's antagonist gefapixant (MK-7264/AF-219). The release of ATP may occur following activation of TRPV4; however, the downstream signalling mechanism connecting the two is not yet fully understood. Previous studies have shown that activation of TRPV4 by hypotonic stimulation led to activation of RhoA followed by Rho kinase-dependent myosin light chain (MLC) phosphorylation (Seminario-Vidal et al., 2011). It has also been shown that ATP release by hypotonic stimulation occurred via pannexin-1 channel (PNX-1) opening, whereby knockdown reduced ATP release by 50%. Here, we suggest a potential secondary mechanism of ATP release following hypotonic stimulation and show the integral components involved in ATP release in the airway in an in vitro cell model.

Experimental Approach: An immortalised alveolar epithelial (A549) cell line was pre-incubated with inhibitors to TRPV4 (10-µM HCO67047), RhoA (1-µM H-1152), MLC (1-µM ML-7), pannexin-1 (10-µM carbenoxolone [CBX]), or calcium-calmodulin kinase II (10-µM CamKII [KN93]) and then subjected to 33% hypotonic stimulation. ATP release was measured using a commercially available luminescent-based kit.

Key Results: Data were reported as percentage change and AUC from control hypotonic stimulation. Inhibition of MLC (via MLCK) and PNX-1 (CBX) significantly reduced peak ATP release following hypotonic stimulus alone, 21.79% and 29.82% reduction, respectively ($P < .05$). TRPV4 inhibition (HCO67047) did not affect peak ATP release but caused a delayed response. We also found that inhibition of CamKII alone resulted in the largest inhibition from a single antagonist, 23.75% reduction, of ATP release ($P < .0001$). Collective inhibition of CamKII and PNX-1 resulted in the largest reduction in peak ATP release, 22.89% reduction ($P < .001$), and overall ATP release, 400% reduction ($P < .0001$), in comparison to hypotonic stimulation alone.

Conclusion and Implications: We propose that ATP release by hypotonic stimulation is largely mediated by CamKII activity and therefore intracellular calcium.

REFERENCE

1. Seminario-Vidal, L., Okada, S. F., Sesma, J. I., Kreda, S. M., van Heusden, C. A., Zhu, Y., ... Lazarowski, E. R. (2011). Rho signaling regulates pannexin 1-mediated ATP release from airway epithelia. *The Journal of Biological Chemistry*, 286, 26277–26286.

P040 | Pharmacological characterisation of the human P2X4 receptor

Anna Fortuny-Gomez; Samuel Fountain

University of East Anglia

Background and Purpose: P2X receptors are ligand-gated ion channels activated by extracellular ATP. Activation causes membrane depolarisation and elevation in cytoplasmic Ca^{2+} (Samways et al., 2014). P2X4 receptors are involved in both health and disease (e.g., pain, inflammation, and cardiovascular disease). Hence, P2X4 receptor is a promising drug target. This project aims to characterise the pharmacological profile of human P2X4 receptor amid some recent advances in small molecule development (Stokes et al., 2017).

Experimental Approach: 1321N1 human astrocytoma cells stably expressing the human P2X4 receptor were loaded with Fura-2 and stimulated with agonists and antagonists. Receptor activity was measured as intracellular Ca^{2+} influx using a FlexStation3 instrument. Data were expressed as mean ± SEM, and N represents the number of repeats. Concentration–response curves were fitted by a Hill equation and used to obtain EC_{50} and IC_{50} values. Statistical analysis was assessed by two-tailed *t* test or a Mann–Whitney *U* test.

Key Results: All agonists tested evoked a calcium response in a dose-dependent manner and were ranked in order of potency (EC_{50}) and

TABLE 1 Summary of human P2X4 receptor agonists EC_{50} and E_{max} and antagonists IC_{50} values

Agonists	EC_{50} (µM)	E_{max} (F_{ratio})	Antagonists	IC_{50} (µM)
ATP (N = 7)	0.704 ± 0.15 ^a	1.465 ± 0.15 ^d	BX430 (N = 5)	0.426 ± 0.13
2-mSATP (N = 5)	1.732 ± 0.27 ^b	0.767 ± 0.10	5-BDBD (N = 5)	1.243 ± 0.19 ^f
CTP (N = 6)	12.67 ± 2.82 ^c	0.817 ± 0.14	PSB12062 (N = 5)	0.237 ± 0.03
α,β-mATP (N = 6)	7.612 ± 6.83	0.162 ± 0.03 ^e	PPADS (N = 5)	33.89 ± 16.6 ^g
			Suramin (N = 5)	–

^a $P < .05$ versus each agonist.

^b $P < .05$ versus CTP and α,β-mATP.

^c $P < .05$ versus α,β-mATP.

^d $P < .05$ versus each agonist.

^e $P < .01$ versus CTP and 2-mSATP.

^f $P < .01$ versus BX430 and PSB12062.

^g $P < .05$ versus each antagonist.

efficacy (E_{max}) (Table 1). Selective antagonists and PPADS showed inhibitory effects on human P2X4 receptor activity and were ranked in order of potency (IC_{50}). Suramin did not block receptor activity at all concentrations tested (Table 1).

Conclusion and Implications: ATP acts as a full agonist at the human P2X4 receptor, whereas CTP, 2-mSATP (2-methylthio-ATP), and α,β -mATP (α,β -methylene-ATP) acted as partial agonists. BX430 (1-(2,6-dibromo-4-isopropyl-phenyl)-3-(3-pyridyl)urea) and PSB12062 (*N*-(*p*-methylphenylsulfonyl)phenoxazine) were significantly the most potent antagonists, followed by 5-BDBD (5-(3-bromophenyl)-1,3-dihydro-2*H*-benzofuro[3,2-*e*]-1,4-diazepin-2-one) and PPADS (pyridoxal phosphate-6-azophenyl-2',4'-disulfonic acid). Data also suggest that human P2X4R is insensitive to blockade by the broad-spectrum antagonist suramin.

REFERENCES

1. Samways, et al. (2014). *Frontiers in Cellular Neuroscience*, 8, 1–18.
2. Stokes, et al. (2017). *Frontiers in Pharmacology*, 8, 1–15.

P041 | Structure–activity relation of ivermectin: A positive allosteric modulator of the human P2X4 receptor

Jessica Meades; Samuel Fountain

University of East Anglia

Background and Purpose: Ivermectin (IVM) is as a positive allosteric modulator of the P2X4 receptor, a ligand-gated ion channel activated by ATP. Various features restrict IVM as a viable pharmacological tool for P2X4 receptor modulation, including its ability to

bind and modulate other mammalian ion channels. Lack of selective modulators for P2X4 channels has hindered research advancement, despite the growing evidence implicating P2X4 as a feasible therapeutic target in several cardiovascular and neurological disorders.

This study aims to investigate the structure–activity relationship of IVM using a range of structural analogues at the human P2X4 receptor. This information will be used to refine the SAR information for positive allosteric modulation of P2X4 and provide insight for developing drugs that can target this receptor with increased potency and selectivity.

Experimental Approach: Fura-2-loaded 1321N1 astrocytoma cells stably expressing the human P2X4 receptor were used to assay ATP-evoked intracellular Ca^{2+} responses using a FlexStation III instrument. IVM analogues were tested for their ability to modulate maximal and potency of ATP. Data was expressed as mean \pm SEM, and *n* represents the number of biological repeats. Dose–response curves were fitted to the Hill1 sigmoidal equation and used to determine EC_{50} and maximum response (R_{max}). Statistical significance was determined using an unpaired two sample *t* test or Mann–Whitney *U* test where appropriate.

Key Results: ATP elicited intracellular Ca^{2+} responses in a concentration-dependent fashion ($EC_{50} = 0.45 \pm 0.032 \mu M$, *n* = 5). Concentration–response curves for IVM, together with all structural analogues, demonstrated a dose-dependent enhancement in ATP-evoked intracellular Ca^{2+} response. All compounds investigated were ranked in order of potency and efficacy (Table 1). As seen in Table 1, there are some significant differences in the EC_{50} and R_{max} values between the test compounds.

Concentration–response curves for ATP in the presence and absence of test compound demonstrated that IVM, and a range of structural analogues, caused a leftward shift in the dose–response

TABLE 1 Rank order for potency (EC_{50}) and efficacy (R_{max}) for IVM and its structural analogues

Potency rank		Efficacy rank	
Test compound	EC_{50} (μM)	Test compound	R_{max} (%)
Eprinomectin (<i>n</i> = 6)	$1.56 \pm 0.25^{*,\alpha,\beta}$	Abamectin (<i>n</i> = 7)	$968.3 \pm 61.4^{*,\beta}$
Selamectin (<i>n</i> = 5)	$0.97 \pm 0.11^{\alpha,\beta}$	Nemadectin (<i>n</i> = 5)	$781.8 \pm 59.9^{*,\gamma,\delta,\epsilon,\eta}$
Milbemectin (<i>n</i> = 7)	$0.90 \pm 0.18^{\alpha,\beta}$	Doramectin (<i>n</i> = 5)	660.8 ± 28.9
Ivermectin (<i>n</i> = 7)	0.75 ± 0.07	Ivermectin (<i>n</i> = 7)	546.6 ± 49.8
Nemadectin (<i>n</i> = 5)	$0.72 \pm 0.05^{\alpha,\beta}$	Moxidectin (<i>n</i> = 5)	$524 \pm 48.7^{\alpha,\beta}$
Moxidectin (<i>n</i> = 5)	$0.47 \pm 0.06^{*,\gamma,\delta,\eta}$	Eprinomectin (<i>n</i> = 6)	$521 \pm 29.3^{\alpha,\beta,\delta}$
Abamectin (<i>n</i> = 7)	$0.42 \pm 0.09^*$	Milbemectin (<i>n</i> = 7)	$439 \pm 41.2^{\alpha,\beta}$
Doramectin (<i>n</i> = 5)	$0.40 \pm 0.03^*$	Selamectin (<i>n</i> = 5)	$423.7 \pm 13.4^{*,\alpha,\beta}$

**P* < .05 versus ivermectin.

^α*P* < .05 versus abamectin.

^β*P* < .05 versus doramectin.

^γ*P* < .05 versus eprinomectin.

^δ*P* < .05 versus selamectin.

^ε*P* < .05 versus milbemectin.

^η*P* < .05 versus nemadectin.

curve accompanied by a decrease in ATP EC₅₀ value and an increase in maximum Ca²⁺ response in the presence of compound.

Conclusion and Implications: All structural analogues of IVM investigated potentiate the intracellular Ca²⁺ response through hP2X4 channels and can be ranked in terms of their potency and efficacy. Overall, the data suggest that IVM and several structural distinct analogues investigated in this study act as positive allosteric modulators of human P2X4 and provide new chemical information.

P042 | Direct vasorelaxant effect of the selective P2Y2 receptor antagonist AR-C118925XX in mesenteric arteries: Constitutive release of purines

Aali Alqarni¹; Putcharawipa Maneesai²; William Dunn¹; Vera Ralevic¹

¹University of Nottingham; ²Khon Kaen University

Background and Purpose: Adipocyte constitutive ATP release and subsequent activation of P2Y2 receptors have recently been shown to regulate basal lipolysis in human adipocytes (Ali, Turner, & Fountain, 2018). This study investigated the possibility that UTP and ATP are released constitutively from perivascular adipose tissue (PVAT) to regulate the vascular tone of mesenteric arteries.

Experimental Approach: Mesenteric arteries with and without PVAT were obtained from large white hybrid pigs and were prepared for isometric tension recording. Mesenteric small arteries (second order and fat free) isolated from male Sprague-Dawley rats (250–300 g) were set up for recording using pressure myography. After precontraction with the Tx A2 receptor agonist U46619, the selective P2Y2 receptor antagonist AR-C118925XX (10 μM) was added for 60 min. The non-selective P2 receptor antagonist suramin (100 μM) was also added to the porcine mesenteric artery. UTP (1–300 μM) was applied cumulatively to porcine mesenteric artery to study the effect of exogenous UTP.

Key Results: Both suramin (100 μM) and AR-C118925XX (10 μM) caused a significant relaxation of U46619-precontracted vascular tone in porcine mesenteric arteries 26.27 ± 2.2% (n = 7) and 25.98 ± 1.6% (n = 8), respectively. The time course and relaxation response to suramin and AR-C118925XX were very similar in both fat and fat-free mesenteric arteries. AR-C118925XX at 1 μM did not alter the vascular tone in porcine mesenteric arteries. UTP induced a concentration-dependent contraction, which was not affected by both suramin and AR-C118925XX in both fat and fat-free porcine mesenteric arteries. In rat mesenteric arteries without PVAT, which were pre-contracted with U46619, 10-μM AR-C118925XX elicited relaxation of 70.79 ± 13.44% (n = 4), which was significantly different to

relaxation by its solvent, 0.001% DMSO, at 16.92 ± 9.55% (n = 4) (P < .05); 1-μM AR-C118925XX also elicited relaxation of 15.03 ± 9.67% (n = 3) in rat mesenteric arteries.

Conclusion and Implications: These data show a direct vasorelaxant effect of two structurally unrelated P2 receptor antagonists on vascular tone of precontracted mesenteric arteries. The evidence thus far suggests that this does not involve PVAT. It points to a possible involvement of endogenously released ATP or UTP, acting via vasocontractile P2 receptors, which are blocked by the antagonists to cause vasorelaxation, but further investigation is needed.

REFERENCE

1. Ali, S., Turner, J. J. O., & Fountain, S. J. (2018). *Journal of Cell Science*, 131, jcs221994.

P043 | PGE₂ sensitizes the cough reflex centrally via activation of EP3 receptors but independently of TRPV1 and TRPA1 channels

Ahmed El-Hashim; Al-Shaimaa Al-Kandery

Kuwait University

Background and Purpose: PGE₂ is an inflammatory mediator with established roles in the induction/sensitization of the cough reflex through a peripheral action. However, whether PGE₂ can sensitize the cough reflex via a central action is not known. In this study, using conscious guinea pig model of cough, we investigated whether PGE₂ can sensitize the cough reflex via a central action and if so through which mechanisms.

Experimental Approach: Drugs were administered to guinea pigs via an intracerebroventricular route 1 week following stereotaxic surgery. Aerosolized citric acid (CA, 0.2 M) was used to induce cough in a whole-body plethysmograph following drug infusion, and coughs were recorded with an automated analyzer.

Key Results: PGE₂ dose-dependently enhanced the CA-induced cough. A similar effect was seen with the non-selective EP1/EP3 agonist, sulprostone. Pretreatment with the EP1 antagonist, ONO-8130, did not alter the sulprostone-induced sensitization, whilst the EP3 receptor antagonist, L-798,106, dose-dependently inhibited this effect. Treatment with either EP2 receptor agonist, butaprost, or the EP4 agonist, L-902,688, had no effect on the CA-induced cough. Pretreatment with the TRPV1 antagonist, JNJ-17203212, or TRPA1 antagonist, HC-030031, did not alter the PGE₂-enhanced CA-induced cough.

Conclusion and Implications: This study shows that PGE₂ can sensitize the cough reflex through a central mechanism of action via activation of central EP3 receptors and independently of TRPV1/TRPA1 channels activation.

Drug	Control	Dose 1	Dose 2	Dose 3
	Cough, mean \pm SEM	Cough, mean \pm SEM	Cough, mean \pm SEM	Cough, mean \pm SEM
PGE ₂	2.75 \pm 0.94 (n = 12)	0.3 mg·ml ⁻¹	0.6 mg·ml ⁻¹	1 mg·ml ⁻¹
		5.25 \pm 1.53 (n = 8)	7.58 \pm 1.28 (n = 12) [*]	16.31 \pm 3.16 (n = 13) ^{***}
Sulprostone	3.44 \pm 1.3 (n = 9)	0.1 mg·ml ⁻¹	0.3 mg·ml ⁻¹	1 mg·ml ⁻¹
		6 \pm 2.2 (n = 8)	8.29 \pm 1.9 (n = 7) [†]	10.3 \pm 1.33 (n = 9) ^{**}
ONO-8130	15.8 \pm 5.67 (n = 10)	1 mg·ml ⁻¹	5 mg·ml ⁻¹	–
		15.71 \pm 2.92 (n = 7)	16.83 \pm 4.45 (n = 6)	
L-798,106	16.3 \pm 3.49 (n = 10)	2.5 mg·ml ⁻¹	5 mg·ml ⁻¹	–
		8.29 \pm 1.69 (n = 7)	6.2 \pm 1.88 (n = 10) [*]	
Butaprost	2.27 \pm 0.93 (n = 11)	0.3 mg·ml ⁻¹	1 mg·ml ⁻¹	–
		2.5 \pm 1.56 (n = 8)	2.6 \pm 1.1 (n = 10)	
L-902,688	2.29 \pm 1.25 (n = 7)	0.3 mg·ml ⁻¹	1 mg·ml ⁻¹	–
		2.33 \pm 1.29 (n = 9)	2.38 \pm 0.92 (n = 8)	
JNJ-17203212	12.1 \pm 1.92 (n = 10)	0.4 mg·ml ⁻¹	1.3 mg·ml ⁻¹	–
		11 \pm 4.55 (n = 10)	8.5 \pm 1.68 (n = 8)	
HC-030031	14.25 \pm 2.29 (n = 8)	0.02 mg·ml ⁻¹	0.05 mg·ml ⁻¹	–
		11.57 \pm 3.6 (n = 7)	13 \pm 3.48 (n = 6)	

*P value <.05.

**P value <.01.

***P value <.001.

P044 | Increased PFKL and PFKM expression underlies increased glycolysis in pulmonary arterial smooth muscle cells from patients with pulmonary arterial hypertension

Jeries Abu-Hanna; Evangelos Anastasakis; Jan-Willem Taanman; Markella Ponticos; David Abraham; Lucie Clapp

University College London

Background and Purpose: Pulmonary arterial hypertension (PAH) is a rare, progressive, life-threatening disease of the pulmonary vasculature (Paulin and Michelakis, 2014). A key cellular event in PAH is the switching of pulmonary arterial smooth muscle cells (PASCs), resident within the medial layers of small pulmonary arteries, from a quiescent and contractile phenotype to a proliferative and synthetic one (Paulin and Michelakis, 2014). The mechanisms that underlie this phenotypic switch remain unclear and are thought to involve a metabolic switch from mitochondrial respiration to glycolysis as postulated by the metabolic theory of PAH (Paulin and Michelakis, 2014). Phosphofructokinase 1 (PFK1) catalyses the phosphorylation of fructose-6-phosphate to fructose-1,6-bisphosphate, which constitutes the rate-limiting step in cytosolic glycolysis, and its levels are correlated with glycolytic flux (Mor et al., 2011). PFK1 is a tetramer composed of three different subunits PFKP, PFKM, and PFKL, encoded by three different genes

(Mor et al., 2011). We therefore sought to investigate whether the expression of PFKP, PFKM, and PFKL is increased in PAH PASCs.

Experimental Approach: PASCs isolated from the lungs of controls or patients with PAH (both adults and children) were grown to full confluency in 10% FBS in six-well plates, serum starved in 0.1% FBS for 48 hr, and lysed for protein. Western blotting in conjunction with densitometry was performed to determine the relative protein levels of PFKP, PFKM, and PFKL. Lung tissue sections from control and PAH patients were stained for PFKM and PFKL using immunohistochemistry and imaged using the Nanozoomer Digital Scanner. Seahorse XFp Glycolysis Stress Test was used to measure extracellular acidification rates (ECARs) in control and PAH PASCs. ECARs were normalised to protein content, which was quantified by the Pierce BCA Protein Assay. Unpaired *t* test was used, and statistical significance was indicated by *P* < .05.

Key Results: The relative protein levels of the PFK1 subunits PFKL and PFKM, but not PFKP, were significantly increased in PAH PASCs compared to their control counterparts. Moreover, in contrast to control PASCs, PASCs from PAH patients exhibited markedly increased ECARs, including those associated with glycolysis, non-glycolytic acidification, glycolytic capacity, and glycolytic reserve. Lung tissue sections from PAH patients stained more strongly for both PFKL and PFKM than those derived from controls. As an example, immunoblotting and immunohistochemical staining of PFKL are shown above.

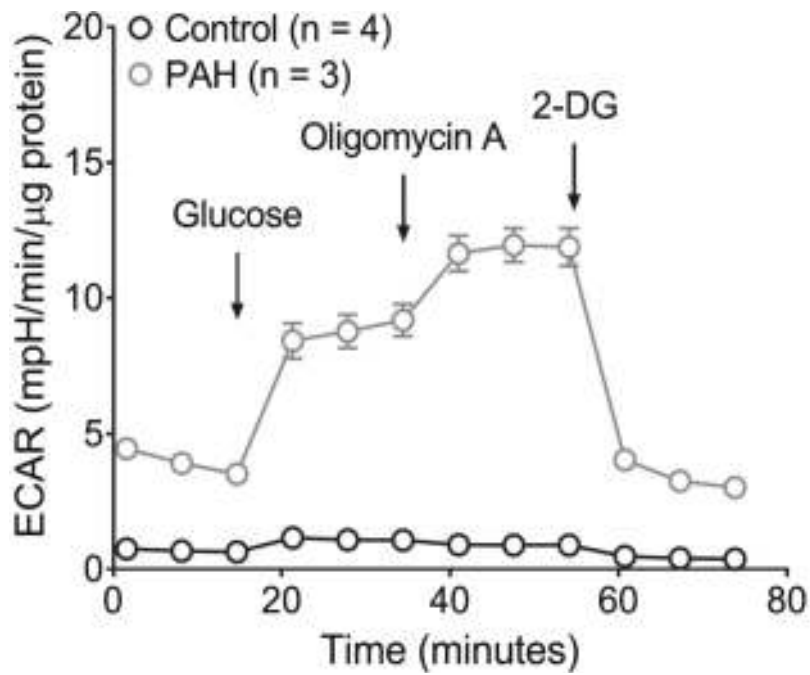
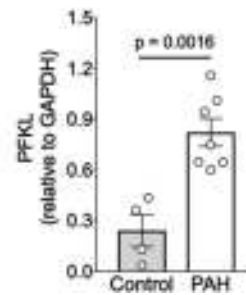
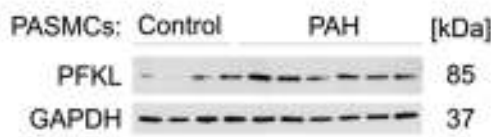
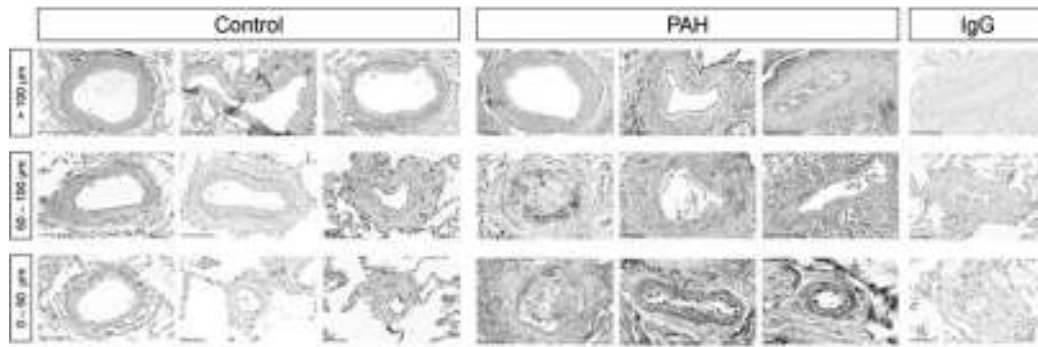


FIGURE 1

Conclusion and Implications: Taken together, these results show that glycolytic flux is markedly increased in PAH PASMCS, when compared to control PASMCS, and suggest that increased expression of the PFK1 subunits PFKL and PFKM, but not PFKP, may underlie this increased glycolytic flux.

REFERENCES

- Mor, I., Cheung, E. C., & Vousden, K. H. (2011). Control of glycolysis through regulation of PFK1: Old friends and recent additions. *Cold Spring Harbor Symposia on Quantitative Biology*, 76(211), 216.
- Paulin, R., & Michelakis, E. D. (2014). The metabolic theory of pulmonary arterial hypertension. *Circulation Research*, 115(1), 148-164.

P046 | Understanding the synergy between polymyxin B and ivacaftor against cystic fibrosis *Pseudomonas aeruginosa*: An untargeted metabolomics study

Elena Schneider-Futschik¹; Rafah Allowabi¹; Drishti Ghelani¹; Maytham Hussein¹; Jian Li²; Tony Velkov¹

¹The University of Melbourne; ²Monash University

Background and Purpose: Polymyxins are used to treat multidrug-resistant *Pseudomonas aeruginosa* lung infections in cystic fibrosis (CF) patients. As resistance to polymyxins can rapidly emerge in *P. aeruginosa* with monotherapy, combination therapy is often the only remaining treatment option.

Experimental Approach: In the present study, we employed metabolomics to investigate the synergistic mechanisms of polymyxin B in combination with the cystic fibrosis transmembrane conductance regulator (CFTR) ivacaftor against polymyxin-susceptible and -resistant *P. aeruginosa* isolates from the lungs of CF patients. The in vitro synergistic activity of polymyxin B combined with ivacaftor was assessed using checkerboard and static time-kill assays against a panel of isolates from the lungs of CF patients. The metabolomes of two *P. aeruginosa* strains (PA14 PMB MIC = 2 mg·L⁻¹; PA-06 MIC = 8 mg·L⁻¹) were analysed following treatment with polymyxin B, ivacaftor, and the combination for 1, 3, and 6 hr.

Key Results: Polymyxin B and ivacaftor were ineffective when used individually. However, when used together, the combination of clinically relevant concentrations of polymyxin B (2 mg·L⁻¹) combined with ivacaftor (8 mg·L⁻¹) displayed synergistic killing activity. Polymyxin B monotherapy induced significant perturbations in glycerophospholipid (GPL) metabolism, pentose phosphate pathway, citric acid cycle, pyrimidine ribonucleotide biogenesis, guanine ribonucleotide biogenesis, and histidine degradation pathways in the polymyxin-susceptible strain and minimal perturbation in polymyxin-resistant strain. The synergy appears to be ivacaftor driven affecting the lipid pathway (figure).

Conclusion and Implications: Overall, these novel findings demonstrate that the disruption of key metabolic features associated with synergistic bacterial killing by the combination against *P. aeruginosa* in CF.

REFERENCES

- Hussein, M., Han, M. L., Zhu, Y., Schneider-Futschik, E. K., Zhou, Q. T., Lin, Y. W., ... Velkov, T. (2018 Nov 10). Mechanistic insights from global metabolomics studies into synergistic bactericidal effect of a polymyxin B combination with tamoxifen against cystic fibrosis MDR *Pseudomonas aeruginosa*. *Computational and Structural Biotechnology Journal*, 16, 587–599.
- Schneider, E. K., Azad, M. A., Han, M. L., Tony Zhou, Q., Wang, J., Huang, J. X., ... Velkov, T. (2016 Jul 8). An “unlikely” pair: The antimicrobial synergy of polymyxin B in combination with the cystic fibrosis transmembrane conductance regulator drugs KALYDECO and

ORKAMBI. *ACS Infectious Diseases*, 2(7), 478–488. <https://doi.org/10.1021/acsinfecdis.6b00035> Epub 2016 May 17

P047 | Oestrogen metabolism in idiopathic pulmonary arterial hypertension

Nina Denver¹; Natalie Homer²; Eric Austin³; Ruth Andrew²; Margaret MacLean¹

¹Strathclyde University; ²University of Edinburgh; ³Vanderbilt University

Background and Purpose: Endogenous sex hormone exposure represents a risk factor in pulmonary arterial hypertension (PAH) where there is a female predominance. Females, however, have a greater survival time than males following diagnosis. This suggests a potential role for sex hormones in disease pathogenesis and right ventricular compensation (Austin et al., 2013). The main circulating oestrogens, oestrone (E1) and oestradiol (E2), can be converted to 16-hydroxyoestrogens (16OHE1 and 16OHE2), shown to contribute to disease progression via proliferative pathways (Hood et al., 2016). Alternatively, methoxyoestrogen metabolites (4MeOE1, 2MeOE2, and 4MeOE2) are emerging as anti-proliferative agents, potentially protective and with therapeutic benefit (Docherty, Nilsen, Maclean, 2019). 2MeOE1 is thought inactive. We hypothesised that the oestrogen metabolite profile is altered towards mitogenic metabolites in PAH contributing to disease phenotype.

Experimental Approach: Serum was collected with ethical approval from Vanderbilt Medical Center, USA, for blinded analysis of oestrogen levels between idiopathic (iPAH) patients ($n = 11, 12$) compared to non-PAH control ($n = 17, 17$) (female and males, respectively). We applied our novel validated LC-MS/MS method coupled with derivatisation to profile oestrogen metabolites in PAH (Denver et al., 2019). Results are shown as the mean \pm SEM in non-PAH versus iPAH with P values following Kruskal-Wallis non-parametric statistical tests applying Bonferroni's post hoc tests for significant changes. Values below the confirmed limit of quantification (LOQ) were inserted as the LOQ. Correlations of metabolite concentrations with age and BMI were tested with Spearman's correlations.

Key Results: In comparison to controls, concentrations of E1 (24.8 ± 2.4 vs. 41.9 ± 8.0 pg·ml⁻¹, $P = .05$), E2 (15.1 ± 1.5 vs. 23.3 ± 2.5 pg·ml⁻¹, $P = .02$), and 16OHE1 (25.8 ± 2.8 vs. 76.8 ± 12.0 pg·ml⁻¹, $P = .01$) were elevated in male iPAH. However, in females, concentrations of E1 were reduced (48.8 ± 8.0 vs. 22.7 ± 5.7 pg·ml⁻¹, $P = .01$) with an increase in 16OHE1 (26.3 ± 4.7 vs. 36.5 ± 6.0 pg·ml⁻¹, $P = .04$) and 16OHE2 (12.2 ± 2.8 vs. 18.1 ± 12.0 pg·ml⁻¹, $P = .001$) in iPAH. There was a correlation between 16OHE2 concentrations with age in female iPAH patients ($R^2 = .7$, $P = .04$) and with BMI in male controls ($R^2 = .8$, $P = .03$).

Conclusion and Implications: We identify evidence of disturbed oestrogen metabolism in iPAH patients with sex-dependent increases in formation of 16-hydroxylated metabolites. Furthermore, parent oestrogens, E1 and E2, were elevated in males, while E1 was reduced

in females. Sex-dependent alterations in oestrogen production and metabolism may underpin the pathobiology of idiopathic PAH.

REFERENCES

1. Austin, E. D., Lahm, T., West, J., Tofovic, S. P., Johansen, A. K., Maclean, M. R., ... Oka, M. (2013). Gender, sex hormones and pulmonary hypertension. *Pulmonary Circulation*, 3, 294–314.
2. Denver, N., Khan, S., Stasinopoulos, I., Church, C., Homer, N. Z., MacLean, M. R., & Andrew, R. (2019). Derivatization enhances analysis of estrogens and their bioactive metabolites in human plasma by liquid chromatography tandem mass spectrometry. *Analytica Chimica Acta*, 1054, 84–94.
3. Docherty, C. K., Nilsen, M., & Maclean, M. R. (2019). Influence of 2-methoxyestradiol and sex on hypoxia-induced pulmonary hypertension and hypoxia-inducible factor-1. *Journal of the American Heart Association*, 1–10.
4. Hood, K. Y., Montezano, A. C., Harvey, A. P., Nilsen, M., Maclean, M. R., & Touyz, R. M. (2016). Nicotinamide adenine dinucleotide phosphate oxidase-mediated redox signaling and vascular remodeling by 16 α -hydroxyestrone in human pulmonary artery cells. *Hypertension*, 68, 796–808.

P048 | Cardiac MRI and haemodynamic assessment of macitentan in a sugen/hypoxic rat model of pulmonary hypertension

Gerard Murphy¹; Geeshath Jayasekera¹; James Mullin²; Lindsay Gallagher²; Yvonne Dempsey¹; David J. Welsh¹

¹Glasgow Caledonian University; ²University of Glasgow

Background and Purpose: Macitentan is a dual endothelin receptor antagonist used in the treatment of pulmonary arterial hypertension (PAH) that has been shown to reduce morbidity and mortality in PAH patients (Pulido et al., 2013). Using cardiac MRI (CMR) and pulmonary haemodynamic measurements, we determined the effect of macitentan therapy on the right ventricle (RV) in the Sugén 5416 combined with chronic hypoxia (Su/Hx) model of pulmonary hypertension (PH).

Experimental Approach: Four-week-old male Sprague Dawley rats received a subcutaneous injection of Sugén 5416 (20 mg·kg⁻¹), followed by 3-week hypobaric hypoxia (550 mbar), then 2 weeks in normoxic conditions (1,013 mbar). Normoxic rats were maintained over the same time course without receiving Sugén. Rats subsequently received macitentan (30 mg·kg⁻¹) or vehicle (gelatin) via daily oral gavage for a further 3 weeks. Pulmonary haemodynamics were determined using the Mikro-Tip[®] Pressure Volume System, measuring right ventricular systolic pressure (RVSP). Remodelled pulmonary arteries were indicated by the presence of a double elastic lamina, shown by elastin–Picrosirius Red. Separately, CMRs using a Bruker PharmaScan 7T system were taken before treatment, at week 5 (baseline), at week 7, and at week 8. Planimetry determined RV and left ventricle (LV) volumes and ventricles mass, which were indexed to total body surface area (TBSA). RVSP and remodelling were analysed using an ordinary one-way ANOVA or a repeated measures one-way ANOVA/mixed effects analysis for CMR data, both ANOVAs were followed by Tukey's post hoc test.

Key Results: Using repeat CMR, we determined that 2 weeks of macitentan treatment led to a decrease in RV mass by 22.1% ($P < .01$ vs. baseline). At 3 weeks, RV mass had decreased by 28.3% ($P < .05$ vs. baseline) (Figure 1). Su/Hx led to an increase in RVSP from 28.73 ± 1.25 to 52.18 ± 3.89 mmHg ($n = 4$; $P < .001$ normoxic vehicle vs. Su/Hx vehicle). Macitentan treatment reduced RVSP to 32.74 ± 1.09 mmHg ($n = 4$; $P < .001$ Su/Hx vehicle vs. Su/Hx macitentan) (Figure 2). The percentage of remodelled pulmonary arteries were also increased from $10.69 \pm 1.35\%$ to $41.4 \pm 1.93\%$ ($n = 6$; $P < .0001$ normoxic vehicle vs. Su/Hx vehicle). Macitentan reduced remodelling to $34.4 \pm 1.79\%$ ($n = 6$; $P < .05$ Su/Hx vehicle vs. Su/Hx macitentan).

Conclusion and Implications: Macitentan treatment resulted in lower RVSP, lower pulmonary artery remodelling, and lower RV mass, suggesting improved RV structure and function in a Su/Hx rat model of PH. Evidence of direct macitentan action on the RV requires further research.

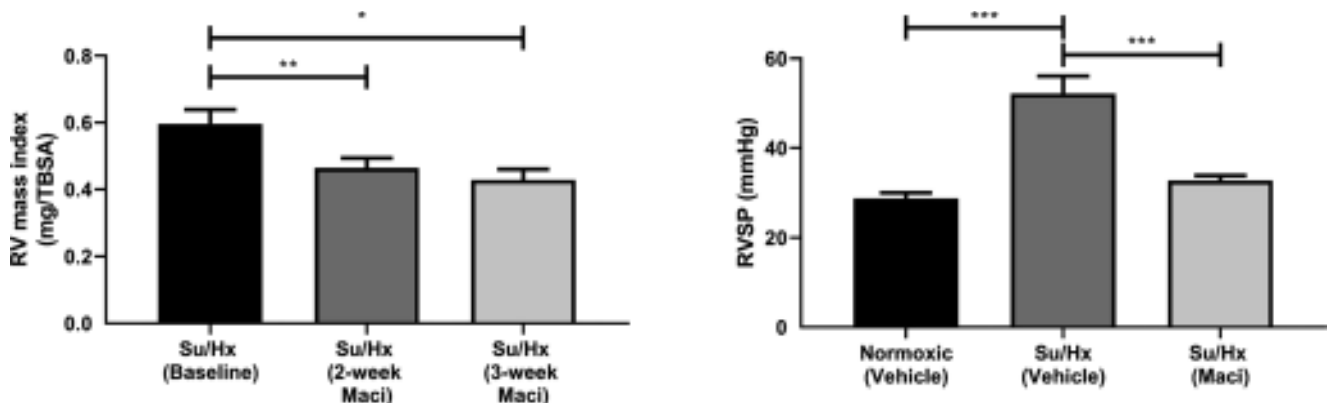


FIGURE 1. Effect of macitentan on RV mass in Su/Hx rats determined by repeat CMR. Data expressed as mean \pm SEM. * $P < .05$, ** $P < .01$, $n = 5-6$

REFERENCE

1. Pulido, T., et al. (2013). Macitentan and morbidity and mortality in pulmonary arterial hypertension. *The New England Journal of Medicine*, 369 (9), 809–818.

P049 | Mitochondrial biogenesis and function are increased in pulmonary arterial smooth muscle cells isolated from patients with pulmonary arterial hypertension

Jeries Abu-Hanna; Evangelos Anastasakis; Jan-Willem Taanman; Markella Ponticos; David Abraham; Lucie Clapp

University College London

Background and Purpose: Pulmonary arterial hypertension (PAH) is a rare, progressive, life-threatening disease of the pulmonary vasculature (Paulin and Michelakis, 2014). Central to the pathogenesis of PAH is the switching of pulmonary arterial smooth muscle cells (PASMCs), which reside within the medial layers of small pulmonary arteries, from a quiescent and contractile phenotype to a proliferative and synthetic one (Paulin and Michelakis, 2014). The mechanisms underlying this phenotypic switch remain poorly understood and are thought to involve changes in mitochondrial activity and dynamics as postulated by the metabolic theory of PAH (Paulin and Michelakis, 2014). We therefore sought to investigate whether mitochondrial biogenesis and function are altered in PASMCs from patients with PAH compared to their control counterparts.

Experimental Approach: PASMCs derived from the lungs of controls

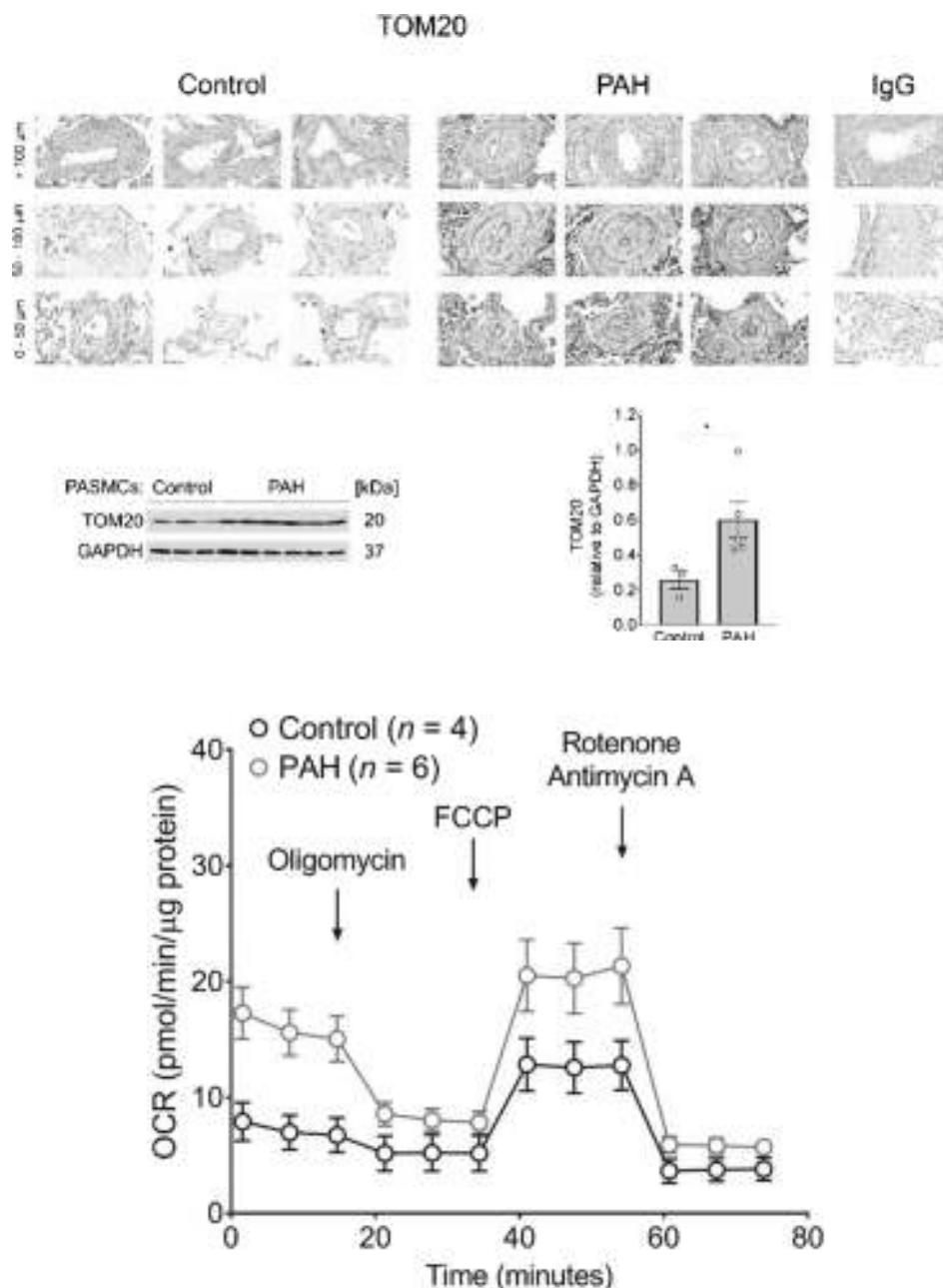


FIGURE 1

or patients with PAH (diagnosed as mean pulmonary arterial pressure >25 mmHg) were grown to full confluency in 10% FBS in six-well plates, quiesced in 0.1% FBS for 48 hr, and lysed for protein. Western blotting together with densitometry was performed to determine the relative protein levels of transcriptional regulators of mitochondrial biogenesis (e.g., PGC1 α , NRF1, NRF2, and TFAM; Hock and Krallie, 2009) and markers of mitochondrial mass (e.g., SDHA, TOM20, VDAC, and MTCO2). Lung tissue sections from control and PAH patients were stained for PGC1 α , SDHA, and TOM20 using immunohistochemistry and imaged using the Nanozoomer Digital Scanner. Seahorse XFp Mito Stress Test was used to measure oxygen consumption rates (OCRs) in control and PAH PSMCs. OCRs were normalised to protein content, which was quantified using Pierce BCA Protein Assay. Unpaired *t* test was used and statistical significance indicated by *P* < .05.

Key Results: The relative protein levels of the mitochondrial biogenesis regulators PGC1 α , NRF1, NRF2, and TFAM were significantly increased in PAH PSMCs compared to their control counterparts, indicative of increased mitochondrial biogenesis in PAH PSMCs. Moreover, the relative protein levels of the mitochondrial mass markers SDHA, TOM20, VDAC, and MTCO2 were elevated in PAH PSMCs, suggesting increased mitochondrial mass in PAH PSMCs. Lung tissue sections from PAH patients stained more strongly, particularly in the medial layers of small pulmonary arteries, for PGC1 α , SDHA, and TOM20 than those derived from controls. As an example, immunoblotting and immunohistochemical staining for TOM20 are shown above. In contrast to control PSMCs, PSMCs from PAH patients exhibited increased OCRs, as shown above, including those associated with basal respiration, ATP production, and maximal respiration.

Conclusion and Implications: Taken together, these results suggest that mitochondrial biogenesis is increased in PAH PSMCs, leading to increased mitochondrial mass and respiration. This provides evidence against the depressed mitochondrial function that was previously proposed for PAH PSMCs.

REFERENCES

Hock, M. B., & Krallie, A. (2009). Transcriptional control of mitochondrial biogenesis and function. *Annual Review of Physiology*, 71(177), 203.
 Paulin, R., & Michelakis, E. D. (2014). The metabolic theory of pulmonary arterial hypertension. *Circulation Research*, 115(1), 148-164.

Poster Session: Drug Discovery, Development and Evaluation 1

P050 | **Measuring inflammatory oedema formation and neutrophil accumulation in dorsal skin: Refining a method to reduce the number of mice used**

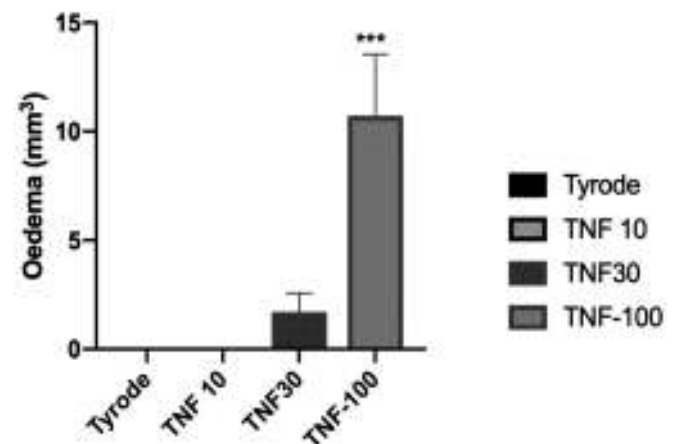
Ali Zarban; Hiba Chaudhry; Susan Brain
 King's College London

Background and Purpose: Minimising the number of animals used is a key goal of experimental design. We have refined a model for measuring inflammatory oedema formation in mouse dorsal skin where intravenously injected Evans Blue dye (which binds to albumin) acts as an oedema marker (Sawyer et al., 2011). In the absence of Evans Blue, no oedema formation can be measured. Neutrophil-dependent oedema formation is under investigation, and myeloperoxidase (MPO, primarily localised to neutrophils) is assayed to assess neutrophil accumulation in dorsal skin (Bradley et al., 1982; Cao et al., 2000). It would reduce numbers of mice used if both assays can be performed on the same skin site. We hypothesise that this is feasible and that Evans Blue dye does not interfere with the MPO assay absorbance readings.

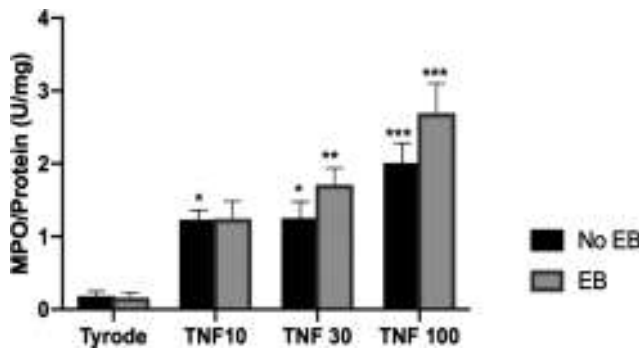
Experimental Approach: Procedures were performed according to the UK Home Office Animals (Scientific Procedures) Act 1986. CD1 male mice (8-10 weeks old) were divided into two groups, transiently anaesthetised with isoflurane (induced at 5% and maintained at 2%) and injected intravenously with either Evans Blue (5 mg·kg⁻¹) or vehicle. Both groups received intradermal injections (50 μ l) of substance P (SP 300 pmol) + CGRP (20 pmol) and/or TNF- α (10, 30, and 100 ng) and vehicle control (Tyrode) according to a randomised balanced site design. After 4 hr, the mouse was humanely killed, and the dorsal skin was collected. The ellipsoid shaped sites were assessed as volume of oedema by calculation of $(\pi/6) \times \text{length} \times \text{width} \times \text{depth}$ (Kodji et al., 2013). The sites were then punched out (16-mm diameter) and homogenised for measurement of MPO using the MPO assay described here (Cao et al., 2000), with absorbance read at 620-nm wavelength.

Key Results: The results (Figure 1) show that significant oedema formation was observed in the Evans Blue injected mice with SP + CGRP (used as a neutrophil-independent oedema positive control) and TNF- α . Assay of MPO showed TNF- α -induced significant neutrophil accumulation over 4 hr in a similar manner in both groups, whilst no MPO was observed in the SP + CGRP site as expected.

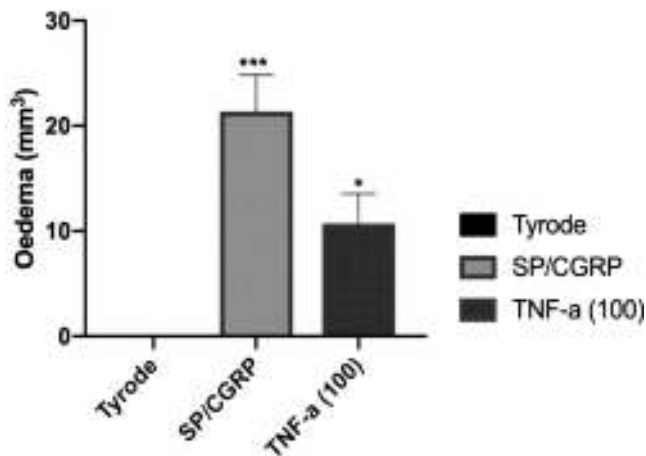
(a)



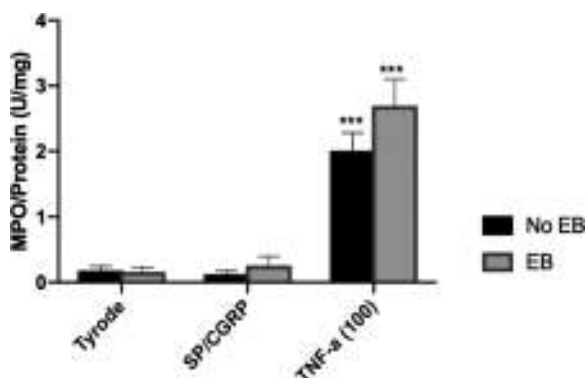
(b)



(c)



(d)



Conclusion and Implications: The Evans Blue dye does not interfere with the absorbance readings from the MPO assay. Our findings suggest that the same mouse can be used for both assays, thus reducing the mice used by 50%.

ACKNOWLEDGEMENTS

A.Z. is funded by Jazan University, Saudi Arabia, and H.C. is funded by BHF.

REFERENCES

- Bradley, et al. (1982). *Journal of Investigative Dermatology*, 78, 206–209.
- Cao, et al. (2000). *Journal of Immunology*, 164, 5424–5429.
- Kodji, et al. (2013). *Pharmacology*. pa2online.org/abstract/abstract.jsp?abid=31265
- Sawyer, et al. (2011). *PLoS ONE*, 6e114671.

P051 | In silico pharmacological assessment of mibefradil in single detrusor smooth muscle cell towards understanding the urinary bladder overactivity

Chitaranjan Mahapatra; Rohit Manchanda

Indian Institute of Technology Bombay

Background and Purpose: Enhanced spontaneous contraction of the detrusor smooth muscle (DSM) cells, which is also known as DSM instability, is associated with overactive bladder (OAB), a pathophysiological syndrome affecting millions of individuals socially (Brading & Brain, 2011). Due to the adverse side effects of conventional anticholinergic drugs, researchers are focusing on novel drug compounds with high specificity. Understanding the drug effects with respect to various ion channels offers additional possibilities for safety pharmacological assessment. Here, our overarching objective was to utilize computational approaches to simulate the effects of the T-type Ca^{2+} channel blocker mibefradil on the DSM cell action potential (AP) and subsequent DSM cell excitability.

Experimental Approach: The DSM cell model is described as an equivalent electrical circuit consisting of a membrane capacitance connected in parallel with a number of variable conductances representing two voltage-gated Ca^{2+} (T type and L type) channels, two voltage-gated potassium (Kv and KCNQ) channels, three calcium-dependent potassium (BK, IK, and SK) channels, an ATP-dependent potassium channel, and an inward rectifying cation channel (Mahapatra, Brain, & Manchanda, 2018). A drug model for mibefradil was simulated by multiplying the maximal conductance of T-type Ca^{2+} channel with a scaling factor between 0 and 1 to mimic the drug concentration.

Key Results: In this model, all ionic conductances were tuned to set the resting membrane potential (RMP) at -50 mV. A synaptic input for 15 ms was injected to evoke the AP. The maximum conductance value of the T-type Ca^{2+} channel (\bar{g}_{CaT}) was set to $0.0006 \text{ S}\cdot\text{cm}^{-2}$. Adding mibefradil by 50% of its control value reduced the peak

amplitude of AP and inward current. However, the addition of mibefradil by 100% resulted in no AP and zero inward currents. The T-type Ca^{2+} conductance was varied by up to $\pm 50\%$ of the control value in discrete steps to study the RMP sensitivity analysis. Note that RMP varies at most by up to $+10\%$ and -15% , indicating T-type Ca^{2+} conductance-dependent DSM cell excitability. These results show that T-type Ca^{2+} channels play an important role in generating AP and deactivation of T-type Ca^{2+} channels decrease the excitability of DSM cell.

Conclusion and Implications: We investigated the ability of the mibefradil to modulate DSM cell's AP using our computational model, which provides a virtual electrophysiological workbench. This *in silico* assessment showed that inhibition of T-type Ca^{2+} channels hyperpolarized the RMP eliminated the AP and reduced DSM cell excitability. This study suggests that a compound, such as mibefradil, may form a part of a new pharmacological strategy in the treatment of OAB.

REFERENCES

1. Brading AF, Brain K.L. (2011). Ion channel modulators and urinary tract function. In *Urinary tract* (pp. 375–393). SpringerBerlin Heidelberg.
2. Mahapatra, C., Brain, K. L., & Manchanda, R. (2018). A biophysically constrained computational model of the action potential of mouse urinary bladder smooth muscle. *PLoS ONE*, 13(7), e0200712.

P052 | Analysing the factors that regulate expression of blood–brain barrier drug transporter proteins

Yu Siong Ho¹; Pablo Torres-Vergara²; Jeffrey Penny¹

¹University of Manchester; ²University of Concepción

Background and Purpose: The ATP-binding cassette (ABC) efflux transporters, ABCB1, ABCG2, and ABCC5, expressed in the blood–brain barrier (BBB) have greatly impaired the pharmacotherapy of brain disorders by reducing drug entry into the CNS (Shubbar & Penny, 2018). The nuclear receptors pregnane X receptor (PXR), constitutive androstane receptor (CAR), and the retinoid X receptor (RXR) are master regulators of ABC efflux transporter activities, and their mechanisms of actions are tightly regulated by the glucocorticoid receptor (GR) in hepatocytes (Hunter et al., 2017). Hence, a better understanding of how nuclear receptors regulate the BBB transporters may help improve therapeutic drugs delivery into the CNS.

Experimental Approach: Primary porcine brain capillary endothelial cells (PBECs) were isolated based on the method previously described (Rubin et al., 1991). Transporter (ABCB1, ABCG2, and ABCC5) activities were determined by measuring intracellular accumulation of fluorescent probes in cells pretreated with the transporter inhibitors. Western blotting was used to determine transporters and nuclear receptors (PXR, CAR, RXR, and GR) expression. The regulatory role of nuclear receptors on transporter activities and expressions was

investigated using pharmacological inducers and inhibitors. All data are reported as mean \pm SD for $n \geq 3$ independent experiments with statistical significance indicated by one-way ANOVA, Tukey's post hoc test.

Key Results: In PBECs pretreated with ABCB1 inhibitor (10- μM verapamil), ABCG2 inhibitor (0.5- μM Ko143) or ABCC5 inhibitor (25- μM Mk147) for 30 min significantly increased ($P < .005$) intracellular accumulation of calcein, Hoechst-33342, and CMFDA (5-chloromethylfluorescein diacetate), respectively. Western blotting confirmed the expression of all the investigated transporters and nuclear receptors in PBECs. Treatment with 10- μM rifampicin (PXR inducer) for 24 hr significantly increased ($P < .05$) all three transporter activities and expressions. The reverse was true for 5- μM L-sulforaphane (PXR inhibitor), 5- μM CITCO (CAR inducer), and 10- μM meclizine (CAR inhibitor). Treatment with 10- μM dexamethasone and hydrocortisone (GR inducers), for 24 hr, significantly enhanced ($P < .05$) the activity and expression of all the transporters and nuclear receptors investigated.

Conclusion and Implications: Key drug efflux transporters (ABCB1, ABCC5, and ABCG2) and regulatory nuclear receptors (PXR, RXR, CAR, and GR) known to be expressed in the BBB *in vivo* are expressed in PBECs. Furthermore, these components of BBB xenobiotic-sensing/detoxification system are functionally active. All three transporter activities are significantly influenced by the activation and inhibition of PXR, CAR, and RXR. These three nuclear receptors are regulated by the activation of GR. Future studies will investigate the intracellular signalling pathways governing BBB transporter expression and activity.

REFERENCES

1. Hunter, S. R., et al. (2017). *Drug Metabolism and Disposition*, 45(2), 118–129.
2. Rubin, L. L., et al. (1991). *The Journal of Cell Biology*, 1991(115), 1725–1735.
3. Shubbar, M. H., & Penny, J. I. (2018). *Biochimica et Biophysica Acta - General Subjects*, 862(10), 2314–2322.

P053 | Using immobilised artificial membrane HPLC to probe the “micro PK/PD” of adenosine receptor ligands

Jack Lochray; Stephen Briddon; Steven Charlton

University of Nottingham

Background and Purpose: This group has previously shown, using fluorescence correlation spectroscopy (FCS), that ligands can concentrate around the phospholipid membrane where their cognate receptors reside, possibly distorting observed pharmacology parameters such as affinity values and association rates (Gherbi, Briddon, & Charlton, 2018). However, FCS has limited direct use in drug discovery as it is time consuming and unable to be used on unlabelled compounds. Here, an immobilised artificial membrane HPLC (IAM-HPLC)

TABLE 1 Previously obtained local concentrations and kinetic values for fluorescent adenosine receptor ligands compared to physicochemical measurements of lipophilicity (cLogD) and membrane interaction (LogkIAM)

Compound	Structure	Concentration 2 μm above membrane (nM) (n = 8)	k_{off} (min^{-1}) (n = 4)	k_{on} ($\text{min}^{-1}\cdot\text{mM}^{-1}$) (n = 4)	K_{d} (nM) (n = 4)	cLogD	LogkIAM (n = 3)
XAC-X-BY	XAC-X-BY630	1,024.6 \pm 347.4	0.55 \pm 0.23	16,700 \pm 8,030	36.0 \pm 6.4	3.39	3.2 \pm 0.05
CA200645	XAC-BY630	62.3 \pm 9.5	0.57 \pm 0.17	1,330 \pm 175	461 \pm 10.7	2.39	2.81 \pm 0.04
AV075	XAC-asn-ala-X-BY630	111.3 \pm 30.1	0.17 \pm 0.10	791 \pm 36.4	346 \pm 30.2	0.87	2.86 \pm 0.02

assay has been assessed as a potential surrogate for determining membrane affinity for three fluorescent xanthine amine congener (XAC)-based adenosine receptor ligands. This has been compared to previous kinetic binding rates and local concentration data to better understand how physicochemical properties of ligands could affect their micropharmacokinetics/micropharmacodynamics.

Experimental Approach: Twenty microlitres of 10- μM compound was injected into an HPLC system containing a 30-mm IAM.PC.DD2 column mimicking cell membranes, at a flow rate of 0.5 $\text{ml}\cdot\text{min}^{-1}$ using a combination of 50-mM ammonium acetate pH 7.4 as the aqueous phase and acetonitrile as organic phase. Retention factors (kIAM) were calculated as $(T_r - T_0)/T_0$, where T_r is the retention time between injection of compound and detection by a photodiode array detector (600–650 nm) and T_0 (dead time) as the retention time of citric acid, which has effectively no affinity for the column. In order to detect the compounds in a reasonable time, an isocratic elution was repeated at several concentrations of acetonitrile and data extrapolated to get kIAM values in 0% organic solvent. Calculated log values of partition between octanol and water at pH 7.4 (cLogDpH7.4) were obtained from Chemicalize online software. In all cases, data presented mean \pm SEM (n experiments).

Key Results: Previous data indicated that XAC-X-BY had a greater propensity to concentrate in the local vicinity of the receptor over CA200645 and AV075 when all added at 0.1xKd (Table 1). Calculated LogD values suggest that CA200645 is over an order of magnitude more lipophilic compared to AV075. However, experimentally derived kIAM values suggest that their affinity for membrane is more similar.

Conclusion and Implications: kIAM values appear to better explain the difference in local concentration compared to more traditionally used cLogD values. This could be due to more complicated interactions with charged phospholipid head groups as a pose to simple partition between octanol and water. As such, kIAM-HPLC assays could be useful in estimating and accounting for local ligand concentration in drug discovery.

REFERENCE

Gherbi, K., Briddon, S., & Charlton, S. (2018). Micro-pharmacokinetics: Quantifying local drug concentration at live cell membranes. *Scientific Reports* Feb 22, 8(1), 3479.

P055 | Structure-based development of novel chemical scaffolds as inhibitors of the store-operated calcium entry pathway

Sinayat Mahzabeen¹; Aneesh Chandran²; Jack Greenhalgh¹; Saifur Rahman¹; Taufiq Rahman¹

¹University of Cambridge; ²IIT Madras

Background and Purpose: The "store-operated calcium entry" (SOCE) pathway is almost ubiquitous and triggered when intracellular calcium stores (e.g., endoplasmic reticulum [ER]) are depleted physiologically or pharmacologically. SOCE is mediated by the pore-forming Orai1 protein, which is activated by aggregated, ER membrane-localised Stim proteins acting as the ER calcium sensor. Aberrant SOCE activity seems to underlie various diseases including cancer, inflammation, and acute pancreatitis. There have been efforts in the academia as well as the industry to develop SOCE modulators, and few hits have emerged and are in early phases of clinical trial. Most of the existing SOCE inhibitors originate from phenotypic screening and derivatisation of some initial hits; that were not much selective against the SOCE and non-SOCE pathway. Recently, few structures of the *Drosophila* Orai (DmOrai) have been published, and we sought out to explore whether we can identify novel SOCE-inhibitory chemical scaffolds utilising a more targeted approach utilising the available DmOrai structure.

Experimental Approach: We built a homology model of human Orai1 (hOrai1) using DmOrai structure (pdb: 4HKR). We then chose few known SOCE inhibitors that are proven to act via Orai1 and docked them blindly (i.e., unbiasedly) with AutoDockVina against the hOrai1 model in several independent docking runs. From the docked poses, we identified few potential pockets to which these inhibitors could bind. We then virtually screened the Enamine Diversity library against those pockets using FRED (OpenEyesTM) and then re-docked by GOLD (CCDC, Cambridge). We then purchased top 11 hits and tested them using Fura-2-based calcium imaging of RBL-1 cells (Rahman & Rahman, 2017). The true positives from calcium assay were tested using NFAT assay using previously published protocols (Gwack et al., 2006). HeLa cells stably expressing human NFAT1(1-460)-GFP were used to evaluate inhibition of thapsigargin-evoked nuclear translocation of NFAT.

Key Results

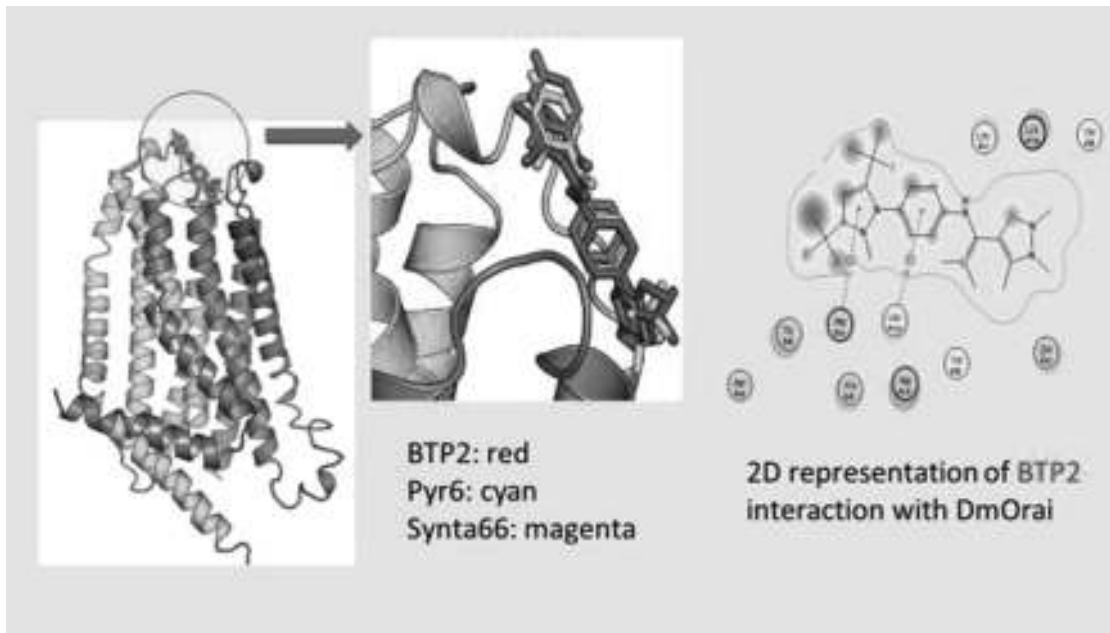


FIGURE 1 A potential site for inhibitor binding on Orai1 has been shown based on Chemgauss (FRED) and ChemPLP (GOLD) score and blind docking with AutoDock Vina

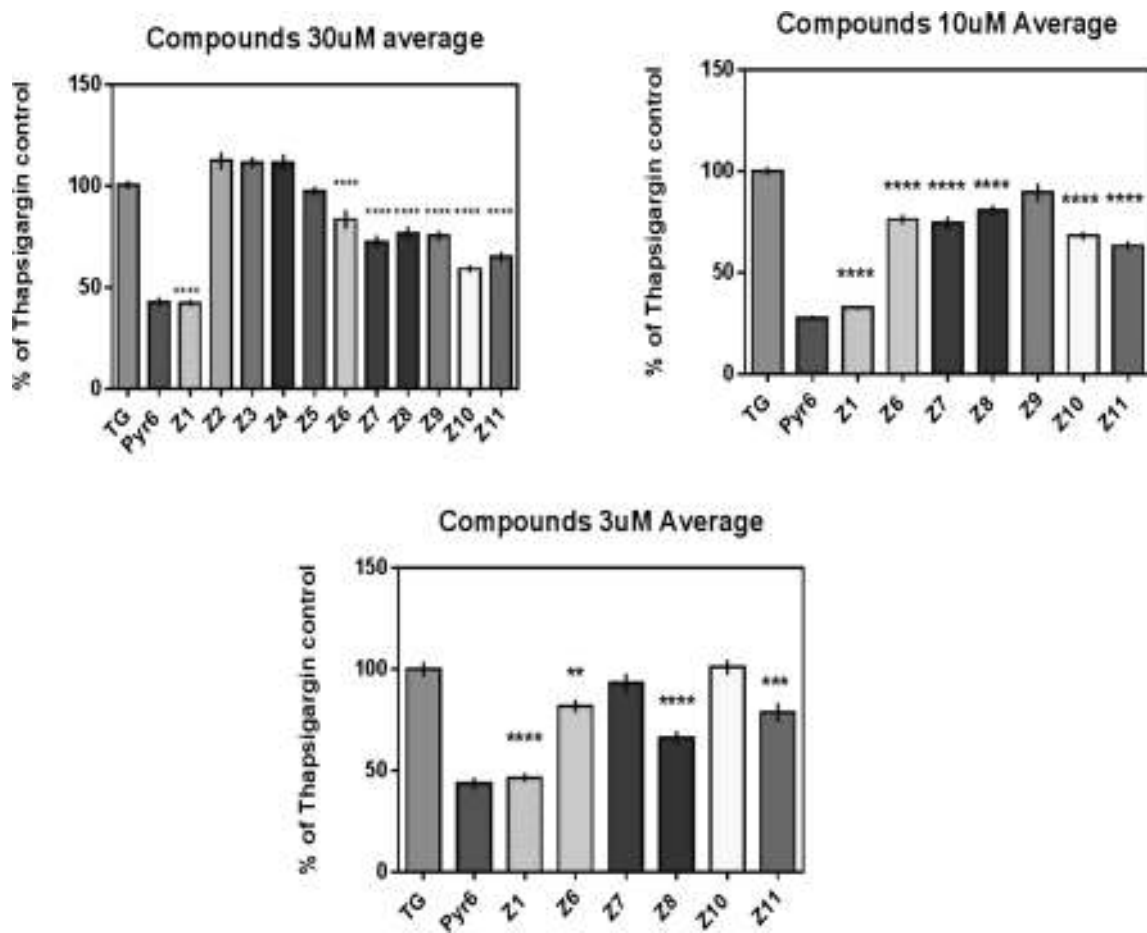


FIGURE 2 Effect of chosen compounds at different concentrations on thapsigargin (TG)-evoked Ca^{2+} entry in RBL-1 cells. Bar diagram showing fluorescence ratio relevant to the peak Ca^{2+} entry signals evoked by Tg in these cells under different conditions. Data represented as mean \pm SEM. The cell numbers (n) for control and each compound treatment group were ≥ 40 . Experiments were done in triplicates on three independent days. One-way ANOVA followed by Dunnett's test was used. **** $P < .0001$, *** $P < .001$, and ** $P < .01$

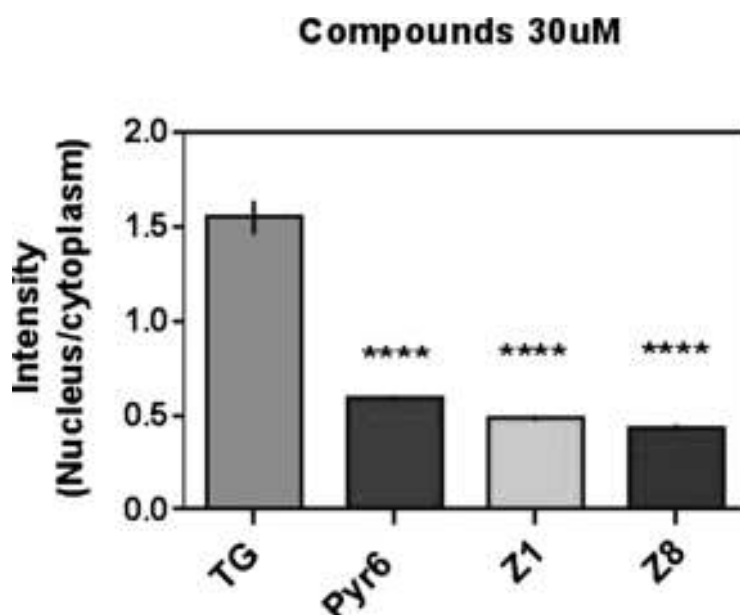


FIGURE 3 Effect of the selected compounds at 30- μ M concentration on thapsigargin (TG)-induced nuclear translocation of NFAT-GFP in HeLa cells. All the test compounds showed significant inhibition of NFAT translocation. Each bar shows mean intensity (nucleus/cytoplasm) \pm SEM ($n \geq 40$ cells) representing degree of NFAT-GFP translocation to the nucleus in various groups. Statistical significance compared with thapsigargin control for the compounds was determined by one-way ANOVA followed by Dunnett's test. Experiments were done in triplicates on three independent days. **** $P < .0001$

1. Potential site for inhibitor binding on Orai1 was identified and virtually screened (Figure 1).
2. Two of the purchased compounds retained significant SOCE inhibitory properties at lower concentration in single-cell Fura-2-based calcium imaging using RBL-1 cells (Figure 2).
3. The true positives in calcium assay inhibited nuclear translocation of NFAT in HeLa cells (Figure 3).

Conclusion and Implications: Our *in silico* approach seemed to be successful in providing two interesting SOCE-inhibitory small-molecule scaffolds that are novel in structures. Future studies include structure-activity relationship for hit to lead optimisation and evaluation of selectivity over other ion channels.

REFERENCES

- Gwack, et al. (2006), doi:<https://doi.org/10.1038/nature04631>.
 Rahman & Rahman (2017), doi:<https://doi.org/10.1038/s41598-017-13343-x>.

P056 | Conformational dynamics of bovine rhodopsin in SMALPs, SMILPs, and DIBMALPs

Rachael L. Grime¹; Richard T. Logan¹; Philip J. Reeves²; Mark Wheatley³

¹University of Birmingham; ²University of Essex; ³Coventry University

Background and Purpose: The fundamental importance of membrane proteins has driven a marked increase in the use of membrane-mimetic approaches for studying and exploiting these proteins. Nano-encapsulation strategies that preserve the native lipid bilayer are particularly attractive. Consequently, the use of amphipathic polymers such as styrene-maleic acid (SMA), styrene-co-maleimide (SMI), and diisobutylene-maleic acid (DIBMA) have been widely adopted to solubilise proteins directly from cell membranes by spontaneously forming "SMA/SMI/DIBMA lipid particles" (SMALPs/SMILPs/DIBMALPs) (Stroud, Hall, & Dafforn, 2018). Each polymer possesses unique properties that altogether forms a toolbox of experimental devices. Negatively charged SMA and positively charged SMI both share the same hydrophobic component in the form of an aromatic styrene ring and form nanodiscs of the same size (~10 nm). DIBMA possesses the same hydrophilic component as SMA—the maleic acid, but forms larger nanodiscs (~20 nm). Here, we have compared and characterised SMA, SMI, and DIBMA with previously characterised DDM for the extraction of bovine rhodopsin (bRho) from rod outer segment (ROS) membranes.

Experimental Approach: ROS membranes were incubated in PBS containing 1% DDM, 2.5% SMA, 2.5% SMI, or 5% DIBMA, in the dark for 1 hr, 20°C. Insoluble material was sedimented via centrifugation at 45,000 \times g, 1 hr, 4°C. Supernatants were gel filtered (Sephadex G-25) to remove free polymer and analysed by UV-Vis absorbance spectroscopy to determine the extent of extraction of rhodopsin ($A_{500\text{ nm}}$). For photobleaching experiments, samples were illuminated directly using a fibre optic light guide (SCHOTT KL1500

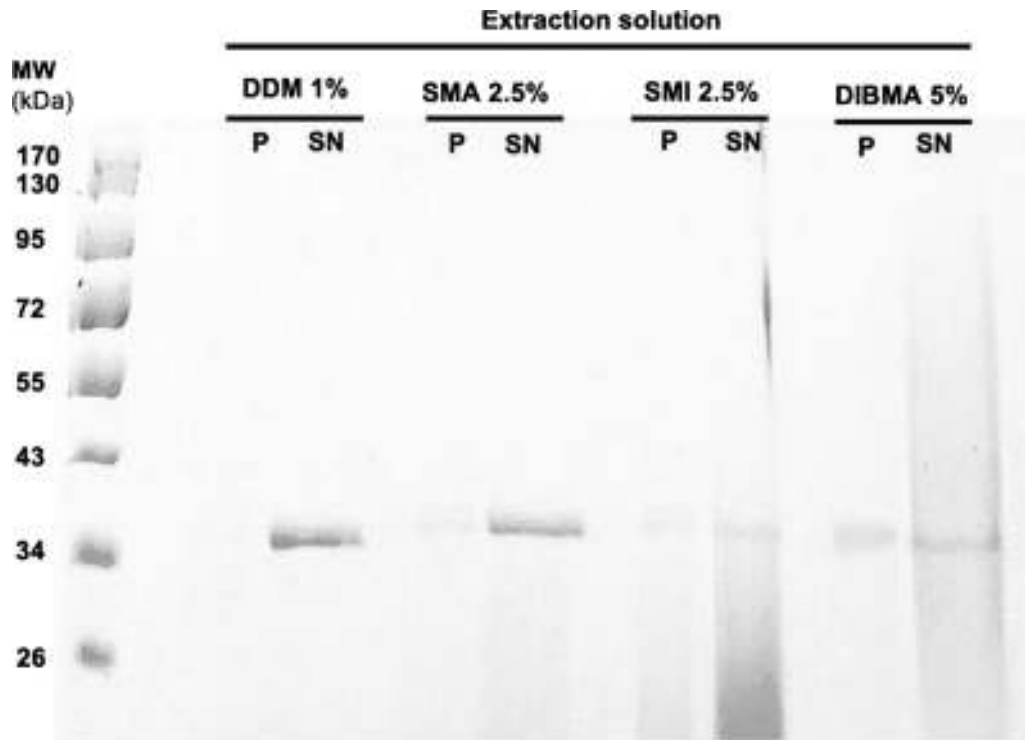


FIGURE 1 Representative SDS-PAGE of bovine rhodopsin (bRho) extractions from rod outer segments (ROS), utilising varying solubilisation conditions. Pellet (p) and supernatant (SN) were compared after extraction with DDM, SMA, SMI, and DIBMA. The diffuse bands seen result from polymer interaction in the gel

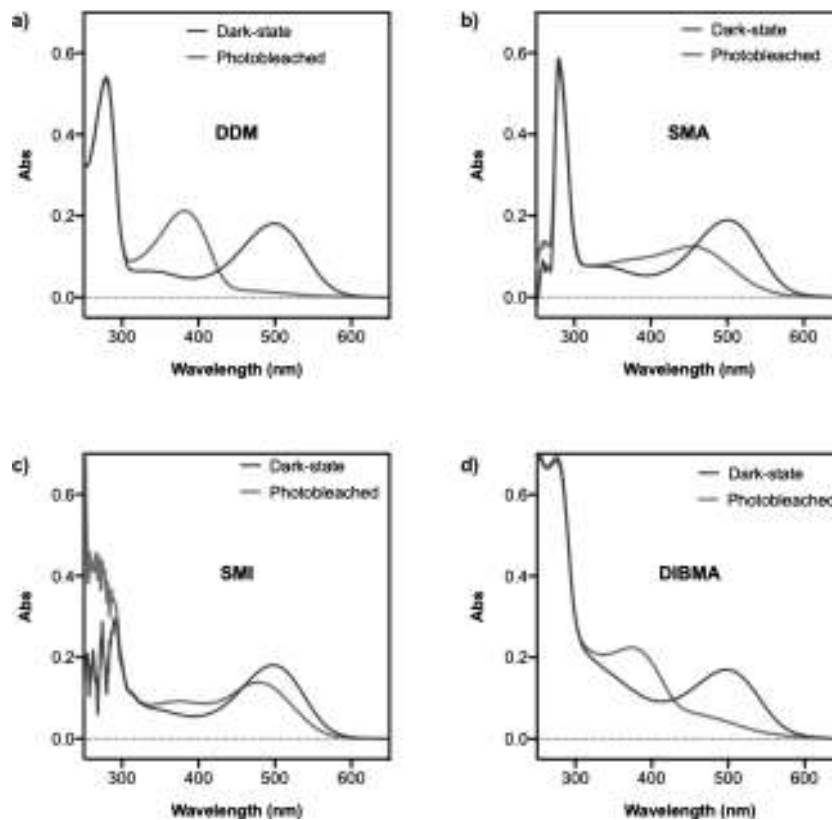


FIGURE 2 Absorption spectra for rhodopsin, solubilised in varied conditions. (a) 1% DDM, (b) 2.5% SMA, (c) 2.5% SMI, and (d) 5% DIBMA. Extractions were analysed in dark state and after photobleaching. Rhodopsin absorbs maximally at 500 nm. Light activation of rhodopsin proceeds through several meta-stable intermediates, finalising in a fully active meta II state, which absorbs maximally at 380 nm

Compact) fitted with a >495-nm long-pass filter. Extractions were also analysed via SDS-PAGE.

Key Results: SMA, SMI, and DIBMA are all effective at extracting rhodopsin from ROS, as demonstrated by comparable rhodopsin pigment yields shown at $A_{500\text{ nm}}$ (Figure 2) and SDS-PAGE (Figure 1). Isomerisation of 11-*cis*-retinal is evident upon photo-bleaching with all three polymers (Figure 2); however, with SMA- and SMI-extracted bRho, photoconversion does not go beyond meta I state ($A_{478\text{ nm}}$). Both DIBMA- and DDM-extracted rhodopsin demonstrated photoconversion to fully active meta II ($A_{380\text{ nm}}$) (Figure 2).

Conclusion and Implications: Previous biophysical data have demonstrated that styrene moiety in a SMALP/SMILP intercalates between lipid and acyl chains. This may account for the inability of the bRho to reach meta II. It is possible that the aromatic ring restricts movement of the lipid-acyl chains or is interacting directly with the TM bundle, preventing conformational changes. DIBMA interacts in a fundamentally different way, and the data show that the receptor is not conformationally restricted.

REFERENCE

Stroud, Z., Hall, S. C. L., & Dafforn, T. R. (2018). Purification of membrane proteins free from conventional detergents: SMA, new polymers, new opportunities and new insights. *Methods*, 147, 106-117.

P057 | Novel sildenafil nanoformulation as a potential therapy for pulmonary arterial hypertension

Nura Mohamed¹; Haissam Abou Saleh²; Yu Kamen¹; Isra Marei¹; Gilberto de Nucci³; Blerina Ahmetaj-Shala¹

¹Imperial College of London; ²Qatar University; ³eDepartment of Pharmacology, Faculty of Medical Sciences, State University of Campinas (UNICAMP), Campinas

Background and Purpose: Pulmonary arterial hypertension (PAH) is an incurable disease, although symptoms are treated with a range of vasodilator drugs. Despite their clinical benefits, these drugs are limited by systemic side effects. It is therefore increasingly recognized that using targeted drug delivery with nanoformulation platforms may overcome these limitations (Mohamed et al., 2017). This study evaluates one particular nanoformulation (the highly porous iron-based metal-organic framework (MOF), nanoMIL-89 (Horcajada et al., 2010)) as a carrier for the PAH drug sildenafil. We have previously shown that nanoMIL-89 is relatively non-toxic in vitro and well-tolerated in vivo (Mohamed et al., 2017).

Experimental Approach: In this study, nanoMIL-89 was prepared, characterized (Horcajada et al., 2010), and charged with a payload of sildenafil by incubating the two components in PBS at room

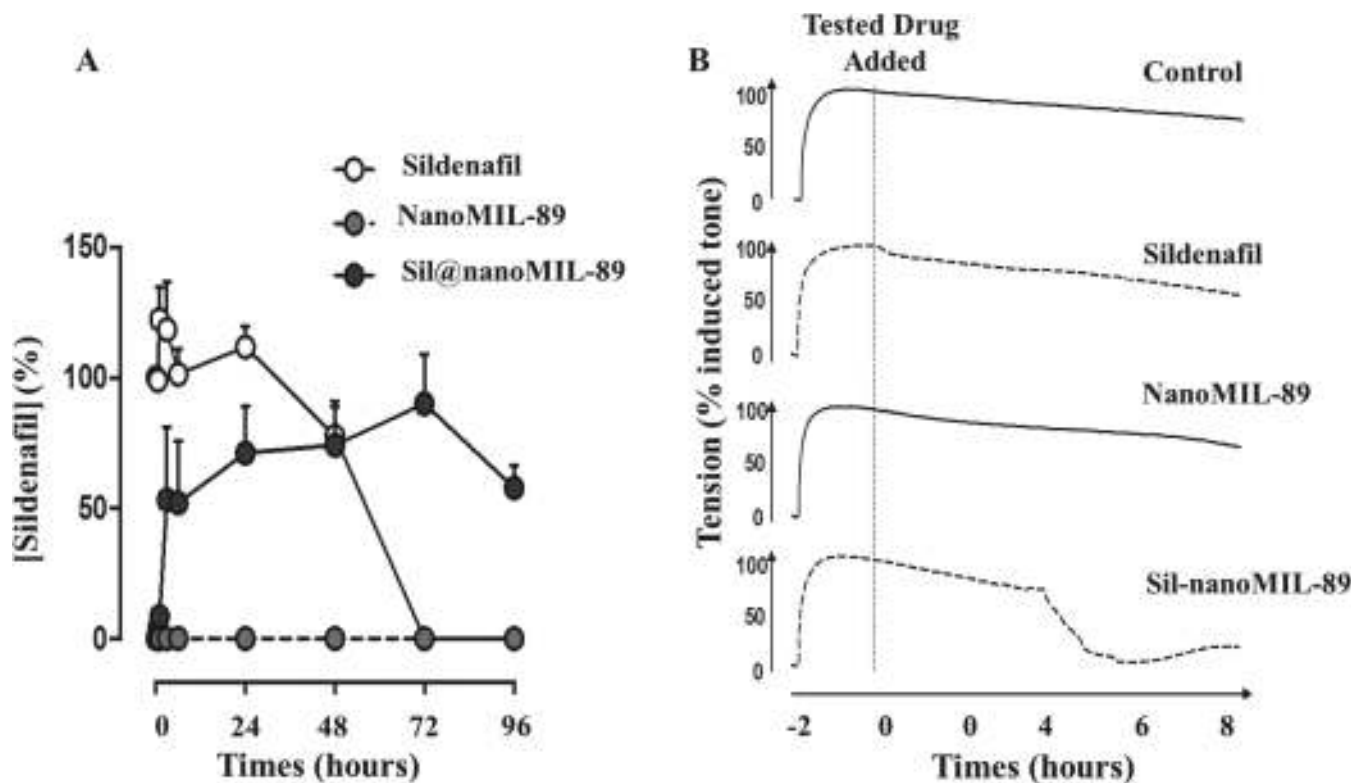


FIGURE 1 Sildenafil release by sil@nanoMIL-89 and vasodilator effects of sildenafil ($10\ \mu\text{M}$), nanoMIL-89 ($10\ \mu\text{g}\cdot\text{ml}^{-1}$), and sil@nanoMIL-89 ($10\ \mu\text{g}\cdot\text{ml}^{-1}$) on pre-contracted mouse aorta. (a) Sildenafil levels in plasma were measured from incubations of sil@nanoMIL-89 ($4\ \text{mg}\cdot\text{ml}^{-1}$) and nanoMIL-89 ($4\ \text{mg}\cdot\text{ml}^{-1}$) at 37°C over 96 hr; $n = 6$; $P < .05$ by two-way ANOVA followed by Bonferroni's posttest. (b) Representative traces of mouse aorta contracted with U46619 ($10\ \text{nM}$) before and following addition of sildenafil, nanoMIL-89, and sil@nanoMIL-89

temperature for 16–18 hr (generating sil@nanoMIL-89). Sildenafil release was measured in human plasma by ELISA, and dilator function in mouse (C57Bl/6) aorta was assessed using wire myography (Harrington et al., 2010).

Key Results: Sil@nanoMIL-89 released sildenafil in a biphasic manner with an initial rapid release over 6 hr followed by a more sustained release over 72 hr (Figure 1a) and induced vasodilation (% induced tone) over a period consistent with drug release kinetics ($t = 2$ hr, 9.61 ± 6.9 ; $t = 4$ hr, 43.53 ± 29.76 ; and $t = 8$ hr, 86.04 ± 26.71 ; Figure 1b).

Conclusion and Implications: Herein, we have produced a nanoformulation of sildenafil, sil@nanoMIL-89, displaying delayed drug release corresponding to vasodilator activity. Further pharmacological assessment of sil@nanoMIL-89, including in PAH models, is now required and constitutes the subject of an ongoing investigation.

REFERENCES

- Harrington, L. S., Moreno, L., Reed, A., et al. (2010). The PPAR β/δ agonist GW0742 relaxes pulmonary vessels and limits right heart hypertrophy in rats with hypoxia-induced pulmonary hypertension. *PLoS ONE*, 5, e9526.
- Horcajada, P., Chalati, T., Serre, C., et al. (2010). Porous metal–organic-framework nanoscale carriers as a potential platform for drug delivery and imaging. *Nature Materials*, 9, 172–178.
- Mohamed, N. A., Davies, R. P., Lickiss, P. D., et al. (2017). Chemical and biological assessment of metal organic frameworks (MOFs) in pulmonary cells and in an acute in vivo model: Relevance to pulmonary arterial hypertension therapy. *Pulmonary Circulation*, 7, 643–653.

P058 | Solubilisation and characterisation of the β_2 -adrenoceptor in the polymer diisobutylene maleic acid

Clare Harwood; David Sykes; Stephen Briddon; Dmitry Veprintsev
University of Nottingham

Background and Purpose: The β_2 -adrenoceptor (β_2 AR) is a well-established target in asthma and a prototypical GPCR for biophysical studies. Solubilisation of membrane proteins has classically used detergents. However, detergents are known to destabilise membrane proteins. In addition, detergent environments differ from the native plasma membrane. Recently, a number of polymers, such as diisobutylene maleic acid (DIBMA), have been developed to extract membrane proteins from the plasma membrane with retention of native lipids in discrete protein–lipid particles. Here, we compared solubilisation efficiency, ligand binding kinetics, and the thermostability of DIBMALP- β_2 AR to that of the conventional detergent *n*-dodecyl- β -D-maltopyranoside (DDM)-solubilised β_2 AR.

Experimental Approach: HEK293TR cells, stably expressing Twin-Strep and SNAP-tagged β_2 AR, were labelled with SNAP–Lumi4–Tb labelling reagent (Cisbio, UK) for 1 hr at 37°C and 5% CO₂. Membrane fractions were prepared and incubated with 3% DIBMA for 1 hr at room temperature or 4°C or 1% DDM for 1 hr at 4°C. Time-resolved

FRET (TR-FRET) between carazolol–BY630/650 and Lumi4–Tb-tagged receptor was used to investigate ligand binding. Assay buffer consisted of 20-mM HEPES, 10% glycerol, 150-mM NaCl, and 0.5% BSA, with a total assay volume of 40 μ l.

For thermostability assays, DIBMALP- β_2 AR was incubated with 10- μ M BODIPY™ FL L-cystine dye for 15 min on ice. Twenty-microlitre samples were added to each well of a 96-well plate and incubated for 30 min over a temperature gradient of 20–78°C across the two plates in a two-block PCR machine. Fifteen-microlitre samples were transferred to 384-well ProxiPlate and TR-FRET between BODIPY™ FL L-cystine dye and Lumi4–Tb using PHERAstar FSX plate reader.

Key Results: β_2 AR solubilisation efficiency of 1% DIBMA was determined as $20 \pm 0.2\%$ compared to $58 \pm 0.8\%$ for 1% DDM. Binding of 100-nM carazolol–BY630/650 was observed using DIBMALP- β_2 AR via TR-FRET ligand binding assay, and the specificity of this binding was confirmed in the presence of 3- μ M cyanopindolol. TR-FRET thermostability assays gave a melting temperature (T_m) of 70°C for DIBMALP- β_2 AR compared to $36 \pm 1^\circ\text{C}$ for DDM-solubilised β_2 AR.

Conclusion and Implications: Overall, we show the successful solubilisation of the β_2 AR with the polymer DIBMA. DIBMALP- β_2 AR was functional, and stability was dramatically improved compared to the DDM-solubilised receptor, making DIBMA-solubilised receptor an attractive alternative for future biophysical studies.

P059 | Validation of a label-free assay to determine chemokine responses in primary human neutrophils

Lisa Stott; Greg Osborne; Kirstie Bennett; Simon Poulter;
Catherine Hutchings; Matt Barnes
Sosei Heptares

Background and Purpose: Neutrophils are the most abundant circulating leukocyte, forming an important part of the innate immune system. They express several GPCRs, including the chemokine receptors CXCR1 and CXCR2. CXCR2 is a potential therapeutic target for numerous indications, including several inflammatory disorders and cancers (Cheng et al., 2019). In order to investigate chemokine signalling in neutrophils, we established label-free, dynamic mass redistribution (DMR) assays and compared results to those from functional cAMP assays in a stable CHO–CXCR2 cell line to test whether responses translate from recombinant to primary cells.

Experimental Approach: Neutrophils were isolated from whole blood by dextran sedimentation and density gradient centrifugation, before the removal of contaminating red blood cells with osmotic shock. Isolated cells were seeded onto uncoated 384-well Epic® plates for 2 hr. Plates were read using the Corning Epic® BT System, which detects cellular responses as a change in the

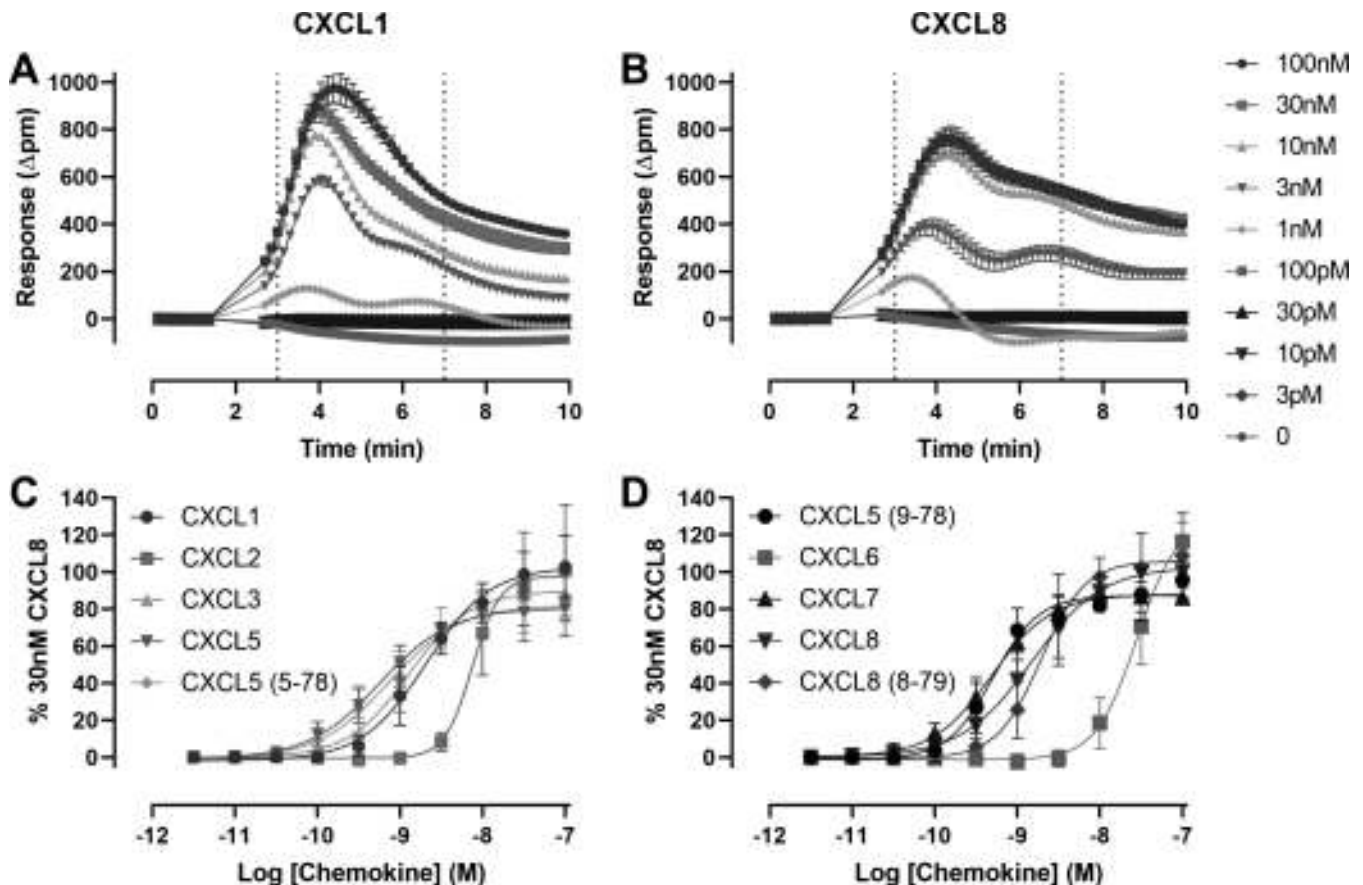


FIGURE 1 Chemokine responses in neutrophil DMR assays. Representative (mean \pm SD in duplicate) DMR kinetic traces of CXCL1 (a) and CXCL8 (b) in neutrophil DMR. Peak response between 3 and 7 min was extracted (c, d). Data shown are pooled (mean \pm SD) from at least four individual donors, normalised to 30-nM CXCL8 response. Data are summarised in Table 1

TABLE 1 Chemokine data summary from neutrophil DMR assays

Chemokine	pEC ₅₀	E _{max} (% 30-nM CXCL8)	n
CXCL1	8.92 \pm 0.19	92 \pm 17	9
CXCL2	8.11 \pm 0.12	100 \pm 29	4
CXCL3	8.92 \pm 0.19	90 \pm 7	4
CXCL5	9.14 \pm 0.21	80 \pm 12	9
CXCL5 (5-78)	9.13 \pm 0.13	82 \pm 8	4
CXCL5 (9-78)	9.28 \pm 0.17	88 \pm 8	4
CXCL6	7.55 \pm 0.12	129 \pm 7	4
CXCL7	9.31 \pm 0.15	88 \pm 2	4
CXCL8	9.02 \pm 0.15	104 \pm 4	9
CXCL8 (8-79)	8.69 \pm 0.15	106 \pm 16	4

Note. Data shown are pooled (mean \pm SD) from at least four individual donors, normalised to 30-nM CXCL8 responses.

wavelength of refracted light. For cAMP assays, stably expressing CHO-CXCR2 cells were seeded overnight in white 384-well plates. Media were replaced with assay buffer for 1 hr prior to addition of chemokine, in the presence 1- μ M forskolin and 0.5-mM IBMX, for 5 min. cAMP was detected using a cAMP Gi kit (Cisbio) according

to the manufacturer's instructions. Plates were read on a PHE-RAsstar FS plate reader, using standard HTRF settings. All data analysis was performed in GraphPad Prism.

Key Results: All CXCR1/2 chemokines demonstrated a large, positive deflection in neutrophil DMR that peaked rapidly within 3 min of agonist addition (Figure 1). This response was inhibited by pre-treatment of the CXCR1/2 antagonist compound 19 (Dwyer et al, 2006), demonstrating the specificity of the responses. Chemokine potencies were very consistent over donors (Table 1), and assays displayed excellent signal window and Z'. When compared to chemokine potencies in recombinant CXCR2 cells, there was a moderate correlation between the assays ($R^2 = .64$, $P < .01$, Pearson's correlation coefficient).

Conclusion and Implications: Functional chemokine responses can be reproducibly measured in primary human neutrophils using DMR, providing a robust, high-throughput, primary cell screening assay, which could be used to support drug discovery programmes. There was a moderate correlation in chemokine potencies between the primary and recombinant cell assays, which may be influenced by the dual expression of CXCR1 and CXCR2 on neutrophils.

REFERENCES

Cheng, et al. (2019). *Biochimica et Biophysica Acta, Reviews on Cancer*, 1871, 289–312.
 Dwyer, et al. (2006). *Journal of Medicinal Chemistry*, 49, 7603–7606.

P060 | Extracellular albumin covalently sequesters selenium compounds and determines cytotoxicity

Wenyi Zheng¹; Roberto Boada²; Tingting Xiao²; Fei Ye³; Manuel Valiente²; Moustapha Hassan¹

¹Karolinska Institutet; ²Autonomous University of Barcelona; ³Royal Institute of Technology

Background and Purpose: Selenium compounds (SeCs) are well-known nutrients and promising drug candidates for the treatment of several diseases including cancer and neurodegenerative disorders. Unfortunately, treatment efficacy is very heterogeneous and the mechanism of action is not fully understood (Fernandes & Gandin, 2015). Several SeCs have been reported to have high-albumin binding, which is an important factor for the determination of the treatment efficacy of many drugs.

Experimental Approach: In the present investigation, we hypothesized that extracellular albumin is involved in determining the cytotoxicity of SeCs. Four SeCs representing distinct categories were selected to investigate their cytotoxicity in vitro. X-ray absorption spectroscopy and hyphenated MS were used to study selenium speciation in cell culture medium, which contains BSA. Intracellular selenium element was measured by atomic emission spectroscopy.

Key Results: Concurrent administration of albumin greatly decreased the cytotoxicity and the cellular uptake of SeCs. Using both X-ray absorption spectroscopy and hyphenated MS (Zheng et al., 2017), we confirmed the formation of macromolecular SeC-BSA conjugate.

Although SeC-BSA was still internalized possibly via albumin scavenger receptors expressed on cell surface, the uptake was strongly inhibited by the excess of BSA.

Conclusion and Implications: Generally, we revealed an overlooked mechanism—extracellular albumin binding—behind the miscellaneous effects of SeCs, which could instruct further investigations on SeCs as cancer therapy.

REFERENCES

Fernandes, A. P., & Gandin, V. (2015 Aug). Selenium compounds as therapeutic agents in cancer. *Biochimica et Biophysica Acta*, 1850(8), 1642–1660.
 Zheng, W., et al. (2017 Jul 18). Rapid and robust quantification of p-xyleneselenocyanate in plasma via derivatization. *Analytical Chemistry*, 89(14), 7586–7592.

P062 | New metal peroxide complexes obtaining for natural metal enzymes mechanism of action modelling

Mikhail Sharipov¹; Anna-Mariia Oleksienko²; Gleb Butyagin³; Maksim Myshakin²

¹Kurnakov Institute of General and Inorganic Chemistry; ²D. Mendeleev University of Chemical Technology of Russia; ³Oakham School

Background and Purpose: Metal peroxide complexes play a key role in the oxidative transformation of organic substrates by metal enzymes. However, it must be emphasized that aryl and alkyl peroxide complexes are much less recognized than hydroperoxide complexes. Therefore, this field of science is the subject of advanced research. Being analogues of metal hydroperoxide complexes, in some cases, their affinity for biological targets is an order of magnitude greater. Thus, such compounds are key ones in a wide range of biological

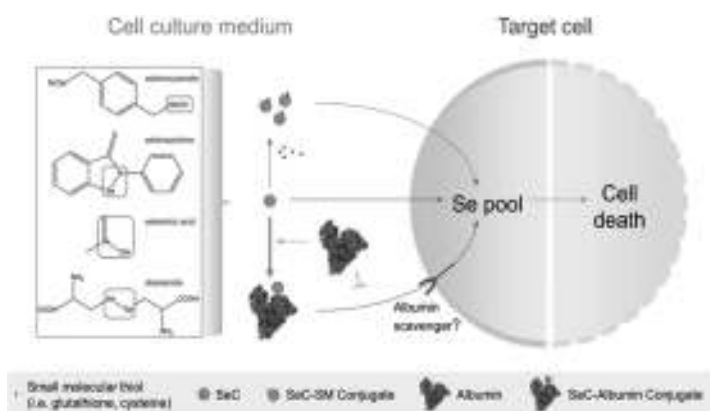


FIGURE 1

oxygen-centric processes (Special thematic issue, 1996). Our research group develop methods for producing stable peroxide complexes, as well as study the stability of obtained coordination compounds in comparison with the initial ligands and search for criteria that affect the stability of the obtained compounds.

Experimental Approach: The composition and structure of the obtained peroxide complexes were examined by chromatographic and spectral (NMR and IR) methods. The stability of the obtained structures was studied by differential scanning calorimetry. The data obtained for crystalline structures by means of X-ray diffraction analysis made it possible to study the geometric structural features of peroxide complexes.

Key Results: New metal peroxide complexes were obtained and characterized. These structures can be used as model compounds in a number of biological oxygen-centric processes. Of special interest are chain polymers based on bisperoxide salts. New materials are potential from the point of view of further use in medicine.

Conclusion and Implications: An approach to the creation of synthetic analogues of active centres of metal enzymes is proposed. This is one of the rapidly developing areas of modern chemistry, located at the junction of bioorganic chemistry, coordination chemistry, and biochemistry. The obtaining of stable, that is, secreted and stable during storage under standard conditions, peroxide complexes could open the door to a number of new applications for such an important class of compounds as peroxides.

ACKNOWLEDGEMENT

This work was supported by the grant of the President of the Russian Federation MK-2947.2019.3.

REFERENCE

Special thematic issue. (1996). Bioinorganic enzymology. *Chemical Reviews*, 96, 2237–3042.

P063 | Using continuous glucose monitoring to determine the accuracy of single time-point measurements and the effect of common in vivo techniques in unrestrained mice

Matilda Kennard; Manasi Nandi; Aileen King

King's College London

Background and Purpose: Blood glucose concentrations are a vital endpoint in diabetes research with current ranges and normoglycaemic cut-offs, such as <11.1 mM, often being determined by glucometer at single time-points, which necessitate animal restraint and tail prick. Using continuous blood glucose radio-telemetry, we aimed to determine how accurately single time-point measurements represent glycaemic control in mice. In addition, we investigated the effects of common in vivo techniques on blood glucose concentrations.

Experimental Approach: Seven male 8- to 10-week-old C57Bl/6J mice were implanted with HD-XG glucose telemetry devices and recovered for 7 days. Blood glucose concentrations were continuously measured via the aortic arch in unrestrained mice with averages recorded every 10 s. Baseline normoglycaemia was measured for 13 days, and a normal target range for each animal was determined by calculating 25% above and below the 24-hr median blood glucose concentrations. The effect of the following was subsequently investigated: (a) disturbance through waking the animals without handling, (b) picking up mice via the tail, (c) standard glucometer measurements, and (d) intraperitoneal injection.

Key Results: The average normal target range measured by telemetry was 4.9–8.2 mM with mice spending at least 80% of time within this range. Mice spent 99.7% of time with blood glucose values <11.1 mM, and blood glucose only varied from the mean by a maximum of 2.6 mM. Overall blood glucose was consistent, but there was inter-animal variability with regard to measures of glycaemic variability such as SD. Mouse disturbance resulted in ~1-mM blood glucose increase for at least 15–30 m (6.80 ± 0.21 and 6.73 ± 0.16 vs. 5.92 ± 0.14 mM, $P < .05$, one-way RM ANOVA with Holm-Sidak's post hoc test, $n = 7$). Handling increased blood glucose by ~2.2 mM with effects also lasting up to 60 m (8.48 ± 0.48 vs. 6.26 ± 0.44 mM). Glucometer readings did not increase blood glucose beyond handling, but increases were prolonged with return to baseline at 90 m. Saline injection resulted in a blood glucose increase of ~2.9 mM, which lasted up to 120 m (8.66 ± 0.33 vs. 5.81 ± 0.99 mM).

Conclusion and Implications: Standard single time-point measurements with a normoglycaemic cut-off of <11.1 mM correctly represent overall normoglycaemia in male C57Bl/6J mice but cannot determine glycaemic variability which differed between animals. Common in vivo procedures including handling and glucometer readings cause a transient but significant increase in blood glucose concentration with degree of stress being cumulative alongside degree of disturbance and experimentation. Therefore, continuous glucose monitoring allows comprehensive measurement of blood glucose concentrations and glycaemic variability in undisturbed mice, helping to optimise preclinical models for future drug testing.

P064 | Penetration of flurbiprofen from a locally acting sore throat lozenge and spray into human pharynx tissue: A novel ex vivo model and microautoradiography method

Oluwajoba Adegoke¹; Robert Turner²; Sean Robert Wevrett²; Suzanne Edmunds²; Marc Brown²

¹Reckitt Benckiser; ²MedPharm Ltd

Background and Purpose: Patients with sore throat experience pain/discomfort resulting from inflammation in the pharynx.

TABLE 1 Tissue thickness and percentage of applied dose of flurbiprofen recovered within pharynx tissue

Parameter	Lozenge (n = 1)	Lozenge (n = 3)	Lozenge (n = 4)	Lozenge (n = 5)	Lozenge (n = 6)	Spray (n = 1)	Spray (n = 2)	Spray (n = 3)	Spray (n = 4)	Spray (n = 5)	Spray (n = 6)
Tissue thickness (mm)	3.81	5.16	3.99	3.30	2.64	2.07	2.73	2.40	1.89	1.83	2.37
Total flurbiprofen applied (µg)	17.6	17.6	17.6	17.6	17.6	195.4	195.4	195.4	195.4	195.4	195.4
Total flurbiprofen detected within pharynx tissue (µg)	3.1	8.7	4.3	4.6	6.2	67.6	63.9	55.7	28.2	17.5	42.1
Percentage of applied dose recovered (%)	17.8	49.2	24.7	26.2	35.1	34.6	32.7	28.5	14.4	9.0	21.5

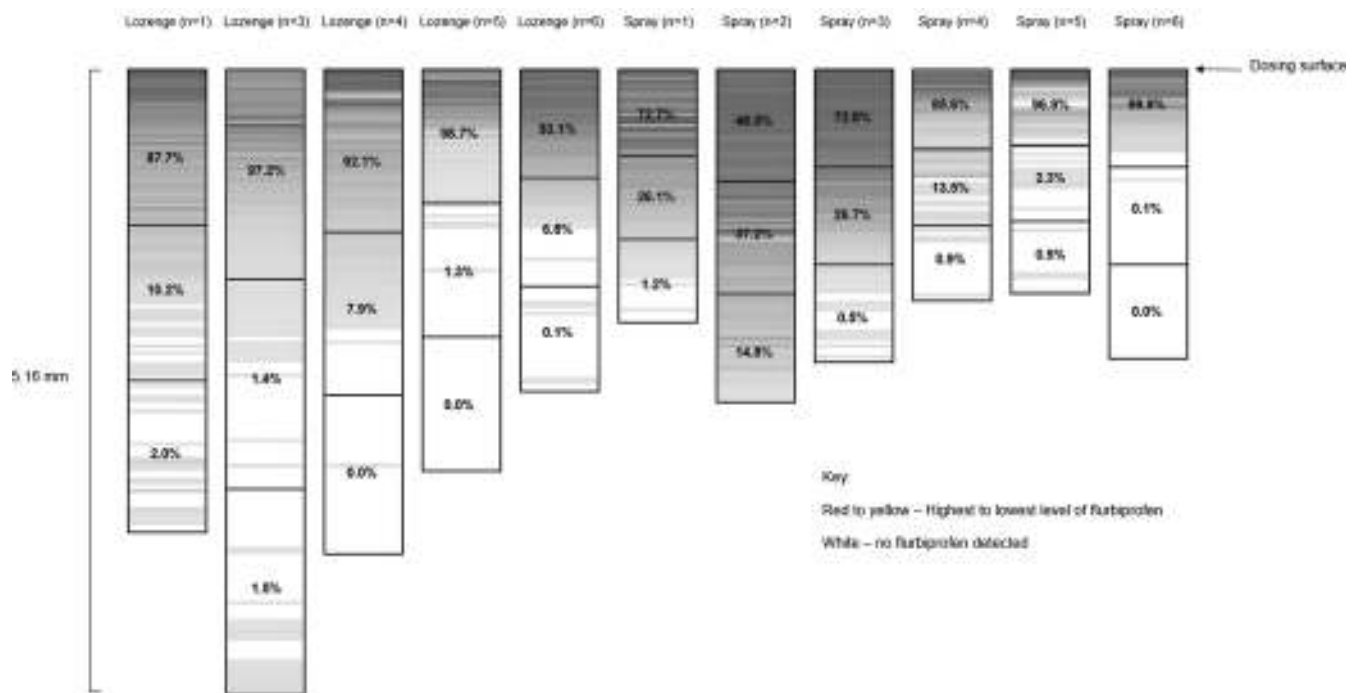


FIGURE 1 Distribution of flurbiprofen within pharynx tissue (percentage of total flurbiprofen detected within pharynx tissue). Each tissue sample has been split into thirds. Height of tissue pieces is scaled according to the actual depth of tissue

Symptom relief can be provided by local or systemic non-steroidal anti-inflammatory drugs (NSAIDs). This study aimed to quantify the depth penetration of the NSAID flurbiprofen (8.75-mg spray and lozenge formulations) into human pharynx tissue using microautoradiography.

Experimental Approach: The ex vivo Franz diffusion cell model was used to mimic physiological and anatomical conditions of human pharynx tissue in situ (Turner et al., 2019). Human pharynx tissue from cadavers was mounted between the donor and receiver compartment. A penetration experiment utilised radiolabelled flurbiprofen in spray and lozenge dosing solutions with a specific activity of 20 µCi·ml⁻¹. Doses of 195.4 µg (n = 6) and 17.6 µg (n = 5) of flurbiprofen were applied to the pharynx tissue from spray and lozenge formulations, respectively (Table 1), to reflect the anticipated

amount that could come into contact with the pharynx tissue based on posology and format. Following incubation of the dosing solution and pharynx tissue, the tissue was frozen and sectioned vertically and horizontally. Radiolabelled flurbiprofen within each section was imaged and quantified (horizontal section only) using a scintillation counter.

Key Results: Radiolabelled flurbiprofen was present in the top sections of pharynx for all replicates (spray and lozenge) and decreased in intensity through the tissue. Thickness of pharynx tissue samples, total amount of flurbiprofen applied, total amount of flurbiprofen detected within tissue, and percentage recovery of applied dose of flurbiprofen are shown in Table 1 for all replicates. Quantification of flurbiprofen within pharynx tissue demonstrated a general trend of higher flurbiprofen levels (48.0–99.9% of flurbiprofen detected within

pharynx tissue) in the top third of the tissue (close to the dosing site) and a lower amount of flurbiprofen (0.0–14.8% of flurbiprofen detected within pharynx tissue) in the bottom third of the tissue (Figure 1).

Conclusion and Implications: Flurbiprofen from 8.75-mg spray and lozenge formulations penetrated human pharynx tissue. Radiolabelled flurbiprofen was observed in the top sections of the pharynx for all replicates (spray and lozenge) and decreased in intensity through the tissue.

REFERENCE

Turner, R., et al. (2019). *Biomedical Chromatography*, 33, e4499.

P065 | The Effect of a humanized anti-cocaine monoclonal antibody on the in vitro metabolism of cocaine by liver carboxylesterase I

Mackenzie Turner¹; Tiffany Bell-Horwath¹; Chris Crutchfield¹; Hanna Wetzel²; Andrew Norman¹

¹University of Cincinnati; ²University of Cincinnati/Xavier University

Background and Purpose: The humanized anti-cocaine monoclonal antibody (mAb), h2E2, is a prime candidate for treating cocaine-use disorders and relapse. When cocaine binds to h2E2, it is likely not available for hydrolysis or metabolism by endogenous esterases. Therefore, the antibody is expected to slow or prevent the clearance of cocaine. However, PK studies in rats and mice demonstrate an apparently unchanged elimination half-life of cocaine in the presence of h2E2. To investigate this paradoxical finding, we determined the effect of h2E2 on the in vitro metabolism of cocaine by liver carboxylesterase I (CES1), which hydrolyses cocaine to benzoylecgonine (BE).

Experimental Approach: A solution of cocaine HCl (0.5 mM) was combined with a range of 0.1- to 0.4-M liver carboxylesterase I (in PBS, pH 7.4) in the presence and absence of an equimolar concentration of h2E2. The solution was incubated at 37°C. Samples were collected in triplicate over 6 hr and were aliquoted into tubes containing concentrated HCl to stop the reaction. The samples were then frozen at –80°C until analysis. Cocaine and metabolite concentrations were measured using LC-MS/MS.

Key Results: In the absence of h2E2, there was a time-dependent formation of benzoylecgonine, the concentrations of which eventually exceed the upper limit of detection of the instrument. h2E2 dramatically decreased the production of benzoylecgonine by greater than 90% over 6 hr compared to reactions in the absence of h2E2, concomitant with a decrease in cocaine concentration (data not shown). Other metabolite concentrations were examined, but only ecgonine methyl ester was found in detectable amounts.

Figure 1. The effect of h2E2 on the carboxylesterase-mediated formation of BE in vitro

Conclusion and Implications: The drastic inhibition of carboxylesterase-mediated metabolism of cocaine in the presence of the antibody is consistent with h2E2 acting as a chemical antagonist of cocaine. The seemingly paradoxical elimination of cocaine from the plasma in the presence of h2E2 in vivo may be resolved by investigating whether the observed decline in plasma concentration actually represents a slowed distribution phase (Wetzel et al., 2017).

REFERENCES

- Norman, A. B., Gooden, F. C. T., Tabet, M. R., & Ball, W. J. (2014). A recombinant humanized anti-cocaine monoclonal antibody inhibits the distribution of cocaine to the brain in rats. *Drug Metabolism and Disposition*, 42, 1125–1131.
- Wetzel, H. N., Zhang, T., & Norman, A. B. (2017). A mathematical model of a recombinant humanized anti-cocaine monoclonal antibody's effects on cocaine pharmacokinetics in mice. *Life Sciences*, 184, 81–86.

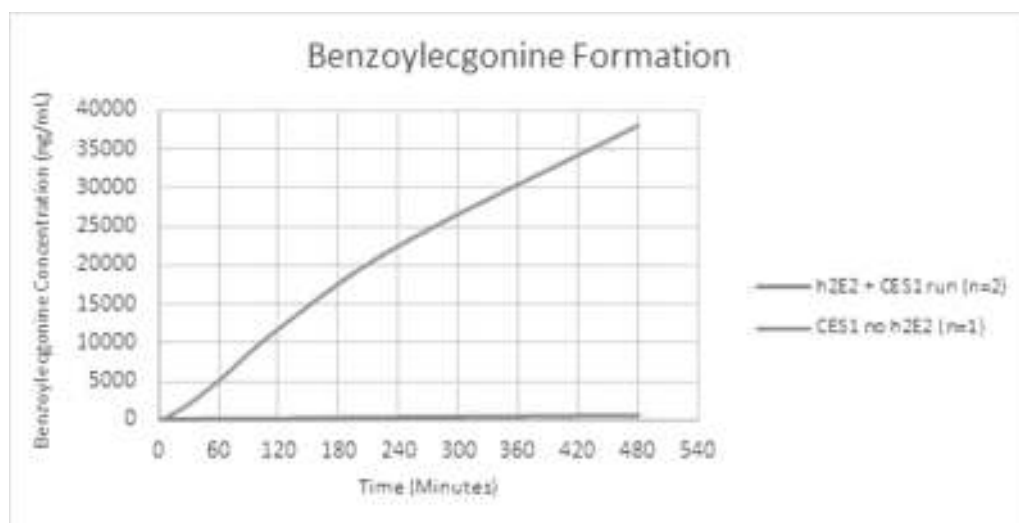


FIGURE 1 Preliminary data showing benzoylecgonine production ($\text{ng}\cdot\text{ml}^{-1}$) over time. Samples containing CES1, h2E2, and cocaine ($n = 3$) are shown in orange. The non-h2E2 group ($n = 5$) is shown in grey

P066 | Characterization of biopesticides as potential antifungal and antiaphid agents

Rehana Badar¹; Asma Ahmed¹; Shamma Firdous²;
Mehmooda Munazir³; Faisal Gulzar⁴

¹Institute of Molecular Biology and Biotechnology (IMBB), The University of Lahore, Lahore; ²Pakistan Council for Scientific and Industrial Research (PCSIR), Lahore, Pakistan; ³Department of Botany, Government College Women University Sialkot, Sialkot, Punjab, Pakistan; ⁴Department of Pharmacy, The University of Lahore, Lahore, Pakistan [Correction added on 20 June 2020, after first online publication: author affiliation (3) has been corrected in this current version.]

Background and Purpose: Pesticides are used in agriculture for plant protection. The use of chemical-based materials to control pests is becoming common and had negative impact on ecosystem. So there is great pressure to replace chemically synthesized pesticides with eco-friendly green/bio-pesticides.

Experimental Approach: The present study was designed to synthesize bio-pesticide as insecticide (against *Aphis solanella*) and fungicide (against wheat fungus, *Puccinia recondita* f.sp. *tritici* (Rust) and *Ustilago tritici* (Smut)). Fresh leaves of neem (*Azadirachta indica* L.), tobacco (*Nicotiana tabacum* L.), and rhizomes of garlic (*Allium sativum* L.) and ginger (*Zingiber officinale* L.) were collected from local area of Lahore and processed by preparing Formulation 1 and Formulation 2 with the same ratio. Neem, garlic, and tobacco were fermented for 1 week (Formulation 1), while ginger was used in Formulation 2 instead of garlic. Both formulations were subjected for FTIR and HPLC analysis.

Key Results: Results showed that Formulation 1 was also efficacious in aphid reduction after 24, 48, 72, 96, and 144 hr ($21.72 \pm 0.5\%$, $20.19 \pm 0.2\%$, $24.08 \pm 0.4\%$, $28.78 \pm 0.4\%$, and $34.32 \pm 0.2\%$) than Formulation 2 while the same results against fungus, that is, Formulation 1 (4.5-cm ZI against rust while 5.0-cm against smut) was more effective than Formulation 2 (3.00-cm ZI against rust and 3.5-cm ZI against smut). Phytochemical analysis showed that garlic has organosulfur compounds (11–35 mg·g⁻¹ of fresh garlic), arginine, oligosaccharides, flavonoids, and selenium. The pesticidal and fungicidal importance of neem, *N. tabacum*, and *Z. officinale* was due to azadirachtin, nicotine, and α -pinene, respectively.

Conclusion and Implications: Outcomes of the present formulations were in favour that these plant-based pesticides could be used for farming as an alternative to chemical pesticides for pest and fungal control.

P068 | Testing inhibitory drugs of the human UPR sensor IRE1 on *Aspergillus fumigatus*

Katherine Deck¹; Jose Guirao Abad²; David Askew²

¹John Brown University; ²University of Cincinnati

Background and Purpose: Immunocompromised individuals are at risk of life-threatening pulmonary infection from the common mould

Aspergillus fumigatus. Current antifungal treatments are limited, making new molecular targets necessary (Van de Veerdonk et al., 2017). The fungal unfolded protein response pathway (UPR) is key to its virulence, and inhibitors of the corresponding human UPR pathway have been developed for cancer therapy but were untested on *A. fumigatus* (Jiang, Niwa, & Koong, 2015; Krishnan & Askew, 2014). Here, the ability of two of the inhibitors, toyocamycin and STF 083010, to inhibit the fungal UPR pathway and reduce the fitness of *A. fumigatus* was investigated.

Experimental Approach: Every experiment was grown at 37°C using strains akuA, genotype Δ akuA::ptrA, and CEA10, a clinical isolate. Concentrations of 0.8 to 400 μ M of toyocamycin or STF 083010 were dissolved in DMSO. Minimum inhibitory concentration (MIC) with resazurin was performed using the protocol standardized by the Clinical and Laboratory Standards Institute and by incubating the 96-well plates for 24 hr. Effects of the drugs when the UPR is required were observed in various conditions created by adding 0.05- μ M calcofluor white, 0.02- μ M Congo red, 0.5-mM carvacrol, or 0.2- μ M hygromycin B to agarose plates or by replacing the 1% glucose in the media with cellulose; plates were spotted with 10^5 to 10^1 conidia and incubated for 48–96 hr. Finally, real-time quantitative PCR (qPCR) was performed using 10^6 conidia grown in flasks for 20 hr that had combinations of 1-mM DTT, to induce the UPR, with 20–120 μ M of STF 083010 added for 1 hr before the quantity of *HacA^u*, *HacAⁱ*, and *bipA*, genes involved in the UPR pathway, was measured.

Key Results: Toyocamycin from 0.8 to 400 μ M had no effect on the metabolic activity or the growth of the fungus under conditions that require UPR intervention. On the other hand, STF 083010 had a MIC of 120 μ M, is fungistatic, and inhibited colony growth from 20 to 120 μ M. STF 083010 at 20–120 μ M, combined with conditions that require the UPR, caused greater inhibition of fungal growth. qPCR demonstrated that STF 083010 blocks the ability of DTT to induce the expression of *hacAⁱ* and *bipA* in a dose-dependent manner.

Conclusion and Implications: These results demonstrate that pharmacological inhibition of the UPR pathway is feasible in *A. fumigatus*, and this loss of fitness by STF 083010 could be a novel approach to antifungal therapy.

REFERENCES

- Jiang, D., Niwa, M., & Koong, A. (2015). Targeting the IRE1 α -XBP1 branch of the unfolded protein response in human diseases. *Seminars in Cancer Biology*.
- Krishnan, K., & Askew, D. S. (2014). The fungal UPR: A regulatory hub for virulence traits in the mold pathogen *Aspergillus fumigatus*. *Virulence*.
- Van de Veerdonk, F., Gresnigt, M., Mark, S., Romani, L., Netea, M., & Latge, J. (2017). *Aspergillus fumigatus* morphology and dynamic host interactions. *Microbiology*.

P070 | Repurposing FDA-approved drugs as potential PARP inhibitors

Maria Eznarriaga; Taufiq Rahman

Department of Pharmacology, University of Cambridge

Background and Purpose: The PARP protein family catalyses the polymerization of poly (ADP-ribose) and covalent attachment of these to proteins and as such plays important role in various DNA damage repair pathways. The discovery that loss of PARP activity triggers cytotoxicity in cells deficient in homologous recombination has sparked a decade of translational research efforts that culminated in the FDA approval of olaparib for clinical use in patients with ovarian and breast cancer harbouring BRCA1/2 mutations (Fang et al., 2014). In recent time, drug repurposing has been gathering momentum as an attractive approach that could potentially offer accelerated establishment of new therapeutics at a much lower cost and risk.

Experimental Approach: Using available structures of PARP-1 with bound inhibitors, we explored an up-to-date library of FDA-approved drugs (DrugBank[®]) through a combination of ligand and structure-guided virtual screening approach. Six best hits were purchased and subjected to an In Cell Western™ (ICW) assay that involved monitoring of H₂O₂-induced PARYlation in A549 cells as an initial reporter of PARP activity. Upon completing the assays in triplicate at various concentrations of tested molecules, semi-logarithmic concentration-response plots were generated and fitted using four-parameter logistic equation implemented in GraphPad™ Prism v.8. To further characterize hits, nuclear PARYlation was measured using confocal microscopy and data plotted as mean nuclear intensity/nuclei number. Statistical significance was determined using one-way ANOVA followed by Tukey's post hoc test.

Key Results: Of all drugs tested using ICW assay, fluvastatin appeared to be reducing PARYlation with a potency of 1.63 μM. In confocal imaging, it also showed significant reduction of nuclear PARYlation, comparable to the known PARP-1 inhibitor olaparib.

Conclusion and Implications: Our in silico screening protocol has been able to identify fluvastatin to be significantly reducing PARYlation. Experiments are underway to assess whether fluvastatin could bind to purified PARP-1 protein, inhibit its catalytic function, and have any

TABLE 1 IC₅₀ determination of potential PARP-1 inhibitors using ICW™ cell-based assay

Drug name	IC ₅₀ (M), n ≥ 3	PIC ₅₀
Olaparib	2.01e – 008 ± 0.000000018	7.69
Rucaparib	1.05e – 008 ± 0.000000023	7.97
Veliparib	7.81e – 009 ± 0.000000013	8.10
Niraparib	3.83e – 007 ± 0.000000017	6.40
Fluvastatin	1.63e – 006 ± 0.000000023	5.70
Bazedoxifene	>50	>4.3

Note. Data represent mean ± SD (from n ≥ 3 independent experiments).

selectivity over any other PARP isoforms and related protein family members.

REFERENCE

Fang, B. (2014). Development of synthetic lethality anticancer therapeutics. *Journal of Medicinal Chemistry*, 57(19), 7859–7873.

P072 | Novel determinants of agonist selectivity in nicotinic ACh receptors

Teresa Minguéz¹; A.S.F. Oliveira²; D.K. Shoemark³; A.J. Mulholland²; I. Bermudez¹; T. Gallagher²

¹Department of Biological and Medical Sciences, Oxford Brookes University; ²School of Chemistry, University of Bristol; ³School of Biochemistry, University of Bristol

Background and Purpose: Activation of α4β2 nicotinic ACh receptors (nAChR) by agonists, particularly partial agonists, is a valid strategy to intervene therapeutically in nicotine addiction. The design of α4β2-specific agonists is however problematic, mainly because of the highly conserved nature of the aromatic box that binds agonists in the nAChR family. For example, ligands that aid smoking cessation, such as varenicline or cytisine, partially activate α4β2 nAChR but behave as full agonists at α7 nAChRs, and this may underlie the off-target effects of these compounds. We have recently describe a series of C(10)-cytisine derivatives that retain the affinity and partial agonism for α4β2 but that have no effects on α7 nAChR at physiologically relevant concentrations (<1 mM) (Rego-Campello et al., 2018). Here, we have investigated the structural determinants that may contribute to the specificity of the C(10)-cytisine derivatives.

Experimental Approach: A multidisciplinary experimental strategy was used for addressing this question. Docking and molecular dynamic simulations were combined with mutagenesis and two-electrode voltage clamping on *Xenopus laevis* oocytes.

Key Results: Comparison of the crystal structure of the α4β2 nAChR with a homology model of the α7 nAChR indicated that non-aromatic residues in loop B differ in the α4 and α7 subunits: α4-KFGSWTYDK versus α7-KFGWSYGG. Molecular dynamic simulations indicated that the aspartate residue in loop B of the α4β2 nAChR influences the electrostatic environment of the upper region of the agonist binding site. In the α7 nAChR, there is a glycine at the equivalent position of the aspartate in α4 (shown in bold in the sequence). We hypothesised this that the glycine to aspartate exchange may affect how agonists interact with the critical loop B in the α7 nAChR. We found that mutating the glycine in α7 nAChR to an aspartate increased the sensitivity of this receptor to activation by cytisine (wild-type EC₅₀ = 30 ± 0.13 μM; mutant EC₅₀ = 9 ± 0.083 μM; n = 11; two-tailed Student's t test, P < .001) or C(10) cytisine derivative (wild-type EC₅₀ = 643 ± 0.17; mutant EC₅₀ = 140 ± 0.19; n = 9; two-tailed Student's t test, P < .001).

Conclusion and Implications: Together, our findings highlight the importance of the electrostatic landscape around the conserved aromatic residues of loop B for agonist effects on nAChRs.

REFERENCE

Rego-Campello, H., Del Villar, S., Honraedt, A., Minguéz, T., Oliveira, A. S. F., Ranaghan, K. E., et al. (2018). Unlocking nicotinic selectivity via direct C–H functionalization of (–)-cytisine. *Chem*, 4(7), 1710–1725.

P073 | Tonantzitolone is a novel potent agonist of transient receptor potential canonical 1/4/5 channels

Hussein Nori Rubaiy¹; Dietmar Wolf²; John A. Beutler³; David J. Beech¹

¹University of Leeds; ²AnalytiCon Discovery GmbH; ³National Cancer Institute

Background and Purpose: Calcium (Ca²⁺)-permeable non-selective cationic channels are known to be involved in maintaining normal cell function by regulation of two parameters: the concentration of free cytosolic calcium and the voltage across the plasma membrane. The transient receptor potential (TRP) family of membrane proteins is one of several superfamilies of Ca²⁺ permeable and in mammals. There are 28 genes encoding TRP proteins, and these channels are widely expressed with diverse functions. The canonical or classical transient receptor potential (TRPC) is a subfamily of TRP proteins with seven members (TRPC1–TRPC7). TRPC4 and TRPC5 assemble as homomers or heteromerize with TRPC1 protein to form functional channels with high calcium permeability. Recent studies suggest that the TRPC1/4/5 channel complexes are potential drug targets for cancer, epilepsy, anxiety, pain, and cardiac remodelling. Tonantzitolone (TZL) is a natural product, which displays cytotoxicity towards certain types of cancer cell such as renal cell carcinoma cells (A498, natively expressing TRPC1 and TRPC4) (Rubaiy et al., 2017; Rubaiy, 2019). The aim of this study was to investigate whether TZL targets the TRPC1/4/5 channels.

Experimental Approach: The effects of TZL on A498 cells, modified HEK293 cells overexpressing TRPC4, TRPC5, TRPC4–TRPC1 or TRPC5–TRPC1 concatemer, TRPC3 or TRPM2, or CHO cells overexpressing TRPV4, were studied by determining changes in intracellular Ca²⁺, or whole-cell or excised membrane patch-clamp electrophysiology (Rubaiy et al., 2018).

Key Results: TZL induced an elevation of intracellular Ca²⁺ in A498 cells and also activated overexpressed channels with EC₅₀ values of 123 nM (TRPC4), 83 nM (TRPC5), 140 nM (TRPC4–TRPC1), and 61 nM (TRPC5–TRPC1). These effects of TZL were reversible on wash-out and potently inhibited by the TRPC1/4/5 inhibitor Pico145 (Rubaiy et al., 2017). Notably, even at 1 μM, TZL failed to activate other members of the TRP superfamily, TRPC3, TRPV4, and TRPM2, suggesting that TZL has specificity for TRPC1/4/5 channels.

Conclusion and Implications: Taken together, we report that TZL is a novel and selective agonist of TRPC1/4/5 channels, and importantly, such an activator is a useful pharmacological tool for testing the functionality of these channels. In addition, TZL is also important for high-throughput screening assays where robust channel activation is a requisite.

REFERENCES

Rubaiy, H. N. (2019). Treasure troves of pharmacological tools to study transient receptor potential canonical 1/4/5 channels. *British Journal of Pharmacology*, 176(7), 832–846.

Rubaiy, H. N., Ludlow, M. J., Henrot, M., et al. (2017). Picomolar, selective, and subtype-specific small-molecule inhibition of TRPC1/4/5 channels. *Journal of Biological Chemistry*, 292(20), 8158–8173.

Rubaiy, H. N., Ludlow, M. J., Siems, K., et al. (2018). Tonantzitolone is a nanomolar potency activator of transient receptor potential canonical 1/4/5 channels. *British Journal of Pharmacology*, 175(16), 3361–3368.

P074 | Punicalagin regulates apoptosis–autophagy switch via modulation of annexin A1 in colorectal cancer cell line

Ajantha Sinniah; Thanusha Ganesan;
Mohammed Abdullah Mahdi Alshawsh; Zamri Chik
University Malaya

Background and Purpose: Colorectal cancer (CRC) is the third most common cancer globally; however, current treatment options fail to exert selective cytotoxicity, paving way for alternative therapeutic options. Pomegranate-derived punicalagin (PU) is proven to have apoptosis and autophagic cell death on various cancers, including CRC (Aqil et al., 2012). Annexin A1 (Anx-A1), an anti-inflammatory protein, is known to possess both anti-cancer and pro-cancer effects (Zhu et al., 2018). Therefore, the aim of this study is to investigate apoptosis–autophagic switch of PU via Anx-A1 modulation.

Experimental Approach: MTT assay was performed on colorectal cancer cell line, HCT-116, treated with various concentrations (0.3–100 μg·ml⁻¹) of PU. To assess the apoptosis inducing ability of PU, annexin V and cell cycle analysis were performed using flow cytometry. Confocal microscopy was used to investigate the permeabilization of cytochrome C in these cells. Proteome profiler using the human apoptosis array kit was used to determine the apoptosis-linked proteins. ELISA was performed to determine the expression of Anx-A1, while the autophagic expression was determined using Autophagy Detection Kit. Assays were conducted in triplicate, and three independent experiments were performed. Data are given as mean ± SEM, and analysis was performed using one-way ANOVA and Bonferonni's post hoc test.

Key Results: MTT assay showed that PU has IC₅₀ of 87 ± 4.4 μg·ml⁻¹ against HCT 116 cells and does not exert cytotoxicity on normal colon epithelium, CCD 841 cells at 72 hr post-treatment. Annexin V apoptosis data demonstrated that HCT-116 entered early apoptosis (11.933 ± 0.949%) that involves disruption of cell membrane integrity.

ELISA revealed that PU down-regulated Anx-A1 in HCT 116 (untreated: 21.14 ± 0.5875 ng·ml⁻¹ vs. PU-treated: 2.963 ± 0.9057 ng·ml⁻¹) and quantitative analysis showed that HCT 116 cells treated with PU and Anx-A1 inhibitors undergo prominent DNA damage and increase in cytochrome C release. Autophagy flux analysis showed significant autophagosome degradation proving involvement of autophagy. Proteome profiling also demonstrated significant involvement of HSP 27, HSP 60, catalase, and TNF RI/TNFRSF1A proteins associated with both apoptosis and autophagy mechanisms.

Conclusion and Implications: Based on these findings, we suggest that PU induces autophagy while maintaining basal level of apoptosis as the main mechanism of cytotoxicity via modulation of Anx-A1 expression in HCT 116 cells and thus has a promising translational potential.

REFERENCES

- Aqil, F., et al. (2012). Anti-proliferative activity and protection against oxidative DNA damage by punicalagin isolated from pomegranate husk. *Food Research International (Ottawa, Ont)*, 49(1), 345–353.
- Zhu, J.-F., et al. (2018). Annexin A1-suppressed autophagy promotes nasopharyngeal carcinoma cell invasion and metastasis by PI3K/AKT signaling activation. *Cell Death & Disease*, 9(12), 1154.

P075 | Ligand-specific differences in protease-activated receptor 2 relaxation of mouse mesenteric arteries

John McGuire; Cheng Yen Lim; Qing Zhong; Rithwik Ramachandran

Western University

Background and Purpose: Recently, ligand-selective signal transduction responses of several protease-activated receptor 2 (PAR2) activating peptides in cell culture were identified (LeSarge, Thibeault, Milne, Ramachandran, & Luyt, 2019). Here, we extend these data on PAR2 agonist biased signalling to functional selectivity in blood vessels from mice.

Experimental Approach: Blood vessel relaxation bioassays for test compounds were performed in small calibre mesenteric arterial ring preparations using wire myographs. Arteries were contracted with phenylephrine before the addition of test compounds. Bioassays were

conducted in replicate from a minimum of three animals. Analyses of test compounds' concentration–relaxation response curves were conducted by non-linear regression and sigmoidal dose–response relationships to determine the best fit curves, $-\log EC_{50}$, Hill slope, and maximum responses (E_{max}). Statistical significance was determined using an F test on the best fit curves.

Key Results: All the PAR2 ligands caused relaxation of mesenteric arteries. There were significant differences in the concentration–response relationships between the PAR2 ligands with a rank order of potency in mesenteric arteries of 5-isoxazoyl-Cha-Chg-AR = 5-isoxazoyl-Cha-Chg > 2-furoyl-LIGRLO > 2-furoyl-LAAAAI. Interestingly, 5-isoxazoyl-Cha-Chg produced a biphasic relaxation response with a 1,000-fold difference in EC_{50} values (M) for the two phases; 5-isoxazoyl-Cha-Chg-AR also caused a biphasic response but was characterized by a second contraction phase at concentrations larger than 100 nM.

Conclusion and Implications: We identify significant differences in the PAR2 agonist concentration–relaxation responses in mouse mesenteric arteries. Overall, the rank-order potency for mesenteric artery relaxation correlated with the reported biased activation of non-calcium signal transduction in cell culture (LeSarge et al., 2019), which demonstrates in mesenteric arteries that PAR2 ligands exhibit agonist functional selectivity.

REFERENCE

- LeSarge, J. C., Thibeault, P., Milne, M., Ramachandran, R., & Luyt, L. G. (2019). High affinity fluorescent probe for proteinase-activated receptor 2 (PAR2). *ACS Medicinal Chemistry Letters*, 10(7), 1045–1050.

P076 | Human breast cancer cell line-dependent differences in responses to a trace amine (TA₁) receptor agonist

Mark Berry¹; Josh McShane¹; Zachary Porter¹; Marius Hoener²; Sherri Christian¹

¹Memorial University of Newfoundland; ²F. Hoffmann-La Roche

Background and Purpose: We have previously shown that expression of TA₁ varies between human breast cancer cell lines at mRNA, protein, and sub-cellular distribution levels (Pitts, McShane, Hoener,

TABLE 1 Concentration–relaxation response curves for different PAR2 ligands

	Potency $-\log EC_{50}$ (M)	Relaxation E_{max} (%)	Hill slope
5-Isloxazoyl-Cha-Chg-AR (n = 16)	8.8 ± 0.1	89 ± 3	0.9 ± 0.2
5-Isloxazoyl-Cha-Chg (n = 6)	First phase, 8.4 ± 0.2	First phase, 37 ± 5	First phase, 1.2 ± 0.5
	Second phase, 5.4 ± 0.1	Second phase, 90 ± 1	Second phase, 1.9 ± 0.7
2-Furoyl-LIGRLO (n = 16)	7.95 ± 0.02	85 ± 4	1
2-Furoyl-LAAAAI (n = 15)	6.09 ± 0.03	80 ± 3	1.3 ± 0.1

Note. All peptides tested were amides.

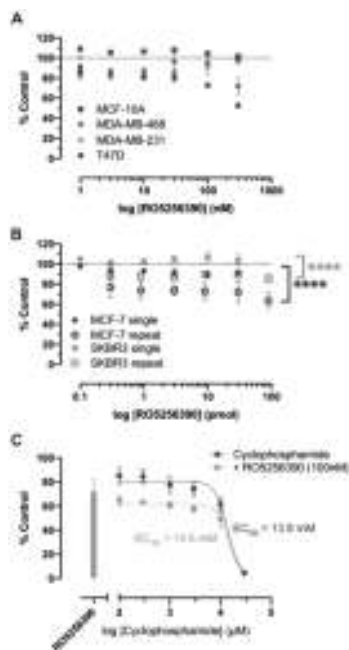


FIGURE 1 Effects of RO5256390 on breast cancer cell line metabolic viability. (a) Cells were treated with a single administration of RO5256390, and metabolic viability was determined 72 hr later. (b) Cells were treated with RO5256390 concentrations indicated in (a) either once or repeated every 24 hr. Shown data are corrected for total drug administered. **** $P < .0001$, two-way ANOVA, single versus multiple administration determined for data expressed as concentrations. (c) MCF-7 cells were treated with a single administration of cyclophosphamide in the absence or presence of repeated administration of 100-nM RO5256390. EC_{50} values were calculated using the log agonist response function of GraphPad Prism. In all panels, data represent mean \pm SEM of triplicate observations in 3–4 independent experiments

Christian, & Berry, 2019). Here, we extend these studies to examine whether such variability affects cellular responses to RO5256390, a highly selective TA_1 agonist.

Experimental Approach: In 12-well plates, 10,000 Her2+ (BT474 and SKBR3), hormone receptor-positive (T47D and MCF-7), triple negative (MDA-MB-231 and MDA-MB-468), or phenotypically normal (MCF-10A) cells per well were grown for 24 hr and then treated with RO5256390 (1–300 nM) or vehicle (0.1% DMSO), either once or every 24 hr. Seventy-two hours after the first administration, metabolic viability was assessed by MTT assay as per manufacturer's instructions. The effect of repeated administration of 100-nM RO5256390 on cyclophosphamide toxicity was also determined in MCF-7 cells. Assays were conducted in triplicate in ≥ 3 independent experiments. Single versus repeated administration was compared by two-way ANOVA. EC_{50} values for cyclophosphamide toxicity \pm RO5256390 were compared using GraphPad Prism. Whole transcriptome data retrieved from the Gene Expression Omnibus database were robust multi-chip average normalized, and relative expression for uridine 5'-diphosphoglucuronyltransferase (UGT) enzymes was obtained by fitting normalized data to a linear model.

Key Results: Single administration of RO5256390 had no effect on metabolic viability except in T47D and MDA-MB-468 cells where concentration-dependent decreases occurred (Figure 1a). Repeated administration, however, also significantly reduced metabolic viability in MCF7 and SKBR3 cells (Figure 1b) even after correction for total pmol administered, suggesting metabolism of RO5256390 in these cell lines. Based on known metabolism of structural analogues (Fowler et al., 2015), bioinformatic analysis of UGT enzymes identified UGT2B4 as a potential contributor to RO5256390 metabolism. Repeated administration of RO5256390 did not affect cyclophosphamide EC_{50} (Figure 1c). No clear correlation between responses and breast cancer phenotype was observed.

Conclusion and Implications: TA_1 activation has cell line-dependent effects on human breast cancer cells due to combinations of variable receptor expression levels and sub-cellular localization, and agonist metabolism, but not breast cancer phenotype. Ongoing research will identify downstream responses to TA_1 activation, including possible effects on cell cycle progression, in each cell line.

REFERENCES

Fowler, S., Kletzl, H., Finel, M., Manevski, N., Schmid, P., Tuerck, D., ... Iglesias, V. A. (2015). A UGT2B10 splicing polymorphism common in African populations may greatly increase drug exposure. *The Journal of Pharmacology and Experimental Therapeutics*, 352, 358–367.
 Pitts, M. S., McShane, J. N., Hoener, M. C., Christian, S. L., & Berry, M. D. (2019). TAAR1 levels and sub-cellular distribution are cell line but not breast cancer subtype specific. *Histochemistry and Cell Biology*, 152, 155–166.

P078 | Mapping signalling profiles downstream of the murine free-fatty acid receptor 4 using label-free methods

Elisa Alvarez-Curto¹; Aska Inoue²; Graeme Milligan¹

¹University of Glasgow; ²Tohoku University

Background and Purpose: Agonists of the murine free-fatty acid receptor 4 (mFFAR4) including long-chain fatty acids (LCFAs) elicit the rapid phosphorylation of specific residues within its C-terminus (Prihandoko et al., 2016). This promotes arrestin 2/3 recruitment to the receptor-G-protein complex and subsequent receptor desensitisation and internalisation (Alvarez-Curto et al., 2016). Activation of mFFAR4 also triggers the activation of $G_{q/11}$ heterotrimeric G proteins, an effect that promotes ERK phosphorylation (Alvarez-Curto et al., 2016). It is therefore anticipated that the balance between G-protein and arrestin-mediated signalling will dictate the outcome of receptor activation (Alvarez-Curto et al., 2016). However, assays to detect specifically arrestin signalling have not been forthcoming (Grundmann et al., 2018). Here, we address this using a collection of HEK293 cell lines lacking arrestin 2/3 (arrestin 2/3-KO cells), $G_{q/11}$ ($G_{q/11}$ -KO cells) (Alvarez-Curto et al., 2016), or all of the G_α subunits ($G_{s/olf/q/11/12/13/i/o} = G_{\alpha all}$ -KO cells) generated by CRISPR-Cas9-mediated genome editing and analyse the

dynamics of signalling using a label-free assay based on changes to cellular impedance using an xCELLigence RTCA system (ACEA Biosciences, Inc).

Experimental Approach: Cells were transfected with 5 µg of a FLAG-mFFAR4-eYFP plasmid in a 1:6 ratio using polyethylenimine; 24 hr after transfection, cells were seeded onto poly-D-lysine-coated E-plates at 60,000 cells per well and grown for 16–20 hr before ligand addition in the xCELLigence RTCA station. Cells were treated with agonist TUG-891 ([3-(4-((4-fluoro-4'-methyl-[1,1'-biphenyl]-2-yl)methoxy)phenyl)propanoic acid)] plus/minus the G_{q/11} inhibitor (UBO-QIC [FR900359]), and cell index values were obtained following ligand stimulation every 30 s for 60 min. Raw cell index values were normalised by dividing the cell index at the time of ligand addition and baseline corrected by subtracting the cell index obtained in vehicle-treated conditions.

Key Results: Activation of mFFAR4 expressed in HEK293 cells with the synthetic agonist TUG-891 reveals an integrated and time-dependent signalling profile consisting of a transient negative phase that rapidly reverts into a positive slope recovery phase. Deviations from this found in some dynamic features of the profiles obtained in the HEK293 were detected in the presence of UBO-QIC and in the arrestin 2/3-KO, G_{q/11}-KO, and G_{αall}-KO cells used in this study highlighting the contribution of these components to integrated signalling.

Conclusion and Implications: Here, we report a novel method to elucidate a signature profile of FFAR4-mediated arrestin 2/3 versus G-protein-dependent signalling that can be extended to other GPCRs and to primary cell culture studies.

REFERENCES

- Alvarez-Curto, E., Inoue, A., Jenkins, L., Raihan, S. Z., Prihandoko, R., Tobin, A. B., & Milligan, G. (2016). *The Journal of Biological Chemistry*, 291(53), 27147–27159.
- Grundmann, M., Merten, N., Malfacini, D., Inoue, A., Preis, P., Simon, K., ... Kostenis, E. (2018). *Nature Communications*, 9(1), 341.
- Prihandoko, R., Alvarez-Curto, E., Hudson, B. D., Butcher, A. J., Ulven, T., Miller, A. M., ... Milligan, G. (2016). *Molecular Pharmacology*, 89(5), 505–520.

P079 | Serine⁴⁵¹ confers ACh potency and efficacy at the M₁ mAChR

Karen Thompson¹; Deryn Teoh En-Jie¹; Geoff Thompson²;
Celine Valant²; Arthur Christopoulos²; Andrew Tobin¹

¹University of Glasgow; ²Monash Institute of Pharmaceutical Sciences

Background and Purpose: The M₁ muscarinic ACh receptor (M₁ mAChR) is implicated in numerous neurological functions, most notably learning and memory. Binding of an agonist to the M₁ mAChR induces rapid phosphorylation of 14 intracellular sites on the receptor (Benovic, Strasser, Caron, & Lefkowitz, 1986)—12 located in the third intracellular loop and two in the C-terminal tail (Butcher et al., 2016).

Recent studies show that transgenic mice expressing a M₁ phosphorylation-deficient (PD) mAChR—with mutations of all 14 sites—are prone to seizures, while M₁-PD mAChRs do not internalise. To assess the precise contribution of each of these sites to seizure and lack of desensitisation, we have engineered cell lines expressing single alanine mutation of either of the two C-terminal tail serines. Here, we present evidence that Ser⁴⁵¹, one of the two C-terminal phosphoserines, contributes to ligand potency and efficacy—but not affinity or internalisation—at the hM₁ mAChR.

Experimental Approach: Cell Lines

CHO cells were stably transfected with either wild-type human M₁ mAChR (hM₁-WT) or human M₁ mAChR with an alanine mutation at Ser⁴⁵¹ (hM₁-S451^A).

[³H]-N-Methylscopolamine (NMS) Assays

Confluent monolayers of Flp-In CHO cells stably expressing hM₁-WT or hM₁-S451^A were incubated in Krebs buffer with [³H]-NMS at (a) increasing concentrations (saturation) or (b) K_D concentration with increasing unlabelled ligand concentrations (inhibition) for 2 hr at 37°C. For internalisation assays, cells were incubated in 100-µM ACh over a 1-hr time course, washed, and then incubated with 3-nM [³H]-NMS overnight at 4°C. Liquid scintillation counting determined bound radioactivity. *Functional assays* were performed with IP₁ accumulation (as a surrogate of Gq-mediated signalling) and ERK1/2 phosphorylation; pERK1/2 (Thr²⁰²/Tyr²⁰⁴) kits (Cisbio, France). For IP₁, confluent monolayers of cells were incubated in stimulation buffer with ligands for 1 hr at 37°C. For pERK1/2, serum-starved cells were stimulated for 5 min at 37°C and then lysed. IP₁ accumulation or pERK1/2 levels were determined with cryptate/D2 antibodies and HTRF. Data Analysis

All non-linear regression and statistical analyses were performed using GraphPad Prism 7.

Key Results: Saturation binding indicated no significant difference in [³H]-NMS K_D between hM₁-WT and hM₁-S⁴⁵¹A (0.71 ± 0.14 vs. 0.69 ± 0.23 nM, respectively; n = 3), while inhibition binding assays indicated no difference in the affinity of the endogenous agonist, ACh, between hM₁-WT and hM₁-S⁴⁵¹A (pK_i = 4.62 ± 0.19 vs. 4.51 ± 0.16, respectively; n = 3). Both hM₁-WT and hM₁-S⁴⁵¹A internalised to an equivalent degree over 1 hr with 100-µM ACh (64.5 ± 4.47% vs. 66.9 ± 3.27%, respectively; n = 3).

However, functional assays revealed differences in ACh potency and efficacy. IP₁ accumulation assays indicated a 10-fold increase in ACh potency at hM₁-WT versus hM₁-S⁴⁵¹A (pEC₅₀ = 6.83 ± 0.23 vs. 7.3 ± 0.12, respectively; n = 7). Meanwhile, only a threefold increase was observed for ACh in pERK1/2 assays at hM₁-WT versus hM₁-S⁴⁵¹A (pEC₅₀ = 5.77 ± 0.14 vs. 6.29 ± 0.24, respectively; n = 4). While ACh was a full agonist at hM₁-WT, only partial agonism was seen at hM₁-S⁴⁵¹A. The operational model of agonism indicated that, although ACh activated IP₁ to a similar extent in hM₁-WT and hM₁-S⁴⁵¹A (log_{tau} = 2.5 ± 0.2 vs. 2.8 ± 0.9; n = 7), hM₁-S⁴⁵¹A phosphorylation of Thr²⁰²/Tyr²⁰⁴ was substantially reduced in comparison to hM₁-WT (log_{tau} = 0.4 ± 0.9 [S⁴⁵¹A] vs. 1.6 ± 0.2 [WT]; n = 3).

Conclusion and Implications: Mutated hM₁-S⁴⁵¹A does not affect orthosteric agonist affinity or internalisation. Functional assays

indicate a gain in ACh potency but reduction in ERK1/2 phosphorylation activation. Therefore, Ser⁴⁵¹ may be crucial for the full induction of specific second messenger pathways.

REFERENCES

- Benovic, J. L., Strasser, R. H., Caron, M. G., & Lefkowitz, R. J. (1986). β -Adrenergic receptor kinase: Identification of a novel protein kinase that phosphorylates the agonist-occupied form of the receptor. *Proceedings of the National Academy of Sciences of the United States of America*, 83, 2797–2801.
- Butcher, A. J., Bradley, S. J., Prihandoko, R., Brooke, S. M., Mogg, A., Bourgognon, J. M., ... Tobin, A. B. (2016). An antibody biosensor establishes the activation of the M₁ muscarinic acetylcholine receptor during learning and memory. *Biological Chemistry*, 291(17), 8862–8875.

P080 | Pharmacological characterisation of the LPS challenge assay for conformation of target engagement of EP₄ antagonists in human whole blood

Hannah Neale; Sue Brown; Kirstie Bennett; Jason Brown;
Matt Barnes

Sosei Heptares

Background and Purpose: PGE₂ expression correlates with the progression of many epithelial cancers (Nakanishi et al., 2013) and may play a role in reducing inflammatory cytokine release in the tumour micro-environment. The reversal of PGE₂ inhibition of TNF- α in LPS-stimulated human whole blood (LPS-HWB) has been used as a target engagement marker for antagonists of the PG receptor 4 (EP₄) (Jin et al., 2018), with the effect thought to be mediated primarily by monocytes (Murase et al., 2008). However, there are conflicting data as to whether the LPS-HWB assay can also measure an EP₂ response (Meja et al., 1997). The aim of this study was to characterise the PGE₂ response in both an immortalised monocytic cell line (THP-1) and an LPS-HWB assay.

Experimental Approach: In THP-1 cells, a G_s cAMP assay was performed to manufacturer's instructions (Cisbio); relative expression of PG receptors was characterised using qRT-PCR. The LPS-HWB was performed following literature methods (Nakanishi et al., 2013), with antagonists pre-incubated (37°C at 5% CO₂) for 30 min prior to agonist addition. Four hours after LPS addition (10 $\mu\text{g}\cdot\text{ml}^{-1}$), TNF- α concentration was measured via ELISA following manufacturer's conditions (DY210 R&D Systems DuoSet). Concentration–response curves were fitted using a sigmoidal four-parameter fit (GraphPad Prism).

Key Results: In THP-1 cells, EP₄ expression was 50-fold higher than EP₂, and the selective EP₄ agonist, KAG308, was found to elicit a G_s cAMP response (pEC₅₀ 8.3 \pm 0.1; n = 3), which could be dose-dependently inhibited by the EP₄ antagonist ONO-AE3-208 but not by EP₂ antagonist PF-04418948. EP₂ agonist AH13205 was found to be inactive at concentrations below 1 μM . In the LPS-HWB assay, PGE₂ inhibition of TNF- α release (pIC₅₀ 9.1 \pm 0.36, n = 3) exhibited a shallow Hill slope (0.62 \pm 0.22), suggesting activity on multiple

receptors. PGE₂ inhibition of TNF- α release could be reversed by the EP₄ antagonist ONO-AE3-208 but not by the EP₂ antagonist PF-04418948. EP₂ agonist AH13205 was found to be inactive in the LPS-HWB assay at concentrations up to 1 μM .

Conclusion and Implications: These data suggest that in both the THP-1 cells and the LPS-HWB assay, EP₂ agonists and antagonists have little activity, in contrast to published data (Murase, et al. 2008). The LPS-HWB assay is an appropriate assay to measure EP₄ responses.

REFERENCES

- Jin, Y., et al. (2018). *Clinical and Translational Science*, 11, 46–53.
- Meja, K. K., et al. (1997). *British Journal of Pharmacology*, 122(1), 149–157.
- Murase, A., et al. (2008). *Life Sciences*, 82, 226–232.
- Nakanishi, M., et al. (2013). *Seminars in Immunopathology*, 35(2), 123–137.

P081 | GPR35 selectivity between the G proteins G α 12 and G α 13 is defined by a single leucine to isoleucine variation

Tezz Quon; Amanda MacKenzie; Brian Hudson; Laura Jenkins;
Andrew Tobin; Graeme Milligan

University of Glasgow

Background and Purpose: The C-terminal α 5 helix of the G α subunit of heterotrimeric G proteins plays an important role in coupling to and activation by GPCRs (Inoue et al., 2019). GPR35 has been shown to preferentially couple to G α 13 over the closely related G α 12 despite minimal differences in the α 5 helix. Here, we dissect the selectivity determinants in the α 5 helix, which allows GPR35 preferentially couple to G α 13 over G α 12.

Experimental Approach: Systematic protein affinity strength modulation (SPASM) intramolecular biosensors (Malik et al., 2013) containing human GPR35 followed by YFP, a flexible linker, nanoluciferase, and the α 5 helix of G α subunits, along with full-length G α 12 and G α 13 BRET-based sensors, were generated (Mackenzie et al., 2019). Following stable expression in parental and G α 12/13 knockout HEK293 cells and treatment with varying concentrations of Iodoxamide, zaprinast, pamoic acid, or bufrolin, changes in BRET ratio were monitored. Each experiment was repeated at least three times, and the pooled data were used for analysis.

Key Results: Single and double residue swaps between the G α 12 and G α 13 α 5 helix sequence revealed that GPR35 selectivity is largely due to a single leucine at position G.H5.23 in G α 13. Indeed, any substitution to this residue resulted in almost complete loss of coupling to GPR35 (P < .0001, Figure 1). The importance of this leucine residue was further highlighted when leucine replaced the equivalent residue of G α q. This resulted in a substantial gain of function (P < .0001), whereas wild-type G α q was unable to couple effectively to GPR35.

Conclusion and Implications: These studies demonstrate the high level of selectivity GPR35 has for G α 13 over its closely related family

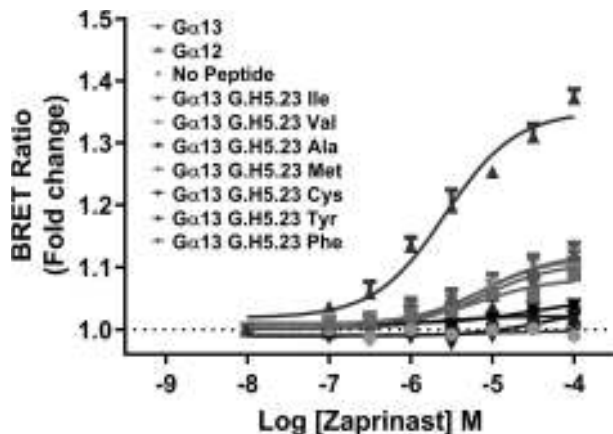


FIGURE 1 GPR35 SPASM sensors with $G\alpha_{12}$ and $G\alpha_{13}$ $\alpha 5$ helix with and without substitutions of the leucine residues

member $G\alpha_{12}$, despite minimum sequence difference and that this selection is largely mediated by a single amino acid variation.

REFERENCES

- Inoue, A., Raimondi, F., Kadji, F. M. N., Singh, G., Kishi, T., Uwamizu, A., ... Russell, R. B. (2019). Illuminating G-protein-coupling selectivity of GPCRs. *Cell*, 177.
- Mackenzie, A. E., Quon, T., Lin, L. C., Hauser, A. S., Jenkins, L., Inoue, A., ... Milligan, G. (2019). Receptor selectivity between the G proteins $G\alpha_{12}$ and $G\alpha_{13}$ is defined by a single leucine-to-isoleucine variation. *The FASEB Journal*, 33.
- Malik, R. U., Ritt, M., DeVree, B. T., Neubig, R. R., Sunahara, R. K., & Sivaramakrishnan, S. (2013). Detection of G protein-selective G protein-coupled receptor (GPCR) conformations in live cells. *The Journal of Biological Chemistry*, 288.

P083 | Extracellular loop 1 of the calcitonin receptor-like receptor is required for agonist-mediated cAMP production

Rachael L. Grime¹; David R. Poyner²; Mark Wheatley³

¹University of Birmingham; ²Aston University; ³Coventry University

Background and Purpose: The calcitonin receptor-like receptor (CLR) is a family B GPCR that interacts with the different receptor activity-modifying proteins (RAMPs) to yield distinct receptor phenotypes. When associating with RAMP 1, it acts as the CGRP receptor. When in association with RAMP 2 or 3, CLR forms the adrenomedullin receptors 1 (AM1R) and 2 (AM2R), respectively (Poyner et al., 2002). Key residues within extracellular loop one (ECL1) have been elucidated via systematic deletion scan. Significant alterations in both CGRP-mediated and adrenomedullin (AM)-mediated cAMP signalling were observed for a number of residues, including V205 Δ , which has been previously implicated in subfertility and miscarriage at the AM1R (Mackie et al., 2018).

Experimental Approach: Site-directed mutagenesis was employed to generate mutagenic constructs that incorporated residue deletions from Asn200 to Asn208. DNA sequences were confirmed by automated fluorescence DNA sequencing, in both sense and anti-sense directions. Constructs were transiently transfected into COS-7 cells for characterisation. Cell surface expression was assessed using ELISA exploiting either an N-terminus HA-tag on the CLR or FLAG-tag on RAMP. cAMP accumulation was assessed using competitive ELISA. Data are expressed as mean \pm SEM and representative of at least three independent experiments.

Key Results: With regard to the AM1R, cell surface expression studies found that deletion at any residue did not significantly impair either receptor or RAMP 2 trafficking (Table 1). N201 Δ , Q202 Δ , A203 Δ , L204 Δ , A206 Δ , and T207 Δ all showed significantly reduced AM₁₃₋₅₂ potency (table 1). V205 Δ demonstrated an 8.8-fold loss in potency, though this did not reach a significant level. Both L204 Δ and A206 Δ demonstrated a significant reduction in maximum response (68% and 65%, respectively), as well as their 10-fold loss in potency. All other constructs demonstrated near-WT-like potency and maximum response.

Conclusion and Implications: These results suggest that ECL1 plays little involvement in trafficking of the receptor to the cell surface; however, ECL1 is crucial for cAMP signalling. This corroborates with the most recent cryo-EM structure of the active, G_s -protein complexed, human CGRP receptor, which identified ECL1 to be in close proximity to the peptide ligand but far from the RAMP binding site (Liang et al., 2018). Characterisation with RAMP 1 and CGRP-mediated cAMP signalling is currently being assessed, as well as loop length requirement, as CLR possesses one of the shortest ECL1s for all family B GPCRs.

TABLE 1 Pharmacological characterisation of CLR-RAMP 2 mutations

Construct	Cell surface expression (%)	cAMP production	
		pEC ₅₀	E _{max} (%)
WT	100 \pm 0	9.5 \pm 0.3	92 \pm 1
N201 Δ	112 \pm 8	7.7 \pm 0.03**	100 \pm 1
Q202 Δ	76 \pm 12	7.3 \pm 0.1***	78 \pm 2*
A203 Δ	116 \pm 10	7.7 \pm 0.1**	100 \pm 4
L204 Δ	95 \pm 3	8.3 \pm 0.4 [†]	68 \pm 4****
V205 Δ	66 \pm 13	8.6 \pm 0.3	88 \pm 2
A206 Δ	95 \pm 19	8.5 \pm 0.2 [†]	65 \pm 5****
T207 Δ	115 \pm 22	7.7 \pm 0.1**	100 \pm 3

REFERENCES

- Liang, Y. L., et al. (2018). Cryo-EM structure of the active, G_s -protein complexed, human CGRP receptor. *Nature*, 561(7724), 492–497.
- Mackie, D. I., et al. (2018). hCALCRL mutation causes autosomal recessive nonimmune hydrops fetalis with lymphatic dysplasia. *The Journal of Experimental Medicine*, 215(9), 2339–2353.

Poyner, D. R., et al. (2002). International Union of Pharmacology. The mammalian calcitonin gene-related peptides, adrenomedullin, amylin, and calcitonin receptors. *Pharmacological Reviews*, 54(2), 233–246.

P213 | Phosphorylation of the M₁ muscarinic ACh receptor mediates neuroprotection

Miriam Scarpa; Colin Molloy; Lisa Finlayson; Andrew B. Tobin; Sophie J. Bradley

University of Glasgow

Background and Purpose: Pharmacological activation of the M₁ muscarinic ACh receptor (mAChR) was proven to improve cognitive deficits and exert beneficial disease-modifying effects in animal models of neurodegeneration and Alzheimer's disease (AD) (Bradley et al., 2017). However, little is known about the M₁ mAChR signalling mechanism interfering with disease progression. This study provides evidence that the phosphorylation-dependent pathway of the M₁ mAChR mediates neuroprotection in prion neurodegeneration.

Experimental Approach: Phosphorylation-deficient M₁ mAChR (M₁-PD) was generated by alanine substitutions of the recognised 14 phosphorylation sites (Butcher et al., 2016). HA-tagged wild-type (WT) and M₁-PD receptors were knocked-in into the natural M₁ mAChR gene locus of C57BL/6 mice. Mice were inoculated with 1% brain homogenate infected with Rocky Mountain Laboratories prion or control. Symptoms were scored according to the appearance of early indicators and confirmatory signs of disease. Hippocampal function was assessed using burrowing test from 9 weeks post-inoculation (w.p.i.) and repeated weekly. Western blots were performed on dissected, frozen tissue (hippocampus and cortex). Immunohistochemical staining was performed on slices of perfused, paraffin-waxed brains. Biochemical and immunohistochemical analyses on hippocampus and cortex used antibodies against HA (receptor expression), GFAP and IBA1 (astroglisis), prion protein (PrP), and APO-E.

Key Results: All mouse strains expressed the receptor at equal levels. M₁-PD mice with prion showed earlier symptom onset (WT: 22 w.p.i.; M₁-PD: 20 w.p.i.) and faster decline in hippocampal function compared to WT ($P < .05$). Prion-infected M₁-PD mice showed higher level of misfolded PrP, spongiosis, and astroglisis compared to WT with prion at the same disease time-point (16 and 18 w.p.i.). APO-E, a hallmark of AD, was up-regulated in diseased M₁-PD mice but not in WT ($P < .01$). Prion-infected M₁-PD mice reached terminal disease significantly earlier than WT with prion (WT: 25 w.p.i.; M₁-PD: 21 w.p.i.).

Conclusion and Implications: Phosphorylation-dependent signalling of the M₁ mAChR plays a neuroprotective role in the neurodegeneration of murine prion disease. This suggests that M₁-activating ligands for treatment of neurodegenerative disorders with a signalling bias towards the phosphorylation-dependent signalling pathway of the M₁ mAChR are more likely to slow down and potentially prevent astroglisis, spongiosis, and accumulation of misfolded proteins compared to G-protein-biased ligands.

REFERENCES

- Bradley, S. J., Bourgognon, J.-M., Sanger, H. E., Verity, N., Mogg, A. J., White, D. J., ... Tobin, A. B. (2017). M₁ muscarinic allosteric modulators slow prion neurodegeneration and restore memory loss. *The Journal of Clinical Investigation*, 127(2), 487–499.
- Butcher, A. J., Bradley, S. J., Prihandoko, R., Brooke, S. M., Mogg, A., Bourgognon, J.-M., ... Tobin, A. B. (2016). An antibody biosensor establishes the activation of the M₁ muscarinic acetylcholine receptor during learning and memory. *The Journal of Biological Chemistry*, 291(17), 8862–8875.

P216 | New mefenamic acid derivative disrupts aggregation of amyloid- β peptide

Atheer Al-Zurfi; Sally Freeman; Harnesh Aojula; Jeffrey Penny

The University of Manchester

Background and Purpose: Alzheimer's disease is an age-related, irreversible, progressive brain disease and is characterised by extracellular accumulation of amyloid- β_{1-42} ($A\beta_{1-42}$) peptide with subsequent formation of plaques (Möller & Graeber, 1998). Disruption of amyloid- β aggregation may therefore prove beneficial when devising an approach to treat Alzheimer's disease.

Non-steroidal anti-inflammatory drugs (NSAIDs) are among the most commonly prescribed drugs in modern medicine (Vonkeman & van de Laar, 2010). While the demand for NSAIDs is on the rise, their clinical usefulness is limited owing to gastrointestinal side effects. Epidemiological observations indicate that long-term treatment with NSAIDs results in reduced risk and delayed onset of Alzheimer's disease (Daniels et al., 2016; Hirohata et al., 2005; In't Veld et al., 2001; Joo et al., 2006; Weggen et al., 2001). It has been proposed that NSAIDs exert their beneficial effects in part by decreasing neurotoxic inflammatory responses in the brain; however, this mechanism has not been proved (Weggen et al., 2001). Mefenamic acid has been reported recently to inhibit the NLRP3 inflammasome (Daniels et al., 2016). NSAIDs dose dependently inhibit formation of $A\beta$ fibrils and destabilise preformed $A\beta$ fibrils, and studies report that NSAID may reduce the amount of $A\beta_{1-42}$ in the brain; however, the mechanism is unknown (Hirohata et al., 2005).

The objective of this study was to investigate the ability of a novel mefenamic acid conjugate to disrupt $A\beta_{1-42}$ aggregation.

Experimental Approach: $A\beta_{1-42}$ was purchased from Cellmano Biotech Limited, China. Mefenamic acid was purchased from Sigma-Aldrich.

The effects of mefenamic acid and a novel mefenamic acid-peptide conjugate on aggregation of $A\beta_{1-42}$ monomers were investigated at an $A\beta_{1-42}$: compound ratio of 1:20. $A\beta_{1-42}$, 100 μ M, was incubated with compounds, at 2 mM. $A\beta_{1-42}$ aggregation size was monitored by NanoSight NS300 DLS system. Atomic force microscopy (AFM) was used to study the morphology of aggregation overtime.

Key Results: Dynamic light scattering (DLS) studies confirmed that mefenamic acid (at a 1:20 peptide: NSAID ratio) may promote the

formation of large globular, non-toxic aggregates of A β ₁₋₄₂, which are likely to be non-amyloidogenic. At almost all time points over the initial 12-hr incubation period, the mean hydrodynamic diameter of aggregates treated with mefenamic acid was significantly higher than in the control condition, while with the mefenamic acid conjugate, the size significantly decreased over 96 hr. Furthermore, atomic force microscopy revealed that incubation with mefenamic acid conjugate significantly changed the morphology of A β ₁₋₄₂.

Conclusion and Implications: The current study indicates that this novel mefenamic acid conjugate disrupts aggregation of A β ₁₋₄₂, which could be a potential future approach for the management and/or treatment of Alzheimer's disease.

REFERENCES

- Daniels, M. J. D., et al. (2016). Fenamate NSAIDs inhibit the NLRP3 inflammasome and protect against Alzheimer's disease in rodent models. *Nature Communications*, 7, 12504.
- Hirohata, M., et al. (2005). Non-steroidal anti-inflammatory drugs have anti-amyloidogenic effects for Alzheimer's β -amyloid fibrils in vitro. *Neuropharmacology*, 49(7), 1088–1099.
- In'T Veld, B. A., et al. (1998). NSAIDs and incident Alzheimer's disease. The Rotterdam study. *Neurobiology of Aging*, 19(6), 607–611.
- In't Veld, B. A., et al. (2001). Nonsteroidal antiinflammatory drugs and the risk of Alzheimer's disease. *New England Journal of Medicine*, 345(21), 1515–1521.
- Joo, Y., et al. (2006). Mefenamic acid shows neuroprotective effects and improves cognitive impairment in in vitro and in vivo Alzheimer's disease models. *Molecular Pharmacology*, 69(1), 76–84.
- Möller, H.-J., & Graeber, M. B. (1998). The case described by Alois Alzheimer in 1911. *European Archives of Psychiatry and Clinical Neuroscience*, 248(3), 111–122.
- Vonkeman, H. E., & van de Laar, M. A. F. J. (2010). Nonsteroidal anti-inflammatory drugs: Adverse effects and their prevention. *Seminars in Arthritis and Rheumatism*, 39(4), 294–312.
- Weggen, S., et al. (2001). A subset of NSAIDs lower amyloidogenic A β ₄₂ independently of cyclooxygenase activity. *Nature*, 414(6860), 212–216.

P227 | Assessing the effects of plant-based therapeutics on TLR2-mediated microglial activation

Maitiú ó Murchú; Breandán N. Kennedy; Derek A. Costello

University College Dublin

Background and Purpose: Toll-like receptor 2 (TLR2) is known to mediate much of the inflammation and neuronal dysfunction associated with Alzheimer's disease (AD). Brain-derived neurotrophic factor (BDNF) is a major contributor to neuronal development and neurogenesis, via interaction with the TrkB receptor. No cure or universal treatment for AD currently exists. However, strategies that target neuro-inflammatory processes and drugs that mimic the role of BDNF are among the most promising candidates for therapeutic intervention. The current study aimed to examine the capacity of a small-molecule activator of TrkB, to alleviate TLR2-mediated inflammatory responses in microglia. In addition, we assessed the anti-inflammatory properties of an unknown naturally occurring compound, routinely used in Chinese herbal medicine.

Experimental Approach

7,8,3-Trihydroxyflavone (7,8,3-THF) is a small-molecule activator of TrkB. Although reported to promote neuronal survival, its anti-inflammatory capacity remains poorly explored. BV2 microglial cells were exposed to the TLR2 agonist lipoteichoic acid (LTA; 5 $\mu\text{g}\cdot\text{mL}^{-1}$) for 24 hr, in the presence of 7,8,3-THF (20 μM), the novel research compound XF2 (5 μM), or vehicle control. Supernatants were subsequently harvested for analysis of pro-inflammatory cytokines TNF- α and IL-6 by ELISA and nitrite concentration using Griess assay. Cells were stored to assess the expression of iNOS using Western immunoblot. Statistical differences were determined by one-way ANOVA, followed by Newman-Keuls posttests.

Key Results: LTA induced a robust increase in supernatant concentration of both TNF- α and IL-6, relative to vehicle-treated cells ($P < .001$; $n = 3$). Application of 7,8,3-THF did not alter the release of TNF- α but significantly attenuated the LTA-mediated increase in IL-6 ($P < .001$; $n = 3$). Co-application of LTA with XF2 significantly attenuated the expression of both TNF- α and IL-6, compared with cells exposed to LTA alone ($P < .001$; $n = 3$). LTA-mediated production of NO was determined by increased expression of iNOS, and supernatant concentration of nitrite, relative to untreated cells ($P < .001$; $n = 3$). The presence of 7,8,3-THF significantly reduced the LTA-induced expression of both iNOS and nitrite ($P < .001$; $n = 3$). Similarly, the presence of XF2 attenuated the expression of iNOS ($P < .01$; $n = 3$) and nitrite ($P < .001$; $n = 3$), compared to cells exposed to LTA alone. Interestingly, XF2 reduced nitrite release to a greater extent than that seen in the presence of 7,8,3-THF ($P < .001$; $n = 3$).

Conclusion and Implications: Both 7,8,3-THF and XF2 can alleviate the TLR2-mediated release of cytokines and production of NO from

TABLE 1 TLR2-mediated inflammatory changes in BV2 cells

Marker (relative to control)	LTA (mean \pm SEM)	LTA + 7,8,3-THF (mean \pm SEM)	LTA + XF2 (mean \pm SEM)
TNF- α	5.2 \pm 0.3 ^{***}	4.8 \pm 0.3	4.1 \pm 0.3 ^{***}
IL-6	24.7 \pm 0.6 ^{***}	21.2 \pm 0.2 ^{***}	20.1 \pm 0.03 ^{***}
Nitrite	6.8 \pm 0.3 ^{***}	5.4 \pm 0.2 ^{***}	3.8 \pm 0.3 ^{***}
iNOS	4.6 \pm 0.5 ^{***}	2.2 \pm 0.3 ^{***}	2.9 \pm 0.5 ^{**}

*** $P < .001$, compared to control. ** $P < .01$, compared to LTA. *** $P < .001$, compared to LTA.

microglial cells. This supports the further exploration of these plant-based compounds as potential therapies for neuro-inflammatory conditions such as AD, associated with TLR2 activation.

Poster Session: Molecular and Cellular Pharmacology 1

P002 | Antagonist binding kinetics at the human D1 dopamine receptor determined by HTRF assay

Kathy Sengmany; Ka-Wing Wong; Steven Charlton; Nicholas Holliday

Excellerate Bioscience

Background and Purpose: The binding kinetics of ligands, described by their association (k_{on}) and dissociation (k_{off}) rate constants at the target receptor, significantly influence drug action. For example, recent studies on the D2 dopamine receptor correlate antipsychotic side effects with association rates and their potential influence on rebinding (Sykes et al., 2017). The D1 receptor (D1R) offers an alternate target in ameliorating symptoms of schizophrenia (Beaulieu & Gainetdinov, 2011), and while functional effects of D1R antagonists have previously been assessed (Beaulieu & Gainetdinov, 2011), less is known about their binding kinetics. Here, we develop a homogenous time-resolved fluorescence (HTRF) D1R binding assay and demonstrate its applicability in measuring antagonist kinetic parameters by the competition association method (Motulsky & Mahan, 1984).

Experimental Approach: Terbium-labelled SNAP-tagged human D1R membranes were generated as previously described (Sykes et al., 2017), and binding assays were carried out in LabMed (Cisbio, supplemented with 1% DMSO, 100 $\mu\text{g}\cdot\text{ml}^{-1}$ of saponin, 100- μM GTP, and 0.02% pluronic acid) using SKF83566-green (F-SKF) as the fluorescent tracer acceptor (with HTRF measured on a BMG Pherastar FSX). F-SKF k_{on} and k_{off} were determined by global fitting of a one-site model (Graphpad Prism) to its association kinetics at different tracer concentrations. Competition association kinetic assays were initiated by adding membranes to a mix of F-SKF (300 nM) and increasing concentrations of unlabelled antagonist, from which competing

ligand k_{on} and k_{off} were determined by the Motulsky-Mahan (MM) model (Motulsky & Mahan, 1984).

Key Results: The F-SKF k_{on} was $3.17 \pm 0.12 \times 10^6 \text{ M}^{-1}\cdot\text{min}^{-1}$, its k_{off} $0.41 \pm 0.01 \text{ min}^{-1}$, and equilibrium dissociation constant K_D $139.1 \pm 5.0 \text{ nM}$ ($n = 4$), measured at the D1R. Using the MM approach, the kinetics of representative D1 antagonists SCH-23390, ecopipam (SCH-39166), and clozapine were also derived as shown in Table 1.

Conclusion and Implications: HTRF screening using the F-SKF tracer offers a robust method to assess antagonist binding kinetics at D1R, with a homogenous, medium throughput format allowing implementation of such studies at an early stage in compound profiling.

REFERENCES

- Beaulieu, J. M., & Gainetdinov, R. R. (2011). The physiology, signaling and pharmacology of dopamine receptors. *Pharmacological Reviews*, 63(1), 182–217.
- Motulsky, H. J., & Mahan, L. C. (1984). The kinetics of competitive radioligand binding predicted by the law of mass action. *Molecular Pharmacology*, 25(1), 1–9.
- Sykes, D. A., Moore, H., Stott, L., Holliday, H., Javitch, J. A., Lane, J. R., & Charlton, S. J. (2017). Extrapyramidal side effects of antipsychotics are linked to their association kinetics at dopamine D2 receptors. *Nature Communications*, 8(1), 763.

P004 | Hyperglycaemia elicits up-regulation of the histamine H₄ receptor in human retinal Müller cells in vitro

Natalie Young¹; Linh Pham¹; Ibrahim Alrashdi²; Ilona Obara²; Vsevolod Telezhkin²; Paul Chazot¹

¹Durham University; ²Newcastle University

Background and Purpose: Diabetic retinopathy is one of the leading causes of blindness, with the pathogenesis associated with histamine, histamine is known to have an involvement in the breakdown of the blood-retinal barrier (BRB), and recent evidence has specifically implicated an important role of the histamine H₁ receptor in vascular permeability. Müller cells are the primary glial cells of the retina and are pivotal for the normal functioning of the retina, and we have demonstrated, for the first time, the presence of the histamine H₄ receptor on murine Müller cells, particularly on the end feet of these cells. Therefore, the aim of this investigation was to initially confirm the presence of the histamine H₄ gene in the human retina and then secondly compare the expression between cells that were grown in standard glucose to those grown in a high-glucose environment.

Experimental Approach: Using an in vitro model of the human retina, RT-PCR was performed using mRNA extracted from Mio-M1 Müller cells, to see the expression of the four histamine receptors in the human retina. Müller cells were also exposed to a high-glucose environment (4.5 g·L⁻¹) for 1 week prior to extraction of RNA, to compare the histamine H₄ levels to control. RT-PCR expression data were quantified by densitometry using ImageJ, expressed as fold change

TABLE 1 Association, dissociation, and equilibrium dissociation constants of D1 antagonists

Compound	k_{on} ($\times 10^7 \text{ M}^{-1} \text{ min}^{-1}$)	k_{off} (min^{-1})	K_D (nM)
SCH-23390 ($n = 3$)	8.89 ± 1.01	0.21 ± 0.004	3.2 ± 0.3
SCH-39166 ($n = 3$)	8.82 ± 0.63	0.35 ± 0.02	4.2 ± 0.2
Clozapine ($n = 3$)	1.68 ± 0.25	5.96 ± 0.61	452.4 ± 51

compared to control, and statistical significance was determined by unpaired *t* tests.

Key Results: RT-PCR of the four histamine genes revealed that bands of relevant sizes were present in the cells, indicative of a positive result for the expression of the histamine receptors; H₁-H₄, in the Müller cells. Histamine H₄ expression revealed a significantly stronger expression when exposed to the high-glucose environment, with a 5.8-fold increase in the receptor expression, compared to control.

Conclusion and Implications: These data serve to demonstrate that the Müller Mio-M1 cell line positively expresses the four histamine receptors; therefore, this cell line is a viable model to characterise the whole family of histamine receptors within the human retina. These data have demonstrated a profound increase in expression of the histamine H₄ receptor when exposed to a high-glucose environment; this up-regulation of H₄ has also been demonstrated using immunofluorescence analysis; therefore, both of these findings indicate a therapeutic potential of neutral H₄ receptor antagonists in diabetic retinopathy.

ACKNOWLEDGEMENTS

This study was supported by Virulite Ltd, RISE, and MRC. The Mio-M1 cells were a kind gift from Professor GA Limb (UCL).

P005 | The influence of cytokines on the transcriptional regulation of the human CCR4 receptor gene

Alessia Carta¹; Michael Portelli²; Joseph Vella¹; Vanessa Petroni Magri¹; Anthony Fenech¹

¹Department of Clinical Pharmacology & Therapeutics, University of Malta, Msida; ²Division of Respiratory Medicine, School of Medicine, University of Nottingham

Background and Purpose: The CCR4 receptor is a 360-amino acid GPCR receptor protein. In asthmatic patients, high expression has been reported in Th₂ lymphocytes. Activation of this receptor by specific endogenous ligands, such as CCL17 (TARC) and CCL22 (MDC), promotes the inflammatory process by contributing to the trafficking of dendritic cells and the localization of T cells to the airways. The main objectives are to (a) identify whether asthma-related cytokines

TABLE 1 Cytokines and concentrations used in cell culture

Cytokine	Concentration (pg·ml ⁻¹)
IL-2	35
IL-5	20
IL-9	30
IL-10	5
IL-1β	250
TNF-α	150

influence the activity of the two known CCR4 promoters in an airway cell line model and (b) explore the major transcription factors that potentially contribute to CCR4 transcriptional regulation through transcription factor binding motif mapping.

Experimental Approach: A panel of 15 pGL3E luciferase reporter deletion constructs previously generated from the two known CCR4 promoters were co-transfected with pGL4.70 [hRluc] into H460 cells. These were exposed to six asthma-relevant cytokines at concentrations (Table 1) based on literature-reported data obtained from bronchoalveolar lavage fluid collected from airways of asthmatic patients suffering acute exacerbations.

Dual-luciferase reporter assays were carried out to study promoter activity under cytokine-exposed and cytokine-free environments. Biological triplicates of each experiment were carried out. Transcription factor promoter mapping was subsequently carried out on the two promoter sequences.

Key Results: The region spanning 1,288 base pairs of promoter A, upstream of transcription start site 1 (TSS1) was the most active, in a basal, as well as in a cytokine-stimulated environment. The most active segment of CCR4 promoter B spanned a region of 1,511 base pairs upstream of TSS2. The activity of both regions was enhanced under the influence of IL-9 and TNF-α (*P* < .05, *n* = 3). Additionally, IL-1β stimulated the most active region of promoter B (*P* < .05, *n* = 3). Transcription factor mapping at a stringency level of 0.85 identified motifs for activator protein 1 (AP-1), CAAT/enhancer-binding protein β (C/EPB), and nuclear factor 1 (NF-1), within the regions of both CCR4 promoters.

Conclusion and Implications: Both promoters are functional transcriptional regulators of the CCR4 gene, and their activity is significantly increased by specific cytokines, at concentrations present in the airways of patients with asthma. This potentially augments the airway inflammatory response. The identification of multiple AP-1 binding sites within both promoters suggests that CCR4 transcriptional expression may be negatively regulated by glucocorticoids.

P006 | Inhibition of cyclic nucleotide accumulation induced by pyridopyrimidine derivatives: Analysis of MD simulations for peptide STa, enzyme PDE5, and sGC

Ivan Pires de Oliveira; Gilberto De Nucci

University of São Paulo

Background and Purpose: Some pyridopyrimidine derivatives (PPDs) have been recently suggested to be potential drugs for the treatment of secretory diarrhoea (Kots et al., 2008). This proposition is due to their ability to inhibit cyclic nucleotide accumulation. The mechanisms causing the decreasing levels of the second messengers (cGMP and cAMP), induced by the mentioned compounds, are not fully understood, and some pharmacological targets have been used to explain the experimental findings (Tanifum et al., 2009; Zaminelli et al., 2019).

Looking for molecular interactions that may justify the pharmacological behaviour of PPDs, this study applied molecular dynamic (MD) simulations to discuss the following three important protein targets directly associated with cGMP synthesis/degradation: (a) heat-stable enterotoxin a (STa), (b) PDE type 5 (PDE5), and (c) soluble guanylate cyclase (sGC).

Experimental Approach: MD simulations were performed from the crystal structure of the peptide from *Escherichia coli* (codeID:1ETN), PDE5 (codeID:1XOZ), and sGC, $\alpha\beta$ -domain (codeID:4NI2), all obtained from the Protein Data Bank. Trajectories were performed with NAMD

software, with isothermal-isobaric ensemble, 310.15 K, and 1 atm, and density closes to $\sim 1 \text{ g}\cdot\text{ml}^{-1}$. Analyses were performed using MDAnalysis and VMD tools. The CHARMM36 force field was used for all the molecules applying the TIP3 model for water. The compounds adopted here were chosen according to the experimental results published by our research group and/or by other researchers, which pointed out the following molecules as potential commercial drugs: BPIPP-(5-(3-bromophenyl)-1,3-dimethyl-5,11-dihydro-1H-indeno-[20:10:5,6]pyrido[2,3-d]pyrimidine-2,3,6-trione) (Kots et al., 2008); CMP23-(5-(3-fluoro,5-trifluoromethylphenyl)-1,3-dimethyl-

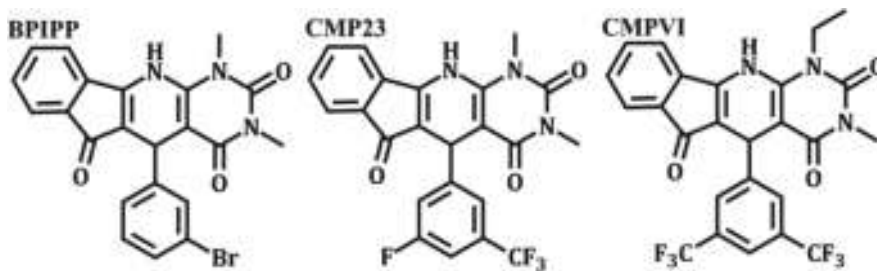


FIGURE 1 Pyridopyrimidine derivatives (PPDs)

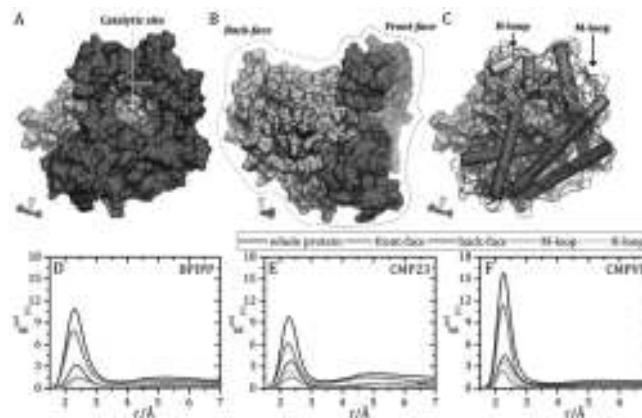


FIGURE 2 PPD compounds deposited in each part of the PDE5 enzyme

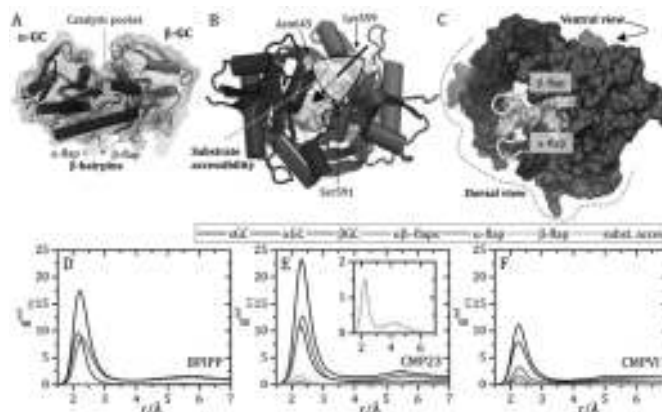


FIGURE 3 Quantitative distribution of PPDs around some domains of the sGC enzyme

5,11-dihydro-1*H*-indeno-[2',1':5,6]pyrido[2,3-*d*]pyrimidine-2,3,6-trione (Tanifum et al., 2009), and CMPVI-(5-(3,5-bistrifluoromethylphenyl)-1-ethyl-3-methyl-5,11-dihydro-1*H*-indeno-[2',1':5,6]pyrido[2,3-*d*]pyrimidine-2,4,6-trione) (Zaminelli et al., 2019) (Figure 1). Quantitative analyses were performed by minimum-distance distribution functions ($g_{(r)}^{\text{md}}$ or MDDF) (Martínez et al., 2017), an adequate tool for non-spherical solute and/or solvent interaction, where $g_{(r)}^{\text{md}} = 1.0$ showed a concentration of PPDs at r similar to the solution bulk. $g_{(r)}^{\text{md}} > 1.0$ indicated accumulation, and $g_{(r)}^{\text{md}} < 1.0$ showed exclusion of the PPD from the protein neighbourhood at distance r .

Key Results: The evaluated compounds were found to be highly accumulated on the STa surface, caused by the pyridopyrimidine group, which has more significant contributions to PPDs-STa interactions than the indenone moiety. Hydrogen bonds were observed with the backbone and/or side chain of the following STa residues: proline, cysteine, alanine, leucine, and asparagine. The $g_{(r)}^{\text{md}}$ curves calculated for PDE5 clearly provided a response pattern for PPDs accumulation, resulting in the following suggestions: (a) all compounds are found to be accumulated close to the enzyme; (b) CMPVI is more accumulated than BPIPP and CMP23 on the protein surface; (c) accumulation is mainly due to front-face contributions; and (d) there are similar concentrations closest to the H loop and M loop (Figure 2). The deposition of compounds closest to the H-M loops is indicative of the favouring of the “open” state of the catalytic groove due to the change on the free-energies gap between opened and closed states, as shown previously for two α -helix in proteins (Pires de Oliveira et al., 2017). Moreover, the affinities between sGC and PPDs may disturb the entrance of the GTP substrate, avoiding cGMP synthesis. This was evaluated for sGC ($\alpha\beta$ -GC portion) and is shown in Figure 3. All PPDs were found to be close to whole protein, with similarities in the accumulations on the α -GC and β -GC domains, except for CMPVI, where it was most concentrated on the α -subunit. Interactions were observed between CMP23 and residues allocated on the entrance gate of the catalytic site, promoting a steric effect that displaces the GTP, avoiding cGMP synthesis.

Conclusion and Implications: From the MD simulations coupled with $g_{(r)}^{\text{md}}$ functions, we quantitatively showed the accumulation of PPDs closest to important protein targets and their structural domains. All compounds were attracted to the STa surface due to the high contribution of the pyridopyrimidine groups. The H loop and M loop are structures from PDE5 that are related to the opening of the catalytic site, and they were surrounded by PPDs, inferring stabilisation of the “active” state. The compound CMP23 was docked in the entrance of the catalytic pocket of sGC, possibly avoiding substrate accessibility. A recent pharmacological approach of these compounds for diarrhoea treatment seems complex at the molecular level, and their accumulation around STa, PDE5, and sGC can help us to understand their biological behaviour.

ACKNOWLEDGEMENT

This study was supported by FAPESP (Process No. 2017/02201-4).

REFERENCES

- Kots, A. Y., et al. (2008). Pyridopyrimidine derivatives as inhibitors of cyclic nucleotide synthesis: Application for treatment of diarrhea. *Proceedings of the National Academy of Sciences of the United States of America*, 105, 8440–8445.
- Martínez, L., et al. (2017). Molecular Interpretation of preferential interactions in protein solvation: A solvent-shell perspective by means of minimum-distance distribution functions. *Journal of Chemical Theory and Computation*, 13, 6358–6372.
- Pires de Oliveira, et al. (2017). Molecular mechanism of activation of *Burkholderia cepacia* lipase at aqueous-organic interfaces. *Physical Chemistry Chemical Physics*, 19, 31499–31507.
- Tanifum, E. A., et al. (2009). Novel pyridopyrimidine derivatives as inhibitors of stable toxin a (STa) induced cGMP synthesis. *Bioorganic & Medicinal Chemistry Letters*, 19, 3067–3071.
- Zaminelli, T., et al. (2019). Synthesis and pharmacological screening of pyridopyrimidines as effective anti-diarrheal agents through the suppression of cyclic nucleotide accumulation. *ChemistryOpen*, 8, 464–475.

P008 | Development and application of a kinetic ligand binding assay for the cannabinoid receptor 1 using resonance energy transfer approaches

Bradley Hoare¹; David Sykes²; Thais Gazzi³; Marc Nazare³; Uwe Grether⁴; Dmitry Veprintsev²

¹University of Nottingham; ²Centre of Membrane Proteins and Receptors (COMPARE), University of Birmingham and University of Nottingham, Midlands and School of Life Sciences, University of Nottingham, Nottingham, United Kingdom; ³Leibniz-Institut für Molekulare Pharmakologie; ⁴Roche Pharma Research & Early Development

Background and Purpose: Robust assays for quantifying ligand binding kinetics at GPCRs are important for novel drug discovery. Resonance energy transfer (RET) methodologies have recently been employed widely (Sykes et al., 2019), often where the extracellular N-terminus of recombinantly expressed GPCR is fused to a RET donor (e.g., terbium cryptate-labelled SNAP tag) in conjunction with a RET acceptor (i.e., fluorescent tracer ligand). The proximity between receptor-fused donor and receptor bound acceptor is usually sufficient to satisfy the distance dependence of RET (usually occurring within <10 nm) to provide a specific binding signal in a homogenous assay set-up; however, this is not always the case. The cannabinoid

TABLE 1 Kinetic rate constants and K_D of three fluorescent cannabinoid compounds at CB₁₍₉₁₋₄₇₂₎ obtained by RET measurements

Compound	k_{on} (M ⁻¹ .min ⁻¹)	k_{off} (min ⁻¹)	Kinetic K_D (k_{off}/k_{on} ; nM)	Equilibrium K_D (nM)	Max RET signal
RO7288472	$7.29 \pm 0.90 \times 10^5$	0.70 ± 0.03	987 ± 115	$1,012 \pm 65$	14,289
RO7304841	$6.23 \pm 0.48 \times 10^5$	0.44 ± 0.05	706 ± 29	712 ± 57	21,320
RO7234691	$5.91 \pm 0.64 \times 10^5$	0.45 ± 0.06	755 ± 17	558 ± 6	1,802

Note. Data are from at least three experimental replicates and represent mean \pm SEM.

receptor 1 (CB₁) is a therapeutically relevant drug target (Mackie et al., 2006) that contains an unusually long extracellular domain (~116 residues), precluding the potential of RET. To develop a RET-based kinetic binding assay for the cannabinoid receptor 1 (CB₁), we truncated its N-terminal domain and characterized the binding kinetics of several experimental fluorescent cannabinoid ligand tracers.

Experimental Approach: All receptor constructs were transfected and expressed in HEK293 cells. SNAP-fused CB₁ in pcDNA4/TO was truncated by 90 residues to produce SNAP-CB₁₍₉₁₋₄₇₂₎, and both receptor constructs were also cloned with a C-terminally fused NanoLuc luciferase. Appropriate effector coupling of CB₁₍₉₁₋₄₇₂₎ compared to full-length CB₁ was assessed by co-expression of NanoLuc-fused receptor with Venus-tagged minimized G α_i (miniG_i), where cells were incubated in white 96-well plates for 1 hr at 37°C with varying concentrations of HU210 or anandamide before measurement. Kinetic binding assays were performed at room temperature in white 384-well plates using membrane preparations from a stable-expressing terbium-labelled SNAP-CB₁₍₉₁₋₄₇₂₎ HEK293 cell line. Fluorescent cannabinoid compounds were provided by Roche Pharmaceuticals.

Key Results: Truncation of CB₁ N-terminal domain did not affect the coupling of miniG_i when stimulated with agonists HU210 (pEC₅₀ = 9.1 ± 0.1 and 9.3 ± 0.1 for CB₁ and CB₁₍₉₁₋₄₇₂₎, respectively; $n = 3$) or anandamide (pEC₅₀ = 6.5 ± 0.1 and 6.3 ± 0.2 for CB₁ and CB₁₍₉₁₋₄₇₂₎, respectively; $n = 3$), suggesting that this domain is not involved in ligand binding. Data from kinetic association assays using three different fluorescent cannabinoid compounds fit well to a one-site binding model providing rate constant and affinity estimates (Table 1).

Conclusion and Implications: A RET-based kinetic ligand binding assay was successfully established for CB₁ by truncating the N-terminal domain, enabling sufficient proximity between RET donor and acceptor. This assay can be used in future for determining kinetic constants for unlabelled cannabinoids, as well as for compound screening efforts in novel drug discovery platforms.

REFERENCES

- Mackie, K. (2006). Cannabinoid receptors as therapeutic targets. *Annual Review of Pharmacology and Toxicology*, 46, 101–122.
- Sykes, D. A., et al. (2019). Binding kinetics of ligands acting at GPCRs. *Molecular and Cellular Endocrinology*.

P011 | GPR84 antagonists display marked species orthologue selectivity

Sarah Mancini¹; Juan Carlos Mobarec²; Matt Barnes²; Andrew Tobin¹; Graeme Milligan¹

¹University of Glasgow; ²Sosei Heptares

Background and Purpose: The orphan GPCR GPR84 is reported to be a pro-inflammatory receptor expressed on immune cells and adipocytes; thus, there is considerable interest in targeting GPR84 in a range of conditions. Understanding the function of this orphan receptor has proved challenging due to the lack of potent and selective ligands. GPR84 sequence is highly conserved between human and mouse (85%); however, other related orphan receptors have displayed profound species selectivity with regard to ligand binding (Jenkins et al., 2017). The aim of this study was to assess whether GPR84 ligands display species selectivity and therefore their usefulness in probing GPR84 function in non-human cells and tissues.

Experimental Approach: GPR84 antagonists 837 (UofG unpublished, orthosteric) and 104 ((9-(5-cyclopropyl-[1,2,4]oxadiazol-3-ylmethoxy)-2-((R)-1-[1,4]dioxan-2-ylmethoxy)-6,7-dihydro-pyrimido[6,1-a]isoquinolin-4-one (Mahmud et al., 2017), allosteric) were screened against an EC₈₀ concentration of the orthosteric agonist 2-HTP (2-(hexylthiol) pyridimine-4,6-diol) (Liu et al., 2016). Membranes were prepared from Flp-In™ T-REx 293™ cells stably expressing either the human or mouse doxycycline-inducible GPR84-G₁₂ fusion protein and utilised in a [³⁵S]GTPγS incorporation assay to assess receptor activation. Assays were carried out in duplicate, with four biological replicates per experiment. Site-directed mutagenesis was performed to “humanise” extracellular loops (ECL) 2 and 3 of mouse GPR84 to identify residues involved in antagonist binding.

Key Results: 2-HTP displayed equipotent agonist activity at the human and mouse orthologues of GPR84 (pEC₅₀ = 7.59 ± 0.07 and 7.50 ± 0.12 , respectively). In contrast, 104 antagonised 2-HTP-stimulated mouse GPR84 activation with reduced potency (pIC₅₀ = 6.06 ± 0.09) was compared with effects at the human receptor (pIC₅₀ = 7.53 ± 0.09). By contrast, 837 was completely inactive at mouse GPR84 (pIC₅₀ at human GPR84 = 8.18 ± 0.04). Systematically mutating residues in ECL2 and ECL3 of mGPR84 to their human equivalent had no effect on antagonist activity at the mouse receptor, suggesting the key residue(s) that determine species selectivity may lie in the transmembrane region and impact receptor confirmation.

Conclusion and Implications: Despite human and mouse orthologues of GPR84 having a high degree of overall sequence homology, there is marked species selectivity of antagonist, but not agonist, ligands at this receptor. This highlights the challenges associated with selecting ligands for poorly characterised receptors in order to probe their biology and therapeutic potential.

REFERENCES

- Jenkins, L., Harries, N., Lappin, J. E., MacKenzie, A. E., Neetoo-Isseljee, Z., Southern, C., ... Milligan, G. (2017). Antagonists of GPR35 display high species ortholog selectivity and varying modes of action. *JPET*, *343*, 683–695.
- Liu, Y., Zhang, Q., Chen, L. H., Yang, H., Lu, W., Xie, X., & Nan, F. J. (2016). Design and synthesis of 2-alkylpyrimidine-4,6-diol and 6-alkylpyridine-2,4-diol as potent GPR84 agonists. *ACS Medicinal Chemistry Letters*, *7*, 579–583.
- Mahmud, Z. A., Jenkins, L., Ulven, T., Labéguère, F., Gosmini, R., De Vos, S., ... Milligan, G. (2017). Three classes of ligands each bind to distinct sites on the orphan G protein-coupled receptor GPR84. *Scientific Reports*, *7*, 17953.

P012 | Hydroxycarboxylic acid receptor 2 signalling at endosomal compartments

Shannon O'Brien; Emma Tripp; Davide Calebiro

University of Birmingham

Background and Purpose: Hydroxycarboxylic acid receptor 2 (HCA2) is highly expressed in adipose tissue, where it has been shown to maintain metabolic homeostasis under changing metabolic and dietary conditions. Key intermediates of energy metabolism are shown to directly activate HCA2 and exert antilipolytic effects. The classical view that GPCR signalling occurs exclusively at the cellular membrane has been challenged by the discovery that GPCRs can signal via G proteins at intracellular sites (Calebiro et al., 2009; Godbole, Lyga, Lohse, & Calebiro, 2017). Previous studies suggest that subcellular confinement of signalling events downstream of GPCR activation—for example, cAMP production and PKA activation—influences adipocyte development and lipolysis (Rogne & Tasken, 2014). However, it is unknown whether HCA2 signals at intracellular sites and whether this accounts for specific biological effects. Here, we use highly inclined and laminated optical sheet (HILO) microscopy and BRET to elucidate the relationship between HCA2 internalisation, trafficking, and signalling.

Experimental Approach: To investigate HCA2 signalling at intracellular sites, a BRET-based assay was used to quantitatively monitor, in living cells and in real time, the recruitment of G proteins to subcellular compartments. HEK293T cells were transiently transfected with HCA2, $G\alpha_i$ protein probes tagged with NanoLuc luciferase, and intracellular markers of interest tagged with YFP or GFP. To visualise HCA2 and $G\alpha_i$ trafficking, HEK293T cells were transiently transfected with YFP-tagged HCA2 or $G\alpha_i$ and visualised using HILO microscopy.

Key Results: Our results indicate that, in HEK293T cells, HCA2 is predominantly coupled to $G\alpha_i$ and efficiently internalises to early endosomes upon stimulation with the full agonist nicotinic acid (NA). Additionally, we find that, following stimulation with NA, HCA2 recruits mini $G\alpha_i$ protein probes to membranes of early endosomes and possibly other endosomal compartments, indicating that HCA2 remains active following internalisation. Interestingly, a cell-impermeable HCA2 agonist (monomethyl fumarate) was also found to mediate $G\alpha_i$ signalling following receptor internalisation, albeit to a lesser extent (approximately 30% of the response to NA). This suggests that an intracellular pool of HCA2 may contribute to the response to NA.

Conclusion and Implications: Our results provide evidence that HCA2 is active at endosomal compartments and that an intracellular pool of HCA2 likely contributes to the overall response induced by NA. Further experiments include investigating the functional consequences of HCA2 endosomal signalling downstream of G-protein activation and its implications in adipocyte metabolism. A better knowledge of the mechanisms implicated in the regulation of adipocyte metabolism will be crucial to develop innovative therapeutic strategies for metabolic diseases.

REFERENCES

- Calebiro, D., Nikolaev, V. O., Gagliani, M. C., De Filippis, T., Dees, C., Tacchetti, C., ... Lohse, M. J. (2009). Persistent cAMP-signals triggered by internalized G-protein-coupled receptors. *PLoS Biology*, *7*(8), e1000172.
- Godbole, A., Lyga, S., Lohse, M. J., & Calebiro, D. (2017). Internalized TSH receptors en route to the TGN induce local G_s -protein signaling and gene transcription. *Nature Communications*, *8*(1), 443.
- Rogne, M., & Tasken, K. (2014). Compartmentalization of cAMP signaling in adipogenesis, lipogenesis, and lipolysis. *Hormone and Metabolic Research*, *46*(12), 833–840.

P014 | Oligomeric structure of the CXCR4 chemokine receptor determined by fluorescence fluctuation analysis

Richard Ward; John Pediani; Graeme Milligan

University of Glasgow

Background and Purpose: CXCR4 is a GPCR of the class A (rhodopsin-like) group and plays key roles in cancer metastasis and HIV infection. Various reports, including a number of X-ray crystallographic structures (Wu et al, 2010), have suggested that CXCR4 is a constitutive dimer. Herein, we investigate the oligomeric structure of CXCR4, with particular emphasis on the effects of ligand binding.

Experimental Approach: We use fluorescence fluctuation analysis-based techniques, particularly Spatial Intensity Distribution Analysis (SpIDA) to investigate receptor oligomerisation. Confocal microscopy images of cells expressing the receptor fused to monomeric eGFP (mEGFP) are collected. Regions of interest (ROIs) are then analysed using software that can determine values for the quantal brightness of

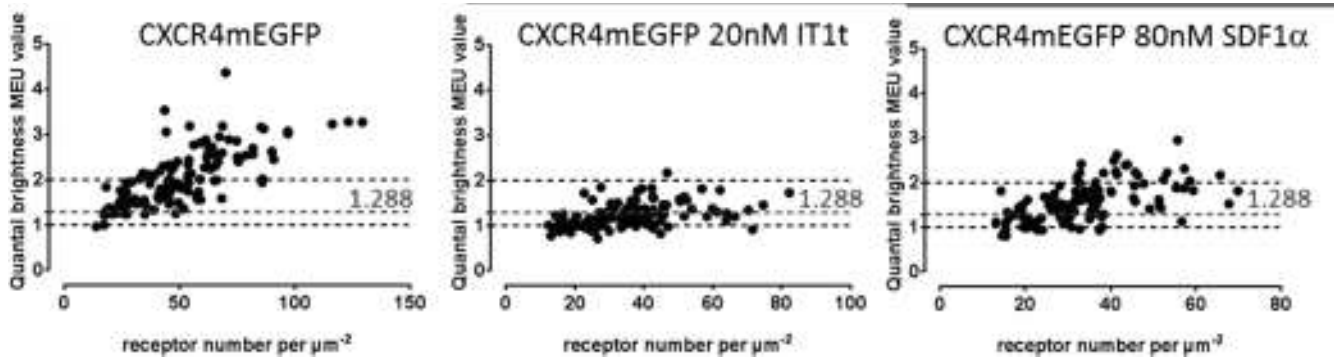


FIGURE 1 Spatial intensity distribution analysis of a cell line expressing CXCR4mEGFP. Left-hand panel shows the untreated quaternary structure of the receptor plotted as receptor number- μm^{-2} against quantal brightness. The MEU value refers to monomeric equivalent unit and is derived from the quantal brightness of the same fluorophore in a known monomeric system. The value of 1.288 as the border between monomer and dimer is similarly based upon the sum of the mean MEU value for the monomeric fluorophore and $1.5\times$ the SD. The centre panel shows the effect of treating the cell line with 20-nM IT1t (an antagonist), which results in a largely monomeric quaternary structure for CXCR4. The right-hand panel shows the effect of treatment with SDF1 α (an agonist), which reduces the oligomeric complexity of CXCR4, but to a lesser degree than IT1t

the fluorophore, which is then compared to those of mEGFP linked to a known monomeric system and consequently the oligomeric structure can be determined. This is supported by the use of Blue Native PAGE gels in which the quaternary structure of protein complexes is preserved.

Key Results: Initial SpIDA results suggest that the CXCR4 receptor is indeed largely dimeric (8.3% monomeric:91.7% dimeric/oligomeric, $n = 120$ ROIs; Figure 1), and it appears that it may be driven to more complex oligomerisation states by increasing expression, particularly when cells are treated with sodium butyrate, which is known to increase the expression level of some receptors (Ward et al, 2017). Treatment with the CXCR4 antagonist IT1t changes the oligomeric structure to one largely composed of monomers (67.5% monomeric:32.5% dimeric/oligomeric, $n = 120$ ROIs; Figure 1), whereas treatment with the agonist SDF-1 α (CXCL12) also reduces the oligomeric complexity, but to a lesser degree (21.7% monomeric:72.3% dimeric/oligomeric, $n = 120$ ROIs; Figure 1). Resolution via Blue Native PAGE produced similar outcomes. Analysis of a CXCR4 mutant that abolishes signalling (N119K) was also seen to result in a largely monomeric state (25%:75%, respectively, $n = 56$ ROIs).

Conclusion and Implications: We have confirmed the dimeric/oligomeric nature of the CXCR4 receptor and shown that it can be modified by ligand treatment. We intend to expand this analysis to include further mutants and ligands and also to make use of a similar, though more comprehensive technique, fluorescence intensity fluctuation spectroscopy, as described by Stoneman et al. (2019).

REFERENCES

- Stoneman, et al. (2019). *Nature Methods*, 16, 493–496.
Ward, et al. (2017). *Biochemical Journal*, 474, 1879–1895.
Wu, et al. (2010). *Science*, 330, 1066–1071.

P015 | Molecular dynamic simulations of morphine in the active and inactive μ -opioid receptor

Nokomis Ramos-Gonzalez; Katy J. Sutcliffe; Graeme Henderson; Eamonn Kelly; Richard B. Sessions

University of Bristol

Background and Purpose: Molecular dynamic simulations of morphine using the active and inactive crystal structures of the μ -opioid receptor were carried out in order to determine whether the interaction of morphine with the receptor is activity dependent.

Experimental Approach: Morphine was first docked into the active (PDB: 5C1M) (Huang et al., 2015) and inactive (PDB: 4DKL) (Manglik et al., 2012) μ -opioid receptor using the Bristol University Docking Engine (BUDE). The 30 lowest energy poses of morphine in each structure were then assessed to give three chosen poses for each of the active and inactive structures; 125-ns molecular dynamic simulations were then carried out for each of these poses. Of these, one pose was chosen for the active and inactive structures, based on the stability of the receptor in each 125-ns simulation, the stability of the

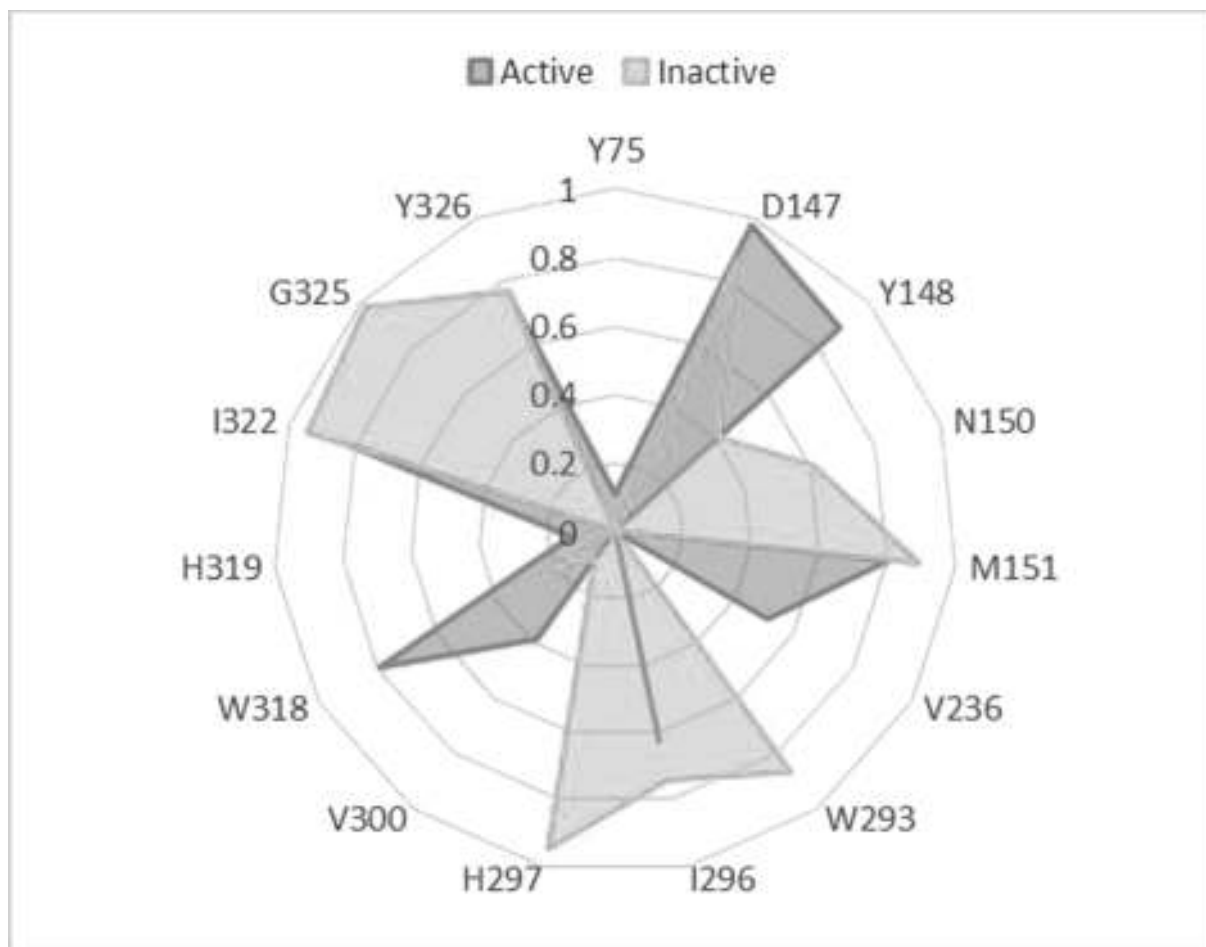


Figure 1. Radar showing residues that reside within 4 Å of morphine during the simulation in the active and inactive μ -opioid receptor; the axis (0–1) indicates the fraction of the total simulation time that morphine is within 4 Å of these residues

ligand itself, and its interaction with the conserved residue aspartate 147 (D147). For the active and inactive structure, seven frames were taken evenly across the initial 125-ns simulation for the chosen pose, and further 125-ns simulations were run from each of these starting points and combined to give 1 μ s of data for each of the active and inactive μ -opioid receptor structures.

Key Results: Morphine simulated in the active μ -opioid receptor structure maintained a tight interaction with D147, whilst in the inactive structure, this interaction was more erratic. In the inactive μ -opioid receptor structure, morphine sat slightly lower in the binding pocket and interacted with the residue tryptophan 293 (W293). Within the binding pocket of the active and inactive μ -opioid receptor structure, morphine interacted with common residues and also with distinct residues in each conformation (Figure 1).

Conclusion and Implications: Molecular dynamic simulations of morphine in the active and inactive μ -opioid receptor structures indicated that morphine interacts with common, as well as distinct residues in the two structures. We are currently undertaking principal component analysis to determine the conformational effects of morphine on the two receptor states.

REFERENCES

- Huang, W., Manglik, A., Venkatakrisnan, A. J., et al. (2015). Structural insights into μ -opioid receptor activation. *Nature*, 524, 315–321.
- Manglik, A., Kruse, A. C., Kobilka, T. S., et al. (2012). Crystal structure of the μ -opioid receptor bound to a morphinan antagonist. *Nature*, 485, 321–326.

P016 | Mathematical models in receptor theory: Dynamics, cooperativity, linearity, and identifiability

Lloyd Bridge

University of the West of England

Background and Purpose: A mathematical understanding of binding and signalling dynamics in pharmacology is needed to characterise and quantify ligand–receptor interactions from the abundant experimental time course data now available and to make predictions through simulation. We extend classical receptor theory (beyond equilibrium analysis of ligands binding monomeric receptors and the operational model of agonism) to simple mathematical models that can

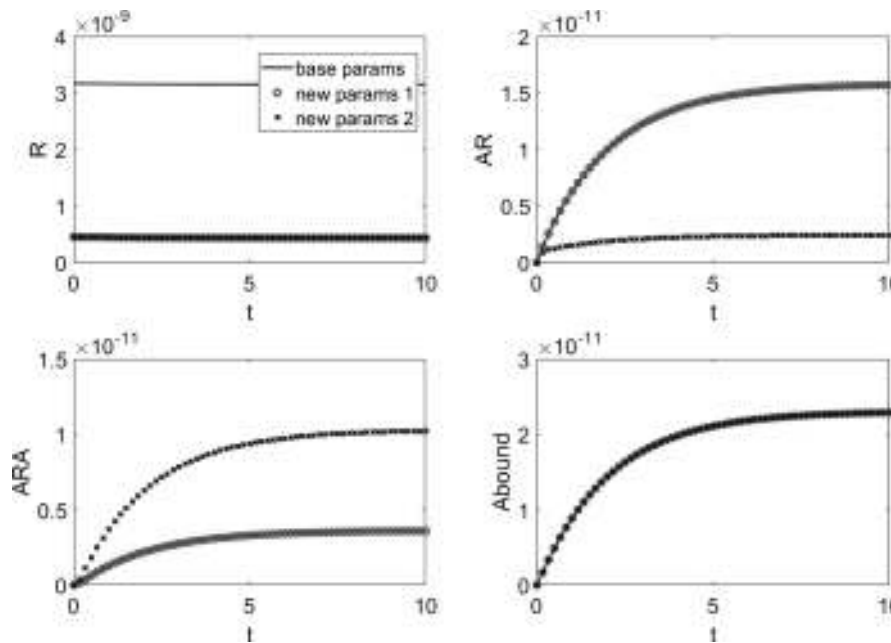


FIGURE 1 Structural non-identifiability for a model of ligand binding dynamics with homo-dimerised receptor. Three different parameter sets give the same observed output (total ligand bound) time course, but via different underlying species concentrations. Parameter fitting results must be treated with caution for such experiments

capture binding and functional dynamics profiles. These models are low-dimensional compared with systems biology studies, offering accessible and potentially powerful models for the non-mathematician. Linearity is a key concept. In particular, low-dimensional linear models yield explicit analytical solutions that are amenable to analysis by hand calculation (Motulsky & Mahan, 1984; White & Bridge, 2018) and simulation (including sensitivity analysis, particularly focussed on cooperativity effects in binding and activation dynamics) in basic data analysis packages.

Structural identifiability analysis (SIA) is crucial in determining which pharmacologically relevant parameters are theoretically estimable from a given data set. SIA may be challenging, even for simple models, and is often overlooked. Here, we outline an SIA approach for linear, drawing on similarly structured pharmacokinetics models, and illustrate the approach applied to receptor theory.

Experimental Approach: We formulate mathematical models for ligand-receptor interactions and functional responses. These models comprise systems of ordinary differential equations. Linear models are solved analytically, while non-linear models are reduced to linear systems, using rapid equilibrium and quasi-steady-state assumptions. SIA is performed on linear models, using the transfer function method. All simulations are performed in MATLAB and parameter fitting in MATLAB and COPASI. Further, we implement new simulations in GraphPad Prism.

Key Results: Analytical expressions have been found for single-ligand and two-ligand competition binding dynamics at monomeric and dimeric receptors and for pathway activation dynamics. These solutions have enabled sensitivity analyses to investigate the effect of pharmacological kinetic parameters on time course features such as decay rates. Further, SIA has determined parameter combinations that

are identifiable from single time course outputs and revealed experimental strategies for identifying all parameters.

Conclusion and Implications: Linear differential equations provide new insights into receptor dynamics through mathematical analysis and simulation. Analytical solutions are especially valuable in assessing identifiability properties of model/experiment combinations and may be used to guide experimental strategy.

REFERENCES

Motulsky, H. J., & Mahan, L. C. (1984 Jan 1). The kinetics of competitive radioligand binding predicted by the law of mass action. *Molecular Pharmacology*, 25(1), 1-9.
 White, C., & Bridge, L. J. (2018 Jan). Ligand binding dynamics for pre-dimerised G protein-coupled receptor homodimers: Linear models and analytical solutions. *Bulletin of Mathematical Biology*, 18, 1-33.

P018 | PARPi-FL, a fluorescent version of the PARP inhibitor olaparib, exhibits decreased potency but similar efficacy compared to olaparib in a cell-based assay

Saheed Benson; Fyaz Ismail; Amos Fatokun

Liverpool John Moores University

Background and Purpose: Fluorescent ligands enable visualisation and quantification of molecular mechanistic events and are thus a powerful pharmacological tool. However, the addition of a fluorophore to a non-fluorescent (parent) ligand to generate its fluorescent derivative could alter the pharmacological properties of the

TABLE 1 EC₅₀ values (mean ± SEM) for olaparib and its fluorescent derivative (PARPi-FL)

	EC ₅₀ (nM)	
	MTT	CTG
Olaparib	45.3 ± 6.6 (n = 4)	38.9 ± 4.2 (n = 3)
Fluorescent olaparib (PARPi-FL)	95.7 ± 9.7 (n = 5)**	123.5 ± 12.6 (n = 6)**
Fold change in EC ₅₀ (decreased potency)	2.1	3.2

**P < .01 versus olaparib for the same assay.

ligand. It is therefore important to characterise a fluorescent ligand to identify any such potential changes. We are interested in using fluorescent ligands to investigate mechanisms of cell death mediated by the nuclear enzyme, PARP. Olaparib is an inhibitor of PARP and is currently used in targeted therapy to treat cancers harbouring mutations in their tumour suppressor genes (e.g., *BRCA1* and *BRCA2* genes), which are very sensitive to PARP inhibition. We, therefore, tested whether or not PARPi-FL, a fluorescent (BODIPY-FL) derivative of olaparib (Thurber, Reiner, Yang, Kohler, & Weissleder, 2014), retains the potency and efficacy of the parent ligand (non-fluorescent olaparib) in a cell-based assay.

Experimental Approach: PARP-dependent cell death (as surrogate for PARP activity) was induced in cultured human cervical adenocarcinoma cells (HeLa) by treatment with the alkylating agent *N*-methyl-*N'*-nitro-*N*-nitrosoguanidine (MNNG) (50 μM, 25 min) (Fatokun, Liu, Dawson & Dawson, 2013). The ability of olaparib and PARPi-FL (each up to 10 μM) to protect against the cell death (as evidence of PARP inhibition) was then assessed, 24-hr post-MNNG treatment, by quantifying cell viability using two different viability reagents—MTT (absorbance based) and CellTiter-Glo (CTG, luminescence based). EC₅₀ values were determined using GraphPad (Version 8.2.0) (log [inhibitor] vs. response-variable slope [four parameters]). Bright-field images of treatment-induced morphological changes were also acquired. Results are reported as means ± SEM for n = 3–6 independent experiments. Statistical analyses were done using, as appropriate, *t* test or one-way ANOVA with Tukey's post hoc test, with *P* < .05 considered statistically significant.

Key Results: Olaparib and PARPi-FL elicited concentration-dependent protection against MNNG-induced reduction in cell viability. The EC₅₀ values for PARPi-FL were significantly higher than for olaparib, with respect to both the MTT assay and the CTG assay (*P* < .01) (Table 1), resulting in PARPi-FL being twice and thrice less potent than olaparib in the MTT and the CTG assays, respectively. However, there were no differences in their efficacies. Viability data were supported by changes to cell morphology revealed in the photomicrographs.

Conclusion and Implications: The fluorescent version of olaparib (PARPi-FL) exhibits decreased potency but similar efficacy compared to the parent olaparib in a cell-based assay, although both potencies were in the nanomolar range. This, to our knowledge, is the first direct comparison of olaparib and PARPi-FL in a functional, cell-based assay

model of parthanatos, as opposed to cell-free systems. Our findings are useful in guiding the use of PARPi-FL in cell-based versus cell-free scenarios.

REFERENCES

- Fatokun, A. A., Liu, J. O., Dawson, V. L., & Dawson, T. M. (2013). *British Journal of Pharmacology*, 169, 1263–1278.
- Thurber, G. M., Reiner, T., Yang, K. S., Kohler, R. H., & Weissleder, R. (2014). Effect of small-molecule modification on single-cell pharmacokinetics of PARP inhibitors. *Molecular Cancer Therapeutics*, 13, 986–995.

P019 | Possible involvement of hydrogen sulfide in the therapeutic effects associated to clodronate therapy

Vincenzo Brancaleone¹; Rosangela Montanaro¹; Alessio D'Addona²; Andrea Izzo²; Carlo Ruosi²; Giuseppe Cirino³

¹Dept. Science, University of Basilicata; ²Orthopaedic Unit, Public Health Dept, University of Naples Federico II; ³Dept. Pharmacy, University of Naples Federico II

Background and Purpose: Hydrogen sulfide (H₂S) is a gaseous mediator involved in many pathophysiological events, including vascular relaxation and inflammation (Cirino, Vellecco, & Bucci, 2017; Kanagy, Szabo, & Papapetropoulos, 2017). In particular, H₂S has been shown to have anti-inflammatory effects as it reduces paw oedema and blocks leukocyte infiltration in different pharmacological models (Zanardo et al., 2006). In addition, it also displays proresolutive properties by triggering activation of AnxA1 pathway (Brancaleone, Miti-dieri, Flower, Cirino, & Perretti, 2014). Inflammation represents a crucial core for several diseases, in particular for patients suffering osteoarticular alterations. Such alterations are, sometimes, very common in arthritis or other bone disease like Paget's syndrome. In the latter case, bisphosphonates are used as therapeutical agents, although this is not the unique case (Fleish, 1991; Rodan & Balena, 1993). Indeed, bisphosphonates are mostly used in osteoporosis as they prevent the loss of bone density, and this class is divided into two subclasses, that is, nitrogen-containing BP (NBP) and nitrogen free (BP). Clodronate represent a typical BP that is till used in therapy. Based on some reports highlighting differences in side effects between NBP and BP (Itoh, Aoyagi, Kusama, Kojima, & Kogo, 2004) and on some cases where BP like clodronate suppressed inflammation, we decided to investigate whether clodronate could supply additional beneficial effects, besides the classical anti-osteoclast activity, and if these effects were somehow related to H₂S.

Experimental Approach: In order to pursue our aim, we used fibroblast-like synoviocyte (FLS) cell line (K4IM) cultured in Iscove's medium supplemented with 10% FBS, and we induced inflammation by administration of TNF-α (10 ng·ml⁻¹, 6 hr). The effect of clodronate (0.1–10 μM) on these cells was addressed by using Western blot analysis to determine expression of iNOS, COX-2, and

CSE. Relative expression (OD) was obtained against expression tubulin used as housekeeping gene. Measurement of H₂S levels was also performed by using fluorometric assay and SF7AM as a specific H₂S probe. H₂S biosynthesis was expressed as nmol of H₂S × mg⁻¹·min⁻¹. In addition, a semi-quantitative determination of multiple cytokines was carried out by using multicytokine panel array. Statistical significance was determined by using ANOVA followed by a Dunnett's post hoc test on raw data. Statistical significance was reached for values of $P < .05$.

Key Results: The first set of data showed that FLS treated with TNF- α had increased expression of COX-2 and iNOS as indication of an active inflammatory process. The administration of clodronate (Clo) together with TNF- α in a range of 0.1–10 μ M did not have any effect on COX-2 increase, while a reduction of iNOS expression was observed (80% of decrease, $P < .05$). In the same experiments, we also measured levels of H₂S and CSE expression. Thus, TNF- α administration induced a slight reduction of CSE enzyme and a significant suppression of H₂S biosynthesis (30% of suppression, $P < .05$). Interestingly, administration of clodronate at 10 μ M brought H₂S levels back to those observed in the non-inflamed cells (1.8 for TNF- α to 2.3 for Clo, $P < .05$). In addition, expression of CSE was also restored when clodronate was given 1 hr before addition of TNF- α , rather than the same time ($P < .05$), and these data were paralleled by H₂S levels. Administration of clodronate, 24 hr before administration of TNF- α , did not show any significant effect on CSE expression. In order to further investigate on possible anti-inflammatory activity exerted by clodronate, we also measured some relevant interleukin/chemokine levels by using a semi-quantitative array. Levels of proinflammatory cytokine IL-1 α were enhanced by TNF- α administration (100% increase, $P < .05$), and this effect was counteracted by clodronate (20% reduction, $P < .05$). In addition, anti-inflammatory cytokine IL-10 levels were down-regulated by TNF- α (30% reduction, $P < .05$), while clodronate was able to bring them back to physiological amount ($P < .05$).

Conclusion and Implications: Our data, altogether, suggest a possible anti-inflammatory effect driven by clodronate and that this action involves somehow H₂S biosynthesis and, in turn, its levels. These findings could highlight novel perspectives for therapeutic use of clodronate in bone diseases, since its possible anti-inflammatory action could allow a single drug treatment rather than associations, thus preserving patients from undesirable effects.

REFERENCES

- Brancaleone, V., Mitidieri, E., Flower, R. J., Cirino, G., & Perretti, M. (2014). Annexin A1 mediates hydrogen sulfide properties in the control of inflammation. *The Journal of Pharmacology and Experimental Therapeutics*, 351(1), 96–104.
- Cirino, G., Vellecco, V., & Bucci, M. (2017). Nitric oxide and hydrogen sulfide: The gasotransmitter paradigm of the vascular system. *British Journal of Pharmacology*, 174(22), 4021–4031.
- Fleish, H. (1991). Bisphosphonates: Pharmacology and use in the treatment of tumor-induced hypercalcaemic and metastatic bone disease. *Drugs*, 42, 919–944.
- Itoh, F., Aoyagi, S., Kusama, H., Kojima, M., & Kogo, H. (2004). Effects of clodronate and alendronate on local and systemic changes in bone metabolism in rats with adjuvant arthritis. *Inflammation*, 28(1), February.
- Kanagy, N. L., Szabo, C., & Papapetropoulos, A. (2017). Vascularbiology of hydrogen sulfide. *American Journal of Physiology. Cell Physiology* May 1, 312(5), C537–C549.
- Rodan, G. A., & Balena, R. (1993). Bisphosphonates in the treatment of metabolic bone disease. *Annals of Medicine*, 25, 373–337.
- Zanardo, R. C., Brancaleone, V., Distrutti, E., Fiorucci, S., Cirino, G., & Wallace, J. L. (2006). Hydrogen sulfide is an endogenous modulator of leukocyte-mediated inflammation. *FASEB J*, 20(12), 2118–2120.

P020 | Efficacy of progestin as a local therapy for endometriosis

Debbie Fischer¹; Sara Santorelli¹; Mohamed Elsaywy¹; Aline Miller²; Kay Marshall¹

¹University of Manchester; ²Manchester BIOGEL/University of Manchester

Background and Purpose: Oral progestin-only pills are recommended as the first-line hormonal treatment for symptoms of endometriosis (Andres et al., 2019). By inhibiting ovulation, progestins suppress the growth of endometrial-like cells within the pelvic cavity, reducing chronic inflammation and pain (Angioni et al., 2019). One major concern is suitability for women wishing to conceive. To alleviate systemic side effects, the efficacy of a peptide hydrogel (HG) system for local delivery of etonogestrel (ENG, a third-generation progestin) was assessed using in vitro and in vivo models of endometriosis (Wilkosz et al., 2011).

Experimental Approach: Uterine fragments from female C57/6J mice in proestrus were sutured onto the parietal peritoneum of recipient mice ($n = 24$). Mice were treated with either daily subcutaneous injection of vehicle or ENG (0.08 mg·kg⁻¹) or during surgery 100- μ l vehicle-HG (DMSO) or ENG-HG (17.6 μ g·ml⁻¹) (Manchester BIOGEL), which was applied adjacent to implant (lesion) sites. Vehicle and ENG were prepared in 5% (v/v) ethanol/95% (v/v) sesame oil. Vaginal lavage was performed to monitor oestrous cycle changes. After 20 days, lesions were weighed and examined by histology and qRT-PCR. Effects on cell viability were also assessed using primary mouse endometrial cells. All experiments were conducted in accordance with Home Office regulations. Data were analysed using Kruskal-Wallis with Dunn's test or two-way ANOVA with Bonferroni's post hoc test.

Key Results: Treatments were well tolerated by the mice. Only systemic delivery of ENG temporarily disrupted the oestrous cycle and caused uterine hyperaemia. In vehicle groups, lesions developed into fluid-filled cysts infiltrated by leukocytes ($n = 36$). Half did not form cysts when treated with ENG and ENG-HG ($P < .01$). ENG treatments increased lesion PPAR γ expression by 1.8-fold and 6-fold, respectively ($n = 6$ /group; $P < .001$), and both reduced COX-2 mRNA compared to vehicle ($P < .05$). Nuclear factor (NF- κ B) and steroid receptor transcripts did not change. High ENG concentrations caused a decline in

endometrial cell viability ($n = 4$; pEC_{50} : 4.9 ± 0.05 M), whereas vehicles and ENG-HG showed no cytotoxic effect.

Conclusion and Implications: ENG attenuated lesion formation in our mouse model of endometriosis regardless of delivery route. Local ENG-HG application avoided systemic ENG effects on ovarian activity and demonstrated good biocompatibility. ENG potentiated PPAR γ expression in lesions, which can decrease inflammation and COX-2 signalling and induce endometrial cell atrophy (Lebovic et al., 2013). The use of this drug delivery system could represent an attractive novel strategy for endometriosis treatment.

REFERENCES

- Andres, et al. (2019). *Einstein*, 17(2), 1–6.
 Angioni, et al. (2019). *Gynecological Endocrinology*, 16, 1–3.
 Lebovic, et al. (2013). *Endocrinology*, 154(12), 4803–4813.
 Wilkosz, et al. (2011). *Gynecologic and Obstetric Investigation*, 72(2), 90–97.

P021 | Novel histamine-binding protein rEV131 attenuates itch in mice: Comparison of local and systemic effect

Ibrahim Alrashdi¹; Paul Chazot²; Miles Nunn³;
 Wynne Weston-Davies³; Ilona Obara⁴

¹Newcastle University; ²Department of Bioscience, Durham University;

³Akari Therapeutics, London; ⁴Newcastle University Institute of Neuroscience

Background and Purpose: Itch (pruritus), affecting 4% of the population, can be defined as an unpleasant sensation that triggers a desire to scratch. Whilst histamine remains as the best known endogenous agent and serves as a classical experimental inducer of itch, many itch sufferers are resistant to standard anti-histamine treatment. Recent development of novel ligands targeting the histamine system has provided interesting tools for further investigation of the role of histamine in itch. This study explored the anti-pruritic efficacy of rEV131 in mice. rEV131 is a novel centrally sparing and high-affinity ($K_D = 2$ nM) recombinant histamine binding protein that naturally occurs in tick saliva to block the host's immunological response at the tick-feeding site.

Experimental Approach: Adult male C57BL/6J mice ($n \geq 6$) itch was induced by intradermal injection of pruritogens: histamine-dependent compound 48/80 (100 μ g) and histamine-independent chloroquine (chloroquine diphosphate salt, 200 μ g). rEV131 (0.3–20 $mg \cdot kg^{-1}$, s.c., and 1–40 $mg \cdot kg^{-1}$, i.p.) was injected 30 min before pruritogens to determine local and systemic effects of rEV131 on itch. Control mice were treated with saline. Behavioural responses after rEV131 and/or pruritogens were recorded for 40 min and analysed at 5-min intervals. All procedures were carried out in accordance with the Animals (Scientific Procedures) Act 1986 and ASPA Amendment Regulation 2012.

Key Results: Bouts of scratching induced by the histamine-dependent pruritogenic compound 48/80 were significantly reduced by local (s.c., directly into the site of itch) pretreatment with rEV131 (number of scratches—0.3 $mg \cdot kg^{-1}$: 237.7 ± 38.8 [SEM], 1 $mg \cdot kg^{-1}$: 207.7 ± 23.4 [SEM], 3 $mg \cdot kg^{-1}$: 175.2 ± 42.9 [SEM], 10 $mg \cdot kg^{-1}$: 168.5 ± 14.3 [SEM], and saline: 377.6 ± 25.9 [SEM]; $F(5, 33) = 7.8$, $P < .0001$). Histamine-dependent itch was also reduced by systemic (i.p.) pretreatment with rEV131; however, the anti-pruritic effect had shorter duration of action (20 min) (number of scratches—20 $mg \cdot kg^{-1}$: 118 ± 12.05 [SEM], 40 $mg \cdot kg^{-1}$: 114 ± 9.07 [SEM], and saline: 185.9 ± 9.73 [SEM]; $F(5, 41) = 3.495$, $P = .01$). Behavioural observations after systemic pretreatment with rEV131 showed that the response to non-histaminergic stimuli was not modified (number of scratches—20 $mg \cdot kg^{-1}$: 405.8 ± 54.6 [SEM], 40 $mg \cdot kg^{-1}$: 449.0 ± 58.7 [SEM], and saline: 461.6 ± 31.04 [SEM]; $F(5, 48) = 0.6274$, $P > .999$). Potential involvement of histamine H_1 and H_4 receptors were determined by using selective antagonists.

Conclusion and Implications: Our findings provide the first evidence for targeting the peripheral histamine system by a recombinant histamine binding protein as a novel strategy for the control of acute itch. Based on the mechanisms of itch transmission, it is possible that rEV-131 prevents binding of histamine to peripheral H_1R , which results in anti-pruritic efficacy of rEV-131.

REFERENCE

- Weston-Davies, W., Coullin, I., Schnyder, S., Schnyder, B., Moser, R., Lissina, O., ... Ryffel, B. (2005). Arthropod-derived protein EV131 inhibits histamine action and allergic asthma. *Annals of the New York Academy of Sciences*, 1056, 189–196.

P022 | Beneficial effect of fractionated heparin on skeletal muscle tissue recovery after *Cerastes cerastes* viper envenomation

Habiba Oussedik-Oumehdi; Nourredine Fatima-Zohra;
 Fatima Laraba-Djebari

Faculty of Biological Sciences

Background and Purpose: Myonecrosis is a prominent local tissue damage, induced by Viperidae venoms, often leading to tissue mass and function loss (Zornetta et al., 2012). Heparin is known to sequester growth factors and cytokines that are involved in cell proliferation and angiogenesis (Landucci et al., 2000). The aim of this study was to investigate the effect of fractionated heparin (FH) treatment on muscle tissue regeneration after viper envenomation in a murine model.

Experimental Approach: Control animals ($n = 5$) received NaCl (0.15 M) by i.m. route. Envenomed group ($n = 20$) received one LD₅₀ of venom (48 μ g per 20 g of mice body mass) by i.m. route. Heparin

treated group ($n = 20$) received one LD₅₀ of venom followed by an i.v. administration of FH ($10 \mu\text{g}\cdot\text{g}^{-1}$) at 15 min and 4 hr after envenomation. Tissue regeneration was evaluated by histopathological analysis and by creatine kinase, MPO, NO, and HGF evaluation.

Key Results: Deep tissue structure alterations were observed at 24 and 72 hr after envenomation, while heparin-treated animals showed less tissue damage and more preserved cells. Myotoxicity correlated with the increase of creatine kinase levels in sera and was concomitant with their decrease in skeletal muscle homogenates. Tissue regeneration was completed by 2 weeks in heparin-treated group, whereas it was completed by 1 month in the envenomed group. Inflammatory reaction in affected muscle was characterized by oedema and neutrophil infiltrate. FH treatment decreased significantly MPO activity at 24 and 72 hr (0.671 ± 0.022 and 0.430 ± 0.024 UDO $\cdot\text{min}^{-1}$ per 100 g of tissue) compared to the envenomed group (0.954 ± 0.025 and 0.552 ± 0.024 UDO $\cdot\text{min}^{-1}$ per 100 g of tissue) at 24 and 72 hr, respectively. The levels of NO ($2.73 \pm 0.157 \mu\text{M}\cdot\text{mg}^{-1}$ of proteins) and HGF ($3110.66 \pm 557.89 \text{ pg}\cdot\text{ml}^{-1}$) were significantly increased in muscle tissue of heparin group compared to that of the envenomed venom group ($P < .001$).

Conclusion and Implications: Fractionated heparin treatment seemed to have a protective ability against the toxic effects of the venom and improved tissue regeneration. This study suggests that heparin use

could be a promising therapeutic approach in muscle tissue recovery after envenomation.

REFERENCES

Landucci, E. C. T., Toyama, M., Marangoni, S., Oliveira, B., Cirino, G., Antunes, E., & de Nucci, G. (2000). Effect of crotapotin and heparin on the rat paw oedema induced by different secretory phospholipases A₂. *Toxicol: Official Journal of the International Society on Toxicology*, 38, 199–208.

Zornetta, I., Caccin, P., Fernandez, J., Lomonte, B., Gutierrez, J. M., & Montecucco, C. (2012). Envenomations by *Bothrops* and *Crotalus* snakes induce the release of mitochondrial alarmins. *PLoS Neglected Tropical Diseases*, 6, e1526.

P023 | GPCR35 as a target for hepatic steatosis?

Li-Chiung Lin¹; Susanna Engberg²; Andrew Tobin¹; Graeme Milligan¹

¹Institute of Molecular, Cell and Systems Biology, University of Glasgow;

²Discovery Sciences, AstraZeneca

Background and Purpose: Hepatic steatosis is a common chronic liver disease and can further transform into cirrhosis and hepatocellular

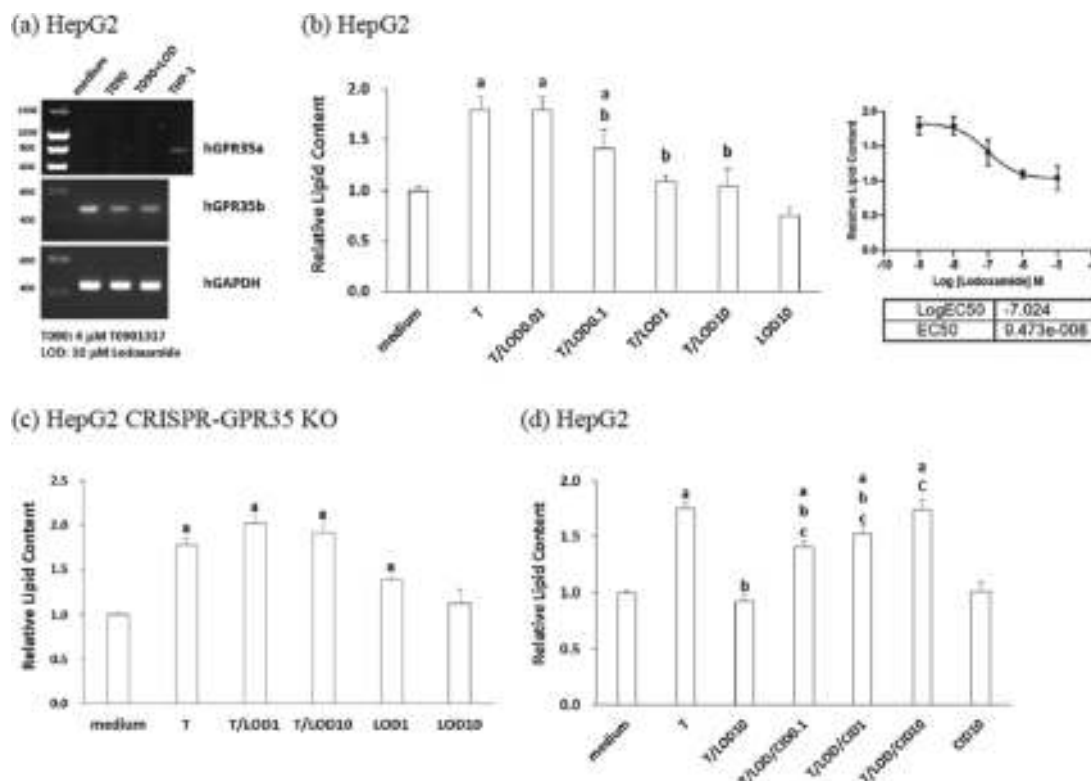


FIGURE 1 The GPR35 agonist lodoxamide can inhibit LXR-induced hepatic lipid accumulation. HepG2 and HepG2 CRISPR-GPR35 KO cells were treated with T0901317 (4 μM), lodoxamide, and/or CID 2745687 for 48 hr. Lipid accumulation was determined by Oil Red O staining. CID0.1, 1, 10, CID 2745687 0.1, 1, 10, lodoxamide 0.1, 1, and 10 μM; LOD0.1, 1, 10, lodoxamide 0.1, 1, and 10 μM; T, T0901317. Data represent mean ± SD in triplicates from each group. ^aSignificant difference compared with medium group ($P < .05$). ^bSignificant difference compared with T0901317 group ($P < .05$). ^cSignificant difference compared with T/L0D10 group ($P < .05$)

carcinoma (Drew, 2017). It is defined as an accumulation of lipid in the liver and is caused by an imbalance of energy homeostasis (Stern et al., 2016). Kynurenic acid, a putative endogenous agonist of GPR35, has been described to induce lipid metabolism and increase energy utilisation through activation of GPR35 in mouse adipose tissue (Agudelo et al., 2018). Whether GPR35 might be a target for treatment of hepatic steatosis is thus worthy of investigation.

Experimental Approach: Oil Red O staining was performed to assess the level of lipid accumulation after drug treatment (Lin et al., 2017). Human HepG2 cells and HepG2 CRISPR-GPR35 KO cells were treated with the liver X receptor (LXR) activator T0901317 and/or the GPR35 agonist Iodoxamide, which has high affinity at human GPR35. PCR was performed using GPR35 isoform selective primers.

Key Results: HepG2 cells express mRNA encoding only the longer (b) isoform of GPR35. In HepG2 CRISPR-GPR35 KO cells, sequencing confirmed lack of expression of full-length receptor mRNA. T0901317 promoted lipid accumulation in both HepG2 and HepG2 CRISPR-GPR35 KO cells. Iodoxamide inhibited this in a concentration-dependent manner in HepG2 cells but lacked this effect in HepG2 CRISPR-GPR35 KO cells. The effect of Iodoxamide in HepG2 cells was also blocked by co-addition of the human orthologue specific antagonist CID 2745687.

Conclusion and Implications: Iodoxamide inhibits LXR-induced lipid accumulation in human HepG2 cells in a GPR35-dependent manner. Because of the marked variation of agonist pharmacology between human and mouse GPR35 and because CID 2745687 does not block mouse GPR35 (Jenkins et al., 2012), translational studies will be conducted using transgenic knock-in "mice" in which we have replaced mouse GPR35 with the human orthologue.

REFERENCES

- Agudelo, et al. (2018). *Cell Metabolism*, 27, 378–392.
 Drew (2017). *Nature*, 550, S103–S103.
 Jenkins, et al. (2012). *The Journal of Pharmacology and Experimental Therapeutics*, 343, 683–695.
 Lin, et al. (2017). *Cancer Letters*, 391, 74–82.
 Stern, et al. (2016). *Cell Metabolism*, 23, 770–784.

P024 | Targeting the protein kinase *Plasmodium falciparum* CLK3 for malaria treatment: TCMDC-135051 blocks asexual parasite progression and malaria transmission

Omar Janha; Ana Sanchez-Azqueta; Mahmood Alam; Andrew Tobin
 University of Glasgow

Background and Purpose: Intervention strategies have significantly contributed to the control of malaria, but the disease still remained a major public health problem killing nearly 500,000 and infecting more than 200 million people annually. This, together with the emerging

resistant parasites to frontline antimalarials, threatened the success in malaria control, hence an urgent need for novel targets offering curative and block transmission opportunities. Here, I show *Plasmodium falciparum* CLK3 (*PfCLK3*) as a therapeutic target meeting these criteria set by medicines for malaria ventures.

Experimental Approach: Kinase activity was measured using a TR-FRET assay run in two steps in the 384-well format. First, in a 10- μ l reaction volume, 5 μ l of 2 \times required enzyme concentration is mixed with 5 μ l of 2 \times substrate solution (2.5 μ l each of 4 \times substrate and inhibitor concentration in inhibition assays) and incubated at 37°C for 1 hr. In the second step, 5 μ l of the stopping solution containing 30-mM EDTA and 3-nM Europium-labelled anti-phospho-specific antibody in Lance detection is added to the reaction and incubated at room temperature for 1 hr to stop the reaction and enhance detection. Further details of the assay are described in Alam et al. (2019).

Key Results: A selective inhibitor TCMDC-135051 was identified specifically inhibiting *P. falciparum* recombinant protein kinase *PfCLK3* activity with an IC_{50} of 0.04 μ M (pIC_{50} = 7.35). TCMDC-135051 blocked parasite transition from rings to *trophozoite* stages and from *trophozoites* to *schizont*. Using standard drug assays, TCMDC-135051 showed high potency against parasites with an IC_{50} of ~200 nM (pIC_{50} = 6.7). To confirm *PfCLK3* as TCMDC-135051 target in parasites, a variant *PfCLK3* mutant (G449P) showed ~3 log shift in sensitivity to TCMDC-135051 (*PfCLK3* pIC_{50} = 7.35 [IC_{50} = 0.04 μ M]; G449P pIC_{50} = 4.66 [IC_{50} = 21.87 μ M]). G449P variant parasites also showed reduced sensitivity to TCMDC-135051 by ~1.5 log units (pIC_{50} in 3D7 wild type, 6.35 [IC_{50} = 0.45 μ M]; in the A3 strain, 4.86 [IC_{50} = 13.80 μ M]), proving that TCMDC-135051 kills parasites via *PfCLK3* inhibition. On different malaria CLK3 orthologues (*PvCLK3* and *PbCLK3*), TCMDC-135051 had near-equipotent inhibition, with pIC_{50} values of 7.47 (IC_{50} = 0.033 μ M) and 7.86 (IC_{50} = 0.013 μ M), respectively. In asexual blood-stage cultures of *P. knowlesi* and *P. berghei*, TCMDC135051 activity showed similar parasitocidal effects in both of these species. Inhibiting *PfCLK3* reduces commitment of asexual parasites to stage II gametocytes (pIC_{50} = 6.04 [IC_{50} = 0.91 μ M]) and significantly reduced maturation of stage II gametocytes to stage V (IC_{50} = 0.8 μ M), significantly decreasing in exflagellation numbers (EC_{50} = 0.2 μ M). These effects combined reduced gametocyte numbers contributed significantly, thus reducing transmission.

Conclusion and Implications: Inhibition of CLK3 can kill multiple blood- and liver-stage parasites across different species as well as block transmission to mosquitoes by preventing gametocyte development. Hence, our data validate CLK3 as prophylactic, curative, and transmission blocking target.

REFERENCE

- Alam, M. M., Sanchez-Azqueta, A., Janha, O., Flannery, E. L., Mahindra, A., Mapesa, K., ... Tobin, A. B. (2019). Validation of the protein kinase *PfCLK3* as a multistage cross-species malarial drug target. *Science*, 365, eaau1682.

P025 | Wnt signalling contributes to cardiomyocyte hypertrophy

Mhairi Paul¹; Emma Hector¹; Erik Ryberg²; Stephen Leslie³; Cherry Wainwright¹; Sarah Walsh¹

¹Robert Gordon University; ²AstraZeneca; ³Raigmore Hospital

Background and Purpose: Cardiac hypertrophy is a key feature of diastolic heart failure and is characterised by reactivation of the cardiac fetal gene programme (Cox & Marsh, 2014). It has emerged that aberrant wntless/int (Wnt) signalling may induce reactivation of fetal genes (Pahnke et al., 2017), and loss of secreted frizzled related protein 1 (sFRP-1), a negative modulator of the Wnt signalling, has been shown to contribute to a hypertrophic phenotype (Sklepkiwicz et al., 2015). The aims of the present study were to characterise the cardiomyocyte-like phenotype of H9c2 cells and examine the hypertrophic potential of Wnt3a.

Experimental Approach: The presence of the cardiomyocyte-specific markers, cardiac troponin T (cTnT), myosin heavy chain 6 (Myh6), cardiac troponin I (cTnI), and Nkx2.5, were examined in both rat myoblast H9c2 cells and rat cardiac tissue. H9c2 cells were cultured in DMEM with 10% FBS and RNA subsequently extracted using TRI reagent. A male Sprague Dawley rat was killed via CO₂ asphyxiation and cervical dislocation, both atrial and ventricular tissues were collected separately, and RNA was extracted. RT-PCR was carried out, and all gels were imaged using the PeqLab Fusion Fx7 system. To induce hypertrophy, H9c2 cells were treated with angiotensin II (AngII; 1 μM) for either 24 or 48 hr in increasing concentrations of FBS (1%, 5%, and 10%). In separate studies, H9c2 cells were treated with Wnt3a (10 and 100 ng·ml⁻¹). The expression of the fetal genes atrial natriuretic peptide (ANP) and brain natriuretic peptide (BNP) was then measured via quantitative RT-PCR. Statistical significance was determined using either a t test or a one-way ANOVA followed by Dunnett's post hoc test.

Key Results: cTnT, cTnI, and Nkx2.5 were all expressed in rat cardiac tissues and H9c2 cells. Treatment of H9c2 cells cultured in 5% FBS with AngII for 24 hr resulted in increases in both ANP (2.43-fold above control; P < .05; n = 3) and BNP (3.58-fold above control; P = .0512; n = 4) expression. Wnt3a (10 ng·ml⁻¹) induced significant increases in both ANP (P < .05) and BNP (P < .01) expression (1.7-fold above control for both; n = 3). At 100 ng·ml⁻¹, Wnt3a appeared to induce hypertrophic responses of greater magnitude than 10 ng·ml⁻¹; however, these responses were much more variable, ranging from 0.15-fold to 7.09-fold above control for ANP and 0.38-fold to 6.75-fold above control for BNP (n = 3; ns).

Conclusion and Implications: Wnt3a induces hypertrophy in the cardiomyocyte-like H9c2 cell line.

REFERENCES

Cox, & Marsh (2014). *PLoS ONE*, 9(3), e92903.
 Pahnke, et al. (2017). *Biochemical and Biophysical Research Communications*, 473(3), 698–703.
 Sklepkiwicz, et al. (2015). *Circulation. Heart Failure*, 8(2), 362–372.

P026 | Role of piperine in chemoresistance of triple-negative breast cancer: Potential modulation of PI3K/Akt/mTOR pathway

Aliaa Abdel Fattah; Amr Zaki; Kohinour Kamel; Lidia Yasser; Marina Barsom; MennatAllah Ahmed; Mohamed Gamal; Andrew Hakeem; Dina El-Kersh; Yasmeen Attia

The British University in Egypt

Background and Purpose: Triple-negative breast cancer (TNBC) is a clinically aggressive type of breast cancer with no targeted therapy available. Conventional chemotherapy remains the mainstay of treatment for TNBC, yet development of intrinsic and de novo resistance

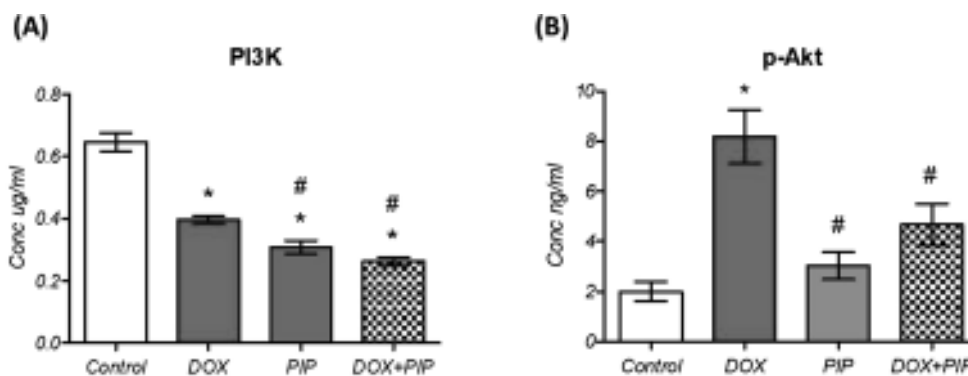


Fig. 1 PI3K and p-Akt protein levels as determined by ELISA in tumor sections of EAC-bearing mice treated with DOX, PIP and DOX+PIP. Significant vs *control and #DOX at P<0.05

FIGURE 1 PI3K and p-Akt protein levels as determined by ELISA in tumor sections of EAC-bearing mice treated with DOX, PIP and DOX+PIP. Significant vs *control and #DOX at P<0.05

represents the main limitation. Adjunct or add-on therapy, therefore, is thought of as an approach to enhance responsiveness and improve prognosis. Previous studies reported the involvement of PI3K/Akt/mTOR signalling pathway in the maintenance and enrichment of cancer stem cells and hence chemoresistance. The present study aimed at investigating the potential effect of piperine (PIP) on enhancing the sensitivity of TNBC cells to doxorubicin (DOX) in vitro on MDA-MB-231 cell line and in vivo in an animal model of Ehrlich ascites carcinoma (EAC) solid tumour.

Experimental Approach: MDA-MB-231 TNBC cells were treated with 50 μM of doxorubicin (DOX), 200 μM of piperine (PIP), and combination of both to investigate the effect on cytotoxicity. Forty EAC-tumour-bearing female mice were randomly allocated into four groups, each containing 10 mice; control, PIP-treated (50 $\text{mg}\cdot\text{kg}^{-1}$, i. p., daily), DOX-treated (4 $\text{mg}\cdot\text{kg}^{-1}$, s.c., once per week), and PIP + DOX-treated groups. All treatments started 5 days after inoculation for 2 weeks. Before termination of experiment, tumour volume was calculated using a digital caliper. Mice were then killed under anaesthesia, and tumour tissues were collected for further analysis. PI3K and p-Akt were determined in tumour sections using ELISA. Data are presented as mean \pm SD ($n = 10$). Statistical significance ($P < .05$) was determined using one-way ANOVA followed by Tukey's post hoc test.

Key Results: Combining PIP to DOX caused 83% significantly higher cytotoxic effect than using DOX alone on MDA-MB-231 cells. Regarding the in vivo experiment, combining DOX to PIP showed a significantly lower tumour size ($88.4 \pm 28.7 \text{ mm}^3$) compared to DOX alone ($717.4 \pm 40.8 \text{ mm}^3$). Moreover, as shown in Figure 1, PI3K and p-Akt levels were significantly lower in DOX + PIP-treated group compared to DOX-treated group.

Conclusion and Implications: Overall, these findings suggest a potential role of PIP in decreasing resistance to DOX in vitro and in vivo, possibly by interfering with the PI3K/Akt/mTOR pathway.

Poster Session: Neuropharmacology 1

P084 | Modulation of human T-type calcium channels by phytocannabinoids in vitro

Somayeh Mirlohi; Mark Connor; Chris Bladen

Macquarie University

Background and Purpose: Low-voltage-activated T-type calcium channels (I_{Ca}), encoded by the genes, $\text{Ca}_v3.1$, $\text{Ca}_v3.2$, and $\text{Ca}_v3.3$, are opened by small depolarizations from the resting membrane potential of diverse cells and are critical for many physiological processes. Their activity contributes to pathophysiological states including cardiac arrhythmia, epilepsy, and pain (Nelson, Todorovic, & Perez-Reyes, 2006). Both endocannabinoids and plant-derived cannabinoids

(phytocannabinoids) modulate T-type current (Ross, Gilmore, & Connor, 2009). The use of phytocannabinoids as therapeutics for pain and epilepsy is dramatically increasing. However, there is no information about the activity of most phytocannabinoids on T-type channels. We therefore examined the potential modulation of T-type I_{Ca} by common phytocannabinoids.

Experimental Approach: We used HEK293 Flp-In-TREx cells stably expressing $\text{Ca}_v3.1$, $\text{Ca}_v3.2$, or $\text{Ca}_v3.3$. A fluorometric (FLIPR) assay was used to screen phytocannabinoid for their ability to block or modulate T-type Ca channels. Whole-cell patch-clamp recordings were made to further investigate cannabinoid modulation of I_{Ca} . Statistical significance was set to $P < .05$.

Key Results: Generally, phytocannabinoids blocked $\text{Ca}_v3.1$ and $\text{Ca}_v3.2$ more potently than $\text{Ca}_v3.3$. In the FLIPR assay, CBGA (cannabigerol acid) and CBDVA (cannabidivarin acid) were the most effective compounds, inhibiting $\text{Ca}_v3.1$ by $97 \pm 1\%$ and $80 \pm 2\%$ at 10 μM ($n = 6$). CBGA blocked $\text{Ca}_v3.2$ by $92 \pm 3\%$, and CBG (cannabigerol) and CBN (cannabinol) also inhibited $\text{Ca}_v3.2$ by more than 50% at 10 μM . Tetrahydrocannabinolic acid (THCA) was the only compound that inhibited $\text{Ca}_v3.3$ by more than 50% ($53 \pm 7\%$) at 10 μM ($n = 6$). The $V_{0.5}$ for steady-state activation and inactivation of $\text{Ca}_v3.1$ was significantly shifted more negative by 300-nM CBGA. THC and THCA blocked $\text{Ca}_v3.1$ with pIC_{50} of -5.72 ± 0.07 and -6.07 ± 0.06 , respectively. THC and THCA produced significant hyperpolarizing shifts in inactivation potential (-7 ± 2 and -7 ± 3 mV) and $\text{Ca}_v3.1$ activation potential (-8 ± 1 and -7 ± 1 mV). THCA (10 μM) produced a significant positive shift in the $\text{Ca}_v3.3$ activation potential and a negative shift in the $\text{Ca}_v3.3$ inactivation ($P < .05$).

Conclusion and Implications: Phytocannabinoids modulate T-type I_{Ca} kinetics in vitro with some causing significant kinetic modulation and I_{Ca} reduction at low μM concentrations. These results extend our knowledge of phytocannabinoids beyond the previously reported effects of THC and CBD (cannabidiol) and suggest that other phytocannabinoids may have potential for therapeutic use in pain and epilepsy via T-type channel modulation.

REFERENCES

- Nelson, M. T., Todorovic, S. M., & Perez-Reyes, E. (2006). The role of T-type calcium channels in epilepsy and pain. *Current Pharmaceutical Design*.
- Ross, H., Gilmore, A. J., & Connor, M. (2009). Inhibition of human recombinant T-type calcium channels by the endocannabinoid N-arachidonoyl dopamine. *British Journal of Pharmacology*.

P085 | A muscarinic M_1 -mEGFP transgenic mouse line to study receptor function and quaternary structure

Sara Marsango; Laura Jenkins; Sophie Bradley; Lisa Finlayson; Andrew Tobin; Graeme Milligan

University of Glasgow

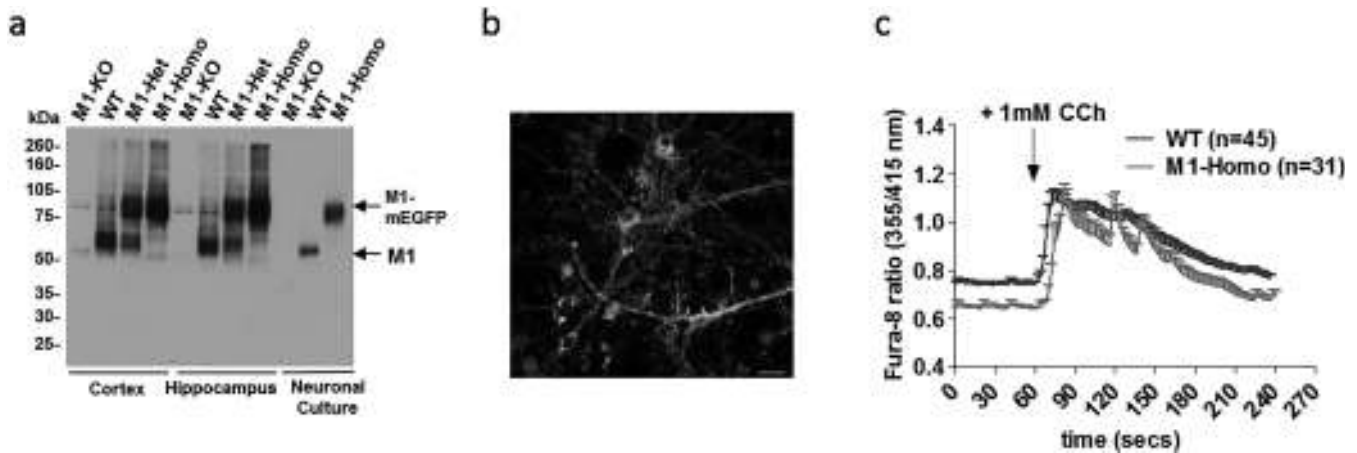


FIGURE 1 Expression and function of M₁-mEGFP in knock-in transgenic mice: (a) Lysates from the indicated tissues or neurons isolated from the indicated mice were resolved by SDS-PAGE and immunoblotted with an anti-M₁ antiserum. (b) Confocal fluorescence images of neurons isolated from homozygous day 16 M₁-mEGFP embryos. Blue, DAPI staining; green, mEGFP. Scale bar = 20 μm. (c) Single-cell Ca²⁺ imaging in neurons isolated from M₁-mEGFP (green) or WT (purple) mice

Background and Purpose: In vitro studies on the quaternary organisation of the muscarinic M₁ receptor (M₁R) have resulted in varying conclusions. It has been described as predominantly monomeric but with a capacity to form dimers, routinely dimeric, or as a mixture of monomers and dimers/oligomers that can be stabilised by binding of selective M₁R antagonists (Marsango et al., 2018). However, to date, no studies have addressed these issues in native cells and tissues. To do so, we have generated a knock-in transgenic mouse line that expresses the M₁R linked in-frame at the C-terminus to monomeric (Lys²⁰⁶Ala) eGFP (M₁R-mEGFP) in place of the wild-type receptor (WT). Here, we characterise this transgenic mouse line.

Experimental Approach: Immunoblotting and signal transduction assays were performed using isolated hippocampus and cortex, or cultured neuronal cells isolated from day 16 embryos and maintained in tissue culture. Behavioural studies were performed in vivo.

Key Results: Lysates from isolated brain regions of each of WT, M₁ knockout (M₁-KO), and both heterozygous and homozygous M₁-mEGFP mice were resolved by SDS-PAGE and immunoblotted with an anti-M₁ antiserum. Specific immunoreactive species of the predicted size were identified. This was also the case where isolated neuronal cultures were used (Figure 1a). Binding studies using the muscarinic receptor antagonist [³H]NMS provided qualitative validation that expression of M₁-mEGFP was at similar levels as the WT receptor in control mice (554 ± 2.3 and 588 ± 35.7 fmol·mg⁻¹, respectively, above M₁-KO line, means ± SEM, n = 2). Confocal imaging of isolated neurons from M₁-mEGFP mice showed the expression of the construct in both the cell body and throughout dendrites (Figure 1b). Addition of the agonist carbachol to neurons from M₁-mEGFP and WT mice resulted in similar elevation of intracellular [Ca²⁺] (Figure 1c). Open field tests showed that locomotion of M₁-mEGFP mice was comparable to WT, with a total distance travelled equal to 24.9 ± 2.7 and 20.8 ± 2.8^{ns} m, respectively. By contrast, M₁-KO mice displayed marked hyperlocomotion (40.7 ± 2.0^{***} m, means ± SEM,

n = 9; ns, not significant; **, P < .001; one-way ANOVA followed by Tukey's multiple comparisons test).

Conclusion and Implications: The M₁-mEGFP mouse line represents a novel and appropriate model for functional and behavioural studies of this receptor as well as to assess M₁ quaternary structure using fluorescence intensity fluctuation spectroscopy (Stoneman et al., 2019) or related methods.

REFERENCE

Marsango, S., et al. (2018). *Neuropharmacology*, 136, 401–410.
Stoneman, M. R., et al. (2019). *Nature Methods*, 16, 493–496.

P087 | Using optogenetics to dissect opioid control of GABAergic inputs to periaqueductal grey neurons that constitute the descending analgesic pathway

Bryony Winters¹; Benjamin Lau²; Christopher Vaughan¹

¹University of Sydney; ²University of Calgary

Background and Purpose: The midbrain periaqueductal grey (PAG) projects via the rostral ventral medulla (RVM) to inhibit nociceptive signals in the spinal cord. Opioids are potent analgesics that activate this descending pathway by inhibiting putative GABAergic interneurons to disinhibit PAG projection neurons (Lau et al., 2014). PAG neurons also receive GABAergic inputs from the medial central amygdala (CeA), which, when activated, engage the descending pathway in an opioid-dependent manner. However, it is unclear whether these GABAergic inputs target interneurons or descending projection neurons. Furthermore, how opioids act at this synapse to facilitate descending analgesia is unknown. The aim of this study was to investigate the effects of opioids on specific

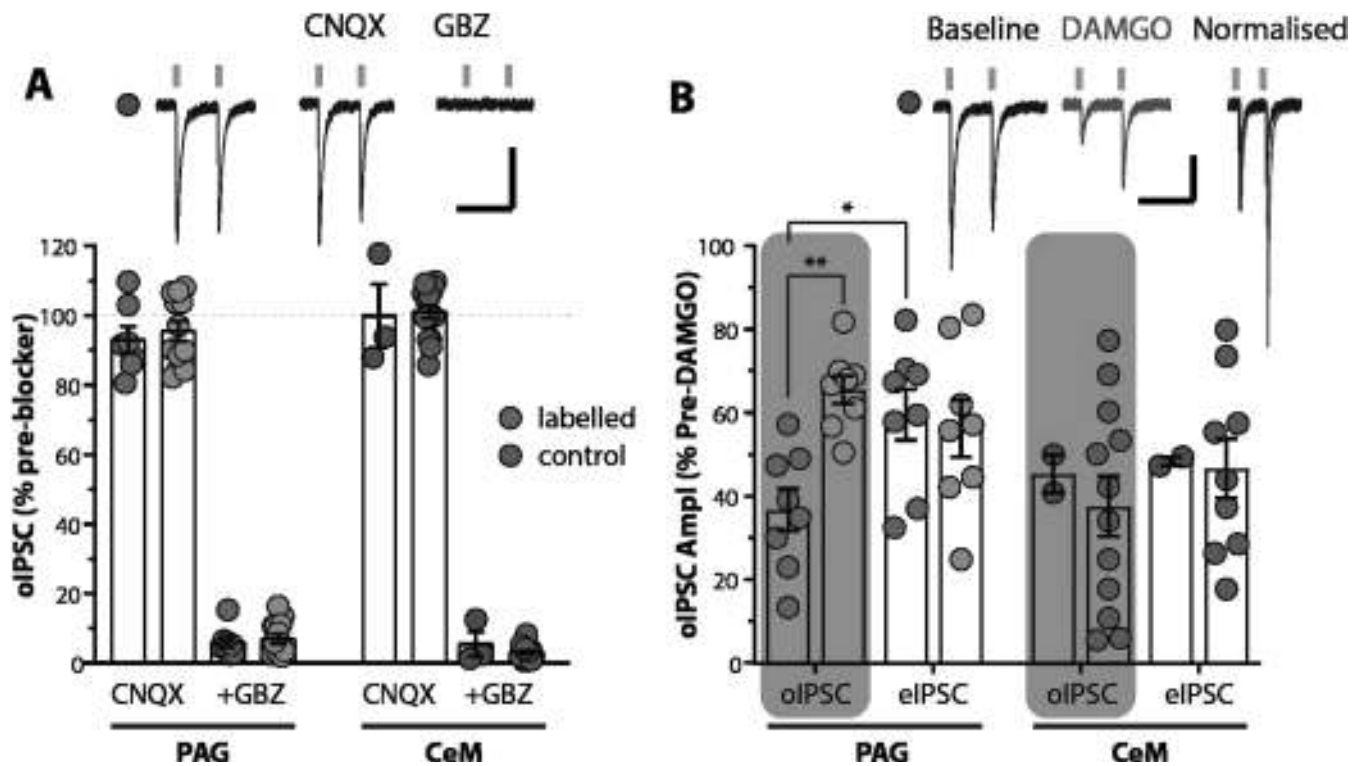


FIGURE 1 (a) Bar chart displaying optically evoked inputs from local interneurons (PAG) and CeM terminals (CeM) that are inhibited by gabazine (GBZ, 10 μ M) but insensitive to CNQX (20 μ M). (b) Bar chart displaying the effect of DAMGO (3 μ M) on optically evoked IPSCs (oIPSC) and electrically evoked IPSCs (eIPSC). ** $P < .01$; * $P < .05$. Above each bar chart are single traces of a representative recording in a retrogradely labelled PAG neuron where CeM terminals were optically activated to evoke oIPSCs

GABAergic inputs to the PAG using an optogenetic, combined with tract-tracing approach.

Experimental Approach: The viral construct AAV-hSyn-ChR2 (H134A)-eYFP was bilaterally injected into either the PAG or CeM of 3- to 4-week-old Sprague Dawley rats. To label PAG projection neurons, rats also received a retrograde tracer injected into the RVM; 8–12 weeks after surgery, whole cell voltage clamp recordings were conducted from retrogradely labelled or control (no tracer injection) PAG neurons in acute brain slices. The effects of DAMGO (3 μ M), a μ -opioid receptor agonist, were studied on optically or electrically evoked responses. All drugs were bath applied, and data were normalised to baseline values and given as mean \pm SEM. Statistical significance was determined using two-way ANOVA with Tukey's post hoc correction.

Key Results: Optical activation of local interneurons evoked inhibitory postsynaptic currents (oIPSC) in all retrogradely labelled ($n = 29$) and control ($n = 21$) PAG neurons, which were abolished by the GABA_A receptor antagonist gabazine but were insensitive to the AMPA receptor antagonist CNQX (Figure 1a). Optical activation of CeM terminals evoked GABAergic oIPSCs in a subpopulation of PAG neurons ($n = 33/93$), some of which were retrogradely labelled ($n = 8/19$). In all cases, DAMGO inhibited optically and electrically evoked IPSCs (Figure 1b). The level of inhibition of CeM inputs to control PAG neurons was highly variable, whilst preliminary data indicate less variability in retrogradely labelled

neurons. These did not differ from electrically evoked IPSCs (eIPSC). In contrast, local interneuron inputs were more sensitive to DAMGO inhibition when recorded in retrogradely labelled PAG neurons, whilst eIPSCs were less sensitive to DAMGO inhibition (Figure 1b).

Conclusion and Implications: Our findings indicate that PAG to RVM projection neurons receive GABAergic inputs both locally from interneurons and extrinsically from the CeM. The relative opioid control of each input appeared to differ with retrograde labelling, with local inputs being particularly sensitive to opioid control.

REFERENCE

Lau, B. K., et al. (2014). *Current Opinion in Neurobiology*, 29, 159–164.

P088 | Targeting adult-born granule cells through GluN2B-containing NMDA receptor antagonist enhances the inhibitory GABA transmission in the dentate gyrus

Julie Doan; Céline Defaix; Alain Gardier; Laurent Tritschler

CESP/UMRS1178, Univ Paris-Sud, Fac Pharmacie, INSERM, Université Paris-Saclay, Châtenay-Malabry, France

Background and Purpose: Major depressive episodes are the most common psychiatric disorder worldwide. Selective serotonin reuptake inhibitors (SSRIs), such as fluoxetine, are the most prescribed antidepressant class. They increase gradually the serotonin transmission.

Chronic antidepressant drug treatments also stimulate adult hippocampal neurogenesis (AHN), the process by which adult-born granule cells (abGCs) are continuously generated in the dentate gyrus (DG). The stimulation of different steps of AHN (proliferation, survival, and differentiation) by SSRIs is necessary to observe antidepressant-like effects in rodents, specifically in behavioural tests such as the novelty-suppressed feeding (NSF) (David et al., 2009).

Our hypothesis: AbGC production induced by a chronic SSRI administration may induce a selective release of neurotransmitters in the DG, which leads to a robust antidepressant-like activity measured in the NSF. Using intracerebral microdialysis in a mouse model of depression based on chronic corticosterone administration,

we evaluated the effect of Ro 25-6981, a selective antagonist of the GluN2B subunit of the NMDA glutamate receptor, which is highly expressed in abGCs. The extracellular concentrations of glutamate ([Glu]_{ext}) and of GABA ([GABA]_{ext}) in the DG have been measured.

Experimental Approach: Male 129/SvPas mice 16–26 weeks of age were treated for 8 weeks with corticosterone (CORT, 35 mg·L⁻¹ in the drinking water) and additionally received fluoxetine (Flx, 160 mg·L⁻¹ in the drinking water) for the last 4 weeks of CORT treatment (David et al., 2009). The latency to feed in the NSF was measured after 24 hr of starvation. The animals were then implanted bilaterally in the DG with microdialysis probes. The following day, the probes were perfused with artificial CSF and local intra-DG administration of Ro 25-6981 (5 nmol in each DG in 12% DMSO) was performed.

Key Results: Fluoxetine treatment decreased the latency to feed in the NSF (Figure 1).

Intra-DG Ro 25-6981 administration induced an increase in [Glu]_{ext} in both fluoxetine- and vehicle-treated animals (Figure 2a) and tended to increase [GABA]_{ext} selectively in fluoxetine-treated animals (Figure 2b).

Conclusion and Implications: Even if they need to be completed, our data showed a [GABA]_{ext} increase in the DG after administration of the antagonist of GluN2B-containing NMDA receptor selectively in fluoxetine-treated mice, which could be a first link between AHN and behaviour.

REFERENCE

David, D. J., Samuels, B. A., Rainer, Q., Wang, J. W., Marsteller, D., Mendez, I., ... Hen, R. (2009). Neurogenesis-dependent and -independent effects of fluoxetine in an animal model of anxiety/depression. *Neuron*, 62(4), 479–493.

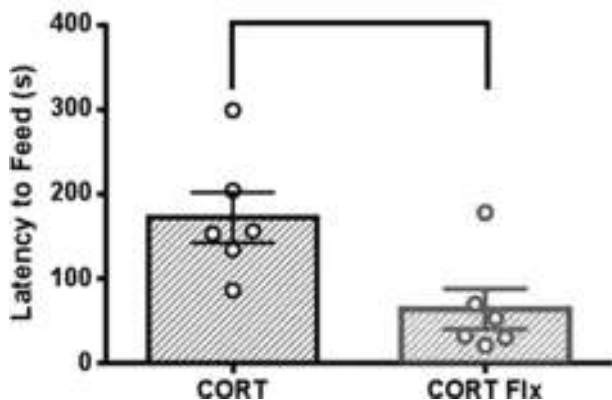


FIGURE 1 Latency to feed in a novel environment in the NSF. One-sample t test: *P < .05

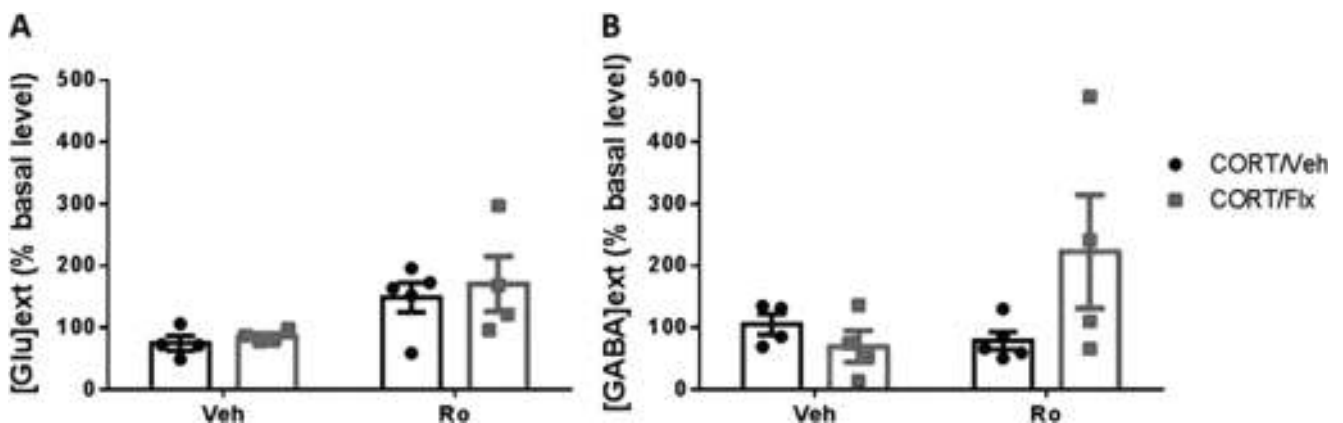


FIGURE 2 Extracellular [GABA] and [Glu] in the ventral DG after administration of Ro 25-6981. Two-way ANOVA: F(1, 13) = 9.35, P < .01, for [Glu]_{ext}; F(1, 13) = 1.90, P = .19, for [GABA]_{ext}

P089 | The interaction of baclofen and 5-hydroxy-L-tryptohan with the LAT1 (SLC7A5) transporter

Mungo Harvey; Waseema Patel; David Dickens

University of Liverpool

Background and Purpose: The strict selectivity of the blood–brain barrier (BBB) is a persistent bottleneck for drugs targeted within the CNS (Pardridge, 2005). A strong understanding of how known compounds cross the BBB, such as 5-HTP and baclofen, can help predict whether novel drugs will have in vivo efficacy. LAT1 (SLC7A5) is highly expressed at the BBB and is a possible target for drug transport into the CNS. Identifying LAT1 substrates enables key pharmacophores for transport to be defined and applied in drug development to improve drug delivery into the CNS.

Experimental Approach: 5-HTP and baclofen uptake was inferred through a trans-stimulation assay (Figure 1) measuring the [³H]-phenylalanine concentration within LAT1-transfected HEK293 cell (Dickens et al., 2013). This considered the effect of drug solutions (1 mM) leucine, baclofen, and 5-HTP, on intracellular [³H]-phenylalanine concentration.

Cells were incubated for two 3-min periods at 37°C: first with [³H]-phenylalanine (0.15 μCi·ml⁻¹) plus unlabelled phenylalanine, up to 1 μM (Figure 1a), and then with a drug treatment (1 mM) (Figure 1b). The reaction was terminated using a cold wash. JPH203 (10 μM), an indirect LAT1 inhibitor, assessed specificity.

Key Results: There was a significant drop in intracellular [³H]-Phe concentration with 5-HTP treatment, 7.39 ± 0.4 pmol per million cells, compared to the control, 30.58 ± 3.1 pmol per million cells (*n* = 4, *P* < .05), indicating that 5-HTP was exchanged for Phe by LAT1. The significant difference in intracellular Phe concentration between 5-HTP treatment, 7.3 ± 0.4 pmol per million cells, and 5-HTP with JPH203 (*n* = 4, *P* < .05), 29.34 ± 12.1 pmol per million cells, demonstrates that the interaction between 5-HTP and LAT1 was the only significant factor reducing intracellular Phe concentration. There was no evidence that baclofen is a LAT1 substrate (Figure 2).

Conclusion and Implications: The evidence indicates that 5-HTP is a substrate for LAT1. Significant differences in the intracellular phenylalanine concentration between 5-HTP versus control and 5-HTP versus 5-HTP + JPH203 (*P* < .05, *n* = 4) suggest that LAT1 was the exchange site for phenylalanine and 5-HTP. The results imply that baclofen is not a substrate for LAT1.

These findings demonstrate carrier-mediated transport of small molecules by a BBB transporter, but further studies are required to characterise the specific interactions and kinetics of 5-HTP with LAT1, as well as with other transporters.

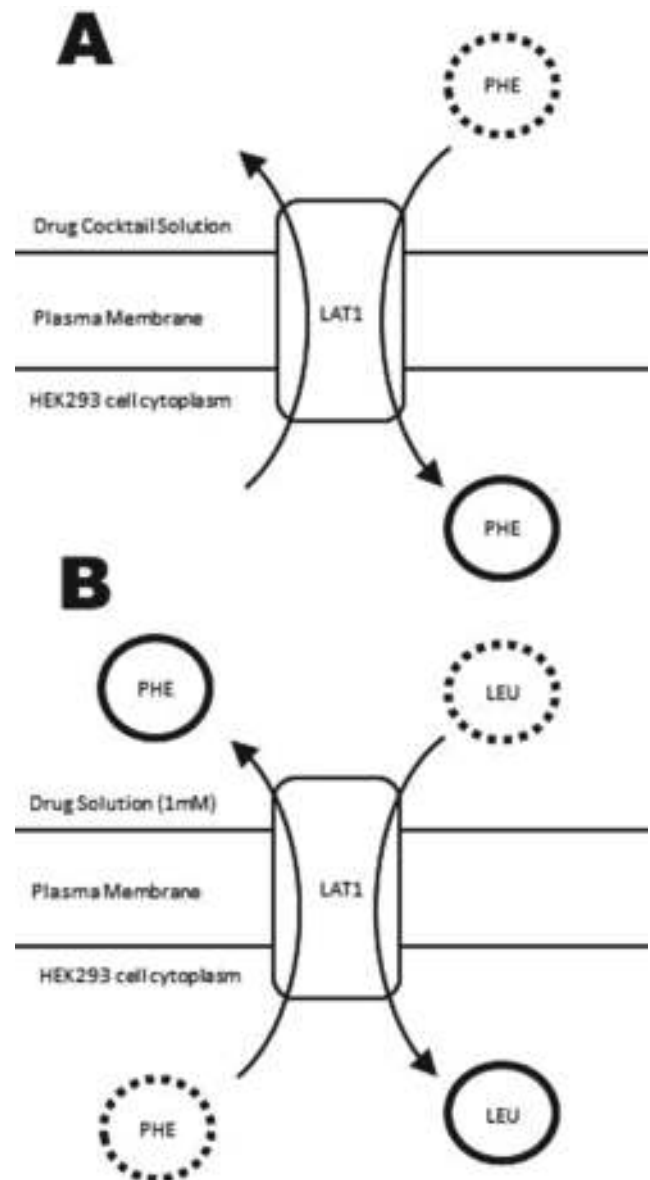


FIGURE 1 Trans-stimulation of LAT1, using the known substrate leucine as an example. LAT1 is an antiporter with 1:1 stoichiometry and will exchange [³H]-phenylalanine for a drug compound, in this assay. (a) At initial 3-min incubation period, phenylalanine, in the drug cocktail, is transported into HEK293 cells via LAT1. (b) During a second incubation period, the drug (leucine in this example) stimulates LAT1 on its extracellular side, whilst phenylalanine stimulates LAT1 on the intracellular side. This causes LAT1 to exchange each substrate moving leucine (or other drug treatments) into the cell and phenylalanine out. Dashed outlines indicate previous position of substrate before exchange by LAT1

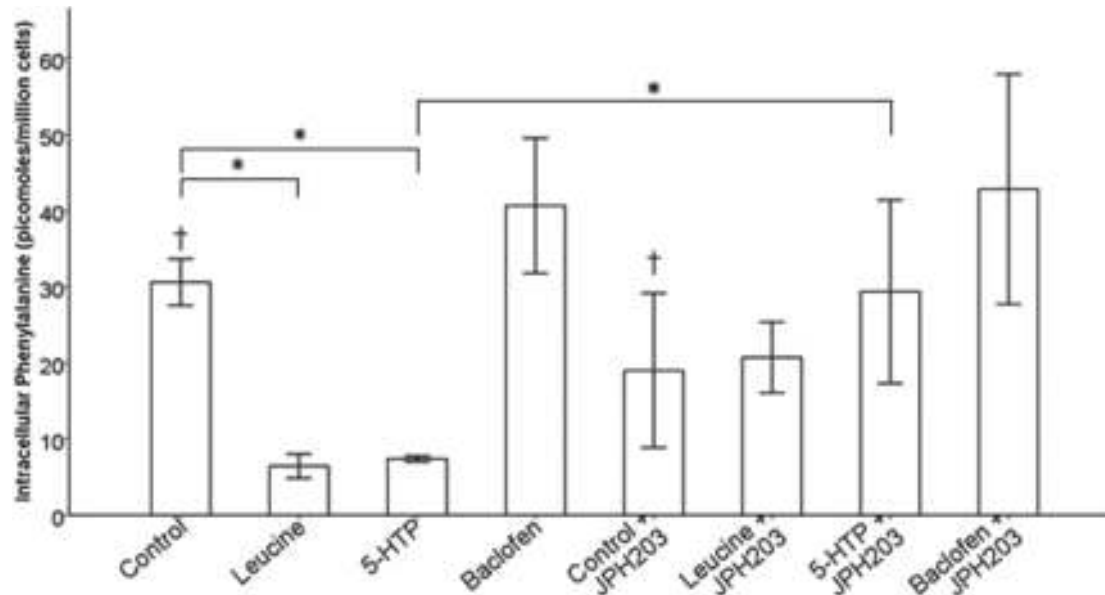


FIGURE 2 Trans-stimulation of LAT1 using phenylalanine and drug treatments: leucine, 5-HTP, and baclofen into HEK293-LAT1 cells, with and without the presence of the JPH203, LAT1. The recorded intracellular phenylalanine concentration is inversely correlated to intracellular drug concentration due to the antiporter and 1:1 stoichiometry property of LAT1. The significant difference, in intracellular phenylalanine concentrations, between 5-HTP, leucine, and the control indicates that they are substrates for LAT1. There is no significant difference between the control group and equivalent JPH203 (10 μM) treatment, showing the transport buffer used had no significant effect on JPH203 activity. There was a significant difference, in the intracellular phenylalanine concentration, between 5-HTP and 5-HTP + JPH203 treatment, suggesting that the predominant mechanism for phenylalanine efflux was via LAT1 exchange with 5-HTP. †No significant difference. *Significant results for $P < .05$. Four independent repeats represented by a mean value ($n = 4$). Error bars represent ± 1 SD

REFERENCES

Dickens, D., Webb, S., Antonyuk, S., et al. (2013). Transport of gabapentin by LAT1 (SLC7A5). *Biochemical Pharmacology*, 85(11), 1672-1683. <https://doi.org/10.1016/j.bcp.2013.03.022>

Pardridge, W. (2005). The blood-brain barrier: Bottleneck in brain drug development. *NeuroRx*, 2(1), 3-14. <https://doi.org/10.1602/neuroRx.2.1.3>

Bolognini et al. (2019) recently employed a novel human (h) FFA2-designer receptor exclusively activated by designer drugs (DREADD) to study the physiological role of FFA2. Here, we describe a novel agonist, 4-methoxy-3-methyl-benzoic acid (MOMBA), for the hFFA2-DREADD variant and use this to further explore physiological roles of FFA2 using mice in which hFFA2-DREADD has replaced the wild-type receptor.

P090 | Identifying and validating a novel agonist for a designer receptor exclusively activated by designer drugs variant of free fatty acid 2 receptor

Natasja Barki; Daniele Bolognini; Laura Jenkins; Brian Hudson; Andrew Tobin; Graeme Milligan

University of Glasgow

Experimental Approach: Following screening of a targeted set of more than 1,200 small molecules, MOMBA was identified as a potential agonist for the hFFAR2-DREADD receptor. (a) The selectivity and potency of MOMBA was assessed initially in β -arrestin-2 recruitment assays. (b) Inhibition of forskolin amplified cAMP levels provided an alternative approach. The effects of MOMBA on tissue from hFFA2-DREADD-expressing animals to release enteroendocrine hormones (GLP-1 and PYY) was assessed on (c) isolated crypts and (d) intact colonic segments and measured by ELISA. (e) A potential role of FFA2 in sensory signalling was investigated in isolated nodose ganglion (NG) and dorsal root ganglion (DRG). Functional activation was assessed by measuring intracellular calcium [Ca^{2+}] levels in cells dissociated from these ganglia.

Background and Purpose: Short-chain fatty acids are produced mainly by the gut microbiota. They mediate a variety of biological effects by acting on at least two GPCRs. These receptors are expressed by various cell types, including in the gut. The exact contribution of free fatty acid 2 receptor (FFA2) in regulating gut physiology is unclear.

Key Results: (a) MOMBA is highly selective for hFFA2 DREAD over each of hFFA2/3 and mFFA2/3. (b) MOMBA inhibits forskolin-stimulated cAMP levels in a concentration-dependent manner in cells

expressing hFFA2-DREADD ($pEC_{50} = 5.24 \pm 0.16$, mean \pm SEM, $n = 3$). (c) MOMBA (1–0.001 mM) induces a FFA2 specific concentration-dependent increase in GLP-1 secretion in colonic crypts. (d) Intraluminal infusion of MOMBA also resulted in a FFA2-mediated increase in GLP-1 and PYY secretion from intact colon. (e) MOMBA also induced a G_q -mediated increase in $[Ca^{2+}]_i$ in cells isolated from hFFA2-DREADD-expressing mice. Conversely, C3 induced a G_i -mediated increase in these cells.

Conclusion and Implications: MOMBA specifically activates hFFA2-DREADD. It is a novel tool ligand to further study the physiological and pathophysiological roles of FFA2 cell and tissues of hFFA2-DREADD-expressing mice.

REFERENCE

Bolognini, D., et al. (2019). Chemogenetics defines receptor-mediated functions of short chain free fatty acids. *Nature Chemical Biology*, 15 (5), 489–498.

P091 | Chebulinic acid alleviates cognitive impairments in AD model of rats via MAPK

Rimpi Arora¹; Rahul Deshmukh²

¹ISF College of Pharmacy; ²MRSP TU Bathinda

Background and Purpose: Stress-activated protein kinases such as p38 MAPK have been implicated in the pathogenesis of Alzheimer's disease (AD). This study was designed to investigate neuroprotective mechanisms. Chebulinic acid (ChA) in ICV-STZ (streptozotocin) and ICV-A β (amyloid- β) induced cognitive deficits, oxidative stress, neuroinflammation, along with altered neurochemistry via p38 MAPK.

Experimental Approach: STZ and A β were infused bilaterally twice at the dose of 3 mg·kg⁻¹ per 1 μ l per 1 min (ICV), on days 1 and 3 and 3 nmol per 3 μ l on day 0 respectively after surgery. ChA (25, 50, and

100 mg·kg⁻¹, p.o.) was administered from the seventh day onwards up to the 21st day following the first STZ and A β infusion. The Morris water maze (MWM) and object recognition task (ORT) were applied to measure cognitive performance. On day 22, all of the rats were killed for evaluation of molecular alterations and neurodegeneration.

Key Results: Rats with ChA showed higher performance in MWM and ORT than rats in the STZ and A β groups whose memory performance declined compared to control group, which correlated with high number of degenerating neurons and increase in p38 MAPK, whereas ChA reversed these STZ- and A β -triggered cognitive and molecular alterations.

Conclusion and Implications: Results of the present study thus demonstrated the role of p38 MAPK in cognitive deficits, neurochemical alterations, and increase in oxidative–nitritive stress and neuroinflammatory markers following STZ and A β . To sum up, we can say that the healing effect of ChA in STZ- and A β -induced neurodegeneration opens a new door for the development of AD treatment as an adjuvant when their action mechanism was explained in detail.

REFERENCES

- Arora, R. B., Kumar, K., & Deshmukh, R. R. (2016). Embelin attenuates intracerebroventricular streptozotocin-induced behavioral, biochemical and neurochemical abnormalities in rats. *Molecular Neurobiology*. <https://doi.org/10.1007/s12035-016-0182-y>
- Chang, C. L., & Lin, C. S. (2012). Phytochemical composition, antioxidant activity, and neuroprotective effect of *Terminalia chebula* Retzius extracts. *Evidence-based Complementary and Alternative Medicine*, 2012, 1–7.

TABLE 1

Groups	MDA (nmol·mg ⁻¹ protein)	Nitrite (μ mol·mg ⁻¹ protein)	GSH (μ mol·mg ⁻¹ protein)
Sham control	0.365 \pm 1.37	7.72 \pm 0.25	2.129 \pm 0.23
ICV-STZ	1.933 \pm 2.44 ^a	26.5 \pm 0.54 ^a	0.029 \pm 0.08 ^a
STZ + ChA (25 mg·kg ⁻¹ , i.p.)	0.930 \pm 2.32 ^b	14.59 \pm 0.33 ^b	0.099 \pm 0.18 ^b
STZ + ChA (50 mg·kg ⁻¹ , i.p.)	0.705 \pm 2.75 ^{b,c}	13.54 \pm 0.21 ^{b,c}	1.026 \pm 0.28 ^{b,c}
STZ + ChA (100 mg·kg ⁻¹ , i.p.)	0.663 \pm 2.35 ^{b,c,d}	10.44 \pm 0.41 ^{b,c,d}	1.070 \pm 0.28 ^{b,c,d}
ICV-A β	1.884 \pm 1.67 [*]	13.92 \pm 1.42 [*]	0.125 \pm 0.17 [*]
A β + ChA (25 mg·kg ⁻¹ , i.p.)	0.850 \pm 2.32 ^{**}	11.85 \pm 0.33 ^{**}	0.183 \pm 0.18 ^{**}
A β + ChA (50 mg·kg ⁻¹ , i.p.)	0.635 \pm 0.75 ^{***}	9.84 \pm 0.34 ^{***}	1.079 \pm 0.88 ^{***}
A β + ChA (100 mg·kg ⁻¹ , i.p.)	0.456 \pm 1.35 ^{*,#}	8.44 \pm 0.41 ^{*,#}	1.156 \pm 0.28 ^{*,#}

Oral Communications, Sunday 15th December, 15:00

Cardiovascular and Respiratory Pharmacology Oral Communications 1

OC002 | Determining the positive allosteric effects of VCP521 on the adenosine A₁ receptor in vitro using NanoBRET and in vivo using Doppler flowmetry

Samantha Cooper; Edward Wragg; Julie March; Stephen Hill; Jeanette Woolard

University of Nottingham

Background and Purpose: Adenosine A₁ receptors offer protection against cardiovascular ischaemia (Burnstock, 2017). However, A₁ receptor agonists are limited by cardiovascular side effects (Burnstock, 2017). A₁ receptor-specific, positive allosteric modulators (PAMs, e.g., VCP521) are considered as therapeutic alternatives. Here, we used (a) a bioluminescence energy transfer (NanoBRET) proximity assay to identify the effect of VCP521 [(2-amino-4-(3,5-bis(trifluoromethyl)phenyl)thiophen-3-yl)(4-chlorophenyl)methanone] on A₁ receptor ligands (Cooper et al., 2019) and (b) in vivo Doppler flowmetry to assess haemodynamic responses to VCP521 in the presence of A₁ receptor ligands.

Experimental Approach: As described previously, specific ligand binding to rat A₁ receptors was measured using NanoBRET (Cooper et al., 2019). Fluorescent antagonist, CA200645, was used to monitor binding of unlabelled ligands. Cells were incubated with drug for 1 hr at 37°C, and the NanoLuc substrate (furimazine) was added 5 min prior to BRET measurement (Cooper et al., 2019). Increasing concentrations of adenosine, CCPA, VCP521, and DPCPX were added simultaneously with CA200645 (25 nM). VCP521 allosteric effects were measured

using increasing concentrations of adenosine or CCPA, in the presence of VCP521 (3–30 μM, n = 5).

Under anaesthesia, Doppler flow probes were implanted in Sprague–Dawley rats for measurement of vascular conductance (VC) in the renal, mesenteric, and hindquarters vascular beds. Heart rate (HR) and mean arterial pressure (MAP) were measured by intra-arterial catheters, and intravenous catheters were implanted for drug administration (Carter et al., 2016). Procedures were approved by the University of Nottingham Animal Welfare Ethical Review Board, under Home Office Project and Personal License Authority. Compounds were prepared in propylene glycol buffer (5% PEG and 2% Tween, in saline). Haemodynamic responses to VCP521 (12–120 μg·kg⁻¹·min⁻¹, n = 8) in the presence of vehicle or DPCPX (0.1 mg·kg⁻¹) and adenosine (30–300 μg·kg⁻¹·min⁻¹) or CCPA (100–1,000 ng·kg⁻¹·min⁻¹) in the presence of vehicle or VCP521 (120 μg·kg⁻¹·min⁻¹, n = 8) were recorded for 4 hr.

Key Results: In vitro, VCP521 demonstrated strong PAM activity through enhancement of adenosine and CCPA binding affinity for the rat A₁ receptor (Table 1). In vivo, VCP521 alone caused a significant bradycardia, which was attenuated by DPCPX, and vasoconstriction in the hindquarters vascular bed. No significant changes were observed in MAP, or the renal and mesenteric VCs. Interestingly, VCP521 did not appear to modulate adenosine- or CCPA-mediated responses.

Conclusion and Implications: These data show that VCP521 is a strong PAM of rat A₁ receptors in vitro. The small in vivo effect of VCP521 alone may be due to a small A₁ receptor agonist effect or a consequence of positive allosterism of endogenous adenosine in vivo. However, enhancement of agonist haemodynamic response was not observed, highlighting the complexity of PAM effects in vivo.

REFERENCES

Burnstock (2017). *Circulation Research*, 120(1), 207–228.
 Carter, et al. (2016). *FASEB*, 31(3), 1193–1203.
 Cooper, et al. (2019). *British Journal of Pharmacology*, 176(7), 864–878.

TABLE 1 The effect of three different concentrations of allosteric modulator (VCP521) on agonist (adenosine and CCPA) pIC₅₀ values, determined by the inhibition of CA200645-specific binding of rat Nluc-A1-AR

VCP521	pIC ₅₀ ± SEM			
	0 μM	3 μM	10 μM	30 μM
Adenosine (n = 5)	4.06 ± 0.15	4.60 ± 0.13	4.91 ± 0.18*	5.18 ± 0.15*
CCPA (n = 5)	6.11 ± 0.07	6.70 ± 0.17	7.12 ± 0.17*	7.37 ± 0.18*

*P < .05, compared to 0 VCP521, one-way ANOVA, post hoc Tukey's test.

OC014 | β_2 -adrenoceptor agonists dephosphorylate ERK in human airway epithelial cells via canonical, cAMP/PKA-dependent signalling: No evidence of a role for β -arrestin-2

Omar Hamed; Radhika Joshi; Mark Giembycz

University of Calgary

Background and Purpose: In addition to promoting β_2 -adrenoceptor (β_2 -AR) internalization, β -arrestin-2 (β -arr2; gene name: ARRB2) can lead to the activation of ERK1 and ERK2. In vivo, β -arr2-dependent ERK1/2 activation in airway epithelial cells (AECs) is proposed to contribute to the adverse effects of chronic β_2 -AR agonist monotherapy in asthma (Nguyen et al., 2017). The present study describes the in vitro effects of β_2 -AR agonists on ERK phosphorylation in AECs and the role of canonical and non-canonical signalling.

Experimental Approach: ERK phosphorylation was measured by Western blotting in human BEAS-2B AECs, human primary bronchial epithelial cells (HBEs), and HEK293 β_2 cells expressing the human recombinant β_2 -AR. Adenovirus-mediated overexpression of an inhibitor (PKI α) of cAMP-dependent protein kinase (PKA) and gene silencing were used to interrogate the role of G_s -dependent signalling. β -arr2-dependent responses were studied in native and clonal BEAS-2B cells in which ARRB2 was deleted by CRISPR/CAS9 gene editing.

Key Results: In unstimulated HEK293 β_2 cells, pERK1/2 was low but was increased in a concentration-dependent manner by the β_2 -AR agonists, salmeterol and formoterol. In contrast, ERK1/2 was partially phosphorylated in BEAS-2B cells and in HBEs, and salmeterol and formoterol paradoxically caused concentration-dependent dephosphorylations (EC_{50} s: \sim 600 and \sim 10 pM, respectively, in both cell types). This effect was rapid, time dependent (Figure 1), antagonized by ICI 118,551, and prevented in cells expressing PKI α . In BEAS-2B cells and HBEs, β_2 -AR agonists up-regulated dual-specificity

phosphatase 1 (DUSP1). This was PKA dependent, and gene silencing established that it was partly responsible for β_2 -AR-mediated ERK dephosphorylation. ERK1/2 was also dephosphorylated in AECs treated with forskolin (10 μ M) and the EP $_2$ and EP $_4$ receptor agonists, ONO-AE1-259 and ONO-AE1-329, respectively. In contrast, EGF (10 ng·ml $^{-1}$, Figure 1), histamine (10 μ M), and carbachol (10 μ M) enhanced ($>$ 2-fold) basal ERK phosphorylation in native and β -arr2 $^{-/-}$ BEAS-2B cells. Moreover, formoterol-induced ERK dephosphorylation was not affected by ARRB2 deletion (Figure 1). Carvedilol, a β_2 -AR antagonist and a β -arr-biased agonist, did not promote ERK phosphorylation in AECs contrary to its effect in HEK293 β_2 cells.

Conclusion and Implications: β_2 -Adrenoceptor agonists inhibit basal ERK phosphorylation in human AECs by a cAMP/PKA signalling mechanism that involves the up-regulation of DUSP1. The absence of β -arrestin-dependent ERK activation indicates that non-canonical signalling is cell-type dependent.

REFERENCE

Nguyen, L. P., Al-Sawalha, N. A., Parra, S., Pokkunuri, I., Omoluabi, O., Okulate, A. A., ... Bond, R. A. (2017). β_2 -Adrenoceptor signaling in airway epithelial cells promotes eosinophilic inflammation, mucous metaplasia, and airway contractility. *Proceedings of the National Academy of Sciences of the United States of America*, 114, E9163–E9171.

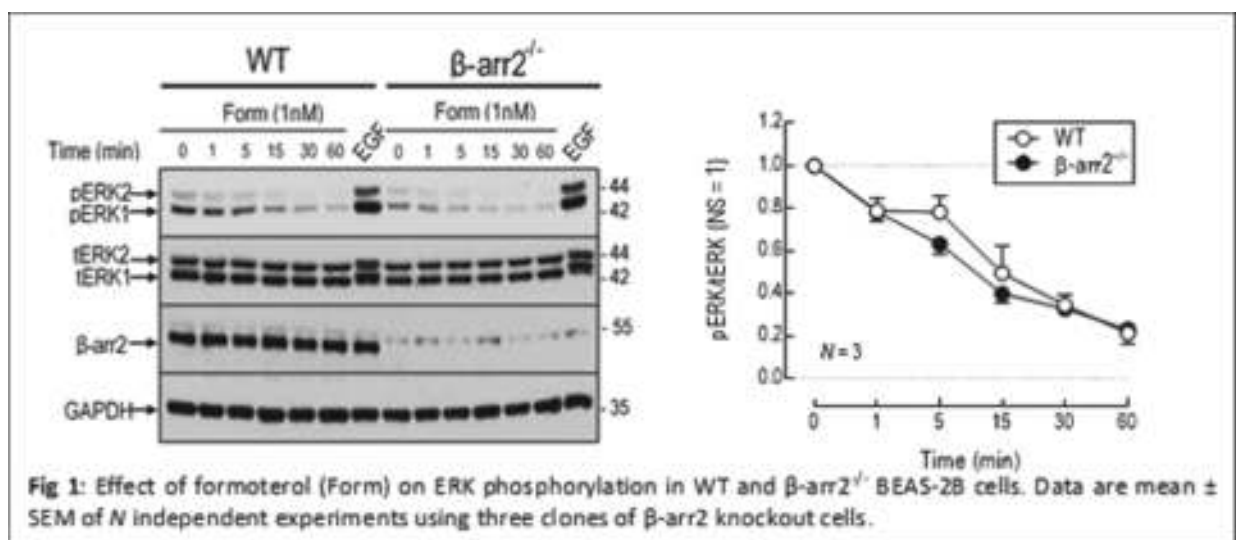
Drug Discovery, Development and Evaluation Oral Communications 1

OC019 | Investigating the relationship between binding kinetics and antagonist action at the β_2 adrenoceptor using luciferase complementation effector recruitment assays

Hannah Lockington; Nicola Dijon; Steven Charlton;

Nicholas Holliday

University of Nottingham



Background and Purpose: NanoLuc-based luciferase complementation assays (NanoBIT; Dixon et al, 2016; Wan et al., 2018) provide new approaches to measure real-time GPCR recruitment of signalling effectors. For example, they allow the kinetics of receptor signalling to these pathways, and the time-dependent effects of

antagonists on these responses, to be monitored continuously within the same assay. Here, we use NanoBIT mini $G\alpha s$ and β -arrestin recruitment assays for the β_2 adrenoceptor (β_2AR) to investigate how the antagonist mode of action at different times relates to ligand binding kinetics.

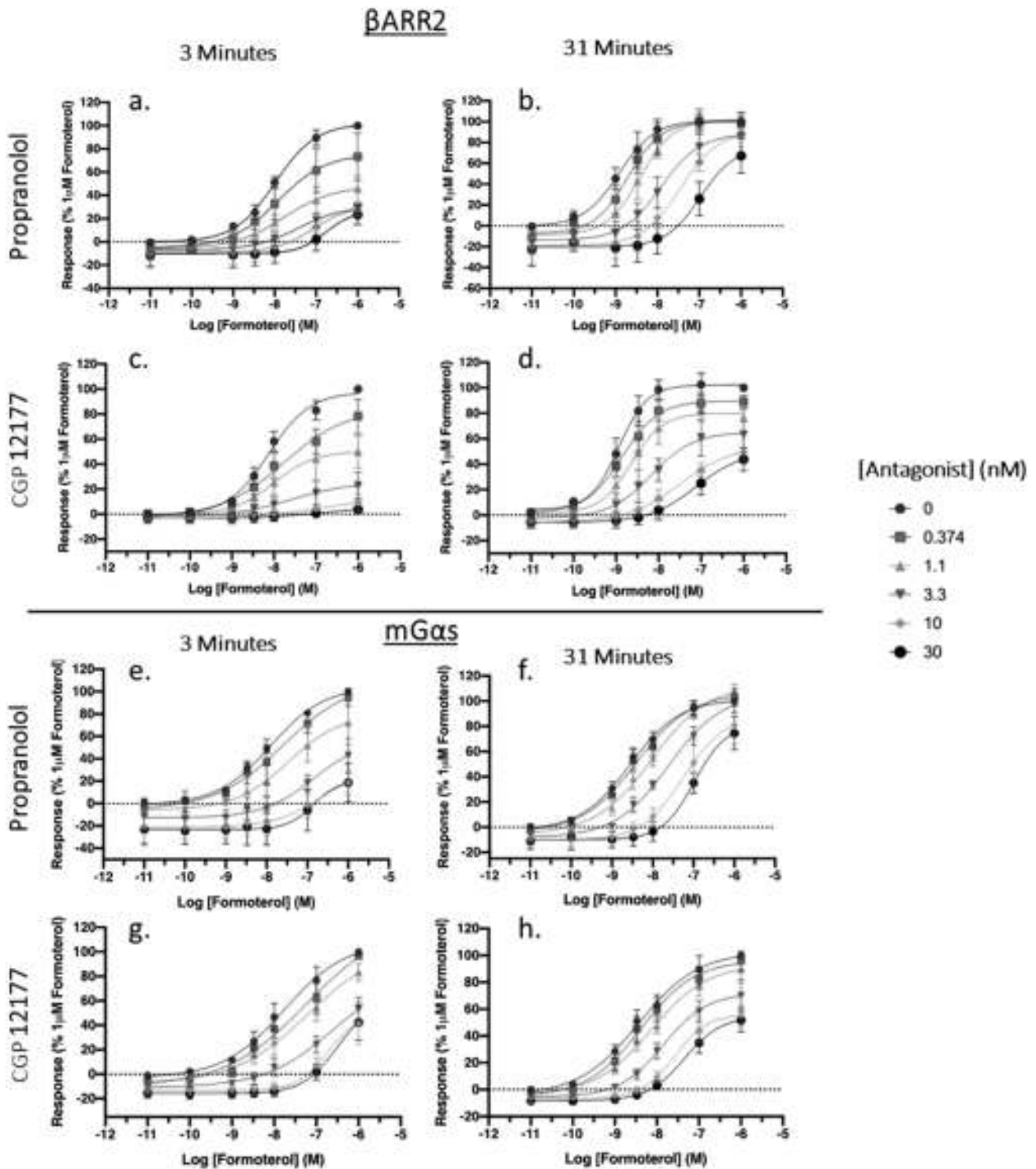


FIGURE 1 Antagonism of formoterol stimulated β -arrestin2 (a.-d.) and $mG\alpha s$ (e.-h.) responses following propranolol (a., b., e. & f.) and CGP12177 (c., d., g. & h.) pre-incuba and 31 minutes following agonist addition. Data represent pooled values (mean \pm s.e. independent experiments performed in duplicate). Relative maximal responses quantified $1\mu M$ formoterol response, in the absence of antagonist.

Experimental Approach: HEK293T cells stably expressed SNAP-tagged β_2 AR fused to C-terminal 18-kDa LgBiT luciferase fragment and the 11-amino acid SmBiT fused to either β -arrestin-2 or an engineered $G_{\alpha s}$ GTPase domain (mini $G_{\alpha s}$; m $G_{\alpha s}$). NanoBiT assays were conducted in cells in 96-well plates in HBSS/0.1% BSA at 37°C. Cells were pre-incubated with propranolol or CGP12177 (0.37–30 nM; 10 min; 37°C), followed by furimazine incubation (5 min; 37°C) and addition of formoterol. Luminescence was monitored for 61 min (BMG Pherastar Platereader, 37°C). Membrane preparations containing Lumi4-Tb-labelled SNAP- β_2 AR-LgBiT receptors were used in time-resolved FRET (TR-FRET) competition association assays (in HBSS; 37°C), to determine kinetic binding parameters of propranolol and CGP12177, using BODIPY-FL-PEG8-(S)-Propranolol as the tracer ligand. Concentration–response curves were fitted in GraphPad Prism v7, with pooled pA_2 and kinetic parameters as mean \pm SEM ($n \geq 4$).

Key Results: Propranolol and CGP12177 both demonstrated insurmountable antagonism when peak formoterol responses were measured at 3 min for β -arrestin-2 and m $G_{\alpha s}$ recruitment, with reduced maximal response observed at higher concentrations of antagonist (Figure 1a,c,e,g). At 31-min post-agonist addition, the antagonism by propranolol was surmountable with pA_2 values of 9.40 ± 0.15 and 8.59 ± 0.09 in β -arrestin-2 and m $G_{\alpha s}$ assays, respectively (Figure 1b,f). However, insurmountable CGP12177 antagonism of formoterol responses persisted at this timepoint. In TR-FRET β_2 AR-LgBiT assays, the CGP12177 dissociation rate constant (k_{off} $0.039 \pm 0.007 \text{ min}^{-1}$) was significantly slower than for propranolol (k_{off} $0.350 \pm 0.044 \text{ min}^{-1}$) with kinetic K_{D5} of 1.79 ± 0.38 and $2.48 \pm 0.71 \text{ nM}$, respectively.

Conclusion and Implications: NanoBiT complementation assays can monitor the transition from insurmountable to surmountable antagonism of agonist responses at the β_2 AR, as equilibrium is approached. The different rates of this transition for propranolol and CGP12177 are consistent with their respective dissociation rates from the β_2 AR.

ACKNOWLEDGEMENT

H.L. was supported by a BPS summer vacation studentship.

REFERENCES

- Dixon, A. S., et al. (2016). *ACS Chemical Biology*, 11, 400–408.
Wan, Q., et al. (2018). *The Journal of Biological Chemistry*, 293(19), 7466–7473.

OC021 | *Lumbriculus variegatus*: A novel in vivo model organism for pharmacology research

Aidan Seeley; Lisa Wallace; Kian Sobhanpanah; Andrew Emm; Mairead Davies

Swansea University

Background and Purpose: Animal models are valuable tools in pharmacological research and drug development. However, due to resource and regulatory constraints, a diminishing number of pharmacologists are adequately trained in the use of in vivo systems (ABPI, 2005, 2008). Here, we propose the use of an aquatic worm, *Lumbriculus variegatus*, as an alternative in vivo drug testing model. This species is not covered under the Animal (Scientific Procedures) Act 1986 and, therefore, presents fewer ethical and regulatory issues.

Experimental Approach: *L. variegatus* have been shown to display two stereotypical behaviours that are easily observed and quantified in a laboratory setting with minimal specialised equipment. Stimulation of the anterior section results in retraction and reversal of body position, while stimulation of the tail elicits helical swimming. We measured the ability of *L. variegatus* to complete these movements after 10 min of exposure to the anaesthetic lidocaine (0–1 mM) or adenosine receptor antagonist, caffeine (0–10 mM). The ability to perform stereotypical movement was graded as 1 = no movement, 2 = partial movement, and 3 = full movement. Statistical significance was determined by a non-parametric paired *t* test or a one-way ANOVA. Using rapid image collection, we also measured free locomotion of the worms before and during drug treatment as well as 10 min and 24 hr after treatment. Statistical significance was determined by a paired *t* test or a one-way ANOVA.

Key Results: For lidocaine, we found that *L. variegatus* body reversal ($P = .031$, $n = 6$) and helical swimming ($P = .031$, $n = 6$) can be inhibited at doses as low as 0.5 mM. We also found that free locomotion was significantly inhibited at 0.5 mM ($P = .008$, $n = 6$) and 1 mM ($P < .001$, $n = 6$). There was no significant difference in locomotor activity between pre-lidocaine and 24 hr after lidocaine treatment ($P = .941$, $n = 6$). The ability to complete stereotypical movements was also tested. For treatment with caffeine, we found that, like lidocaine, it decreased the ability of *L. variegatus* to perform body reversal ($P = .026$, $n = 6$) and helical swimming ($P = .026$, $n = 6$) movements. Moreover, the 10-mM dose of caffeine was shown to have long-term inhibitory effects on body reversal ($P = .029$, $n = 6$) and helical swimming ($P = .042$, $n = 6$) 24 hr after exposure.

Conclusion and Implications: Our data show that behavioural measurements can be performed on *L. variegatus* and that drug treatment can alter these behaviours. This demonstrates the potential for *L. variegatus* for use as a novel in vivo model system. Full development of this model could lead to the reduction or replacement of vertebrate animals in some pharmacological tests, a principle of the NC3Rs.

Molecular and Cellular Pharmacology Oral Communications 1

OC001 | Discovery of a small-molecule toxin with inhibitory activity at human P2X4 ion channels

Lucka Bibic¹; Volker Herzig²; Glenn F. King²; Mark Searcey¹; Leanne Stokes¹

¹University of East Anglia; ²Institute for Molecular Bioscience, University of Queensland

Background and Purpose: Today, one in five adults experience chronic pain, and this figure increases for those >65 years old. However, frustration is mounting over the inadequate treatment for chronic neuropathic pain since its symptoms are difficult to treat and often resistant to opioids. Processing of pain signals relies on the activities of ion channels with some of the P2X receptors being important players (Stokes, Layhadi, Bibic, Dhuna, & Fountain, 2017). Animal venoms can be used to gain insights into potential new modulators for ion channels. We have recently developed and validated a variety of quantitative fluorescent-based high-throughput screening (HTS) cell-based assays for screening animal venoms against P2X receptors (Bibic, Herzig, King, & Stokes, 2019). Here, we extend these data and report a discovery of a novel toxin with inhibitory activity against human P2X4.

Experimental Approach: Using our HTS assays (Fura-2-AM, YOPRO-1, and Calcium 6) on a variety of stable 1321N1 or HEK293 cell lines expressing hP2X3, hP2X4, or hP2X7, we tested 180 crude venoms and performed fractionation on those with either inhibitory or potentiating effects on human P2X4. The mouse BV2 cell line was used as a model of microglia. Fractionation of crude spider venoms was performed using RP-HPLC, and molecular identification of the inhibitory fractions was performed by MALDI-TOF, LC-MS, and MS-MS. We carried out a fragment-based screen and performed chemical synthesis, homology modelling, and in silico ligand docking studies.

Key Results: We found a structurally novel toxin with a potent inhibitory action at hP2X4 with no modulating effect on hP2X7, hP2X3, or hNMDA 1A/2A receptors. Species differences were evident with no effect at rat P2X4 and only modest effect on mouse P2X4. Using the identified toxin (compound 1) as a structural guide, the fragment-based screening was carried out and a number of smaller toxin analogues were chemically synthesized. One of them, LA-3, was found to block the hP2X4 with IC₅₀ of 9.7–18.6 μM and showed selectivity to hP2X4 over hP2X3, hP2X7, and rP2X4 with a modest inhibition at mP2X4 (IC₅₀ = 365.4 μM). Due to the differential sensitivity of LA-3 to block P2X4 orthologues, homology models of human, mouse, and

rat P2X4 were built and the potential binding sites were identified. The validation of the predicted amino acid residues in binding LA-3 is currently in progress.

Conclusion and Implications: We discovered a novel toxin from a spider venom with inhibitory activity at human P2X4 ion channels that shows selectivity at hP2X4 over other P2X receptors. In addition to small molecules, our HTS showed some potential inhibitory peptides that might block hP2X4 receptor. Further characterization and validation is required to understand whether these novel compounds could be useful as analgesics.

REFERENCES

- Bibic, L., Herzig, V., King, G. F., & Stokes, L. (2019). Development of high-throughput fluorescent-based screens to accelerate discovery of P2X inhibitors from animal venoms. *Journal of Natural Products*. accepted
- Stokes, L., Layhadi, J. A., Bibic, L., Dhuna, K., & Fountain, S. J. (2017). P2X4 receptor function in the nervous system and current breakthroughs in pharmacology. *Frontiers in Pharmacology*, 8, 291.

OC003 | Single-nucleotide polymorphisms in GPR75 alter receptor-mediated signalling and localisation

Cameron Malcolm; Jean Iyinnikkel; James Hislop; Fiona Murray

Institute of Medical Sciences, University of Aberdeen

Background and Purpose: GPR75, also known as retinal GPCR, is an orphan GPCR that is highly expressed in the retina (Sauer et al., 2001). Single-nucleotide polymorphisms (SNPs) in the coding sequence of GPR75 are associated with age-related macular degeneration (AMD) (Sauer et al., 2001); AMD is the biggest cause of sight loss in the UK. The retinal expression of GPR75 and GPR75 SNPs associated with AMD suggests that this GPCR could be a novel target for the disease. We aimed to determine the functional significance of AMD-associated GPR75 SNPs.

Experimental Approach: Site-directed mutagenesis (QuikChange II, Agilent Technologies) was used to introduce SNPs (Table 1) into human GPR75 (OriGene). WT-GPR75 and SNPs-GPR75 (subcloned into Flag-tagged pcDNA3.1) were transfected in HEK293 cells (lipofectamine, Thermo Fisher), and GPR75 expression was confirmed using real-time PCR and Western blots. cAMP accumulation was measured using a cAMP ELISA (Enzo Life Sciences) in cells pre-incubated with IBMX (200 μM) and then stimulated with forskolin (1 μM). Proliferation was measured via [³H]-thymidine incorporation (1 μCi·ml⁻¹, PerkinElmer). Dual-colour ratiometric imaging (FLAG-AF594 and Flag-AF-647 antibody) was used to visualise the trafficking of GPR75 (FACS Calibur II). Golgi localisation was determined using pmTurquoise2-Glogi. All data are presented as mean ± SEM and compared via ANOVA or Student's *t* test.

TABLE 1 GPR75 SNPs

SNP	N78K	S108T	T135P	A116T	Q234X
Amino acid change	Asparagine–lysine	Serine–threonine	Threonine–proline	Alanine–threonine	Glutamine–stop
Single base change	(AAC–AAA)	(AGC–ACC)	(ACA–CCA)	(GCT–ACT)	(CAA–TAA)

Key Results: GPR75 RNA and protein were increased in HEK293 cells transfected with WT-GPR75 and SNPs-GPR75. Overexpression of WT-GPR75, T135P, N78K, S108T, and A116T decreased cAMP accumulation (155.7 ± 6.4 , 183.7 ± 8 , 196.3 ± 8.4 , 144 ± 13 , and 191 ± 14.7 , respectively, vs. 251.7 ± 11.5 pmol per million cells, $P < .05$, $n = 3$); however, this was not seen in Q234X (282.3 ± 11.3 vs. 251.7 ± 11.5 pmol per million cells, $n = 3$). Increased WT-GPR75, T135P, N78K, S108T, and A116T increased proliferation of HEK293 cells (732.4 ± 83.7 vs. $1,359.8 \pm 77.3$, $1,472.2 \pm 131.7$, $1,386 \pm 89.3$, $1,438.8 \pm 193.8$, and $1,037.8 \pm 59.7$ cpm, respectively, $P < .05$, $n = 3$), but Q234X did not (732.4 ± 83.7 vs. 799.8 ± 95.3 cpm, respectively, $n = 3$). WT-GPR75, T135P, N78K, and S108T, but not A116T, recycled back to the surface at similar rates ($17.9 \pm 2.1\%$, $23.9 \pm 0.9\%$, $20 \pm 2\%$, $10.9 \pm 2.9\%$, and $4.5 \pm 1.5\%$ of 60-min internalised fraction, $n = 3$). Q234X was not expressed on the plasma membrane but colocalised, in part, with the golgi.

Conclusion and Implications: GPR75, which is constitutively active, decreased cAMP accumulation and increased cellular proliferation. Q234X completely abolished GPR75-mediated signalling and prevented localisation of the receptor to the plasma membrane. In conclusion, GPR75 SNPs associated with AMD are functional and may give potential insight into the pathophysiology of the disease and provide evidence that GPR75 is a novel target for AMD.

REFERENCE

Sauer, C. G., et al. (2001). *British Journal of Ophthalmology*, 85(8), 969–975.

OC004 | Ligand-directed covalent labelling of the adenosine A_{2A} receptor with a fluorescent tag

Leigh Stoddart; Omolade Otun; Nicholas Kindon; Stephen Briddon; Barrie Kellam; Stephen Hill

University of Nottingham

Background and Purpose: To study the localisation of GPCRs in their native cellular environment requires their visualisation through fluorescent labelling. To overcome the requirement for genetic modification of the receptor or the limitations of dissociable fluorescent ligands, we have designed a fluorescent antagonist, NDK174, in which the linker incorporated between pharmacophore (ZM241385) and fluorophore (sulfo-cyanine5) is able to facilitate covalent linking of the fluorophore to the adenosine A_{2A} receptor (A_{2A}R) (Miki et al., 2014). The ligand is designed so that, when bound, a suitably positioned phenyl ester group, with tunable chemical reactivity, is in proximity to a

nucleophilic amino acid (e.g., lysine) with which it reacts and transfers the linker and fluorophore cargo forming a covalent bond. This leaves the fluorophore attached to the receptor and allows dissociation of the antagonist. Here, we characterised the pharmacology and imaging properties of NDK174 at the A_{2A}R to determine its ability to covalently transfer a fluorophore to the receptor.

Experimental Approach: NDK174 was synthesised at the University of Nottingham. Membranes were prepared from HEK293 cells expressing SNAP-tagged A_{2A}R or adenosine A₃ receptor (A₃R) that were labelled with Lumi4Tb as described previously (Sykes & Charlton, 2018). Saturation and dissociation experiments were performed on these resulting membranes and the signal between the donor (Lumi4Tb) and the acceptor (sulfo-cyanine5) monitored by time-resolved FRET (TR-FRET), and data were analysed using GraphPad Prism. Confocal imaging was performed on SNAP-A_{2A}R-expressing HEK293 cells, and images were captured using a Zeiss 880 Laser Scanning Microscope.

Key Results: Saturation TR-FRET experiments showed that the apparent affinity of NDK174 at the A_{2A}R increased with longer incubation periods, with no specific signal seen after 30 min but an apparent pK_D of 7.03 ± 0.07 ($n = 3$) after 5 hr. No significant reduction in the TR-FRET signal was observed 2 hr after addition of 10- μ M ZM241385. No specific binding was observed up to 500-nM NDK174 at A₃R. NDK174 showed clear membrane labelling of the A_{2A}R in live cells using confocal imaging, which was prevented by pre-incubation with 10- μ M ZM241385. This labelling persisted for 60 min following ligand washout or the addition of 10- μ M ZM241385.

Conclusion and Implications: These data suggest that NDK174 is capable of covalently labelling the A_{2A}R with a fluorescent tag in a ligand-directed manner. Further work is required to confirm this labelling such as mutation of the target lysine for covalent attachment of the fluorophore.

REFERENCES

Miki, et al. (2014). *Chemistry & Biology*, 21, 1013–1022.
Sykes, & Charlton (2018). *Methods in Molecular Biology*, 1824, 177–194.

OC005 | Exploring G-protein coupling to smoothed using BRET biosensors

Brian Hudson¹; Alen Pucko¹; Connie Mackinnon¹; Benjamin Myers²

¹University of Glasgow; ²University of Utah School of Medicine

Background and Purpose: Smoothed (SMO) is a GPCR and component of the sonic hedgehog pathway. Dysregulation of the hedgehog

pathway leads to a number of cancers, and SMO inhibitors have become valuable anti-cancer therapeutics. Although SMO is a GPCR, the importance of G-protein coupling to this receptor is not well understood. We have explored whether BRET biosensors can be used to study G-protein interactions with SMO.

Experimental Approach: We have employed “SPASM” BRET biosensors to assess interactions between SMO and the $\alpha 5$ helix of individual $G\alpha$ proteins (Mackenzie et al., 2019; Malik et al., 2013). For all studies, sensors were either transiently transfected into HEK293T cells or stably expressed in Flp-IN T-Rex 293 cells and then used to assess SMO interactions with one of 10 different G peptides (corresponding to all common $G\alpha$ proteins). Time course and concentration–response studies assessed sensor responses to various SMO drugs. The impact of PTCH1, another component of hedgehog signalling, was assessed by co-transfecting Ptch1 with SMO–SPASM sensors. Potency of SMO inhibitors were calculated as pIC_{50} values, while statistical differences between BRET responses were assessed through one-way ANOVA, two-way ANOVA, or *t* test as appropriate.

Key Results: SMO is a constitutively active GPCR, which is kept inactive by PTCH1. To assess interaction of SMO with various G proteins, we measured the basal BRET from 10 different G-peptide sensors in the absence and presence of Ptch1. Co-expression of Ptch1 significantly ($P < .05$) reduced basal BRET for four of the G peptides: Gi1/2 (44%), Gi3 (55%), G14 (30%), and Gz (42%), while Ptch1 had no effect on: Gs, Gq/11, G12, G13, Go, and G16 sensors. Next, we assessed the impact of the SMO inhibitor cyclopamine (cyc), finding that cyc treatment significantly ($P < .05$) reduced the BRET signal for the Gi1/2, Gi3, G14, and Gz sensors. This inhibition was relatively slow, taking ~45 min to reach maximum effect. Cyc had no effect on BRET when Ptch1 was co-expressed with the sensors, presumably because SMO was already inactivated by Ptch1. To assess the ability of these sensors to study ligand pharmacology, concentration–response curves were generated with the Gi1/2, Gi3, and Gz sensor against several Smo ligands (Table 1). These data show that each sensor is able to assess the potency of these antagonists to inhibit Smo G-protein interaction.

Conclusion and Implications: We have used SPASM sensors to demonstrate that SMO interacts with $\alpha 5$ helix of Gi1/2, Gi3, G14, and Gz. We have further shown that these sensors can assess both time course and pharmacology of SMO drugs, suggesting that the sensor will be valuable tools in identifying new SMO targeting therapeutics.

TABLE 1 Assessing ligand pharmacology at SMO BRET SPASM sensor

Drug	Gi1/2 pIC_{50}^a	Gi3 $pEIC_{50}^a$	Gz pIC_{50}^a
KAAD-cyc	7.28 ± 0.17	7.35 ± 0.17	7.30 ± 0.23
SANT-1	7.74 ± 0.10	7.99 ± 0.11	7.84 ± 0.09
PF04449913	8.25 ± 0.11	8.10 ± 0.11	8.23 ± 0.04
Itraconazole	6.38 ± 0.01	6.74 ± 0.15	6.66 ± 0.15
IHR 1	7.30 ± 0.20	7.21 ± 0.12	7.26 ± 0.13

^a pIC_{50} values shown are mean ± SEM.

REFERENCES

Mackenzie, et al. (2019). *The FASEB Journal*, 33(4), 5005–5017.
 Malik, et al. (2013). *JBC*, 288, 17167–17178.
 Molecular and Cellular Pharmacology Oral Communications 2

OC007 | Pharmacoperone rescue of inactivating mutations in the neurokinin B receptor, NK3R

Ross Anderson¹; Zulfiah Mohamed Moosa¹; Yong Bhum Song²; Ursula Kaiser²; Robert Millar¹; Claire Newton¹

¹University of Pretoria; ²Harvard Medical School

Background and Purpose: Neurokinin 3 receptor (NK3R) is a GPCR involved in regulation of the reproductive axis, with inactivating mutations of the NK3R associated with isolated GnRH deficiency (IGD), resulting in failure to progress through puberty. Most inactivating GPCR mutations result in misfolding of the nascent receptor protein, followed by intracellular retention and degradation. Here, we investigate whether cell membrane expression of retained NK3R mutants can be restored by treatment with a small-molecule cell-permeant NK3R antagonist.

Experimental Approach: Plasmids encoding wild-type (WT) and mutant NK3Rs were labelled with an N-terminal HA-epitope tag and were expressed in HEK293 cells in the presence and absence of *N',2*-diphenylquinoline-4-carbohydrazide NK3R antagonist (M8). An ELISA assay using monoclonal anti-HA antibodies was utilised to measure cell surface expression (intact cells) and total receptor expression (permeabilised cells). Posttranslational modification of NK3R was determined by quantitative Western blotting in the presence or absence of deglycosylation enzymes. Experiments were performed a minimum of three times and presented as bar graphs with statistical significance determined by ANOVA followed by Bonferroni's post hoc test. Signalling was determined by inositol phosphate accumulation assay following stimulation with NK3R ligand with data presented as sigmoidal dose–responses using graph-fitting software to determine values for EC_{50} and E_{max} .

Key Results: Six out of seven mutant receptors tested showed significant intracellular retention by ELISA when compared to WT ($P < .001$; G93D, H148L, Y256H, Y267N, and P353S, $P < .01$; Y315C) with M8 treatment increasing cell surface expression of all retained mutants. Four out of six mutants were rescued to WT receptor levels. Western blotting of cell lysates containing WT or mutant NK3Rs indicated that retained mutants had reduced or absent glycosylation that was restored following treatment with M8 to WT levels in five out of seven mutants. Signalling competency following rescue of cell surface expression was determined for all six retained mutants. Five out of six retained mutants had significantly increased signalling response following stimulation with ligand ($P < .01$; vehicle vs. M8 treatment).

Conclusion and Implications: We have shown that a small-molecule NK3R antagonist, M8, can restore cell surface expression of

intracellularly retained NK3R mutants. Increased glycosylation indicates that trafficking of the rescued mutants through the secretory pathway is restored. Five out of six retained mutants showed an increased signalling response following M8 treatment, indicating that these rescued receptors are functional, validating this approach as a therapeutic strategy for restoring function to inactivating NK3R mutations causing poor cell surface expression.

OC008 | Functional rescue of mutant LH receptors with deficiencies in cell surface expression, hormone binding, and hormone signalling

Claire Newton¹; Ross Anderson¹; Annika Kreuchwig²; Gerd Krause²; Arieh Katz³; Robert Millar¹

¹University of Pretoria; ²Leibniz-Forschungsinstitut fuer Molekulare Pharmakologie (FMP); ³University of Cape Town

Background and Purpose: GPCR mutations have been implicated in many diseases. The majority of inactivating mutations cause receptor misfolding, preventing translocation to the cell membrane. Indeed, we have shown that most mutant LH receptors (LHRs) identified in human patients suffering from reproductive dysfunction are poorly expressed at the cell surface (Newton, Anderson, Katz, & Millar, 2016). Some cell-permeant ligands (pharmacological chaperones) can “rescue” cell surface expression of such mutant GPCRs, presumably by stabilising correct folding of the nascent protein. We have identified an LHR pharmacological chaperone (LHR-Chap/Org 42599) (Newton et al., 2011), and here, we examine the scope of intracellularly retained LHR mutations that it can “rescue” and whether this allosteric agonist can also restore function of mutant luteinising hormone receptors with deficiencies in hormone binding or hormone-induced signalling.

Experimental Approach: Eighteen mutant LHRs, characterised as causing impaired cell surface expression (14/18), hormone binding (2/18), or hormone-induced signalling (2/18) were expressed in HEK 293T cells with N-terminal FLAG epitope tags. Receptor cell surface expression/localisation, hormone binding, and hCG/LHR-Chap signalling were determined by FLAG ELISA, [¹²⁵I]-hCG binding, and G α_{16} -linked [³H]-inositol phosphate accumulation respectively in the presence/absence of LHR-Chap. A minimum of three separate assays were performed, each in triplicate. Signalling data were analysed using a sigmoidal concentration–response model to determine EC₅₀ and maximum response (E_{max}). Significance was determined using Student's *t* test (LHR-CHAP vs. vehicle treated) or ANOVA followed by Dunnett's post hoc test (mutants vs. wild-type), as appropriate. In silico molecular modelling predicted LHR-Chap interactions.

Key Results: LHR-CHAP significantly increased cell surface expression of five out of 14 retained mutants (T461I, L502P, A593P, Del L608-V609, and S616Y) from <10% to 20–70% of wild-type levels ($P < .05$ vs. vehicle). For mutants T461I, L502P, and S616Y, hCG

responsiveness was significantly increased from 2–15% to 15–40% of wild-type following treatment ($P < .05$ vs. vehicle). Rescue by LHR-Chap was limited to those mutants located in transmembrane helices predicted to be stabilised by LHR-Chap binding. LHRs with mutations in the hormone-binding site (C131R and I152T) or in the hinge domain important for hormone-binding-induced signalling (E354K) had good cell surface expression but poor response to hormone stimulation. However, they were responsive to allosteric activation by LHR-CHAP with potencies (EC₅₀) not different to the wild-type receptor (50–80 nM; $P > .05$).

Conclusion and Implications: LHR-Chap can functionally rescue intracellularly retained, hormone-binding-deficient or hormone-signalling-deficient mutant LHRs. However, its effectiveness as a pharmacological chaperone is limited to mutations within TM regions stabilised by its binding and which do not otherwise disrupt receptor function.

REFERENCES

- Newton, C. L., Anderson, R. C., Katz, A. A., & Millar, R. P. (2016). Loss-of-function mutations in the human luteinizing hormone receptor predominantly cause intracellular retention. *Endocrinol*, 157(11), 4364–4377.
- Newton, C. L., et al. (2011). Rescue of expression and signaling of human luteinizing hormone G protein-coupled receptor mutants with an allosterically binding small-molecule agonist. *Proceedings of the National Academy of Sciences of the United States of America*, 108(17), 7172–7176.

OC009 | Tubastatin A rescues vision and elicits with neuroprotection in models of inherited blindness

Husvinee Sundaramurthi¹; Sarah Roche²; Guinevere Grice³; Eugene Dillon¹; Ailís Moran¹; Breandán Kennedy¹

¹University College Dublin; ²University College Cork; ³University of Cambridge

Background and Purpose: Classified as rare diseases, the clinical and genetic heterogeneity of inherited retinal dystrophies (IRD) limits the availability of treatment options, causing a clinical need for drug therapies. Preclinical studies in models of inherited blindness reveal that visual function can be rescued by treatment with broad-spectrum histone deacetylase inhibitors (HDACi). However, both beneficial and side effects were reported in retinitis pigmentosa patients (Bhalla et al., 2013). We hypothesized that selective HDAC6 inhibitors (HDAC6i) can restore vision with increased safety/efficacy and postulated that HIF-1 pathway is involved in the disease pathomechanism in our *dye^{UCD6}* zebrafish model of IRD, harbouring a mutation in *atp6v0e1* (Burr et al., 2016; Leyk et al., 2017).

Experimental Approach: *dye^{UCD6}* larvae were treated with 100- μ M tubastatin A (TubA), 10- μ M tubacin, 10- μ M ACY-1215, or 25- μ M NF2373 (Brindisi et al., 2018) ($n = 12$ *dye*) at 3 days post fertilization (dpf). Visual function was assessed 3 days later using optokinetic response assays (OKR). Protein was isolated from the larval eyes and

analysed by MS. Retinal explants from rd¹⁰/rd¹⁰ mice were treated with increasing concentrations of TubA, for 4 days (n = 4). Retinal morphology from all samples was analysed by light/electron microscopy and immunohistochemistry. *atp6v0e1* was knocked-out in HeLa HRE-GFP^{ODD} cells and analysed for HIF1 α expression. Experiments were performed in triplicates; two-tailed Student's *t* test and one-way ANOVA with Dunnett's multiple comparisons were used for statistical analysis.

Key Results: TubA, tubacin, ACY-1215, and NF2373 significantly improved visual capacity from 0.7 saccades·min⁻¹ on average to 7.9 (P < .0001), 4.6 (P = .0002), 2.6 (P = .0042), and 2.3 (P = .0318) saccades·min⁻¹, respectively, in *dye^{UCD6}*. Photoreceptor morphology was well preserved in HDAC6i-treated larvae. A significant increase in cone arrestin-positive cells (P = .0452) and a non-significant increase in rhodopsin-positive cells were detected in the outer nuclear layer of TubA-treated rd¹⁰/rd¹⁰ mice explants. HIF1 α was up-regulated in *atp6v0e1* knockout HeLa HRE-GFP^{ODD} cells. A total of 258 proteins were differentially expressed in TubA-treated *dye^{UCD6}*. Top altered pathways include ubiquitin-proteasome, phototransduction, and phagocytosis.

Conclusion and Implications: Further analysis and validation of proteomics data is required to understand the disease pathomechanism in *dye^{UCD6}* and to elucidate HDAC6i mechanism of action in restoring vision. HDAC6 inhibition restores visual function and is neuro-protective in models of blindness.

REFERENCES

Bhalla, S., et al. (2013). *The British Journal of Ophthalmology*.
 Brindisi, M., et al. (2018). *European Journal of Medicinal Chemistry*.
 Burr, S. P., et al. (2016). *Cell Metabolism*.
 Leyk, J., et al. (2017). *Cell Death & Disease*.

OC010 | Repurposing the Oxford MediStress Leukocyte Coping Capacity™ assay as a novel point-of-care biomarker of neutrophil function

Caitlin Carr-Knox¹; Sara Shaida²; João Oliveira¹; Colin Hamilton-Davies³; Andrew Smith³; James Fullerton¹

¹Division of Medicine, University College London; ²School of Clinical Medicine, University of Cambridge; ³Department of Anaesthetics and Intensive Care, St. Bartholomew's Hospital, London

Background and Purpose: Quantification of immune function is increasingly recognised as an important part of clinical practice allowing both prognostication and tailoring of ongoing care. Oxford MediStress (OMS) have developed the Leukocyte Coping Capacity™ (LCC) test. This assay uses 10- μ l blood acquired from “finger prick,” phorbol 12-myristate 13-acetate (PMA) stimulation and luminol chemiluminescence to describe leukocyte function in 10 min. To date, the LCC has been marketed as a test of “stress.” This study sought to independently confirm the biological basis of the assay and assess whether the LCC could be repurposed as a dynamic biomarker of neutrophil function.

Experimental Approach: Blood was obtained from a pool of healthy volunteers (male and female, 18–65, n = 10 total, n = 3–5 per experiment) via finger prick (10 μ l via standard lancet) and/or venepuncture. Either whole blood (variably anticoagulated) or its components including leukocyte subgroups formed the substrate of the LCC. The latter were obtained via density gradient centrifugation using Ficoll-Paque PLUS™. The LCC was supplied by OMS as freeze-dried pellets reconstituted in PBS prior to use. After combination of reagents with substrate, samples were incubated for 10 min at 37.5°, before chemiluminescence was quantified (expressed as relative light units [RLU]).

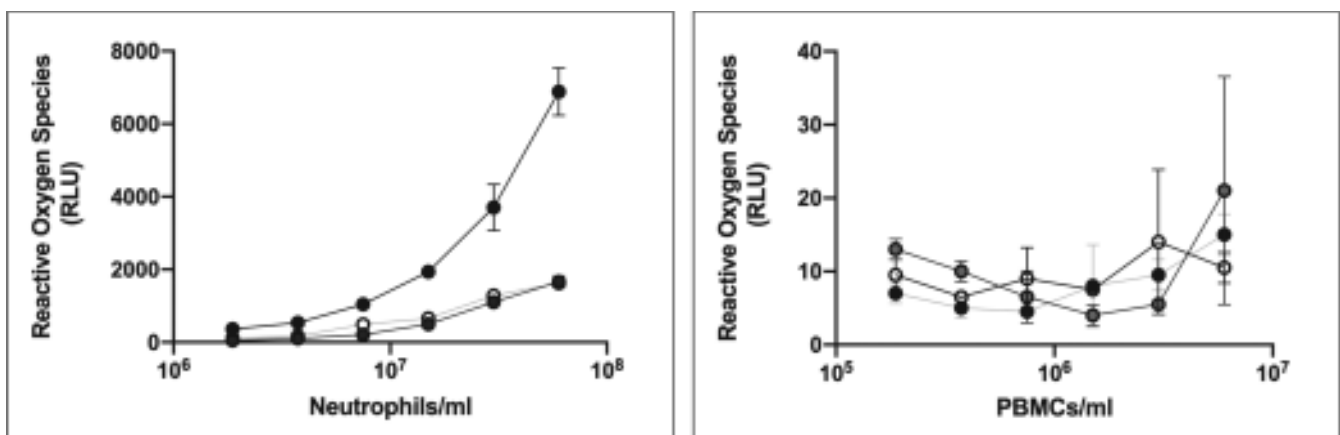


FIGURE 1 Mean ROS production (±SD) at various concentrations of isolated neutrophils and peripheral blood mononuclear cells (PBMCs), expressed as relative light units (RLU). The three lines represent readings from individual subjects (n = 3)

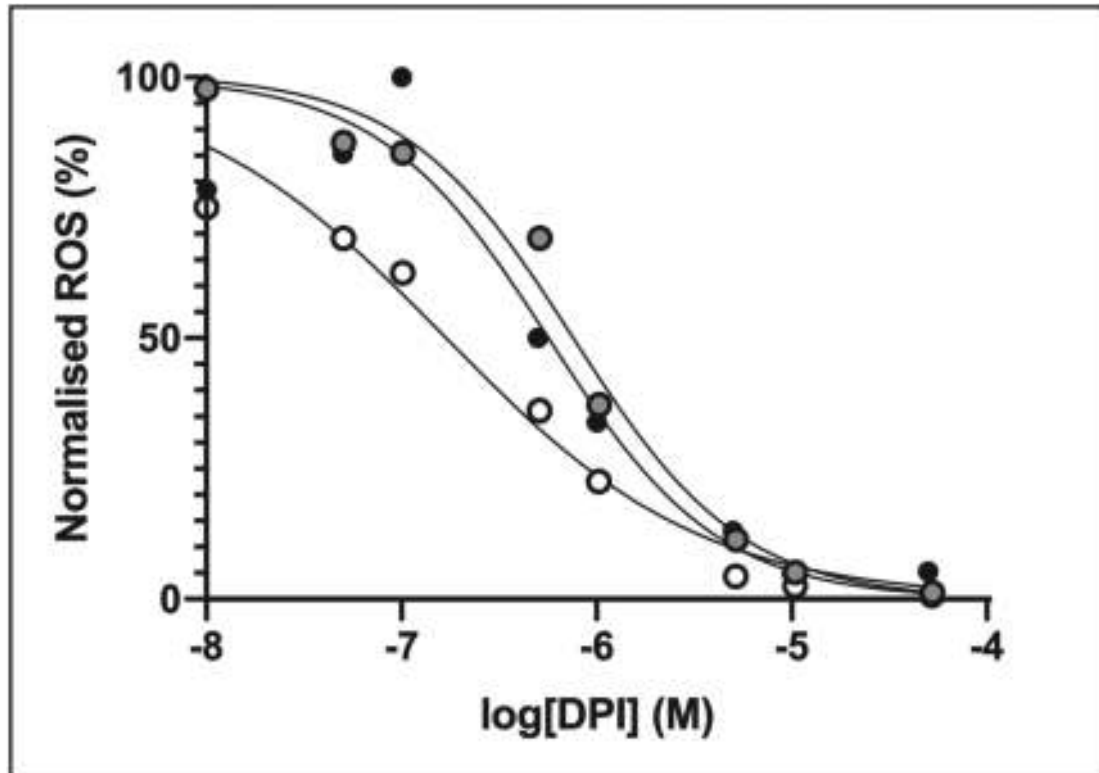


FIGURE 2 ROS production by $10^6 \cdot \text{ml}^{-1}$ neutrophil sample, with dose-dependent inhibition by DPI. Readings normalised to value in absence of DPI. Each line represents an individual subject ($n = 3$)

Diphenyleioidonium chloride (DPI) was used as an inhibitor of neutrophil NADPH oxidase. Ethical approval was granted by the UCL Research Ethics Committee (5060/002).

Key Results: Employing erythrocytes and plasma as substrate for the LCC generated negligible luminescence. Separation of leukocytes into neutrophil and PBMC fractions indicated that the former contributed the entirety of the observed signal in a cell number-dependent manner (Figure 1). This could be inhibited via the addition of DPI (IC_{50} 715 nM) indicating ROS dependence. Non-significant differences were seen between capillary (finger prick) and venous blood or between un-anticoagulated or anti-coagulated (lithium heparin, EDTA, and sodium citrate) samples. Equally, time after bloodletting was not associated with significant signal change (0–240 min). No significant variation was observed in individual healthy volunteer's readings over 1 week (bled day 0, 1, 3, and 7) nor was a circadian effect noted; 10 min was confirmed as the optimal read-time (IQR = 8.75–10.25 min).

Conclusion and Implications: We have confirmed that the OMS LCC easily, specifically, and rapidly (10 min) quantifies neutrophil ROS release using a small volume of blood obtainable from different sources. Corrected for circulating neutrophil number, this allows a description of neutrophil functional capacity: a known marker of immune competence linked to patient outcomes. The LCC warrants further investigation in the clinical environment.

OC011 | Sex differences in macrophage-mediated endothelin-1 clearance

Greg Sutton; Alicja Czopek; Timm Krueger; Filippo Menolascina; Neeraj Dhaun

University of Edinburgh

Background and Purpose: Hypertension is a major risk factor for cardiovascular and chronic kidney disease. However, its cause remains unclear in most cases. Our recent data suggest that macrophages contribute to, and protect from, hypertension by regulating the endothelin (ET) system (Czopek, *Eur Heart J* 2019). ET-1 is the most potent endogenous vasoconstrictor with pro-inflammatory properties. We have shown that macrophage remove ET-1 through the ET_B receptor (ET_BR). As cardiovascular risk varies between men and women, here, we explored if the expression of the ET system and ET-1 clearance varies between male and female mice and with macrophage phenotype.

Experimental Approach: Bone marrow-derived macrophage from 9- to 12-week-old male ($n = 5$) and female ($n = 7$) C57B6J mice were cultured in vitro. LPS/IFN- γ were used to polarise macrophage to a pro-inflammatory/ M_1 phenotype and IL-4/IL-13 for anti-inflammatory/ M_2 polarisation. Gene expression was determined using qPCR. ET-1 concentration was measured by ELISA. Macrophage was then exposed to

2 ng·ml⁻¹ of fluorescently labelled ET-1 (fET-1), and the concentration was measured by fluorescence spectrophotometry after 12 hr. Statistical analyses were performed using a two-way ANOVA with Sidak's multiple comparisons method.

Key Results: Unstimulated macrophage

Male macrophage expressed twofold greater ET_BR than females (*P* < .01). There was no difference in ppET-1 expression between the sexes. Neither male nor female macrophage showed net production of ET-1. Whereas male macrophage cleared all extracellular ET-1, females cleared none (*P* < .05).

M₁ macrophage

Both male and female macrophage expressed ET_BR and ppET-1. Whereas ET_BR levels were similar, male macrophage displayed threefold greater ppET-1 than females (*P* < .05). Net ET-1 production was similar between male and female macrophages (~20 pg·ml⁻¹ at 24 hr). However, male macrophage cleared extracellular ET-1 whereas females did not (*P* < .05).

M₂ macrophage

Both male and female macrophage expressed ET_BR and ppET-1 similarly. Neither males nor females demonstrated net ET-1 production or ET-1 clearance.

Conclusion and Implications: Our data suggest a sex difference in ET system expression and in ET-1 clearance by macrophage. The increased clearance seen with male macrophage is consistent with increased ET_BR expression relative to female macrophage. These differences may be important in the cardiovascular risk difference observed between men and women.

OC012 | Investigating the role of actin in the membrane organisation of the adenosine A_{2B} receptor using single-molecule imaging

Evelyn Garlick¹; Jak Grimes¹; Davide Calebiro²; Stephen Briddon³; Steven Thomas²

¹COMPARE, University of Birmingham; ²University of Birmingham;

³University of Nottingham

Background and Purpose: Cellular organisation of GPCRs plays an important role in determining signalling responses and associated pharmacological parameters. There is increasing evidence that this is relevant in disease. However, the molecular determinants of this organisation are not fully understood. Previous work has identified a

role for the actin cytoskeleton in constraining receptor movement and the creation of signalling "hot spots," (Sungkaworn et al., 2017) but little is known about how the dynamics of the cortical actin itself contribute to this phenomenon. Here, we use super-resolution microscopy techniques to investigate the role of cortical actin in the organisation of the human adenosine A_{2B} receptor (A_{2B}R) at a single-molecule level.

Experimental Approach: A549 cells were transiently transfected with an N-terminal SNAP-tagged human A_{2B}R. For live visualisation of the actin network, cells were additionally transfected with LifeAct-mEGFP. For single-molecule localisation microscopy, SNAP-Surface Alexa Fluor 647-labelled cells (1 μM, 22°C, 20 min) were treated with cytochalasin D (CytoD, 1 μM) or vehicle (Veh) for 30 min at 37°C, fixed, and imaged using a Nikon N-STORM system. Resulting data sets were analysed with ToMATo cluster analysis (Pike et al., 2018). For single-particle tracking, transfected cells were allowed to express for 5 hr, labelled with SNAP-Surface 549 as above and treated with CytoD or Veh for 15 min at 37°C. Imaging was performed at 33 fps on a Nikon N-SIM-S system in H-TIRF mode, before spot tracking and msd-based track analysis. Simultaneous receptor imaging and capture of super-resolved actin was achieved through super-resolution radial fluctuations (SRRF) analysis (Gustafsson et al., 2016).

Key Results: Disruption of normal cortical actin by CytoD had no significant effect on A_{2B}R clustering: cluster area (Veh = 6,388 ± 1,832 nm² and CytoD = 6,367 ± 1,771 nm²; *n* = 3, representing 14 cells per condition, mean ± SEM) and density (Veh = 0.016 ± 0.002 detections·nm⁻² and Cyto D = 0.019 ± 0.002 detections·nm⁻²). In contrast, single-particle tracking experiments indicated that actin disruption caused significant reduction in the fraction of immobile A_{2B}R (*n* = 3, 10 cells Veh, 12 cells CytoD, *P* < .001, unpaired *t* test) and an increase in freely diffusing (*P* = .008) and subdiffusive (*P* = .004) fractions (Table 1). Initial experiments incorporating SRRF indicated that super-resolution imaging of actin was possible on a timescale, which allowed concurrent monitoring of A_{2B}R movement.

Conclusion and Implications: These initial experiments indicate a complex role for actin in mediating A_{2B}R membrane organisation, with potential for different regulatory contributions across organisational scales.

REFERENCES

Gustafsson, et al. (2016). *Nature Communications*, 7(12471).
 Pike, et al. (2018). *bioRxiv*, 400275.
 Sungkaworn, et al. (2017). *Nature*, 550(7677), 543–547.

TABLE 1 A_{2B}R particle trajectory categories (mean ± SEM)

	Particle trajectories (%)			
	Immobile	Subdiffusive	Brownian	Superdiffusive
Vehicle	39.0 ± 1.84	27.7 ± 1.36	30.1 ± 1.51	3.2 ± 0.44
Cyto D	23.7 ± 1.70**	33.8 ± 1.32*	38.0 ± 2.10*	4.5 ± 0.43

P* < .01. *P* < .001 versus vehicle.

Neuropharmacology Oral Communications 1

OC024 | Environmental enrichment and stress: How these factors affect BDNF gene expression in mouse prefrontal cortex

Nívea Silva¹; Gabriel Costa¹; Priti Chivers²; Alexis Bailey³; Rosana Camarini¹¹University of São Paulo; ²University of Surrey; ³St George's, University of London

Background and Purpose: While studies show a decrease in BDNF in the prefrontal cortex (PFC) after environmental enrichment (EE) (Rueda, Teixeira, Yonamine, & Camarini, 2012), others mention that there is no significant change in these neurotrophin levels in the PFC (Pautassi et al., 2017). In addition, chronic stress has already shown both decreased and increased BDNF gene expression in the dorsomedial and ventromedial portions of the CBP, respectively (Calabrese et al., 2015). Since the effects of EE and stress on BDNF expression in PFC have been controversial, the objective of this study was to evaluate the BDNF gene expression in PFC of mice submitted to EE and stress.

Experimental Approach: Male Swiss mice (PND = 50) were exposed to two different environmental conditions: non-enriched (NE) and EE. Animals from the NE group were housed in standard polypropylene cages throughout the experiment. EE mice were housed in large polycarbonate cage, with tubes, running wheels, toys, ramps, and houses (objects changed/moved three times a week). Animals were divided into four groups ($n = 10-15$): non-enriched and non-stressed (NE), non-enriched and stressed (NE_S), enriched and non-stressed (EE), and enriched and stressed (EE_S). After 21 days of EE or NE conditions, the animals were submitted to 11 days of chronic unpredictable stress (CUS), which contained stresses such as restraint stress, wet bed, food/water deprivation, and isolation. Mice were killed via guillotine following 32 days (21 days of EE or NE housing conditions and 11 days of stress exposure). Brains were collected, and the PFC was dissected and maintained in RNAlater[®] solution until analysis of BDNF gene expression. To investigate whether EE could induce changes in BDNF gene expression in the prefrontal cortex of stress-exposed animals, specific exons were chosen from the promoter region of the BDNF gene, including exons 4 and 9. DNA and RNA from the sample were extracted. The RNAs were subjected to a reverse transcription process, generating a converted DNA (cDNA). CDNA was prepared for the real-time PCR reaction by the addition of specific primers and then amplified in a real-time quantitative PCR equipment. From the amplified samples, the gene expression of each sequence was analysed. Kruskal–Wallis test was performed using Dunn's post hoc test, with a 5% significance probability, plotted with Prism 5.0[®]. It is important to point out that all results are normalized

to the NE group. All procedures were approved by the Animal Use Ethics Commission (CEUA) of the University of São Paulo (120/2016). **Key Results:** In exon 4, environmental enrichment significantly reduced the gene expression when compared to the NE group ($P < .001$). A similar result was found for EE_S when compared to the NE ($P < .001$). Also, gene expression in the EE group was lower than in the EE_S ($P < .05$) and lower when compared to the NE_S ($P < .001$). In the region 1 of exon 9, stress caused a significant decrease of gene expression (NE_S vs. NE; $P < .01$). Despite EE itself increased gene expression in this exon region, this increase was not significant ($P > .05$). However, when associated the effects of stress and EE, BDNF gene expression in this region of exon 9 significantly decreased when compared to the NE group (EE_S vs. NE; $P < .001$) and to the EE group (EE_S \times EE; $P < .001$). On the other hand, in the region 2 of exon 9, EE per se was able to increase the gene expression when compared to the NE group (NE vs. EE; $P < .05$) and when compared to the NE_S group (EE vs. NE_S; $P < .001$). Finally, the combination of stress and EE reduced gene expression when compared to the NE group (EE_S vs. NE; $P < .01$) and to EE group (EE_S vs. EE).

BDNF gene expression

Group	Exon 4	Exon 9.1	Exon 9.2
NE ($n = 18$)	1.000	1.000	1.000
NE_S ($n = 18$)	0.847	0.763333**	0.725385
EE ($n = 18$)	0.060***\$.+++	2.151111	2.346111*.+++
EE_S ($n = 18$)	0.408***	0.441111***.###	0.628333**###

* $P < .05$ versus NE.** $P < .01$ versus NE.*** $P < .001$ versus NE.\$. $P < .05$ versus EE_S..+++ $P < .001$ versus NE_S.# $P < .05$ versus EE.### $P < .001$ versus EE.

Conclusion and Implications: These results indicate that the combination of environmental enrichment and stress alters BDNF gene expression in the prefrontal cortex, leading to a lower expression of this neurotrophin in the region.

REFERENCES

- Calabrese, F., Van der Doelen, R. H., Guidotti, G., Racagni, G., Kozicz, T., Homberg, J. R., & Riva, M. A. (2015). Exposure to early life stress regulates Bdnf expression in SERT mutant rats in an anatomically selective fashion. *Journal of Neurochemistry*, 132(1), 146–154.
- Pautassi, R. M., Suárez, A. B., Hoffmann, L. B., Rueda, A. V., Marianno, P., & Camarini, R. (2017). Effects of environmental enrichment upon ethanol-induced conditioned place preference and pre-frontal BDNF levels in adolescent and adult mice. *Scientific Reports*, 7(1), 8574.
- Rueda, A. V., Teixeira, A. M., Yonamine, M., & Camarini, R. (2012 Jul). Environmental enrichment blocks ethanol-induced locomotor sensitization and decreases BDNF levels in the prefrontal cortex in mice. *Addiction Biology*, 17(4), 736–745.

OC025 | Cannabidiol antidepressant-like effect is associated with time-dependent changes in monoamine and glutamate levels in the brain

Gabriela Pandini Silote¹; Sâmia Joca^{2,3}; Gregers Wegener⁴

¹University of São Paulo and Aarhus University; ²Department of Physics and Chemistry, School of Pharmaceutical Science of Ribeirão Preto, USP, Ribeirão Preto, Brazil; ³Aarhus Institute of Advanced Studies, AIAS, Aarhus University, Aarhus, Denmark; ⁴Translational Neuropsychiatry Unit, Department of Clinical Medicine, Aarhus University, Aarhus, Denmark

Background and Purpose: Cannabidiol (CBD) is a compound extracted from *Cannabis sativa* L. that produces antidepressant effect in different paradigms in rodents (Sales et al., 2018). Studies have shown that CBD effects are dependent on brain serotonin (5-HT). However, its neurochemistry profile has not yet been fully elucidated. Therefore, the aim of this study was to investigate CBD effects at different time points after treatment and how that is correlated with changes in monoamine and glutamate levels in brain regions with relevance to depression.

Experimental Approach: Adult male Sprague–Dawley rat (8 weeks of age) from Taconic (Copenhagen, DK) were kept under standard laboratory conditions. The animals were exposed to forced swimming test (FST, 15 min; pretest session), and 24 hr later, they received an i.p. injection of CBD (30 mg·kg⁻¹; 1, 2, and 4 hr), S-ketamine (15 mg·kg⁻¹ 1 hr, positive control), or vehicle (VEH; saline and Tween 80 3%; 1 hr) before the behavioural tests: open field test (OFT, 5 min) and FST (test session, 5 min). After the test, the rats were euthanized and the prefrontal cortex (PFC), striatum (ST), midbrain (MID), and dorsal and ventral hippocampus were dissected (DH and VH, respectively). The monoamines, dopamine (DA), noradrenaline (NA), DOPAC, 5-HT, 5-HIAA, and glutamate were measured using ultra-HPLC (UHPLC) with electrochemical and fluorescence detection. The data were analysed using one-way ANOVA followed by a Dunnett's post hoc test comparing with VEH group. Danish National Committee for Ethics in Animal Experimentation (2016-150201-001105).

Key Results: CBD significantly reduced the immobility time after 2 ($P < .05$) and 4 hr ($P < .0001$), similar to S-ketamine ($P < .05$), characterized as antidepressant-like effect. None of the treatments changed the locomotor activity in the OFT (one-way ANOVA: $F(4, 16) = 0.6029$; $P > .05$). CBD effects on brain neurochemistry were complex: PFC decreased NA at 2 and 4 hr ($P < .05$); MID decreased NA, DA, and glutamate at 2 hr ($P < .05$); and VH decreased DOPAC ($P = .07$) at 2 and 4 hr ($P < .05$). On the other hand, S-ketamine increased the 5-HT levels only in the DH ($P = .06$) without significantly changing other neurotransmitter levels.

Conclusion and Implications: CBD produced an antidepressant-like effect, similar to positive control group (S-ketamine), at 2 and 4 hr after its administration. CBD effects in the FST were associated with changes in the levels of monoamines and glutamate the PFC and MID, respectively.

REFERENCE

Sales, A. J., Fogaça, M. V., Sartim, A. G., Pereira, V. S., Wegener, G., Guimarães, F. S., & Joca, S. R. L. (2018). *Molecular Neurobiology*, 1–12.

OC026 | “Compound 1”: An apparent G-protein-biased μ -opioid receptor agonist that induces receptor desensitization through GRK

Sam Groom¹; Yangmei Li²; Graeme Henderson³; Eamonn Kelly³; Chris Bailey¹

¹University of Bath; ²University of South Carolina; ³University of Bristol

Background and Purpose: G-protein-biased μ -opioid receptor (MOPr) agonists have the potential to induce less receptor desensitization and tolerance than traditional opioids. In this study, we characterized the signalling properties of two novel MOPr agonists (PZM21 and “Compound 1” (Tyr-c[D-Lys-Phe-Tyr-Gly])) (Li et al., 2016) and investigated the MOPr desensitization they induce using brain slice electrophysiology.

Experimental Approach: Opioid-induced G-protein activation and arrestin-3 recruitment were studied using BRET techniques in HEK293 cells (Hill et al., 2018).

Male Wistar rats (4 weeks old) were decapitated under general anaesthesia (80 mg·kg⁻¹ of ketamine and 12 mg·kg⁻¹ of xylazine, i.p.), and brains were removed. Brains were sliced to produce 230- μ m-thick brain slices containing locus coeruleus (LC) neurons. Whole-cell voltage-clamped recordings were taken from LC neurons. Opioids were perfused for 10 min, with reductions in evoked current amplitude tracked as a measure of receptor desensitization (Bailey et al., 2009).

Data are presented as mean \pm SEM ($n = 3–6$), and statistical significance ($P < .05$) was assessed using one-way ANOVA with Tukey's multiple comparisons test.

Key Results: Morphine, PZM21, and Compound 1 are partial MOPr agonists, with significantly lower E_{max} values for G-protein activation compared to the full agonist DAMGO (70 \pm 3%, 53 \pm 3%, and 66 \pm 4%, respectively, Figure 1a). Compound 1 has a similar E_{max} for G-protein activation to morphine but a significantly lower E_{max} for arrestin-3 recruitment (morphine = 34 \pm 4% and Compound 1 = 13 \pm 2%, Figure 1b). These data suggest that Compound 1 has an apparent bias towards G-protein coupling.

The amplitude of K^+ currents evoked by morphine, PZM21, and Compound 1 were significantly less than those evoked by DAMGO (Figure 2a). While PZM21 induced less MOPr desensitization than morphine, Compound 1 induced robust MOPr desensitization of greater magnitude than morphine (Figure 2b). The extent of Compound 1-induced MOPr desensitization was unaffected by activation (PMA, $1 \mu\text{M}$) or inhibition (GF109203X, $1 \mu\text{M}$) of PKC but was significantly reduced by inhibition of GRK (Compound 101, $30 \mu\text{M}$)

Conclusion and Implications: Despite Compound 1 coupling weakly to arrestin-3 recruitment, it induced robust MOPr desensitization. Unexpectedly, our data suggest that Compound 1-induced MOPr desensitization is GRK dependent. Investigations are ongoing to further detail the mechanisms of the receptor desensitization induced by Compound 1 and its implications for the long-term functional consequences of biased signalling at MOPr.

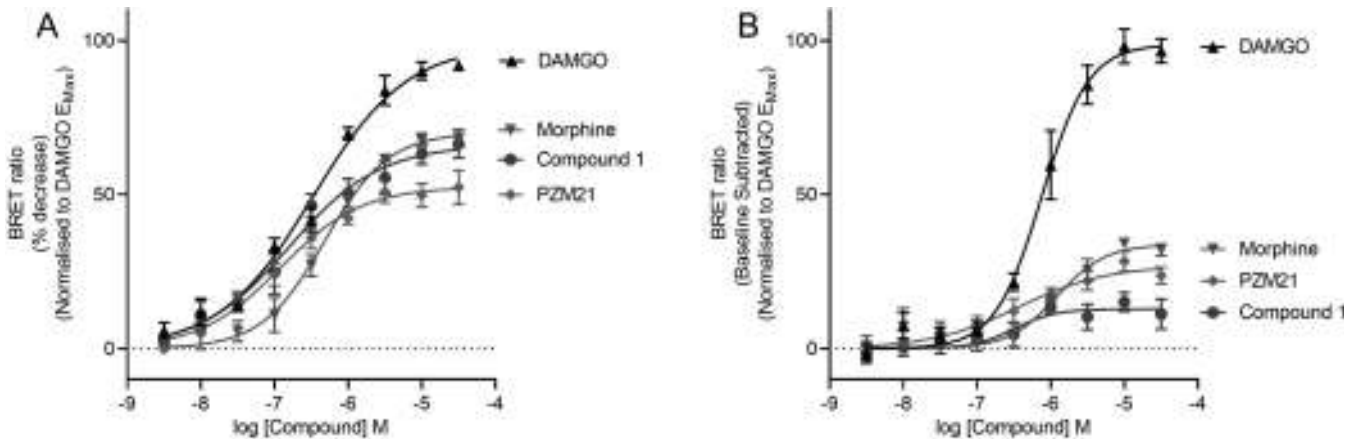


Figure 1. Opioid-induced G_i activation (a) and arrestin-3 translocation (b) in HEK293 cells expressing recombinant MOPrs. Data are presented as mean \pm SEM ($n = 5$) and normalized to E_{max} of DAMGO

(Figure 2c).

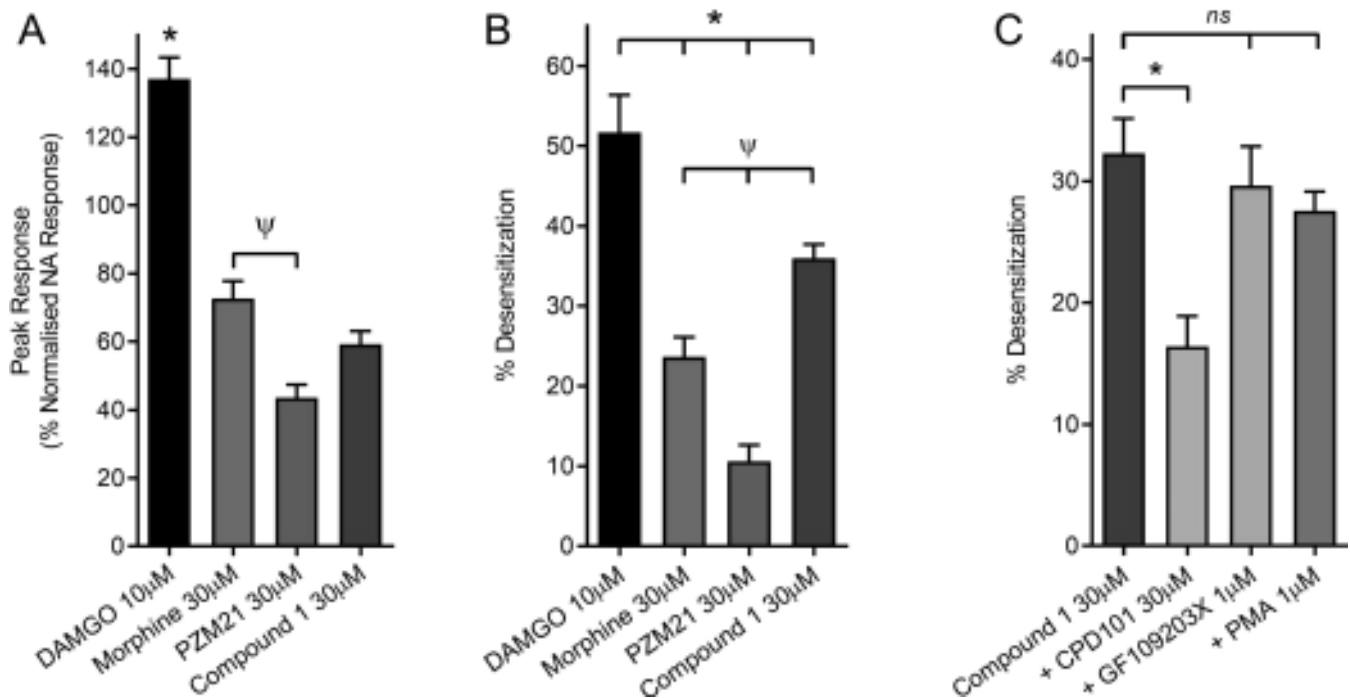


Figure 2. Studying the activity of novel MOPr agonists in rat locus coeruleus neurons. (a) Peak responses elicited by opioids in LC neurons. $^*P < .05$ versus all; $^{\Psi}P < .05$. (b) % Desensitization of opioid-evoked currents. $^*P < .05$ versus DAMGO; $^{\Psi}P < .05$ versus morphine. (c) % Desensitization of Compound 1-evoked currents in the presence of kinase modulators. $^*P < .05$; $^{ns}P > .05$

REFERENCES

- Bailey, et al. (2009). *British Journal of Pharmacology*, 158(1), 157–164.
 Hill, et al. (2018). *British Journal of Pharmacology*, 175(13), 2653–2661.
 Li, et al. (2016). *Journal of Medicinal Chemistry*, 59(3), 1239–1245.

OC028 | The natural product taspine suppresses P2X₄ receptor activity via inhibition of phosphoinositide 3-kinase

Neville Ngum; Izzudin Nadzirin; Samuel Fountain

University of East Anglia

Background and Purpose: P2X receptors are a family of extracellular ATP-gated cationic channels associated with various physiological and pathophysiological processes. An up-regulation of the P2X₄ receptor subtype in activated spinal microglia following peripheral nerve injury is associated with the development of neuropathic pain. This warrants the need for selective molecules capable of antagonising P2X₄-mediated effects. To this end, we have undertaken compound library screens and identified taspine as a novel inhibitor of P2X₄ receptor activity.

Experimental Approach: Fura-2-loaded 1321N1 astrocytoma cells expressing either human or mouse P2X₄ were used for measurement of ATP-evoked Ca²⁺ responses. Whole-cell patch clamp was used to make electrophysiological recordings. Quantitative measurement of cell surface P2X₄ was made by flow cytometry. *in vitro* phosphoinositide 3-kinase inhibition assays were performed using biotinylated phosphoinositol (3,4,5)-triphosphate as a positive reference. Hill's equation was used to determine EC₅₀ and IC₅₀ values, and statistical significance was determined using ANOVA followed by Turkey's post hoc test for parametric data.

Key Results: Taspine inhibited ATP-evoked Ca²⁺ responses at human and mouse P2X₄ with IC₅₀ values of 3.8 ± 0.2 μM (n = 5) and 3.5 ± 0.3 μM (n = 5), respectively. Taspine (10 μM) reduced the maximal response to ATP by approximately 80% but had no significant effect on ATP potency (EC₅₀ 0.47 ± 0.1 μM control vs. 0.48 ± 0.2 μM taspine (n = 5), P > .05), revealing a non-competitive mode of action. P2X₂, P2X_{2/3}, P2X₇, and M2 muscarinic receptors were insensitive to taspine. Taspine (10 μM) treatment has no significant effect on the cell surface expression of P2X₄. Taspine (10 μM, 4 min) significantly decreased ivermectin-potentiated P2X₄ current density (28.8 ± 3.7 vs. 10.39 ± 2.5 pA·pF⁻¹ [n = 9], P < .05), and at concentrations ≥0.1 μM, taspine significantly inhibited more than 60% of phosphoinositide 3-kinase activity with complete enzyme inhibition attained at 1 μM. Effects of taspine on P2X₄ Ca²⁺ response, current density, and on phosphoinositide 3-kinase activity were mimicked by the known phosphoinositide 3-kinase inhibitor LY294002 (Vlahos, Matter, Hui, & Brown, 1994).

Conclusion and Implications: Taspine acts non-competitively to inhibit P2X₄ receptor activity. We suggest that rather than acting directly at the receptor, taspine acts by inhibiting phosphoinositide

3-kinase, causing interference with the documented P2X₄ receptor modulation by phosphoinositides.

REFERENCE

- Vlahos, C. J., Matter, W. F., Hui, K. Y., & Brown, R. F. (1994). A specific inhibitor of phosphatidylinositol 3-kinase, 2-(4-morpholinyl)-8-phenyl-4H-1-benzopyran-4-one (LY294002). *The Journal of Biological Chemistry*, 269, 5241–5248.

Posters, Monday 16th December, 13:30

Poster Session: Integrated Systems

P127 | Inadequate adrenal response in high-fat diet-fed rats with septic shock: The role of 11β-HSD dysregulation

Chiao-Lin Chuang; Hui-Chun Huang; Shao-Jung Hsu; Fa-Yauh Lee; Yi-Hsiang Huang; Ming-Chih Hou

Taipei Veterans General Hospital

Background and Purpose: Non-alcoholic fatty liver disease (NAFLD) is linked with metabolic syndrome. Previous studies showed that obesity may disrupt adrenal function and hypothalamus–pituitary–adrenal (HPA) axis. Subjects with NAFLD also had a blunted suppression of cortisol secretion to low-dose dexamethasone administration, suggesting the possibility of a subtle, chronic HPA axis activation. Adrenal gland is important for vascular counter-regulations against shock, but whether adrenal function and HPA axis abnormalities exist and influence the outcome in NAFLD subjects with or without septic shock remains obscure.

Experimental Approach: Male Sprague–Dawley rats were fed with regular chow diet (control) or high-fat diet (HFD, 60% energy derived from fat). Plasma concentrations of triglyceride, cholesterol, alanine aminotransferase (ALT), aspartate aminotransferase (AST), glucose, insulin, aldosterone, and corticosterone were determined at the end of the fourth, sixth, and eighth weeks, respectively. Three series of experiments were also performed at the end of the eighth week to survey first, changes of haemodynamics, biochemistry parameters, ACTH response and adipose tissue, and adrenal gland 11β-HSD system protein expressions in control and HFD rats without sepsis; second, haemodynamic response, HPA axis, and 11β-HSD system protein expressions in control and HFD rats with LPS-induced sepsis; and third, haemodynamic and ACTH response in control and HFD rats with LPS-induced sepsis. Mean arterial pressure (MAP), portal pressure (PP), and heart rate (HR) were monitored for 120 min after LPS administration.

Key Results: HFD-fed rats exerted the histological features of NAFLD including ballooning change of hepatocytes and increased extent of Oil Red O staining, compatible with liver steatosis. The levels of glucose, insulin, HOMA-IR (the index of insulin resistance), cholesterol, and triglyceride increased significantly in HFD group, which were in line with the endocrine and biochemistry features of NAFLD. HFD-fed rats also had elevated portal pressure as compared with the chow-diet control rats, compatible with the development of portal hypertension.

The plasma ACTH and corticosterone levels increased along with HFD feeding (at the eighth week, ACTH (ng·ml⁻¹): 2.3 ± 0.2 vs. 3.6 ± 0.1, *P* < .001; corticosterone (ng·ml⁻¹): 150 ± 10 vs. 226 ± 16, *P* = .002). In contrast, the corticosterone increment ratio (%) in response to ACTH injection decreased along with the time (at the sixth week, 2.0 ± 0.1 vs. 1.5 ± 0.2, *P* = .079; at the eight week, 2.0 ± 0.1 vs. 1.4 ± 0.1, *P* < .001, *n* = 7, 7). Adipose tissue and adrenal gland 11β-HSD1 and G6PD protein expressions of HFD rats were significantly up-regulated than control rats, whereas 11β-HSD2 expressions were significantly down-regulated.

In parallel groups, although shock was induced immediately after LPS injection, MAP was elevated and stabilized since 60 min after LPS injection in control but not in HFD group. The drop of MAP was significantly more prominent in HFD group at 120 min as well (mmHg): -5.5 ± 5.0 vs. -27.6 ± 3.6, *P* = .002, *n* = 8, 9). HFD rats had excess arterial iNOS expression. In addition, despite HFD rats had a significantly higher baseline corticosterone level (ng·ml⁻¹: 153 ± 11 vs. 234 ± 17, *P* = .003), after shock, the corticosterone levels were not significantly different between control and HFD groups (ng·ml⁻¹: 454 ± 56 vs. 484 ± 26, *P* = .658) and the corticosterone increment ratio after LPS injection was significantly lower in HFD group (3.1 ± 0.2 vs. 2.1 ± 0.3, *P* = .021). Furthermore, the corticosterone increment ratio was lower in HFD rats after ACTH administration. Although in stable condition without sepsis, the 11β-HSD system in the adipose tissue and adrenal gland acts towards corticosterone synthesis in HFD group, the trend changed after sepsis: The 11β-HSD1, G6PD, and 11β-HSD2 protein expressions were not significantly different between the control and HFD groups.

Conclusion and Implications: NAFLD rats exerted a higher HPA axis activity with up-regulation of 11β-HSD1 and G6PD and down-regulation of 11β-HSD2 in adipose tissue and adrenal gland. However, HPA axis reactivity was poorer in NAFLD rats with sepsis. This is, at least partly, due to 11β-HSD dysregulation and iNOS over-production in shock.

REFERENCES

- Jessop, D. S., Dallman, M. F., Fleming, D., & Lightman, S. L. (2001). Resistance to glucocorticoid feedback in obesity. *The Journal of Clinical Endocrinology and Metabolism*, 86, 4109–4114.
- Targher, G., Bertolini, L., Rodella, S., Zoppini, G., Zenari, L., & Falezza, G. (2006). Associations between liver histology and cortisol secretion in subjects with nonalcoholic fatty liver disease. *Clinical Endocrinology*, 64, 337–341.
- Wang, P., Ba, Z. F., Jarrar, D., Cioffi, W. G., Bland, K. I., & Chaudry, I. H. (1999). Mechanism of adrenal insufficiency following trauma and

severe hemorrhage: Role of hepatic 11β-hydroxysteroid dehydrogenase. *Archives of Surgery*, 134, 394–401.

P128 | The role of endogenous H₂S in vasoactive responses of isolated thoracic aorta in hypertriglyceridemic rats as a model of metabolic syndrome

Sona Cacanyiova; Andrea Berenyiova; Samuel Golas

Institute of Normal and Pathological Physiology, Center of Experimental Medicine, Slovak Academy of Sciences, Bratislava

Background and Purpose: Dysfunction of endothelium and/or perivascular adipose tissue (PVAT) as main sources of vasoactive substances such as NO or hydrogen sulfide (H₂S) interferes with the etiopathogenesis of hypertension or metabolic syndrome. In spontaneously hypertensive rats, we confirmed that H₂S signal pathway coupled with PVAT activity could serve as reserved vasorelaxant mechanism during NO deficiency (Berenyiova, Drobna, Cebova, Kristek, & Cacanyiova, 2018; Cacanyiova, Majzunova, Golas, & Berenyiova, 2019). The aim of this study was to evaluate the role of PVAT and endogenously produced H₂S in vasoactive responses of isolated thoracic aorta in hypertriglyceridemic (HTG) rats used as a model of metabolic syndrome.

Experimental Approach: Eighteen- to 20-week-old male normotensive Wistar and HTG rats were used. Systolic BP (sBP) was measured by plethysmography. Triacylglycerol (TAG) and glucose (GLU) levels were determined in plasma. Endothelium-dependent vasorelaxation induced by ACh and noradrenaline (NA)-induced contraction of TA with preserved PVAT+ or denuded PVAT- were recorded as changes in isometric tension. The pretreatment with propargylglycine (PPG, 10 mM) was used to inhibit cystathionine γ-lyase, H₂S-producing enzyme. Statistical significance was determined using an ANOVA followed by Bonferroni's post hoc test on raw data.

Key Results: Compared to Wistar rats, higher amount of visceral fat, increased level of TAG and GLU, higher sBP, and decreased endothelium-dependent relaxation were demonstrated in HTG (Table 1). Endothelial dysfunction was associated with increased contractile responses to exogenous NA. The presence of PVAT revealed inhibitory effect on adrenergic contractile responses in both groups, however, significantly more in HTG rats (Table 1). Unlike in Wistar rats, in HTG group, H₂S produced by aortic wall with removed PVAT reduced maximal endothelium-dependent vasorelaxation (before PPG: 49.03 ± 3.33%; after PPG: 66.08 ± 2.41%; *n* = 9; *P* < .05). On the other hand, the presence of PVAT was associated with anti-contractile action of endogenous H₂S; maximal NA (1 μM)-induced contraction reached 1.12 ± 0.08 g before the pretreatment with PPG and 1.42 ± 0.09 g after the pretreatment with PPG (*n* = 9; *P* < .01).

Conclusion and Implications: Our results confirmed that in a model of metabolic syndrome, endogenous H₂S could manifest dual effect depending on the type of triggered signal pathway. H₂S produced in

TABLE 1 Basic characteristics of Wistar and HTG rats

	sBP (mm Hg)	RFW/TL (mg·mm ⁻¹)	TAG (mM)	GLU (mM)	EDR PVAT- (%)	Cont/PVAT- (g)	Cont/PVAT+ (g)
Wistar (n = 8)	118.48 ± 1.75	2.68 ± 0.28	2.23 ± 0.13	7.48 ± 0.24	69.69 ± 4.58	0.82 ± 0.11	0.51 ± 0.07 [#]
HTG (n = 9)	135.67 ± 2.14 [*]	4.52 ± 0.31 [*]	9.23 ± 0.25 ^{**}	8.49 ± 0.37 ^{**}	10.93 ± 4.73 ^{**}	1.68 ± 0.08 ^{**}	1.19 ± 0.07 ^{###}

Abbreviations: Cont, maximal contraction induced by NA (1 μM); EDR, maximal endothelium-induced relaxation induced by Ach (10 μM); RFW/TL, retro-peritoneal fat weight/tibia length.

^{*}P < .05 versus HTG.

^{**}P < .01 versus HTG.

[#]P < .05 versus Cont/PVAT- in Wistar rats.

^{###}P < .001 versus Cont/PVAT- in HTG rats.

the vessel wall contributed to the endothelial dysfunction; however, the anti-contractile action of PVAT associated with H₂S activity could serve as probable part of compensatory vasoactive mechanisms. Tissue-specific individual parts of sulfide signal pathway might represent as a promising target to affect pathological processes associated with endothelial dysfunction.

REFERENCES

- Berenyiova, A., Drobna, M., Cebova, M., Kristek, F., & Cacanyiova, S. (2018). Changes in the vasoactive effects of nitric oxide, hydrogen sulfide and the structure of the rat thoracic aorta: The role of age and essential hypertension. *Journal of Physiology and Pharmacology*, 69, 4.
- Cacanyiova, S., Majzunova, M., Golas, S., & Berenyiova, A. (2019). The role of perivascular adipose tissue and endogenous H₂S in vasoactive responses of isolated mesenteric arteries in normotensive and spontaneously hypertensive rats. *Journal of Physiology and Pharmacology*, 70, 295–306.

P129 | The impacts of MMP inhibition or deletion on liver cirrhosis and characteristics of portal hypertension in bile duct-ligated animals

Chiao-Lin Chuang; Hsin-Ling Ho; Shao-Jung Hsu; Hui-Chun Huang; Ming-Chih Hou; Fa-Yauh Lee

Taipei Veterans General Hospital

Background and Purpose: Liver cirrhosis and portal hypertension may develop hyperdynamic circulatory dysfunction, angiogenesis, and portosystemic collaterals. The major issue in treatment is to effectively control hepatic fibrogenesis and angiogenesis. Metalloproteinases (MMPs) participate in fibrogenesis and angiogenesis and interact with VEGF, the main growth factor participating in portal hypertension. However, a relevant investigation in cirrhosis is lacking.

Experimental Approach: Liver cirrhosis was induced by common bile duct ligation (BDL) in male Sprague–Dawley rats. Sham operation was surgical control. The influences of (a) minocycline (120 mg·kg⁻¹·day⁻¹, oral gavage for 28 days), an antibiotic possessing MMP inhibition capability or vehicle; (b) SB-3CT (0.16 mg·kg⁻¹·day⁻¹, i.p. for 28 days), an MMP-2 and MMP-9 inhibitor or vehicle; and (c) MMP-9 knockout

(KO) or wild-type (ST) mice were evaluated. On the 29th day, three series of experiments were performed to survey:

First series, (a) body weight, systemic and splanchnic haemodynamic parameters, including mean arterial pressure (MAP), cardiac output (CO), cardiac index (CI), systemic vascular resistance (SVR), portal pressure (PP), superior mesenteric arterial (SMA) blood flow, and SMA resistance; (b) mesenteric vascular density with CD31 immunofluorescent staining; (c) plasma VEGF, alanine transaminase (ALT), aspartate transaminase (AST), total bilirubin, blood urea nitrogen (BUN), and creatinine concentrations; (d) mesenteric vascular morphology with immunofluorescent staining; (e) hepatic fibrogenesis factor protein expressions with Western blotting; and (f) mesenteric angiogenesis factor protein expressions with Western blotting.

Second series, portosystemic shunting determination with colour microsphere technique.

Third series, (a) the hepatic vascular responsiveness to endothelin-1 (ET-1) with an in situ liver perfusion model and (b) the splanchnic vascular responsiveness to arginine vasopressin (AVP) with an in situ SMA perfusion model.

Key Results: Minocycline reduced CO, CI, PP, and SMA flow, mesenteric vascular density, and plasma VEGF, AST, and total bilirubin levels in BDL rats. Minocycline induced higher mesenteric perfusion pressure change to AVP at the concentration of 3×10^{-9} M ($P < .05$). Furthermore, SB-3CT did not influence the systemic and portal haemodynamic parameters but reduced CO, CI, PP, and SMA flow in BDL rats. SB-3CT elicited lower hepatic perfusion pressure changes to ET-1 in both sham and BDL rats, which might be related to the SB-3CT-induced down-regulation of liver fibrogenesis-related protein expressions and thus reduction of hepatic resistance. SB-3CT did not influence the splanchnic vascular responsiveness to AVP and the mesenteric vasoactive factor protein expressions. Furthermore, the SB-3CT-treated cirrhotic rats had lower shunting degree, mesenteric vascular density, plasma VEGF concentration, and mesenteric VEGF protein expression, suggesting that SB-3CT may ameliorate angiogenesis via VEGF down-regulation. This also contributes to the reduced SMA flow. In combination with the reduced hepatic resistance, the PP was also reduced.

Finally, as compared with the corresponding sham groups, both MMP-9 KO and WT mice that underwent BDL had significantly decreased MAP and elevated PP, ALT, AST, bilirubin, and Sirius Red-

stained area of the liver, indicating significant portal hypertension, liver injury, and fibrosis. The MMP-9 KO-BDL mice had significantly lower PP and Sirius Red-stained area of the liver as compared with those of the WT-BDL mice. BDL up-regulated hepatic α -SMA protein expression in the WT mice, but not in KO mice. The WT-BDL mice had significantly higher α -SMA protein expression as compared with the MMP-9 KO-BDL mice. The MMP-9 KO-BDL mice also had significantly lower p-eNOS expression and p-eNOS/eNOS ratio as compared with the WT-BDL and MMP-9 KO-sham mice. Furthermore, the WT mice with BDL had significantly higher p-VEGFR2 expression as compared with the WT-sham and KO-BDL mice ($P < .05$).

Conclusion and Implications: MMP-9 inhibition or deletion ameliorates the severity of portal hypertension, liver fibrosis, and the relevant derangements, showing the role of MMP-9 in the pathogenesis of liver cirrhosis and portal hypertension. MMP-9 may be targeted in the treatment of liver cirrhosis and portal hypertension.

REFERENCES

- Bergers, G., Brekken, R., McMahon, G., et al. (2000). Matrix metalloproteinase-9 triggers the angiogenic switch during carcinogenesis. *Nature Cell Biology*, 2, 737–744.
- Iwakiri, Y., & Groszmann, R. J. (2007). Vascular endothelial dysfunction in cirrhosis. *Journal of Hepatology*, 46, 927–934.
- Kossakowska, A. E., Edwards, D. R., Lee, S. S., et al. (1998). Altered balance between matrix metalloproteinases and their inhibitors in experimental biliary fibrosis. *The American Journal of Pathology*, 153, 1895–1902.

P130 | Mechanism of neuropeptide Y mediated potentiation of P2X1 receptor-dependent vasoconstriction in human and mouse small arteries

Maria del Carmen Gonzalez-Montelongo¹; Samuel J. Fountain²

¹University of East Anglia; ²School of Biological Sciences, University of East Anglia

Background and Purpose: Neuropeptide Y (NPY) is co-released with ATP and norepinephrine by sympathetic nerves that innervate arteries. Here, we explore the mechanism by which NPY can augment vasoconstriction mediated by activation of the P2X1 receptor for ATP.

Experimental Approach: Patients Small arteries (500–200 μ m) from subcutaneous abdominal adipose tissue samples were obtained from normotensive female volunteers.

Animals Mesenteric arteries (<200 μ m) from male C57BL/6 mice were used.

Isometric contractility measurements were made on arterial rings by wire myography. Neurogenic responses were elicited by electrical field stimulation. Data are expressed as mean \pm SEM, and n represents the number of animals. Analysis was performed using ANOVA or Kruskal–Wallis test followed by a Student–Newman–Keuls t test, post hoc Tukey honestly significant difference test, or Mann–Whitney

U test where appropriate. Comparison between segments from the same samples was assessed by a paired t test or a Wilcoxon signed-rank test.

Key Results: Human arteries

Purinergic agonist α , β -methylene ATP (α , β -meATP; 300 nM) evoked contractions that were potentiated by NPY (10 nM) in arteries (potentiation = 198%; $P < .01$; $N = 9$). In addition, NPY (1 nM–100 μ M) evoked concentration-dependent contractions on basal tone with functional and non-functional endothelium ($EC_{50} = 1.25 \times 10^{-8} \pm 4.09 \times 10^{-9}$ M; $P < .05$; $N = 6$; and $EC_{50} = 1.69 \times 10^{-8} \pm 4.24 \times 10^{-9}$ M; $P < .05$; $N = 5$, respectively). α , β -meATP-evoked responses were sensitive to suramin ($IC_{50} = 1.28 \times 10^{-6} \pm 2.82 \times 10^{-7}$ M; $P < .05$; $N = 3$), and a selective P2X₁ receptor antagonist (NF449; [100 nM]) was sufficient to completely block of α , β -meATP-induced contractions (inhibition = 85%; $P < .005$; $N = 5$). NPY-induced potentiation on α , β -meATP-evoked contractions was not reduced by selective NPY1R antagonism (BIBO3304 [10 nM]; n.s.; $N = 5$) or NPY2R antagonism (BIIE0246 [100 nM]; n.s.; $N = 5$). However, NPY-induced potentiation was abolished when both antagonists were applied together (inhibition = 58%; $P = .059$; $N = 3$).

Mouse arteries Previous results showed that nifedipine (100 nM) does not block α , β -meATP (100 nM) peaks; however, nifedipine inhibits NPY potentiation of α , β -meATP contractions (inhibition = 49%, $P < .05$; $N = 10$). In addition, purinergic and adrenergic contractile responses induced by EFS were blocked by TTx (1 μ M; inhibition ~75% to 64 Hz, $P < .01$; $N = 7$) and guanethidine (10 μ M; inhibition ~60% to 64 Hz; $P < .05$; $N = 10$), respectively, and also of the partial inhibition of the selective P2X1R (NF449 [3 μ M]; inhibition ~40% to 64 Hz; $P < .05$; $N = 6$).

Conclusion and Implications: Data suggest that NPY exerts a positive modulatory effect on α , β -meATP-evoked contractions by combined activation of NPY1R and NPY2R in human and mice vascular tissue and requires L-type Ca²⁺ channel activity.

P131 | Tangeretin improves reproductive dysfunction in L-NAME-induced hypertensive male rats

Petcharat Chiangsaen¹; Upa Kukongviriyapan¹; Wannapa Settheetham-Ishida¹; Terdthai Tong-un¹; Parichat Prachaney²; Pongrat Pakdeechote¹

¹Department of Physiology, Faculty of Medicine, Khon Kaen University;

²Department of Anatomy, Faculty of Medicine, Khon Kaen University

Background and Purpose: Tangeretin, a flavonoid found in citrus fruit peels, has been reported to have antioxidation and anti-inflammatory effects (Lee et al., 2016). This study investigated the effect of tangeretin on reproductive dysfunction in *N*_ω-nitro-L-arginine methyl ester hydrochloride (L-NAME)-induced hypertensive male rats.

Experimental Approach: Male Sprague-Dawley rats were induced hypertension using L-NAME (40 mg.kg⁻¹) in drinking water for 5 weeks. The hypertensive rats were treated with tangeretin at dose 15 or 30 mg.kg⁻¹ or sildenafil (10 mg.kg⁻¹) for the last 2 weeks. Mean arterial pressure (MAP), intracavernosal pressure (ICP) response to cavernous nerve stimulation (1–4 V, 15 Hz, for 1 min), tissue malondialdehyde (MDA), and plasma NO metabolites (NOx) were analysed. Sperm concentration and motility were counted. Furthermore, endothelial NOS (eNOS) and steroidogenic acute regulatory (StAR) protein expressions in penile and testicular tissues were evaluated. Serum testosterone and testicular morphology were evaluated. Statistical significance was determined using an ANOVA followed by a Fisher's LSD post hoc test.

Key Results: L-NAME hypertensive rats had high BP, decreased ICP/MAP ratio, poor sperm quality, and changes of seminiferous tubule morphology (*P* < .05). eNOS and StAR expressions in reproductive tissues were suppressed (*P* < .05). An increase in tissue MDA and decrease in plasma NOx and serum testosterone were shown in hypertensive rats (*P* < .05). Tangeretin significantly reduced MAP, improved male reproductive dysfunction (Tables 1 and 2), mitigated alterations of seminiferous tubule morphology, and restored eNOS expression in penile and testicular tissues as well as StAR protein expression in testicular tissue in hypertensive rats (*P* < .05). These

were consistent with increases in plasma NOx and serum testosterone levels (Table 2) and decrease in tissue MDA in hypertensive rats treated with tangeretin (*P* < .05). Sildenafil also had the beneficial effect on BP and male reproductive dysfunction as tangeretin did but not for erectile responses in hypertensive rats.

Conclusion and Implications: These findings could suggest that tangeretin reduces BP and improves male reproductive dysfunction in NO-deficient hypertension. The underlying mechanism might involve restoration of eNOS and StAR protein expressions, along with increased NO bioavailability resulting from reducing oxidative stress.

REFERENCE

Lee, Y. Y., Lee, E.-J., Park, J. S., Jang, S. E., & Kim, D. H. (2016). Kim HS (2016) Anti-inflammatory and antioxidant mechanism of tangeretin in activated microglia. *Journal of NeuroImmune Pharmacology*, 11, 294–305.

P132 | Cannabidiol and cannabigerol inhibit spontaneous contractions in the mouse isolated uterus

James Brown; Georgieva Teodora; Roshni Rajendran; Brigitte Gyeke; Kirsten Handy; Mohsen Seifi

University of Portsmouth

Background and Purpose: The production of endocannabinoids and the presence of cannabinoid receptors in mouse uterus have

TABLE 1 Effect of tangeretin and sildenafil on erectile responses in hypertensive male rats

Voltages	Maximum ICP/MAP (%)				
	Control + vehicle	L-NAME + vehicle	L-NAME + tangeretin (15 mg.kg ⁻¹ .day ⁻¹)	L-NAME + tangeretin (30 mg.kg ⁻¹ .day ⁻¹)	L-NAME + sildenafil (10 mg.kg ⁻¹ .day ⁻¹)
1 V	9.16 ± 2.29	3.51 ± 1.23 ^a	4.07 ± 1.03 ^a	4.35 ± 0.98 ^a	3.76 ± 1.05 ^a
2 V	18.44 ± 5.91	4.80 ± 1.28 ^a	5.18 ± 1.73 ^a	9.43 ± 1.50	4.40 ± 1.06 ^a
3 V	22.13 ± 5.34	4.97 ± 2.25 ^a	3.69 ± 0.61 ^a	13.36 ± 2.15 ^{a,b}	4.27 ± 0.92 ^a
4 V	39.37 ± 4.40	6.02 ± 1.47 ^a	8.04 ± 1.56 ^a	17.46 ± 1.91 ^{a,b}	6.73 ± 2.37 ^a

Note. Data are expressed as mean ± SEM (n = 6–8 per group).

^a*P* < .05 versus control.

^b*P* < .05 versus L-NAME.

TABLE 2 Effect of tangeretin and sildenafil on sperm quality in hypertensive male rats

Parameters	Control + vehicle	L-NAME + vehicle	L-NAME + tangeretin (30 mg.kg ⁻¹ .day ⁻¹)	L-NAME + sildenafil (10 mg.kg ⁻¹ .day ⁻¹)
Caudal epididymal sperm concentration (× 10 ⁶ .ml ⁻¹)	19.07 ± 1.02	14.10 ± 0.65 ^a	15.77 ± 0.96 ^b	17.28 ± 0.59 ^b
Sperm motility (%)	63.48 ± 2.05	42.85 ± 1.96 ^a	57.88 ± 2.57 ^b	60.67 ± 0.66 ^b
Serum testosterone levels (pg.ml ⁻¹)	170.50 ± 20.57	73.19 ± 26.27 ^a	164.21 ± 39.23 ^b	150.35 ± 28.75 ^b

Note. Data are expressed as mean ± SEM (n = 6–8 per group).

^a*P* < .05 versus control.

^b*P* < .05 versus L-NAME.

previously been reported (Pagano et al., 2017). Furthermore, we have reported how uterine tissue harvested from early gestation mice (5–9 days) spontaneously contracts when bathed in a high Ca^{2+} (1.5 mM) containing physiological solution (Francis et al., 2003). In this study, we investigate the effect of the phytocannabinoids cannabidiol (CBD) and cannabigerol (CBG) on these contractions.

Experimental Approach: Uterine horns were harvested from pregnant mice (C57BL6 strain; 5–9 days of gestation) and incubated at 37°C in a 10-ml organ bath with modified De Jalon's solution containing 2.5-mM Ca^{2+} aerated with 95% O_2 /5% CO_2 . Spontaneous contractions commenced and were allowed to equilibrate for 30 min before drug additions. Studies were performed in accordance with the Animals (Scientific Procedures) Act 1986/ASPA Amendment Regulations 2012. All drugs were obtained from Tocris and dissolved in DMSO with the final concentration of DMSO in the bath being less than 0.01% v/v. All control data were obtained in the presence of the corresponding percentage DMSO (% v/v). Recordings were captured using Labchart 8 (ADI; V8.13) and analysed by measuring the AUC (g.s) using the integral relative to minimum method to take into account changes in both force and frequency of contraction. Cumulative additions of drugs (concentration range 10^{-10} to 10^{-5} M) were made every 20 min, and the AUC was measured during the final 10 min of each addition. Uterine tissue was also harvested following in vivo perfusion, and the location of CB_1 receptors was identified using immunohistochemistry and laser scanning confocal microscopy.

Key Results: The non-psychoactive phytocannabinoids CBD and CBG produced a concentration-dependent inhibition of spontaneous contractions with IC_{50} s of 421 and 15.5 nM, respectively ($n = 6-9$). Furthermore, the fatty acid amyl hydrolase (FAAH) inhibitor JNJ1661010 also produced a concentration-dependent inhibition of spontaneous contractions with an IC_{50} of 367 nM. Finally, the CB_1 and GPR55 receptor antagonist AM251 (Tocris) inhibited the effects of JNJ1661010 with a pA_2 of 9.036 and a slope of 0.969. Finally, CB_1 receptors appear to be located within both circular and longitudinal murine uterine muscles.

Conclusion and Implications: These data suggest a role for both endocannabinoids and phytocannabinoids in the control of uterine smooth muscle contractions. Whilst the precise mechanism through which these inhibitory effects are mediated is currently unclear, it is likely to involve CB_1 receptors.

REFERENCES

- Francis, M., Arkle, M., Martin, L., Butler, T. M., Cruz, M. C., Opare-Aryee, G., ... Brown, J. F. (2003). Relaxant effects of parathyroid hormone and parathyroid hormone-related peptides on oviduct motility in birds and mammals: Possible role of nitric oxide. *General and Comparative Endocrinology*, 133, 243–251.
- Pagano, E., Orlando, P., Finizio, S., Rossi, A., Buono, L., Iannotti, F. A., ... Borrelliet, F. (2017). Role of the endocannabinoid system in the control of mouse myometrium contractility during the menstrual cycle. *Biochemical Pharmacology*, 124, 83–93.

P133 | Effects of cannabidiol and cannabigerol on isolated intestinal smooth muscle preparations from the mouse

James Brown; Amasha Bellange; Bernardette Dwimoh; Fateha Asha; Neamatullah Niazi; Simran Patel

University of Portsmouth

Background and Purpose: The production and action of endocannabinoids and the presence of cannabinoid receptors in the gastrointestinal tract have been comprehensively reviewed (Lee, Jo, Chung, Pothoulaki, & Im, 2016). Furthermore, a role of CB_1 receptors in the gastric fundus and intestinal smooth muscle have previously been reported (Garella & Baccari, 2012; Makwana, Molleman, & Parsons, 2010). In this study, we explore the effect of the phytocannabinoids cannabidiol (CBD) and cannabigerol (CBG) on either spontaneous or electrical field stimulation-evoked contractions in isolated tissue preparations from the mouse.

Experimental Approach: Gastric fundic strips, distal ileum, and proximal colon were harvested from C57BL6 strain mice and incubated at 37°C in a 10-ml organ bath with Krebs–Henseleit solution aerated with 95% O_2 /5% CO_2 . Studies were performed in accordance with the Animals (Scientific Procedures) Act 1986/ASPA Amendment Regulations 2012. Fundic strips were pre-contracted with carbamylcholine (10^{-5} M) prior to application of electrical field stimulation (EFS), which was applied at a frequency of 4, 8, and 16 Hz at 60 V with a pulse width of 0.5 ms for 10-s duration. Distal ileum and proximal colon produced regular pendula spontaneous contractions that were allowed to equilibrate for 30 min prior to drug additions. All drugs were obtained from Tocris and dissolved in DMSO with the final concentration of DMSO in the bath being less than 0.01% v/v. All control data were obtained in the presence of the corresponding percentage DMSO (% v/v). Recordings were captured using LabChart 8 (ADI) and analysed by measuring the AUC (g.s) using the integral relative to minimum method (LabChart Reader V8.1.13) to take into account changes in both force and frequency of contraction. Cumulative additions of drugs (concentration range 10^{-10} to 10^{-5} M) were made every 20 min, and the AUC was measured during the final 10 min of each addition.

Key Results: In the fundic strips, the non-psychoactive phytocannabinoid CBD (10^{-6} M) significantly enhanced the EFS stimulated relaxation at every frequency ($n = 5$; analysed by a two-way ANOVA and Bonferroni's multiple comparisons post hoc test on original non-normalised data). In distal ileum and proximal colon, CBD, CBG, the fatty acid amyl hydrolase (FAAH) inhibitor JNJ1661010, and anandamide produced concentration-dependent inhibition of spontaneous contractions; data are summarised in Table 1.

Conclusion and Implications: These data suggest a role for both endocannabinoids and phytocannabinoids CBD and CBG in the control of intestinal smooth muscle contractions. Whilst the precise mechanism through which these inhibitory effects are mediated is currently unclear, it is likely to involve CB_1 receptors.

TABLE 1 Summary of effects of cannabinoids (CBD, CBG, and anandamide) and the FAAH inhibitor JNJ1661010 on intestinal smooth muscle contractions

Tissue	CBD	CBG	JNJ1661010	Anandamide
Fundus	Significantly increased EFS relaxation at all frequencies (4, 8, and 16 Hz) at 10^{-6} M (n = 5)	ND	ND	ND
Ileum	IC ₅₀ = 850 nM (n = 11)	IC ₅₀ = 120 nM (n = 3)	IC ₅₀ = 1.97 μM (n = 3)	ND
Colon	IC ₅₀ = 329 nM (n = 6)	IC ₅₀ = 116 nM (n = 3)	ND	IC ₅₀ = 212 nM (n = 3)

Abbreviation: ND, not determined.

REFERENCES

Garella, R., & Baccari, M. (2012). Endocannabinoids modulate non-adrenergic, non-cholinergic inhibitory neurotransmission in strips from the mouse gastric fundus. *Acta Physiologica*, 206(1), 80-87.

Lee, Y., Jo, J., Chung, H. Y., Pothoulaki, C., & Im, E. (2016). Endocannabinoids in the gastrointestinal tract. *The American Journal of Physiology*, 311(4), G655-G666.

Makwana, R., Molleman, A., & Parsons, M. (2010). Pharmacological characterization of cannabinoid receptor activity in the rat-isolated ileum myenteric plexus-longitudinal muscle preparation. *British Journal of Pharmacology*, 159(8), 1608-1622.

P134 | Effects of a *Thymus vulgaris* L. extract on the nonadrenergic noncholinergic relaxation of the rat gastric fundus

Diego Curro¹; Giovanna Nicotra²

¹Institute of Pharmacology, School of Medicine, Catholic University of the Sacred Heart; ²EPO S.r.l.

Background and Purpose: Gastric accommodation dysfunction is a known pathogenetic mechanism of functional dyspepsia. Thyme preparations are traditionally used in some countries for the relief of digestive disorders. Thus, we aimed to evaluate whether the beneficial digestive effects of thyme preparations could be attributable to an increase in the NANC relaxation of the rat proximal stomach, an in vitro model of the gastric accommodation.

Experimental Approach: Longitudinal muscle strips from the gastric fundus of Wistar rats were placed inside 5-ml organ baths containing Krebs solution maintained at 37°C and bubbled with carbogen under isotonic (1-g load) and NANC (1-μM atropine + 5-μM guanethidine) conditions. The effects of a *Thymus vulgaris* L. extract (1-300 μg.ml⁻¹) on the NANC relaxations of U46619 (0.1 μM)-precontracted strips induced by low-frequency (2 Hz) and high-frequency (13 Hz) electrical field stimulation (EFS; 2 min) were studied. The amplitude of the initial rapid component of the 2-Hz EFS-induced relaxation measured at 10 s is completely due to nitric oxide (NO), whereas the AUC of 13-Hz EFS-induced relaxation is largely due to vasoactive intestinal polypeptide (Currò, Ipavec, & Preziosi, 2008). All responses were normalized by dividing them for the maximal relaxation induced by papaverine (300 μM). The results were evaluated by means of one-way ANOVA or paired Student's t test. The extract (Thymox[®], EPO S. r.l., Milan, Italy) was characterized according to the European

Pharmacopoeia 9 and standardized to contain min. 0.3% thymol according to DAB 2007.

Key Results: The thyme extract (1-300 μg.ml⁻¹) significantly reduced the peak amplitude of EFS (2 Hz)-induced relaxation at all concentrations tested, with the maximal reduction of 18.2 ± 2.4% (P < .001) of controls observed at 300 μg.ml⁻¹ (n = 4). The extract (3, 10, and 300 μg.ml⁻¹) significantly reduced by 30.2 ± 10.3% (P < .05), 37.3 ± 10.2% (P < .01), and 27.0 ± 3.7% (P < .05) of controls, respectively (n = 4), the 2-Hz EFS-induced relaxation measured at 10 s. The extract (100-300 μg.ml⁻¹) relaxed the strips by 4.8 ± 1.2% and 17.3 ± 1.6% (n = 4), respectively. The extract (100 μg.ml⁻¹) did not significantly affect the AUC of 13-Hz EFS-induced relaxation (109.7 ± 4.2% of controls, n = 4).

Conclusion and Implications: The thyme extract slightly reduces the NANC relaxation of the proximal stomach induced by low-frequency neuronal activation, mainly by inhibiting the NO-mediated component. It also relaxes the smooth muscle of the proximal stomach, and this action could be responsible for its beneficial digestive effects.

REFERENCE

Currò, D., Ipavec, V., & Preziosi, P. (2008). *European Review for Medical and Pharmacological Sciences*, 12(Suppl 1), 53-62.

P135 | Effect of vildagliptin in treatment of experimentally induced ulcerative colitis in rats

Marina Ramsis¹; Rania Salama¹; Ayman El-Sahar²; Hala Zaki²

¹Misr International University; ²Cairo University

Background and Purpose: Ulcerative colitis (UC) is a chronic and progressive inflammatory disorder that is characterized by diffused mucosal inflammation of the distal colon and rectum. Pro-inflammatory cytokines and ROS are involved in the intestinal ulceration and mucosal disruption (Soliman, Keshk, Rizk, & Ibrahim, 2019). Vildagliptin (Vilda), a dipeptidyl peptidase IV inhibitor, has an anti-inflammatory activity manifested through reduction of TNF-α and NO levels. Yet its possible protective effect in UC has not been elucidated (El-Marasy, Abdel-Rahman, & Abd-Elsalam, 2018). Thus, the present study aims to

TABLE 1 Effect of different doses of vildagliptin on DAI and biochemical markers in acetic acid-induced ulcerative colitis in rats

Parameter	Control	Vilda	AA	AA + Vilda (5 mg)	AA + Vilda (10 mg)	AAA + Sulfa
DAI	0.18 ± 0.04 [#]	0.13 ± 0.05 [#]	1.720 ± 0.117 [*]	0.870 ± 0.163 ^{*,#}	0.807 ± 0.179 ^{*,#}	0.813 ± 0.209 ^{*,#}
p-PI3K (Tyr607)/total PI3K	1.00 ± 0.005 [#]	1.01 ± 0.008 [#]	5.920 ± 0.928 [*]	1.974 ± 0.121 ^{*,#}	1.665 ± 0.306 [#]	2.129 ± 0.778 ^{*,#}
p-Akt (Thr450)/total Akt	1.013 ± 0.015 [#]	1.010 ± 0.009 [#]	7.230 ± 0.859 [*]	2.700 ± 0.283 ^{*,#,@}	1.643 ± 0.306 [#]	2.005 ± 0.782 ^{*,#}
cyt Nrf2/β-actin	1.01 ± 0.009 [#]	1.02 ± 0.019 [#]	6.171 ± 0.109 [*]	1.813 ± 0.466 ^{*,#}	1.313 ± 0.181 [#]	1.818 ± 0.215 ^{*,#@}
nuc Nrf2/β-actin	1.033 ± 0.036 [#]	1.079 ± 0.086 [#]	0.201 ± 0.081 [*]	0.803 ± 0.030 ^{*,#@}	0.916 ± 0.058 ^{*,#}	0.771 ± 0.058 ^{*,#@}
p-CREB (Ser133)/total CREB	1.003 ± 0.004 [#]	1.025 ± 0.047 [#]	0.247 ± 0.035 [*]	0.830 ± 0.138 ^{*,#@}	0.935 ± 0.021 [#]	0.786 ± 0.079 ^{*,#@}
HO-1 mRNA expression	1.048 ± 0.058 [#]	1.06 ± 0.101 [#]	0.204 ± 0.034 [*]	0.770 ± 0.175 ^{*,#}	0.882 ± 0.024 ^{*,#}	0.838 ± 0.056 ^{*,#}
NQO1 mRNA expression	1.013 ± 0.01282 [#]	1.010 ± 0.009258 [#]	0.2875 ± 0.1035 [*]	0.7238 ± 0.05097 ^{*,#}	0.8000 ± 0.05855 ^{*,#}	0.7500 ± 0.03207 ^{*,#}
miR-146A mRNA expression	1.024 ± 0.04596 [#]	1.016 ± 0.01923 [#]	9.688 ± 0.9702 [*]	3.730 ± 1.125 ^{*,#@}	2.713 ± 0.1642 ^{*,#}	3.650 ± 0.4567 ^{*,#}
lnc IFNG-AS1 mRNA expression	1.015 ± 0.012 [#]	1.06 ± 0.15 [#]	7.075 ± 0.19 [*]	3.28 ± 0.248 ^{*,#@}	1.891 ± 0.201 ^{*,#}	3.103 ± 0.68 ^{*,#@}
TNF-α (pg·mg ⁻¹ protein)	19.09 ± 1.814 [#]	19.11 ± 0.164 [#]	67.19 ± 1.514 [*]	35.23 ± 2.311 ^{*,#@}	19.61 ± 2.044 [#]	36.63 ± 2.032 ^{*,#@}
NF-κB (pg·mg ⁻¹ protein)	177.8 ± 272.1	82.24 ± 2.526	200.0 ± 1.297	109.0 ± 3.445	90.31 ± 2.239	110.1 ± 0.3137
BAX (pg·mg ⁻¹ protein)	66.44 ± 2.384 [#]	65.18 ± 3.421 [#]	125.7 ± 3.353 [*]	87.93 ± 1.399 ^{*,#@}	67.98 ± 2.268 [#]	84.73 ± 5.107 ^{*,#@}
BCL2 (pg·mg ⁻¹ protein)	161.1 ± 18.13 [#]	167.1 ± 6.370 [#]	74.60 ± 1.151 [*]	135.4 ± 2.281 ^{*,#@}	164.8 ± 2.050 [#]	140.4 ± 2.662 ^{*,#@}
Caspase-3 activity DEVD-pNA cleavage	2.136 ± 0.117 [#]	1.989 ± 0.063 [#]	9.450 ± 0.823 [*]	3.455 ± 0.204 ^{*,#@,-}	2.826 ± 0.184 ^{*,#}	4.071 ± 0.034 ^{*,#@}

Note. Data are presented as mean ± SD (n = 8), one-way ANOVA followed by Tukey's multiple comparisons test.

Abbreviations: AA, acetic acid; Akt, PKB; BAX, BCL2-associated X protein; BCL2, B-cell lymphoma protein 2; CREB, cAMP response element-binding protein; cyt Nrf2, cytosolic nuclear factor erythroid 2-related factor 2; DAI, disease activity index; HO-1, haem oxygenase 1; lnc IFNG-AS1, long non-coding RNA IFNG-AS1; miR-146A, microRNA 146 A; NQO1, NAD(P)H quinone oxidoreductase 1; nuc Nrf2, nuclear nuclear factor erythroid 2-related factor 2; Sulfa, sulfasalazine; Vilda, vildagliptin.

*P < .05 versus control.

#P < .05 versus AA.

@P < .05 versus AA + Vilda (10 mg).

-P < .05 versus AA + Sulfa.

investigate the possible beneficial effect of different doses of Vilda against acetic acid (AA)-induced UC in rats.

Experimental Approach: Male Wistar albino rats were randomly allocated into six groups each composed of eight rats that were treated as follows: control (saline only), Vilda (10 mg·kg⁻¹·day⁻¹), AA and AA + Vilda (5 mg·kg⁻¹·day⁻¹) (El-Marasy et al., 2018), AA + Vilda (10 mg·kg⁻¹·day⁻¹) (El-Marasy et al., 2018), and AA + sulfasalazine (Sulfa) (100 mg·kg⁻¹·day⁻¹) (Soliman et al., 2019). Vilda and Sulfa were orally administered for 7 days before induction of UC. On the eighth day, colitis was induced intra-rectally by a single dose of 2 ml of 3% (v/v) AA in 0.9% sodium chloride (Soliman et al., 2019) followed by

14 days of treatment of the drugs. The rats were anaesthetized by urethane (1.3 g·kg⁻¹, i.p.) and then killed 24 hr after the last treatment, and their colon tissues were collected for histopathological and biochemical assessment.

Key Results: Low- and high-dose Vilda and Sulfa groups showed improvement in the disease activity index (DAI) and inflammatory, oxidative stress and apoptosis markers (Table 1).

Histological examination with Harris haematoxylin and eosin (H&E) revealed intact histological structures in the treated groups when compared to AA group (Figure 1).

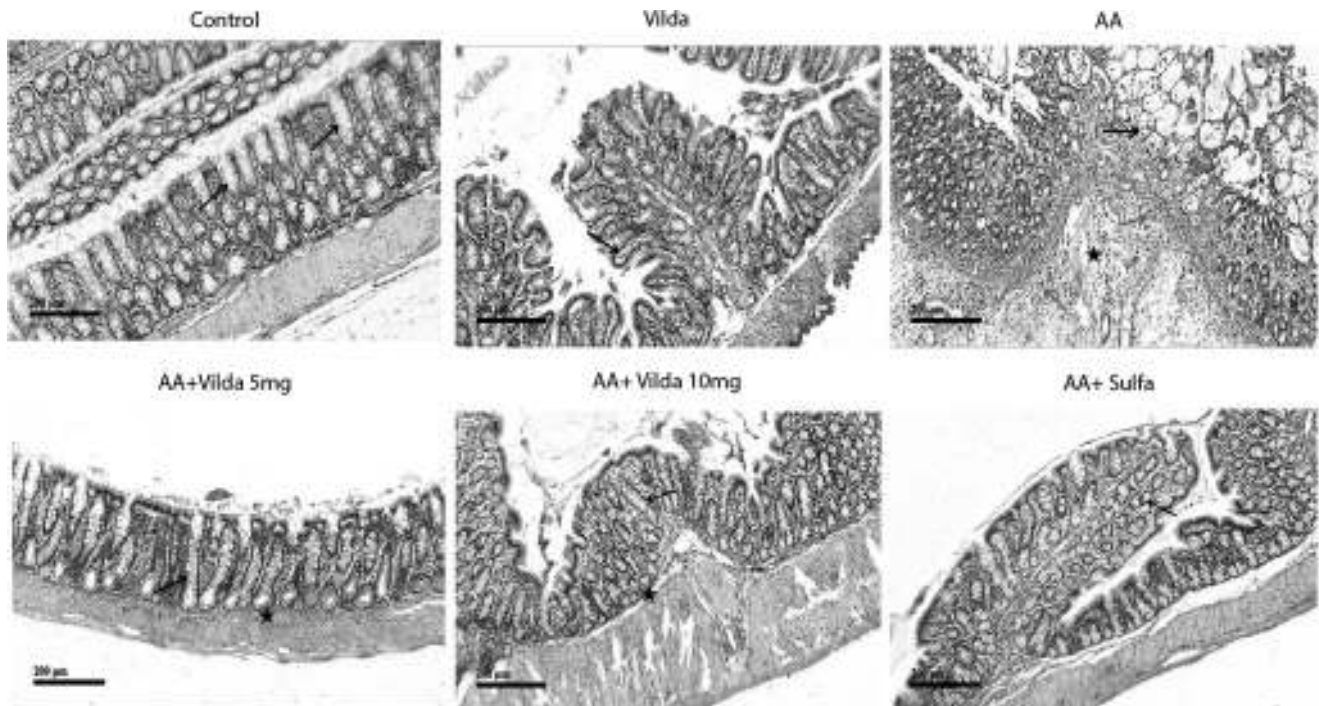


Figure 1. Photomicrographs of colon sections from all experimental groups. AA, acetic acid; Vilda, vildagliptin. H&E stain × 100

Conclusion and Implications: Vilda has anti-inflammatory, antioxidant, and anti-apoptotic effects showing better results with the high dose against low dose and Sulfa. Consequently, it can be concluded that Vilda is effective in the treatment of experimentally induced UC in rats.

REFERENCES

El-Marasy, S., Abdel-Rahman, R., & Abd-Elsalam, R. (2018). Neuroprotective effect of vildagliptin against cerebral ischemia in rats. *Naunyn-Schmiedeberg's Archives of Pharmacology*, 391(10), 1133-1145. <https://doi.org/10.1007/s00210-018-1537-x>

Soliman, N., Keshk, W., Rizk, F., & Ibrahim, M. (2019). The possible ameliorative effect of simvastatin versus sulfasalazine on acetic acid induced ulcerative colitis in adult rats. *Chemico-Biological Interactions*, 298, 57-65. <https://doi.org/10.1016/j.cbi.2018.11.002>

P136 | The effect of the hypoxia mimetic agent, L-mimosine, on potassium- and carbachol-induced contractility in isolated rat colon

John O'Connor; Eimear O'Riordan; Sam Bolger; Deirdre Campion
 University College Dublin

Background and Purpose: L-Mimosine is a non-protein amino acid derived from tropical leguminous shrubs *Mimosa pudica* and *Leucaena leucocephala*. L-Mimosine has been proposed as a potential drug of interest for treatment of a diverse range of clinical conditions, including cancer and inflammatory conditions (Nguyen & Tawata, 2016). The anti-inflammatory effects of L-mimosine are generally considered to be due to inhibition of prolyl hydroxylases (Warnecke et al., 2003). Although targeting hypoxia-sensitive pathways with prolyl hydroxylase inhibitors is a therapeutic approach in the treatment of inflammatory bowel disease, limited research has been conducted to investigate the effects of prolyl hydroxylase inhibitors on gastrointestinal smooth muscle contractility.

Experimental Approach: Male and female Wistar rats ranging from 50 to 120 g were humanely killed following Department of Health and institutional ethics approval. Tissue rings from the proximal and distal colon were dissected and individually mounted in organ baths, bathed in physiological saline maintained at 37°C, and gassed with a 95% O₂/5% CO₂ mixture. Tissues were allowed to equilibrate for 40-60 min before an initial KCl (100 mM) contracture was induced. A second KCl-induced contraction was carried out following 60-min incubation with 10-µM L-mimosine. Responses were expressed as a percentage of the pretreatment contraction and compared with untreated controls.

Separately to assess agonist-induced responsiveness of distal colon rings, an initial concentration of the muscarinic agonist, carbachol (100 μ M), was added, followed by a cumulative response curve (0.1 to 100 μ M). Carbachol-induced contractility was measured using the square root of the mean of squares (RMS) of the gram tension, to allow for both contraction amplitude and frequency. The cumulative response to carbachol in the presence and absence of 10- μ M L-mimosine was expressed as a % of the initial carbachol stimulus and then analysed using non-linear regression [log (agonist) versus response].

Key Results: Incubation with L-mimosine (10 μ M) did not affect KCl-induced (100 mM) contraction amplitude in proximal colon ($n = 5$). However, contraction amplitude was significantly reduced in the treated distal colon rings ($68.1 \pm 7.5\%$, $n = 6$, $P < .05$, Mann-Whitney U test) in comparison with the initial contraction and compared with untreated controls ($109.3 \pm 13.3\%$, $n = 11$). Using comparison of fit analysis with base constrained to zero, the cumulative response curve to carbachol differed significantly (<0.001) in the presence of L-mimosine ($pEC_{50} 5.10 \pm 0.33$, plateau at $47.3 \pm 9.9\%$, $n = 6$) compared with untreated controls ($pEC_{50} 5.10 \pm 0.19$, plateau at $85.1 \pm 10.3\%$, $n = 6$).

Conclusion and Implications: Incubation with L-mimosine significantly reduced the contractile response to carbachol-induced contraction and to a potassium-depolarising stimulus in distal rat colon. These results suggest a putative role for prolyl hydroxylase domain-containing proteins in normal gut motility.

REFERENCES

- Nguyen, B. C., & Tawata, S. (2016). The chemistry and biological activities of mimosine: A review. *Phytotherapy Research*, 30(8), 1230–1242.
- Warnecke, et al. (2003). Activation of the hypoxia-inducible factor-pathway and stimulation of angiogenesis by application of prolyl hydroxylase inhibitors. *FASEB*, 17(9), 1186–1188.

Poster Session: Molecular and Cellular Pharmacology 2

P095 | Development of histamine H₄ receptor target engagement assays in immune cell populations involved in atopic dermatitis pathophysiology

Eugenia Sergeev; Susan Brown; Kirstie Bennett; Greg Osborne; Richard May; Matt Barnes

Sosei Heptares

Background and Purpose: Atopic dermatitis (AD) is a chronic inflammatory skin condition with limited options for long-term disease management. Leukocytes in inflamed skin tissue are involved in the pathophysiology of AD, and several populations express the histamine H₄ receptor (H₄R) (Schaper-Gerhardt, 2018). H₄R activation exacerbates pro-inflammatory processes; hence, H₄R antagonists are being considered as AD therapeutics (Schaper-Gerhardt, 2018). With the aim to develop a clinically translatable target engagement assay in healthy human blood, we assessed the effect of H₄R ligands on eosinophil shape change, a process underlying eosinophil migration (Willets, 2014), and the secretion of IL-31, a cytokine linked to pruritus (Gibbs, 2019), from T helper type 2 (Th2) cells.

Experimental Approach: The eosinophil shape change assay was performed as described (Ling, 2004). Data were analysed using a four-parameter sigmoidal concentration-response model to determine IC₅₀, EC₅₀, and maximum response (E_{max}). For the IL-31 assay, peripheral blood mononuclear cells (PBMCs) were isolated from human blood by density gradient centrifugation on Lymphoprep™ and processed using the EasySep™ Naïve CD4⁺ T Cell Isolation Kit. Naïve CD4⁺ T cells were polarised using the ImmunoCult™ Th2 Differentiation Supplement Protocol, and polarisation was confirmed by a CD4⁺CCR4⁺CD45RO⁺IL 4⁺/CD45RA⁻IFN- γ ⁻ expression profile. Th2 cells were treated with 10 nM- to 10- μ M H₄R ligands for 16 hr or positive control 25 ng·ml⁻¹ of PMA and 1 μ g·ml⁻¹ of ionomycin for 2 hr, with 5 μ g·ml⁻¹ of brefeldin A added during the last 2 hr. IL-31 expression was evaluated by flow cytometry.

Key Results: H₄R agonist histamine induced eosinophil shape change, albeit with a lower potency and efficacy than the positive control, CCR3 agonist eotaxin. Increasing concentrations of selective H₄R antagonists resulted in inhibition of eosinophil shape change following histamine challenge, and pIC₅₀ values obtained are consistent with literature data showing approximately 10-fold higher affinity of ZPL-3893787 for H₄R compared to toreforant (Paul Chazot, 2019). Naïve CD4⁺ T cells from healthy donors were successfully polarised into Th2 cells; however, neither treatment with non-specific agonist histamine, H₄R-specific agonist 4-methylhistamine, nor positive control PMA/ionomycin was able to induce a consistent increase in IL-31 expression across five donors.

Conclusion and Implications: The eosinophil shape change assay produced useful potency data and would be clinically translatable. Indeed, it has been applied to characterise a H₄R antagonist in phase I trials (Thurmond, 2014). The ability of H₄R agonists to increase IL-31 expression in Th2 cells from healthy donors appears donor-to-donor dependent. However, H₄R agonists have been shown to be more efficacious in inducing IL-31 expression in PBMCs from AD patients compared to healthy volunteers (Gutzmer, 2009), which could be an area to explore in the future.

TABLE 1 Eosinophil shape change in response to H₄R ligand treatment

H ₄ R agonism			H ₄ R antagonism ^a	
Compound	pEC ₅₀	E _{max} (% change)	Compound	pIC ₅₀
Histamine (mean ± SD; n = 3)	7.5 ± 0.3	22 ± 6	ZPL-3893787 (n = 3)	8.4 ± 0.4
Eotaxin ^b (mean ± SD; n = 3)	9.7 ± 0.5	32 ± 5	Toreforant (n = 3)	7.6 ± 0.4

^aInhibition of histamine EC₈₀ challenge concentration determined for each donor (68–198 nM).

^bCCR3 agonist used as positive control.

REFERENCES

- Gibbs, B. F. (2019). Role of the pruritic cytokine IL-31 in autoimmune skin diseases. *Frontiers in Immunology*, 10, 1383.
- Gutzmer, R. (2009). The histamine H₄ receptor is functionally expressed on T_H2 cells. *Journal of Allergy and Clinical Immunology*, 123(3), 619–625.
- Ling, P. (2004). Histamine H₄ receptor mediates eosinophil chemotaxis with cell shape change and adhesion molecule upregulation. *British Journal of Pharmacology*, 142(1), 161–171.
- Paul Chazot, P. (2019). Histamine receptors: H₄ receptor. IUPHAR/BPS Guide to PHARMACOLOGY. Retrieved from <http://www.guidetopharmacology.org/GRAC/ObjectDisplayForward?objectId=265#>
- Schaper-Gerhardt, K. (2018). The role of the histamine H₄ receptor in atopic dermatitis and psoriasis. *British Journal of Pharmacology*, Epub Ahead of Print. <https://doi.org/10.1111/bph.14550>
- Thurmond, R. L. (2014). Clinical and preclinical characterization of the histamine H₄ receptor antagonist JNJ-39758979. *Journal of Pharmacology and Experimental Therapeutics*, 349(2), 176–184.
- Willets, L. (2014). Eosinophil shape change and secretion. *Methods in Molecular Biology*, 1178, 111–128.

P096 | A hydrogen sulfide-releasing dexamethasone derivative attenuates atopic dermatitis severity signs and the associated oxidative stress markers in mice

Silvia Abigail Coavoy-Sánchez¹; Vincenzo Santagada²;
Giuseppe Caliendo²; Soraia Katia Costa¹; Beatrice Severino²;
Marcelo Nicolás Muscará¹

¹Department of Pharmacology, Institute of Biomedical Sciences, University of São Paulo, São Paulo, Brazil; ²Department of Pharmacy, Università degli Studi di Napoli Federico II, Napoli, Italy

Background and Purpose: Atopic dermatitis (AD) is a highly prevalent chronic inflammatory skin disease characterized by pruritus and eczematous skin lesions. Considering that hydrogen sulfide (H₂S) is produced in the skin and participates of several processes, such as the regulation of inflammation, pruritus, scarring, and angiogenesis (Coavoy-Sánchez, Costa, Muscará, 2019), we decided to test the effects of a H₂S-releasing dexamethasone (Dexa) derivative in a murine model of AD.

Experimental Approach: The experimental protocol was approved by our Local Ethics Committee for Animal Experimentation (CEUA-ICB/USP; no. 129/2016). Female BALB/c mice (6- to 8-week-old) had the dorsal hair shaved, and 2,4-dinitrochlorobenzene (DNCB) was topically applied on days 1–3. On days 15, 17, 19, and 22, the mice were topically challenged with DNCB on both the dorsal skin and the right ear. On days 19–23 after sensitization, the animals were topically treated with either dexamethasone (Dexa) or the H₂S-releasing thiobenzamide (TBZ)-dexamethasone derivative (Dexa-TBZ; both at 250 nmol per mice), or TBZ (1 μmol per mice). Skin severity score and scratching behaviour were assessed before each challenge and on day 24 before the animal euthanasia. Blood samples were collected for cell counting, and dorsal skin samples were collected for analysis of oxidative stress markers (3-nitrotyrosine [3NT]- and carbonyl group-containing proteins) and antioxidant enzymes. Results are shown as mean ± SEM. Differences among the experimental groups were analysed by one-way ANOVA followed by the Tukey's test for multiple comparisons.

Key Results: Topical DNCB induced AD-like skin lesions, scratching behaviour, ear oedema, and eosinophilia. Similarly to Dexa, topical treatment with Dexa-TBZ significantly reduced the skin severity score (average 27.9%; *P* < .001; *n* = 5), scratching behaviour (88.8%; *P* < .001; *n* = 5), and ear oedema (98.8%; *P* < .05; *n* = 5) and decreased the number of eosinophils to values lower than those observed in the animals without AD. Both 3-NT and carbonyl groups were increased in the AD skins, and treatment with Dexa-TBZ (but not Dexa) resulted in significant reduction of these markers (by average 59% and 100%, respectively; *P* < .05; *n* = 5) in addition to increased glutathione peroxidase activity (by 22.3%; *P* < .05; *n* = 5) in comparison with Dexa.

Conclusion and Implications: The addition of a TBZ moiety to dexamethasone does not interfere with the beneficial effects of this parent corticosteroid and adds the advantage of stimulating antioxidant defences in the animals with AD, thus evidencing the therapeutical potential of this new molecule for the clinical treatment of AD.

ACKNOWLEDGEMENTS

This study was supported by FAPESP (Process 2017/16409-6), CNPq, and CAPES.

REFERENCE

Coavoy-Sánchez, S. A., Costa, S. K. P., & Muscará, M. N. (2019). Hydrogen sulfide and dermatological diseases. *British Journal of Pharmacology* May 3. <https://doi.org/10.1111/bph.14699>

P097 | Synthetic analogues of ferulic acid exert anti-inflammatory and antioxidant effects in human monocytic cells

Nursabah Atli¹; James Harvey¹; Colin Kay²; Richard Draijer³; Mark Searcey¹; Maria O'Connell¹

¹School of Pharmacy, University of East Anglia, Norwich; ²Plants for Human Health Institute, Kannapolis, NC; ³Unilever R&D Vlaardingen B.V

Background and Purpose: Flavonoid-rich food and beverage consumption is correlated with a reduced risk of developing cardiovascular disease, potentially due to anti-inflammatory and antioxidative mechanisms in vascular cells. In the gut, flavonoids are extensively metabolised into phenolic acids (PA) via bacterial catabolism. We have previously found that specific flavonoids and metabolites at physiological concentrations modestly inhibit TNF- α secretion and induce haem oxygenase-1 (HO-1) expression in monocytes. In this study, we investigated whether the anti-inflammatory and anti-oxidative effects of three common PA could be enhanced by esterification in THP-1 monocytes.

Experimental Approach: 4-Hydroxy-3-methoxycinnamic acid (FA), 3,4-dihydroxybenzoic acid (PCA), and 4-hydroxy-3-methoxybenzoic acid (VA) and their esters FA methyl (FA-ME), FA propyl (FA-PE), FA hexyl (FA-HxE), PCA methyl (PCA-ME), PCA ethyl (PCA-EE), PCA propyl (PCA-PE), PCA hexyl (PCA-HxE), and VA hexyl (VA-HxE) were utilised. Cell viability was measured by MTS assay (Promega). TNF- α secretion was measured by ELISA (di Gesso et al., 2015), and NQO1 enzyme activity was assessed as previously described (Prochaska & Santamaria, 1988). HO-1 protein expression was measured by a DuoSet[®] IC ELISA (R&D Systems) and Nrf2 DNA-binding by ELISA (TransAM[®] Nrf2, Active Motif), all according to the manufacturer's instructions. TNF- α , HO-1, and NADPH quinone oxidoreductase (NQO1) mRNA expressions were measured by quantitative real-time PCR as described earlier (di Gesso et al., 2015).

Key Results: Parent and esterified phenolic acids were screened at 10 μ M for their effects on LPS-induced TNF- α secretion in THP-1 cells. None of the parent compounds significantly affected LPS-induced TNF- α secretion. FA-PE and FA-HxE significantly inhibited TNF- α secretion in a concentration-dependent manner (19% and 39% reduction at 20 μ M, respectively) but had no effect on TNF- α mRNA expression. FA-PE and FA-HE also significantly induced HO-1 protein expression (2.6 and 3.7 \times basal control, respectively) and NQO1 enzymatic activity (1.3 and 1.3 \times basal control). FA-HxE significantly increased HO-1 mRNA expression (1.88 \times basal control) but neither affected HO-1, NQO1 mRNA, or Nrf2 activation.

Conclusion and Implications: Esterification of FA enhanced its anti-inflammatory and anti-oxidative effects in THP-1 cells, with the longer

hexyl ester exerting more inhibitory effects than the shorter propyl ester, suggesting enhanced cellular uptake due to increased lipophilicity. The effect of FA-HxE and FA-PE on TNF- α and NQO1 secretion appears to be post-translational, as mRNA expression was not affected. Furthermore, the effects on HO-1 and NQO1 are independent of Nrf2 activity, similarly to the mechanisms of other common flavonoid metabolites in human monocytic cells.

REFERENCES

di Gesso, J., et al. (2015). *Molecular Nutrition & Food Research*, 59, 1143–1154.
Prochaska, H., & Santamaria, A. (1988). *Analytical Biochemistry*, 169(2), 328–336.

P098 | Immunomodulatory effects of alarmins on human monocytes

Jon Whitby¹; Qing Xue¹; João Oliveira¹; Ashley Smaje²; James Fullerton¹

¹University College London; ²University College London Hospitals

Background and Purpose: Alarmins or “damage-associated molecular patterns” (DAMPs) comprise a heterogeneous group of endogenous biomolecules released in response to tissue damage. Classically thought to function as “danger” signals to the immune system, recent evidence has associated high plasma levels after cardiac arrest, trauma, and surgery with immunoparalysis. Murine studies suggest that they may induce a “tolerance-like” state in mononuclear cells, including to bacterial motifs; however, whether this occurs in man is unknown.

In this pilot study, the effect of individual alarmins on healthy volunteer monocyte function—either independently or on subsequent LPS challenge—was evaluated.

Experimental Approach: Heparinised whole blood from healthy volunteers ($n = 3$) was combined with alarmin solutions at a range of physiological and pathophysiological concentrations (1 ml, 48-well plate, triplicate). Alarmins investigated included calprotectin, heparin-binding protein, HMGB1, heat shock protein 70 (HSP70), IL-33, procalcitonin, and S100A12. After 30-min incubation at 37°C, LPS (1 ng·ml⁻¹) was either added or not before incubating for further 4 hr. Monocyte function was quantified using both TNF- α release (R&D DuoSet ELISA) and HLA-DR expression (BD Quantibrite™ system): gold standard assays for identification of clinically relevant immunoparalysis. Ethical approval was granted by the UCL Research Ethics Committee (5060/002). Statistical analysis was conducted in GraphPad Prism using one-way ANOVA (Dunnett's multiple comparisons test) with unstimulated control and LPS-stimulated control as baseline reference.

Key Results: HSP70 alone independently stimulated TNF- α release (Figure 1); mean release was increased by 339 pg·ml⁻¹ (95% CI [152, 526], $P = .0002$) and 2,126 pg·ml⁻¹ (95% CI [1,939, 2,313], $P < .0001$) at 10 and 100 ng·ml⁻¹ of HSP70, respectively.

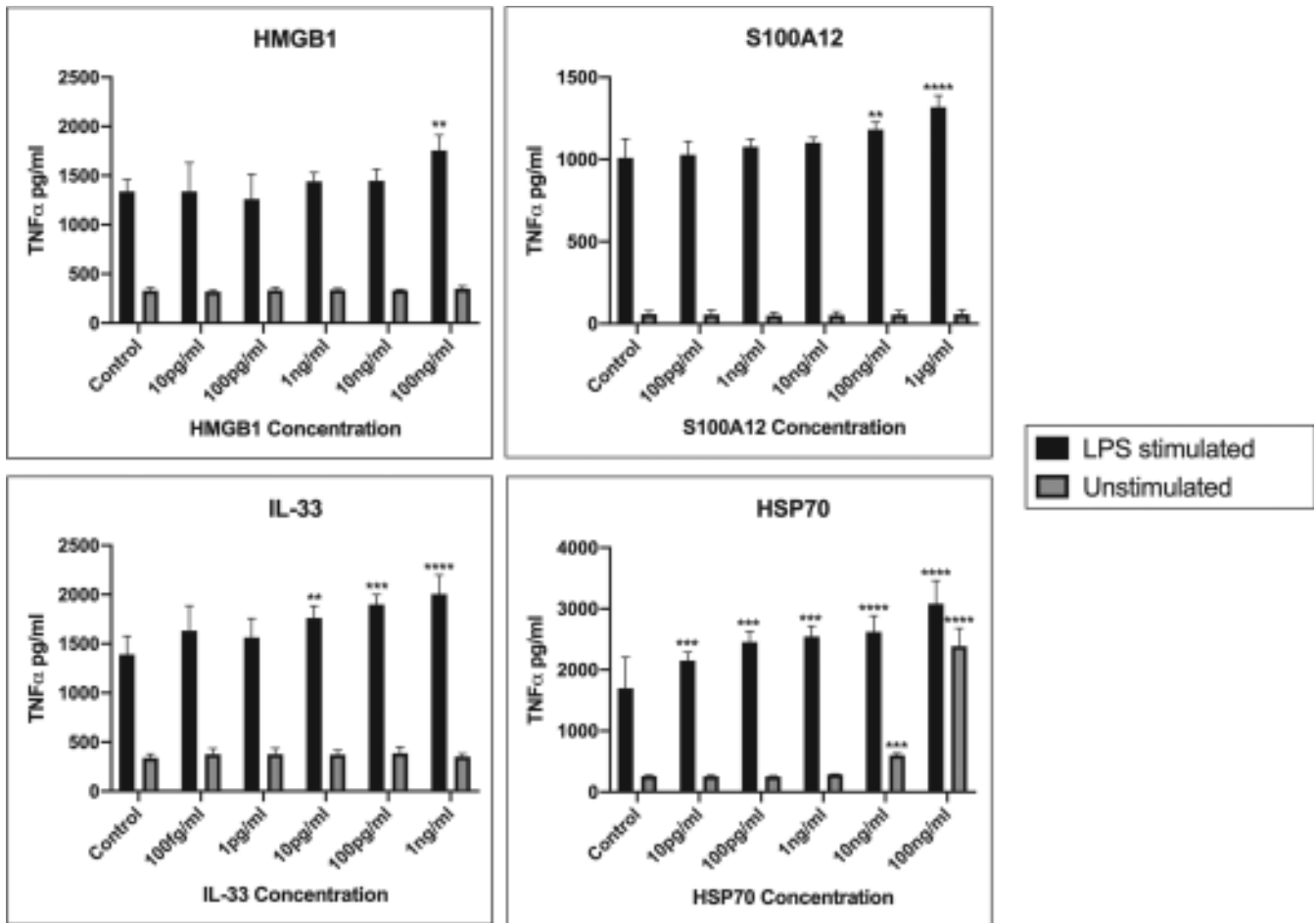


Figure 1. Mean TNF- α release in $\text{pg}\cdot\text{ml}^{-1}$ (\pm SEM) with and without LPS stimulation at a range of concentrations of (a) HMGB1, (b) S100A12, (c) IL-33, and (d) HSP70. Representative data from individual healthy volunteers. *P* values for one-way ANOVA (Dunnett's multiple comparisons test) represented as **P* \leq .05, ***P* \leq .01, ****P* \leq .001, and *****P* \leq .0001. Unstimulated and LPS-stimulated controls were used as baseline comparator

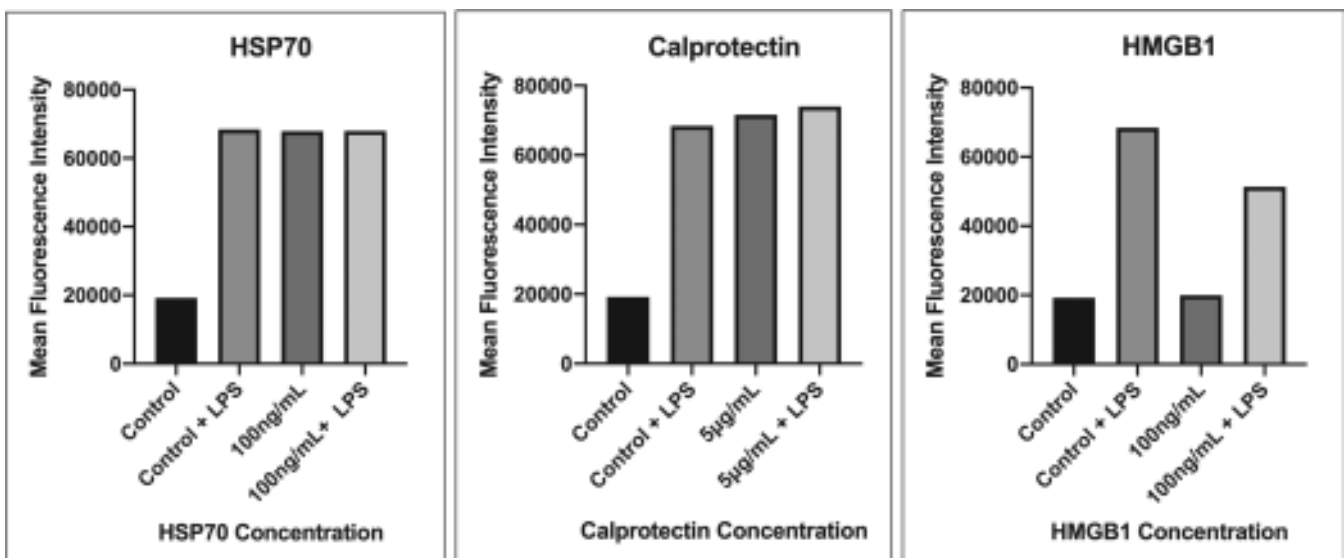


Figure 2. HLA-DR expression on CD14⁺ monocytes from a single healthy volunteer, following stimulation with (a) HSP70, (b) calprotectin, and (c) HMGB1, with and without LPS

HMGB1, HSP70, IL-33, and S100A12 increased TNF- α release from LPS-stimulated blood when compared to LPS-stimulated control (Figure 1). At maximum tested concentrations, mean TNF- α release was increased by 416 pg·ml⁻¹ for HMGB1 (95% CI [130, 703], $P = .0026$), 1,384 pg·ml⁻¹ for HSP70 (95% CI [920–1,849], $P < .0001$), 616 pg·ml⁻¹ for IL-33 (95% CI [336, 897], $P < .0001$), and 308 pg·ml⁻¹ for S100A12 (95% CI [198, 417], $P < .0001$).

HSP70 and calprotectin independently increased HLA-DR expression on CD14⁺ monocytes, while HMGB1 appears to reduce up-regulation of HLA-DR expression in response to LPS stimulation (Figure 2).

Conclusion and Implications: Contrary to recent clinical reports and animal data, we did not find evidence of a negative immunomodulatory effect of the tested alarmins on human circulating monocytes. While responses were inevitably not uniform, several alarmins—most notably HSP70, IL-33, HMGB1, S100A12, and calprotectin—appeared independently stimulatory to monocytes or enhanced the response to subsequent LPS challenge. This preliminary exploration requires further verification.

REFERENCES

- Frazier, W. J., & Hall, M. W. (2008). Immunoparalysis and adverse outcomes from critical illness. *Pediatric Clinics of North America*, 55(3), 647–668xi. <https://doi.org/10.1016/j.pcl.2008.02.009>
- Segre, E., & Fullerton, J. N. (2016). Stimulated whole blood cytokine release as a biomarker of immunosuppression in the critically ill: The need for a standardized methodology. *Shock*. <https://doi.org/10.1097/SHK.0000000000000557>
- Vourc'h, M., Roquilly, A., & Asehnoune, K. (2018). Trauma-induced damage-associated molecular patterns-mediated remote organ injury and immunosuppression in the acutely ill patient. *Frontiers in Immunology*, 9, 1330. <https://doi.org/10.3389/fimmu.2018.01330>

P099 | Examining the role of transient receptor potential canonical 5 in osteoarthritis

Joao de Sousa Valente; Xenia Kodji; Sabah Bharde; Patrik Keringer; Susan Brain

King's College London

Background and Purpose: We have recently shown that genetic deletion (transient receptor potential canonical 5 [TRPC5] knockout [KO]) or pharmacological blockade of the TRPC5 receptor in a joint inflammation model resulted in marked exacerbation of hyperalgesia and critically increased localised inflammation in the synovium (Alawi et al., 2017). Further mRNA expression of TRPC5 was reduced in the synovium from patients with osteoarthritis (OA), highlighting a

potential role for TRPC5 in OA (Alawi et al., 2017). Here, we examine the development of monoiodoacetate (MIA)-referred mechanical hypersensitivity and joint pathology in wild-type (WT) and TRPC5 KO mice.

Experimental Approach: WT and TRPC5 KO 129S1/SvIm mice were intra-articularly injected with 1-mg MIA or vehicle (10 μ l per saline), seven to eight mice per group. Hind-paw mechanical thresholds were measured using calibrated Von Frey hairs and weight bearing changes using a weight incapitance tester regularly for 28 days. Knee joint cartilage degradation was analysed using Safranin O staining. RNA from ipsilateral synovial membrane and L3–L5 dorsal root ganglia was extracted using RNeasy Plus Mini Kit (Qiagen), reverse-transcribed using SuperScript ViLO cDNA synthesis reagents (Invitrogen). Gene expression was determined using PowerUp SYBR Green Master Mix kit and 7900HT Real-Time PCR instrument (Applied Biosystems). All statistical significance was determined using ANOVA plus Tukey's test.

Key Results: Both TRPC5 KO and WT mice developed referred mechanical hypersensitivity and weight bearing asymmetries following MIA injection, with faster onset (Day 3 vs. Day 7) in TRPC5 KO mice. Twenty-eight days after MIA injection, mechanical hypersensitivity had reached similar levels in TRPC5 KO and WT mice (Figure 1). Twenty-eight days after MIA injection, the joints of TRPC5 KO mice showed increased signs of cartilage degradation compared to TRPC5 KO saline-treated mice (0.59 ± 0.21 vs. 2.83 ± 0.74 , $n = 8$ and 7 , respectively, $^*P = .02$). Further, TRPC5 KO MIA-treated mice showed increased expression of MMP2 and MMP13, ADAMTS4, and CD117 in the synovium and ATF3, CSF1, galanin, and CGRP in the DRG (Table 1).

Conclusion and Implications: This study suggests that deletion of the TRPC5 receptor signalling is associated with a faster onset of pain-like behaviour in a model of OA which correlates with increased expression of enzymes involved in cartilage remodelling and inflammatory cells in the synovium and increased neuronal activation and injury in the DRG. The relationship of joint cartilage degradation to nociceptive hypersensitivity of TRPC5 KO mice in the MIA model will be established in future studies.

ACKNOWLEDGEMENT

This research was supported by Versus Arthritis (ARUK 21524).

REFERENCE

- Alawi, K. M., et al. (2017). *Annals of the Rheumatic Diseases*.

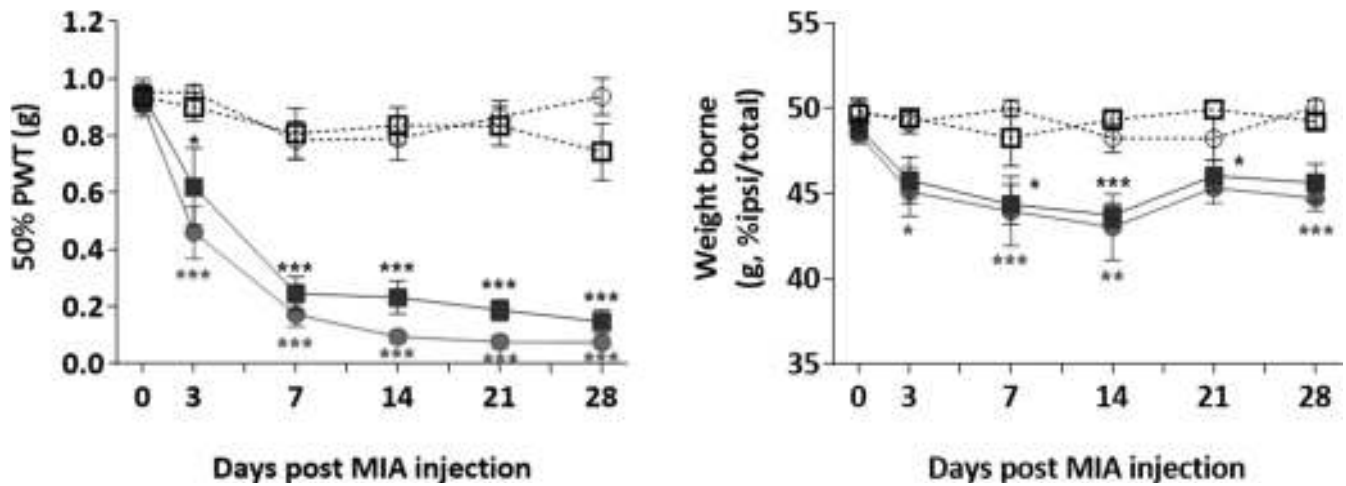


Figure 1. MIA-induced mechanical hypersensitivity and weight bearing deficits. (a) Mechanical thresholds following intra-articular injection of monosodium iodoacetate (MIA) (1 mg per mouse) or saline (10 ml per saline). Data are mean ± SEM of seven to eight mice per group. RM two-way ANOVA followed by Bonferroni's test. (b) Weight bearing asymmetries following intra-articular injection of monosodium iodoacetate (MIA; 1 mg per mouse) or saline (10 ml per saline). Data are mean ± SEM of seven to eight mice per group. RM two-way ANOVA followed by Bonferroni's test

Tissue	Gene	WT saline (n = 8)	WT MIA (n = 8)	TRPC5 KO saline (n = 8)	TRPC5 KO MIA (n = 7)
Synovium	MMP13	1.00 ± 0.23	1.56 ± 0.60	2.59 ± 0.87	4.31 ± 1.55*
	MMP2	1.00 ± 0.18	1.01 ± 0.15	1.28 ± 0.29	2.19 ± 0.52*.#
	ADAMTS4	1.00 ± 0.20	0.89 ± 0.26	0.69 ± 0.24	2.58 ± 0.68*.#,\$
	CD117	1.00 ± 0.08	1.09 ± 0.14	0.83 ± 0.13	1.67 ± 0.34\$
	TRPC5	1.00 ± 0.25	2.17 ± 0.70	0.08 ± 0.06#	0.29 ± 0.15#
DRG	ATF3	0.97 ± 0.16	2.26 ± 0.43	1.06 ± 0.16	3.79 ± 1.36*
	CSF1	1.04 ± 0.10	1.37 ± 0.12	1.25 ± 0.19	1.78 ± 0.30*
	Galanin	0.95 ± 0.10	1.24 ± 0.12	1.07 ± 0.10	2.28 ± 0.65*
	CGRP	1.03 ± 0.09	1.07 ± 0.12	1.25 ± 0.17	1.67 ± 0.17*.#
	TRPC5	1.02 ± 0.07	1.41 ± 0.12*	0.01 ± 0.00***.###	0.03 ± 0.02***.###

Note. Expression was calculated using the $2^{-\Delta\Delta Ct}$ method against to housekeeping genes, $\beta 2$ macroglobulin, and HPRT and normalised to WT saline group. Values are mean ± SEM, ANOVA + Tukey's post hoc test.

Abbreviations: ADAMTS4, a disintegrin and metalloproteinase with thrombospondin motifs 4; ATF3, cAMP-dependent transcription factor ATF-3; CD117, cluster of differentiation 117; CSF1, colony-stimulating factor 1; MMP13, matrix metalloproteinase 13; MMP2, matrix metalloproteinase 2; TRPC5, transient receptor potential canonical 5.

*P < .05 versus WT saline group.

***P < .001 versus WT saline group.

\$P < .05 versus TRPC5 saline group.

#P < .05 versus WT MIA group.

###P < .001 versus WT MIA group.

P100 | Therapeutic fasting mitigates metabolic and cardiovascular dysfunction in a prediabetic rat model: Possible role of adipose inflammation

Haneen Dwaib¹; Maha Taher²; Nahed Mogharbil³; Omar Obeid³; Ahmed El-Yazbi³

¹American University of Beirut; ²Lebanese University; ³AUB

Background and Purpose: The risk of cardiovascular complications in type 2 diabetes increases as early as in the prediabetic stage. Our previous studies showed that perivascular adipose tissue inflammation contributes to vascular and cardiac autonomic dysfunction in prediabetic rats. Intermittent fasting has been extensively studied in the management of metabolic diseases. Here, we aim to examine the impact of therapeutic fasting (TF) on the metabolic and cardiovascular stress among MHC-fed prediabetic rats.

Experimental Approach: SD male rats (4–5 weeks) were randomly allocated into three dietary groups: control diet (C), high-calorie

(HC) diet, and HC diet with TF, for 24 weeks. Rats were fed ad libitum in the first 12 weeks. Afterwards, the TF group was subjected to daily fasting from 7.00 p.m. to 7.00 a.m. (during the dark period) for 12 weeks with free access to water and to HC diet during the light phase. Daily food intake, body weight (BW), blood glucose (fasting FBG and random RBG), body composition (BC) (using NMR), HbA1c, serum insulin levels, echocardiographic parameters, and non-invasive BP were measured. At Week 24, rats were catheterized for invasive haemodynamic examination. Cardiac autonomic neuropathy (CAN) was assessed by measuring baroreceptor sensitivity (BRS) using the vasoactive method. After sacrifice, aortic contractility and endothelial function were measured using organ bath experiments.

Key Results: No difference was recorded in body weight, blood glucose level, HbA1c, and glucose tolerance. Daily calorie intake was higher in the HC group compared to control. TF did not reduce caloric intake. Similar to our previous observations, HC feeding led to an increased fat/lean ratio, increased serum insulin level and insulin resistance, increased vascular reactivity, and reduced endothelium-dependent relaxation, parameters that were reversed by TF. As well, SBP was higher in the HC-fed rats (137.7 vs. 119 mmHg), which was reversed in TF rats. This could be explained based on the observed increase in vascular sensitivity to phenylephrine-induced contraction (pEC₅₀ 5.95 vs. 5.53) and a reduced ACh-mediated endothelium-dependent relaxation in HC rats. Both observations were normalized in TF rats. Moreover, HC-fed rats showed parasympathetic CAN manifesting as reduced BRS (DMAP vs. DHR slope decreased from -0.4 to -0.15) that was reversed in TF.

Conclusion and Implications: HC feeding induces vascular and cardiac autonomic dysfunction secondary to perivascular adipose inflammation. TF reverses signs of cardiovascular impairment. Future studies will be conducted to assess the effect of TF on PVAT inflammation.

P101 | Study of inflammasome activation in the intestine and lymph node during pathogenic and non-pathogenic SIV infection in macaques and African green monkeys

Emma Booth¹; Michaela Muller-Trutwin²; Béatrice Jacquelin²; Nicolas Huot²; Thalia Garcia-Tellez²; Philippe Rasclé²

¹University of Glasgow; ²Institut Pasteur

Background and Purpose: Chronic inflammation and macrophage activation in HIV/Simian immunodeficiency virus (SIV) infection persist under combination anti-retroviral therapy and correlate with disease progression in untreated and higher risk of non-communicable diseases in treated patients. SIVagm-infected African green monkeys (AGMs) have the capacity to efficiently resolve SIV-induced inflammation. We previously reported lower levels of plasma IL-18 in AGM than in pathogenic SIV infection in macaques (MAC) (Jacquelin et al.,

2014), which might indicate less inflammasome activation in macrophages during SIVagm infection. We investigated this here.

Experimental Approach: We analysed inflammasome activation in AGM and MAC during SIV infection in the gut, lymph node, and plasma. Using confocal microscopy, we examined how macrophages and IL-18 and IL-1 β expressing cells were distributed. The levels of plasma IL-18 and IL-1 β were analysed longitudinally by Luminex and ELISA with their respective antagonists, IL-18BPa and IL-1RA. An array targeting 45 genes was designed and put in place for our nonhuman primate model, along with methods to isolate macrophages and epithelial cells from the gut. Assays were included to confirm microscopy results and analyse inflammasome and regulator expression.

Key Results: Plasma IL-1 β was produced earlier (Day 2 p.i.) in AGM ($n = 6$) when compared to MAC ($n = 6$). However, plasma IL-18 was higher in MAC (peak 270 pg·ml⁻¹ in MAC, 100 pg·ml⁻¹ in AGM), with IL-18BPa and IL-1RA present in higher concentrations in AGM throughout the infection. Fluorescence staining revealed weak IL-18 and IL-1 β in the jejunum of MAC ($n = 4$) and AGM ($n = 3$) at baseline, that seemed to increase with infection in MAC only ($n = 3$ for MAC and AGM). Preliminary PCR analysis of gut macrophages indicates an increase of IL-1 β transcription in acute phase in MAC only ($n = 1-7$). Preliminary image analysis of gut-associated lymph nodes indicates an increase of IL-18 and IL-1 β in MAC in acute phase, particularly in the B-follicles for IL-1 β ($n = 1-2$).

Conclusion and Implications: In conclusion, MAC displayed higher levels of systemic IL-18 and IL-1 β in SIV infection compared to AGM. This production is reflected by results in the mesenteric lymph node and gut. It could be better regulated in AGM via antagonists in the plasma. Altogether, this suggests a stronger activation of the inflammasome in MAC in SIV infection, with fewer control mechanisms, such as antagonists, when compared to AGM.

REFERENCE

Jacquelin, B., Petitjean, G., Kunkel, D., Liovat, A.-S., Jochems, S. P., Rogers, K. A., et al. (2014). Innate immune responses and rapid control of inflammation in African green monkeys treated or not with interferon- α during primary SIVagm infection. *PLoS Pathogens*, 10(7).

P103 | Investigating the role of the anti-cell death protein myeloid cell leukaemia 1 in macrophage-mediated chemoresistance in acute myeloid leukaemia

Mark Williams¹; Jennifer Duncan²; Stefan Corradini¹; Helen Wheadon³; Simon Barry⁴; Monica Guzman⁵

¹Glasgow Caledonian University; ²University of St Andrews; ³University of Glasgow; ⁴AstraZeneca; ⁵Cornell University

Background and Purpose: Chemoresistance is a major contributing factor towards poor survival in acute myeloid leukaemia (AML). Our preliminary findings show that M2-like (potentially leukaemia supporting) CD163⁺CD206⁺ macrophages are elevated in AML

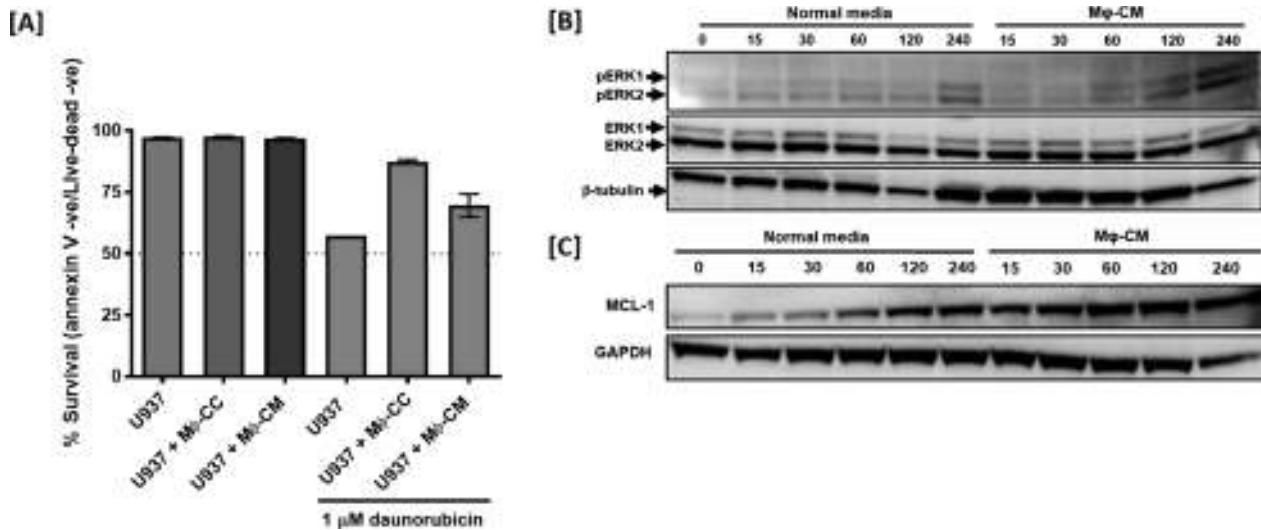


Figure 1: Macrophage-mediated protection of AML cells is associated with up-regulation of the ERK1/2-MCL-1 axis. (a) U937 cells were directly co-cultured with Mφs (Mφ-CC), or exposed to normal media (NM), 50% Mφ conditioned media (Mφ-CM), and cultured in the absence or presence of 1-μM daunorubicin for 24 hr. Apoptosis was assessed by annexin V/live-dead staining (FACS). % survival of viable (annexin V⁻/live-dead⁻) cells was graphed. Data represent mean ± SEM, and two independent experiments (n = 2). (b) Levels of phosphorylated ERKs 1 and 2 (pERK1/2), total ERK1/2, and β-tubulin (loading control) were visualized via the LI-COR Odyssey Fc imaging system. (c) MCL-1 and GAPDH (loading control) were determined as above. Immunoblots are representative of two independent experiments (n = 2)

patients, with others showing that macrophages limit the effect of chemotherapy in a murine model of AML (Keech, McGirr, Winkler, & Levesque, 2017). However, it is unknown if macrophages protect human AML cells from chemotherapy-induced apoptosis. In other leukaemias, the anti-apoptotic protein, myeloid cell leukaemia 1 (MCL-1), is up-regulated by macrophages (Van Attekum et al., 2017). The study objectives were to determine if M2-like macrophages protect AML cells from daunorubicin-induced apoptosis and to ascertain the role of MCL-1.

Experimental Approach: U937 AML cell lines were exposed to daunorubicin (0–10 μM) for 24 hr with % survival determined via annexin V/live-dead assay and flow cytometry (FACS). Conditions were performed in duplicate four separate times (n = 4). The IC₅₀ value (1 μM) was determined using a variable slope (four parameters) model. Monocyte-derived M2-like macrophages were generated from healthy blood donors. U937 cells were cultured with macrophages (Mφ-CC), or exposed to normal media (NM), 50% macrophage conditioned media (Mφ-CM), and exposed to 1 μM daunorubicin for 24 hr. Apoptosis was assessed by annexin V/live-dead staining (FACS) and detection of cleaved caspase-3 (immunoblotting). To assess activation of ERK1/2 (potential positive regulator of MCL-1) and MCL-1 protein levels, U937 cells were exposed to NM or 50% Mφ-CM for 0–240 min, and immunoblotting was performed. Conditions were performed in duplicate, two separate times (n = 2).

Key Results: Mφ-CC and Mφ-CM increased the % survival of U937 cells in the context of daunorubicin versus U937 monoculture (Figure 1a). U937 cells exposed to daunorubicin in the presence of Mφ-CM exhibited reduced cleaved caspase-3 levels, which was associated with increased MCL-1 protein levels. Mφ-CM induced a 2.6-fold increase in p-ERK1/2 and MCL-1 levels in U937 cells at 240 min (Figure 1b,c).

Conclusion and Implications: We are the first to show that M2-like Mφs protect AML cells from chemotherapy-induced apoptosis via cell-to-cell contact and secreted factors and that this chemoprotection is associated with up-regulation of ERK1/2 and MCL-1. This provides a rationale for utilizing drugs targeting ERK1/2 (e.g., AZD6244) and MCL-1 (AZD5991), as therapeutic strategies to circumvent macrophage-mediated chemoprotection.

REFERENCES

Keech, T., McGirr, C., Winkler, I. G., & Levesque, J. P. (2017). Macrophage involvement in the response of acute myeloid leukaemia to chemotherapy. *Blood*, 130, 5069.
 Van Attekum, M. H. A., et al. (2017). Macrophages confer survival signals via CCR1-dependent translational MCL-1 induction in chronic lymphocytic leukemia. *Oncogene*, 36, 3651–3660.

P104 | Understanding the cone-specific visual cycle to develop treatments for inherited blindness

Aimee Frazer; Rebecca Ward; Breandán Kennedy

UCD

Background and Purpose: The visual cycle is the process by which light-sensitive vitamin A is regenerated, subsequently allowing photo-transduction to continuously take place. Understanding the visual cycle is essential as many complex retinal disorders arise from inherited defects within this cycle. The canonical pathway takes place in the RPE where Rpe65 acts as the sole isomerase and supplies both rods and cones with 11-cis-retinal, whereas the cone-specific pathway

is believed to take place in retinal Müller glia. The cone-specific cycle is not as well characterised, and the key isomerase has been coined as isomerase II; however, its identity is not known. Des1, an enzyme involved in ceramide synthesis, has been identified as a putative isomerase II. This project aimed to further understand the role of Des1 and Rpe65 in the cone-specific chromophore synthesis pathway.

Experimental Approach: A Des1 CRISPR knockout was generated in zebrafish larvae, a cone-dominant model, and injected larvae were functionally analysed using visual motor response (VMR) and optokinetic response (OKR). *des1* expression in microdissected mouse ocular tissue was also evaluated by RT-PCR. Visual function analysis of *rpe65a*^{-/-} larvae was carried out to examine the role of Rpe65, a key enzyme in the canonical pathway, in the cone-specific cycle.

Key Results: *des1* is expressed in the eyes and trunks of wild-type larvae at 5 days post fertilisation (5 dpf), suggesting that it may play a role in zebrafish vision and other non-ocular roles. *des1* expression in microdissected mouse ocular tissue showed highest expression in the iris and RPE, with lowest expression somewhat surprisingly in the murine retina. CRISPR/Cas9 technology was used to create a 484-bp deletion in the *des1* gene. The *des1* knockout was viable in the "mosaic" F₀ knockouts. Behavioural analysis revealed that the mosaic knockout had no robust effects on visual function when examined by VMR and OKR. The *rpe65a*^{-/-} knockout was found to significantly reduce the VMR of the larvae whereas their OKR response remained normal. This indicated that the knockout may cause a delayed light adaptation in the larvae.

Conclusion and Implications: These findings suggested that further studies in the isogenic F2 *des*^{-/-} line are essential as the role of Des1 in the cone-specific visual cycle remains elusive and that Rpe65 may play a role in cone-mediated vision of zebrafish larvae.

P108 | Phasic and tonic components to adrenergic contractions in rat portal vein

James Docherty¹; Hadeel A. Alsufyani²

¹Royal College Surgeons, Ireland; ²Physiology, KAU, Jeddah

Background and Purpose: The portal vein carries blood at low pressure from the capillaries of the gastrointestinal tract to the liver capillaries, and flow is aided by peristaltic contractions. Contractions to adrenergic agonists in rat portal vein involve phasic and tonic components, and responses are reported to be α_{1A} -adrenoceptor mediated (Marshall et al., 1996). In this study, we have investigated the receptor subtypes involved in contractions to phenylephrine.

Experimental Approach: Male Wistar rats (250–300 g) were killed by CO₂ overdose, and portal veins were mounted longitudinally in organ baths under 0.5-g tension and bathed with Krebs–Henseleit solution at 37°C. Tissues were contracted with cumulative additions of phenylephrine in 0.5 log unit increments, over the concentration range 10⁻⁸–10⁻³ M. Two concentration response curves were carried out: control and in the presence of antagonist or distilled water vehicle.

Key Results: Portal veins exhibited spontaneous phasic contractions. Phenylephrine, in low concentrations, increased the amplitude of these phasic contractions (pD₂: 6.52 ± 0.17, -log M, n = 5) and, in high concentrations, produced tonic contractions (pD₂: 5.30 ± 0.22, -log M, n = 5).

The α_{1D} -adrenoceptor antagonist BMY7378 (10⁻⁷ M) did not significantly affect tonic or phasic contractions to phenylephrine. The α_{1A} -adrenoceptor antagonist RS100329 (3 × 10⁻⁹ M) shifted both phasic and tonic responses to phenylephrine but produced a significantly more marked shift of phasic (log [DR-1]: 1.99 ± 0.22, n = 5) than tonic (log [DR-1]: 1.26 ± 0.20, n = 5) contractions to phenylephrine (*P* < .01, repeated measures ANOVA). The non-selective α_1 -adrenoceptor antagonist prazosin (3 × 10⁻⁸ M) produced similar shifts in the phasic (log [DR-1]: 1.33 ± 0.21, n = 5) and tonic (log [DR-1]: 1.31 ± 0.19, n = 5) contractions to phenylephrine (no significant difference).

Conclusion and Implications: It is concluded that there is no evidence for involvement of α_{1D} -adrenoceptors in responses of rat portal vein to phenylephrine, but phasic responses were markedly shifted by RS100329, suggesting involvement of α_{1A} -adrenoceptors. Since RS100329 was less potent against tonic contractions, these may involve α_{1B} -adrenoceptors probably in addition to α_{1A} -adrenoceptors.

REFERENCE

Marshall, I., et al. (1996). *British Journal of Pharmacology*, 119, 407–415.

P110 | Differential effects of HIV antiretroviral drugs upon pro-inflammatory and cardioprotective properties of vascular endothelial cells

Akif Khawaja¹; Kirk Taylor¹; Andrew Lovell¹; Marta Boffito²; Michael Emerson¹

¹Imperial College London; ²Chelsea and Westminster NHS Trust

Background and Purpose: Cardiovascular disease (CVD) is more prevalent among people living with HIV (PLHIV) for unclear reasons; however, certain antiretroviral drugs (ARVs) have been associated with increased CVD risk. Studies demonstrate that some ARVs can enhance platelet and leukocyte activation; however, their effects upon the endothelium are not as well characterised. The vascular endothelium influences CVD through expression of adhesion molecules, coagulation factors, and secretion of membrane-enclosed microparticles (EMPs), which facilitate cellular crosstalk. Our objective was to compare the effects of different ARVs upon endothelial inflammatory responses to better understand the causes of increased CVD in PLHIV.

Experimental Approach: HUVECs were treated with plasma C_{max} concentrations of the clinically used ARVs abacavir sulphate (ABC, 8.96 µM), tenofovir disoproxil fumarate (TDF, 0.52 µM), or tenofovir alafenamide (TAF, 0.46 µM) 2 days prior to experimentation

(90 min·day⁻¹) and stimulated with 10 ng·ml⁻¹ TNF- α . Adhesion molecule, tissue factor (TF) and ectonucleotidase expression, and EMP characterisation were assessed by flow cytometry. PRP was pre-incubated with 50,000 EMP·ml⁻¹ for 30 min, and platelet activation monitored by real-time flow cytometry following ADP (10 μ M), collagen (10 μ g·ml⁻¹), or thrombin receptor activator peptide (TRAP)-6 (10 μ M) stimulation. Statistical significance was tested by one-way ANOVA with Tukey's multiple comparisons test.

Key Results: HUVEC treated with ABC had greater levels of TNF- α -induced ICAM-1 and TF expression compared to both TDF (+1.85-fold and +1.18-fold, $n = 5$, $P < .05$ and $P < .01$) and TAF (+1.86-fold and +1.16-fold, $n = 5$, $P < .05$ and $P < .01$). In contrast, HUVEC treated with TDF or TAF displayed greater ectonucleotidase expression compared to vehicle (+1.44-fold and +1.46-fold, $n = 5$, $P < .05$), whilst ABC had no significant effect. We also noted greater numbers of ICAM-1+ and TF+ EMP in ABC-treated cells compared to TDF-treated (+2.06-fold and +3.34-fold, $n = 5$, $P < .05$) and TAF-treated (+2.24-fold and +3.48-fold, $n = 5$, $P < .05$) cells. Moreover, following normalisation, EMP isolated from ABC-treated endothelium significantly enhanced collagen-evoked, but not ADP- or TRAP-6-evoked, platelet integrin activation (+1.67-fold and +1.87-fold, $n = 5$, $P < .05$) and α -granule release (+1.42-fold and +1.45-fold, $n = 5$, $P < .05$).

Conclusion and Implications: The ARVs ABC, TDF, and TAF differentially affect the endothelial inflammatory response. ABC enhanced ICAM-1 and TF expression, which may confer greater pro-inflammatory and pro-thrombotic properties. In contrast, TDF and TAF increased ectonucleotidase-positive endothelial populations, which may indicate cardioprotective effects through the increased degradation of platelet agonists. Further work is required in more relevant cell types and in clinical settings with approved ARV combinations to establish whether these inflammatory changes elucidate mechanisms by which ARVs may affect CVD in PLHIV.

P111 | Influence of adenosine deaminase 2, on the angiogenic function of blood outgrowth endothelial cells

Loryn Halliday¹; Paul Brogan²; Nicholas Freestone³; Francesca Arrigoni³

¹Kingston University London; ²UCL, Great Ormond Street, Institute of Child Health; ³Kingston University

Background and Purpose: Adenosine deaminase 2 (ADA2), usually released from circulating leukocytes, has recently become a therapeutic target in treating children with systematic vasculitis due to autosomal recessive loss-of-function mutations in the ADA2 gene (formerly known as *CECR1*). Children with a deficiency in ADA2 (DADA2) exhibit inflammation, endothelial damage, and elevated plasma

adenosine levels, although the direct influence of ADA2 on the endothelium is unclear.

Experimental Approach: Our aim was to investigate the influence of ADA2 in the presence of its substrate, adenosine, on the proliferation and migration of blood outgrowth endothelial cells (BOECs), which are endothelial progenitors isolated and cultured from healthy donors ($n = 5$). PBMCs were extracted from whole blood, cultured in EBM-2 media on collagen-coated plates for 7–21 days, until the formation of colonies with characteristic cobble-shaped morphology. BOECs were confirmed to have classical endothelial cell surface marker expression (CD31, CD144, low CD34) using flow cytometry. BOECs were then treated with increasing concentrations of adenosine (from 10 nM to 100 μ M) with and without ADA2 (10 U·L⁻¹) for 24 hr before being assessed for changes in cell proliferation (Colorimetric BrdU ELISA) or cell migration (scratch wound assay).

Key Results: ADA2 treatment of BOEC decreased both growth rate of BOECs and migration ($-18 \pm 7.4\%$, at 18 hr, $n = 5$, $P < .05$). Adenosine influenced endothelial proliferation in a dose-dependent manner increasing BOEC cell proliferation at lower concentrations (10 nM–0.5 μ M) and reduced proliferation at higher concentrations (1–100 μ M). ADA2 did not influence the proliferation of BOEC in the presence of adenosine, except at 0.5 μ M, where it created a significant spike in endothelial cell growth ($+65 \pm 17.4\%$, $n = 5$, $P < .01$).

Conclusion and Implications: This is the first time that the influence of adenosine and ADA2 has been studied on these cells. We demonstrated that physiological concentrations of ADA2 alone inhibited both endothelial cell proliferation and migration of BOECs; however, in the presence of adenosine, these changes were absent. In addition, the combination of physiological levels of ADA2 in the presence of 0.5- μ M adenosine created significant increases in BOEC proliferation. We believe that these data strongly provide evidence of one mechanism by which ADA2, in the presence of adenosine, can promote endothelial health and repair and therefore in ADA2-deficient, DADA2 patients, might contribute to the endothelial damage and ensuing inflammation and vasculitis that is observed.

P112 | Prostanoid inhibition of IL-6 signalling and function in pulmonary arterial endothelial cells

Gillian Durham¹; Tim Palmer¹; Talat Nasim²; Claire Rutherford³

¹University of Hull; ²University of Bradford; ³University of Glasgow

Background and Purpose: IL-6 has been highlighted as a key inflammatory factor in pulmonary arterial hypertension (PAH) development (Jasiewicz et al., 2014) due to IL-6-mediated JAK/STAT signalling to induce transcription of pro-inflammatory and pro-angiogenic genes. IL-6 also induces the transcription of suppressor of cytokine signalling 3 (SOCS3) which limits IL-6 signalling (Babon et al., 2014). Current

TABLE 1 STAT3 Tyr705 phosphorylation post-prostanoid treatment alongside IL-6 versus treatment with IL-6 alone (100%)

	AS-M.5 WT	AS-M.5 SOCS3 KO
BPS	60 ± 21%**	72 ± 19%#
Treprostinil	65 ± 21%*	79 ± 20%#

Note. Quantification for $n = 5$ experiments.

* $P < .05$.

** $P < .01$.

#Not significant.

PAH therapies target the symptoms of PAH and include prostanoid drugs which induce vasodilation via stimulating cAMP (Lau et al., 2017). However, other mechanisms of prostanoids have not been investigated. As cAMP also induces SOCS3 (Sands et al., 2006), we hypothesised that an important mechanism by which cAMP-mobilising prostanoid drugs could limit PAH is via SOCS3 inhibition of IL-6 induced JAK/STAT signalling.

Experimental Approach: Immunoblotting was used to determine the effects of beraprost sodium (BPS) (10 μ M), treprostinil (10 μ M), and the selexipag metabolite ACT-333679 (1 μ M) on SOCS3 expression and inhibition of IL-6 *trans*-signalling activity, measured via STAT3 Tyr705 phosphorylation, in human pulmonary arterial endothelial cells (HPAECs) and angio-sarcoma (AS-M.5) cells. Induction of SOCS3 gene transcription was also measured via qPCR. A FITC-dextran cell permeability assay was utilised to measure the ability of prostanoids to inhibit an IL-6-induced increase in cell permeability. Statistical significance was determined using one-way ANOVA and the Bonferroni post hoc test using Prism5 software (GraphPad).

Key Results: BPS and treprostinil each stimulated SOCS3 protein expression in HPAECs in a time-dependent manner with maximum protein accumulation detectable after by 2 hr while ACT-333679 treatment induced maximal SOCS3 protein expression in HPAECs after 4 hr. BPS induced a transient increase in SOCS3 mRNA levels that peaked 1 hr post-treatment, suggesting that prostanoid drugs increased SOCS3 gene transcription.

IL-6 mediated Tyr705 phosphorylation of STAT3 in HPAECs was inhibited after 4 hr of treatment with BPS (55 ± 14% vs. IL-6 alone, $P < .01$), treprostinil (58 ± 5%, $P < .01$), and ACT-333679 (27 ± 10%, $P < .001$). Experiments in AS-M.5 SOCS3 KO cells suggested that this was due in part to SOCS3 as STAT3 phosphorylation was significantly inhibited in AS-M.5 wild-type (WT) cells but not AS-M.5 SOCS3 KO cells (Table 1).

BPS also rescued HPAECs from increased cell permeability resulting from treatment with IL-6/sIL-6R α (67 ± 7% vs. IL-6 alone, $P < .05$).

Conclusion and Implications: Our results indicate that prostanoid drugs used to treat PAH each induce SOCS3 expression and limit IL-6 *trans*-signalling sufficiently to limit IL-6-mediated increases in endothelial cell permeability. From these and future studies, it is anticipated that more effective strategies will emerge with which to target the IL-6/JAK/STAT signalling pathway in PAH.

REFERENCES

1. Babon, J. J., et al. (2014). *Seminars in Immunology*, 26, 13–19.
2. Jasiewicz, M., et al. (2014). *Cytokine*, 76, 187–192.
3. Lau, E. M. T., et al. (2017). *Nature Reviews. Cardiology*, 14, 603–614.
4. Sands, W. A., et al. (2006). *Molecular and Cell Biology*, 26, 6333–6346.

P113 | Antiproliferative effects of PDE1 inhibition in human pulmonary artery smooth muscle cells

Zaher Al Bakour¹; James Guy Breitenbacher²; Fiona Murray¹

¹University of Aberdeen; ²Convelo Therapeutics

Background and Purpose: Pulmonary arterial hypertension (PAH) is a disease characterized by increased pulmonary vascular resistance and remodelling in the pulmonary artery. We have previously shown that PAH is accompanied with increased PDE1C (catalyses the hydrolysis of cAMP and cGMP), which in part accounts for lower cyclic nucleotide levels and increased proliferation of pulmonary artery smooth muscle cells (PASMCs) isolated from PAH patients. Recently, new selective PDE1 inhibitors have been developed for CNS disorders and tested in preclinical studies. We aimed to provide evidence for the utility of such selective PDE1 inhibitors for PAH.

Experimental Approach: Human PASMCs (Lonza) were treated for 24–72 hr with 10- μ M 16K (with/without 1–1,000 nM of selexipag or iloprost) in the presence/absence of hypoxia (1% O₂, 72 hr). Proliferation was measured by MTS assay (Promega) and cAMP accumulation by ELISA in the presence/absence of forskolin (1 μ M, Enzo Life Science). PCNA and pVASP were detected by Western blot. Experiments were performed three times, and data presented as means ± SEM and compared by ANOVA or Student's *t* test.

Key Results: Proliferation of PASMCs with hypoxia (72 hr, 1% O₂) correlated with increased PDE1C expression (7.6 ± 0.9, $n = 3$, $P < .05$). In parallel, G1-arrested PASMCs showed decreased PDE1C expression levels. The novel PDE1 inhibitor, 16K (10 μ M), reduced the proliferation of hypoxic-PASMC (21 ± 2.4% decrease, $n = 3$, $P < .05$), which was associated with decreased PCNA levels. 16K increased forskolin-stimulated cAMP levels (151 ± 8.6 pmol·mg⁻¹, forskolin vs. 224 ± 16.8 pmol·mg⁻¹, forskolin + 16K, $n = 3$, $P < .01$) and pVASP. Importantly, we found that 16K enhanced the response of selexipag and iloprost (prostacyclin receptor agonists) by enhancing pVASP and decreasing PASMC proliferation.

Conclusion and Implications: PDE1 inhibition restored cAMP accumulation and reduced the proliferation of PASMC alone and in combination with current clinically used drugs (selexipag and iloprost); therefore, our data provide evidence for PDE1 inhibitors for PAH treatment.

REFERENCE

1. Murray, F., et al. (2007). *American Journal of Physiology - Lung Cellular and Molecular Physiology*, 292(1), L294–L303.

P114 | Tangeretin alleviates L-NAME-induced high BP and left ventricular remodelling in rats via suppressing AT₁R/pERK1/2 pathway

Putcharawipa Maneesai; Chutamas Wunpathé;
Poungnat Pakdeechote; Siwayu Rattanakanokchai
Khon Kaen University

Background and Purpose: Several biological activities of tangeretin (TG), a citrus flavonoid, has been reported (Lee et al., 2016). This study aims to evaluate the effect of T on BP and left ventricular (LV) remodelling in L-NAME-induced hypertensive rats.

Experimental Approach: Male Sprague-Dawley rats were divided into five groups: control group, L-NAME (40 mg·kg⁻¹·day⁻¹) group, L-NAME groups treated with TG (15 mg·kg⁻¹) or T (30 mg·kg⁻¹), or captopril (5 mg·kg⁻¹) (n = 8 in each group). After 5 weeks of the experiment, BP measurement, cardiac morphometry study, and western blot analysis of AT₁R and pERK1/2 protein expression were performed. Statistical significance was analysed using one-way ANOVA followed by LSD tests.

Key Results: L-NAME-treated rats had high BP (120.39 ± 2.33 vs. 197.31 ± 6.64 mmHg) comparing to those of control rats (P < .05). In addition, LV remodelling was found in L-NAME group as evidenced by increases in HW/BW, LVW/BW ratio, wall thickness, and the cross-sectional area, and decrease in luminal area of the LV (Table 1). Subsequently, LV fibrosis was accumulated in L-NAME hypertensive rats comparing to those of the control group (Table 1, P < .05). Moreover, the up-regulation of AT₁R and pERK1/2 protein expression was found in cardiac tissue from L-NAME rats. Supplementation with TG or captopril significantly reduced BP, alleviated left ventricular alterations, and restored AT₁R and pERK1/2 protein expression in L-NAME rats (P < .05).

Conclusion and Implications: TG supplementation reduces BP and alleviates LV remodelling in L-NAME-induced hypertensive rats. These effects are involved in the suppression of an AT₁R/pERK1/2 signalling cascade in L-NAME-induced hypertensive rats.

REFERENCE

- Lee, Y. Y., Lee, E.-J., Park, J.-S., Jang, S.-E., Kim, D.-H., & Kim, H.-S. (2016). Anti-inflammatory and antioxidant mechanism of tangeretin in activated microglia. *Journal of Neuroimmune Pharmacology*, 11, 294–305.

P240 | IL-13 and IL-4 induce 5-HT-mediated airway hyperreactivity in mouse trachea

Willem Abma; Jesper Säffholm; Craig Wheelock; Sven-Erik Dahlen; Mikael Adner

Karolinska Institutet

Background and Purpose: Inflammation plays a key role in the pathophysiology of asthma. Two important cytokines are IL-4 and IL-13. We have previously shown that exposure to these ILs leads to airway hyperreactivity in human bronchi. We now set out to translate this effect into a mouse model looking at the effect of IL-4/IL-13 on contractions evoked by activation of two different contractile GPCRs, namely, 5-HT_{2a} and the TP receptor in mouse trachea.

Experimental Approach: Tracheae from naïve, male BALB/c mice (n = 4, 8–10 weeks old) were dissected free from connective tissue and divided into four intact ring segments. The segments were incubated in DMEM for 4 days in the presence of IL-4 (100 ng·ml⁻¹) or IL-13 (100 ng·ml⁻¹) in combination or alone. Fresh DMEM and cytokines were added every day. On the fourth day, the segments were mounted in a myograph, and 5-HT and U46619 concentration-response curves were obtained in the presence of indomethacin (3 µM). The data are represented as mean ± SEM and normalised against carbachol (10 µM). The data were analysed using one-way ANOVA.

Key Results: In cultured control segment, 5-HT caused a concentration-dependent contraction reaching a maximal response (E_{max}) of 18.6 ± 4.7%. Both IL-4 and IL-13 alone, or in combination, increased the E_{max} of 5-HT to 36.8 ± 4.3%, 55.9 ± 3.5%, and 46.3 ± 3.6% (P < .05), respectively. U46619 caused a much stronger contraction than 5-HT reaching an E_{max} of 80.2 ± 5.0% in the control

TABLE 1 Effects of tangeretin and captopril on cardiac mass indices and cardiac morphometry in L-NAME-induced hypertensive rats

Parameter	Control	L-NAME	L + TG15	L + TG30	L + Cap
HW/BW (mg·g ⁻¹)	2.65 ± 0.03	2.97 ± 0.02 [†]	2.61 ± 0.02 [#]	2.46 ± 0.05 [#]	2.62 ± 0.04 [#]
LVW/BW (mg·g ⁻¹)	1.86 ± 0.03	2.15 ± 0.03 [†]	1.85 ± 0.02 [#]	1.75 ± 0.02 [#]	1.75 ± 0.03 [#]
LV wall thickness (mm)	2.45 ± 0.06	3.34 ± 0.07 [†]	2.63 ± 0.10 [#]	2.61 ± 0.06 [#]	2.60 ± 0.03 [#]
LV cross-sectional area (mm ²)	51.72 ± 1.18	69.72 ± 1.82 [†]	49.69 ± 0.36 [#]	48.47 ± 1.45 [#]	53.34 ± 1.53 [#]
LV luminal area (mm ²)	11.37 ± 0.80	6.75 ± 0.32 [†]	9.49 ± 0.88 [#]	9.74 ± 0.46 [#]	9.35 ± 0.23 [#]
LV fibrosis (%)	0.39 ± 0.08	1.37 ± 0.15 [†]	0.55 ± 0.05 [#]	0.47 ± 0.08 [#]	0.77 ± 0.15 [#]

Note. Data are expressed as means ± SEM (n = 8 per group).

Abbreviations: BW, body weight; Cap, captopril; HW, heart weight; LV, left ventricular; LVW, left ventricular weight; TG, tangeretin.

*P < .05 versus control.

[#]P < .05 versus L-NAME.

segments, and this response was unaffected by IL-13 ($74.1 \pm 5.2\%$), IL-4 ($60.5 \pm 5.1\%$), or IL-13 + IL-4 ($74.5 \pm 3.6\%$).

Conclusion and Implications: In mouse trachea, both IL-4 and IL-13 cause 5-HT-mediated airway hyperreactivity without having an additional effect when combined. The model is found appropriate to investigate signalling mechanisms in type 2-induced airway inflammation.

Poster Session: Neuropharmacology 2

P116 | Investigating $\alpha 7$ nicotinic receptors as a target to prevent relapse in drug-induced conditioned place preference

Maria Giulia Coccia¹; Sue Wonnacott¹; David Heal²; Christopher P. Bailey¹

¹University of Bath; ²RenaSci LTD

Background and Purpose: Chronic exposure to drugs of abuse induces the formation and maintenance of maladaptive drug cue-context associations that can induce relapse. The ventral hippocampus (vHip) is involved in associative memory and drug-related emotional behaviours. The cholinergic system plays a key role in neuronal activity and synaptic plasticity in the vHip (Luchicchi et al., 2014). Inhibiting $\alpha 7$ nicotinic ACh receptors ($\alpha 7$ nAChRs) in vHip with the antagonist methyllycaconitine (MLA) selectively attenuated priming-induced reinstatement in morphine conditioned place preference (CPP) (Wright et al., 2019). Hence, the aims of this study are to investigate if $\alpha 7$ nAChRs contribute to heroin- and cocaine-CPP in mice and to examine c-Fos expression in vHip after drug priming-induced reinstatement.

Experimental Approach: Male C57BL/6J mice (6–7 weeks old) underwent heroin- or cocaine-induced CPP (heroin: $2 \text{ mg}\cdot\text{kg}^{-1}$, i.p.; cocaine: $15 \text{ mg}\cdot\text{kg}^{-1}$, i.p.), followed by extinction training. Drug-primed reinstatement was induced by a single injection of heroin (heroin: $1 \text{ mg}\cdot\text{kg}^{-1}$, i.p.; cocaine: $2 \text{ mg}\cdot\text{kg}^{-1}$, i.p.) with prior injection of MLA ($4 \text{ mg}\cdot\text{kg}^{-1}$, s.c.) or saline controls (Wright et al., 2019). All drugs were prepared in saline. Immediately following reinstatement, mouse brains were perfusion fixed for immunohistochemistry (Ziminski et al., 2018) (anaesthetic used 2% pentobarbital, i.p.); 40- μm coronal brain slices containing vHip were taken to quantify c-Fos expression.

Key Results: MLA prevented reinstatement of heroin-primed CPP, in comparison with saline controls ($P < .05$, Student's *t* test) and c-Fos

expression in vHip after heroin-primed reinstatement was reduced in animals pretreated with MLA ($P < .001$, Student's *t* test). In contrast, MLA did not significantly inhibit cocaine-primed CPP or c-Fos expression following cocaine-primed reinstatement (see Table 1).

Conclusion and Implications: Reinstatement of heroin-CPP and c-Fos expression in the vHip in mice were both inhibited by MLA. This suggests that blockade of $\alpha 7$ nAChRs reduces reinstatement-induced neuronal activation in the vHip that is relevant to addiction-related behaviour. In contrast, MLA did not significantly affect cocaine-primed CPP reinstatement or c-Fos expression, suggesting that $\alpha 7$ nAChRs may play a role in modulating addiction-related behaviour for opioids, but not psychostimulants.

REFERENCES

- Luchicchi, A., et al. (2014). *Frontiers in Synaptic Neuroscience*, 6, 24.
- Wright, V. L., et al. (2019). *Addiction Biology*, 24, 590–603.
- Ziminski, et al. (2018). *Neuropsychopharmacology*, 43, 718–727.

P118 | Protracted environmental enrichment can alter gene expression but not methylation status on Bdnf gene promoter region in the prefrontal cortex

Gabriel Costa¹; Pritilata Chivers²; Nivea Karla Silva¹; Alexis Bailey³; Rosana Camarini¹

¹University of Sao Paulo; ²University of Surrey; ³St Georges University of London

Background and Purpose: Environmental enrichment (EE) is a housing condition characterized by key factors such as social contact, novelty and complexity in the environment, and voluntary exercise (Nithianantharajah & Hannan, 2006). EE interacts with brain-derived neurotrophic factor (BDNF) levels (Rueda, Teixeira, Yonamine, & Camarini, 2012) which performs a key role in neuronal signalling. Strategies that alter neuronal activity, such as EE, can induce changes in the Bdnf gene which is controlled by a complex regulatory region that has nine promoting regions (Aid, Kazantseva, Piirsoo, Palm, & Timmusk, 2007). Among these regions, exon IV locus is related to important changes environmental related, and DNA methylation in this region has been related to this gene expression in important conditions that can alter the neuronal physiology.

Experimental Approach: C57BL male mice were randomly divided and maintained in an enriched (EE, $n = 10$) or non-enriched condition (NE, $n = 10$) to evaluate whether EE can induce epigenetic

TABLE 1 Conditioned place preference and subsequent c-Fos in vHIP investigation

	Heroin reinstatement: CPP (s)		Heroin reinstatement: c-Fos expression (cells·mm ⁻²)		Cocaine reinstatement: CPP (s)		Cocaine reinstatement: c-Fos expression (cells·mm ⁻²)	
	Saline	MLA	Saline	MLA	Saline	MLA	Saline	MLA
Mice <i>n</i>	8	8	4	4	7	8	7	6
Mean \pm SEM	70 \pm 20	-2 \pm 23	333 \pm 19	139 \pm 25	93 \pm 3	43 \pm 35	234 \pm 15	220 \pm 31

modifications in the Bdnf gene. To this purpose, DNA methylation and gene expression at the BDNF exon IV promoter region were analysed in prefrontal cortex brain tissues. Gene expression and methylation status were analysed in exon IV for both groups (Mann-Whitney *U* test). Additionally, BDNF protein expression was accessed by a western blot assay (unpaired *t* test).

Key Results: Gene expression analysis showed a significant increase in exon IV expression for enriched mice compared with the non-enriched group (NE:171,0000; EE:495,0000; *p*:0,00000004). For methylation status (NE:164,0000; EE:136,0000; *p*:0,4428) and BDNF protein level (NE:100 ± 45,6; EE:147 ± 53,94; *p*:0,5326), no significant difference was found.

Conclusion and Implications: Exon IV is a CpG-rich locus, being a target of the methylation process. However, although DNA methylation correlates with gene repression, it will not necessarily be translated into changes in protein expression, as several factors can interfere in this process and BDNF has a complex gene expression which can be affected by several promoters.

REFERENCES

1. Aid, T., Kazantseva, A., Piirsoo, M., Palm, K., & Timmusk, T. (2007). Mouse and rat BDNF gene structure and expression revisited. *Journal of Neuroscience Research*, 85(3), 525–535.
2. Nithianantharajah, J., & Hannan, A. J. (2006). Enriched environments, experience-dependent plasticity and disorders of the nervous system. *Nature Reviews. Neuroscience*, 7, 697–709.
3. Rueda, A. V., Teixeira, A. M., Yonamine, M., & Camarini, R. (2012). Environmental enrichment blocks ethanol-induced locomotor sensitization and decreases BDNF levels in the prefrontal cortex in mice. *Addiction Biology*, 17(4), 736–745.

P119 | Comparison of the pharmacokinetics and time course of effect of the Fab fragment of a humanized anti-cocaine monoclonal antibody in rats

Jordan Marckel; Hanna Wetzel; Tiffany Bell-Howarth; Mackenzie Turner; Rose Webster; Andrew Norman
University of Cincinnati

Background and Purpose: We have developed a humanized anti-cocaine monoclonal antibody, h2E2, that has high affinity for cocaine and a long terminal elimination half-life (7.8 days). Although the

traditional approach to determine the pharmacokinetic profile of a drug is to measure drug concentration in timed blood or plasma samples, the time course of a drug effect can also provide vital information to accelerate drug development. Fab fragments generally have shorter terminal elimination half-lives compared to their whole antibody counterparts. Using self-administration as an *in vivo* assay system, we investigated the time course of effect of the Fab fragment of h2E2 which provided a comparison to the traditional pharmacokinetic method.

Experimental Approach: Pharmacokinetic Study: Rats were injected with Fab fragment (82 mg·kg⁻¹, *i.v.*, pH = 7.4, PBS) (*n* = 3), and blood samples collected from the tip of the tail at designated time points over 3 days. Fab concentrations in blood samples were quantified using an ELISA assay.

Self-Administration Behaviour Study: Rats self-administered cocaine HCl for 15–20 presses/injections at a dose of 300 mmol·kg⁻¹ cocaine (*i.v.*). When intervals stabilized, rats were injected with Fab fragment (82 mg·kg⁻¹, 1 ml·min⁻¹, pH = 7.4, PBS, *i.v.*) (*n* = 7). Infusions lasted approximately 180–240 s or less than the average inter-injection interval of 280 s. After the end of the injection, rat resumed self-administration behaviour for 5 hr. Vehicle control (*n* = 7) was administered at an equal volume as Fab injections, based on weight. Some rats were used in both control and Fab treatment groups.

Key Results: Pharmacokinetic Study: The pharmacokinetic profile of Fab fragment shows two phases (Figure 1). The Fab fragment has a mean distribution half-life (*t*_{1/2a}) of 24.0 ± 3.6 min and a terminal elimination half-life (*t*_{1/2b}) of 6.9 ± 1.1 hr (Table 1, Figure 1).

Self-Administration Behaviour Study: After the injection of Fab, cocaine self-administration rate increased, consistent with the effect of the intact antibody, h2E2 (Figure 2a) (Wetzel, Tsubulsky, & Norman, 2016). However, the effect of half-life of the Fab fragment on self-administration behaviour was determined to be approximately 101 min (1.68 hr) (Table 2) which is shorter than the typically reported pharmacokinetic terminal elimination half-life of 7.1 hr (Figure 1). Vehicle injections did not alter self-administration behaviour (Figure 2b).

Conclusion and Implications: The half-life of the effect of the Fab fragment more closely correlates to the distribution half-life. Therefore, it is likely that the initial decline in Fab fragment concentrations in the blood represents elimination as well as distribution. Self-administration behaviour is a useful assay to examine relevant pharmacokinetic parameters of an antagonist and can help inform the interpretation of traditional pharmacokinetic data.

TABLE 1 The pharmacokinetics of the Fab fragment in male rats

Parameter				
Rat #	<i>t</i> _{1/2a} (min)	<i>t</i> _{1/2b} (hr)	<i>V</i> _D (L·kg ⁻¹)	AUC (mg·min ⁻¹ ·ml ⁻¹)
1	21.6 ± 3.0	7.9 ± 6.9	0.28 ± 0.22	1,212 ± 219
2	28.2 ± 13.8	6.9 ± 37.5	0.38 ± 1.76	778 ± 642
3	22.8 ± 6.6	5.7 ± 4.9	0.41 ± 0.27	959 ± 236
Average	24.0 ± 3.6	6.9 ± 1.1	0.35 ± 0.07	938 ± 218

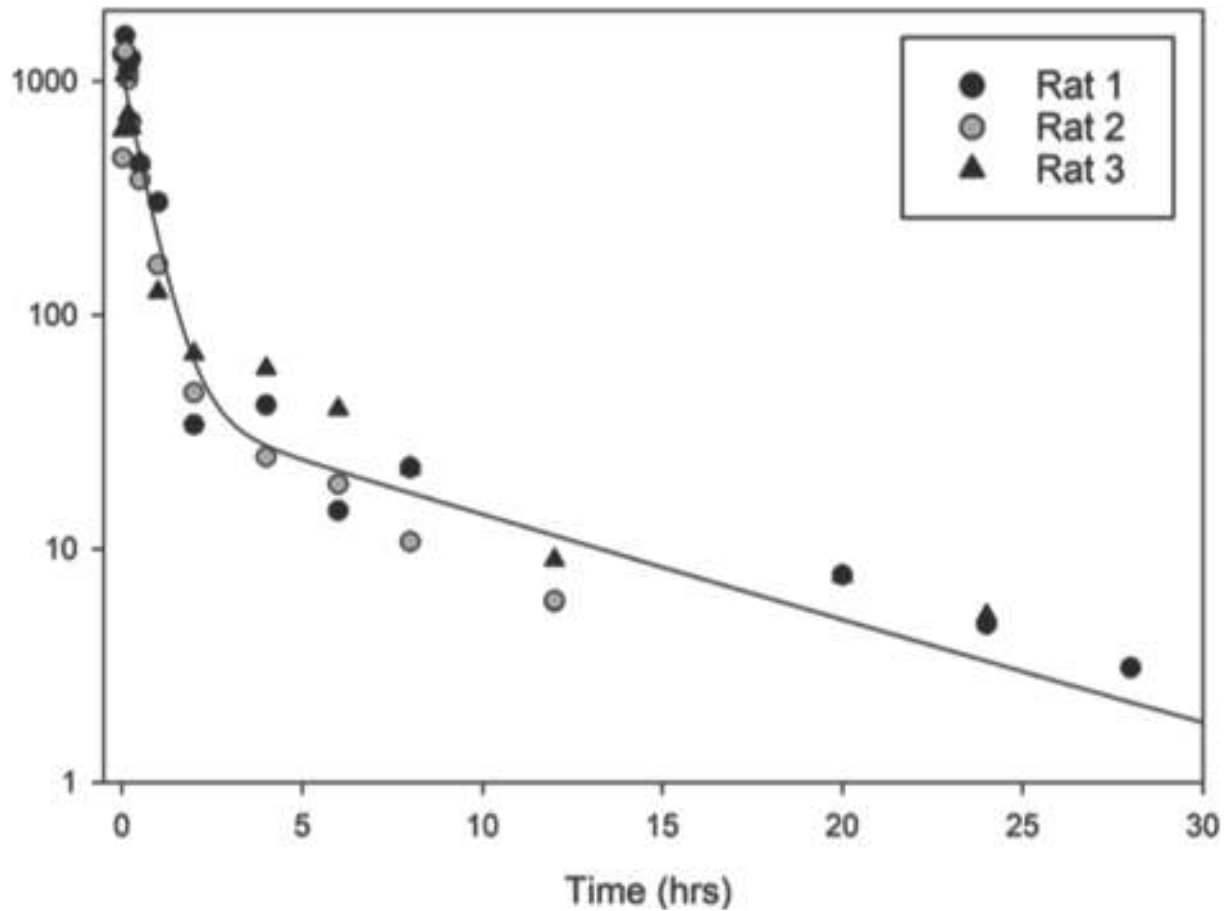


FIGURE 1 The pharmacokinetics of the Fab fragment in male rats

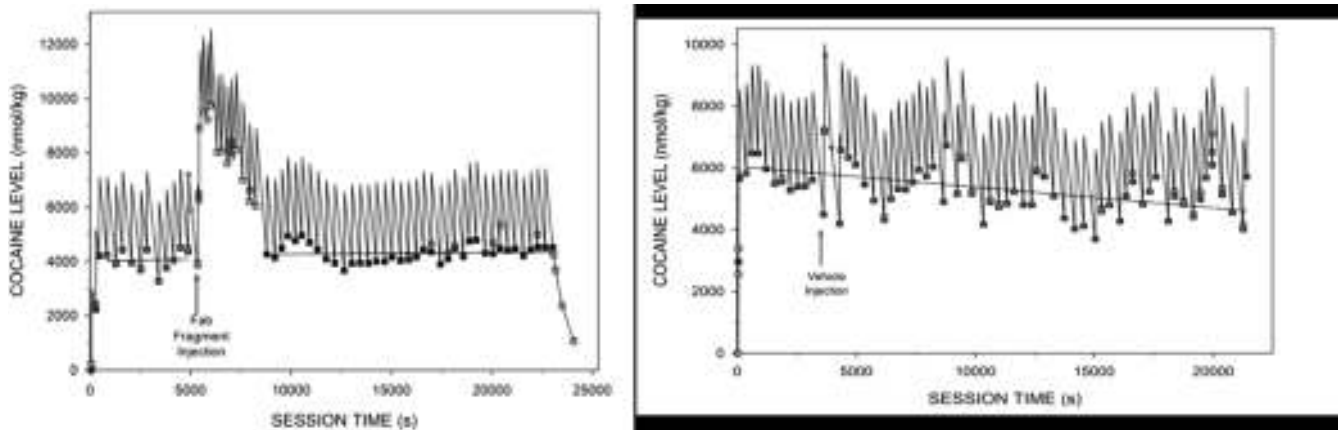


FIGURE 2 The effects of the (a) Fab fragment and (b) vehicle on cocaine self-administration

TABLE 2 Fab fragment in vivo effect pharmacokinetics

Parameter	Average	SD	SEM	n
Effect $t_{1/2}$ (min)	100.8	64.8	24.5	7
Peak ratio	1.9	0.3	0.1	7
t_{max} (min)	19.4	11.2	4.2	7

REFERENCES

- Tsibulsky, V. L., & Norman, A. B. (2005). Real time computation of in vivo drug levels during drug self-administration experiments. *Brain Research. Brain Research Protocols*, 15, 38–45.
- Wetzel, H. N., Tsibulsky, V. L., & Norman, A. B. (2016). The effects of a repeated dose of a recombinant humanized anti-cocaine monoclonal antibody on cocaine self-administration in rats. *Drug and Alcohol Dependence*, 168, 287–292.

P120 | AMPK, mTORC1, protein synthesis, and the regulation of opioid tolerance

Amal Alsubaiyel; Amal Alsubaiyel; Ilona Obara
Newcastle University

Background and Purpose: We previously showed that the mammalian target of rapamycin complex 1 (mTORC1), a kinase which controls protein synthesis, also regulated nociceptor sensitivity and modulated opioid efficacy. A novel aspect of our research identified that metformin, a widely used anti-diabetic drug, regulated opioid tolerance, potentially acting via activation of the 5'-AMP-activated protein kinase (AMPK) and inhibition of mTORC1. Here, we extended our observations and further determined the importance of AMPK, mTORC1, and protein synthesis in the development of morphine tolerance in naïve mice.

Experimental Approach: In adult male C57BL/6J mice (n = 6-8), opioid tolerance was induced by morphine (20 mg.kg⁻¹, i.p.) given twice daily at 12-hr intervals for nine consecutive days. The influence of AMPK activation was assessed by repeated injection of AMPK activator A-769662 (30 mg.kg⁻¹, i.p.) once daily, 20 hr before the morning morphine injection, on each testing day. Using a similar treatment schedule, ascomycin (FK520, 10 mg.kg⁻¹, i.p.) and anisomycin (150 mg.kg⁻¹, i.p.) were also injected. To determine the effect of a single injection of all three drugs on restoring the analgesic effect of morphine, separate groups of mice, tolerant to morphine, received a single injection of A-769662/ascomycin/anisomycin, 20 hr before the subsequent morphine dose. Pain threshold was assessed by tail-flick daily 30 min after morphine injection. All procedures were carried out in accordance with the Animals (Scientific Procedures) Act 1986 and ASPA Amendment Regulation 2012.

Key Results: Our study showed, for the first time, that the AMPK activator A-769662, that is known to produce mTORC1 inhibition, blocked the development and maintenance of morphine tolerance in naïve mice, $F(4, 319) = 757.60, P < .0001$. Furthermore, pretreatment with anisomycin, a known protein synthesis inhibitor, resulted in reduction of morphine tolerance, $F(4, 285) = 1238, P < .0001$. Both drugs when injected singly in tolerant mice fully restored the analgesic

effect of morphine ($P < .05$). In contrast, ascomycin, which binds to FKBP12 but does not inhibit mTORC1, did not regulate the morphine analgesic effect ($P > .05$).

Conclusion and Implications: Our findings provide further evidence that mTORC1 may represent a novel and tractable target for the improvement of opioid analgesic efficacy, particularly in conditions when long-term treatment with opioids is required. An important aspect of our current observations is related to the better understanding of the roles for AMPK, mTORC1, and protein synthesis in regulation of opioid efficacy, and, therefore, our studies provide a novel insight into the complexity of the adaptive molecular mechanisms that underlie opioid treatment.

REFERENCE

Xu, J. T., Zhao, J. Y., et al. (2014). Opioid receptor-triggered spinal mTORC1 activation contributes to morphine tolerance and hyperalgesia. *The Journal of Clinical Investigation*, 124(2), 592-603.

P121 | The changes of protein kinases activities in the brain structures after ghrelin antagonists administration in previously stressed *Danio rerio*

Alexandra Blazhenko; Platon Khokhlov; Ilia Tissen; Andrey Lebedev; Eugeny Bychkov; Petr Shabanov
Institute of Experimental Medicine

Background and Purpose: Nowadays, there are a lot of data to suggest about a key role of ghrelin signalling system in stress response and reinforcement mechanisms. There is a common opinion that a protein kinase system plays a role of a second intracellular messenger for ghrelin system (Portelli & Smolders, 2014). So the aim of our study was to measure the total protein kinase activity in the brain structures of *Danio rerio*.

Experimental Approach: All the procedures have been held according to the Local Ethical Committee of Institute of Experimental Medicine. In our study, 50 specimens of *D. rerio* 6-8 months of age have been used. A predator (*Hypsophrys nicaraguensis*) has also been used.

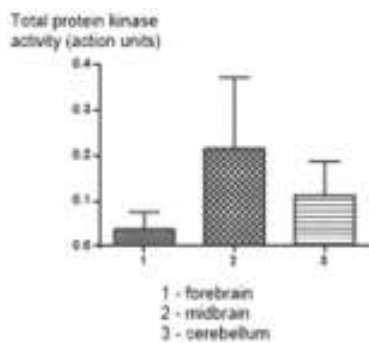


FIGURE 1 Control group

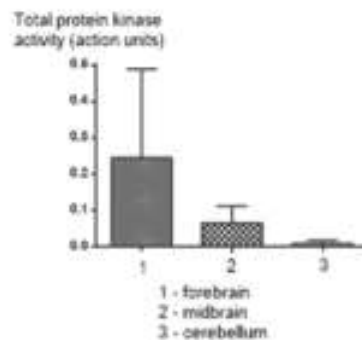


FIGURE 2 Predator exposure

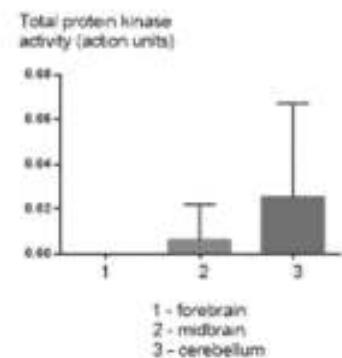


FIGURE 3 Agrelax administration

During the experiment, a fish has been firstly placed into a tank of water with a dissolved pharmacological substance for 5 min and then transferred into a tank with predator also for 5 min. Two ghrelin antagonists have been used in our experiment in $0.333 \text{ mg}\cdot\text{L}^{-1}$ dosage ([D-Lys3]-GHRP-6 and Agrelax, a recombinant peptide analogue of ghrelin with MW 3500 KD, which has been invented in our institute but has not been patented yet). The brain has been divided into three anatomical parts: forebrain, midbrain, and cerebellum. After that, the material for kinase activity assay was made (ADP-sensor Universal Kinase Activity Assay kit, BioVision). We have also used GraphPad Prism 6 for statistical estimation. Kolmogorov–Smirnov test and Mann–Whitney *U* test have been used as statistical tests.

Key Results: In the control group, the kinase activity has been determined in all tested brain structures. The highest level of kinase activity has been determined in the midbrain. After predator exposure, the kinase activity has significantly changed compared to the control group, and the highest level of kinase activity has been in the forebrain of *D. rerio* (Figure 2). After [D-Lys3]-GHRP-6 administration, there has not been determined any protein kinase activity in all brain structures. In the cerebellum, the kinase activity has been the highest after Agrelax administration.

Conclusion and Implications: Protein kinase system demonstrates significant stress response. Pharmacological action on ghrelin receptors leads to changes in kinase system in *D. rerio*'s brain structures.

REFERENCE

Portelli, J., & Smolders, I. (2014). Central functions of the ghrelin receptor. <https://doi.org/10.1007/978-1-4939-0823-3>

P122 | Neuroprotection by CB₁ agonist, arvanil

Alaa Al-Hindawi; Olumayokun Olajide; Karl Hemming

University of Huddersfield

Background and Purpose: Neuroinflammation in Alzheimer's disease (AD) participates in the disease pathogenesis as much as do tangles and plaques themselves (Zhang et al., 2013). However, none of the current pharmacological therapies for AD decrease or prevent the destruction and damage to neurons. In neurodegenerative diseases, the endocannabinoid is known to play a role in disease progression. In the present study, we evaluated inhibition of neuroinflammation by a CB₁ agonist, arvanil, in LPS-activated BV-2 microglia.

Experimental Approach: LPS-stimulated BV2 microglia cells were treated with arvanil (1, 2.5, and 5 μM), followed by stimulation with LPS ($100 \text{ ng}\cdot\text{ml}^{-1}$). Cell viability was assessed by XTT and LDH assays while levels of nitrite production were detected with the Griess assay. Secretion of pro-inflammatory cytokines TNF- α and IL-6 levels was measured by ELISA. Furthermore, western blotting was used to detect the expression of iNOS and COX-2 proteins. Data were expressed as mean \pm SEM and analysed by one-way ANOVA followed by Dunnett's multiple comparisons test.

Key Results: Results show that arvanil did not affect the viability of cells when used at a concentration of 1, 2.5, and 5 μM . Treatment with arvanil resulted in a significant ($P < .001$) decrease in the release of both TNF- α and IL-6 into culture supernatants following stimulation of BV-2 cells with LPS (Figure 1). Treatment with 2.5 and 5 μM of arvanil also significantly inhibited COX-2 ($P < .01$) and iNOS ($P < .001$) protein expression and reduced elevated NO production (Figure 2) in LPS-stimulated BV2 cells.

Conclusion and Implications: These results show that that arvanil produce an anti-inflammatory effect in LPS-stimulated BV2 microglia cells, thus showing potential promise in AD therapeutics.

REFERENCE

Zhang, B., Gaiteri, C., Bodea, L.-G., Wang, Z., McElwee, J., Podtelezhnikov, A. A., ... Dobrin, R. (2013). Integrated systems approach identifies genetic nodes and networks in late-onset Alzheimer's disease. *Cell*, 153(3), 707–720.

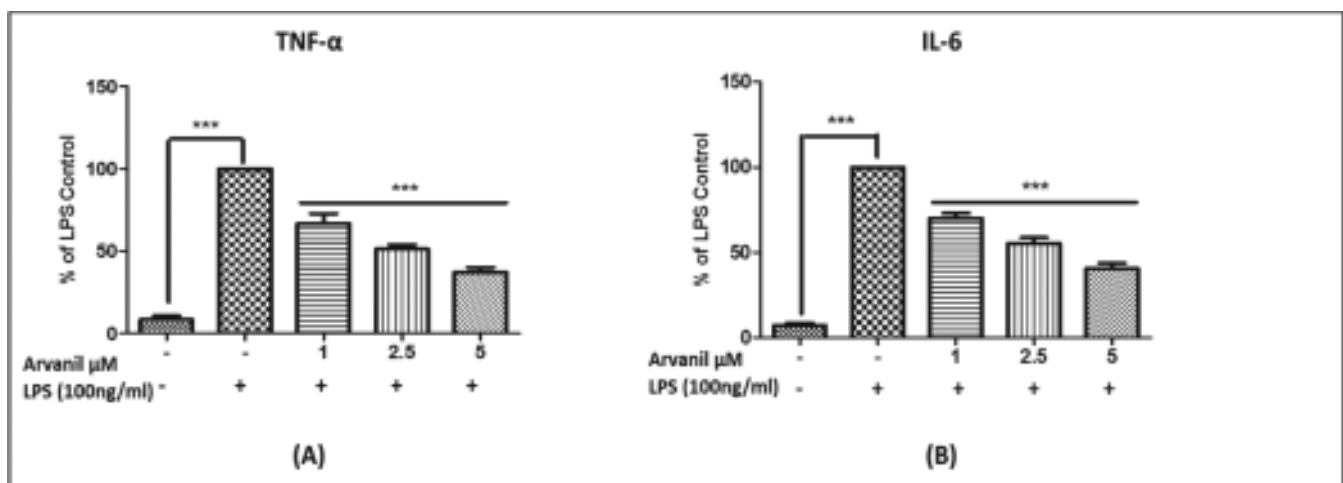


FIGURE 1 ELISA assay for determining (a) TNF- α and (b) IL-6 level after treatment with 1, 2.5, and 5 μM of arvanil followed by stimulation with LPS for 24 hr. *** $P < .001$ versus LPS-stimulated cells

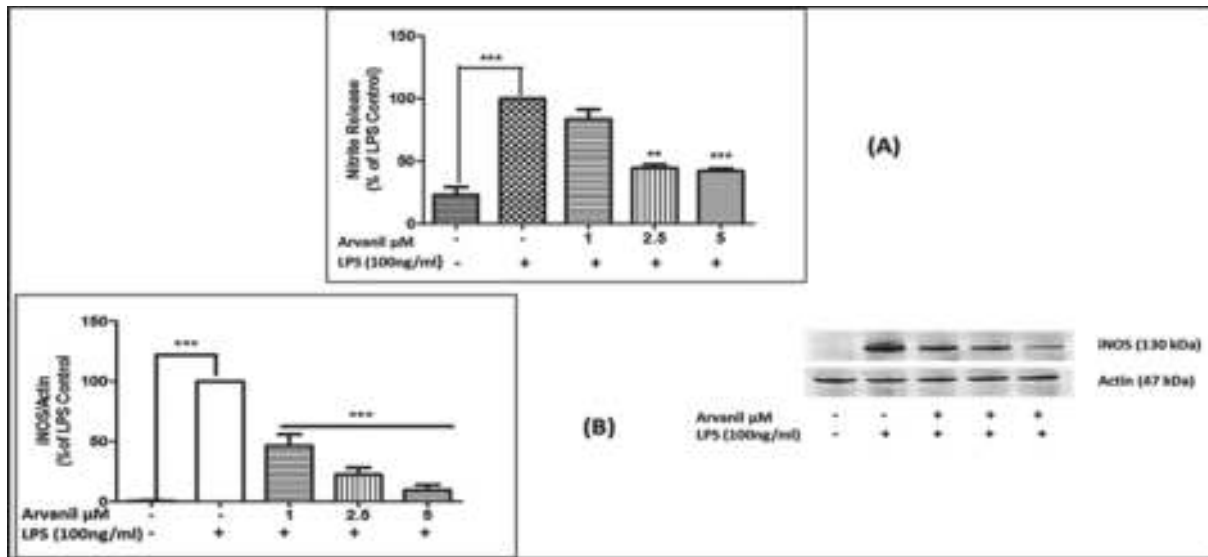


Figure 2 Effects of 1, 2.5, and 5 μ M of arvanil treatment on (a) nitrite release level and (b) iNOS protein expression in the stimulated BV2 cells. ** $P < .01$ and *** $P < .001$ versus LPS-stimulated cells

P123 | The effect of Δ^9 -THC and CBD on DOI-induced head twitches in juvenile mice

Victoria Gorberg; Peter McCaffery; Sharon Anavi-Goffer
University of Aberdeen

Background and Purpose: Administration to adult mice of 2,5-dimethoxy-4-iodoamphetamine (DOI), a potent agonist of the serotonin 5-HT_{2A}/5-HT_{2C} receptors, increases head twitch response (HTR). DOI-induced HTR has been proposed to model motor tics of Tourette syndrome. Tourette syndrome is a neuropsychiatric disorder which is defined as part of the tic disorder spectrum. It affects about 1% of the general population and has a childhood onset. It has been previously shown in other studies that Δ^9 -tetrahydrocannabinol (Δ^9 -THC) reduces DOI-induced HTR in adult rodents, further supporting reports describing a significant amelioration of symptoms when cannabis was used by adult patients with Tourette syndrome. However, the effects of Δ^9 -THC and CBD in the mouse DOI model of Tourette syndrome have not yet been investigated in juvenile mice.

Experimental Approach: Drugs were dissolved in DMSO and injected (i.p.) 60 min before the DOI (1 mg.kg⁻¹; saline; i.p.) to juvenile male C57BL/6J mice (n = 4-6 in each group). After 5-min habituation in a clear glass cage, the number of head twitches was counted for 15 min. The results were analysed with two-way ANOVA followed by Bonferroni's test for multiple comparisons performed by GraphPad Prism version 7. $P < .05$ was considered statistically significant.

Key Results: In the presence of DOI, Δ^9 -THC (0.2-5 mg.kg⁻¹) showed a significant decrease of HTR ($P < .001$). Compared to Δ^9 -THC, CBD at doses of 5 and 10 mg.kg⁻¹ had a small, but significant, decrease of HTR ($P < .05$). But CBD at a dose of 1 mg.kg⁻¹ had no significant effect on DOI-induced HTR in juvenile mice. However, in the absence of DOI, Δ^9 -THC at a dose of 5 mg.kg⁻¹ induced a cataleptic behaviour

in healthy juvenile mice ($P < .05$). Surprisingly, CBD alone significantly increased the HTR in healthy juvenile mice.

Conclusion and Implications: These results show that in juvenile mice, although Δ^9 -THC significantly reduces motor tic-like behaviour, it can also induce a side effect similar to catalepsy. In addition, these results show that CBD has a minor reverse effect on motor-like tics which are mediated by 5-HT_{2A}/5-HT_{2C} receptors. These results suggest that the dose of Δ^9 -THC for the treatment of children should be regulated. Moreover, these results imply that CBD may not effectively treat motor tics in children and may even exacerbate tics in a population of patients.

ACKNOWLEDGEMENT

We acknowledge the Research Grant Award, Tourette Association of America (S.A.-G. and P.M.).

Oral Communications, Monday 16th December, 14:30

Cardiovascular and Respiratory Pharmacology Oral Communications 2

OC029 | Exploring the haemodynamic effects of adenosine A_{2B} receptor ligands in conscious, freely moving rats

Edward Wragg; Samantha Cooper; Julie March; Marleen Groenen; Stephen Hill; Jeanette Woolard

University of Nottingham

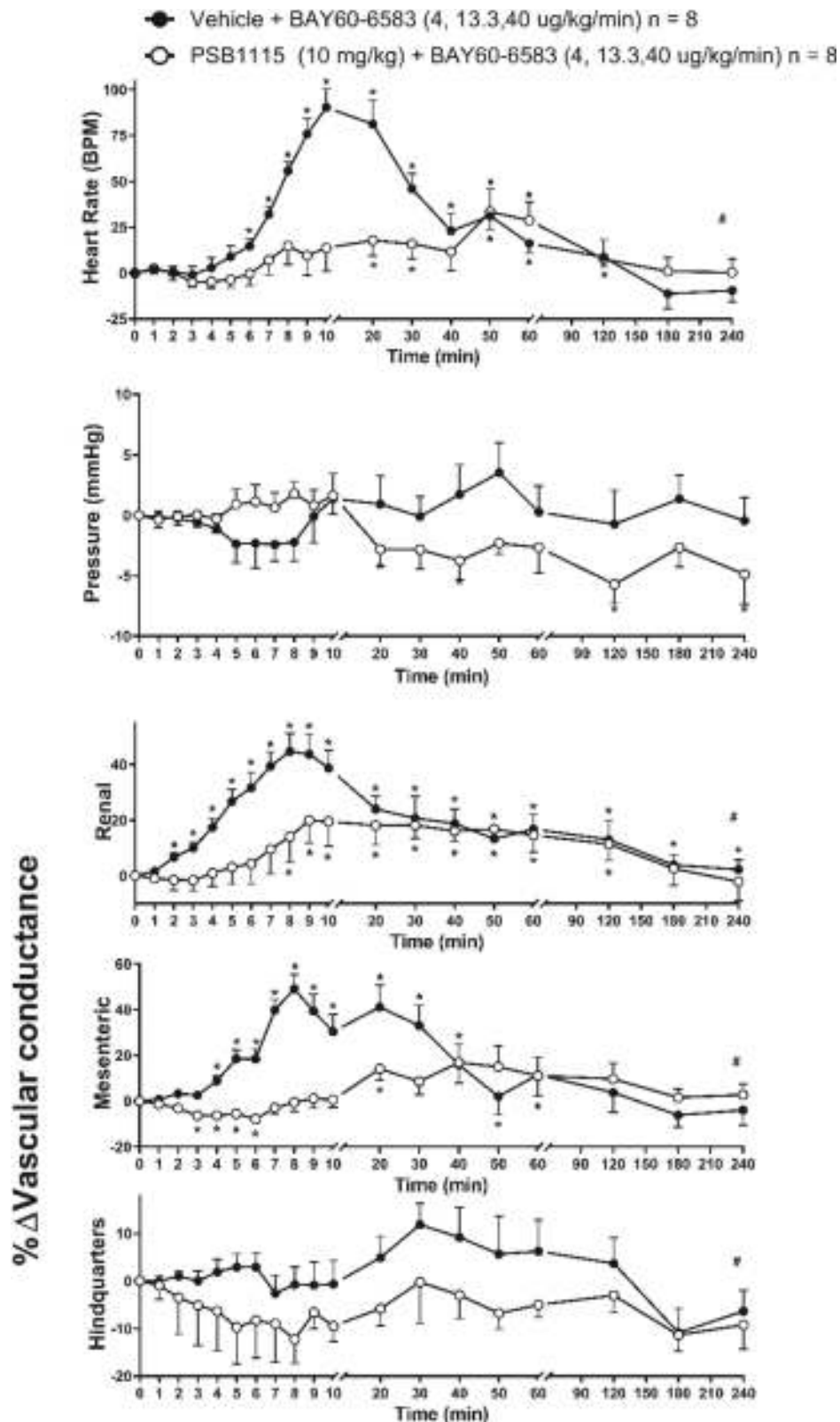


Figure 1 Systemic and regional haemodynamic effects of a 10-min IV infusion of BAY60-6583, in the presence or absence of PSB1115, in conscious, freely moving rats. An IV bolus of either PSB1115 (10 $\text{mg}\cdot\text{kg}^{-1}$) or polyethene glycol vehicle was given 10 min before a low, medium, and high dose (4, 13.3, and 40 $\mu\text{g}\cdot\text{kg}^{-1}\cdot\text{min}^{-1}$) of BAY60-6583 was administered, each for 3 min, respectively. Each rat was given drugs across two experimental days, with the administration of the second IV bolus that was not given on the previous experimental day given on the subsequent day, allowing each rat to act as their own control. *Friedman's test, $P < .05$ accepted for statistical significance for each time point. #Mann-Whitney U test, $P < .05$ accepted for significant difference across all measurements. Error bars \pm SEM, $n = 8$

Background and Purpose: The adenosine A_{2B} receptor ($A_{2B}R$) has been shown to have roles in pathological conditions involving the cardiovascular system, including ischaemia-reperfusion injury and cancer (Vecchio, White, & May, 2019). Thus, there is an interest in targeting the $A_{2B}R$ for potential novel therapeutics (Sorrentino & Morello, 2017). However, the systemic effects of $A_{2B}R$ ligands on the cardiovascular system have not been determined. This project explored the systemic and regional haemodynamic responses to $A_{2B}R$ ligands in conscious, freely moving rats.

Experimental Approach: Adult, Sprague-Dawley rats were anaesthetised, before implantation with pulsed Doppler flow probes to facilitate the measurement of vascular conductance in mesenteric, renal, and hindquarter vascular beds. Subsequently, intra-arterial and intra-venous catheters were implanted, allowing measurements of heart rate (HR) and mean arterial pressure (MAP), and drug administration, respectively. Compounds were prepared in propylene glycol buffer (5% PEG, 2% Tween, 0.9% saline). Twenty-four hours after surgery, a bolus of either the $A_{2B}R$ antagonist PSB1115 ($10 \text{ mg}\cdot\text{kg}^{-1}$) or vehicle was administered. Ten minutes later, a low, medium, and high dose of the $A_{2B}R$ -selective agonist BAY60-6583 was infused, each for 3 min, respectively, and recordings were made for a further 4 hr. Each rat was administered the $A_{2B}R$ agonist on two separate experimental days, in the presence or absence of PSB1115, allowing each rat to act as their control. A group size of 8 was required. Procedures were approved by the University of Nottingham Animal Welfare Ethical Review Board, under Home Office Project and Personal License Authority.

Key Results: Infusion of BAY60-6583 ($4, 13.3, \text{ and } 40 \mu\text{g}\cdot\text{kg}^{-1}\cdot\text{min}^{-1}$) caused a dose-dependent increase in HR, but no significant change to MAP. This was accompanied by a dose-dependent increase in renal and mesenteric vascular conductance, but no significant change in hindquarter vascular conductance (Figure 1). The observed effects were attenuated by PSB1115 ($10 \text{ mg}\cdot\text{kg}^{-1}$), confirming that the responses are caused by agonism of $A_{2B}R$ (Figure 1).

Conclusion and Implications: BAY60-6583 caused a dose-dependent increase in HR and an increase in renal and mesenteric vascular conductance. However, no changes to MAP were observed. This tachycardic response could be indicative of baroreceptor reflex mediated countermeasures to maintain MAP in the presence of vasodilations in the renal and mesenteric vascular beds.

REFERENCES

- Sorrentino, C., & Morello, S. (2017). Role of adenosine in tumor progression: Focus on A_{2B} receptor as potential therapeutic target. *Journal of Cancer Metastasis and Treatment*, 3, 127–138.
- Vecchio, E. A., White, P. J., & May, L. T. (2019). The adenosine A_{2B} G protein-coupled receptor: Recent advances and therapeutic implications. *Pharmacology & Therapeutics*, 198, 20–33.

OC030 | The effect of isoliquiritigenin on the hERG potassium channel

Minahil Mujahid; Taiyi Wang; Clive Ellory; Robert Wilkins; Yu-Ling Ma

Department of Physiology, Anatomy and Genetics, Oxford University

Background and Purpose: Xin Su Ning (XSN) is an herbal anti-arrhythmic medicine formulated with 11 Chinese herbal medicines. It has been shown to prolong action potential duration and to block potassium and sodium channels of isolated cardiac myocytes, which implies the property of class I and III anti-arrhythmic medicine. Isoliquiritigenin (ISL) is a constituent compound of XSN shown to have anti-inflammatory, anti-angiogenic, and anti-cancer activities. We aim to extend the current understanding of the anti-arrhythmic mechanism of XSN by identifying any effect of ISL on the hERG potassium channel.

Experimental Approach: Electrophysiological assays were conducted with Axopatch 200B patch clamp system on a CHO (CHO-K1) cell line stably transfected with the human isoform of the hERG channel. Solutions were prepared as previously described (Ma et al., 2019). Drug was perfused to cells at room temperature. ISL (a bioactive chalcone compound), at various concentrations, was applied to cells, and the effects on peak channel amplitude were measured ($n = 6$). Furthermore, the effects of ISL on activation and deactivation kinetics of the hERG channels were studied, respectively, by applying a range of voltage clamp protocols to assess the binding property of ISL on hERG channels ($n = 8$).

Key Results: ISL inhibited the amplitude of the maximum hERG channel potassium current in a dose-dependent manner. ISL blocks hERG in a bi-sigmoidal fashion; the sigmoid at low concentrations (Figure 1a) has $EC_{50} 0.16309 \pm 0.02832$ and at high range (Figure 1b) has $EC_{50} 8.53946 \pm 2.06073$. The bi-sigmoid suggests that ISL binds to both the oestrogen site ($0.01\text{--}1 \mu\text{m}$) and the channel pore site ($1\text{--}400 \mu\text{m}$). ISL caused a significant leftward shift of the activation curve (Figure 1c), indicating that the compound binds to the channel in the open state; there was no statistically significant difference in the deactivation kinetics of the channel (Figure 1d). ISL reduced the current within a wide range of membrane potentials of -80 to $+50 \text{ mV}$ (Figure 1f).

Conclusion and Implications: ISL blocks hERG channel in a dose-dependent manner with affinity for the activated state. Any drug that blocks hERG channels would be expected to prolong action potential duration of the cardiac myocytes. Our results imply that ISL would contribute to the class III anti-arrhythmic action of XSN as one of the active components. Further study into the anti-arrhythmic actions of XSN could prove beneficial in understanding the action of multi-component anti-arrhythmic drugs.

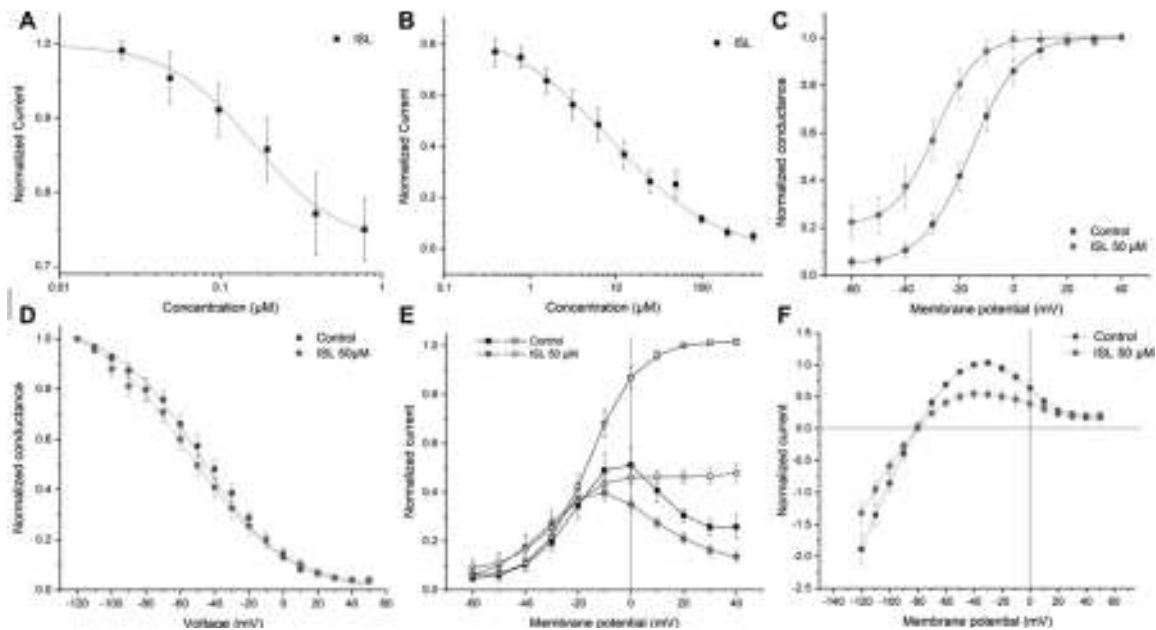


Figure 1 Acute effects of ISL on hERG current in CHO-K1 cell line. (a and b) Dose–response curves of the inhibition on human hERG channel by ISL at low range and high range ($n = 6$). Normalised and averaged current values for each concentration plotted to produce a dose–response curve fitted with the Hill equation. The inhibitory effect of ISL was reversed with washout. (c and d) Normalised current values were plotted and fitted with the Boltzmann equation to show effects of 50- μM ISL on activation and deactivation kinetics ($n = 8$). Derived from averaged I–V curves of the tail currents generated by “activation” and “inactivation” pulse protocols. (e and f) Normalised and averaged I–V relationships. I–V curves in (e) are for the maximal tail currents at repolarisation potential of -55 mV (open symbols) and for currents at the end of the depolarising pulse (solid symbols) against the pulse potential. In (f), the I–V curves are for the maximal repolarisation-evoked tail currents against repolarisation potential

REFERENCE

Ma, Y., et al. (2019). Ion channel targeted mechanisms of anti-arrhythmic Chinese herbal medicine Xin Su Ning. *Frontiers in Pharmacology*, 10, 70.

OC031 | The effect of a selective phosphoinositide 3-kinase- α inhibitor in vascular inflammation

Hiba Chaudhry¹; Ali Zarban¹; Fulye Argunhan¹; Xenia Kodji¹; Anne Ridley²; Susan Brain¹

¹King's College London; ²University of Bristol

Background and Purpose: Cardiovascular inflammation is associated with endothelial cell (EC) damage, resulting in leukocyte trafficking and oedema formation (Cerutti & Ridley, 2017). Inflammation disrupts EC junctions, increasing microvascular permeability, and resulting in a positive-feedback loop of inflammatory events. The phosphoinositide 3-kinase pathway stimulates this endothelial response (Cain et al., 2010), and this study examined the actions of BYL-719, a PI3K- α -selective inhibitor (Juric et al., 2018), on inflammatory responses.

Experimental Approach: Confocal imaging using immunofluorescence and permeability assays were undertaken to quantify the effect of inflammatory cytokines, TNF- α and IL-1 β , in the presence of the PI3K inhibitor using fluorescein isothiocyanate-dextran (40 kDa, 0.1 mg·ml⁻¹) on human microvascular endothelial cells (HMVECs)

(Lonza, derived from dermal tissue). Cells were treated with either of the cytokines for 16–18 hr, followed by a 1-hr treatment of drug and a final 1-hr treatment with FITC-dextran. *in vivo* analysis was carried out per the UK Home Office Animals (Scientific Procedures) Act 1986. Male WT CD1 mice were anaesthetised initially using 5% isoflurane and maintained at 2% for procedures, to test BYL-719 in a model of dorsal skin inflammation, to determine neutrophil accumulation (measured by myeloperoxidase) and oedema formation (measured by Evans Blue accumulation) (Sawyer et al., 2011). All statistical significance was determined using one-way or two-way ANOVA followed by Tukey's post hoc test.

Key Results: BYL-719 significantly reduced cytokine-induced EC permeability and shape changes, including cell area and elongation (Table 1), impeding *in vitro* cytokine-induced inflammation. The inhibitor abrogated effects of the inflammatory cytokines *in vivo* of both TNF- α and IL-1 β but interestingly had no effect on the neutrophil accumulation or oedema formation in the presence of C5a (Figure 1).

Conclusion and Implications: Our findings show that the PI3K- α inhibitor, BYL-719, reduces endothelial activation and inhibits inflammatory oedema formation in the presence of TNF- α and IL-1 β . We conclude that there is a potential for PI3K inhibitors to act as anti-neutrophil and oedema agents in cardiovascular-related inflammatory conditions.

ACKNOWLEDGEMENT: We thank the British Heart Foundation (BHF) for funding this work.

TABLE 1 Effect of BYL-719 in vitro on cell permeability

Condition	% permeability	
	TNF- α	IL-1 β
Control (DMSO)	101.1799	100.9394
Control (BYL-719)	114.5761	101.8357
Cytokine only (TNF- α or IL-1 β)	187.2436****	170.7179****
Cytokine + 0.1- μ M BYL-719	174.8551	162.0197
Cytokine + 1- μ M BYL-719	145.8654#	125.3866###
Cytokine + 10- μ M BYL-719	116.2207###	97.8358####

Note. HMVECs treated with TNF- α or IL-1 β for 16–18 hr, followed by 1-hr treatment of BYL-719 at 0.1, 1, and 10 μ M and permeability quantified using FITC-dextran. Values are mean \pm SEM, one-way ANOVA by Tukey's test. $n = 6$ independent experiments in duplicates.

**** $P < .0001$ between control (DMSO) and cytokine only groups.
 # $P < .05$ between cytokine only and cytokine + BYL-719 drug groups.
 ### $P < .001$ between cytokine only and cytokine + BYL-719 drug groups.
 #### $P < .0001$ between cytokine only and cytokine + BYL-719 drug groups.

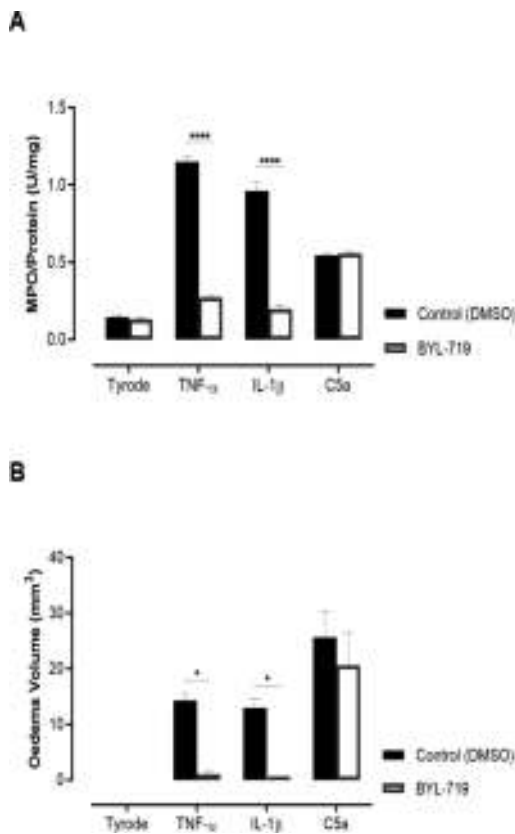


Figure 1 The effect of BYL-719 in the dorsal skin inflammation model. Mice were pretreated with 50 mg·kg⁻¹ BYL-719 intraperitoneally for 30 min, injected intravenously with Evans Blue dye, and intradermally injected with TNF- α (100 ng per 50 μ l), IL-1 β (10 ng per 50 μ l), and C5a (300 ng per 50 μ l) for 4 hr, followed by ex vivo MPO assay (a) and oedema volume measurements (b). Data are mean \pm SEM, two-way ANOVA by Tukey's test. $n = 6$ independent experiments in duplicates; * $P < .05$ and **** $P < .0001$ between control (DMSO) and BYL-719-treated groups

REFERENCES

Cain, et al. (2010). *The Journal of Cell Biology*, 188, 863–876.
 Cerutti, & Ridley (2017). *Experimental Cell Research*, 358, 31–38.

Juric, et al. (2018). *Journal of Clinical Oncology*, 36, 1291–1299.
 Sawyer, et al. (2011). *PLoS ONE*, 6, e14671.

OC032 | Trace amine-induced vasoconstriction: Are trace amine-associated receptors responsible?

Alex Voisey; Kenneth Broadley; William Ford
 Cardiff University

Background and Purpose: Trace amines are monoamines closely related to the classical monoamines (Gainetdinov et al., 2018), nor-adrenaline, dopamine, and 5-HT. They were considered to be indirectly acting sympathomimetics, although it is now known that trace amines can induce vasoconstriction independent of α_1 -adrenoceptors (Broadley et al., 2013). Mounting evidence suggests that trace amine-associated receptors (TAARs) could mediate this response (Broadley et al., 2013). This study investigates the role of TAARs in trace amine-induced vasoconstriction.

Experimental Approach: Aortic rings (5 mm) from male Sprague Dawley rats were immersed in Krebs' bicarbonate solution gassed with CO₂/O₂ (5%/95%) at 37°C under 1.5 g of resting tension. The absence of endothelium was confirmed by a lack of relaxation to 100- μ M carbachol of rings pre-constricted with 60-mM KCl. Cumulative concentration–response curves (CRCs) for β -phenylethylamine (β -PEA), the selective TAAR1 agonist RO5256390, 5-HT, and the α_1 -adrenoceptor agonist phenylephrine were obtained following a 1-hr equilibration period. CRCs were generated in the presence or absence of endothelium, the α_1 -adrenoceptor antagonist, prazosin (1 μ M), the 5-HT₂ receptor antagonist, cinanserin (100 nM), or the TAAR1-selective antagonist, EPPTB (1 μ M). Isometric contractions reported as a percentage of the contraction obtained with 60-mM KCl were measured using Power Lab, Chart 5 software (ADInstruments). Means were compared using Student's unpaired t test. Statistical significance was accepted for $P \leq .05$.

Key Results: β -PEA and RO5256390 induce concentration-dependent vasoconstriction of rat aorta. Endothelium removal significantly potentiated the maximum contractile response of β -PEA from $53 \pm 10\%$ to $85 \pm 7\%$ and RO5256390 from $11 \pm 2\%$ to $60 \pm 6\%$. Prior addition of prazosin ($1 \mu\text{M}$) induced a slight but significant rightward shift of the β -PEA in the absence of endothelium. The apparent dissociation constant (K_B) of prazosin based on the observed shift of the β -PEA CRC was 680 nM , significantly lower than that calculated from the shift for phenylephrine of 430 pM . Conversely, prazosin did not induce any shift of CRCs for RO5256390 and did not significantly shift the β -PEA CRC when endothelium was present. Pre-incubation with cinanserin (100 nM) did not induce any shift in the CRCs generated for β -PEA. RO5256390 CRCs were not affected by the prior addition of EPPTB ($1 \mu\text{M}$).

Conclusion and Implications: Trace amine-induced vasoconstriction is not mediated through α_1 -adrenoceptors or 5-HT_2 receptors. As EPPTB did not inhibit contractile responses, this suggests that TAAR1 is not involved, although its selectivity for rat TAAR1 is unknown.

REFERENCES

- Broadley, K. J., et al. (2013). *European Journal of Pharmacology*, 715, 370–380.
Gainetdinov, R. R., et al. (2018). *Pharmacological Reviews*, 70, 549–620.

OC033 | α CGRP can act independently of NO to rescue blood flow in the mesenteric microvasculature in vivo

Fulye Argunhan¹; Dibesh Thapa¹; Aisah A. Aubdool²; Susan D. Brain¹
¹King's College London; ²Queen Mary University London

Background and Purpose: Endogenous α CGRP protects against exacerbated hypertension in *N*-nitro-L-arginine methyl ester (L-NAME) murine model where NO generation is inhibited to simulate conditions of endothelial dysfunction (Argunhan et al., 2017), extending our knowledge of CGRP cardiovascular protective properties (Aubdool et al., 2017). We hypothesised that α CGRP acts on mesenteric resistance microvessels, independently of NO and hereby investigated this in vivo.

Experimental Approach: All procedures were carried out according to the UK Home Office Animals (Scientific Procedures) Act 1986. Male C57BL/6J WT and global α CGRP KO mice (10–12 weeks old) received L-NAME ($120 \text{ mg}\cdot\text{kg}^{-1}$) in drinking water (1). Mice were anaesthetised 6 weeks after treatment onset with ketamine ($75 \text{ mg}\cdot\text{kg}^{-1}$) and medetomidine ($1 \text{ mg}\cdot\text{kg}^{-1}$) for non-recovery. A sub-cohort of WT mice were pretreated with the CGRP receptor antagonist BIBN4096BS ($0.3 \text{ mg}\cdot\text{kg}^{-1}$, i.v.). Their small intestine (4 cm^2) was exteriorised (Sand et al., 2015). Blood flow was measured simultaneously in first-, second-, and third-order arterioles using a laser

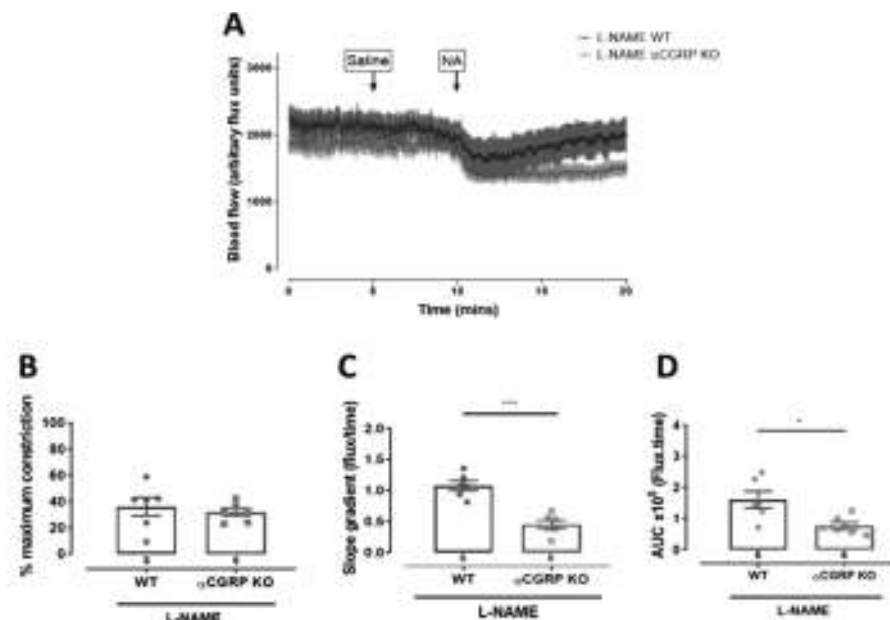


Figure 1 – Investigating changes in blood flow recovery in 1st order mesenteric arterioles after administration of noradrenaline (NA) in L-NAME-treated WT and α CGRP KO anaesthetised mice. A) Mean blood flow trace of 1st order mesenteric arterioles at baseline (0–5 minutes), in response to saline administration (5–9 minutes), followed by response to noradrenaline-mediated constriction (10 minutes) and blood flow recovery (10–20 minutes). B) Percentage of maximum constriction calculated from immediately before noradrenaline administration to maximum point of constriction. C) Slope of recovery calculated as the difference in flux from point of maximum constriction to 8 minutes thereafter, divided by the time. D) Area under the curve (AUC) of the recovery phase after noradrenaline-mediated constriction. AUC was calculated from the maximum point of constriction to 8 minutes thereafter. Values represent mean \pm SEM, $n=6$. * $p<0.05$, ** $p<0.001$ between indicated groups. Two-tailed unpaired Student T-test.

speckle imager. Baseline blood flow was determined (10 min), and then the sympathetic constrictor agent noradrenaline (NA, 0.75 μg per 100 μl) was applied topically. Results presented as (i) % constriction, (ii) recovery as AUC for 8 min from maximum constriction, and (iii) slope of recovery. Data were expressed as mean \pm SEM ($n = 6-8$), statistical analysis by two-way ANOVA and Bonferroni's test or unpaired Student's *T* test.

Key Results: A dose of NA was chosen where vasoconstriction, then substantial recovery was seen in WT mice, irrespective of treatment. αCGRP KO mice demonstrated a similar constrictor response to NA (Figure 1a,b) but significantly impaired blood flow recovery, with a significantly lower recovery slope in first-order vessels than WT counterparts (0.45 ± 0.07 vs. 1.08 ± 0.08 , $n = 6$, $***P < .001$; Figure 1c). Additionally, the AUC of L-NAME αCGRP KO mice was significantly reduced ($0.77 \times 10^5 \pm 0.12 \times 10^5$ flux units per time) when compared to L-NAME WT mice ($1.61 \times 10^5 \pm 0.27 \times 10^5$ flux units per time, $n = 6$, $^*P < .05$; Figure 1d). These findings were supported with significantly lower AUC and slope of recovery values obtained from L-NAME WT mice pretreated with the CGRP receptor antagonist BIBN4096BS.

Conclusion and Implications: The first-order mesenteric vessels are involved in the protective effect of αCGRP . Our findings suggest that endogenous αCGRP supports the recovery of mesenteric vasoconstriction, when endothelial dysfunction associated with reduced NO production exists. These *in vivo* results support that targeting of the CGRP pathway for novel treatments of cardiovascular disease.

ACKNOWLEDGEMENT: F.A. is funded by KCL MRC-DTP.

REFERENCES

- Argunhan, F. et al., Pharmacology 2017 (BPS, London UK). <http://www.pa2online.org/abstract/abstract.jsp?abid=33556&author=argunhan&cat=-1&period=>
- Aubdool, A. A., et al. (2017). *Circulation*, 136, 367–383.
- Sand, C. A., et al. (2015). *Journal of Applied Physiology*, 118, 344–354.

Drug Discovery, Development and Evaluation Oral Communications 2

OC035 | Development of new bicyclic analogue of sulforaphane as potent nuclear factor erythroid 2-related factor inducer

Kit-Kay Mak¹; Mallikarjuna Rao Pichika¹; Ola Epemolu²; Alben T. Dinkova-Kostova³; Maureen Higgins³

¹International Medical University; ²Wellcome Centre for Anti-infectives Research, Drug Discovery Unit, School of Life Sciences, University of Dundee; ³Jacqui Wood Cancer Centre, Division of Cellular Medicine, School of Medicine, University of Dundee

Background and Purpose: Sulforaphane is a well-known nuclear factor erythroid 2-related factor (NRF2) activator, but it is not a drug-like molecule (Dinkova-Kostova, Fahey, Kostov, & Kensler, 2017). Here, we report the development of bicyclic analogue of sulforaphane possessing major NRF2 inducer activity with optimum drug metabolism and pharmacokinetic (DMPK) properties.

Experimental Approach: The bicyclic analogue of sulforaphane, 4,5,6,7-tetrahydrobenzo[*b*]thiophene (THBT), was designed with the objective of developing drug-like NRF2 inducer. THBT was synthesised and characterised using spectroscopic techniques. Its *in vitro* DMPK properties were determined using reported methods. NRF2 inducer activity was determined via the determination of NAD(P)H quinone oxidoreductase 1 (NQO1) enzyme activity (Dinkova-Kostova & Talalay, 2010) in Hepa 1c1c7 murine hepatoma cells, GSH assay and KEAP1:NRF2 inhibitor screening assay kit (Kandasamy et al., 2019).

Key Results: THBT was synthesised with a good yield (85%) and characterised using ¹H and ¹³C NMR spectroscopy. The purity and mass of the compound was determined using HPLC-mass spectroscopy (LC-MS) technique. In human, rat, and mouse, its intrinsic clearance ($\text{ml}\cdot\text{min}^{-1}\cdot\text{g}^{-1}$ liver) in hepatocytes was 0.86, 2.33, and 3.95; in microsomes without CYP450 inhibitor, it was 1.73, 2.34, and 7.1; in microsomes with CYP450 inhibitor, it was 0.74, 0.78, and 2.46; and in cytosol, it was 0.0001, 0.007, and 0.004, respectively. The stability of THBT in human and rat plasma was found to be >180 min either in the presence or absence of inhibitor (PMSF, 4-bis-phenyl-nitrophosphate; 500 μM), whilst its stability in mouse plasma was 141.7 and >180 min in the presence and absence of inhibitor, respectively. Its per cent binding to mouse plasma proteins was 85.5%; aqueous solubility was 78.1 μM , lipophilicity was 3.7, permeability at pH 7.4 was 149.9 $\text{nm}\cdot\text{s}^{-1}$, and it was non-cytotoxic in HEPG2 cells with a value of >100 μM . The IC_{50} value in inhibiting the interactions between NRF2 and KEAP1 was 2.17 ± 0.34 μM . The NQO1 activity was concentration dependent, with a CD (concentration that doubles the specific enzyme activity) value of 9.5 μM .

Conclusion and Implications: We have successfully developed a novel drug-like bicyclic analogue of sulforaphane (THBT) with robust NRF2 inducer activity, which is comparable in potency to that of dimethyl fumarate, the only marketed NRF2 inducer.

REFERENCES

- Dinkova-Kostova, A. T., Fahey, J. W., Kostov, R. V., & Kensler, T. W. (2017 Nov). KEAP1 and done? Targeting the NRF2 pathway with sulforaphane. *Trends in Food Science and Technology*, 69(Pt B), 257–269.
- Dinkova-Kostova, A. T., & Talalay, P. (2010 Sep). NAD(P)H:quinone acceptor oxidoreductase 1 (NQO1), a multifunctional antioxidant enzyme and exceptionally versatile cytoprotector. *Archives of Biochemistry and Biophysics*, 501(1), 116.
- Kandasamy, M., Mak, K.-K., Devadoss, T., Thanikachalam, P. V., Sakirolla, R., Choudhury, H., & Pichika, M. R. (2019). Construction of

novel quininoxaline as a new class of Nrf2 activator. *BMC Chemistry*. <https://doi.org/10.21203/rs.2.12921/v1>

OC036 | TRPV1 modulation of MOP signalling and regulation

Julie Sanchez; Wai Fung; J. Robert Lane; Meritxell Canals

University of Nottingham

Background and Purpose: Pain dysregulation underlies major diseases, affecting 20% of the population. Opioids are still the mainstay treatments for severe acute pain. However, their use is associated with abuse and severe adverse effects. Despite significant research in developing G protein biased agonists (able to promote analgesia without eliciting adverse effects), the search for safer opioids has not been successful yet. Thus, in recent years, novel strategies involving promoting G protein signalling while sparing the regulation processes associated with tolerance (Scherer et al., 2017) are being explored. Transient receptor potential channel subfamily vanilloid member 1 (TRPV1), the ion channel activated by capsaicin (the pungent component of chili peppers), has been proposed to modulate the μ -opioid receptor (MOP) regulation (Basso et al., 2019); however, the cellular mechanisms involving MOP/TRPV1 regulation are not yet understood.

Experimental Approach: Here, we used cellular models (transfected HEK 293 cells) to investigate how expression and/or activation of TRPV1 affects MOP signalling and regulation using a range of BRET sensors and ELISA ($n \geq 3$ for all experiments). DAMGO (0.01 nM–10 μ M) was used as a MOP agonist, and capsaicin (0.01 nM–10 μ M) was used as a TRPV1 agonist. Cells were transfected in 10-cm dishes using polyethylenimine (1 to 6 DNA:PEI ratio) and then replated in 96- or 48-well plates coated with poly-D-lysine, and experiments were performed 48 hr post-transfection. Statistical significance was determined using two-way ANOVA (multiplicity correction using the Tukey method).

Key Results: BRET assays showed that activation of TRPV1 with capsaicin blocks DAMGO-induced arrestin recruitment at the MOP, significantly reduces DAMGO-mediated G protein activation (GPA), and

induces translocation of GRK5 away from MOP-RLuc8 in a concentration-dependent manner. TRPV1 activation does not influence the recruitment of a conformationally selective nanobody (Nb33) or mini Gi protein recruitment, showing that the MOP and the G proteins can still be activated.

Conclusion and Implications: Our results suggest that TRPV1 activation, in addition to modulating receptor internalization, also modulates signalling pathways downstream of G protein activation without directly affecting MOP activation.

REFERENCES

- Basso, et al. (2019). TRPV1 promotes opioid analgesia during inflammation. *Science Signaling*, 12(575).
Scherer, et al. (2017). TRPV1 is a physiological regulator of μ -opioid receptors. *PNAS*, 114(51).

OC037 | Single-molecule imaging of wild-type β_2 -adrenergic receptors with a novel fluorescent antagonist

Jak Grimes¹; Mark Soave²; Zsombor Koszegi¹; Davide Calebiro¹; Barrie Kellam²; Stephen J. Hill²

¹University of Birmingham; ²University of Nottingham

Background and Purpose: A well-orchestrated activation of GPCRs is required for achieving efficient and specific responses to hormones and drugs (Sungkaworn et al., 2017). However, the exact organisation of GPCRs on the plasma membrane is poorly understood. This is mainly due to the lack of adequate tools to study receptors in living cells with sufficient spatio-temporal resolution. Here, we used a novel, fluorescent β_2 -adrenergic ligand, based on the high-affinity, selective antagonist ICI 118,551, to image β_2 adrenergic receptors in living cells with single-molecule sensitivity.

Experimental Approach: CHO cells were transfected with wild-type β_2 -adrenergic receptor cDNA (or mock transfected) and labelled 4 hr after transfection with 10 nM of a fluorescent ICI 118,551 derivative. Cells were then imaged with a custom-built total internal reflection fluorescence microscope, equipped with an EMCCD camera, a

TABLE 1 MOP activation data in the presence of TRPV1

Assay	Ligand	pEC ₅₀	EC ₅₀ (nM)	E _{max} (%)
β Arr2	DAMGO	6.59 ± 0.15	258.5	100
	DAMGO + 1- μ M capsaicin	Did not fit		
Nb33	DAMGO	7.00 ± 0.13	99.81	100
	DAMGO + 1- μ M capsaicin	7.02 ± 0.09	94.66	138.9 ± 1.5
Mini Gi	DAMGO	7.38 ± 0.06	41.54	100
	DAMGO + 1- μ M capsaicin	6.74 ± 0.06	181.5	91.7 ± 1.5
GPA i2	DAMGO	8.37 ± 0.04	4.251	100
	DAMGO + 1- μ M capsaicin	7.22 ± 0.12*	60.87	35.5 ± 1.1*

*P < .05 compared to DAMGO.

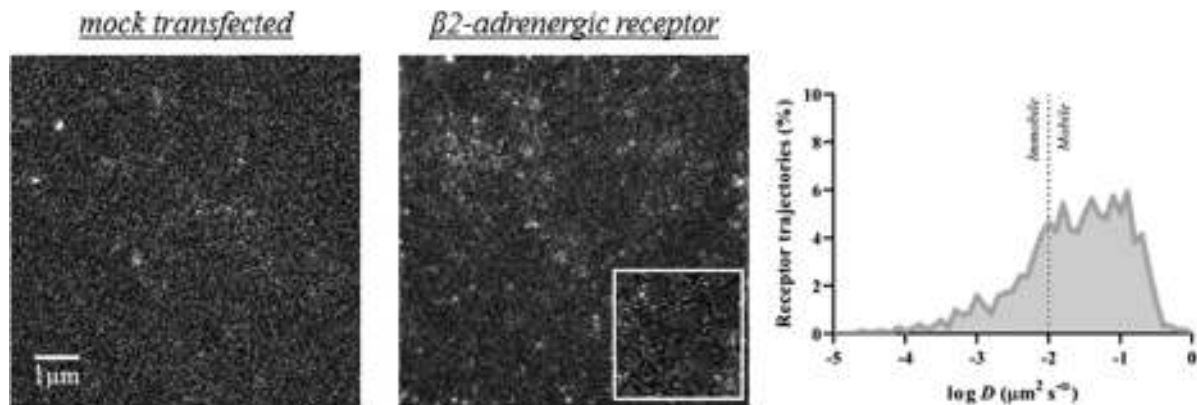


Figure 1. Left panel: Representative images from tracked movies of cells mock transfected or transfected with β_2 -adrenergic receptor; cells were labelled with 10-nM fluorescent ICI 118,551 and imaged on a custom-built TIRF microscope. Right panel: Distribution of diffusion coefficient (D) based on an MSD analysis of >10,000 β_2 -adrenergic receptor trajectories ($n = 15$ cells)

637-nm diode laser, and a 100 \times /1.49 NA oil-immersion objective. Single-molecule image sequences were acquired every 30 ms for 400 frames (12 s total). Image sequences were analysed with an automated particle detection and tracking algorithm (μ -track) (Jaqaman et al., 2008) in the MATLAB environment. A mean squared displacement (MSD) analysis of the obtained receptor trajectories was used to categorise them according to their diffusion.

Key Results: Using the fluorescent ICI 118,551 derivative, we were able to image and track individual β_2 -adrenergic receptors expressed in CHO cells at low/physiological densities (~ 0.4 receptor- μm^{-2}). Non-specific binding was negligible, as indicated by the absence of detectable fluorescent spots in mock transfected cells. An MSD analysis on the trajectories revealed a heterogeneous distribution, with a mixture of freely diffusing ($27.4\% \pm 5.6\%$), confined ($36.3\% \pm 7.0\%$), and immobile ($32.4\% \pm 7.1\%$) receptors ($n = 15$ cells from three experimental replicates; data represented as mean \pm SD).

Conclusion and Implications: Our results provide a proof of principle that our novel, fluorescent β_2 -adrenergic ligand can be used to directly visualise and track wild-type β -adrenergic receptors expressed at low levels in a simple cell system. In the future, we aim to extend this approach to image endogenous β_2 -adrenergic receptors and investigate their spatio-temporal dynamics in primary cells and tissues.

REFERENCES

Jaqaman, K., et al. (2008). Robust single-particle tracking in live-cell time-lapse sequences. *Nature Methods*, 5, 695–702.
 Sungkaworn, T., et al. (2017). Single-molecule imaging reveals receptor-G protein interactions at cell surface hot spots. *Nature*, 550, 543–547.

OC038 | Evaluation of AF647-CXCL8 as a fluorescent tracer for developing kinetic binding TR FRET assay for the human CXCR2 receptor

Desislava Nesheva; Steven Charlton; Shailesh Mistry; Nicholas Holliday

University of Nottingham

Background and Purpose: The chemokine receptor CXCR2 is involved in different inflammatory pathologies (Helen et al., 2017). Here, we compare whole-cell imaging and time-resolved FRET (TR FRET) approaches to develop a whole-cell fluorescent ligand binding assay for CXCR2, using CXCL8 labelled at its C terminal lysine with Alexa Fluor (AF) 647.

Experimental Approach: All assays used HEK293 cells stably transfected with N-terminal SNAP-tagged and C-terminal His-tagged human CXCR2 cDNA. For whole-cell imaging experiments, cells were labelled with 0.2- μM membrane-impermeable SNAP surface AF488 for 30 min at 37 $^\circ\text{C}$, prior to incubation in HBSS/0.1% BSA containing Hoechst 33342 ($2 \mu\text{g}\cdot\text{ml}^{-1}$) for 10 min at room temperature. AF647 CXCL8 (0.01–10 nM) was added in the absence/presence of 10-nM CXCL8 or 1- μM intracellular modulator SB265610, and cells were imaged on a confocal plate reader at 10-min time intervals. Image analysis to quantify binding and obtain saturation binding curves was performed as described (Liu et al., 2016). For TR FRET assays, cells were labelled with Lumi4-Tb for 60 min at 37 $^\circ\text{C}$ in LABMED buffer. A range of concentrations of AF647-CXCL8 were then added with or

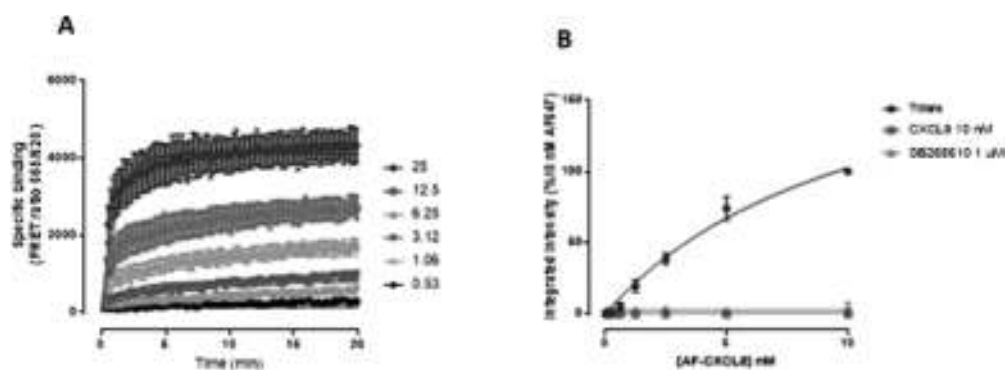


Figure 1. A) Association binding kinetics of a range of AF647-CXCL8 concentrations at CXCR2 receptor obtained using TR FRET ($n \geq 3$; error bars = SEM). B) Saturation binding of AF647-CXCL8 at 20 minutes at CXCR2 receptor obtained by whole-cell imaging analysis at 20 minutes ($n=3$, error bars = SEM)

without pretreating with 1- μ M unlabelled CXCL8 to define non-specific binding. Signal detection was performed using a BMG Pstar over 60 min, with ligand association globally fitted using a one-site model to obtain k_{on} and k_{off} constants and kinetic K_d values (GraphPad Prism).

Key Results: In whole-cell imaging assays, specific binding of AF647-CXCL8 was initially observed at the cell surface with a redistribution to intracellular compartments over time. This binding was inhibited in the presence of 10-nM CXCL8 or 1- μ M SB265610. Saturation analysis based on the quantified images provided an AF647-CXCL8 pK_d estimate of 7.52 ± 0.14 ($n = 3$) at 20 min and 8.44 ± 0.12 at 60 min ($n = 3$). When measuring AF647-CXCL8 in whole-cell binding by TR FRET, two phases were observed, including a secondary rising phase evident from 20 to 60 min of incubation. Analysis of the initial 20-min time course yielded AF647-CXCL8 k_{on} $1.83 \times 10^7 \pm 0.71 \text{ M}^{-1} \cdot \text{min}^{-1}$, k_{off} $0.56 \pm 0.21 \text{ min}^{-1}$, and kinetic pK_d of 7.53 ± 0.14 ($n \geq 3$).

Conclusion and Implications: AF647-CXCL8 is a high-affinity fluorescent ligand for the CXCR2 receptor which binding can be detected by both cellular imaging and TR FRET approaches. In whole cells, internalisation of the ligand over time occurs in a receptor-specific manner, and this component could be eliminated by using membrane preparation or purified receptor systems.

REFERENCES

- Helen, H., et al. (2017). Inflammatory diseases. *Theranostics*, 7(6), 1543–1588.
Liu, M., et al. (2016). *Journal of Medicinal Chemistry*, 59(13), 6059–6069.

Posters, Tuesday 17th December, 13:15

Poster Session: Cardiovascular and Respiratory Pharmacology 2

P184 | Pharmacological or genetic inhibition of soluble epoxide hydrolase demonstrates cardioprotection following myocardial infarction in aged female mice

Lockhart Jamieson¹; Zamaneh Kassiri¹; Gavin Oudit¹; Darryl Zeldin²; Bruce Hammock³; John Seubert¹

¹University of Alberta; ²NIH/NIEHS; ³University of California, Davis

Background and Purpose: Ischaemic heart disease accounts for a significant proportion of death and disability in aged individuals. The influence of age and sex on the development and presentation of heart disease is often underestimated in drug development (Merz & Cheng, 2016). CYP450 metabolism of polyunsaturated fatty acids (PUFAs) generates numerous metabolites, epoxy lipids, that exhibit a wide range of cellular effects. Previous studies demonstrate that epoxy lipids can regulate and protect mitochondria resulting in preserved cardiac function following ischaemic injury. The epoxy lipids are further metabolised by soluble epoxide hydrolase (sEH) into corresponding diol products with differing activities. Our first aim was to characterise epoxy lipid metabolism and sEH expression in tissues obtained from the human left ventricle (LV). And second, we aimed to

assess whether pharmacological inhibition or genetic deletion of sEH preserves cardiac and mitochondrial function post-ischaemia in aged mice.

Experimental Approach: Human tissues were obtained from male ($n = 12$) and female ($n = 5$) patients with a previous MI as part of the Human Explanted Heart Program (HELP), and non-failing control ($n = 10$) heart tissues were obtained from the Human Organ Procurement and Exchange (HOPE) programme at the University of Alberta. Male and female C57BL6 (WT) and sEH null mice averaging 15 months old underwent permanent occlusion of the left anterior descending coronary artery (LAD) (Kolk et al., 2009). Pharmacological inhibition of sEH was achieved by giving vehicle (0.1% DMSO) or sEH inhibitor trans-4-[4-(3-adamantan-1-yl-ureido)-cyclohexyloxy]-benzoic acid (tAUCB, $10 \text{ mg}\cdot\text{ml}^{-1}$ in 0.1% DMSO) to WT mice in the drinking water 4 days before or on the day of surgery ($n = 5-26$) (Liu et al., 2009) and continued ad libitum for 28 days. Cardiac function was assessed at baseline, 7 days, and 28 days post-MI by echocardiography and ECG. LVs were assessed for changes to protein expression and mitochondrial enzymatic activity; cardiac fibres were used to assess mitochondrial respiration. Human heart tissue was assessed for changes to the PUFA metabolite profile by LC-MS/MS.

Key Results: Individuals with a previous MI had significantly elevated levels of sEH expression correlating with changes to the PUFA metabolite profile and decreases in mitochondrial function. In mice, genetic deletion or treatment with the sEH inhibitor tAUCB significantly preserved cardiac function and increased survivability following MI. Importantly, these cardioprotective effects were only observed in aged female mice.

Conclusion and Implications: In summary, these data suggest that sEH is a potential pharmacological target for humans who had experienced a previous MI and suffer from heart failure. Moreover, the mouse data indicate an age-dependent sex difference, suggesting that targeting sEH may be more effective in improving post-ischaemic heart function in aged females.

REFERENCES

- Kolk, M. V., Meyberg, D., Deuse, T., Tang-Quan, K. R., Robbins, R. C., Reichenspurner, H., & Schrepfer, S. (2009). LAD-ligation: A murine model of myocardial infarction. *Journal of Visualized Experiments*.
- Liu, J. Y., Tsai, H. J., Hwang, S. H., Jones, P. D., Morisseau, C., & Hammock, B. D. (2009). Pharmacokinetic optimization of four soluble epoxide hydrolase inhibitors for use in a murine model of inflammation. *British Journal of Pharmacology*, 156, 284–296.
- Merz, A. A., & Cheng, S. (2016). Sex differences in cardiovascular ageing. *Heart*, 102, 825–831.

P186 | Cannabidiol exerts species selective cardioprotective effects in anthracycline-induced cardiotoxicity

Sarah Walsh; Gemma Barron; Cherry Wainwright

Robert Gordon University

Background and Purpose: Anthracyclines such as doxorubicin are effective chemotherapy agents; however, a severe and common side effect of this treatment is anthracycline-induced cardiotoxicity (AIC), which can lead to heart failure. At present, limiting anthracycline exposure is the only proposed strategy for reducing the risk of developing AIC; however, it is not entirely effective. Cannabidiol (CBD), a component of the cannabis plant, has recently been licensed for the treatment of spasticity in patients with multiple sclerosis and is currently being trialled as an anti-epileptic agent. Previous work has shown that CBD is cardioprotective in rodent models of AIC; however, it is unknown whether these findings extrapolate to humans. The aim of the present study was to investigate the effects of CBD in both rat and human in vitro models of AIC.

Experimental Approach: Rat H9c2 myoblast cells and human-induced pluripotent stem cell cardiomyocytes (HiPSC-CM) were plated for the assessment of cell viability using the MTT (3-(4,5-dimethylthiazol-2-yl)-2,5-diphenyl tetrazolium bromide) assay. Concentration-response curves were carried out to calculate the IC_{50} for doxorubicin (10^{-9} – 10^{-4} M) for each cell type, and this concentration was subsequently used to investigate the effects of CBD (0.1–10 μM) on AIC. Following treatment with pharmacological agents, media was stored for the measurement of cardiac troponin I (cTnI) via ELISA (HiPSC-CMs only), and an MTT assay carried out on the cells. All curves were constructed using non-linear regression and data compared using either a Student's *t* test or one-way ANOVA (with Dunnett's post hoc test).

Key Results: Both the potency (1.59 μM vs. 0.26 μM ; $P < .01$; $n = 3$) and efficacy ($46 \pm 2\%$ vs. $20 \pm 4\%$ cell viability; $P < .01$; $n = 3$) of doxorubicin were reduced in HiPSC-CMs compared with H9c2 cells. CBD alone was not toxic to H9c2 cells up to 10 μM ; however, in HiPSC-CMs, 10- μM CBD induced an increase in cTnI release ($1,738 \pm 161$ vs. $899 \pm 35 \text{ pg}\cdot\text{ml}^{-1}$; $P < .05$; $n = 3$) and a reduction in cell viability ($76 \pm 5\%$ vs. 100% ; $P < .05$; $n = 3$). In cells treated with both CBD and doxorubicin, 1- μM CBD protected H9c2 cells ($74 \pm 4\%$ vs. $62 \pm 3\%$ cell viability; $P < .05$; $n = 3$) but not HiPSC-CMs ($60 \pm 1\%$ vs. $65 \pm 3\%$ cell viability; $n = 3$) from the toxic effects of doxorubicin. Furthermore, 10- μM CBD enhanced the cardiotoxic effects of doxorubicin in HiPSC-CMs as evidenced by both an increase in cTnI release ($3,403 \pm 219$ vs. $1,379 \pm 246 \text{ pg}\cdot\text{ml}^{-1}$; $P < .001$; $n = 3$) and a reduction in cell viability ($48 \pm 4\%$ vs. $65 \pm 3\%$; $P < .05$; $n = 3$) compared with controls.

Conclusion and Implications: The cardioprotective effects of CBD in AIC appear to be species dependent and are not evident in human cardiomyocytes.

P187 | Assay development for measurement of the sulfhydrylation in the pig heart as a potential signalling pathway of hydrogen sulfide

Yasir Al-Taie¹; Stephen Alexander²; Richard Roberts²; Michael Garle²

¹University of Nottingham/Medical School; ²Life Sciences/Medical School/University of Nottingham

Background and Purpose: Hydrogen sulfide (H₂S) is a biomodulator signalling molecule, which belongs to the gasotransmitters, NO and CO (Meng et al., 2017). H₂S is mainly biosynthesised in mammalian tissues, and it was implicated in many physiological and pathological conditions (Sen, 2017). There detailed signalling pathways of H₂S in the heart are not yet clear (Yasir et al., 2016). The aim of this study was to develop an assay to measure the sulfhydrylation (SH) in the myocardium.

Experimental Approach: Porcine hearts were dissected, and the left ventricle was homogenised in Tris-HCl buffer (pH 7.4) (Yasir et al., 2017). Next, the porcine heart homogenate (PHH) was subjected to biotin switch assay (BSA) in which unmodified cysteines of proteins are blocked by the methiolating (alkylating) agent: methyl methanethiosulfonate (22 mM, MMTS). Next, sulfhydrylated cysteines are labelled with biotin (4 mM) which can be readily purified by streptavidin-agarose and then run biotinylated protein (sulfhydrylated) by Western blotting by probing with GAPDH (1:5,000) or MEK1 (1:1,000) antibody (Mustafa et al., 2009). In the red maleimide assay (RMA) (Sen, 2017), the PHH was incubated with Na₂S (1 mM, sodium sulfide, H₂S donor) for 30 min in 37°C incubator. Second, the PHH was incubated with the red maleimide (2 μM) for 2 hr at 4°C with slow-speed upside-down shaker. Then the PHH was exposed to DTT (1 mM) for 1 hr at 4°C on slow-speed shaker. Next, the PHH was diluted 1:1 with a non-reducing solubilising buffer (2× SB). Then the PHH was run by Western blotting. Subsequently, the gel was scanned for the red maleimide signal and then probed by incubation with GAPDH (1:5,000) or MEK1 (1:1,000) antibody to measure the level of sulfhydrylation. All values were expressed as means ± SEM. Comparisons between more than two data groups were made using ANOVA followed by Sidak's post hoc test. For comparisons between two data sets, a two-tailed unpaired/paired Student's *t* test was used. *P* value of less than .05 indicated a significant difference between the data sets; *n* = number of animals.

Key Results: There was a significant increase in sulfhydrylation with Na₂S (1 mM, H₂S donor) (709,222 ± 163,347 vs. 1,100,000 ± 330,213; *n* = 6) and non-significant increase with H₂O₂ (1 mM, oxidising agent)

(*n* = 3). There was more sulfhydrylation by MEK1 than GAPDH (*n* = 6). The RMA results showed obvious/significant decrease of RMA signal with DTT in many places (wherever they are) (595,300 ± 260,948 vs. 1,030,800 ± 294,676; *n* = 5) and consistent shifting of the double band of GAPDH and MEK1 to low MW in the presence of Na₂S (1 mM, H₂S donor) and DTT (1 mM, reducing agent). Moreover, there was a shifting of double band to low MW, which is potentially sulfhydrylated.

Conclusion and Implications: In short, SH was present in the heart. The BSA was kind of working for the detection of sulfhydrylated protein, but the results were variable. In BSA, MEK1 may be more susceptible to sulfhydrylation than GAPDH. RMA produced consistent results, and it may be promising and robust assay to measure the SH rather than BSA in the heart.

REFERENCES

- Meng, et al. (2017). *British Journal of Pharmacology*.
Mustafa, et al. (2009). *Science Signaling*.
Sen (2017). *Journal of Molecular Biology*.
Yasir, et al. (2016). *BPS Winter Meeting*.
Yasir, et al. (2017). *BPS Winter Meeting*.

P188 | Methamphetamine induces sex-dependent hypertrophic changes in the right ventricle

Hicham Labazi; Margaret Nilsen; Margaret MacLean

University of Strathclyde

Background and Purpose: Methamphetamine (MA) is a highly addictive drug, and MA abuse is associated with increased risk of developing pulmonary arterial hypertension (PAH). Interestingly, a recent clinical study demonstrated that the female sex is the main factor associated with MA-induced PAH. The mechanisms associated with increased prevalence and severity of MA-PAH in females versus males are still unclear. Here, we hypothesized that MA may promote changes in gene expression in the heart and/or the lung contributing to the development and/or worsening of PAH in females.

Experimental Approach: Male (M) and female (F) C57BL/6 mice were divided into two groups: MA groups receiving i.p. injections of low dose of MA (0.5 mg·kg⁻¹, 5 days·week⁻¹) for 3 weeks and vehicle groups (0.2% to 0.3% methanol). After 3 weeks, right and left ventricular systolic pressures (RVSP and LVSP, respectively) were assessed under terminal anaesthesia (isoflurane, 1% to 1.5%), and tissue samples were collected for gene expression using real-time PCR.

Key Results: LVSP and RVSP were not significantly different between the two female groups (98.62 ± 2.403 mmHg in F-MA [female-MA] vs. 86.25 ± 10.50 mmHg in F-V [female-vehicle]; *n* = 4–6 and 23.83 ± 1.41 mmHg in F-MA vs. 24.66 ± 0.61 mmHg in F-V; *n* = 5–6, respectively). In females, the right ventricular (RV) weight and Fulton index were significantly increased in the F-MA group, compared to F-V; RV: 19.90 ± 1.16 mg versus 16.48 ± 0.68 mg, respectively; *n* = 6,

$P < .05$; Fulton index: 0.24 ± 0.02 in F-MA versus 0.20 ± 0.01 in F-V; $n = 6$, $P < .05$, Student's t test. These changes were not observed in male mice. Our data suggest that, contrary to males, MA-dosed female mice developed RV hypertrophy independent of increases in RVSP. Also, in the females, while lung gene expression was not affected by MA, MA-induced RV hypertrophy was associated with increased expression of brain natriuretic peptide (BNP) gene (0.08 ± 0.02 in F-MA vs. 0.03 ± 0.01 in F-V, $n = 6$, $P < .05$, Student's t test). Expression of members of the TGF- β receptor signalling pathway such as TGF- β receptor-1 and smad3 and smad7 genes was also increased by MA. In male mice, we did not observe any changes in gene expression in either the lung or RV.

Conclusion and Implications: Our results suggest that MA may cause RV hypertrophy, which precedes the development of PAH in female mice, but not in males. If this translates to PAH patients, it might explain the poor outcome observed in MA-associated female PAH patients.

P189 | Mechanisms of sex hormones induced porcine coronary artery relaxation

Musaad Althobaiti; Musaad Althobaiti; Michael Garle;
Richard Roberts; Michael Randall

University of Nottingham

Background and Purpose: Sex hormones have significant roles in the regulation of a wide range of physiological processes. There is a growing body of evidence to suggest that sex steroids regulate vascular tone and affect the health of the cardiovascular system particularly at young ages. The incidence of cardiovascular diseases (CVDs) differs significantly between male and female as it has been revealed by several clinical studies. In premenopausal women, cardiovascular incidence is very low comparing with men at similar age. It has been reported that sex hormones have genomic and rapid non-genomic mechanisms in regulating cardiovascular system. This study aimed to investigate the mechanisms of sex hormones (estradiol and testosterone) induced porcine coronary artery relaxation (Miller & Duckles, 2008; Orshal & Khalil, 2004).

Experimental Approach: An isometric tension recording system was used to investigate the alterations in porcine coronary arterial (PCA) tone. Segments of PCA with or without endothelium were set up in isolated tissue baths and contacted by the Tx mimetic, U46619, followed by cumulative concentrations to estradiol (1 nM–30 μ M) or testosterone (1 nM–50 μ M). PCAs were contracted with U46619 in the presence and absence of 300- μ M L-NAME (nitric oxide synthase inhibitor) or 10- μ M indomethacin (COX inhibitor), followed by cumulative concentrations of estradiol (1 nM–30 μ M) or testosterone (1 nM–50 μ M) in other experiments. PCAs were washed with Ca $^{2+}$ free buffer several times and contracted by cumulative concentrations of CaCl $_2$ (1 μ M–1 mM) in the presence and absence of 10- μ M estradiol or 10- μ M testosterone. PCAs were contracted by cumulative

concentrations of the calcium channel activator BAY-K8644 (1–300 nM) in the presence and absence of 10- μ M estradiol or 10- μ M testosterone.

Key Results: PCA relaxation to testosterone was not affected by removing the endothelium ($E_{\max} = 103\% \pm 7$) compared to PCA relaxation with intact endothelium ($E_{\max} = 97\% \pm 1$) (both $n = 6$). Similarly, no differences were revealed in the estradiol-induced relaxation in the denuded PCA ($E_{\max} = 88\% \pm 7$) compared to the intact PCA ($E_{\max} = 91\% \pm 4$; $n = 6$). The presence of 300- μ M L-NAME did not affect PCA relaxation to estradiol ($E_{\max} = 92\% \pm 7$) comparing to PCA relaxation in the absence of 300- μ M L-NAME ($E_{\max} = 104\% \pm 2$; $n = 6$). Similarly, 300- μ M L-NAME had no effect on PCA relaxation to testosterone ($E_{\max} = 99\% \pm 4$ in the absence of L-NAME, comparing to $E_{\max} = 97\% \pm 3$; $n = 6$). PCA relaxation to estradiol was not affected by the presence of 10- μ M indomethacin ($E_{\max} = 108\% \pm 4$) comparing with PCA relaxation to estradiol in the absence of 10- μ M indomethacin ($E_{\max} = 103\% \pm 5$; $n = 6$). Similarly, relaxation of the PCAs to testosterone was not affected by the presence of 10- μ M indomethacin ($E_{\max} = 108\% \pm 5$) compared with relaxation of PCAs to estradiol in the absence of 10- μ M indomethacin ($E_{\max} = 99\% \pm 6$; $n = 6$). Contractile responses of PCAs to BAY-K8644 were affected by the presence of 10- μ M estradiol ($E_{\max} = 38\% \pm 4$) compared to its absence ($E_{\max} = 38\% \pm 9$; $n = 5$). Similarly, contractile responses to BAY-K8644 were affected by the presence of 10- μ M testosterone ($E_{\max} = 50\% \pm 4$) compared to its absence ($E_{\max} = 54\% \pm 2$; $n = 6$). However, the PCAs contractile responses to CaCl $_2$ were significantly reduced in the presence of 10- μ M estradiol ($E_{\max} = 59\% \pm 5$) comparing with the absence of estradiol ($E_{\max} = 89\% \pm 7$; $n = 7$). Similarly, PCAs contractile response to CaCl $_2$ was reduced in the presence of 10- μ M testosterone ($E_{\max} = 68\% \pm 4$) comparing with its absence ($E_{\max} = 97\% \pm 7$; $n = 6$).

Conclusion and Implications: This study indicates that sex hormones induce PCAs relaxation independent of the endothelium, nitric oxide, or COX pathway. The presence of estradiol or testosterone did not show any effect on PCAs contractile responses to BAY-K8644 cumulative concentrations. However, contractile responses following reintroduction of Ca $^{2+}$ to calcium-free buffer in the presence of high KCl were significantly inhibited by both estradiol and testosterone which indicates that sex hormones might inhibit Ca $^{2+}$ influx. However, more investigations are required to understand the mechanisms of sex hormones induced PCA relaxation.

REFERENCES

- Miller, V. M., & Duckles, S. P. (2008). Vascular actions of estrogens: Functional implications. *Pharmacological Reviews*, 60(2), 210–241.
- Orshal, J. M., & Khalil, R. A. (2004). Gender, sex hormones, and vascular tone. *American Journal of Physiology - Regulatory, Integrative and Comparative Physiology*, 286(2), R233–R249.

P190 | Prescribing a single inhaler type: Audit of inhaler prescribing in two London general practices

Fatima Rashid¹; Srutti Suresan¹; Patricia McGettigan²

¹Barts and The London, School of Medicine and Dentistry; ²The William Harvey Research Institute - Barts and The London

Background and Purpose: Inhaled medicines are a mainstay of treatment for asthma and chronic obstructive pulmonary disease (COPD). Multiple inhaler devices are available, and techniques for use differ. The British Thoracic Society (BTS) and Scottish Intercollegiate Guidelines Network (SIGN) recommend prescribing the same type of inhaler device (e.g., pressurised metered-dose inhaler [pMDI] or dry powder inhaler [DPI]) where possible for individual patients in order to optimise outcomes (BTS/SIGN Guideline for the management of asthma, 2019). In retrospective audits based in primary care, we assessed prescribers' adherence to the guidelines.

Experimental Approach: Eligible patients were registered at two London general practices during March 2019, were 16 years or older, and were prescribed at least one inhaler. EMIS database searches identified a combined total of 1,520 patients meeting these criteria, and a sample of 266 records was randomly selected for audit. Anonymised data including age, sex, respiratory diagnosis, spirometry, lung function, and most recent inhaler prescription information (name/s and dose/s) were extracted under general practitioner supervision for each patient. The RightBreathe website (<https://www.rightbreathe.com/>) was used to categorise inhaler types and U.K. availability of devices. Ethics approval was not required as this was an audit.

Key Results: Seventy-nine patients (30%) had a prescription for a single inhaler while 187/266 (70%) were prescribed >1 inhaler: 165/266 (62%) patients, 2 inhalers; 19 (7%), 3 inhalers; 2 (<1%), 4 inhalers; and 1 (<1%) patient had 5 inhalers. The most commonly prescribed device was the pMDI with 251 (94%) patients prescribed at least one.

Sixty-two per cent (116/187) of patients prescribed ≥ 2 inhalers had the same type of device, but 84% (157/187) could have had the same device. Patient records included no explanation for discrepant device choices. Patients prescribed 2 inhalers were more likely to be prescribed the same type of device than those with >2 devices.

Conclusion and Implications: In our audit, prescribers did not adhere consistently to national guidelines regarding inhaler prescribing. This was a small audit, but if our findings apply generally, it suggests a gap between guidance for optimising treatment effectiveness and practice in community care. Online tools are available that might help close this gap (RightBreathe (<https://www.rightbreathe.com/>) and ADMIT (inHalers4u)). Correct inhaler technique is essential for effective disease management, and future audits should determine practices' assessment of technique and spacer prescription for specific patients.

REFERENCES

BTS/SIGN *Guideline for the management of asthma* 2019 <https://www.brit-thoracic.org.uk/quality-improvement/guidelines/asthma/inHalers4u> <https://www.inhalers4u.org/index.php/choosing-inhalers/> <https://www.rightbreathe.com/>

P191 | Biochemical analysis of atorvastatin and amlodipine in single and combination therapy

Mehjabeen Mehjabeen¹; Noor Jahan²; Farah Owais¹

¹Federal Urdu University of Arts and Sciences; ²Dow University of Health Sciences

Background and Purpose: Amlodipine (antihypertensive agent) and atorvastatin (antihyperlipidemic agent) are widely used either as a single drug therapy or combination therapy for patients suffering from cardiovascular problems. Besides valuable medications, both drugs have some complications or side effect such as hepatotoxicity. Therefore, the present study is designed to investigate the effect of atorvastatin and amlodipine in single and combination therapy on biochemical and histological parameters in rabbits.

Experimental Approach: The animals (rabbits) are divided into Group 1 (0.5 ml of saline), Group 2: atorvastatin ($0.57 \text{ mg}\cdot\text{kg}^{-1}$), Group 3: amlodipine ($0.15 \text{ mg}\cdot\text{kg}^{-1}$), and Group 4: combination of atorvastatin and amlodipine ($0.57 + 0.15 \text{ mg}\cdot\text{kg}^{-1}$). The drugs were administered orally for a period of 90 days followed by blood sample collection for biochemical analysis and tissue histology of stomach, liver, heart, and kidney.

Key Results: The results showed that in combination of both drugs, uric acid ($P < .0001$) and SGOT level ($P < .0003$) increased significantly while cholesterol level was reduced, whereas SGPT and alkaline phosphatase markedly increased in all treated groups. Tissue histology revealed mild to moderate inflammation with both atorvastatin and amlodipine in kidney and liver tissues while no significant alterations were observed in stomach and cardiac tissues.

Conclusion and Implications: It could be concluded that prolong use of combination of atorvastatin and amlodipine may induce inflammatory changes in liver and kidney and increased uric acid level which needs a careful monitoring.

TABLE 1 Effect of atorvastatin and amlodipine and its combination on blood chemistry

Biochemical parameter	Control	Atorvastatin	Amlodipine	Atorvastatin + amlodipine
Cardiac enzymes				
LDH	371 ± 2.65	385 ± 3.12	380 ± 1.95	350 ± 2.21
CPK	933 ± 1.23	832 ± 0.95	756 ± 1.17	860 ± 1.54
CK-MB	20 ± 0.65	28.4 ± 1.58	27 ± 2.12	23 ± 1.12
Kidney function test				
Uric acid	0.04 ± 0.01	1.23 ± 1.17 ^a †	0.085 ± 0.01	3.41 ± 0.91 ^{**} †
Urea	59 ± 1.45	57 ± 1.87	64.5 ± 1.69	64.3 ± 1.63
Creatinine	1.57 ± 0.04	1.55 ± 0.05	2.045 ± 0.02	1.81 ± 0.26
Liver function test				
Total bilirubin	0.12 ± 0.02	0.40 ± 0.02	0.37 ± 0.01	0.31 ± 0.02
Direct bilirubin	0.05 ± 0.01	0.10 ± 0.01	0.07 ± 0.02	0.12 ± 0.02
SGPT	20 ± 1.21	32 ± 1.21	31 ± 0.87	30 ± 0.58
Alkaline phosphatase	36 ± 1.4	47 ± 1.16	59 ± 2.17	47 ± 2.37
Lipid profile				
Cholesterol HDL ratio	4.2 ± 2.56	4.68 ± 1.58	5.35 ± 0.96	4.4 ± 0.52
Cholesterol (mg·dl ⁻¹)	139 ± 1.38	133.2 ± 19.97	141 ± 7.22	122.6 ± 17.90
Triglycerides (mg·dl ⁻¹)	169 ± 2.51	163.2 ± 26.75	162 ± 0.71	156.60 ± 24.02
HDL (mg·dl ⁻¹)	33 ± 1.14	27.6 ± 2.46	26 ± 0.89	28.40 ± 2.23
LDL (mg·dl ⁻¹)	120 ± 1.34	109 ± 26.43	95.6 ± 21.71	40 ± 6.32
VLDL (mg·dl ⁻¹)	34 ± 0.71	32.4 ± 5.32	32 ± 0.55	31 ± 4.83

Note. Values are expressed in mean ± SEM; n = 5; ANOVA.

^aAtorvastatin.

^bAmlodipine.

*P < .05 is significant.

**P < .001 is highly significant.

REFERENCE

Jukema, J. W., & Van Der Hoorn, J. W. (2004). *Expert Opinion on Pharmacotherapy*, 5, 459–468.

P192 | Canagliflozin, dapagliflozin, and empagliflozin exerted antiplatelet activity

Caroline Honaiser Lescano; Pedro Henrique Portugal Torres; Edson Antunes; Fabíola Zakia Mónica

University of Campinas

Background and Purpose: Sodium-glucose co-transporter 2 inhibitors, also known as gliflozins (canagliflozin, dapagliflozin, and empagliflozin), are drugs approved for the treatment of type II diabetes. Clinical studies have shown that diabetic patients who have received gliflozins had better cardiovascular outcomes evaluated by lower number of deaths from cardiovascular causes and fewer hospitalizations for congestive heart failure (Neal, 2017; Wiviott et al. 2019; Zinman, 2015). Since gliflozins have beneficial responses in the cardiovascular system and platelets participate in the pathophysiology of cardiovascular diseases, including coronary artery disease and ischaemic stroke, this study is aimed to characterize the role of gliflozins on human platelets obtained from healthy volunteer.

Experimental Approach: The experimental protocols were approved by the Human Ethics Committee of the University of Campinas (CAAE number 72739517.9.0000.5404). PRPs and washed platelets (WPs) were pre-incubated with gliflozins (1–100 μM) and stimulated with ADP (10 or 30 μM), U-46619 (2 or 4 μM), or collagen (COL, 2 μg·ml⁻¹). The levels of Tx B₂ (TXB₂), cyclic nucleotides, and calcium (Ca²⁺) mobilization were determined. All the protocols were carried out in the presence of sub-maximal concentrations of sodium nitroprusside (SNP 10 or 100 nM) and iloprost (ILO 0.1 or 10 nM). The effect of gliflozins was determined in comparison with platelets stimulated with the vehicle (DMSO, 1%) in the presence of SNP and ILO. Non-parametric Friedman followed by post hoc Nemenyi test with N = number of patients was performed.

Key Results: The aggregations induced by collagen, U-46619, or ADP were significantly reduced by gliflozins in both PRP and WP (Figure 1, N = 23, P < .0001 vs. vehicle). The Ca²⁺ mobilization (N = 14) and TXB₂ levels (N = 27), respectively, were also significantly reduced (P < .0001) in the presence of canagliflozin (33.1 ± 2.5% and 58.1 ± 5.1%), dapagliflozin (34.1 ± 2.4% and 47.1 ± 7.2%), or empagliflozin (30.5 ± 2.5% and 43.4 ± 9.2%). Gliflozins did not interfere in the intracellular levels of cAMP or cGMP.

Conclusion and Implications: Our findings showed that gliflozins inhibited human platelet aggregation induced by different agonists, decreased Ca²⁺ mobilization, and TXA₂ synthesis. Our study opens

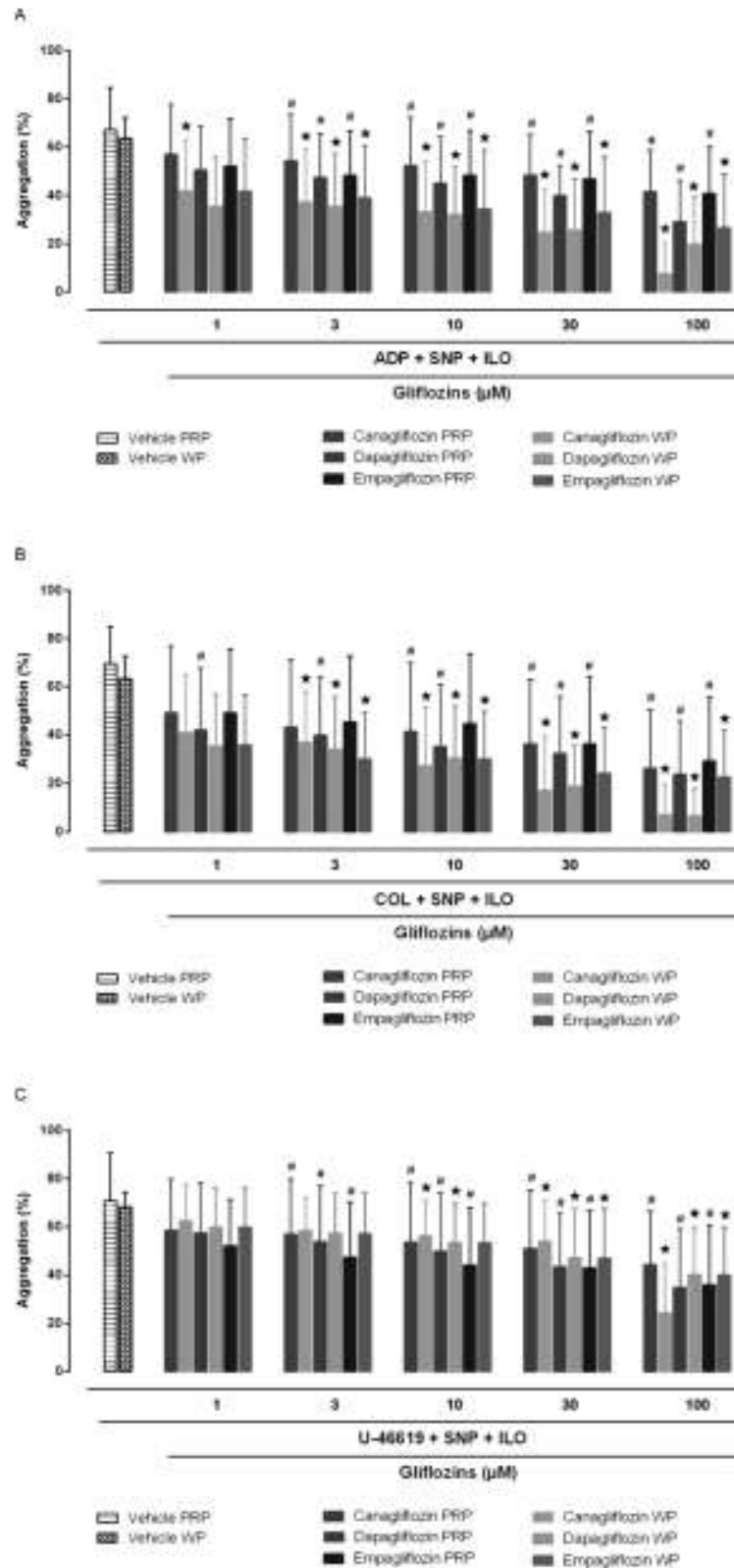


Figure 1. Effects of gliflozins on PRPs and washed platelets (WPs) in the presence of sodium nitroprusside (10 nM for WP or 100 nM for PRP) and iloprost (0.1 nM for WP or 10 nM for PRP). PRP and WP were pre-incubated with gliflozins (1–100 μM) followed by stimulation with ADP (10 or 30 μM) (a) or collagen (2 $\mu\text{g}\cdot\text{mL}^{-1}$) (b) or U-46619 (2 or 4 μM) (c). Data represent the mean values \pm SD, $\#P < .05$ compared with vehicle PRP; $*P < .05$ compared with vehicle WP

the possibility to verify the effect of gliflozins in combination with antiplatelet substances for the treatment of patients with arterial thromboembolic diseases.

ACKNOWLEDGEMENTS: This study was supported by FAPESP (Processes 2017/26687-3, 2017/15175-1, and 2018/21880-2) and CAPES.

REFERENCES

- Neal, B. (2017). Canagliflozin and cardiovascular and renal events in type 2 diabetes. *The New England Journal of Medicine*, 377, 644–657.
- Wiviott, S. D., et al. (2019). Dapagliflozin and cardiovascular outcomes in type 2 diabetes. *The New England Journal of Medicine*, 380, 347–357.
- Zinman, B., et al. (2015). Empagliflozin, cardiovascular outcomes, and mortality in type 2 diabetes. *The New England Journal of Medicine*, 373, 2117–2128.

P193 | Hepatocyte growth factor, IL-6, and cell matrix interactions in A549 adenocarcinoma growth

Griselda Awanis; Sathuwarman Raveenthiraraj;
Anastasia Sobolewski
University of East Anglia

Background and Purpose: Within the tumour micro-environment, cytokines such as hepatocyte growth factor (HGF) and IL-6 are mutationally up-regulated in non-small cell lung cancer (NSCLC) (Awad et al. 2016; Lee et al. 2016). In NSCLC, remodelling of the lung extracellular matrix proteins such as collagen IV and laminin occurs (Yan et al. 2006). Integrins, receptors to the extracellular matrix (ECM), facilitate pro-tumourigenic signalling through crosstalk with other pathways such as the HGF/c-Met pathway (Barrow-McGee et al. 2016). Therefore, we investigated the potential additive or synergistic effect between HGF, IL-6, and the ECM proteins in potentiating A549 growth.

Experimental Approach: A549 cells, which are human lung adenocarcinoma epithelial cells, were seeded in media containing 10% FBS. After 24 hr, cells were treated with HGF or IL-6 for a further 24 hr, and the number of cells present in the wells was counted using a haemocytometer. For ECM experiments, wells were pre-coated with laminin and collagen IV for an hour before addition of A549 cells. To establish the synergistic or additive effects of HGF and IL-6 with collagen IV, cell counts were carried out as above utilising the maximal concentrations. Determination of significance in all growth data was assessed with one-way ANOVA and Turkey's multiple comparisons test.

Key Results: HGF, IL-6, collagen IV, and laminin increased the proliferation in a concentration-dependent manner with an EC_{50} value of $1 \text{ ng}\cdot\text{ml}^{-1}$, $0.5 \text{ ng}\cdot\text{ml}^{-1}$, $0.3 \text{ }\mu\text{g}\cdot\text{ml}^{-1}$, and $0.4 \text{ }\mu\text{g}\cdot\text{ml}^{-1}$, respectively ($n = 3$, $P < .05$). A549 cells pre-coated with collagen IV and treated with HGF and IL-6 induced an additive effect in proliferation compared to A549 cells grown on plastic control.

Conclusion and Implications: Collagen IV functions as a platform for HGF and IL-6 to achieve A549 growth, thus highlighting its potential signalling cooperation. Future work will identify whether β 1-integrins are involved in regulating the HGF, IL-6, and ECM-induced A549 growth.

REFERENCES

- Awad, M. M., et al. (2016). MET exon 14 mutations in non-small-cell lung cancer are associated with advanced age and stage-dependent MET genomic amplification and c-Met overexpression. *American Society of Clinical Oncology (ASCO)*.
- Barrow-McGee, R., et al. (2016). Beta 1-integrin-c-Met cooperation reveals an inside-in survival signalling on autophagy-related endomembranes. *Nature Communications*, 7, 11942.
- Lee, S. O., et al. (2016). IL-6 promotes growth and epithelial-mesenchymal transition of CD133+ cells of non-small cell lung cancer. *Oncotarget*, 7 (6), 6626.
- Yan, X., et al. (2006). Expression of collagen IV, fibronectin, laminin in non-small cell lung cancer and its correlation with chemosensitivities and apoptosis. *The Chinese-German Journal of Clinical Oncology*, 5(1), 58–62.

P194 | Differential regulation of baculoviral repeat-containing protein 2 and 3 by inflammatory stimuli and glucocorticoids

Andrew Thorne; Robert Newton
University of Calgary

Background and Purpose: Glucocorticoids (GCs) repress expression of many inflammatory genes and are widely used to treat inflammatory diseases. However, GCs also induce expression of other inflammatory genes. Examples include baculoviral repeat-containing protein 3 (BIRC3) and the closely related homologue BIRC2. While it is unclear why GCs may up-regulate inflammatory genes, BIRC2 and BIRC3 are suggested to be functionally redundant E3 ubiquitin ligases that contribute to inflammatory signalling cascades. The current study therefore characterises the expression of BIRC2 and BIRC3 in the context of inflammatory stimuli and GCs using pulmonary A549 cells as a model of airway epithelial cells.

Experimental Approach: A549 cells were treated for various times with dexamethasone (Dex), budesonide (Bud), IL1B, and TNF alone or in combination with GC. Concentration-response analyses established maximally effective concentrations for Dex ($1 \text{ }\mu\text{M}$), Bud (333 nM), IL1B ($1 \text{ ng}\cdot\text{ml}^{-1}$), and TNF ($10 \text{ ng}\cdot\text{ml}^{-1}$). Roles for GR and the NF- κ B pathway were interrogated by gene silencing, the GR receptor antagonist, Org34517, or ATP binding site I κ B kinase (IKK) inhibitors. Cells were harvested for (i) total RNA, prior to cDNA synthesis and qPCR analysis of gene expression; or (ii) total proteins and western blot analysis. All data are $N = 4$ – 9 independent experiments.

Key Results: Low baseline expression of BIRC3 mRNA was induced 60-fold, 25-fold, or 10-fold by IL1B, TNF, or GCs, respectively. Peak mRNA expression was at 4 hr for IL1B and TNF, but at 6–24 hr for GCs. In each case, maximal BIRC3 protein expression occurred

6–24 hr post-treatment, and this was unaffected by combination treatment (IL1B/Dex or TNF/Dex). While BIRC2 mRNA was modestly induced by all stimuli (<5-fold), protein expression was constitutive. Gene silencing and receptor antagonism by Org34517 confirmed a role for GR in BIRC3 expression induced by GCs. Likewise, silencing of the NF- κ B subunit, RELA, and the IKK2-selective inhibitor, PS-1145, reduced BIRC3 expression induced by IL1B.

Conclusion and Implications: Our data support a possible acute role for BIRC2 in signalling events, but the later induction of BIRC3 expression via an NF- κ B-dependent mechanism suggests delayed and/or possibly nonredundant functions relative to BIRC2. The modest induction of BIRC3 expression by GCs involves the GR but is currently of unclear significance. Functional explanations for these differential effects will require a more detailed molecular assessment of the relative roles of BIRC2 and BIRC3 in the context of inflammatory stimulation and GCs.

P195 | Does sacubitril/valsartan have an impact on cardiac function through β -ARs in high-fat diet + low-dose streptozotocin diabetes model?

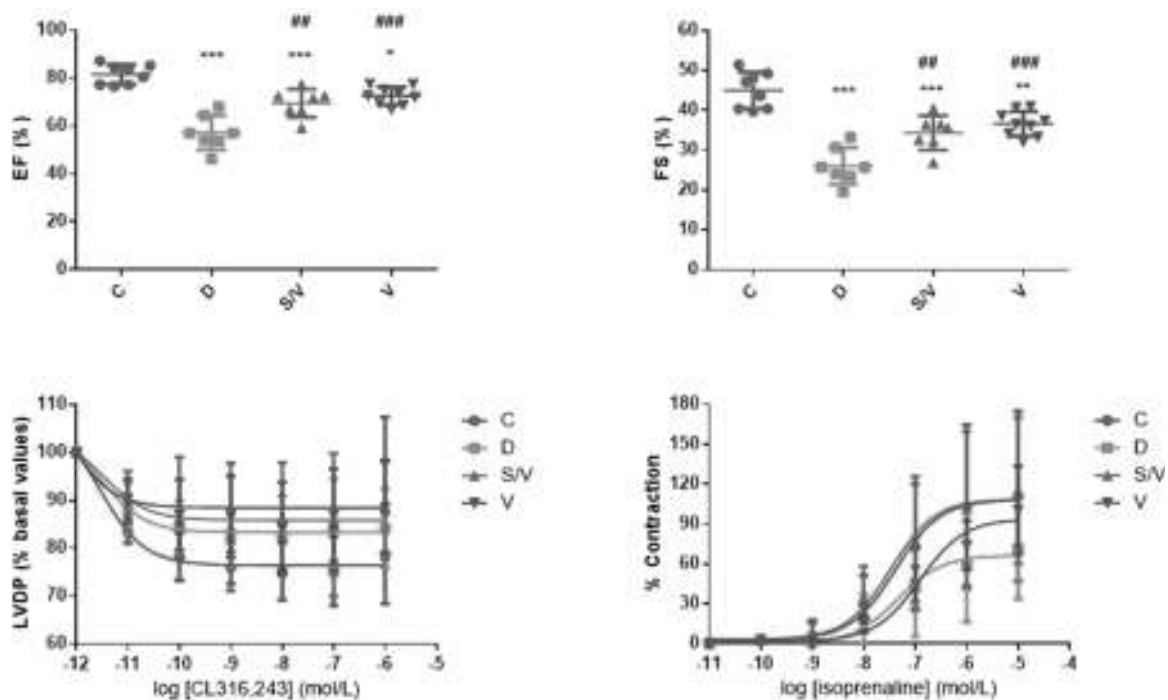
Betul Rabia Erdogan; Zeynep Elif Yesilyurt; Irem Karaomerlioglu; Ayhanim Elif Muderrisoglu; Kadir Sevim; Ebru Arioglu Inan
Ankara University

Background and Purpose: Cardiac dysfunction is the most important cause of diabetic morbidity and mortality. It has been reported that β -adrenergic responsiveness is reduced in diabetic heart (Dinçer et al.,

2001; Yu & McNeill, 1991). Development of new drugs targeting cardiac dysfunction in diabetes becomes increasingly significant. Sacubitril/valsartan has been approved for the treatment of heart failure in 2015. There are limited data about the effects of this combination on cardiac function in diabetic animals. Thus, our aim was to investigate the possible beneficial effects of sacubitril/valsartan comparatively to valsartan on diabetic heart by evaluating β -AR-mediated responses.

Experimental Approach: Four-week-old (100–150 g) Sprague Dawley rats were allocated into four groups (control, diabetic, sacubitril/valsartan-treated diabetic, and valsartan-treated diabetic with randomization). Some of the rats were put on high-fat diet (HFD) (45% kcal fat) whereas the others were put on a control diet (CD). Four weeks later, the rats on the HFD received intraperitoneal 30 mg·kg⁻¹ streptozotocin (STZ); rats on control diet received vehicle injection. One week after STZ injection, the rats had >200 mg·dl⁻¹ blood glucose levels considered as a diabetic. After 10-week diabetes period, some rats were treated with valsartan (31 mg·kg⁻¹·day⁻¹, oral gavage) or sacubitril/valsartan (68 mg·kg⁻¹·day⁻¹, oral gavage) for 4 weeks. At the end of the treatment period, echocardiography, PV loop analysis, papillary muscle (β 1-AR-mediated responses), and Langendorff (β 3-AR-mediated responses) experiments were performed under 2% isoflurane anaesthesia.

Key Results: Ejection fraction (EF) and fractional shortening (FS) have been reduced significantly in diabetic rats (^{***}*P* < .001 vs. control) in vivo echocardiography experiments, and both drugs improved cardiac dysfunction with similar efficacy (^{##}*P* < .01; ^{###}*P* < .001 vs. diabetic) (*n* ≥ 7). On the other hand, same parameters measured by in vivo PV loop analysis were comparable among the groups (*n* ≥ 4). Contraction response mediated by isoprenaline was blunted in diabetic group which was improved after sacubitril/valsartan and



valsartan treatment ($n \geq 5$). There was no significant difference in $\beta 3$ -AR-mediated response among the groups ($n \geq 5$).

Conclusion and Implications: The results of echocardiography experiments have revealed that in vivo cardiac function was improved with both valsartan and sacubitril/valsartan at a similar extent. However, PV loop analysis was failed to demonstrate the beneficial effect of both drugs. Despite of comparable $\beta 3$ -AR-mediated responses among the groups, $\beta 1$ -AR-mediated contractility was ameliorated by both valsartan and sacubitril/valsartan. According to our results, the beneficial effects of this combination on diabetic heart might be mediated by $\beta 1$ -ARs. Nonetheless, further molecular studies could help to clarify the underlying mechanisms.

REFERENCES

Diñçer, Ü. D., Bidasee, K. R., Güner, Ş., Tay, A., Özçelikay, A. T., & Altan, V. M. (2001). The effect of diabetes on expression of $\beta 1$ -, $\beta 2$ -, and $\beta 3$ -adrenoreceptors in rat hearts. *Diabetes*, 50(2), 455–461.
 Yu, Z., & McNeill, J. H. (1991). Altered inotropic responses in diabetic cardiomyopathy and hypertensive-diabetic cardiomyopathy. *The Journal of Pharmacology and Experimental Therapeutics*, 257(1), 64–71.

P197 | Hesperidin mitigates signs of metabolic syndrome, cardiac remodelling, and dysfunctions in rats with high-fat diet-induced metabolic syndrome

Patoomporn Prasatthong; Putcharawipa P. Maneesai; Parichat Prachaney; Poungrat Pakdeechote
 Khon Kaen University

Background and Purpose: Metabolic syndrome (MS) is a cluster of at least three of five following conditions, central obesity, insulin resistance, impaired glucose tolerance, hypertension, and dyslipidaemia. MS is believed to contribute to cardiac remodelling and dysfunction. Hesperidin is a major bioflavonoid found in citrus fruits. It exerts anti-hypertensive, anti-inflammation, and antioxidant effects (Maneesai

et al., 2018). This study investigates whether hesperidin could improve signs of metabolic syndrome, cardiac remodelling, and dysfunction in high-fat diet (HFD)-induced metabolic syndrome in rats.

Experimental Approach: Male Sprague-Dawley rats were divided into five groups ($n = 8$). A control group was fed with standard chow diet (SCD) and distilled water while MS rats were fed with HFD and 15% fructose in drinking water for 16 weeks in order to induce MS rats. After 12 weeks of induction, MS rats were subdivided into three groups and fed with hesperidin (15 or 30 mg.kg⁻¹) or metformin (100 mg.kg⁻¹) for further 4 weeks. Body weight, food intake, and BP were measured. At the end of experiment, cardiac function, blood glucose, serum insulin, and lipid profiles were measured. Histomorphometry of cardiac tissue was evaluated. Protein expression of insulin receptor substrate (p-IRS), p-AKT, and GLUT4 in heart tissue was determined using western blot analysis. Statistical significance was analysed using one-way ANOVA followed by a Fisher's LSD post hoc test.

Key Results: MS rats showed signs of MS such as insulin resistance, dyslipidaemia, increases in weight gain, and BP ($P < .05$) (Table 1). Furthermore, ventricular hypertrophy and dysfunction ($P < .05$) (Table 2) and down-regulation of insulin signalling pathway were observed in MS rats ($P < .05$). Hesperidin and metformin supplementation significantly reduced weight gain and BP and alleviated dyslipidaemia and insulin resistance ($P < .05$) (Table 1) and up-regulated insulin signalling pathway expression in cardiac tissue in MS rats ($P < .05$). Alterations of cardiac morphology and function were ameliorated in MS rats treated with hesperidin or metformin ($P < .05$) (Table 2).

Conclusion and Implications: Hesperidin was effective in reducing signs of metabolic syndrome in HFD-induced MS rats. It also alleviated ventricular remodelling and dysfunction via restoration of insulin signalling pathway in cardiac tissue in HFD-induced MS rats.

REFERENCE

Maneesai, P., Bunbupha, S., Potue, P., Berkban, T., Kukongviriyapan, U., Kukongviriyapan, V., et al. (2018). Hesperidin prevents nitric oxide deficiency-induced cardiovascular remodeling in rats via suppressing TGF- $\beta 1$ and MMPs protein expression. *Nutrients*, 10(10), 1549.

TABLE 1 Effect of hesperidin and metformin on signs of MS in HFD-induced MS rats

	Control	MS	MS + hesperidin (15 mg.kg ⁻¹)	MS + hesperidin (30 mg.kg ⁻¹)	MS + metformin (30 mg.kg ⁻¹)
LVIDd (cm)	0.699 ± 0.028	0.607 ± 0.028 ^a	0.627 ± 0.024	0.666 ± 0.041	0.697 ± 0.030 ^b
LVIDs (cm)	0.446 ± 0.020	0.431 ± 0.032	0.422 ± 0.025	0.427 ± 0.037	0.452 ± 0.029
EDV (ml)	0.789 ± 0.086	0.540 ± 0.073 ^a	0.590 ± 0.064	0.712 ± 0.116	0.790 ± 0.083 ^b
ESV (ml)	0.225 ± 0.027	0.217 ± 0.044	0.198 ± 0.032	0.216 ± 0.050	0.243 ± 0.039
SV (ml)	0.568 ± 0.062	0.323 ± 0.032 ^a	0.393 ± 0.043 ^a	0.496 ± 0.069 ^b	0.547 ± 0.054 ^{b,c}
EF (%)	71.629 ± 1.372	62.075 ± 3.503 ^a	66.850 ± 2.873	71.686 ± 2.553 ^b	70.363 ± 2.807 ^b
FS (%)	36.214 ± 1.059	29.575 ± 2.318 ^a	32.850 ± 2.164	36.414 ± 1.936 ^b	35.550 ± 2.076 ^b

Note. Data are expressed as mean ± SEM ($n = 8$).

^a $P < .05$ versus control.

^b $P < .05$ versus MS.

^c $P < .05$ versus MS + hesperidin (15 mg.kg⁻¹).

TABLE 2 Effect of hesperidin and metformin on cardiac function in HFD-induced MS rats

	Control	MS	MS + hesperidin (15 mg.kg ⁻¹)	MS + hesperidin (30 mg.kg ⁻¹)	MS + metformin (30 mg.kg ⁻¹)
LVIDd (cm)	0.699 ± 0.028	0.607 ± 0.028 ^a	0.627 ± 0.024	0.666 ± 0.041	0.697 ± 0.030 ^b
LVIDs (cm)	0.446 ± 0.020	0.431 ± 0.032	0.422 ± 0.025	0.427 ± 0.037	0.452 ± 0.029
EDV (ml)	0.789 ± 0.086	0.540 ± 0.073 ^a	0.590 ± 0.064	0.712 ± 0.116	0.790 ± 0.083 ^b
ESV (ml)	0.225 ± 0.027	0.217 ± 0.044	0.198 ± 0.032	0.216 ± 0.050	0.243 ± 0.039
SV (ml)	0.568 ± 0.062	0.323 ± 0.032 ^a	0.393 ± 0.043 ^a	0.496 ± 0.069 ^b	0.547 ± 0.054 ^{b,c}
EF (%)	71.629 ± 1.372	62.075 ± 3.503 ^a	66.850 ± 2.873	71.686 ± 2.553 ^b	70.363 ± 2.807 ^b
FS (%)	36.214 ± 1.059	29.575 ± 2.318 ^a	32.850 ± 2.164	36.414 ± 1.936 ^b	35.550 ± 2.076 ^b

Note. Data are expressed as mean ± SEM (n = 8).

^aP < .05 versus control.

^bP < .05 versus MS.

^cP < .05 versus MS + hesperidin (15 mg.kg⁻¹).

P198 | Effect of diosmetin on high-fat diet-induced metabolic syndrome and cardiac remodelling and dysfunction in rats

Sariya Meeapat¹; Pucharawipa Maneesai²; Parichat Prachaney²; Poungrat Pakdeechote²

¹Department of Physiology, Faculty of Medicine; ²Khon Kaen University

Background and Purpose: Metabolic syndrome (MS) is an importance of risk factors including obesity, insulin resistance, dyslipidaemia, elevated BP, and glucose intolerance. MS increases the risk for cardiac dysfunction and type 2 diabetes. Diosmetin is an aglycone part of the flavonoid glycosides diosmin that occurs naturally in citrus fruits. It exerts antihypertensive, antioxidant, and hypoglycaemic effects (Yu et al., 2014). This study aims to explore the effect of diosmetin on

cardiac dysfunction and signs of MS in high-fat diet (HFD)-induced MS in rats.

Experimental Approach: Male Sprague-Dawley rats were randomly divided into five groups (n = 8). Control group was fed with standard chow diet and distilled water. MS rats were fed with HFD and 15% fructose drinking water for 16 weeks to induce MS. After 12 weeks, MS rats were treated with diosmetin (20 or 40 mg.kg⁻¹) or metformin (100 mg.kg⁻¹). Body weight and food intake were measured throughout experimental period. At the end of experiment, cardiac function, BP, blood glucose, serum insulin, lipid profiles, oxidative stress markers, and histomorphometry of left ventricle (LV) were measured. Statistical significance was analysed using one-way ANOVA with LSD post hoc test.

Key Results: Rats that received HFD had weight gain, insulin resistance, glucose intolerance hypertension (Table 1), and dyslipidaemia (Figure 1a-c) (P < .05). Increases in LV wall thickness and LV muscle fibre cross-sectional area (CSA) were shown in MS rats. Impairment of

TABLE 1 Effect of diosmetin on metabolic syndrome and cardiac function parameters in all groups

	Control	MS	MS + diosmetin (20 mg.kg ⁻¹)	MS + diosmetin (40 mg.kg ⁻¹)	MS + metformin (100 mg.kg ⁻¹)
BW (g)	678.00 ± 21.38	812.17 ± 38.74 [*]	794.38 ± 34.94 [*]	825.13 ± 29.68 [*]	766.13 ± 31.24
AUC of OGTT (mg.dl ⁻¹ per 180 min)	21,493.13 ± 485.75	26,394.38 ± 796.01 [*]	21,746.25 ± 636.96 [#]	22,355.63 ± 414.86 [#]	22,222.5 ± 559.61 [#]
Serum insulin (mg.ml ⁻¹)	6.62 ± 1.07	19.81 ± 1.72 [*]	15.29 ± 2.08 [*]	10.42 ± 1.42 [#]	8.61 ± 1.44 [#]
SBP (mmHg)	117.94 ± 3.70	152.52 ± 3.78 [*]	130.26 ± 3.21 ^{*,#}	117.47 ± 3.59 ^{*,#}	124.71 ± 4.77 [#]
EDV (ml)	0.83 ± 0.08	0.59 ± 0.05 [*]	0.58 ± 0.08 [*]	0.78 ± 0.08	0.74 ± 0.11
ESV (ml)	0.24 ± 0.03	0.22 ± 0.02	0.15 ± 0.02 [*]	0.13 ± 0.01 [*]	0.21 ± 0.05
SV (ml)	0.60 ± 0.06	0.37 ± 0.03 [*]	0.43 ± 0.06	0.65 ± 0.08 ^{*,#}	0.53 ± 0.06
FS (%)	37.63 ± 1.18	30.41 ± 0.80 [*]	37.57 ± 2.54 [#]	45.87 ± 2.26 ^{*,#}	37.74 ± 1.79 ^{*,#}
EF (%)	71.8 ± 0.96	63.81 ± 1.3 [*]	72.93 ± 2.95 [#]	81.87 ± 2.01 ^{*,#}	73.33 ± 2.36 ^{*,#}

Note. Data are expressed as mean ± SEM (n = 8).

^{*}P < .05 versus control.

[#]P < .05 versus MS.

[†]P < .05 versus MS + diosmetin (20 mg.kg⁻¹).

[‡]P < .05 versus MS + diosmetin (40 mg.kg⁻¹).

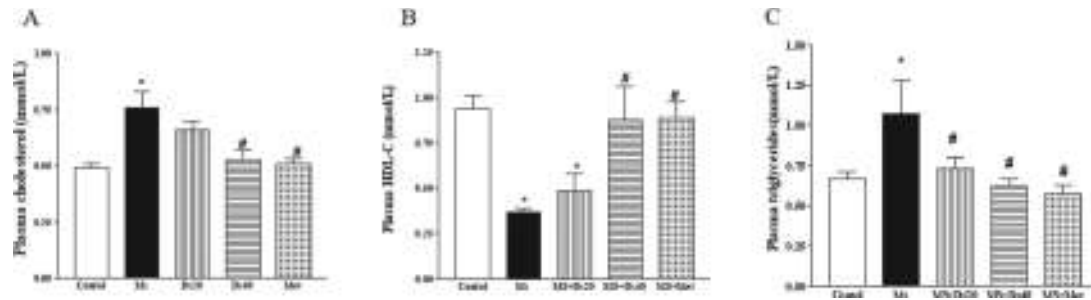


Figure 1. Effect of diosmetin on lipid profiles in HFD-induced metabolic syndrome in rats. Data are expressed as mean ± SEM (n = 8), *P < .05 versus control, #P < .05 versus MS

cardiac function indicated by decreasing fraction shortening and ejection fraction was observed in MS rats (P < .05). Additionally, vascular superoxide production and MDA level significantly increased in MS rats (P < .05). Diosmetin and metformin significantly alleviated signs of MS as well as cardiac remodelling and dysfunction and reduced oxidative stress markers in MS rats (P < .05).

Conclusion and Implications: Diosmetin alleviates signs of MS and improves cardiac dysfunction in HFD-induced MS rats. These effects may involve its antioxidant and hypoglycaemic effects of diosmetin.

REFERENCE

Yu, G., Wan, R., Yin, G., Xiong, J., Hu, Y., Xing, M., et al. (2014). Diosmetin ameliorates the severity of cerulein-induced acute pancreatitis in mice by inhibiting the activation of the nuclear factor-κB. *International Journal of Clinical and Experimental Pathology*, 7(5), 2133–2142.

P199 | Decreased contribution of K_{Ca}2.3 channels to endothelium-dependent relaxation in erectile tissue from diabetic (db/db) mice

Simon Comerma Steffensen¹; Susie Mogensen¹; Judit Prat Duran¹; Rafael Fais²; Lilliana Beck¹; Ulf Simonsen¹

¹Aarhus University; ²Sao Paulo University

Background and Purpose: Activation of endothelial small conductance calcium-activated K⁺ channels (K_{Ca}2.3 or SK3) and intermediate conductance calcium-activated K⁺ channels (IK or K_{Ca}3.1) leads to

vascular relaxation. Our previous studies have shown that K_{Ca}2.3 down-regulation diminishes erectile function (Comerma-Steffensen et al., 2017). In the present study, we hypothesized that K_{Ca}2.3 channel function is altered in erectile tissue of type 2 diabetic animals.

Experimental Approach: All animal experimentation are over n = 4 and followed the EU Directive 2010/EU/63 regulation. Erectile function was measured in anaesthetized (pentobarbital 50 mg.kg⁻¹) diabetic db/db mice (n = 12) and was compared to heterozygous animals (db/+) (n = 11). Corpus cavernosum strips were mounted for isometric tension recording, and they were stored in RNA later solution or frozen in liquid nitrogen for, respectively, qPCR and Western blotting. Statistical significance (P < .05) was determined by Student's t test or ANOVA followed by Tukey's post hoc test.

Key Results: In anaesthetized diabetic db/db mice, erectile function was markedly decreased compared to control animals. Thus, 16-Hz stimulation increased erectile function, measured as peak increase in intracavernous pressure over mean arterial pressure (PICP/MAP), respectively, 30.46 ± 4.49 (n = 5) and 17.72 ± 3.21 (P < .05, n = 5) in control (db/db+) versus diabetic db/db mice. In corpus cavernosum strips from db/db mice, the sensitivity towards noradrenaline was unaltered, while maximal contraction was increased in corpus cavernosum from db/+ compared to db/db mice. ACh relaxations were unaltered compared to strips from control mice. NS309 (0.5 μM), an activator of K_{Ca}2 and K_{Ca}3.1 channels, leftward shifted concentration–response curves for ACh in corpus cavernosum from control mice, but this was not the case in corpus cavernosum from db/db mice. Apamin, a blocker of K_{Ca}2 channels, inhibited ACh relaxation in corpus cavernosum from db/db and control animals, being less effective in db/db compared to control animals. The NO donor,

TABLE 1 pD₂ and E_{max} comparisons of corpus cavernosum from db/db mice versus control (db/+)

	db/+		db/db	
	pD ₂ (mean ± SEM)	E _{max} (mean ± SEM)	pD ₂ (mean ± SEM)	E _{max} (mean ± SEM)
NA (n = 6)	5.73 ± 0.12	0.42 ± 0.04	5.65 ± 0.14	0.6 ± 0.06
ACh (n = 5 and 6)	6.91 ± 0.18	85.87 ± 6.19	6.91 ± 0.13	89.17 ± 4.74
ACh + apamin (n = 4 and 6)	5.69 ± 0.25	70.15 ± 11.41	6.36 ± 0.14	65.97 ± 4.94
ACh + NS309 (n = 5 and 6)	6.98 ± 0.06	95.64 ± 2.23	7.05 ± 0.08	87.29 ± 2.75
SNP (n = 6)	6.48 ± 0.19	100	6.55 ± 0.08	100

Note. E_{max} for NA was expressed as g.mg⁻¹ and for ACh and SNP as percentage of NA contraction. *P < .05, Student's t test.

sodium nitroprusside (SNP), induced comparable relaxations in corpus cavernosum from db/db and control animals (Table 1). $K_{Ca}2.3$ gene and protein expression was increased in corpus cavernosum from db/db mice; nevertheless, protein expressed in aorta was unchanged.

Conclusion and Implications: Our results suggest that despite increased expression of $K_{Ca}2.3$ channels in erectile tissue, the contribution of the $K_{Ca}2.3$ channels to relaxation in corpus cavernosum is markedly reduced. The impaired $K_{Ca}2.3$ channel function may contribute to the increased noradrenaline contraction and impaired erectile function in diabetes.

REFERENCE

Comerma-Steffensen, S., Kun, A., Hedegaard, E. R., Mogensen, S., Aalkjaer, C., Köhler, R., ... Simonsen, U. (2017). Down-regulation of $K_{Ca}2.3$ channels causes erectile dysfunction in mice. *Scientific Reports*, 7, 3839.

P200 | The effects of perivascular adipose tissue on vascular control in the porcine coronary artery

Imogen Bacon; Michael Randall

University of Nottingham

Background and Purpose: Perivascular adipose tissue (PVAT) releases vasoactive mediators, inducing a net vasorelaxant response (Gollasch, 2012). Phenotypic changes of PVAT in metabolic syndrome are linked to vascular dysfunction and may contribute towards the development of cardiovascular disease (CVD). This study aimed to elucidate PVAT's effect on vascular tone in response to contractile mediators in the porcine coronary artery (PCA), hypothesising that PVAT would exert an anti-contractile effect on the arteries. The relationship between PVAT and hyperglycaemia, as well as the PPAR- γ agonist, rosiglitazone, on control of the vasculature, was explored.

Experimental Approach: Studies were carried out on isolated 5-mm sections of porcine coronary arteries (PCAs) which were studied under isometric conditions, in vitro in 20-ml organ baths, bathed with Krebs-Henseleit buffer (at 37°C and gassed with 95% O_2 /5% CO_2). Arteries were either with PVAT intact and denuded (controls). Contractile responses were recorded to 60-mM KCl and cumulative concentrations (10–300 nM) of the Tx mimetic, U46619. In subsequent experiments, the responses to KCl and U46619 responses were determined in PCAs incubated for 2 hr in 25-mM glucose Krebs' (hyperglycaemia) and were then compared to those in 11-mM glucose Krebs'. In some experiments, 10- μ M rosiglitazone was added to PCAs pre-contracted submaximally with U46619 and observed for 2 hr to determine its effects on vascular tone in the absence and presence of PVAT.

Concentration response curves were fitted to sigmoidal curves using three-parameter logistic equation, and the R_{max} and pEC_{50} values were determined. Statistical significance was determined using a Student's t test.

Key Results: Tension increase in response to 60-mM KCl in controls was 9.08 ± 0.34 g (mean \pm SEM), compared to 7.55 ± 0.27 g in PVAT-intact PCAs ($P < .001$; $n = 72$). Adherent PVAT reduced the concentration-dependent contraction to U46619; R_{max} in controls was $130 \pm 9\%$ and $79.7 \pm 8.5\%$ in PVAT-intact PCAs ($P < .001$; $n = 18$). Incubation with 25-mM glucose abolished the anticontractile effects of PVAT on responses to KCl; however, it did not affect responses to U46619. The presence of rosiglitazone enhanced the PVAT-induced time-dependent relaxation. The difference was significant ($P < .05$; $n = 7$) at 50 and 60 min with a relaxation in PVAT vessels with ethanol of $18.9 \pm 5.1\%$ (50 min) and $23.1 \pm 6.1\%$ (60 min) compared to $43.4 \pm 10.6\%$ (50 min) and $50.0 \pm 13.2\%$ (60 min) in PVAT vessels with rosiglitazone.

Conclusion and Implications: These findings highlight the importance of PVAT in control of vascular tone, demonstrating an anti-contractile effect in response to KCl and U46619. This response to KCl was attenuated by hyperglycaemia. PVAT-induced relaxation was enhanced by rosiglitazone. Maintaining PVAT function could provide a novel therapeutic target in the treatment of CVDs.

REFERENCE

Gollasch, M. (2012). Vasodilator signals from perivascular adipose tissue. *British Journal of Pharmacology*, 165, 633–642.

P201 | Perivascular adipose inflammation underlies early vascular dysfunction in the course of metabolic deterioration

Mohammed Elkhatab¹; Ali Mroueh²; Rim Rafeh²; Fatima Sleiman²; Ahmed El-Yazbi²

¹Faculty of Pharmacy, Alexandria University; ²Faculty of Medicine, The American University of Beirut

Background and Purpose: Despite significant advances in pharmacotherapeutic options, type 2 diabetes remains a major cause of cardiovascular mortality and morbidity with a high risk of microvascular and macrovascular complications. While hyperglycaemia is traditionally thought to be the instigating factor of the vascular detrimental phenotype, a significant proportion of diabetic patients exhibit microvascular complications at initial diagnosis without prolonged exposure to hyperglycaemia, and patients with impaired glucose tolerance and normal plasma glucose levels also carry a high risk of cardiovascular disease. As such, it is highly likely that a mechanism other than elevated blood glucose level underlies the early vascular dysfunction. Whereas adipose tissue inflammation has been implicated in the pathogenesis of diabetes, its role in mediating vascular dysfunction early in the course of the metabolic insult remains unclear. Here, we developed a rat model of a mild metabolic challenge and delayed onset of diabetes, with isolated perivascular adipose tissue (PVAT) inflammation to study its role as a predisposing factor for diabetic vascular impairment.

Experimental Approach: Male Wistar rats weighing 180–200 g were randomly divided into five groups (each has eight rats) as follows: (1) rats fed normal chow (NC, 3 kcal·g⁻¹), (2) rats fed mild hypercaloric diet (HC, 4.035 kcal·g⁻¹), (3) rats fed HC diet and treated with metformin (HC + Met), (4) rats fed HC diet and treated with pioglitazone (HC + Pio), and (5) rats fed HC diet and then switched to normal chow diet (HC-NC). HC feeding continued for 12 weeks, then rats were killed, and isolated rat aortic rings were used to study vascular function. Different adipose pools were dissected and used for PCR, immunohistochemistry, and western blotting.

Key Results: Following 12 weeks of HC feeding, rats did not show an increase in body weight, BP, blood glucose level, or glucose tolerance. An increase in serum insulin was observed indicative of insulin resistance. Aortic tissues showed hypercontractility in response to phenylephrine stimulation, which was dependent on increased Rho kinase-mediated calcium sensitization. Vascular inflammation was detected in the form of increased inflammatory cytokines expression associated with signs of isolated PVAT inflammation. Involvement of other adipose pools was not detected. Amelioration of PVAT inflammation via drug treatment or switch to normal chow improved vascular function.

Conclusion and Implications: Our study is the first to implicate isolated PVAT inflammation as an underlying cause of vascular dysfunction in the course of development of type 2 diabetes. Early intervention to treat this condition might help prevent or reverse diabetic vascular complications.

P202 | Role of perivascular adipose tissue as a calcium store

Musaad Althobaiti; Michael Garle; Richard Richard; Michael Randall

University of Nottingham

Background and Purpose: Perivascular adipose tissue (PVAT) which surrounds blood vessels is now recognised as a physiologically and metabolically active layer releasing a wide range of adipokines in paracrine and endocrine manners. These adipokines augment vasorelaxation or vasoconstriction to various compounds in several vascular beds of various species (Owen et al., 2013). In obesity, PVAT is associated with ultrastructural and biochemical alterations, including cholesterol crystals and accumulation of calcium (Giordano et al., 2013). Clinical studies indicate that PVAT is associated with coronary artery calcification (Lehman et al., 2010). Therefore, calcium released from PVAT could contribute to the tone of the underlying blood vessel. The aim of this study was to determine whether calcium released from PVAT could contribute to the contraction of porcine coronary arteries (PCAs).

Experimental Approach: Five-millimetre segments of PCA were set up isometric recording in organ baths and were bathed in oxygenated Krebs–Henseleit buffer at 37°C. Contractile responses to KCl and the Tx mimetic, U46619, were measured in the presence or absence of

0.5 g re-added PVAT (+PVAT) in calcium-free buffer. Data are presented as mean + SEM, and statistical significance was determined by two-way ANOVA.

Key Results: In calcium-free buffer, addition of 60-mM KCl did not show any effect on PCA tone. However, in the presence of +PVAT, 60-mM KCl in calcium-free buffer caused a contraction of 56% ± 3 of that in the presence of calcium ($P < .001$; $n = 6$). The contraction to 60-mM KCl in the absence of calcium was still enhanced in the presence of +PVAT when the NaCl concentration was reduced to maintain osmolality (83% ± 6 in the presence of +PVAT compared to 25% ± 4 in absence of +PVAT) ($P < .001$; $n = 6$). The enhanced contraction to KCl in the presence of PVAT was completely inhibited in the presence of 10-μM nifedipine (L-type calcium channel inhibitor) and in the presence of 1-mM EGTA ($P < .001$; $n = 6$). The contraction to the Tx mimetic U46619 was reduced in the absence of calcium to 24% ± 3. However, in the presence of +PVAT, this calcium-free contraction was enhanced to 68% ± 9.

Conclusion and Implications: This study demonstrates that the presence of PVAT enhances the contractions to KCl and U46619 in the absence of extracellular calcium in the buffer. This contraction was prevented by the presence of EGTA or nifedipine, indicating that the contraction is likely to be due to influx of extracellular calcium released from the PVAT. However, more investigation is required to confirm Ca²⁺ efflux from PVAT and understand the clinical relevance of this phenomenon.

REFERENCES

- Giordano, A., et al. (2013). Obese adipocytes show ultrastructural features of stressed cells and die of pyroptosis. *Journal of Lipid Research*, 54(9), 2423–2436.
- Lehman, S. J., et al. (2010). Peri-aortic fat, cardiovascular disease risk factors, and aortic calcification: The Framingham Heart Study. *Atherosclerosis*, 210(2), 656–661.
- Owen, M. K., et al. (2013). Perivascular adipose tissue potentiates contraction of coronary vascular smooth muscle: Influence of obesity. *Circulation*, 128(1), 9–18.

P203 | Adipose tissue enhances nitrite-mediated vascular relaxation in conditions of hypoxia

Andy MacKenzie; Ayoub Akhtar; Nicholas Sculthorpe; Chris Easton

University of the West of Scotland

Background and Purpose: Nitrite is an important source of NO, particularly when production from endothelial cells (EC) is compromised, for example, during hypoxia (Mills et al., 2017). Adipose tissue, for example, white (WAT) and perivascular (PVAT), modulates a variety of vascular parameters. Here, we aim to determine if PVAT and WAT influence nitrite-mediated vascular reactivity.

Experimental Approach: Aortic rings from male C57BL/6 mice were denuded of EC. PVAT was maintained on some segments while removed from others; rings were then mounted for tension recording.

Three groups of ring were created: smooth muscle cells alone (SMC), SMC + PVAT, and SMC + PVAT + WAT (in which segments of inguinal WAT were cohabited with SMC + PVAT rings in the myograph bath). Tissues were gassed with 5% CO₂ in oxygen (control) or 5% CO₂ in nitrogen (hypoxia) for 2 hr (Maenhaut et al., 2010). Responses to sodium nitrite (1 nM–1 mM) were generated following contraction with phenylephrine. Hydroxocobalamin (HXO; 1 mM) and 1*H*-[1,2,4]oxadiazolo[4,3-*a*]quinoxalin-1-one (ODQ; 10 μM) determined the influence of NO and soluble GC (sGC), respectively. Statistical significance was determined by two-way ANOVA.

Key Results: In control oxygen, nitrite produced a concentration-dependent relaxation of SMC rings (maximum 69.9 ± 9.2%, *n* = 6) that was not different from that found in either SMC + PVAT (80.0 ± 4.9%, *n* = 6) or SMC + PVAT + WAT (80.9 ± 3.5%, *n* = 6) groups. The relaxation produced in all groups was abolished (*P* < .001) following treatment with either HXO or ODQ, demonstrating that nitrite-mediated relaxation was reliant on NO generation and sGC activation. In conditions of hypoxia, the magnitude of the nitrite-induced response was not changed in either SMC or SMC + PVAT groups compared to that found with control oxygen; however, the relaxation found in SMC + PVAT + WAT rings was substantially greater (97.5 ± 1.1%, *n* = 5, *P* < .001). In hypoxic conditions, HXO and ODQ continued to eliminate relaxation in SMC and SMC + PVAT tissues. In contrast, nitrite-induced relaxation in SMC + PVAT + WAT rings persisted in the presence of HXO although this was substantially impaired (39.0 ± 11.6%, *n* = 5, *P* < .01) compared to that found in control conditions. ODQ still obliterated the nitrite-mediated relaxation in this group.

Conclusion and Implications: In conditions of abundant oxygen, adipose tissue (PVAT or PVAT + WAT) has no influence on the magnitude or character of nitrite-induced relaxation to SMC. However, in conditions of low oxygen, the presence of PVAT + WAT both enhanced the scale and character of the response, thus demonstrating that adipose tissue in hypoxic conditions does indeed modulate nitrite-mediated relaxation.

REFERENCES

- Maenhaut, N., et al. (2010). *European Journal of Pharmacology*, 641, 207–212.
Mills, C. E., et al. (2017). *British Journal of Clinical Pharmacology*, 83, 140–151.

Poster Session: Drug Discovery, Development and Evaluation 2

P077 | Palmitate-induced lipotoxicity alters 5-HT receptor expression in pancreatic BRIN-BD11 beta cells

Chinmai Patibandla; Zahidul Islam Khan Md; Steven Patterson

Glasgow Caledonian University

Background and Purpose: Serotonin (5-HT) is a monoamine neurotransmitter expressed in the CNS and also in peripheral tissue. Interestingly, pancreatic beta cells produce 5-HT, and it is co-localised with insulin in the secretory vesicles and secreted alongside insulin in response to glucose stimulation (Cataldo Bascuñan, Lyons, Bennet, Artner, & Fex, 2019). It is known that 15 subtypes (5-HT1–7) of G protein-coupled (except 5-HT3) 5-HT receptors are expressed in human islets and their expression is altered in type 2 diabetes mellitus, although beta cell-specific changes and their implications are unclear (Cataldo Bascuñan et al., 2019). The current study aimed to determine the expression of the 5-HT receptors in the clonal rat BRIN-BD11 beta cell line. Since lipotoxicity plays a role in beta cell dysfunction, we also investigated the effects of palmitate culture on 5-HT receptor expression and examine the potential role of 5-HT7 receptors in beta cell.

Experimental Approach: BRIN-BD11 cells were cultured in RPMI 1640 medium supplemented with FBS (10%, v/v), 50 U·ml⁻¹ penicillin/streptomycin at 37°C (5% CO₂ and 95% air). Cell viability was measured by MTT assay. Intracellular calcium levels were measured in FURA-2AM loaded cells. Total RNA was extracted from the BRIN-BD11 cells, after 24-hr treatment with 125-μM palmitate or 5-HT7 receptor agonist LP-44, cDNA was synthesised, and changes in mRNA levels was measured by qPCR.

Key Results: BRIN-BD11 cells expressed mRNA for 12 different 5-HT receptors along with Tph1, Sert, MaoA, and MaoB. Palmitate treatment (125 μM) for 24 hr reduced BRIN-BD11 cell viability by 50% (*n* = 4, *P* < .0001). Palmitate treatment enhanced Htr1a, Htr1b, Htr2c, and Htr4 expression (*n* = 3, *P* < .05) along with Htr2a, Htr6, and Htr7 (*n* = 3, *P* < .01), while Htr3a, Tph1, and Maob expression were down-regulated (*n* = 3, *P* < .01, .05, and .01, respectively). Acutely, 5-HT7 receptor agonist, LP-44, enhanced intracellular Ca²⁺ levels in BRIN-BD11 cells at both low (1.1 mM) and high (16.7 mM) glucoses. Longer term culture (24 hr) with LP-44 did not affect cell viability, nor expression of specific beta cell genes Ins1, Pdx1, Mafa, and Gck (*n* = 3).

Conclusion and Implications: Current results suggest that serotonin receptor expression is altered by chronic exposure to free fatty acid palmitate in BRIN-BD11 beta cells. 5-HT7 receptor agonist LP-44 raises intracellular calcium levels in BRIN-BD11 cells. Further study is warranted to establish the specific beta cell changes in 5-HT receptors and their potential role in islets function and dysfunction in obesity and type 2 diabetes.

REFERENCE

- Cataldo Bascuñan, L. R., Lyons, C., Bennet, H., Artner, I., & Fex, M. (2019). Serotonergic regulation of insulin secretion. *Acta Physiologica*, 225, e13101.

P204 | Investigations of thiolated chitosan for intranasal delivery of sumatriptan succinate for migraine

Rimpi Arora; Vishavprabhjot Kaur

ISF College of Pharmacy

Background and Purpose: The nasal route has been used for delivery of drugs for local treatment of diseases like nasal congestion and allergy conditions. Nasal route has been recognized as important route for systemic delivery of neurological drugs due to favourable anatomical and physiological characteristics of nasal mucosa. As the nasal cavity mucosa offers direct access to the CNS through olfactory region of nasal cavity, hence by passing the brain barrier. Intranasal delivery provides a practical, non-invasive method for delivering therapeutic agents to the brain because of the unique anatomical connections provided by the olfactory and trigeminal nerves. By using nanotechnology, it is possible to deliver the drug to the targeted tissue across the BBB, release the drug at a controlled rate, and avoid degradation processes. Efforts have been made to deliver various drugs, especially peptides and proteins, through nasal route for systemic use.

Experimental Approach: The derivatized chitosan, thiolated chitosan, has gained popularity due to their pH-independent solubility and higher permeation enhancing characteristics. The nanoparticles were formed to resolve the issue of sumatriptan succinate bio-availability.

The natural and synthetic polymers were used for preparation of nanoparticles by ionic gelation technique. Chitosans (Chs) have been widely studied as drug carrier for nose to brain delivery utilizing olfactory pathway. However, Ch has pH-dependent solubility limitation, which restricts its applications of drug delivery via intra-nasal route. In linked with this derivative Ch, thiolated Ch has gained popularity due to their pH-independent solubility and higher permeation enhancing characteristics. Nose to brain delivery of nanoparticulates loaded with drugs of low partition co-efficient utilizing olfactory pathway has emerged as an alternative to IV delivery of drug for increasing their brain uptake by overcoming P-GP efflux and also protects drugs from enzymatic degradation.

Key Results: Nanoparticles (NPs) of thiolated chitosan were prepared by ionic gelation method. The NPs were optimized for processing parameters based on particle size, zeta potential, and entrapment efficiency (EE). EE was found to be fairly good for thiolated chitosan NPs. After optimization, the surface morphology was checked with the help of SEM.

Conclusion and Implications: The study is focused on the evaluation of the bioadhesive behaviour of Ch and thiolated Ch in nasal delivery and enhancement of transport of sumatriptan for migraine.

REFERENCES

Bernkop-Schnurch, A., Hornof, M., & Gugli, D. (2004). Thiolated chitosans. *European Journal of Pharmaceutics and Biopharmaceutics*, 57, 9–17.

Goadsby, P. J., Lipton, R. B., & Ferrari, M. D. (2002). Migraine: Current understanding and treatment. *Journal of Medical Sciences*, 346, 257–270.

P205 | New insights in autonomic disorder therapy: Effect of various botulinum neurotoxin serotypes in a model of autonomic nervous system hyperactivity

Jacque Maignel; Johannes Krupp; Matthew Beard; Fraser Hornby

IPSEN

Background and Purpose: In contrast to skeletal neuromuscular junctions, the autonomic nervous system (ANS), while targeted clinically, is less explored in botulinum neurotoxin (BoNT) research. One model of ANS hyperactivity is the isolated bladder strip preparation, where electrical stimulation induces hyperactivity of detrusor smooth muscle. This study directly compared potencies of BoNT/A, B, and F on human and rodent bladder muscle activity *ex vivo*.

Experimental Approach: Detrusor strips prepared from C57Bl6 mouse, WKY rat, and human bladders were tensed in organ baths and submitted to electrical field stimulation to generate neurogenic contractions. Purified natural BoNT/A, B, or F was added, and signals were recorded for 4 hr. Potency was expressed as time to reach half-paralysis (t50). A histological study of the samples for BoNT receptors and substrates was also performed in mouse and rat tissues.

Key Results: BoNT/F was the most potent toxin in each preparation. In the mouse, BoNT/B was more potent than BoNT/A in inhibiting neurogenically induced contractions. In contrast, BoNT/A and B were approximately equipotent in the human preparation. Interestingly, rat bladder was totally resistant to BoNT/B, even though rat vesicle-associated membrane protein (VAMP)2—which is cleaved by BoNT/B—was detected in addition to VAMP1, which is not cleaved by BoNT/B.

Conclusion and Implications: Human bladder is equally sensitive to BoNT/A and B. This finding is at odds with the established relative resistance of human skeletal muscle to BoNT/B and lower affinity for the human form of its receptor Syt1. A preference of BoNT/B for the ANS over skeletal muscle has been noted previously and is supported by the finding that BoNT/B is more potent than A in mouse bladder strips. Syt1 and VAMP1 seem to drive parasympathetic-driven contractions of the detrusor, with VAMP2 likely involved in another aspect of bladder innervation. These data highlight the interest of using BoNT serotypes other than A to dampen autonomic disorders.

REFERENCES

Jin, R., et al. (2006). *Nature*, 444(7122), 1092–1095.
Maignel-Ludop, J., et al. (2017). *Pharmacology Research & Perspectives*, 5(1), e00289.
Weisemann J, et al. *Toxins (Basel)*. 7(12):5035–54 (2015)
Schiavo, G., et al. (1992). *Nature*, 359, 832–835.
Matarasso, S. L. (2003). *Dermatologic Surgery* Jan, 29(1), 7–13.

P206 | Deficiency of the anaphylatoxin receptors C5aR2 and C3aR aggravates hypertensive renal injury

Heimo Ehmke¹; Marlies Bode¹; Catherine Meyer-Schwesinger¹; Christian Kurts²; Joerg Koehl³; Ulrich Wenzel¹

¹University Medical Centre Hamburg-Eppendorf; ²University Clinic of Bonn; ³University of Lübeck

Background and Purpose: Hypertension and hypertensive end-organ damage are mediated not only by haemodynamic injury but also by innate and adaptive immune responses. The complement is an important part of the immune system, which drives the host defence against microbes and mediates inflammatory responses. Recent experimental data support a role for complement activation in arterial hypertension. During the activation and amplification of the complement cascade, the anaphylatoxins C3a and C5a are released and trigger pro-inflammatory signalling through their corresponding receptors. We recently identified a protective effect of C5a receptor 1 (C5aR1) deficiency on hypertensive renal injury (Weiss et al., 2016). Here, we investigate the role of the second C5a receptor (C5aR2) and the C3a receptor (C3aR) in hypertensive end-organ damage.

Experimental Approach: Expression of C5aR2 and C3aR on infiltrating and resident renal cells were determined using tandem tomato knock-in mice for either C3aR or C5aR2 by flow cytometry and confocal microscopy. The hypertension model of angiotensin II (Ang II) infusion in combination with unilateral nephrectomy and high-salt diet was induced in Balb/c wild-type and C5aR2- as well as C3aR-deficient mice. Arterial BP, GFR, albuminuria, and morphological damage were determined.

Key Results: Flow cytometric analysis of leukocytes isolated from the kidney of reporter mice showed that C5aR2 is expressed on dendritic cells (34%), macrophages (30%), and neutrophils (14%), whereas C3aR is predominantly expressed in dendritic cells (90%). C5aR2 and C3aR were also detected by confocal microscopy in the kidney only on infiltrating cells. Both C5aR2- and C3aR-deficient mouse lines exhibited significantly increased renal injury compared to wild-type mice in response to Ang II-induced hypertension. Consistent with our previous observations, additional genetic deletion of C5aR1 by use of C3aR-C5aR1 double knockout mice rectified the higher sensitivity to renal injury in C3aR-deficient mice.

Conclusion and Implications: Our data identify C5aR2 and C3aR expression on infiltrating (mainly dendritic cells) but not on resident cells in the kidney. Deficiency of C5aR2 or C3aR aggravates hypertensive renal injury. Together, these findings indicate that C5aR2 and C3aR mediate protective or homeostatic effects in hypertensive renal injury.

REFERENCE

Weiss, S., Rosendahl, A., Czesla, D., Meyer-Schwesinger, C., Stahl, R. A., Ehmke, H., ... Wenzel, U. O. (2016). The complement receptor C5aR1 contributes to renal damage but protects the heart in angiotensin II-

induced hypertension. *American Journal of Physiology. Renal Physiology*, 310, F1356-65.

P207 | Cysteinyl LT receptor expression and potential as a therapeutic target in uveal melanoma

Kayleigh Slater¹; Helen Kalirai²; Sarah Coupland²; Breandán Kennedy¹

¹University College Dublin; ²University of Liverpool

Background and Purpose: Uveal melanoma is a rare, but often devastating form of ocular cancer that will metastasize to the liver in 50% of patients. Uveal melanoma and its associated liver metastasis are known to respond extremely poorly to currently available chemotherapeutic drugs, with no proven standard of care available for metastatic patients. Unfortunately, as few as 8% of patients will survive beyond 2 years once the disease has spread (Kuk et al., 2016), highlighting the unmet clinical need for alternative therapeutic targets. Although considered a rare disease, Ireland has a higher incidence of the disease per capita than the United States or the United Kingdom (1.3 cases per 100,000 per year in Ireland vs. 0.52 cases per 100,000 per year in the United States) (Slater et al., 2018).

The cysteinyl leukotrienes are a group of inflammatory, lipid mediators that exert their biological effects via binding to GPCRs, the cysteinyl LT receptors (CysLT₁ and CysLT₂). This research investigates the role of both cysteinyl LT receptors (CysLT₁ and CysLT₂) in uveal melanoma. Both receptors have been implicated in various cancers, and *CYSLTR2* has been identified as a uveal melanoma oncogene in a small subset of patients (Moore et al., 2016). We have previously shown that cysteinyl LT receptor antagonists attenuate developmental and pathological angiogenesis in the eye (Reynolds et al., 2016) and show anti-angiogenic and anti-tumourigenic activity in *in vivo* models of colorectal cancer (Adrian et al., 2016).

Experimental Approach: Western blot and qPCR analyses were used to analyse the expression of both receptors in primary and metastatic uveal melanoma cell lines ($n \geq 3$, Mel285, Mel270, and OMM2.5 cell lines). Immunohistochemical staining was conducted on UM patient samples ($n = 50$) to analyse the expression of both receptors and their relationship to matched clinical data and patient survival. Additionally, the effectiveness of cysteinyl LT targeting drugs (at 10, 20, and 50 μ M) has been analysed in survival and long-term proliferation assays ($n \geq 3$) to determine their effectiveness in uveal melanoma cell lines.

Key Results: Both receptors were found to be expressed in all cell lines and patient tumour samples that were analysed. Interestingly, high CysLT₁ expression was found to have a statistically significant association with ciliary body involvement, a poor prognostic indicator in the disease. Similarly, this receptor showed an interesting relationship with patient survival. In keeping with these findings, drugs that specifically target CysLT₁, but not those targeting CysLT₂, block long-

term proliferation and cell viability in both primary and metastatic uveal melanoma cell lines in a time- and dose-dependent manner.

Conclusion and Implications: These results highlight the importance of CysLT signalling in uveal melanoma and its role as a potential novel therapeutic target in the disease.

REFERENCES

- Kuk, D., Shoushtari, A. N., Barker, C. A., Panageas, K. S., Munhoz, R. R., Momtaz, P., ... Postow, M. A. (2016). Prognosis of mucosal, uveal, acral, nonacral cutaneous, and unknown primary melanoma from the time of first metastasis. *The Oncologist*, 21(7), 848–854.
- Moore, A. R., Ceraudo, E., Sher, J. J., Guan, Y., Shoushtari, A. N., Chang, M. T., et al. (2016). Recurrent activating mutations of G-protein-coupled receptor CYSLTR2 in uveal melanoma. *Nature Genetics*, 48(6), 675–680.
- Murphy, A. G., Casey, R., Maguire, A., Tosetto, M., Butler, C. T., Conroy, E., ... O'Sullivan, J. (2016). Preclinical validation of the small molecule drug quininiB as a novel therapeutic for colorectal cancer. *Scientific Reports* Volume 6, Article number: 34523.
- Reynolds, A. L., Alvarez, Y., Sasore, T., Waghorne, N., Butler, C. T., Kilty, C., ... Merrigan, S. (2016). Phenotype-based discovery of 2-[(E)-2-(quinolin-2-yl)vinyl]phenol as a novel regulator of ocular angiogenesis. *Journal of Biological Chemistry*, 291(14), 7242–7255.
- Slater, K., Hoo, P. S., Buckley, A. M., Piulats, J. M., Villanueva, A., Portela, A., & Kennedy, B. N. (2018). Evaluation of oncogenic cysteinyl leukotriene receptor 2 as a therapeutic target for uveal melanoma. *Cancer and Metastasis Reviews*, 37, 335.

P208 | Hollow fibre infection model for investigating the long-term culture of trypanosome parasites and their response to therapy

Rebecca Sterritt¹; Suresh Lakshminarayana²; Manuel Saldivia²; Debjani Patra²; Srinivasa Rao²; Colin Osborne²

¹Royal Veterinary College; ²Novartis Institute for Tropical Diseases

Background and Purpose: Trypanosome parasites are the causative agents of diseases such as human African trypanosomiasis (HAT, *T. brucei gambiense* and *T. b. rhodesiense*, about 4,000 new cases each year, (https://www.who.int/trypanosomiasis_african/country/en/)) and Chagas disease (*T. cruzi*, 8 million people infected, (<https://www.who.int/chagas/epidemiology/en/>)). Current treatment options for such diseases are limited. To aid in drug discovery efforts, here, we used a hollow fibre culture model as an alternative means of investigating long-term in vitro growth of parasites, the infection kinetics, and the parasite response to therapy.

Experimental Approach: A C2011 medium, polysulfate, hollow fibre cartridge (Fibercell Systems Inc) was used as the culture system. The cartridge was primed with PBS and serum free media before inoculation with parasites (*T. cruzi*, approximately 3×10^5 parasites-ml⁻¹; *T. brucei*, approximately 1×10^5 parasites-ml⁻¹). The media used to maintain the culture were Hyclone RPMI-1640 (*T. cruzi*) and IMDM (*T. brucei*) supplemented with FBS. In addition, for *T. cruzi* culture only, the reactor was prepopulated with 3T3/NIH fibroblast cells 6 days prior to infection. After infection, the culture system was serially sampled, and the parasite burden determined microscopic count using a haemocytometer. The parasite response to therapy using commercially available compounds, benznidazole and nifurtimox (*T. cruzi*) and acoziborole and suramin (*T. brucei*), was investigated using the Buckner assay method (Buckner et al., 1996) (*T. cruzi*) and cell titre glow assay (*T. brucei*) to determine IC₅₀ values.

Key Results: Parasites were continuously cultured for over 120 and 60 days for *T. cruzi* (Figure 1) and *T. brucei*, respectively. Parasites density reached up to 1×10^8 parasites-ml⁻¹ for *T. cruzi* and 1×10^7 parasites-ml⁻¹ for *T. brucei*. Parasite responses to therapy for both hollow fibre infection models were similar to values obtained from standard culture methods, within a twofold to fourfold range observed in IC₅₀ values.

Conclusion and Implications: Hollow fibre systems provide a robust means of providing long-term parasite culture to a high density. Such

methods can now be used to help better understand the pharmacodynamic and pharmacokinetic properties of anti-parasitic therapies aiding drug discovery efforts against diseases such as HAT and Chagas.

REFERENCES

https://www.who.int/trypanosomiasis_african/country/en/
<https://www.who.int/chagas/epidemiology/en/>
 Buckner, F. S., et al. (1996). *AAC*, 40, 2592–2597.

P209 | Effect of empagliflozin, sitagliptin, and cholestyramine on streptozotocin-induced diabetic rats: Cardiovascular fortification in tandem with glucose lowering

Danish Ahmed; Mohd Ibrahim Khan

Sam Higginbottom University of Agriculture, Technology and Sciences

Background and Purpose: Diabetes is one of the most common metabolic diseases with a complex, multifactorial aetiology and has varied clinical and biochemical investigations. Recent data report the efficacy of the three selected drugs, namely, empagliflozin, sitagliptin, and cholestyramine, which ameliorates the glucotoxicity via different mechanisms in type 2 diabetes (Hebatollah et al., 2019; Moustafa Ahmed, Shehata Messiha, El-Sayed El-Daly, & Abo-Saif, 2019; Noriyasu & Katsuo, 2000). To strengthen the data, the present research exertion aims to investigate the combinatorial effect of the three drugs, namely, empagliflozin, sitagliptin, and cholestyramine, on glucotoxicity, inflammation, lipid profile, and cardiovascular complications in the streptozotocin (STZ)-induced neonatal rats (N2-STZ model). Selected drugs were evaluated as monotherapy and in different plausible combinations.

Experimental Approach: Neonatal rats (N2-STZ model) were used as a model of type 2 diabetes. Type 2 diabetes was induced in the neonatal rats that were 2-day-old pups by a single shot of STZ (60 mg·kg⁻¹, i.p.) dissolved in 0.1-M citrate buffer, pH 4.5. The pups were weaned after 21 days and maintained on AIN-93G/M diet in individual cages throughout the experimental period. Empagliflozin (10 mg·kg⁻¹, p.o.), sitagliptin (10 mg·kg⁻¹, p.o.), and cholestyramine (240 mg·kg⁻¹, p.o.) were administered via drinking water for 8 weeks.

Key Results: Treatment with empagliflozin + sitagliptin + cholestyramine when given together has marked effect on glucotoxicity (129.20 ± 4.85) when compared to empagliflozin (152.6 ± 6.05), sitagliptin (151.0 ± 4.49), cholestyramine (154 ± 5.38), empagliflozin + sitagliptin (135.6 ± 3.75), empagliflozin + cholestyramine (154.6 ± 8.03), and sitagliptin + cholestyramine (145.4 ± 6.78). Triple combinatorial therapy is proved to be beneficial in plummeting the total cholesterol, namely, empagliflozin + sitagliptin + cholestyramine (141.4 ± 3.59), when compared to the double therapy and monotherapy, namely, empagliflozin (168.8 ± 6.47), sitagliptin (163.6 ± 6.32), cholestyramine (184.8 ± 5.51), empagliflozin + sitagliptin

(149.0 ± 3.71), empagliflozin + cholestyramine (161.8 ± 4.86), and sitagliptin + cholestyramine (158.0 ± 10.02).

TABLE 1

Group	Blood glucose level (mg·dl ⁻¹) (mean)	Blood glucose level (mg·dl ⁻¹) (SD)	Blood glucose level (mg·dl ⁻¹) (SEM)
Normal	109	9.617692	4.312866
Toxic control	257	29.2831	13.13144
Empagliflozin (10 mg·kg ⁻¹ , p.o.)	152.6	13.50185	6.054642
Sitagliptin (10 mg·kg ⁻¹ , p.o.)	151	10.02497	4.495502
Cholestyramine (240 mg·kg ⁻¹ , p.o.)	154	12	5.381166
Empagliflozin (10 mg·kg ⁻¹ , p.o.) + sitagliptin (10 mg·kg ⁻¹ , p.o.)	135.6	8.38451	3.75987
Empagliflozin (10 mg·kg ⁻¹ , p.o.) + cholestyramine (240 mg·kg ⁻¹ , p.o.)	154.6	17.92484	8.038046
Sitagliptin (10 mg·kg ⁻¹ , p.o.) + cholestyramine (240 mg·kg ⁻¹ , p.o.)	145.4	15.12614	6.783021
Empagliflozin (10 mg·kg ⁻¹ , p.o.) + sitagliptin (10 mg·kg ⁻¹ , p.o.) + cholestyramine (240 mg·kg ⁻¹ , p.o.)	129.2	10.82589	4.854661

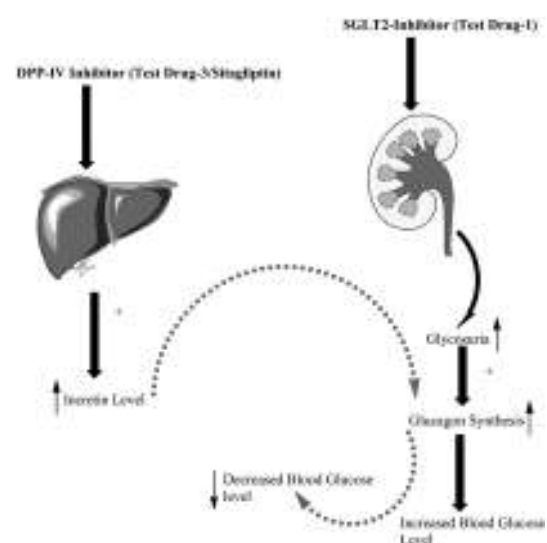


FIGURE 1 Schematic representation of synergistic hypothetical approach of Test Drug-1 and Test Drug-3 (Sitagliptin)

Conclusion and Implications: Expression of GLU-1, GLUT-2, and GLUT-3 was determined by the Western blot analysis. GLUT-3 and GLUT-4 were increased in the group that received the triple therapy as compared to the monotherapy and double therapy. Triple combination of the hypoglycaemic drugs mitigates the development of type 2 diabetes through improved expression of GLUT receptors involved in the transportation of glucose. Histopathological investigation of cardiovascular walls of the triple therapy-treated group was analysed and was found to be improved when compared to the STZ-induced immunohistochemical and histopathological alterations.

REFERENCES

Hebatollah, E. E., Yousreya, A. M., Noha, F. A., Amina, A., Gamal, D., Manal, A. B., & Sanaa, A. K. (2019). Modulating impacts of quercetin/sitagliptin combination on streptozotocin-induced diabetes mellitus in rats. *Toxicology and Applied Pharmacology*, 365, 30–40.

Moustafa Ahmed, Y., Shehata Messiha, B. A., El-Sayed El-Daly, M., & Abo-Saif, A. A. (2019). Effects of ticagrelor, empagliflozin and tamoxifen against experimentally-induced vascular reactivity defects in rats in vivo and in vitro. *Pharmacological Reports* in press June 2019.

Noriyasu, K., & Katsuo, K. (2000). Contractile responses in spontaneously diabetic mice: II. Effect of cholestyramine on enhanced contractile response of aorta to norepinephrine in C57BL/KsJ (db/db) mice. *General Pharmacology: The Vascular System*, 35(6), 319–323.

P210 | Investigating the chemical reactivity, stability, and mechanisms of hydrogen sulfide (H₂S) generation moieties commonly used in H₂S-releasing drug hybrids

Roberta Torregrossa¹; Mark Wood²; Matt Whiteman³
¹University of Exeter; ²Biosciences, College of Life and Environmental Sciences, University of Exeter; ³University of Exeter Medical School

Background and Purpose: Several compounds able to release hydrogen sulfide have been studied in vitro and in vivo in several disease models. Among these, 1,2-dithiolethiones (such as ADTOMe; Figure 1) and thioamides (like HTB; Figure 1) (Gerö et al., 2016; Le Trionnaire et al., 2014; Latorre et al., 2018) are recognised for their biological activity established through H₂S release. We recently reported another H₂S donor based on 1,2-dithiolones (ADOMe; Figure 1) (Gerö et al., 2016; Le Trionnaire et al., 2014; Latorre et al., 2018). ADTOMe, HTB, and ADOMe have been linked to a mitochondria-targeting moiety (Gerö et al., 2016; Le Trionnaire et al.,

2014; Latorre et al., 2018) and clinically used drugs (e.g., NSAIDs) (Wallace et al., 2007) forming drug-H₂S donor hybrid compounds. However, despite their clear pharmacological effects, the chemical mechanisms by which they release H₂S have never been appropriately studied. Moreover, the structures of the decomposition products obtained after these compounds release H₂S, and their biological

TABLE 1 Reaction tests on ADTOMe, HTB, and ADOMe

H ₂ S adduct	Solvent(s) and reagent(s)	Time	T (°C)	Product(s)	
ADTOMe	4-DMSO, 2:0:25 % 4-DMSO, 2:0:25 % DMSO, H ₂ O (25 %)	36 days 32 days 48 h	20 50 120	ADTOMe (No reaction) ADOMe and ACTOMe (7:1) ADOMe 14 %	
	PhEt or H ₂ O or 1,4-Dioxane, H ₂ O (25 %) or DMSO anhydrous	48 h	120	2 (trace) ADTOMe = 81 % (No reaction)	
	DMSO, H ₂ O (25 %) DMSO/H ₂ O-H ₂ O (1:1.1 % - 12.5 %)	48 h 48 h	120 120	ADOMe 70 % (Main product) ADOMe + GADOMe (1:1)	
	NaOH (3 eq) in EtOH	48 h	Reflux	1:0.5 %; 2:20 %	
	EtOH, PhEt (pH=4) or -Cl (3 eq) in THF	7 days	Reflux	ADTOMe = 41 % (No reaction)	
	H ₂ O (3 eq) in DCM, H ₂ O (25 %)	72 h	20	ADOMe 17 %; 2:15 %	
	NaOH (2.5 eq) in EtOH, H ₂ O	72 h	Reflux	2:2 %; ADTOMe 25 %	
	1,4-Dithiolethione (10 eq) in EtOH, PhEt (pH=8) N-(tert-Butylcarbamoyl)-L-cysteine methyl ester (10 eq) in EtOH, PhEt (pH=8)	7 days 7 days	Reflux Reflux	1:81 %; ADTOMe 39 % ADOMe 85 %; ADTOMe 52 %	
	HTB	4-DMSO, 2:0:25 % 4-DMSO, 2:0:25 %	36 days 32 days	20 50	HTB (No reaction) HTB and HTB 3 (trace)
		4-DMSO, 2:0:25 % DMSO, PhEt (25 %) or DMSO or PhEt or EtOH	48 h	Reflux	HTB 5 (3) 3 = 30 %
NaOH (3 eq) in EtOH HCl (3 eq) in EtOH		48 h 48 h	20 20	HTB 57 %; 3:38 % HTB 88 % (No reaction)	
H ₂ O (3 eq) in DCM, H ₂ O (25 %)		48 h	20	4:18 %; 3:22 %	
1,4-Dithiolethione (5 eq) in EtOH, PhEt (pH=4) or -Cl (3 eq) in EtOH		4 days	20	5:8 % HTB = 70 % (No reaction)	
ADOMe		DMSO, PhEt (25 %) NaOH (3 eq) in EtOH	72 h 48 h	120 Reflux	ADOMe 80 % (No reaction) 1:30 %; 2:8 %; ADOMe 17 %
	EtOH, PhEt (pH=4) or -Cl (3 eq) in EtOH	72 h	Reflux	ADOMe = 81 % (No reaction)	
	H ₂ O (3 eq) in DCM, H ₂ O (25 %)	7 days	20	ADOMe 86 % (No reaction)	
	NaOH (2.5 eq) in EtOH or 1,4-Dithiolethione (5 eq) in EtOH, PhEt (pH=8) CH ₃ COCH ₃ (1.5 eq), NH ₄ Cl (5 eq) in NaOH-THF (1:1)	5 days 48 h	Reflux 50	1 = 30 %	
				4:7 % 1:16 %	

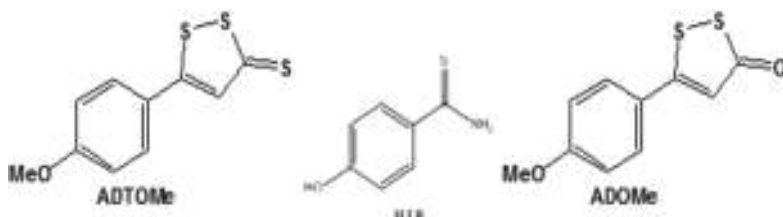


Figure 1. H₂S-releasing adducts

activity, have never been explored, despite the fact that their identification is essential for therapeutic use.

Experimental Approach: Each compound was synthesised in-house (Gerö et al., 2016; Le Trionnaire et al., 2014; Latorre et al., 2018). Stability/reactivity was examined in the reactions reported in Table 1 and the degradation products obtained characterised using ^1H , ^{13}C -NMR, and MS techniques. Water- ^{18}O was used to determine if the oxygen atom found on hydrolysis products came from solvent (DMSO) or water.

Key Results: The main decomposition products (Table 1) of ADTOME were identified as ADOMe, **1**, and **2** whereas HTB generated primarily **3**, **4**, and **5**. ADOMe formed **1** and **6** (which may be formed with different thiols, e.g., a sulfur-containing amino acid). All the compounds were stable at room temperature in water/DMSO solutions; thus, H_2S formation at room temperature in these solutions may be excluded. Moreover, they were stable at harsh acidic pH and slightly basic pH (pH = 8) but susceptible to hydrolysis at strong basic pH. Thus, in cells environment, ADTOME may react with oxidative species and with sulfur-containing amino acid, while ADOMe may react with reductive species and thiols. HTB may react with oxidants and may be enzymatically hydrolysed probably forming **3**.

Conclusion and Implications: This work, for the first time, has identified and characterised the possible metabolites of major H_2S -releasing moieties which will be useful in elucidating the mechanism of action (and toxicity) of H_2S -releasing drug hybrids. We are currently examining in vitro the effects of these products.

REFERENCES

- Gerö, et al. (2016). *Pharmaceutical Research*, 113, 186.
Latorre, et al. (2018). *Aging (Albany NY)*, 10, 1666.
Le Trionnaire, et al. (2014). *Medicinal Chemistry Communications*, 5, 728.
Wallace, et al. (2007). *Gastroenterology*, 132, 261.

P211 | The potential role of myocardium-mediated hydrogen sulfide in the relaxation response of porcine coronary artery

Yasir Al-Taie¹; Stephen Alexander²; Richard Roberts²;
Michael Garle²

¹University of Nottingham/Medical School; ²Life Sciences/Medical School/University of Nottingham

Background and Purpose: H_2S is an inorganic bio-signalling gasotransmitter (Al-Taie et al., 2018), similar to NO and CO (Wang et al., 2012), and H_2S is present in mammal tissues (Donovan et al., 2017). H_2S is reported in many health and disease conditions (Rashid et al., 2013). Lacking H_2S generating enzymes in mice leads to hypertension and morbid complications (Donovan et al., 2017). The impact of the myocardium is not well established (Donovan et al., 2018). This study aims to gain greater insight into the role of H_2S in the heart to identify whether endogenous H_2S influences tone in the porcine coronary artery (PCA).

Experimental Approach: Five millimetres of proximal PCA segments were mounted for isometric tension recording system in organ bath (Donovan et al., 2017). Assessment of the relaxation responses of myocardium-derived H_2S was done in paired preparations. The relaxation responses were measured after incubation of the PCA with the absence or presence of 0.5 g of the myocardial tissue; myocardial tissue was pre-incubated for 15 min with the absence or presence of 100- μM AOAA (CBS inhibitor), 100- μM PPG (CSE inhibitor), and/or 100- μM CDS (candidate MST modifier/inhibitor). All values were expressed as means \pm SEM. Comparisons between more than two data groups were made using ANOVA followed by Sidak's post hoc test. For comparisons between two data sets, a two-tailed unpaired/paired Student's *t* test was used. A *P* value of less than .05 indicated a significant difference between the data sets; *n* = number of animals.

Key Results: There was a significant relaxation response in U4-precontracted PCA with the myocardial tissue (-5.183 ± 1.171 vs. -57.18 ± 9.744 ; *n* = 6). Moreover, there was a significant decrease in the relaxation with AOAA and PPG (-55.45 ± 12 vs. -12.86 ± 9.394 ; *n* = 6). Intriguingly, there was enhancement of the relaxation with CDS (-47.9 ± 8.07 vs. -98.46 ± 5.437 ; *n* = 6).

Conclusion and Implications: To summarise, H_2S is biosynthesised in the myocardium (may be as a diffusible factor) and has a potential relaxation influence in the PCA.

REFERENCES

- Al-Taie, et al. (2018). Winter meeting.
Donovan, et al. (2017). *Vascular Pharmacology*.
Donovan, et al. (2018). *Acta*.
Rashid, et al. (2013). *British Journal of Pharmacology*, 168, 1902–1910.
Wang, et al. (2012). *Physiological Reviews*, 92, 791–896.

P212 | Safety and mechanism of action of lidocaine N-oxide, a hypoxia-activated prodrug of lidocaine, for the treatment of ischaemia-induced ventricular fibrillation

Louise Hesketh¹; James Winter¹; Markus Sikkel²; Michael Curtis¹

¹King's College London; ²Imperial College London

Background and Purpose: Sudden cardiac death, most commonly resulting from ischaemia-induced ventricular fibrillation (VF) as a result of acute myocardial infarction (AMI), is responsible for approximately 50% of deaths from cardiovascular disease (Kudenchuk et al., 2012). Currently, an effective antiarrhythmic drug capable of preventing VF, devoid of intolerable adverse effects, is not available (Dan et al., 2018). Lidocaine N-oxide is a hypoxia-activated prodrug of lidocaine that has previously demonstrated its potential as an effective and safe anti-VF agent (Hesketh et al., 2017). Further investigations have been undertaken to explore its safety and mechanism of action.

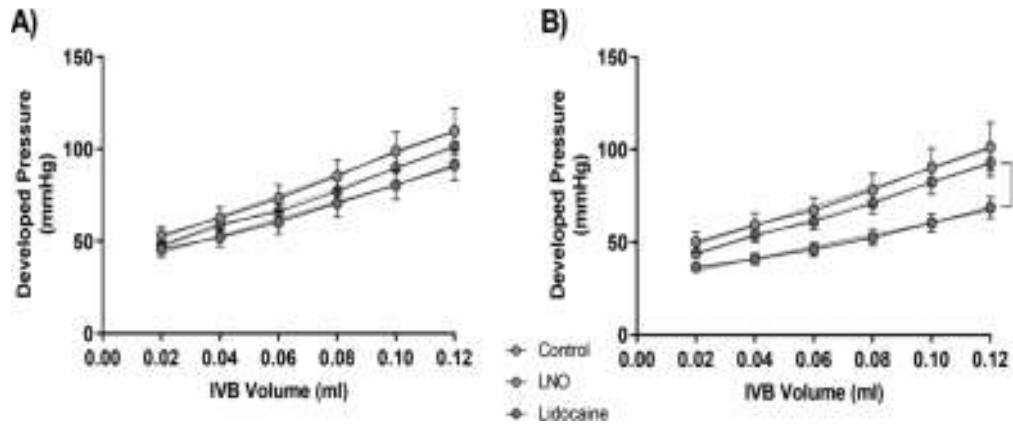


FIGURE 1. A) Starling Curve during baseline Krebs perfusion and B) Starling Curve after solution switch. Linear regression analysis, * $p < 0.05$ (s) vs control, $n = 12$ /group. Values are mean \pm SEM

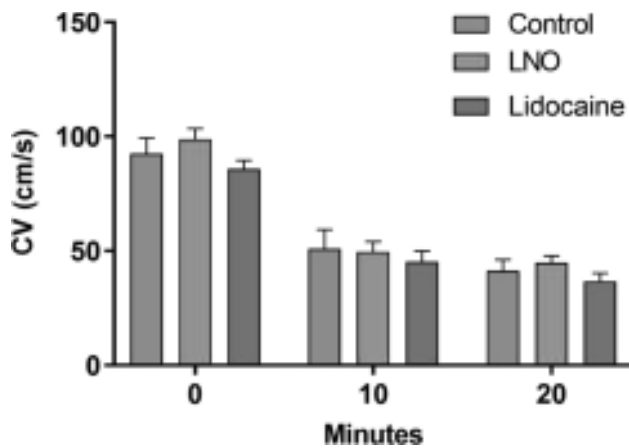


FIGURE 2. Conduction velocity, measured by optical mapping using di-4-ANNEPs, during test solution perfusion prior to (0 minutes) and 10 and 20 minutes into LAD ligation in Langendorff-perfused rat hearts. 1 way ANOVA vs control, * $p < 0.05$ (s), $n = 5$ /group

Experimental Approach: Male Wistar rat (295–510 g) hearts were Langendorff perfused with Krebs' buffer (3-mM K^+ , 37°C) and randomised to switch to vehicle, 15- μ M lidocaine, or 15- μ M lidocaine N-oxide perfusate in three experimental preparations. (i) An intraventricular balloon (IVB) was used to assess left ventricular contractile

function during test solution perfusion ($n = 12$). Gradient between developed pressure (mmHg) and IVB volume (ml) was analysed by linear regression analysis. (ii) Conduction velocity changes were assessed by optical mapping with di-4-ANNEPs during 30 min of left coronary artery (LAD) ligation and constant pacing (400 beats·min⁻¹) ($n = 5$). (iii) Additional hearts were paced at escalating rates (400--900 beats·min⁻¹) at regular intervals during 40 min of LAD ligation ($n = 9$), and the interval (ms) between pacing stimulus and ventricular response (activation time) was determined. Ventricular response failure rate (conduction block) was analysed by Kaplan–Meier analysis. Gaussian distributed data were processed by one-way ANOVA, and, if conditions were met, groups were compared using Tukey's post hoc test.

Key Results: Lidocaine exhibited negative inotropic effects in the non-ischaemic ventricle, whereas lidocaine N-oxide did not (Figure 1). Neither lidocaine nor lidocaine N-oxide decreased conduction velocity during regional ischaemia at a pacing rate representative of a normal sinus rate (Figure 2). Lidocaine increased activation time even in the absence of ischaemia, whereas equivalent effects of lidocaine N-oxide occurred only during ischaemia, most prominently at higher pacing rates (Figure 3). Block of conduction was developed during ischaemia, and this was facilitated to the same extent by lidocaine and lidocaine N-oxide (Figure 3).

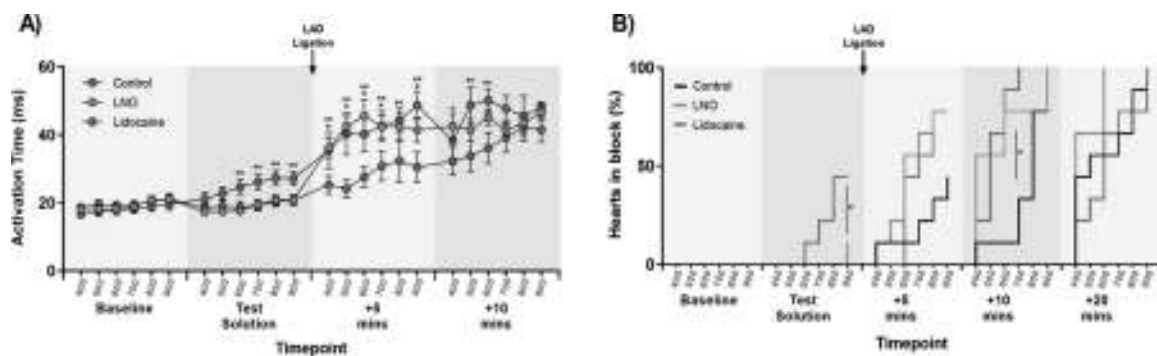


FIGURE 3. A) Activation time at baseline, with test solution perfusion, and at timepoints during ischaemia. 2 way ANOVA * $p < 0.05$ (s) vs control, $n = 9$ /group. Values are mean \pm SEM. B) Incidence of failure of ventricular response to stimulus at pacing protocols at baseline, with test solution perfusion and at time points during ischaemia, at escalating pacing rates (400-900 beats·min⁻¹). Kaplan Meier survival analysis * $p < 0.05$ (s) vs control, $n = 9$ /group

Conclusion and Implications: Lidocaine N-oxide, like lidocaine, prevents ischaemia-induced VF, but, unlike lidocaine, the N-oxide possesses ischaemia selectivity, exemplified by the absence of off-target pharmacological activity, such as adverse effects on cardiac electrophysiology and left ventricular contractile function. Additionally, lidocaine N-oxide appears to achieve its antiarrhythmic benefit selectively within the ischaemic ventricle via the same mechanism of rate-dependent conduction block obtained by lidocaine. Lidocaine N-oxide is a novel effective and safe antiarrhythmic prodrug.

REFERENCES

- Dan, G., et al. (2018). *EP Europace*, 20, 731–732an.
Hesketh, L. M., et al. (2017). BPS pA2online.org 18:1 Abstract 169P.
Kudenchuk, P. J., et al. (2012). *Circulation*, 125, 1787–1794.

P214 | Tetrahydrothiazolo[5,4-c]pyridines as a new class of antiobesity compounds

Mallikarjuna Rao Pichika¹; Thirumurugan Rathinasabapathy²;
Slavko Komarnytsky²; Kimberly M. Palatini Jackson²; Kit-Kay Mak¹;
Puvaneswari Marappan¹

¹International Medical University; ²North Carolina State University

Background and Purpose: 11 β -Hydroxysteroid dehydrogenase type 1 (11 β -HSD1) is an enzyme that converts inactive cortisone to active cortisol. It is highly expressed in fat, liver, and brain (Valsamakis et al., 2004). Inhibition of 11 β -HSD1 has proven to be useful in the treatment of glucocorticoid-associated diseases such as obesity, diabetes, and muscle atrophy (Draper et al., 2003). Here, we report the development of new tetrahydrothiazolo[5,4-c]pyridine (THTP) with optimum in vitro drug metabolism and pharmacokinetics (DMPK) properties possessing significant 11 β -HSD1 inhibitory activity in 3T3-L1 adipocytes and antiobesity activity in C57BL/6J mice.

Experimental Approach: The THTPs were designed using structure-based drug design based on the reported X-ray crystal structure (PDB ID: 2RBE). Thirteen different analogues of THTP were synthesised and characterised using spectroscopic techniques. Ten different analogues of THTP were synthesised and evaluated for in vitro 11 β -HSD1 inhibitory activity in 3T3-L1 adipocytes (Mehra, Macdonald, & Pillay, 2007). The top three most potent compounds were tested for adipogenesis inhibition in 3T3-L1 adipocytes from which the most potent compound (TR-13A) was tested for its influence on adipogenesis markers (PPAR γ and aP2), adipocyte function (Lep, 11 β HSD-1, Sreb, and Fxr), and energy metabolism (Ucp1 and Tgr5), and its in vitro DMPK properties were determined using the reported methods. The antiobesity activity of TR-13A (50 mg·kg⁻¹ body weight) was further investigated in high-fat diet-induced obesity in C57BL/6J mice, and the modulation of genes (in adipocytes) responsible for adipogenesis, adipocyte function, and energy metabolism was investigated. All the animal experimental procedures were approved by the Institutional Animal Care and Research Committee of North Carolina Research Campus and performed in Association for

Assessment and Accreditation of Laboratory Animal Care (AALAC) accredited animal care facility of David H. Murdock (DHM) Research Institute.

Key Results: The TR-13A was synthesised in good yield (75%) and characterised using ¹H and ¹³C NMR spectroscopy. The purity and mass of the compound was determined using HPLC-mass spectrometry (LC-MS) technique. TR-13A showed dose-dependent inhibition of 11 β -HSD1 oxoreductase activity and adipogenesis in 3T3-L1 adipocytes, and they were completely inhibited at 10- μ M concentration. It suppressed the expression of adipogenesis genes (PPAR γ and aP2), up-regulated energy metabolism genes (Ucp1 and Tgr5), and up-regulated adipocyte function gene (Fxr) in 3T-L1 adipocytes. In human, rat, and mouse, its clearance (ml·min⁻¹·g⁻¹ liver) in hepatocytes was 0.61, 0.49, and 0.03; in microsomes, it was 0.25, 0.31, and 0.41; and in cytosol and plasma, it was 0, respectively. After 14 days of dosing of TR-013A at 50 mg·kg⁻¹, p.o., the body weights were reduced by 9% ($P < .05$) and reduces epididymal fat pad weight by 8%. The genes PPAR γ , Sreb, and Fxr expressions were suppressed; Ucp1 and Tgr5 expressions were up-regulated; and there were no changes in expression of 11 β -HSD1. These results suggest that the TR-13A exhibits antiobesity effect through increased energy expenditure in the adipose tissue.

Conclusion and Implications: We successfully designed and synthesised a new THTP (TR-13A) with optimum in vitro DMPK properties possessing significant inhibitory activity on 11 β -HSD1 oxoreductase activity and adipogenesis mediated through suppression of adipogenesis, up-regulation of energy metabolism, and up-regulation of adipocyte function. However, the results showed that TR-13A's antiobesity activity in mice is mediated through energy expenditure without any influence on 11 β -HSD1 expression in adipocytes.

REFERENCES

- Draper, N., Walker, E. A., Bujalska, I. J., Tomlinson, J. W., Chalder, S. M., Arlt, W., ... Stewart, P. M. (2003). Mutations in the genes encoding 11 β -hydroxysteroid dehydrogenase type 1 and hexose-6-phosphate dehydrogenase interact to cause cortisone reductase deficiency. *Nature Genetics*, 34, 434–439.
Mehra, A., Macdonald, I., & Pillay, T. S. (2007). Variability in 3T3-L1 adipocyte differentiation depending on cell culture dish. *Analytical Biochemistry*, 362, 281–283.
Valsamakis, G., Anwar, A., Tomlinson, J. W., Shackleton, C. H., McTernan, P. G., Chetty, R., ... Kumar, S. (2004). 11 β -hydroxysteroid dehydrogenase type 1 activity in lean and obese males with type 2 diabetes mellitus. *The Journal of Clinical Endocrinology and Metabolism*, 89, 4755–4761.

P215 | Differential activation of human mast cells by the antibiotics polymyxin B and colistin

Graham Mackay; Stephanie Zhang; Nithya Fernandopulle;
James Ziogas; Paul Soeding

The University of Melbourne

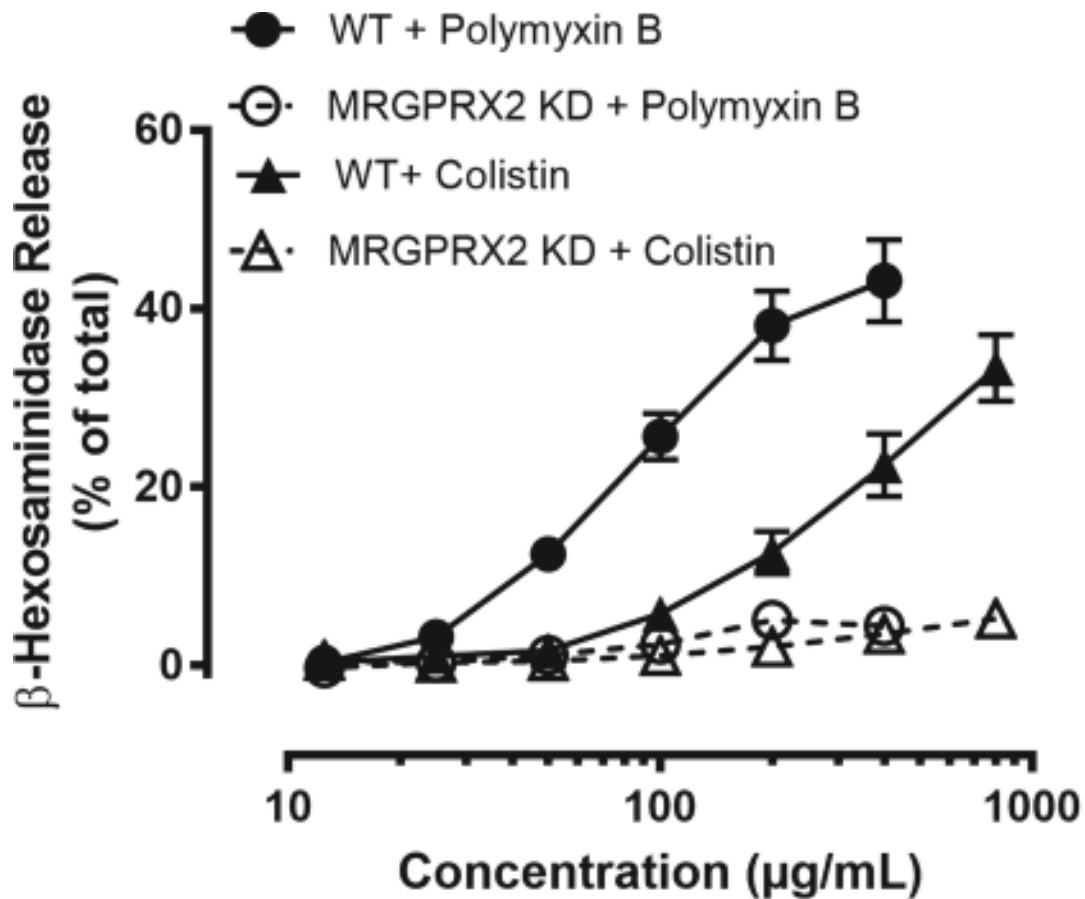


FIGURE 1. Comparison of the activity of polymyxin B and colistin in eliciting degranulation from LAD2 mast cells. The dependence of the degranulation on MRGPRX2 was also examined using receptor knock-down (KD) cells

Background and Purpose: Mast cells have important roles in allergic and inflammatory diseases and can be activated via the classical IgE-dependent pathway and by IgE-independent mechanisms. Recently, the MAS-related GPCR X2 (MRGPRX2) has been shown to mediate IgE-independent mast cell activation to a diverse range of cationic drugs including certain antibiotics and neuromuscular blocking agents (McNeil et al., 2015). As polymyxins are similarly cationic compounds, they have also been hypothesised to activate mast cells through MRGPRX2 which has been recently confirmed (Zhan et al., 2019). In this study, we further characterise the role of MRGPRX2 in the activation of human mast cells comparing the activity of two clinically used polymyxins, polymyxin B and colistin.

Experimental Approach: The FcεRI and MRGPRX2 expressing LAD2 human mast cell line was used to characterise and compare the actions of polymyxin B and colistin. MRGPRX2 knock-down LAD2 cells, generated using CRISPR-Cas9, were also used to examine the importance of MRGPRX2 to the actions of the polymyxins. Mast cell degranulation was measured by quantifying released β-hexosaminidase, CCL2 levels were quantified by commercial immunoassay, and calcium mobilisation was assessed using the calcium indicator Fura-2. Cell viability was determined using both trypan blue exclusion and measurement of LDH release. All experiments were conducted on at least six independent occasions. Statistical significance was

determined using an ANOVA with Bonferroni's post hoc test or Student's *t* test.

Key Results: At the concentrations tested, no cytotoxicity of the polymyxin drugs was observed. Polymyxin B and colistin caused degranulation, calcium mobilisation, and cytokine production in LAD2 mast cells in a concentration-dependent manner. However, as shown in Figure 1, colistin was less potent than polymyxin B in eliciting degranulation. In contrast, the two drugs had equivalent activity in calcium mobilisation and cytokine production. All responses were ablated by more than 90% in the MRGPRX2 knock-down cells.

Conclusion and Implications: Polymyxin B and colistin activation of mast cells was confirmed to be mediated through MRGPRX2 and could contribute to patient hypersensitivity to these drugs. Better understanding the reasons behind the potency difference in mast cell degranulation induced by polymyxin B and colistin might enable more selective use of these drugs in clinical practice.

REFERENCES

McNeil, B. D., Pundir, P., Meeker, S., Han, L., Undem, B., Kulka, M., et al. (2015). Identification of a mast-cell-specific receptor crucial for pseudo-allergic drug reactions. *Nature*, 519, 237–241.
 Zhan, Y., Ma, N., Liu, R., Wang, N., Zhang, T., & He, L. (2019). Polymyxin B and polymyxin E induce anaphylactoid response through mediation of Mas-related G protein-coupled receptor X2. *Chemico-Biological Interactions*, 308, 304–311.

P217 | Paracetamol and dipyrene share an identical pharmacological profile as inhibitors of COX activity in intact and homogenised cell preparations

Jane Mitchell¹; Carina Zhao²; Hime Gashaw²; Plinio Ferreira²; Nicholas Kirkby²

¹Imperial College London; ²Imperial College

Background and Purpose: Paracetamol and dipyrene (also known as metamizole) are first-line therapies for the treatment of pain and fever. Paracetamol is licensed worldwide and features in the world health organisation's list of essential medicines. Whilst dipyrene remains a popular drug in some countries, it is banned in others because of a rare yet life-threatening side effect resulting in severe leukopenia (agranulocytosis). Despite decades of use, the mechanism of action of paracetamol and dipyrene remains the subject of debate. However, although not anti-inflammatory agents, in "low lipid peroxide" bioassay systems, both paracetamol (Lucas, Warner, Vojnovic, & Mitchell, 2005) and dipyrene (Campos et al., 1999) share a common feature with nonsteroidal anti-inflammatory drugs (NSAIDs) of blocking the COX product, PGE₂. NSAIDs are substrate inhibitors at the active site of COX whilst paracetamol is thought to act at the peroxidase (POX) site of the enzyme. Here, we have profiled paracetamol and dipyrene in two pharmacological assays used to differentiate the inhibitory effects of NSAIDs from those of paracetamol on PGE₂ release/formation (Lucas et al., 2005). Specifically, we used a "low lipid peroxide" intact cell assay and a "high lipid peroxide" homogenate assay (Lucas et al., 2005).

Experimental Approach: As we have described previously (Lucas et al., 2005), human A549 cells were treated with drugs for 30 min prior to stimulation with IL-1 β (1 ng·ml⁻¹; 18 hr) to induce COX-2 activity. In separate studies, homogenates of IL-1 β -treated A549 cells

were prepared and incubated with drugs or vehicle (0.1% DMSO) for 30 min before the addition of substrate (arachidonic acid; 30 μ M) (Lucas et al., 2005). PGE₂ release/formation was measured using ELISA. **Key Results:** Each drug caused a concentration-dependent inhibition of PGE₂ release from intact cells (Figure 1a). By contrast, paracetamol and dipyrene stimulated PGE₂ formation in cell homogenates whilst the NSAID, ibuprofen, retained its inhibitory effects (Figure 1b).

Conclusion and Implications: This study suggests that paracetamol and dipyrene have a common mechanism of action as inhibitors of PGE₂ and our results are consistent with the idea that they both work as POX inhibitors. We suggest that these screens could be used to identify novel POX-site inhibitors of COX with improved efficacy and safety profiles compared to paracetamol and dipyrene.

REFERENCES

Campos, C., et al. (1999). *European Journal of Pharmacology*, 378, 339–347.
Lucas, R., Warner, T. D., Vojnovic, I., & Mitchell, J. A. (2005). *The FASEB Journal*, 19.

P218 | Induction of differentiation of human SH-SY5Y neuroblastoma cells by formyl peptide receptor agonist FPR α 14 in culture

Peter Cussell; Margarita Gomez Escalada; Nathaniel Milton; Andrew Paterson

Leeds Beckett University

Background and Purpose: The N-formyl peptide receptors (FPRs) are a family of GPCR that were initially identified in myeloid cells; however, accumulating evidence suggests a nervous function for FPRs (Ho et al., 2018). In a previous study (Cussell et al., 2019), the FPR agonist FPR α 14 induced differentiation of murine Neuro2a neuroblastoma cells. In light of the differences between species in number of FPR family members and agonist preferences (He et al., 2013), this

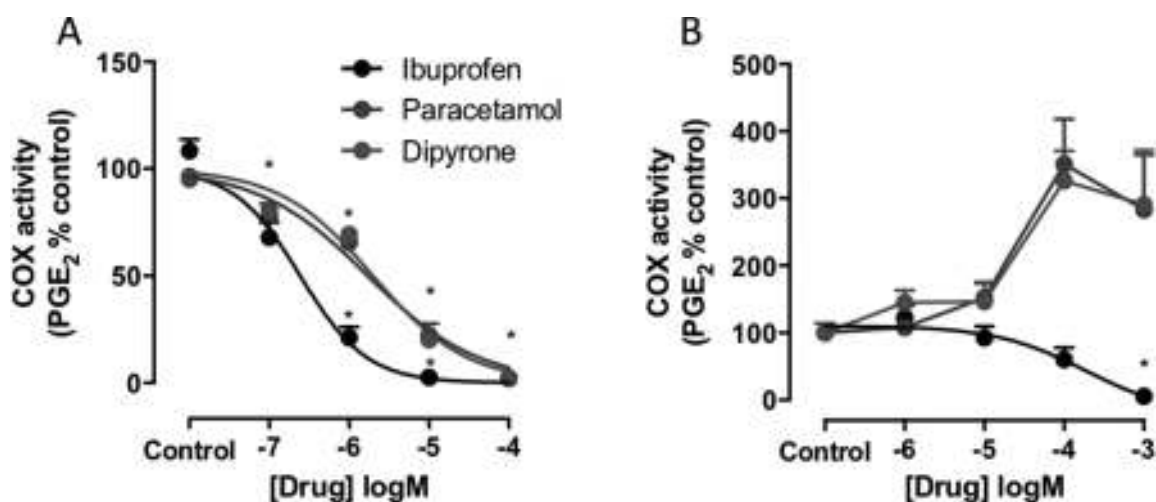


Figure 1: Effect of ibuprofen, paracetamol, and dipyrene on COX activity in intact cells (a) ($n = 8$) and homogenates (b) ($n = 6$). Data are mean \pm SEM. * $P < .05$, two-way ANOVAs followed by Dunnett's post hoc test

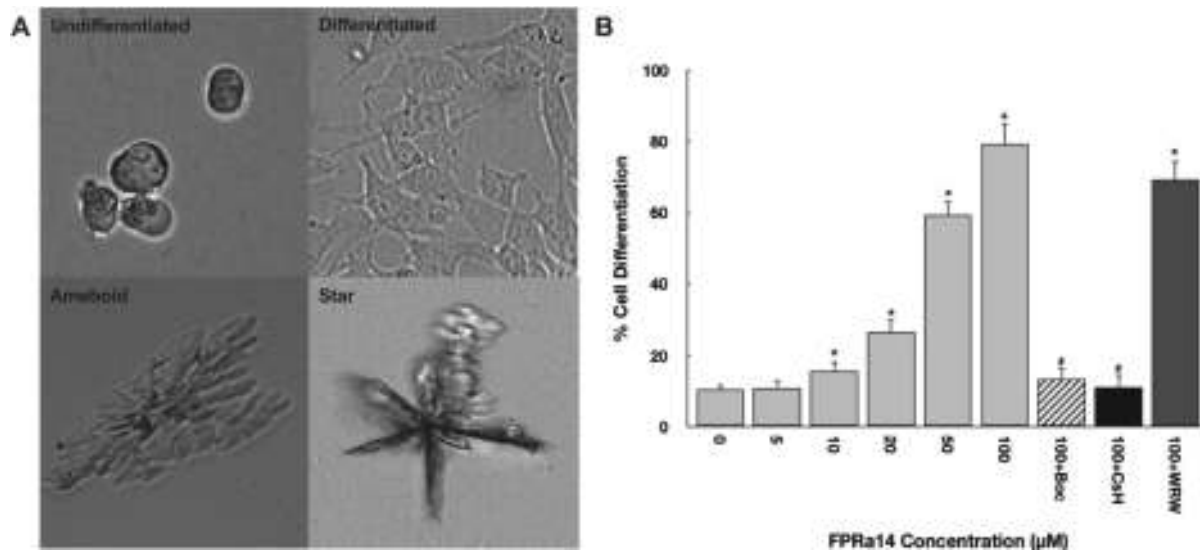


FIGURE 1: (a) Typical phase contrast images exhibiting SH-SY5Y undifferentiated control versus morphology traits following treatment with 100-µM FPRa14. (b) The effect of FPRa14 (5–100 µM and 100 µM following pre-incubation with Boc-MLF, CsH, or WRW4 [50 µM]) on the % of differentiated SH-SY5Y cells. **P* < .05 relative to appropriate incubation control, #*P* < .05 relative to the appropriate FPRa14 concentration (*n* = 246–390)

study assessed FPRa14 for its ability to induce differentiation in human SH-SY5Y neuroblastoma cells.

Experimental Approach: SH-SY5Y cells were seeded into 24-well microtitre plates and exposed to FPRa14 (5–100 µM). Images (×200 magnification) were taken 24 hr following agonist administration and visually assessed for morphological changes. Further differentiation assays were conducted with cells pre-incubated with the FPR antagonists Boc-MLF (50 µM), cyclosporin H (CsH) (50 µM), or WRW4 (50 µM) prior to agonist administration. Data are given as mean ± SEM, and analysis was performed via two-way ANOVA with Dunnett's post hoc test where applicable.

Key Results: SH-SY5Y cells differentiated into three distinct isoforms which presented phenotypic traits similar to those previously observed in FPRa14-induced differentiation of murine Neuro2a cells (Figure 1a). Concentrations of FPRa14 required to produce this effect were approximately 10-fold greater than those required to differentiate murine Neuro2a cells (Cussell et al., 2019). The synthetic FPR agonist FPRa14 induced a significant response in human neuroblastoma SH-SY5Y cells, with % cell differentiation increasing in a dose-dependent fashion. Pre-incubating SH-SY5Y cultures with FPR1-specific agonists Boc-MLF (50 µM) or CsH (50 µM) prior to agonist administration significantly reduced differentiation to near untreated control levels, while WRW4 (50 µM), an FPR2-specific antagonist, did not attenuate differentiation significantly (Figure 1b).

Conclusion and Implications: These results demonstrate that FPRa14 stimulates differentiation in human SH-SY5Y neuroblastoma. This effect was significantly reduced via pre-incubation with FPR1-specific antagonists Boc-MLF and CsH, while FPR2-specific WRW4 had no significant effect upon FPRa14-induced differentiation. This suggests that the SH-SY5Y differentiation response has an FPR1-mediated signalling component. The demonstration of FPR-induced differentiation in a human cell line suggests a nervous role for FPR in the human

setting and highlights the potential of FPRs as a novel target for the treatment of human CNS disorders.

REFERENCES

Cussell, et al. (2019). *PLoS ONE*, 14(6), e0217815.
 He, et al. (2013). *Molecular Pharmaceutics*, 83, 389–398.
 Ho, et al. (2018). *Neurochemical Research*, 43, 1587–1598.

P219 | The antidepressant AV-101 is a substrate for LAT1 (SLC7A5) at the blood–brain barrier

Waseema Patel¹; Mark Smith²; Ralph Snodgrass²; Munir Pirmohamed¹; Ana Alfirevic¹; David Dickens¹

¹University of Liverpool; ²VistaGen Therapeutics

Background and Purpose: Major depressive disorder represents a common mood disorder that is the leading cause of disability worldwide. AV-101 (4-chlorokynurenine), the prodrug of 7-chlorokynurenic acid (7-Cl-KYNA), is currently in phase II clinical trials as an adjunctive antidepressant therapy. The large neutral amino acid transporter (LAT1) has been recognised as a conduit for the passage of neurotherapeutics across the blood–brain barrier (BBB), overcoming a common bottleneck. Thus, we determined whether AV-101 is a substrate of LAT1 and characterised the movement of AV-101 through LAT1.

Experimental Approach: Using [¹⁴C]-AV-101, we followed the uptake of the compound in HEK 293 cells stably overexpressing LAT1 or matched control cells, with the inhibitor JPH203 used to test for specificity.

Key Results: We found AV-101 (10 µM) uptake to be 689.7 ± 69.5 pmol per million cells in LAT1 expressing cells compared to 76.5 ± 9.8 pmol

per million cells ($n = 3$, $P < .05$ vs. control) in control cells. Addition of the LAT1 inhibitor, JPH203 (10 μM), reduced this uptake to 21.8 ± 2.4 pmol per million cells ($n = 3$, $P < .05$ vs. LAT1) and 14.3 ± 1.4 pmol per million cells ($n = 3$, $P < .05$ vs. control) in LAT1 expressing and control cells, respectively, indicating that AV-101 was indeed being transported via LAT1. We also characterised the uptake kinetics of AV-101; the V_{max} was $4,522 \pm 1,016$ pmol per million cells min^{-1} , and the K_m was $1,799 \pm 372.5$ μM . In comparison, the model LAT1 substrate, phenylalanine (10 μM), showed an uptake of 754.2 ± 103.8 pmol per million cells in LAT1 expressing cells compared to 319.8 ± 34.25 pmol per million cells ($n = 3$, $P < .05$ vs. control) in control cells. Overall, AV-101 showed a LAT1-mediated uptake of 613.1 ± 77.8 pmol per million cells whilst phenylalanine had an uptake of 434.4 ± 121.1 pmol per million cells.

Conclusion and Implications: Together with the uptake data, similarities in LAT1-mediated uptake suggested that AV-101 showed a greater selectivity for LAT1 in comparison to phenylalanine. In contrast, 7-CI-KYNA (10 μM) showed no LAT1-mediated uptake (2.7 ± 0.5 pmol per million cells in LAT1 expressing cells compared to 3.6 ± 2.2 pmol per million cells in control cells), validating the use of the prodrug as an approach for delivery of the active drug. Future experiments will determine whether AV-101 is a substrate of other transporters, to further characterise the movement of the drug across the BBB. Additionally, we will perform a genotype to phenotype approach to assess if genetic variants in LAT1 and additional candidate genes correlate with AV-101 efficacy as an adjunct antidepressant therapy (ELEVATE).

ACKNOWLEDGEMENT

This study was funded by VistaGen Therapeutics, Inc. (Clinicaltrials.gov identifier: NCT03078322).

P220 | Effects of riluzole and edaravone in SOD1 and WT spinal motor neurons injured with glutamate: A comparative study

Alexandre Henriques; Clémence Farrugia; Philippe Poindron;
Noëlle Callizot

Neuro-Sys

Background and Purpose: Amyotrophic lateral sclerosis (ALS) is a rare motor neuron disease affecting people between 50 and 70 years old and is characterized by degeneration and loss of upper and lower motor neurons. The loss of motor neurons in ALS is caused by complex and multifactorial pathological events. Some familial cases (fALS) are linked to toxic gain-of-function mutations of SOD type 1 (SOD1), an antioxidant enzyme whose activity is preserved in most mutant forms. Owing to the similarities in sporadic and fALS forms, mutant SOD1 animal and cellular models are useful tool to study the disease. In addition, mutations on genes involved in RNA metabolism (e.g., tarbp/TDP-43) are found in inherited and sporadic forms of ALS,

and aggregates of TDP43 are found in the motor neurons of the majority of ALS patients.

Impairment in glutamatergic system is well documented in ALS patients and animal models. Excess in glutamate in the environment of motor neurons contributes to their hyperexcitability, to the production of ROS, and to neurodegeneration through excitotoxicity.

In this study, the effects of a riluzole (anti-glutamatergic drug) and edaravone (antioxidant drug) were investigated in primary motor neurons from rats transgenic for SOD1^{G93A} injured with glutamate. Non-transgenic primary motor neurons injured with glutamate served as control.

Experimental Approach: Non-transgenic and SOD1^{G93A} rat spinal cord (E14) were cultured as described by Wang et al. (2013) with modifications. Cells were cultured in 96-well plates maintained at 37°C. Glutamate (5 μM , 20 min) was applied on Day 13. Neuron survival, integrity of the neurite network, and TDP43 translocation were studied by immunocytochemistry.

Key Results: We showed that glutamatergic stress induced a clear loss of motor neurons and an abnormal cytoplasmic accumulation of TDP43 in spinal motor neurons. We found that glutamatergic stress was more pronounced in SOD1^{G93A} motor neurons and induced a massive accumulation of TDP43 in the cytoplasm when compared to injured non-transgenic controls. Riluzole and edaravone showed strong neuroprotective effects in the non-transgenic culture and were able to correct the TDP43 cellular distribution. In SOD1^{G93A} cultures, the neuroprotective effects of riluzole and edaravone were confirmed, but interestingly, their efficacy was lower when compared to their neuroprotective effects on WT cultures.

Conclusion and Implications: Altogether, our results clearly indicate that SOD1^{G93A} primary motor neurons were more sensitive to glutamatergic stress and less sensitive to riluzole and edaravone. The massive accumulation of TDP43 in the cytoplasm of SOD1^{G93A} motor neurons may directly contribute to exacerbate neurodegeneration process in this in vitro model of amyotrophic lateral sclerosis.

REFERENCE

Wang, W., Li, L., Lin, W. L., Dickson, D. W., Petrucelli, L., Zhang, T., & Wang, X. (2013 Dec 1). The ALS disease-associated mutant TDP-43 impairs mitochondrial dynamics and function in motor neurons. *Human Molecular Genetics*, 22(23), 4706–4719.

P221 | The cardiac work-loop technique: An in vitro model for profiling drug-induced changes in cardiac contractility using rat papillary muscles

Sophie Fletcher¹; Mayel Gharanei¹; Helen Maddock¹; Rob James²

¹Coventry University/InoCardia Ltd; ²Coventry University

Background and Purpose: Adverse cardiac effects are one of the leading causes of safety-related drug attrition (Wallis, Gharanei, & Maddock, 2015). Drug-induced changes in contractility (inotropy) can

be harmful and can have fatal consequences. Inotropy is, therefore, an important characteristic when assessing preclinical safety of compounds. The cardiac work-loop technique incorporates a sinusoidal length change to mimic intrinsic cardiac muscle movement to enable accurate prediction of the physiological and pharmacological changes in response to drugs. The cardiac work-loop has the potential to be used as a preclinical in vitro assay to assess inotropy (Gharanei, Wallis, Babba, & Maddock, 2016; Wallis et al., 2015).

Experimental Approach: Further optimisation of the work-loop assay (Wallis et al., 2015) and in-house software development was undertaken to enable real-time work-loop data output. Known positive and negative inotropes were used to assess the ability of the cardiac work-loop to identify drug-induced changes in contractility. The compounds used (verapamil, flecainide, atenolol, isoprenaline, digoxin, and dobutamine) have all been previously well characterised. Rat papillary muscles were dissected from the heart and mounted onto a work-loop rig perfused with oxygenated Krebs-Henseleit (KH) buffer (pH 7.40 at 37°C). Following length optimisation, work-loop contractions were carried out every 5 min for 80 min. The first 20 min of the protocol was used to assess baseline performance, followed by 60 min of vehicle control or drug treatment. Statistical significance was determined by comparing drug treatment to the appropriate vehicle control treatment using two-way repeated measures ANOVA followed by post hoc independent samples *t* test. *P* < .05 was determined significant. All results are expressed as mean ± SEM.

Key Results: All drug treatments were compared to an appropriate vehicle control of either KH buffer (*n* = 7) or 0.01% DMSO (*n* = 7). Negative inotropes verapamil (1 µM; *n* = 7), flecainide (3 µM; *n* = 7), and atenolol (20 µM; *n* = 8) significantly reduced the power output of the papillary muscle by $-17 \pm 9\%$, $-16 \pm 6\%$, and $-13 \pm 7\%$, respectively, when compared to vehicle control. Positive inotropes digoxin (1 µM; *n* = 6), dobutamine (1 µM; *n* = 9), and isoprenaline (20 nM; *n* = 7) increased the power output by $+27 \pm 9\%$, $+20 \pm 6\%$, and $+14 \pm 9\%$, respectively, when compared to vehicle control.

Conclusion and Implications: In the current study, the work-loop technique correctly identified significant decreases in muscle performance when treated with negative inotropes and significant increases in muscle performance when treated with positive inotropes. The work-loop technique closely resembles the in vivo characteristics of cardiac muscle function and is thereby able to predict inotropy at clinically effective concentrations.

REFERENCES

- Gharanei, Wallis, Babba, & Maddock (2016). *Journal of Pharmacological and Toxicological Methods* Sep-Oct, 81, 362–363.
Wallis, Gharanei, & Maddock (2015). *Journal of Pharmacological and Toxicological Methods* Sep-Oct, 75, 62–69.

P222 | Novel peptide spexin enhances insulin gene and protein levels in pancreatic BRIN-BD11 beta cells

Md Zahidul Islam Khan; Steven Patterson

Glasgow Caledonian University

Background and Purpose: Spexin has been reported to regulate feeding behaviour, metabolism, and body weight. Significant correlations between spexin, blood glucose, and lipids suggest that this peptide may play a vital role in glucose and lipid metabolism in obesity and type 2 diabetes (Gu et al., 2015). However, the exact role of spexin in insulin secreting pancreatic beta cells remains to be clarified. The aim of this study was to elucidate the expression and possible function of spexin using the BRIN-BD11 beta cell model.

Experimental Approach: BRIN-BD11 were cultured in RPMI 1640 medium (Lonza) and supplemented with 10% FBS and 1% penicillin-streptomycin. Expression of spexin and insulin was determined by immunocytochemistry. Effects of culture (24 and 48 hr) with spexin and exendin-4 on cell growth/viability were determined by MTT. BRIN-BD11 cell-specific gene expressions were quantified by qPCR following 24- and 48-hr treatment of cells with different concentrations of spexin and exendin-4.

Key Results: Spexin was co-expressed with insulin in BRIN-BD11 cells. Treatment (24 and 48 hr) with spexin alone had no effect on BRIN-BD11 cell viability. Exendin-4 (10–500 nM) increased cell viability (*P* < .05–.0001) following 24-hr treatment. Spexin/exendin-4 (1 nM each) combined treatment (24 hr) decreased (*P* < .001) cell viability, while combination (100 nM each) for 48 hr increased (*P* < .001) cell viability. Key beta cell transcription factor MafA was up-regulated following 24 and 48 hr of exposure to spexin (10 nM, *P* < .05) and following 24 hr at 100-nM spexin (*P* < .01). Exendin-4 (10 nM) alone and in combination with spexin (10 nM) increase PDX-1 expression (*P* < .05 and <.01, respectively) after 24 hr. Spexin (10 nM) alone (48 hr) increased PDX-1 expression. Following 48-hr culture with 10-nM spexin, insulin-1 was significantly up-regulated (*P* < .01), while exendin-4 caused down-regulation following 48 hr (*P* < .05). Insulin protein expression was also increased significantly by 24 hr of treatment with spexin alone (10 nM) and spexin and exendin-4 at 100 nM combination.

Conclusion and Implications: Spexin is expressed in BRIN-BD11 cells along with insulin. Treatment of BRIN-BD11 cells with spexin alone or in combination with GLP-1 receptor agonist exendin-4 up-regulates MafA and PDX-1. Spexin also increases the insulin 1 gene expression and protein expression. Further studies into the actions of spexin alone and with known beta cell modulators are required in normal and dysfunctional islets.

REFERENCE

- Gu, L., Ma, Y., Gu, M., et al. (2015). Spexin peptide is expressed in human endocrine and epithelial tissues and reduced after glucose load in type 2 diabetes. *Peptides*, 71, 232–239.

P223 | Immunomodulatory effect of pregabalin derivatives and their metal complexes on ovalbumin-induced acute lung remodelling

Muhammad Shoab Zafar; Muhammad Shahzad

University of Health Sciences, Lahore

Background and Purpose: Pregabalin is a structural analogue of γ -aminobutyric acid approved for partial epilepsy, neuropathic pain, and diabetic peripheral neuropathy. Pregabalin also showed beneficial activity against hyperalgesia after acute joint or paw inflammation and has potential to alleviate the symptoms of asthma to an individual after onset of asthma and prophylactically before the bronchospasm begins in an asthma attack, to prevent its occurrence or to reduce the extent to which it occurs (Schrier & Taylor, 2002). The aim of this study is to evaluate the effect of salicylaldehyde and benzaldehyde derivatives of pregabalin and their metal complexes on ovalbumin-induced acute lung remodelling in rats.

Experimental Approach: Rats were divided into nine groups, except control group; the rats were intraperitoneally sensitized at Days 0 and 14 and then challenged intranasally with OVA for 2 weeks for the induction of lung remodelling. Group III was treated with methylprednisolone $15 \text{ mg}\cdot\text{kg}^{-1}$ b.w. intraperitoneally, while Groups IV and V were treated with salicylaldehyde derivatives of pregabalin (pregsal) and benzaldehyde derivatives of pregabalin (pregbenz) $100 \text{ mg}\cdot\text{kg}^{-1}$ b.w. intraperitoneally, respectively. Groups VI and VII were treated with copper and zinc complex of pregal, respectively, while Groups VIII and IX were treated with copper and zinc complex of pregbenz, respectively. Hydroxyproline and arginase activity was determined in lung homogenate by spectrophotometry. Activity of ornithine decarboxylase (ODC) and osteopontin (OPN) was determined by ELISA. The mRNA expression of proinflammatory markers were measured by reverse transcription PCR.

Key Results: Characteristics of lung remodelling including enhanced inflammatory cells, increased hydroxyproline, arginase, ODC, and OPN level in the lungs of OVA-exposed rats were observed. Pregsal, pregbenz, and their zinc complex suppressed the inflammatory cells infiltration and activity of arginase, hydroxyproline, ODC, and OPN levels. Furthermore, they also abrogated the mRNA expression of TNF- α , IL-4, IL-8, IL-13, arginase I, MMP-9, TIMP-1, and TGF- β , while significantly increased the expression of AQP1 and AQP5.

Conclusion and Implications: Administration of pregal, pregbenz, and their zinc complex significantly reduced the level of OVA-induced lung remodelling by the inhibition of arginase pathways and the expression of cytokines, MMP9, TIMP1, and TGF- β . Our findings suggest that these novel compounds might have useful implications in the treatment of allergen-induced lung remodelling.

REFERENCE

Schrier, D., & Taylor, C. (2002). Method for treating asthma using pregabalin. In: Google Patents.

P224 | Characterising an etonogestrel-loaded hydrogel for use as a localised therapy for endometriosis

Jessica Traynor; Debbie Fischer; Alberto Saiani; Aline Miller; Kay Marshall

University of Manchester

Background and Purpose: Prior studies have demonstrated that etonogestrel (ENG)-loaded peptide hydrogels ($17.6 \mu\text{g}\cdot\text{ml}^{-1}$ hydrogel) displayed therapeutic efficacy in a murine model of endometriosis. The ENG-loaded hydrogel reduced lesion weight and volume compared to hydrogel alone (Santorelli, 2018). Before progressing these studies, the impact of the progestin ENG on the physical and structural properties of this hydrogel was characterised. The chosen hydrogel was the Alpha2 PeptiGel, produced by Manchester BIOGEL, due to its bio-compatibility, biodegradability, and muco-adhesive properties.

Experimental Approach: To examine the physical and structural properties of the hydrogel, oscillatory rheology, Fourier transform IR spectroscopy (FTIR), and transmission electron microscopy (TEM) were conducted using hydrogel alone and loaded with ENG ($17.6 \mu\text{g}\cdot\text{ml}^{-1}$; $n = 3$ per group). For TEM analysis, hydrogels were diluted with water at ratios of 1:10, 1:100, 1:200, 1:500, and 1:1,000. The diameter of the fibrils was analysed using ImageJ 1.48v software and compared using one-way ANOVA with Tukey's multiple comparisons test. Storage modulus (G') was compared using Kruskal-Wallis with Dunn's post hoc test.

Key Results: There was no statistically significant change in G' within the linear viscoelastic region of either gel ($n = 3$). The percentage strain at which "break-point" of the gel occurs did not significantly change with ENG loading: $33.56 \pm 1.96\%$ and $32.05 \pm 0.72\%$ for vehicle and ENG-loaded hydrogel, respectively (mean \pm SEM). Shear recovery experiments showed that both hydrogel formulations were able to recover from high shear strain (100%). FTIR analysis produced a major peak at $1,625 \text{ cm}^{-1}$ and a minor peak at $1,695 \text{ cm}^{-1}$ for both hydrogels. TEM showed comparable network topology between the vehicle and ENG-loaded hydrogel. Both formulations produced images of long, entangled, filamentous fibrils, with no visible helical secondary structures. Fibre diameter of the hydrogels was increased from 3.74 nm in vehicle to 4.29 nm with ENG loading ($P < .05$).

Conclusion and Implications: These data suggest that the addition of ENG at $17.6 \mu\text{g}\cdot\text{ml}^{-1}$ does not induce substantial changes in hydrogel structure and physical properties. ENG did not significantly affect the physio-chemical properties of the hydrogel or its ability to recover from high strain, indicating its suitability for injection. The network topology of both control and ENG-loaded peptide hydrogels showed anti-parallel β -sheet formation. Increase in fibril diameter with ENG could be due to a slight increase in fibril aggregation in order to avoid contact with ENG. This could occur as a result of the hydrophilic fibrils repelling from the hydrophobic ENG. However, this needs to be investigated further.

REFERENCE

Santorelli, S. (2018). *Development of a novel controlled release pelvic drug delivery system to manage endometriosis [traditional]*. Manchester: University of Manchester.

P225 | Targeting bone marrow with CCL2 conjugated cytotoxic NAMPT inhibitors

Joshua Greally; Maria Likhatcheva; Kara Filbey; John Grainger; Annalisa Tirella; Sam Butterworth

University of Manchester

Background and Purpose: Chronic myelomonocytic leukaemia (CMML) is characterised by the aberrant proliferation of monocytic cells. The initial mutations occur within the bone marrow, and treat-

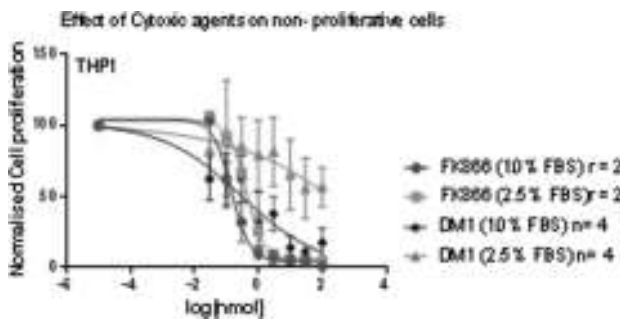


FIGURE 1. Comparison of FK866 (Nampti) with DM-1 (anti-mitotic agent) in both high proliferative (10% FBS) and low proliferative (2.5% FBS) THP1 cells. DM-1 shows large drop off in potency in low proliferative cells while FK866 shows no significant change

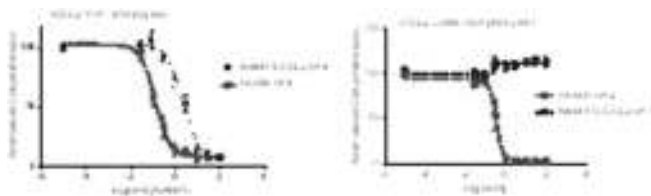


FIGURE 2. Dose-response curve of CCL2-NAMPTi in CCL2-positive THP1 cells (left) and CCL2-negative Jurkat cells (right). CCL2-NAMPTi is shown to be selective towards THP1 cells

ment is palliative due to current drugs only being able to kill cells in the peripheral blood stream. Slow proliferation of bone marrow cells also results in widely used chemotherapy agents that target proliferation being ineffective. Herein, we report a novel CCL2 conjugated drug delivery system that can selectively target cancerous cells involved in CMML, including in bone marrow by utilising a NAMPTi inhibitor as the cytotoxic payload. These compounds are metabolic cytotoxins, allowing induction of apoptosis and cell death in non-proliferating cells.

Experimental Approach: Click protein conjugation was carried out using standard conditions and protein purified and isolated by PD size exclusion chromatography. Samples were analysed by MALDI-TOF and MCP-1 ELISA assay. Conjugate compounds were incubated with THP1 and Jurkat monocytic cells for 48 hr and analysed using a WST-1 cell proliferation assay. *in vivo* mouse studies were undertaken by injecting CCL2-SCY5 into WT and CCR2 KO mice at 1 mg·kg⁻¹ (10 µM in PBS, 0.1% BSA). After 3 hr, samples were taken from bone marrow and blood, labelled for standard markers, and analysed by FACS.

Key Results: High (10% FBS) and low (2.5% FBS) proliferative THP1 were treated with FK866 or the typical cytotoxic ADC payload DM-1. DM-1 showed a large drop off in potency in the slower proliferating THP1 cells in 2.5% FBS, whereas FK866 showed minimal reduction in efficacy.

Following earlier studies on selective uptake of CCL2 conjugates by CCR2+ cells. THP1 and Jurkat cells were incubated for 48 hr with a novel CCL2-NAMPTi, and WST-1 was used as cell proliferation assay, showing that CCL2-NAMPTi is high selectivity for CCR2-expressing cells.

In *in vivo* studies, WT mice showed high levels of Cy5 uptake in the CCR2-positive population in bone marrow as well as in the blood, while no uptake is observed in any cell type for the CCR2^{-/-} mice.

Conclusion and Implications: NAMPT inhibitors are metabolic cytotoxins that can target non-proliferating cells; however, as a result, they have no useful therapeutic window. We have developed CCL2 conjugates that are selectively internalised by CCR2+ cells and are able to target the bone marrow *in vivo*.

Combining these findings with the initial THP1 results gives a very promising basis that a CCL2-NAMPTi inhibitor will be able to target and kill cancerous bone marrow cells in CMML.

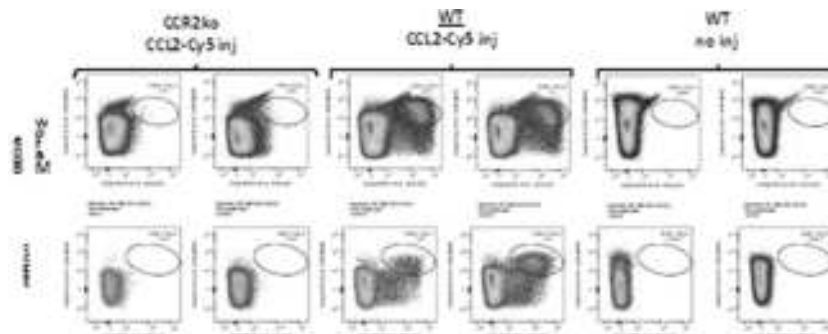


FIGURE 3. Flow cytometry data of *in vivo* mouse study. The data depict significant uptake of CCL2-SCy5 into bone marrow and blood of wild-type mice

REFERENCES

- Deshmane, S. L., Kremlev, S., Amini, S., & Sawaya, B. E. (2009). Monocyte chemoattractant protein-1 (MCP-1): An overview. *Journal of Interferon & Cytokine Research*, 29(6), 313–326.
- Imai, S. (2009). Nicotinamide phosphoribosyltransferase (Nampt): A link between NAD biology, metabolism, and diseases. *Current Pharmaceutical Design*, 15(1), 20–28.
- Patnaik, M. M., & Tefferi, A. (2016). Chronic myelomonocytic leukemia: 2016 update on diagnosis, risk stratification, and management. *American Journal of Hematology*, 91(6), 631–642.

P228 | Novel pharmacology of cannabidivarin, tetrahydrocannabivarin, cannabigerol, and cannabichromene in vitro and in vivo

Robert Laprairie; Kawthar Mohamed; David Kim; Ayat Zagzoog

University of Saskatchewan

Background and Purpose: The two most abundant cannabinoids present in *Cannabis*, the acid forms of Δ^9 -tetrahydrocannabinol (THC) and cannabidiol (CBD), have been extensively studied for their pharmacodynamics activity at the type 1 and 2 cannabinoid receptors (CB_1 and CB_2) (Russo, 2011); but comparatively little is known about the numerous other cannabinoids present in *Cannabis sativa* sp. The purpose of this study was to assess the activity of the less abundant plant cannabinoids cannabidivarin (CBDV), tetrahydrocannabivarin (THCV), cannabigerol (CBG), and cannabichromene (CBC) at CB_1 and CB_2 in vitro and in vivo.

Experimental Approach: In vitro, CHO-K1 cells expressing human CB_1 or CB_2 were treated with CP55,940 (reference agonist), THC, CBDV, THCV, CBG, CBC, or vehicle (1% DMSO in PBS). Inhibition of cAMP (HitHunter; DiscoverRx) (Tham et al., 2018) and β arrestin2 recruitment (PathHunter, DiscoverRx) (Tham et al., 2018) were measured. Data were fit to the operational model of Black and Leff to quantify bias (Tham et al., 2018). In vivo, adult, male, C57Bl/6 mice were injected (i.p.) with THC, CBDV, THCV, CBG, CBC, or vehicle (1:1:18

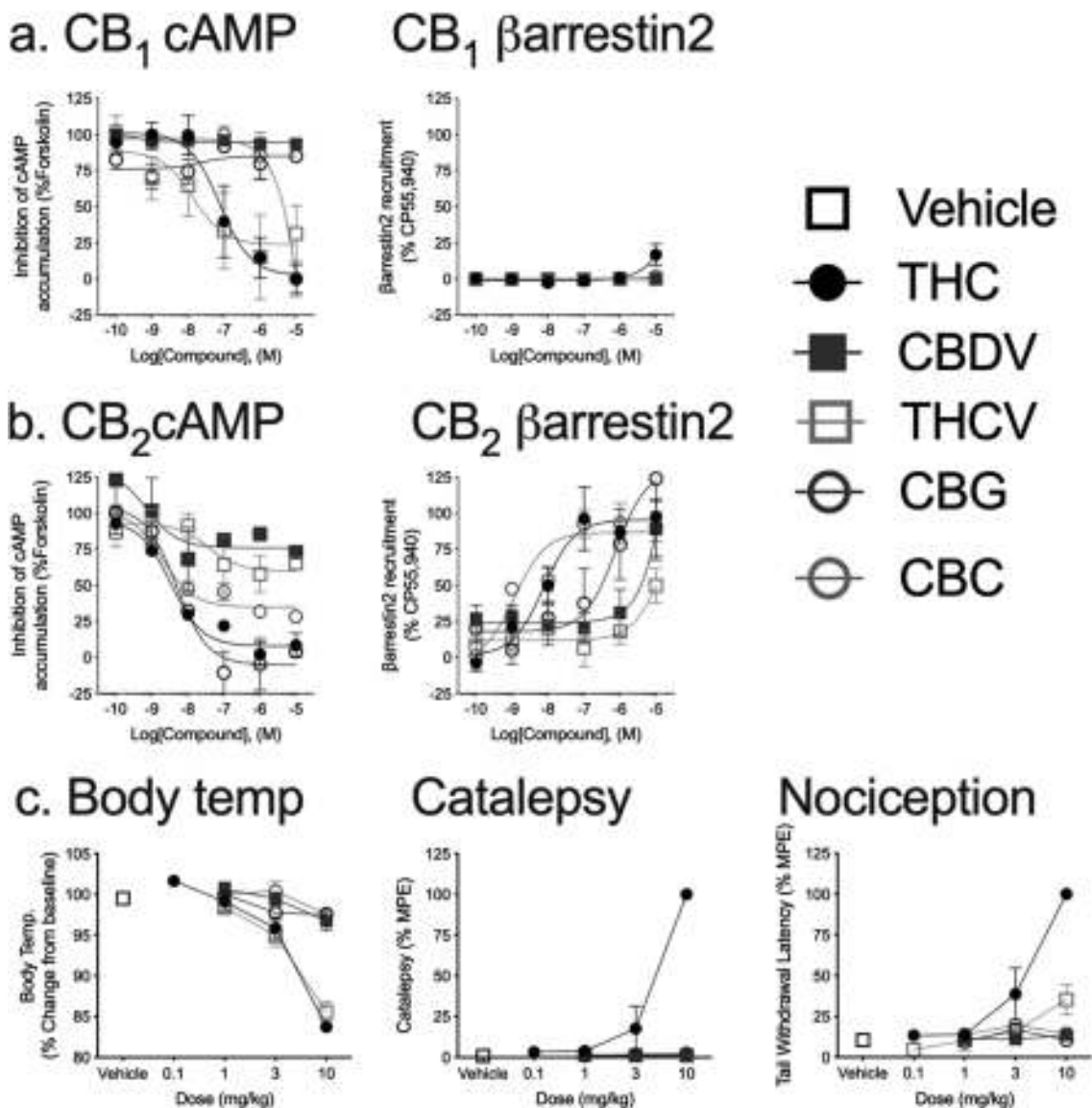


FIGURE 1

cremaphor:ethanol:saline), and body temperature, catalepsy, nociception, and locomotion were quantified according to established triad protocols (Grim et al., 2017).

Key Results: THCv—and not CBDV, CBG, or CBC—were weak partial agonists of cAMP inhibition, but not β arrestin2 recruitment at CB₁ (n = 8; Figure 1a); CBG and CBC were agonists of cAMP inhibition and β arrestin2 recruitment at CB₂; whereas CBDV and THCv were weak partial agonists of cAMP inhibition and β arrestin2 recruitment at CB₂ (n = 8; Figure 1b). THCv produced moderate hypothermic and anti-nociceptive effects, but no other effects were observed for the compounds tested (n = 6; Figure 1c).

Conclusion and Implications: These data support the hypothesis that the less abundant cannabinoids modulate cannabinoid receptor activity in vitro and in vivo (Russo, 2011). Subsequent research is required to determine if (i) these ligands are antagonists or modulators of other cannabinoids, and (ii) the mechanism of these compounds' effects in vivo. This research highlights that the potential effects of less abundant cannabinoids may have on the efficacy of THC and CBD in existing *Cannabis*-based medicines and may lead to the development of new compounds based on the structures and activity of these ligands.

REFERENCES

Grim, T. W., Morales, A. J., Thomas, B. F., Wiley, J. L., Endres, G. W., Negus, S. S., & Lichtman, A. H. (2017). Apparent CB1 receptor rimonabant affinity estimates: Combination with THC and synthetic cannabinoids in the mouse in vivo triad model. *The Journal of Pharmacology and Experimental Therapeutics*, 362, 210–218.

Russo, E. B. (2011). Taming THC: Potential cannabis synergy and phytocannabinoid-terpenoid entourage effects. *British Journal of Pharmacology*, 163, 1344–1364.

Tham, M., Yilmaz, O., Alaverdashvili, M., Kelly, M. E. M., Denovan-Wright, E. M., & Laprairie, R. B. (2018). Allosteric and orthosteric pharmacology of cannabidiol and cannabidiol-dimethylheptyl at the type 1 and type 2 cannabinoid receptors. *British Journal of Pharmacology*, 176, 1455–1469.

P230 | Protective effect of vitamin C on leachate-induced genotoxicity and oxidative stress in the liver and ovary of rat

Oluwatosin Arojjoye; Olajumoke Nwaechefu; Abiola Adeosun; Aminat Alimi

Lead City University, Ibadan, Oyo State, Nigeria

Background and Purpose: Contamination of groundwater by landfill leachate poses potential health hazards for man and his environment. Generally, leachates are composed of heavy metals, organic and inorganic compounds that are sources of ROS. This study investigated the protective effect of vitamin C on leachate-induced genotoxicity and oxidative stress in the liver and ovary of rats exposed to Ajakanga landfill leachate.

Experimental Approach: Sixty female Wistar rats (150–200 g) were divided into 10 groups (A–I) with six rats per group. Group A animals (control) were given distilled water, and Groups B–E animals were given 12.5%, 25%, 50%, and 100% leachate, respectively, via drinking water for 28 days. Animals in Group F were given distilled water plus 100 mg.kg⁻¹ vitamin C while Groups G–I animals were given 100 mg.kg⁻¹ vitamin C plus 12.5%, 25%, 50%, and 100% leachate, respectively. Activities of alanine amino transferase (ALT), aspartate aminotransferase (AST), and γ -glutamyltransferase (GGT) were determined in the serum of rats using enzyme kits. Oxidative stress markers (malondialdehyde, reduced GSH, GSH-S-transferase, superoxide dismutase, and catalase activity) were determined in the liver and ovary of the rats by spectrophotometry. Genotoxicity study was carried out using micronucleus assay.

Key Results: There was increase in the activities of ALT, AST, and GGT in the serum of rats exposed to leachate (Groups B–E) compared with control, but ALT and AST activity decreased in rats exposed to leachate plus vitamin C (Groups G–I). There was an increase in malondialdehyde concentration (index of lipid peroxidation) in the

TABLE 1 Activity of alanine aminotransferase in the serum

Group	Negative control/ leachate-treated group	Positive control/ leachate-treated group + 100 mg.kg ⁻¹ vitamin C
Control	A 69.7 ± 2.9	F 73.8 ± 4.3
12.5% leachate	B 82.2 ± 4.8	G 70.4 ± 4.8 ^β
25% leachate	C 86.3 ± 3.9	H 65.2 ± 3.6 ^β
50% leachate	D 83.3 ± 3.4	I 68.5 ± 3.7 ^β
100% leachate	E 92.8 ± 3.7 ^α	J 71.0 ± 2.7 ^β

Note. The results are expressed as mean ± SD.
^αSignificant when compared with control.
^βSignificant when compared with vitamin C + leachate-treated group at P < .05.

TABLE 2 Lipid peroxidation in the liver

Group	Lipid peroxidation (μmol.mg ⁻¹ protein)	
	Negative control/ leachate-treated group	Positive control/ leachate-treated group + 100 mg.kg ⁻¹ vitamin C
Control	A 72.6 ± 20.9	F 71.1 ± 10.2
12.5% leachate	B 102.3 ± 21.5	G 73.7 ± 12.1
25% leachate	C 125.8 ± 16.8	H 118.6 ± 45.2
50% leachate	D 203.6 ± 55.9 ^α	I 112.0 ± 38.8 ^β
100% leachate	E 302.7 ± 21.7 ^α	J 144.1 ± 112.1 ^β

Note. The results are expressed as mean ± SD.
^αSignificant when compared with control.
^βSignificant when compared with vitamin C + leachate-treated group at P < .05.

TABLE 3 Lipid peroxidation in the ovary

Group	Lipid peroxidation ($\mu\text{mol}\cdot\text{mg}^{-1}$ protein)			
		Negative control/ leachate-treated group		Positive control/ leachate-treated group + 100 mg·kg ⁻¹ vitamin C
Control	A	0.7 ± 0.2	F	0.2 ± 0.1 ^β
12.5% leachate	B	1.1 ± 0.1 ^α	G	0.47 ± 0.1 ^β
25% leachate	C	1.2 ± 0.3 ^α	H	0.99 ± 0.2
50% leachate	D	1.7 ± 3.5 ^α	I	1.25 ± 0.2 ^β
100% leachate	E	2.1 ± 3.3 ^α	J	1.14 ± 0.9 ^β

Note. The results are expressed as mean ± SD.

^αSignificant when compared with control.

^βSignificant when compared with vitamin C + leachate-treated group at $P < .05$.

TABLE 4 Micronuclei formation in the bone marrow of rats

Group	Micronuclei formation			
		Negative control/ leachate-treated group		Positive control/ leachate-treated group + 100 mg·kg ⁻¹ vitamin C
Control	A	72.8 ± 17.2	F	78.8 ± 10.9
12.5% leachate	B	98.3 ± 13.1	G	72.5 ± 8.7 ^β
25% leachate	C	113.0 ± 18.0	H	65.5 ± 4.4 ^β
50% leachate	D	95.0 ± 8.7	I	77.8 ± 8.3
100% leachate	E	74.7 ± 20.1	J	66.8 ± 12.7

Note. The results are expressed as mean ± SD.

^αSignificant when compared with control.

^βSignificant when compared with vitamin C + leachate-treated group at $P < .05$.

liver and ovary of rats in Groups B–E compared with control, but there was a significant decrease in malondialdehyde level in animals treated with vitamin C. There was a decrease in the levels of reduced GSH and SOD in the ovary of rats in Groups B–E, but vitamin C treatment increased the levels of these antioxidants. A significant increase in GSH-S-transferase activity was observed in the liver and ovary of rats in Groups G–I compared with Groups B–E animals. A significant increase in micronucleated polychromatic erythrocytes (MPCEs) was observed in bone marrow of rats exposed to leachate, but there was a decrease in MPCEs in rats treated with vitamin C.

Conclusion and Implications: Vitamin C has a protective effect on leachate-induced genotoxicity and oxidative stress in the liver and ovary of the rats.

REFERENCE

Arojojoye, O. A., & Odunlade, A. K. (2016). Farombi EO (2016). Assessment of the genotoxic potential of Olusosun landfill leachate using plant and animal bioassays. *Journal of Current Topics in Toxicology*, 12, 75–84.

P231 | Revisiting the past to enhance the future: Traditional medicinal plant extracts in the discovery of novel drug lead to target P2X7

Stefan Bidula; Lučka Bibič; Adrienne Moulton; Jiayi Zhang; Leanne Stokes

University of East Anglia

Background and Purpose: P2X7 is an ATP-gated cation channel predominantly expressed on cells of myeloid origin that participates within immunity to pathogens and inflammatory disorders. This is primarily achieved through the production of inflammatory mediators (e.g., IL-1 β), regulation of cell death pathways, and activation of the NLRP3 inflammasome. We recently identified that protopanaxadiol ginsenosides from the traditional Chinese herb *Panax ginseng* function as positive allosteric modulators of P2X7. Therefore, we obtained a large library of plant extracts (>400) used in Traditional Chinese Medicine (TCM) and aimed to identify novel modulators of P2X7.

Experimental Approach: Extracts and agonists were applied to HEK293 cells transfected with human P2X7 (hP2X7-HEK293) in 96-well plates using a Flexstation 3 plate reader. In this protocol, extracts (30 $\mu\text{g}\cdot\text{ml}^{-1}$) were added after 30 s, ATP (1 mM) was added after 90 s, and YOPRO-1 dye fluorescence was read for another 210 s. Hits were counter-screened in THP-1 monocytes via the measurement of IL-1 β (ELISA) and cell viability (AlamarBlue[®]). Individual compounds were docked in silico against homology models of the closed and open states of hP2X7. Purified compounds were tested against receptor function using YOPRO-1 and whole-cell patch-clamp electrophysiology. Data were analysed for statistical significance using either unpaired *t* tests or one-way ANOVA with posttests as appropriate ($n = 3-5$).

Key Results: The initial screen identified 71 negatively modulating (<25% of the 1-mM ATP response) and 29 positively modulating (>150% of the 1-mM ATP response). Counter screens reduced this number to 20 negative and 10 positive extracts. We further identified that only one positive extract could produce concentration-dependent potentiation (*Dioscorea nipponica*). A literature search of the compounds contained in these extracts, combined with in silico molecular modelling, predicted 60 compounds to bind to a previously described inhibitory site. Testing chemically distinct potential inhibitory compounds against P2X7 (berberine, kaempferol, palmitic acid, bergapten, methyl syringate, and scopoletin) indicated that only the known inhibitor berberine could inhibit at physiologically relevant concentrations (3–10 μM). A compound from *D. nipponica* (dioscin) was capable of potentiating ATP-induced YOPRO-1 uptake (2.6-fold increase), cell death (50% reduction), and channel opening (2.7-fold increase). This was predicted to be due to interactions with our recently characterized positive allosteric site.

Conclusion and Implications: There is growing evidence that natural compounds have significant potential for the discovery of novel lead

compounds to target P2X7 and related ion channels. Here, we describe several potential inhibitory compounds and a novel positive modulator for P2X7, but these extracts need investigating in more detail.

P232 | Brain targeting of letrozole nanoemulsion: Pharmacodynamics evaluation of anticonvulsant action against kainic acid-induced status epilepticus in mice

Ramsha Iqbal; Shakeeb Ahmed; Gaurav Jain; Divya Vohora

Jamia Hamdard

Background and Purpose: Status epilepticus (SE) is a serious neurological condition characterized by persistent episodes of seizures. Aromatase is the key enzyme which converts testosterone into 17 β -estradiol in the brain, which enhances brain excitability. Several peripheral adverse effects of letrozole (LET) limit its potential benefit in SE. Intranasal route delivers therapeutic agents directly to the brain by avoiding blood-brain barrier. The objective of the study is brain targeting by direct nose to brain delivery of letrozole nanoemulsion and its evaluation against kainic acid (KA)-induced status epilepticus (SE).

Experimental Approach: Letrozole loaded nanoemulsion (LET-NE) was prepared. LET-NE was studied for droplet size, polydispersity index (PDI), zeta potential, percentage transmittance, drug content, and surface morphology. SE was induced by KA (10 mg·kg⁻¹, i.p.) in Swiss albino mice 60 min after drug treatments. Behavioural seizures were recorded for 120 min and scored according to Modified Racine's scale. Gamma scintigraphy imaging was performed; later animals were killed for biochemical estimations of 17 β -estradiol, 5 α -DHT, and 3 α -Diol and histopathological studies of the hippocampus and was compared against free LET in KA-induced SE in mice.

Key Results: LET-NE was prepared by aqueous microtitration method using Triacetin, Tween 80, and PEG-400 as the oil phase, surfactant, and co-surfactant. The onset time of SE was significantly increased, and % incidence of SE was reduced by intranasal administration of LET-NE. Biochemical estimation revealed that LET-NE effectively reduced levels of 17 β -estradiol ($P < .01$, $n = 4$), while the levels of 5 α -DHT and 3 α -Diol ($P < .01$, $n = 4$) were increased significantly in the hippocampus. Cresyl violet staining showed that LET-NE protected the hippocampus from neurotoxicity induced by KA. In gamma scintigraphy of mouse brain, intranasal administration of nanoemulsion exhibited the presence of a high concentration of letrozole.

Conclusion and Implications: LET-NE protected all animals from the development of seizures and neurodegeneration induced by KA, feasibly by reduction of the transformation of testosterone to 17 β -estradiol, proconvulsant, and redirecting the synthesis of testosterone metabolite 3 α -Diol with known anticonvulsant and neuroprotective action. Thus, LET-NE may be used in the therapy of SE that requires further investigations.

REFERENCES

- Rashid, D., et al. (2015). *Neurochemistry International*, 90, 271–274.
 Reddy, D. S. (2004). *Neuroscience*, 129, 195–207.
 Reddy, D. S., & Mohan, A. (2011). *The Journal of Neuroscience*, 31, 650–658.

P235 | Statin and hypoxia decrease coronary perivascular adipose tissue-induced chemerin release in porcine

Tariq Alsahli; Richard Roberts; Michael Randall

University of Nottingham

Background and Purpose: Statins exert significant effects beyond their impact on lowering cholesterol synthesis including decreasing BP and vascular inflammation. Chemerin is an adipokine secreted from liver and adipose tissue including perivascular adipose tissue (PVAT) (Liao & Laufs, 2005). Chemerin is implicated in BP regulation with well-established roles in inflammation and obesity (Buechler, Feder, Haberl, & Aslanidis, 2019). We have previously demonstrated the release of chemerin by PVAT surrounding porcine coronary artery (PCA). The aim of this study was to determine the effect of statins on chemerin release by coronary PVAT in porcine.

Experimental Approach: A 0.3 g of fresh PVAT was added to a four-channel wire myograph filled with 7.5-ml Krebs–Henseleit solution maintained at 37°C and aerated with a 95% O₂/5% CO₂ gas mixture and left for 2 hr in the presence and absence of 10- μ M simvastatin or 10- μ M pravastatin. In order to examine the effect of hypoxia, the gas cylinder was swapped to 95% N₂/5% CO₂ for 30 min. Electrical field stimulation (EFS) was applied to the PVAT to test the role of sensory nerve activation. Chemerin release in the Krebs–Henseleit was quantified using ELISA. Data were analysed using Student's two-tailed paired *t* test. Data are expressed as mean \pm SEM ($n \geq 6$).

Key Results: Incubation with 10- μ M simvastatin significantly reduced chemerin release from PVAT (0.5 ± 0.1 ng·ml⁻¹ in the presence of simvastatin vs. 0.8 ± 0.1 ng·ml⁻¹ in vehicle control, mean \pm SEM, $n = 10$, $P < .01$) while the presence of 10- μ M pravastatin reduced chemerin release from 1.2 ± 0.1 ng·ml⁻¹ in control to 0.6 ± 0.1 ng·ml⁻¹ (mean \pm SEM, $n = 6$, $P < .001$). Hypoxia induction for 30 min inhibited PVAT-induced chemerin release from 1.2 ± 0.1 to 0.9 ± 0.05 ng·ml⁻¹ (mean \pm SEM, $n = 6$, $P < .05$) whereas EFS had no effect on the amount of chemerin released.

Conclusion and Implications: These data demonstrate that both lipophilic (simvastatin) and hydrophilic (pravastatin) statins could reduce chemerin release from the PVAT surrounding coronary arteries, which may explain some of the pleiotropic effects of statins. Chemerin release is decreased after exposure to conditions of reduced oxygenation, suggesting that part of the vascular response to hypoxia may be due to reduced contraction by chemerin.

REFERENCES

- Buechler, C., Feder, S., Haberl, E. M., & Aslanidis, C. (2019). Chemerin isoforms and activity in obesity. *International Journal of Molecular Sciences*, 20(5), 1128.
- Liao, J. K., & Laufs, U. (2005). Pleiotropic effects of statins. *Rev. Pharmacol. Toxicol.*, 45, 89–118.

Poster Session: Education and Skills

P253 | Minimal nephrotoxicity of amine-modified kaolinite clay, a novel low-cost adsorbent for water treatment in Nigeria

Chiagoziem Otuechere; Adewale Adewuyi; Oghenetega Avwioroko; Egunoluwa Olajide; Beatrice Fadoju

Redeemer's University, Ede, Osun State, Nigeria

Background and Purpose: The quality of water is negatively impacted by heavy metals contamination arising from environmental and industrial exertions. Gradationally, the connection between good health and well-being (Sustainable Development Goal [SDG] 3) and clean water and sanitation (SDG 6) is being drawn more so as exposure to heavy metals in drinking water has been associated with the risk of cancer, diabetes, and kidney malaise. Presently, treatment options for heavy metals contaminated water are either ineffective or unattainably expensive. Hence, the modification of native clay to boost its adsorbent properties and its subsequent toxicity evaluation in renal tissues.

Experimental Approach: In this study, an amine functional group was introduced into kaolinite clay by surface grafting to improve its

surface area and minimize its cation exchange capacity, thereby boosting its efficacy in remediation of metal-polluted water. Characterization studies were performed using Brunauer–Emmett–Teller (BET), X-ray diffractometer, zeta potential analysers, and Fourier transform IR spectrophotometer. Despite the health benefits of clay minerals, chemical modifications could elicit some toxic responses in organisms. Hence, we also conducted a 2-week dose–response study in Wistar albino rats ($n = 5$ per group) at the doses of 1, 2, and 5 mg·kg⁻¹ body weight (p.o.) of amine-modified kaolinite clay.

Key Results: The BET surface area and monomodal pattern peak for the modified kaolinite clay were 13 m²·g⁻¹ and 10 μm, respectively. Furthermore, in the toxicity studies, there were no significant ($P > .5$) changes in levels of albumin, uric acid, triiodothyronine, thyroxine, ratio of triiodothyronine to thyroxine, calcium and potassium electrolytes, and relative kidney organ weight in the rats treated with amine-modified kaolinite clay relative to the controls (Table 1).

Interestingly, treatment of animals with amine-modified kaolinite clay also preserved the renal histoarchitecture and antioxidant enzymes status in the rats.

Conclusion and Implications: This present, therefore, study justifies the potential uses of amine-modified kaolinite clay as a safe, low-cost adsorbent for the treatment of contaminated water in rural areas of Nigeria.

REFERENCES

- Chukwuemeka-Okorie, H. O., Ekemezie, P. N., Akpomie, K. G., & Olikagu, C. S. (2018). Calcined corncob-kaolinite combo as new sorbent for sequestration of toxic metal ions from polluted aqua media and desorption. *Frontiers in Chemistry*, 6, 273. <https://doi.org/10.3389/fchem.2018.00273>
- Unuabonah, E. I., Adewuyi, A., Kolawole, M. O., Omorogie, M. O., Olatunde, O. C., Fayemi, S. O., ... Taubert, A. (2017). Disinfection of water with new chitosan-modified hybrid clay composite adsorbent. *Heliyon*, 3, e00379. <https://doi.org/10.1016/j.heliyon.2017.e00379>

TABLE 1 Kidney organ weight and selected biochemical indices in rats following 14 days of treatment with different doses of amine-modified kaolinite clay (MKC)

Parameter	Control	MKC 1	MKC 2	MKC 3
Absolute kidney weight (g)	1.04 ± 0.09	1.19 ± 0.15	0.97 ± 0.04	0.96 ± 0.03
AST (U·L ⁻¹)	47.6 ± 1.8	48.9 ± 2.2	45.4 ± 2.4	58.54 ± 3.4*
Albumin (g·dl ⁻¹)	14.7 ± 1.2	12.7 ± 1.4	13.3 ± 1.2	14.4 ± 1.2
Uric acid (mg·dl ⁻¹)	2.70 ± 0.4	2.93 ± 0.2	2.77 ± 0.2	2.87 ± 0.3
Total cholesterol (mg·dl ⁻¹)	51.0 ± 5.8	40.7 ± 2.0	37.6 ± 2.0*	32.54 ± 2.8*
Calcium (mg·dl ⁻¹)	13.4 ± 0.7	9.2 ± 0.2	7.5 ± 1.1	7.1 ± 1.3
Potassium (mEq·L ⁻¹)	6.1 ± 0.3	4.7 ± 0.5	4.2 ± 0.1	4.9 ± 0.5
Sodium (mEq·L ⁻¹)	149.4 ± 0.7	141.4 ± 0.8	143.7 ± 3.3	141.1 ± 1.1
Thyroxine (nmol·L ⁻¹)	73.6 ± 3.2	82.3 ± 5.8	81.7 ± 2.6	70.7 ± 1.2
Triiodothyronine (nmol·L ⁻¹)	1.4 ± 0.1	10.02.9 ± 0.1	2.0 ± 0.03	1.6 ± 0.2
Triiodothyronine/thyroxine ratio	0.02 ± 0.001	0.02 ± 0.001	0.02 ± 0.01	0.02 ± 0.002

Note. Values are expressed as mean ± SEM ($n = 5$). MKC 1 (1 mg·kg⁻¹); MKC 2 (2 mg·kg⁻¹), and MKC 3 (5 mg·kg⁻¹).

*Significantly different from control ($P < .01$).

P254 | Guidelines on target validation for innovative therapeutics (GOT-IT)

Michael J. Parnham¹; Christoph H. Emmerich²;
Lorena Martinez-Gamboa³; Martine Hofmann⁴; Anton Bespalov²;
Ulrich Dirnagl³

¹Fraunhofer IME-TMP; ²PAASP GmbH, Heidelberg; ³Charite Universitätsmedizin Berlin; ⁴Fraunhofer IME-TMP, Frankfurt

Background and Purpose: Academic-industrial collaboration is important for the development of novel therapeutics. For various reasons, including lack of resources and incentives, academic research on drug discovery and target validation often does not fulfil the criteria needed for potential commercial exploitation. Consequently, a project group across three centres, supported by the German Ministry of Science and Education (BMBF), aimed to establish a set of flexible guidelines to enable academic researchers to achieve robust target validation.

Experimental Approach: Initially, an extensive literature review of articles was performed to assess the degree to which preclinical target validation criteria are applied in academic research. A final 440 articles were selected. Of these, 35% investigated a single model system, 53% performed only one target manipulation but employed two to four readouts, and only 16% considered development aspects (e.g., safety and biomarkers). To address this incompleteness, but maintain flexibility across different indications and targets, the GOT-IT guidelines are based on several *Building Blocks* (BBs), each covering various aspects of target validation, to be aligned on a case-to-case basis, thereby forming a *Critical Path* for target validation with the aim to meet a number of predetermined milestones (Figure 1). The selection and positioning of relevant BBs is guided by sets of *Guiding Questions*

(GQs). These GQs ensure that only project-relevant BBs are selected and help to identify key gaps and road blocks for a translational target validation project.

The approach proposed was moulded by interviews with target validation experts from academia, industry, CROs, and tech-transfer offices and the opinions of academic researchers and their industry mentors from 11 research projects on target validation initiated by the BMBF. Use of specific examples strengthened the general acceptance of the approach.

Key Results: The GOT-IT concept is being incorporated into a website to be publicly available, providing additional resources. These include a *Critical Path Generator*, with which validation steps can be arranged to support the planning of a project and an *Educational Tool* (in preparation) explaining the application of the guidelines to enable experienced and inexperienced researchers to run studies more efficiently.

Conclusion and Implications: The GOT-IT guidelines are designed to assist in identifying relevant tasks, allocating resources, and prioritizing target validation activities to increase confidence in the target of interest. They also provide practical means to enhance researcher training on target validation and may be a blueprint for similar training tools in other research areas.

P256 | An in silico 360 concept for the triage and selection of drug development compounds

Christopher Southan¹; Per Arvidsson²

¹Deanery of Biomedical Sciences; ²SciLifeLab

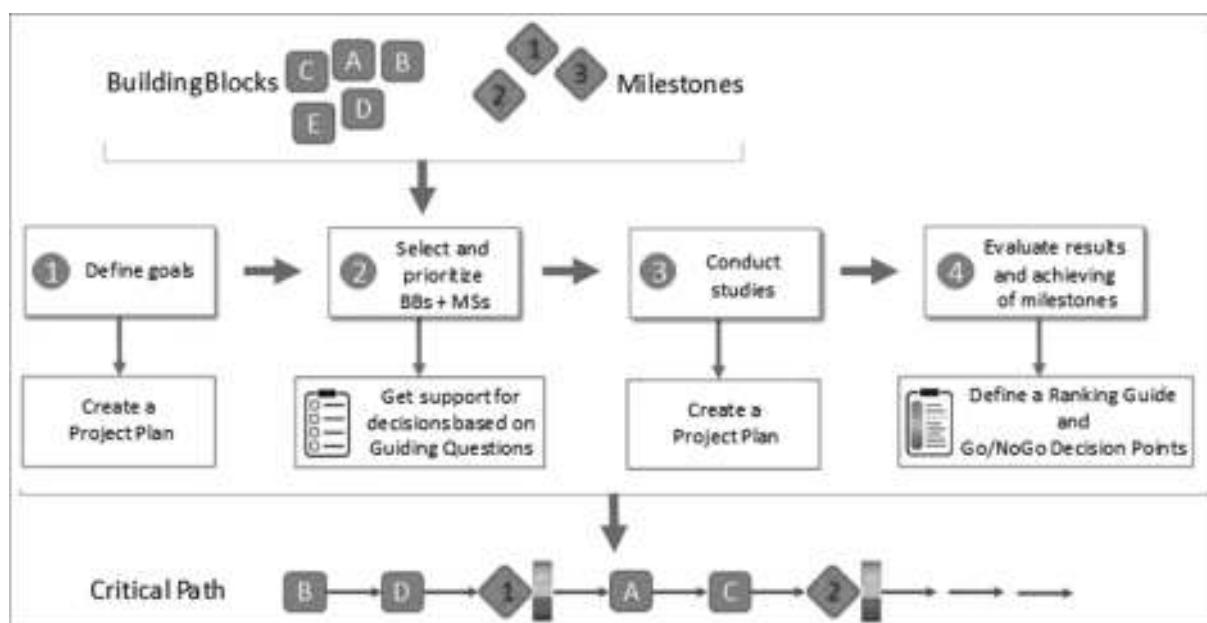


FIGURE 1. Concept for GOT-IT recommendations

Background and Purpose: Consequent to a memorandum of understanding between the Karolinska Institutet and the International Union of Basic and Clinical Pharmacology (IUPHAR) in 2018, a report on academic drug development, including guidelines (ADEV), has been drafted (Southan, 2019). As part of this exercise, we conceived a triage for comprehensive informatics profiling around the compound, target, disease axis. We have termed this “in slico 360” (INS360), the aim of which was to support ADEV teams since they may lack either internal expertise or external support to do this on their own. Indeed, some past SciLifeLab Drug Discovery and Development Platform projects had been halted because of overlooked competitive impingements or insufficient target validation evidence.

Experimental Approach: We assessed the current database landscape, mostly public but including commercial, for potential utility for INS360. We were guided primarily by content coverage, usability, and reputation. We also explored some open property prediction resources for assay interference and toxicological inferences.

Key Results: As a first-stop-shop, we selected the IUPHAR/BPS Guide to PHARMACOLOGY with ~900 ligand–target relationships captured via expert curation of journal papers moving up in scale we evaluated ChEMBL at 1.8 million compounds with 1.1 million assay descriptions and 7,000 targets. With yet another jump, we could search the patent corpus with 18 million extracted compounds in SureChEMBL. We explored PubChem that integrates these three with over 500 other sources linked to 96 million compounds, BioAssay results, and connectivity into the NCBI Entrez system. The final jump in scale for document-to-chemistry navigation was represented by SciFinder with 155 million structures. On the target side, 360 exploration has the need to encompass literature, structure, genetic variation, splicing, interactions, and disease pathways. From their UniProt links, both GtoPdb and ChEMBL provide these entry points. Navigating genetic association data in support of target validation was enabled by the OpenTargets portal and the GWAS Catalog. We also found servers that could produce prediction scores from chemical structures for a range of features important for de-risking development.

Conclusion and Implications: This work scoped out initial resource choices for the INS360. We propose that not only ADEV operations but also essentially any pharmacology research team has much to gain from this approach and many potential pitfalls can consequently be avoided when approaching key checkpoints, such as preparing a publication. However, support may be needed for institutions and teams to get the best out of these complex and feature-rich databases.

REFERENCE

Southan, C. (2019). Towards academic drug development guidelines, ChemRxiv preprint no. 8869574

P257 | Cardiac autonomic neuropathy and haemodynamic dysfunction as a consequence of mild hypercaloric intake: Modification by phosphate supplementation

Ghina Ajouz; Haneen Dweib; Nahed Mogharbil; Marwan Refaat; Omar Obeid; Ahmed El-Yazbi

American University of Beirut

Background and Purpose: Cardiac autonomic neuropathy (CAN) is associated with metabolic syndrome and diabetes. Our previous research showed that prediabetic rats develop CAN in absence of overt signs of metabolic derangement or change in body weight. This was associated with vascular dysfunction and perivascular adipose tissue (PVAT) inflammation. Significantly, PVAT inflammation was related to increased uncoupling protein 1 (UCP1) expression and increased hypoxia and hypoxia-inducible factor (HIF1- α) expression. Recent studies identified phosphate supplementation as a simple intervention to improve body weight, energy metabolism, and glucose tolerance. Moreover, inorganic phosphate acts as a UCP1 inhibitor. Here, we examined the role of phosphate supplementation in ameliorating the early signs of cardiovascular dysfunction.

Experimental Approach: Male SD rats (5–6 weeks) were randomly allocated into four groups fed either control or high-calorie (HC) diet with three levels of dietary phosphate (LP, IP, and HP with 0.37, 0.7, and 1.5 mg·kcal⁻¹, respectively). Daily food intake, body weight, and body composition were recorded. Serum adiponectin, leptin, and insulin were measured by ELISA. Invasive haemodynamic measurements were done following 12 weeks of feeding, and baroreceptor sensitivity (BRS) was assessed by the vasoactive method. After sacrifice, several organs were dissected and used for immunohistochemistry and western blotting.

Key Results: No changes in caloric intake, body weight, BP, serum adipokines, and blood glucose levels were observed following 12 weeks of feeding. However, an increase was observed in fat/lean ratio among rats on HC diet together with an increase in serum insulin level. Consistent with our previous work, HC feeding was associated with reduced parasympathetic BRS. This was observed in the LP and IP (Δ MAP vs. Δ HR slope decreased to 0.14 ± 0.02 and 0.18 ± 0.02 , respectively, vs. 0.37 ± 0.02). This was also accompanied by a reduced left ventricular systolic function (dP/dt_{max} decreasing from 1,940 to 1,288 mmHg·s⁻¹). Interestingly, both observations were reversed in the HP. Nevertheless, Oil Red O stain showed a significant increase in the diameter of PVAT adipocytes in LP arm. IL-1 β was highly expressed in the PVAT among LP and was lower in HP. Moreover, a similar pattern was observed for UCP1 and consequently HIF1- α expression levels. Furthermore, macrophage infiltration was higher in the PVAT and HMS among the LP and lower in HP.

Conclusion and Implications: Our present results highlight a role of phosphate supplementation in the amelioration of the parasympathetic dysfunction. This could be due to the reported ability of dietary

phosphate to improve the assimilation of fat and hence reduce adipose inflammation possibly via UCP1 inhibition.

REFERENCE(S)

P261 | Development of novel TR-FRET-based adenosine A2A binding assays using the polymers SMA and DIBMA

David Sykes¹; Hoare Bradley¹; Romez Uddin²; Mark Soave¹; David Poyner²; Dmitry Veprintsev¹

¹University of Nottingham; ²Aston University

Background and Purpose: Emerging evidence implicates the adenosine A2A receptor (A2AR) in the progression of certain cancers. Administration of antagonists of this receptor is associated with blockade of adenosine-driven angiogenesis and metastasis, warranting the exploration of A2AR antagonist ligand-receptor binding kinetics. The high-throughput characterisation of unlabelled compound kinetics (both fast and slow) is complicated by the injection of non-homogeneous solutions of membranes into the assay plate, leading to inherent assay variability. One solution to this problem is to first solubilise the receptor using either detergent or polymer-based solutions. Here, we describe a novel higher throughput TR-FRET-based method to assess the functionality and stability of the human A2AR under varied solubilisation conditions.

Experimental Approach: Terbium cryptate-labelled HEK293-A2A receptors in standard incubation buffer, 20-mM HEPES, 150-mM NaCl, 5% glycerol, and 0.5% BSA pH 7.5, containing either the detergent 0.1% DDM/0.02% CHS or 0.05% LMNG, or the polymers 0.1% styrene maleic anhydride (SMA) or 0.1% diisobutylene-maleic acid

(DIBMA), were incubated in the presence of the fluorescent ligands, CA200645 (15.6–500 nM, final assay volume of 20 µl) or SCH442416-red (3.1–100 nM) at room temperature. Assays were initiated by the addition of receptors to the fluorescent ligand in a 384-well proxiplate plate, and TR-FRET measurements were taken every 20 s on a PHERAstar FSX (BMG Labtech) using eight flashes of the laser under standard HTRF instrument settings. Kinetic parameters were obtained by fitting specific binding data, defined by the addition of SCH442416 (1 µM), to standard kinetic binding models with equilibrium saturation parameters taken at 60 min. All data were fitted GraphPad Prism 8.0.

Key Results: The kinetics of binding of both fluorescent CA200645 and SCH442416-red were examined with values for their on and off rates achieved under all four experimental conditions. The kinetic off rates of the fluorescent ligand CA200645 closely matched the existing literature value (Chitlangia et al., 2016) with similar dissociation rates observed across the different conditions. Results for CA200645 and SCH442416-red are summarised in Tables 1 and 2, respectively.

Conclusion and Implications: The fluorescent ligands tested displayed binding to the A2AR in both the detergent and polymer-based solubilisation buffers. Receptor stability in the presence of fluorescent CA200645 and SCH442416-red, as judged by the change in B_{max} with time (see Tables 1 and 2), suggests that the SMA polymer is suitable for determining the kinetics of ligand binding using the instrument injectors. The novel methods described have the potential to significantly increase assay throughput enabling the kinetic profiling of unique chemical fragments.

REFERENCE

Chitlangia S et al., (2016). 233P London, UK. Pharmacology 2016. Poster Session: Molecular and Cellular Pharmacology 3

TABLE 1 Kinetic parameters of CA200645

	CA200645					
	k_{off} ($M^{-1} \cdot min^{-1}$)	k_{off} (min^{-1})	Kinetic K_d (nM)	Kinetic B_{max} (30 min)	Saturation K_d	Saturation B_{max} (60 min)
DDM CH	$3.1 \pm 0.8 \times 10^6$	0.87 ± 0.20	375 ± 158	21,753	138 ± 42	12,346
LMNG	$1.2 \pm 0.4 \times 10^6$	0.53 ± 0.18	456 ± 68	6,654	385 ± 144	4,635
SMA	$1.3 \pm 0.7 \times 10^6$	0.53 ± 0.08	937 ± 387	8,895	394 ± 142	5,588
DIBMA	$2.35 \pm 0.58 \times 10^6$	1.26 ± 0.11	687 ± 229	34,799	120 ± 22	5,903

Note. Data are expressed as mean \pm SEM (n = 4).

TABLE 2 Kinetic parameters of SCH442416-red

	SCH442416-red					
	k_{off} ($M^{-1} \cdot min^{-1}$)	k_{off} (min^{-1})	Kinetic K_d (nM)	Kinetic B_{max} (30 min)	Saturation K_d	Saturation B_{max} (60 min)
DDM CH	$3.7 \pm 0.4 \times 10^6$	0.47 ± 0.04	132 ± 16	32,277	94 ± 13	24,586
LMNG	$7.7 \pm 2.4 \times 10^6$	0.41 ± 0.12	58 ± 15	6,639	146 ± 49	8,745
SMA	$3.2 \pm 0.64 \times 10^6$	0.17 ± 0.02	62 ± 16	16,102	53 ± 12	13,882
DIBMA	$8.6 \pm 0.90 \times 10^6$	0.20 ± 0.02	24 ± 5	31,252	16.4 ± 3	20,226

Note. Data are expressed as mean \pm SEM (n = 4).

P236 | Pharmacodynamic analysis of the transcriptomic changes produced by the EP₄-receptor agonist, ONO-AE1-329, in BEAS-2B human bronchial epithelial cells

Radhika Joshi¹; Dong Yan²; Omar Hamed¹; Mark A. Giembycz¹

¹University of Calgary; ²Pfizer

Background and Purpose: Prostanoid EP₄-receptors are highly expressed on human airway epithelial cells (AECs) and typically mediate canonical, Gs-cAMP signalling. EP₄-receptor agonists exhibit bronchodilator and anti-inflammatory activity (Birrell et al., 2015; Buckley et al., 2011) and could represent novel therapeutic candidates to treat obstructive lung diseases. We have reported previously that long-acting β₂-adrenoceptor agonists (LABAs) promote significant gene expression changes in human AECs, which could contribute to their clinical efficacy. In this study, the results of a pharmacodynamics analysis of gene expression changes in BEAS-2B cells produced by the selective EP₄-receptor agonist, ONO-AE1-329, are described and compared to the LABA, vilanterol.

Experimental Approach: BEAS-2B cells were treated for 2 hr with vehicle and two concentrations of ONO-AE1-329 (1 nM, ONO₁; 1,000 nM, ONO_{1,000}). A maximally effective concentration of vilanterol (100 nM, Vil₁₀₀) was included as a comparator and to define maximum responses. Total RNA was extracted (N = 4), and differentially induced genes were determined by RNA sequencing. Simulated E/[A] curves were generated from ONO₁ and ONO_{1,000} data assuming a unity Hill coefficient for each gene expression change (≥3-fold; FDR ≤ 5%). BEAS-2B cells transfected with a cAMP response element (CRE) luciferase reporter were used to determine the affinity (K_A) of ONO-AE1-329 for the EP₄-receptor. This was estimated by operational model fitting of E/[A] curve data before and after fractional receptor depletion using siRNA-mediated

PTGER₄ gene silencing. Occupancy–response relationships for ONO-AE1-329-induced genes were constructed using the simulated E/[A] curves and the K_A value determined in CRE reporter cells.

Key Results: Transcriptomic changes produced by Vil₁₀₀ and ONO_{1,000} were highly correlated (Pearson's $r = .97$), suggesting that the β₂-adrenoceptor and the EP₄-receptor shared a common mechanism of action. Vilanterol was a full agonist on all induced genes whereas ONO-AE1-329 was a partial agonist with intrinsic activity values that depended on the gene of interest and varied from 0.2 to 0.8. The K_A of ONO-AE1-329 was estimated to be 5.48 ± 0.56 nM (N = 5), consistent with a previous radioligand binding study (K_D = 9.7 nM (Suzawa et al., 2000)). ONO-AE1-329-induced genes differed in sensitivity by ~12-fold with NR4A1 and PDE4B representing transcripts at the extremes of this sensitivity spectrum. Accordingly, occupancy–response relationships varied from almost linear (where response is directly proportional to occupancy; e.g., NR4A1) to marked hyperbolic (indicative of a significant receptor reserve; e.g., PDE4B) (Figure 1).

Conclusion and Implications: Differences in the potency and intrinsic activity of ONO-AE1-329 indicate that genes that constitute the EP₄-receptor-regulated transcriptome interpret equivalent degrees of receptor occupancy differently. This may relate to variability in promoter context, which may differentially affect the ability of transcription factors to interact favourably with DNA.

REFERENCES

- Birrell, M. A., Maher, S. A., Dekkak, B., et al. (2015). Anti-inflammatory effects of PGE₂ in the lung: Role of the EP₄ receptor subtype. *Thorax*, 70, 740–747.
- Buckley, J., Birrell, M. A., Maher, S. A., Nials, A. T., Clarke, D. L., & Belvisi, M. G. (2011). EP₄ receptor as a new target for bronchodilator therapy. *Thorax*, 66, 1029–1035.
- Suzawa, T., Miyaura, C., Inada, M., et al. (2000). The role of prostaglandin E receptor subtypes (EP₁, EP₂, EP₃, and EP₄) in bone resorption: An analysis using specific agonists for the respective EPs. *Endocrinology*, 141, 1554–1559.

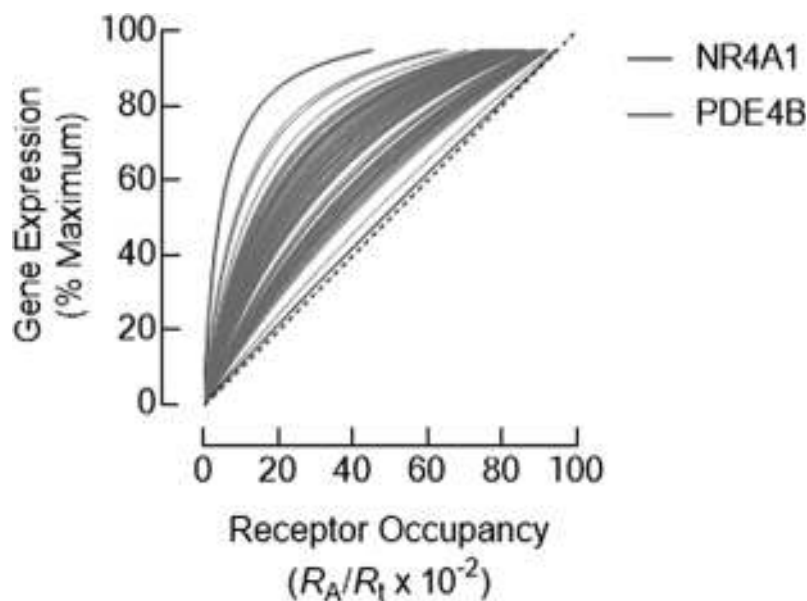


FIGURE 1. Receptor occupancy-response relationship for ONO-AE1-329 induced genes

P237 | Inhibition of Epac reduces inflammatory responses of bronchial epithelial cells to LPSs and cigarette smoke exposure

Susan Leung¹; Peng Zhang¹; Ricky Man¹; Judith Mak^{1,2}

¹Department of Pharmacology and Pharmacy, The University of Hong Kong; ²Department of Medicine, The University of Hong Kong

Background and Purpose: Chronic obstructive pulmonary disease is characterized by airway inflammation, and cigarette smoking is one of the most common risk factors. As the disease progresses, exacerbation (an acute worsening of the respiratory symptoms) occurs more frequently. Exacerbation likely occurs with bacterial infection which causes additional inflammatory responses in the airway. Airway inflammation can be reduced by activation of cyclic AMP (cAMP) pathway. The two major cellular targets of cAMP are PKA and exchange protein directly activated by cAMP (Epac). The present study was designed to examine the relative contribution of PKA and Epac, if any, to the airway epithelial inflammatory responses to cigarette smoke exposure, in the absence or presence of the bacterial endotoxin LPSs.

Experimental Approach: Human bronchial epithelial BEAS-2B cells (Passages 42–49) were incubated for 24 hr with medium containing cigarette smoke extract (CSM, 4%), without or with LPS (10^{-6} to 10^{-4} g·ml⁻¹), in the absence or presence of pharmacological agents targeting cAMP pathway. The levels of the inflammatory mediator IL-8 in the medium were measured with ELISA kit. Data are expressed as percentage of control and given as mean ± SEM (*n* denotes different passages of cells); and analysis was performed using ANOVA followed by the Bonferroni post hoc test or the unpaired Student's *t* test, as appropriate.

Key Results: LPS, at 10^{-5} g·ml⁻¹, enhanced the CSM-induced IL-8 production in BEAS-2B cells (CSM: $785 \pm 240\%$; CSM + LPS: $2,002 \pm 173\%$; *n* = 5). The levels of IL-8 in cells exposed to CSM, alone or in combination with LPS, were increased by SQ22536 (adenylyl cyclase inhibitor, 2×10^{-5} M; *n* = 4–8) and reduced by rolipram (PDE-4 inhibitor, 10^{-4} M; *n* = 8–9), 8-bromo-cAMP (cAMP analogue, 2×10^{-5} M; *n* = 4–7), or 6-bnz-cAMP (PKA activator, 2×10^{-5} M; *n* = 5–6). They were not affected significantly by 8-CPT-2Me-cAMP (Epac activator, 10^{-4} M; *n* = 3) or KT5720 (PKA antagonist, 10^{-6} M; *n* = 4) but was almost abolished by ESI09 (Epac inhibitor, 10^{-5} M), to $8.8 \pm 2.5\%$ (*n* = 8) and $16 \pm 5.2\%$ (*n* = 7) of the levels in cells exposed to CSM and to CSM plus LPS, respectively. The inhibition of IL-8 release by ESI09 was partly reversed by KT5720 in both CSM- and CSM + LPS-exposed cells ($68 \pm 8.7\%$, *n* = 4; and $57 \pm 7.3\%$, *n* = 4, respectively).

Conclusion and Implications: Epac mediates, at least partly, the production of IL-8 induced by CSM, without or with LPS, and its inhibition unmasks the involvement of PKA in the inflammatory responses.

P238 | Cigarette smoke increases β -2 integrin expression, HSP70, and autophagy in THP-1 cells: Possible role of oxidative stress

Piotr Szoka¹; Robert Czarnomysy²; Adam Holownia¹

¹Department of Pharmacology, Medical University of Bialystok;

²Department of Synthesis and Technology of Drugs, Medical University of Bialystok

Background and Purpose: Cigarette smoke (CS) is considered as a critical factor in the progression and pathogenesis of the chronic obstructive pulmonary disease (COPD). Development of COPD is associated with activation of immune response, inflammation, and tissue remodelling in which monocytes/macrophages are essential inflammatory cells. Activated macrophages release inflammatory mediators (i.e., TNF- α and IL-8), chemokines, and MMPs that have distinct effects on structural cells in the airways. The aim of our study was to investigate the impact of acute CS exposition on β -2 integrin adhesion molecules, HSP70 expression, and autophagy in human monocyte/macrophage cell line (THP-1 cells). We have also evaluated the role of oxidative stress in CS-induced effects.

Experimental Approach: CS-conditioned medium (CSM) was prepared using full-strength Marlboro red cigarettes. Smoke was passed through RPMI/FCS culture media (two cigarettes per 50 ml) using a low-pressure vacuum pump. THP-1 cells were pretreated for 24 hr with a redox-active compound decreasing GSH-L-buthionine-(S,R)-sulfoximine (BSO; 100 μ M) or with N-acetylcysteine (NAC; 5 mM). Cells were grown in CSM for 2 hr. To determine the effects of CS on ROS production, 2',7'-dichlorodihydrofluorescein (DCF) assay was used. Effects of CS on adhesion molecules (CD11b; CD18), HSP70, and autophagy (LC3) were assayed using fluorescent monoclonal antibodies and flow cytometry detection.

Key Results: CS induced a significant increase in the expression of CD11b (about 60-fold) and CD18 (about 2.5-fold). We have also observed overexpression of HSP70 (about fourfold increase) and elevated LC3 protein (about fourfold). CS caused a twofold increase in cellular ROS production as compared with control cells. Similar effects were produced after pretreatment of cells with BSO, and it can be suggested that all of the above effects were dependent on oxidative stress. NAC partially attenuated the consequences of CS exposure, normalized ROS production, CD18, HSP70, and LC3 expression.

Conclusion and Implications: The results of the current study indicate even short-term exposure to CS-provoked changes in cell adhesion, proinflammatory response, and stress in THP-1 cells. CS exposition increases ROS production, and NAC only in part prevents CS-induced alterations.

REFERENCES

Holownia, A., Wielgat, P., Rysiak, E., & Braszko, J. J. (2016). Intracellular and extracellular cytokines in A549 cells and THP1 cells exposed to

cigarette smoke. *Advances in Experimental Medicine and Biology*, 910, 39–45.

Yang, D. C., & Chen, C. H. (2018). Cigarette smoking-mediated macrophage reprogramming: Mechanistic insights and therapeutic implications. *Journal of Nature and Science*, 4(11).

P239 | Interrogating the respiratory-analgesia therapeutic window of novel opioids in mice

Rob Hill; Rob Lane; Meri Canals

University of Nottingham

Background and Purpose: In the pursuit of safer opioid medications, greater focus has recently fallen on increasing the therapeutic window between the desired analgesic effects and opioid-induced side effects such as respiratory depression. TRV130 has been suggested as a safer opioid agonist due to G-protein biased signalling whereas tianeptine is a novel opioid agonist with an unknown mechanism to its potentially safer pharmacology. This investigation assessed whether TRV130 and tianeptine possess improved therapeutic separation between antinociception and respiratory depression compared to the prototypical opioid agonist morphine.

Experimental Approach: Whole body plethysmography was used to measure minute volume (MV) respiration in male CD-1 mice breathing air (30 g) (all groups, $n = 6$). Saline (± 1 –4% DMSO), morphine (1 – 30 mg·kg⁻¹), tianeptine (3 – 90 mg·kg⁻¹), and TRV130 (0.2 – 5 mg·kg⁻¹) were administered i.p. in 0.1-ml volumes. Linear regression was used to calculate equi-depressant ($\sim 40\%$ MV) doses for each drug which was verified by plethysmography. Hot plate assessment of nociception (52°C with a 20-s cut-off every 15 min, $n = 10$ all groups) was used to compare the analgesic effect of equi-depressant doses of each opioid calculated and was calculated as per cent maximum possible effect (%MPE).

Key Results: Saline (± 1 –4% DMSO) induced a 10–15% decrease in MV. Morphine, tianeptine, and TRV130 depressed MV in a dose-dependent manner with a peak decrease in MV of 75–85% for the highest dose of each opioid. Equi-depressant calculated doses of morphine (3.44 mg·kg⁻¹), tianeptine (12.74 mg·kg⁻¹), and TRV130 (0.75 mg·kg⁻¹) were found to all depress respiration to 38–42% at peak effect (no significant difference, one-way ANOVA). TRV130 and tianeptine were found to peak at 15 min and return to baseline in <90 min, whereas morphine maintained respiratory depression for the entire 90-min observation period. The same doses of each opioid all induced antinociception in the hot plate assay with each opioid peaking at 30 min (42–55% MPE—no significant difference, one-way ANOVA), with both tianeptine and TRV130 returning to control latencies at 75–90 min post-injection. Morphine maintained effect until the end of observation at 90 min.

Conclusion and Implications: These data suggest no difference in the relative efficacy between morphine, TRV130, and tianeptine to induce respiratory depression or antinociception when considering the peak effect attained, suggesting no increase in therapeutic window with

these novel opioids. However, the decreased duration of effect for TRV130 and tianeptine may still be of use therapeutically where prolonged respiratory depression is a risk factor.

P242 | Molecular pathway underlying suicidal behaviours revealed through systems pharmacology investigation of drugs which trigger suicide

Arash Sadri^{1,2}

¹Faculty of Pharmacy, Tehran University of Medical Sciences, Tehran, Iran; ²Students' Scientific Research Center, Tehran University of Medical Sciences, Tehran, Iran

Background and Purpose: Suicide takes the life of one person every 40 s. Despite its great burden, its molecular pathway remains unknown, and most studies have investigated mainly its general correlates. An innovative method to identify new drug targets using side-effect similarity had been previously published (Campillos, Kuhn, Gavin, Jensen, & Bork, 2008), but in this study, by adding a translational mindset, I aim to introduce a new approach for discovering the molecular pathways mediating such complex phenotypes using systems pharmacology analysis of substances with similar side effects.

Experimental Approach: Drugs reported to have these adverse effects were retrieved from the SIDER database: suicidal ideation, suicidal tendency, suicidal behaviour, suicide attempt, and suicide. Then I acquired the targets of these molecules with their normalized substance–target affinity values based on in vitro and in vivo measurements from Reaxys. Also, I added other putative targets using molecular docking, similarity ensemble approach, and analysis of the drugs' gene expression signatures. Afterward, to get a more holistic view, I gathered the first and second shell interacting proteins of all the targets collected using the previous methods. Each drug–target pair was assigned a value representing both its affinity and weight of evidence. I constructed a network with the network pharmacology of all the drugs using Cytoscape. After analysing the network with NetworkAnalyzer, I created a subnetwork with the most common components.

Key Results: After collecting the drugs from SIDER and removing the duplicates, 123 drugs remained. About 150,000 measurements from their in vitro and in vivo investigations were gathered from Reaxys to determine the targets of each drug. The final acquired subnetwork which represents a possible molecular network mediating suicidal behaviours includes pivotal components like phosphoinositide-specific PLC, 5-HT_{2A} receptor, and various types of ionotropic glutamate receptors and voltage-gated sodium channels.

Conclusion and Implications: A noteworthy validation for this proposed pathway is that most of the drugs used for patients at suicide risk act on one of its most important components: 5-HT_{2A} receptor. This and other observations regarding the down-regulation of this receptor after chronic antidepressant administration (Gray & Roth,

2001) and higher risk for suicide at first weeks after starting antidepressant treatment may suggest the reliability of this model and its potential for facilitating further therapeutic investigations.

REFERENCES

- Campillos, M., Kuhn, M., Gavin, A., Jensen, L., & Bork, P. (2008). Drug target identification using side-effect similarity. *Science*, 321, 263–266.
- Gray, J., & Roth, B. (2001). Paradoxical trafficking and regulation of 5-HT_{2A} receptors by agonists and antagonists. *Brain Research Bulletin*, 56, 441–451.

P243 | The role of α -2c adrenoceptors in ketamine-induced schizophrenia rat model

Nurdan Tekin; Tuğba Karamahmutoğlu; Dilek Akakın;
M. Zafer Gören

Marmara University School of Medicine

Background and Purpose: Adrenoceptors (ARs) play regulatory roles in neurotransmitter release and neuronal firing. α -2c, one of the subtypes of α -AR, is also related to schizophrenia. The disease has three main symptoms like positive, negative, and cognitive symptoms. While the current treatments are effective in controlling the positive symptoms, they often fail to treat negative and cognitive symptoms. Previous experiments have shown that α -2c antagonists have antipsychotic and pro-cognitive effects.

Experimental Approach: In this study, we aimed to show the effects of JP-1302, a selective α -2c antagonist, in a rat model of schizophrenia attained by giving sub-anaesthetic ketamine (25 mg·kg⁻¹, i.p.) for eight consecutive days. At the end of the seventh and eighth days, the behavioural tests were performed. Locomotor activity was tested for the positive symptoms. Negative and cognitive symptoms were assessed by using social interaction and novel object recognition tests, respectively. Upon completion of behavioural tests, the Wistar rats were killed, and [glutamine]/[glutamate] ($n = 6$) in the homogenates were measured by fluorometric HPLC analysis. TH immunohistochemical reactivity (*TH-ir*) was also shown in *striatum* and *nucleus accumbens* in separate group of rats ($n = 6$). All experiments were performed according to the ethical guidelines.

Key Results: Chronic ketamine administration decreased the percentage of resting and increased the percentage of stereotypic behaviour, significantly ($P < .02$; $P < .05$, respectively). Acute JP-1302 administration did not affect these behaviours, significantly. Saline treatment decreased the social interaction time ($P < .0001$), and JP-1302 reversed this in rats receiving ketamine in a dose-dependent pattern. In the novel object recognition test, ketamine-received rats had lower discrimination indices ($P = .0012$), and JP-1302 (10 mmol·kg⁻¹) significantly increased the indices ($P = .0385$). Increased [glutamine]/[glutamate] ratio, an index of decreased glutamergic activity, was observed in ketamine-received control rats. *TH-ir* increased in the nucleus accumbens, and the striata of ketamine-received control rats and JP-1302 significantly reversed the increase in *TH-ir* ($P < .001$).

Conclusion and Implications: These promising results may show that JP-1302 may alleviate the negative and cognitive symptoms of schizophrenia.

REFERENCES

- (2011). *British Journal of Pharmacology*, 164, 1162–1194.
- (2010). *Neuropsychopharmacology*, 35, 2462–2478.

P244 | The proposed multimodal mechanism of action of cannabidiol in epilepsy: Modulation of intracellular calcium and adenosine-mediated signalling

Kathryn Nichol

Greenwich Biosciences Inc

Background and Purpose: Although commonly misunderstood, cannabidiol (CBD) does not act directly through cannabinoid receptors at physiologically achievable concentrations. CBD has shown anticonvulsant properties in non-clinical studies and antiseizure effects in clinical trials of Dravet and Lennox-Gastaut syndromes. We present preclinical evidence for a unique multimodal molecular target profile distinct from other antiepileptic drugs.

Experimental Approach: Preclinical evidence suggests that CBD reduces neuronal hyperexcitability through multiple mechanisms, including modulation of intracellular calcium via GPCR 55 (GPR55), extracellular calcium influx via transient receptor potential vanilloid type 1 (TRPV1) channels, and adenosine-mediated signalling.

Key Results: CBD antagonises GPR55 at excitatory synapses. Inhibition of intracellular calcium release decreases excitatory currents and seizure activity. GPR55-mediated modulation of neurotransmission was potentiated in excitatory neurons and reduced in inhibitory neurons in a chronic epilepsy model. CBD potently blocked GPR55-mediated increase of miniature EPSC frequency in pyramidal neurons in both healthy and epileptic tissues. CBD did not affect GPR55-mediated increase of excitatory neurotransmission in inhibitory neurons in healthy tissue. CBD's anticonvulsant properties were attenuated in GPR55 knockout (KO) animals.

CBD desensitises TRPV1 channels. The resultant decrease in extracellular calcium influx decreases neurotransmission. The dose-dependent, CBD-mediated increase in seizure threshold seen in wild-type mice was significantly attenuated in TRPV1 KO mice. Brain CBD concentrations were consistent with those required for TRPV1 activation and desensitisation irrespective of genotype.

CBD inhibits the equilibrative nucleoside transporter 1 (ENT1), reducing adenosine reuptake. The increase in extracellular adenosine reduces hyperexcitability and neurotransmission. CBD inhibited [³H] adenosine uptake into rat cortical synaptosomes at low micromolar concentrations.

Conclusion and Implications: While the precise mechanisms by which CBD exerts its anticonvulsant properties in humans remain unknown,

growing preclinical evidence suggests that CBD reduces neuronal hyperexcitability through a unique multimodal mechanism of action. CBD antagonises GPR55 at excitatory synapses, desensitises TRPV1 channels, and inhibits adenosine reuptake.

P245 | Comparison of gene expression changes due to exposure to MDMB-CHMICA, 5F-ADB, and THC in stem cell-derived human neuronal brain cells

Israa Al-Banaa¹; Simon Thomas²; Peter Hanson²

¹Newcastle University; ²Medical Toxicology Centre, Newcastle University

Background and Purpose: The abuse of herbal products that contain synthetic cannabinoids (SCs) is an important issue with potential serious public health consequences. Although previously perceived as "safe and legal" alternatives to herbal cannabis, especially by younger people, they can cause serious toxicity. MDMB-CHMICA and 5F-ADB are SCs that have been responsible for hospital admissions and fatalities. The short- and long-term health effects of misuse of SC such as MDMB-CHMICA or 5F-ADB are not fully understood. This study therefore investigated the potential neurotoxicity of MDMB-CHMICA and 5F-ADB to characterise the mechanisms of toxicity in comparison to Δ^9 -tetrahydrocannabinol (Δ^9 -THC).

Experimental Approach: Mature neuronal brain cells, derived from human stem cells, were exposed to 10 nM of MDMB-CHMICA, 5F-ADB, or Δ^9 -THC for 14 days. RNA was then extracted, and samples were prepared using the TruSeq stranded mRNA library preparation kit (Illumina). The potential gene expression changes due to NPS exposure were examined using RNA sequencing performed on an Illumina NextSeq 500 platform.

Key Results: At the mRNA level, gene differential changes detected variations involving genes that belong to very different functional categories. The gene expression analysis revealed that 154 genes were significantly changed in MDMB-CHMICA-exposed cells (98 genes down-regulated; 56 genes up-regulated). In 5F-ADB-treated cells, 20 genes were significantly changed (9 genes down-regulated; 11 genes up-regulated). In THC-exposed cells, 50 genes were significantly changed (22 genes down-regulated; 28 genes up-regulated). The genes most significantly affected from the top 20 were mitochondrial tRNA genes (MT-tRNA). All of these were up-regulated with 1.17-fold to 1.99-fold changes between times. There were four genes that were significantly changed among three groups. All the expressed genes were further analysed by Ingenuity Pathways Analysis (IPA, Redwood City, USA) software to explore the canonical pathway. IPA identified 34 canonical pathways significantly changed ($P < .05$) in MDMB-CHMICA-treated cells, 25 in cells exposed to 5F-ADB, and 17 in THC-exposed cells.

Conclusion and Implications: The results suggest that repeated exposure to the selected cannabinoids in low concentrations modulated

different brain pathways. Many of these changes related to oxidative state, protein synthesis, and perturbed mitochondrial function, thereby leading to subtle but potentially lasting changes in the brain and to behaviour. Further validation studies are required to elucidate these effects, taking into consideration the complexity of the pathways involved.

P246 | The vicissitudes of target validation exemplified by BACE1 for Alzheimer's disease and BACE2 for diabetes

Christopher Southan

Deanery of Biomedical Sciences

Background and Purpose: The β -amyloid (APP) cleaving enzyme (BACE1) was implicated as a drug target for Alzheimer's disease (AD) back in 1999. In 2011, the paralogue, BACE2, became a new proposed target for type II diabetes (T2DM) having been reported to be the TMEM27 secretase regulating pancreatic beta cell function (Southan & Hancock, 2013). By 2019, the accumulated evidence, including a swathe of failed clinical trials for BACE1 inhibitors, has produced a de facto de-validation of both targets in both diseases. As a learning exercise, the series of events leading up to this is reviewed here.

Experimental Approach: Basic information about these two targets and the lead compounds against them were sourced via the IUPHAR/BPS Guide to Pharmacology (GtoPdb) as Target IDs 2330 and 2331, for BACE1 and 2, respectively. This was consolidated by a literature and patent review as well as following them in other databases. The most recent information on clinical trials was sourced from press releases.

Key Results: GtoPdb annotates 24 lead compounds against BACE1 and 12 against BACE2. The corresponding counts mapped to these targets in ChEMBL are 8741 and 1377, making BACE1 one of the most actively pursued enzyme targets ever. Notwithstanding the massive global effort during 2018, Merck's verubecestat and J&J's atabecestat BACE1 inhibitors not only failed their Phase III endpoints but even appeared to worsen cognition in prodromal patients. In 2019, Amgen/Novartis stopped Phase II/III trials of umibecestat that also showed more cognitive decline in the treatment group compared to controls. BACE2 presented an anomalous situation in several ways. By 2016, both Novartis and Amgen declared their inability to reproduce the TMEM27 secretase turnover reported in 2011. Notwithstanding, Novartis and other companies have published patents on BACE2-specific inhibitors over several years, and paradoxically, verubecestat is more potent against BACE2 rather than 1 but was never tested for glucose lowering. Equally puzzling is that one academic group is still publishing BACE2 inhibitors for T2D even after de-validation. One thing both targets have in common is the complete absence of genetic support from genome-wide disease association studies, but this warning sign went unheeded.

Conclusion and Implications: The massive waste of resources on the pursuit of BACE1 as an AD target over the last two decades is catastrophic. This tale of de-validation is compounded for this paralogous pair of enzymes by the fact that the original evidence for BACE2 as a T2D target was eventually refuted. The story of these targets highlights a range of crucial pharmacological pitfalls that must be avoided in the future.

REFERENCE

Southan, C., & Hancock, J. M. (2013). A tale of two drug targets: The evolutionary history of BACE1 and BACE2. *Frontiers in Genetics*, 4, 293.

P248 | Olanzapine alters β catenin dynamics in mouse MIN6 cells to reduce glucose-stimulated insulin secretion

Madeleine Honey; Greg Scutt; Wendy Macfarlane; Adrian Bone; Mark Yeoman

University of Brighton

Background and Purpose: Second-generation antipsychotic drugs are widely prescribed to patients with severe mental illness, yet their use has frequently been associated with the development of diabetes. Olanzapine is a high risk antipsychotic with metabolic side effects including hyperglycaemia often occurring rapidly at the onset of treatment. We hypothesise that olanzapine pharmacologically alters the function of the pancreatic beta cells to secrete insulin in response to glucose. Variations in components of the canonical Wnt pathway such as β catenin and transcription factor-7-like-2 (TCF7L2) have recently been linked to beta cell dysfunction, and olanzapine has been associated with changes in TCF7L2 expression; thus, we aimed to determine the effect of olanzapine on the canonical Wnt pathway related to beta cell function.

Experimental Approach: The mouse MIN6 beta cell line was exposed to olanzapine for 72 hr, followed by 2-hr glucose stimulation. ELISA was used to quantify insulin secretion in response to basal (5 mM) or high (25 mM) glucose with or without 1- μ M glycogen synthase kinase 3 (GSK3) inhibitor 6-bromindirubin-3'-oxime (BIO). Western blot was used to quantify cytoplasmic and nuclear β catenin, TCF7L2, and Axin2. Data are expressed as mean \pm SEM, and statistical analysis was carried out using two-way ANOVA and Bonferroni's posttest.

Key Results: Stimulation with high glucose caused a significant increase in insulin secretion $160.4 \pm 25.0\%$ compared to basal ($n = 3$, $P < .05$). Olanzapine significantly inhibited this increase in secretion ($94.48 \pm 8.3\%$ of basal) ($n = 3$, $P < .01$). Western blot showed that there was significantly less cytoplasmic β catenin following glucose challenge in olanzapine-treated cells ($n = 3$, $P < .05$). Addition of BIO to the glucose challenge resulted in an increase in cytoplasmic β catenin ($n = 3$, $P < .05$) as well as an increase in insulin secretion from $53.92 \pm 9.69\%$ to $97.91 \pm 14.28\%$ compared to control ($n = 4$, $P < .05$). There were also increases in protein concentration of

TCF7L2 and Axin2, suggesting an interaction with the canonical Wnt signalling pathway to decrease free β catenin.

Conclusion and Implications: These data suggest that olanzapine reduces insulin secretion through a reduction in cytoplasmic β catenin concentration, a protein that is thought to be involved in insulin vesicle trafficking. We propose that addition of BIO, a GSK3 inhibitor, is able to correct these changes through disruption of the β catenin destruction complex leading to increases in cytoplasmic accumulation. We conclude that olanzapine alters β catenin/TCF7L2 signalling in beta cells which leads to a decline in function, and we theorise that this increases risk of hyperglycaemia and diabetes.

Poster Session: Toxicology

P249 | Prospective toxic effects of lead acetate and cadmium sulfate on some myogenic function of urogenital tract in male rats

Safaa Taha; Amira Senbel; Tahia Daabees

Alexandria Faculty of Pharmacy

Background and Purpose: Lower urogenital tract disorders such as overactive bladder, premature ejaculation, and prostate myogenic abnormalities are among the most prevalent disorders worldwide. However, shallow information and insufficient data are available regarding the potential contribution of Pb and Cd in the development of such disorders. This study aims at exploring the potential deleterious effect of these metals on urogenital tract in male rats.

Experimental Approach: In vitro tension studies were performed using isolated rat detrusor muscles, vas deferens and prostate, where the effect of acute treatment (10 min) with Pb acetate (10 mM) or Cd sulfate (0.1 mM) on submaximal direct and electrically induced contractions was tested. Male Wistar rats (weighing 250–270 g) were used, and the tissues were fixed at one end between two parallel platinum electrodes and mounted in a 10-ml organ bath containing Krebs solution, kept at 37°C and continuously aerated with 95% O₂ and 5% CO₂.

Key Results: In detrusor muscle, ACh (10⁻⁴ M) and ES (4 Hz)-induced contractions were significantly reduced from 1.53 ± 0.10 and 1.48 ± 0.09 g, respectively, to 0.79 ± 0.09 and 0.85 ± 0.11 g by Pb and to 0.26 ± 0.06 and 0.52 ± 0.07 g by Cd. In vas deferens, Pb and Cd inhibited PE (10⁻⁵ M) response by 90% and 95%, as well as the ES-induced contractions by 74% and 97%, respectively. In the presence of Cd or Pb, the relaxation concentration–response curve of SNP (10⁻⁹–10⁻³ M) on prostate strips precontracted with PE (10⁻⁵ M) was markedly shifted rightward with a significant decrease in E_{max}. ES-induced contractions were also inhibited.

Conclusion and Implications: According to the observed results, Pb and Cd exerted an inhibitory effect on the contraction of detrusor

muscles, vas deferens and prostate, and these tissues seem to be more vulnerable to Cd than Pb. Further investigation will be executed to explore the interaction with the effective signalling pathway in each tissue.

P250 | Regional differences in the action of cisplatin to affect slow waves in the gastrointestinal tract of house musk shrew (*Suncus murinus*)

Julia Y.H. Liu¹; Peng Du²; John A. Rudd¹

¹The Chinese University of Hong Kong; ²Auckland Bioengineering Institute, University of Auckland

Background and Purpose: The treatment of cancer with cisplatin is often associated with nausea, emesis, and disrupted gastric function, including delayed emptying and an eventual loss of slow wave structure. Slow waves are generated by interstitial cells of cajal (ICC) and have different properties relative to their location in the gastrointestinal tract. Common laboratory animals do not vomit. In the present studies, we investigate if cisplatin differentially affects slow waves of the duodenum, ileum, and colon, of the house musk shrew (*Suncus murinus*), using a 60-channel microelectrode array and a spatiotemporal analytical approach.

Experimental Approach: Male *S. murinus* (45–65 g) were used. The intestines were isolated and transferred into Krebs' medium (in mM): NaCl, 115; KCl, 4.7; KH₂PO₄, 1.2; MgSO₄·7H₂O, 1.2; CaCl₂·2H₂O, 2.5; glucose, 10; NaHCO₃, 25, gassed with 95/5% oxygen/carbon dioxide at 37°C; 1-cm lengths of tissue were incubated further with Krebs containing nifedipine (1 μM) for 15 min before the serosal side was placed directly onto the recording field of a microelectrode array (8 × 8 3-D electrodes, diameter of 30 μm, spacing at 200 μm); data were sampled at 1 kHz (MEA1060 1200x, Multichannel systems, Germany). We recorded 5 min of basal activity before incubating further with cisplatin at 1–10 μM for a further 5–6 min.

Key Results: In the duodenum, cisplatin (10 μM) reduced the frequency of slow waves from 26.4 ± 1.8 (mean ± SD) to 24.6 ± 1.4 cpm ($P < .05$, $n = 8$); it also increased the propagation velocity from 35.6 ± 26.3 to 75.4 ± 53.9 mm·s⁻¹ ($P < .05$, $n = 6$). In the colon, cisplatin (10 μM) increased slow wave frequency from 24.9 ± 1.1 to 26.8 ± 1.0 cpm ($P < .001$, $n = 7$), but reduced propagation velocity from 7.3 ± 4.5 to 5.3 ± 1.4 mm·s⁻¹ ($P < .05$, $n = 6$). Conversely, cisplatin did not affect the slow waves recorded from the ileum (basal slow wave frequency was 25.1 ± 2.2 cpm; propagation velocity was 21.9 ± 18.7 mm·s⁻¹).

Conclusion and Implications: Our studies show that cisplatin may have acute actions on slow waves recorded from different regions of the gastrointestinal tract. The mechanism of action to disrupt slow waves is not known, nor is the reason behind the regional differences that we observed.

P251 | Inducing a zebrafish model of visual dysfunction using the anti-malarial amodiaquine dihydrochloride dihydrate

Alison Reynolds; Susan Obaseki

University College Dublin

Background and Purpose: Long-term use of anti-malarials (e.g., amodiaquine hydrochloride and hydroxychloroquine) has previously been reported to cause retinopathies (ref). This preliminary study investigates whether treatment with amodiaquine hydrochloride can induce visual dysfunction in larval zebrafish.

Experimental Approach: Amodiaquine dihydrochloride dihydrate (Sigma) was dissolved in water and diluted into embryo medium for experiments. Wild-type (Tuebingen) zebrafish (*Danio rerio*) were drug treated from 1 to 5 days post fertilization (dpf) by immersion using increasing concentrations (10–100 μM) of amodiaquine ($N = 5$ –10 zebrafish per treatment with three replicates per treatment). Survival and gross morphology were assessed. Visual behaviour was

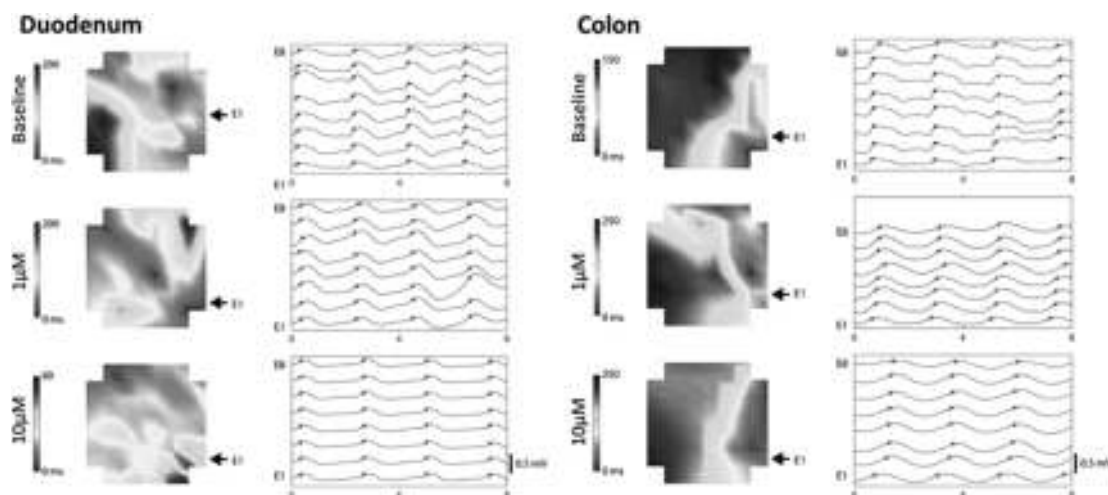


FIGURE 1. Representative activation maps under cisplatin treatment (1–10 μM) in the duodenum and colon of the *Suncus murinus*

investigated using the optokinetic response (OKR) and visual motor response (VMR). Retinal histology (light microscopy) was examined. A one-way ANOVA using Dunnett's post hoc correction was used to compare drug treatments to control.

Key Results: Concentrations of amodiaquine above 70 μM resulted in a shortening of the caudal fin (not quantified), and treatment with 100- μM amodiaquine reduced survival to 73% of control. Treatment with amodiaquine attenuated the optokinetic response in a dose-dependent fashion; 80- μM amodiaquine reduced the OKR from 21.4 (control) to 11.93 saccades- min^{-1} (P value < .001) and 100 μM to 6.8 saccades- min^{-1} (P value < .001) ($N = 5, n = 3$). Preliminary VMR data suggest that 100- μM amodiaquine destroys the visual motor response in all larvae tested. Retinal histology showed that treatment with 100- μM amodiaquine resulted in a shortening of the photoreceptor outer segments in the central retina and a reduction in the number of rows of photoreceptors.

Conclusion and Implications: Preliminary results reveal that concentrations of amodiaquine above 70 μM have a retinotoxic effect on larval zebrafish, resulting in an inhibition of visual behaviour and retinal histology. Further investigation of the effects of amodiaquine on visual function is required. In future, it may be possible to use amodiaquine-induced visual dysfunction in zebrafish to investigate underlying mechanisms of and treatments for retinopathies.

REFERENCES

- Adjei, G. O., Adabayeri, V. M., & Annobil, S. H. (2012). Reversible binocular visual loss in temporal association with artesunate-amodiaquine treatment in a child on mefloquine chemoprophylaxis. *Ghana Medical Journal*, 46(3), 171–173.
- Yusuf, I. H., Sharma, S., Luqmani, R., & Downes, S. M. (2017). Hydroxychloroquine retinopathy. *Eye (London, England)*, 31(6), 828–845. <https://doi.org/10.1038/eye.2016.298>

P252 | Treatment with protocatechuic acid attenuates brain toxicity induced by cisplatin in male albino rats

Adebukola Adeyanju¹; Olorunfemi Molehin²; Babatunde Oso³; Joshua Fadero³; Busayo Odulote³

¹KolaDaisi University Ibadan; ²University of Ado Ekiti, Ekiti, Nigeria;

³McPherson University, Ogun State

Background and Purpose: Cisplatin has demonstrated efficacy against various types of cancers. However, its use in clinical chemotherapy is limited on account of its lethal cytotoxic effects, among which is brain toxicity (Aldossary, 2019). Its mechanism of inducing this toxicity has been associated with oxidative stress. Hence, there is need for effective compounds that can protect against cisplatin toxicity to allow for its safer use in clinical practice. Study has revealed that protocatechuic acid (PCA) contributed to the prevention of oxidative stress in the brain of diabetic rats (Semaming et al., 2015). Here, we

investigate the possible protective effect of protocatechuic acid in brain toxicity caused by cisplatin.

Experimental Approach: Male albino rats in the control group received normal saline while Group II was exposed to single dose of cisplatin (10 $\text{mg}\cdot\text{kg}^{-1}$) intraperitoneally. Groups III and IV received protocatechuic acid at 10 and 20 $\text{mg}\cdot\text{kg}^{-1}$, respectively, for 5 days orally before cisplatin administration. Group V received protocatechuic acid only (20 $\text{mg}\cdot\text{kg}^{-1}$). On the sixth day, animals were killed by cervical dislocation. The brain was removed, minced with scissors in potassium phosphate buffer, pH 7.4, and homogenized. The homogenate was centrifuged at 14,000 rpm for 15 min at 4°C to yield the post mitochondrial fractions which was used for biochemical assays. In addition, immunohistochemical staining was performed on brain samples obtained from rats. Statistical significance was determined using ANOVA and Newman-Keuls multiple comparisons test.

Key Results: Table 1 shows that rats exposed to cisplatin had a decline in the activities of antioxidant enzymes GSH-S-transferase (GST) ($P > .05$), catalase (CAT) ($P < .01$), and SOD ($P > .05$). Reduced GSH level, a non-enzymic antioxidant, was also reduced ($P > .05$), while lipid peroxidation was significantly induced by increase in malondialdehyde (MDA) level. This is an indication of oxidative stress and toxicity by cisplatin in the brain. However, PCA treatment offered protection especially at the dose of 20 $\text{mg}\cdot\text{kg}^{-1}$ by elevating the activities of GST ($P > .05$), CAT ($P < .05$), and SOD ($P > .05$), while GSH level was significantly increased, and lipid peroxidation significantly decreased ($P < .05$). Additionally, the immunohistochemical staining revealed that PCA treatment prevented NF- κB expression in rats.

Conclusion and Implications: Findings suggest that PCA may facilitate antioxidant defence system as well as activate anti-apoptotic signalling pathways in protection against brain toxicity caused by cisplatin.

REFERENCES

- Aldossary, S. A. (2019). Review on pharmacology of cisplatin: Clinical use, toxicity and mechanism of resistance of cisplatin. *Biomedical and Pharmacology Journal*, 12(1), 7–15.
- Semaming, Y., Sripetchwandee, J., Sa-Nguanmoo, P., Pintana, H., Pannangpetch, P., Chattipakorn, N., & Chattipakorn, S. C. (2015). Protocatechuic acid protects brain mitochondrial function in streptozocin-induced diabetic rats. *Applied Physiology, Nutrition, and Metabolism*, 40(10), 1078–1081.

TABLE 1 Effect of treatment with PCA in cisplatin-induced toxicity in rat brain

Group	Treatment group	GST (nmol·g ⁻¹ tissue)	GSH (μg·g ⁻¹ kidney weight)	MDA (nmol·mg ⁻¹ protein)	CAT H ₂ O ₂ (μmol consumed·min ⁻¹)	SOD (U·mg ⁻¹ protein)	NF-κB expression (magnification ×400)
I	Control	1.9 ± 0.49	3.81 ± 1.70	1.36 ± 0.83	5.25 ± 0.11	0.25 ± 0.16	Absent (0)
II	Cisplatin (10 mg·kg ⁻¹)	0.37 ± 0.19	3.11 ± 0.77	4.18 ± 0.84 [#]	1.00 ± 0.01 [*]	0.15 ± 0.02	Weak (+)
III	Cisplatin + PCA (10 mg·kg ⁻¹)	0.63 ± 0.24	3.13 ± 0.45	1.33 ± 0.31 ^{##}	2.20 ± 0.73	0.17 ± 0.03	Absent (0)
IV	Cisplatin + PCA (20 mg·kg ⁻¹)	3.85 ± 0.02	4.58 ± 0.43 ^{##}	3.30 ± 0.62	4.20 ± 0.58 ^{**}	0.33 ± 0.11	Absent (0)
V	PCA only (20 mg·kg ⁻¹)	2.60 ± 0.94	7.93 ± 0.66 [#]	2.74 ± 0.42	5.00 ± 0.71	0.30 ± 0.12	Absent (0)

Note. Values are expressed as mean of five replicates ± SEM.

Abbreviation: PCA, protocatechuic acid.

^{*}Significantly different from control ($P < .01$).

^{**}Significantly different from cisplatin-treated rats ($P < .01$).

[#]Significantly different from control ($P < .05$).

^{##}Significantly different from cisplatin-treated rats ($P < .05$).

Oral Communications, Tuesday 17th December, 14:15

Education and Skills Oral Communications 1

OC073 | Building capacity for laboratory animal sciences and ethics across Africa

Dave Lewis¹; John Chipangura²; Tamsyn Fourie³; Louise F. Martin⁴; Bert Mohr²; Ouajdi Souilem⁵

¹University of Leeds; ²University of Cape Town; ³SAALAS & LAS Veterinary Consultancy; ⁴University of Zurich; ⁵Ecole Nationale de Médecine Vétérinaire de Sidi Thabet

Background and Purpose: African nations face many challenges including the prevention of diseases and promoting sustainable health and well-being in their populations. Many are looking to the development of their Pharma industries both to address these challenges and to create economic development. However, there is a severe shortage across Africa of individuals with the necessary knowledge, skills, and expertise to undertake the required animal studies. There is a substantial need for introductory courses in laboratory animal sciences and ethics, upskilling and continuing professional development for established personnel, and the sharing of good practice. The aim of this project was to create and deliver sustainable “Train the Trainer” programmes in laboratory animal sciences and ethics across Africa.

Experimental Approach: In partnership with African colleagues, animal welfare organisations, and the IUPHAR IOSP initiative, two “Train the Trainer” courses were created and co-delivered in South Africa and Tunisia. Participants (78 from 14 countries) included researchers, vets, animal care staff, and research ethics committee members. Topics covered included animal welfare; 3Rs; legislation; ethical review;

experimental design and reporting; and animal handling. To ensure sustainability and growth of the initiative beyond these two courses, participants were provided with the educational tools and all resources used, the expectation being that they deliver at least two courses in their own networks. In addition, the first guidelines for animal ethics committees in Africa were created. Participants were required to submit a post-course essay in which they reflected on their main learning, the changes they intend to make in their personal and professional practices, and their plans for sharing their knowledge with colleagues.

Key Results: The courses had a significant impact on participants, resulting in them changing their own practices, sharing the good practice with colleagues, and implementing change in their own institutions. They empowered many to speak up for animals facilitating the development of a culture of care. Delivery as “Train the Trainer” courses has ensured that the initiative is not only sustained but also grows, a model that can be used elsewhere in the Emerging World. Given that animal ethics committees are in their infancy or non-existent in many African countries, the developed guidelines will greatly facilitate their introduction and development across the continent, for the betterment of animal welfare and science.

Conclusion and Implications: This intervention clearly demonstrates the benefits of collaborative partnerships between the Emerging and Developed Worlds, sharing good practice and working together to build research capacity and skills in the Emerging World.

Molecular and Cellular Pharmacology Oral Communications 3

OC060 | Cannabinoid sensitive receptors as novel biomarkers and therapeutic targets for chronic lymphocytic leukaemia

Joshua Dyson; Mark Mitra; Charlotte Lennon; Mark Vickers; Roger Pertwee; Fiona Murray

University of Aberdeen

Background and Purpose: Chronic lymphocytic leukaemia (CLL) is a hematologic malignancy, characterized by the accumulation of mature CD11 B cells. Patients can have indolent disease with minimal clinical manifestations or an aggressive form characterized by high mortality. Endocannabinoids, such as anandamide and 2-arachidonoyl glycerol, which are endogenous cannabinoids are anti-proliferative and proapoptotic in lymphoma and leukaemia (McKallip et al., 2006). We aimed to investigate the expression of cannabinoid sensitive receptors in normal and CLL cells (both from indolent and aggressive CLL patients) and determine the response of CLL cells to their ligands.

Experimental Approach: Human B cells were isolated from healthy controls and CLL patients (with indolent and aggressive stages, CLL cells) using anti-CD11 conjugated magnetic microbeads (ThermoFisher). The expression of cannabinoid sensitive receptors was detected using real-time PCR. CLL in the presence/absence of stromal cells were co-cultured for 72 hr in the presence/absence of cannabinoid receptor ligands, and cell viability was investigated using Annexin V FITC and PI (FACs, ThermoFisher) and MTS proliferation assay (Promega). Data are presented as means \pm SEM and compared by ANOVA or Student's *t* test.

Key Results: Real-time PCR showed the relative expression of the cannabinoid sensitive receptors in CLL cells to be GPR18 > CB2 > CB1 > GPR55 > GPR119 ($n = 10$). Of interest, the expression of CB2 was increased in CLL cells (2.6 ± 0.6 -fold, $n = 10$), whereas GPR55 was decreased (20.2 ± 11.4 -fold, $n = 10$) when compared to healthy B cells. CB2 expression was found to be higher in aggressive CLL cells (>4-fold increase) compared to indolent CLL cells (<4-fold increase). A CB2-selective agonist (JWH-133) enhanced the number of viable CLL cells; however, cannabidiol (CBD) induced apoptosis of CLL cells ($82.3 \pm 3.4\%$ viability, $n = 3$, $P < .5$) even in the presence of stromal cells ($88.9 \pm 4.6\%$ viability, $n = 3$, $P < .5$).

Conclusion and Implications: In conclusion, the data show that CB2 expression is up-regulated, whereas GPR55 expression is down-regulated in CLL cells; CB2 may be a novel biomarker for disease progression. Cannabinoids, such as CBD, may have clinical utility for CLL.

REFERENCE

McKallip, et al. (2006). *Molecular Pharmacology*, 70, 897–908.

OC061 | Potential role of farnesoid X receptor activation in non-alcoholic steatohepatitis-associated hepatocellular carcinoma

Yasmeen Attia¹; Rasha Tawfiq¹; Aya Ali¹; Abdullah Gibriel¹; Olfat Hammam²; Mohamed Elmazar¹

¹The British University in Egypt; ²Theodor Bilharz Research Institute

Background and Purpose: Non-alcoholic steatohepatitis (NASH) has recently become the main aetiology for hepatocellular carcinoma (HCC) although historically, viral hepatitis was the main cause for the disease. NASH is also becoming a top indication for liver transplantation since global prevalence is rapidly growing. Besides the well-known effects of farnesoid X receptor (FXR), a bile-acid-activated nuclear receptor, on metabolic disorders including NASH, its role as a tumour suppressor was recently described. Moreover, the FDA-approved FXR agonist, obeticholic acid (OCA), has demonstrated anti-proliferative effects on HCC cell lines by interfering with IL-6/STAT3 pathway (Attia et al., 2017). Herein, we expand on these findings investigating the effect of OCA in an in vivo model of NASH-associated HCC (Attia et al., 2019).

Experimental Approach: Three-week-old Swiss albino male mice were randomly allocated into normal, control untreated, and OCA-treated groups. Mice in control and treated groups received a one-time i.p. injection of 25 mg·kg⁻¹ diethyl-nitrosamine and was kept on a high-fat choline-deficient diet during the entire experimental period. Normal group received vehicles and was kept on a balanced diet. Treatment with OCA (10 mg·kg⁻¹·day⁻¹, p.o.) was initiated after 20 weeks of induction for a duration of 8 weeks. Histopathological analysis was conducted. Immunohistochemical staining (IHC) of liver sections using monoclonal antibodies against α -fetoprotein (AFP) and STAT3 was also performed. IHC results were analysed in a blinded semi-quantitative manner. Tissue levels of IFN- γ were also determined using ELISA. Additionally, gene expression analysis of tissue FXR and p53 was performed using qRT-PCR. Data are presented as mean \pm SD ($n = 10$). Statistical significance ($P < .05$) was determined using one-way ANOVA followed by Tukey's post hoc test.

Key Results: Histopathological evaluation showed that OCA caused an amelioration in dysplastic foci. Immunostaining showed a significant decrease in the percentage of AFP positively stained liver cells in OCA-treated group ($32.6 \pm 5.7\%$) compared to control ($64.2 \pm 4.3\%$). Also, a significant decrease in STAT3 immunohistochemical expression was reported in OCA-treated group ($46.8 \pm 4.7\%$) compared to control ($62 \pm 2.1\%$). OCA significantly reduced IFN- γ hepatic levels (61.4 ± 45.3 ng·ml⁻¹) relative to control (324.3 ± 36.4 ng·ml⁻¹). Moreover, OCA caused an up-regulation in both FXR and p53 genes (Table 1).

Conclusion and Implications: Activation of FXR by OCA attenuated the development and progression of NASH-dependent HCC. These

TABLE 1 Gene expression analysis using qRT-PCR for FXR and p53 as fold change normalized against normal

Group	Gene expression (fold change normalized against normal expressed as mean \pm SD)	
	FXR	P53
Control untreated	0.07 \pm 0.06	0.85 \pm 0.42
OCA treated	2.9 \pm 1.62*	9.18 \pm 1.6*

*Significant at $P < .05$ versus control untreated group.

findings suggest its use in NASH patients to impede its progression to HCC.

REFERENCES

- Attia, Y. M., et al. (2017). *Scientific Reports*, 7(1), 12502.
 Attia, Y. M., et al. (2019). *Journal of Hepatology*, 70(1), e520. EASL meeting 2019

OC062 | Anti-cancer effects of differentiation-inducing factor-1 in triple negative breast cancer 4T1/Luc cell

Fumi Tetsuo¹; Masaki Arioka¹; Fumi Takahashi-Yanaga²; Shunichi Kajioaka¹; Fusanori Nishimura¹; Toshiyuki Sasaguri¹

¹Kyushu University; ²School of Medicine, University of Occupational and Environmental Health

Background and Purpose: Triple negative breast cancer (TNBC) is the most aggressive subtype of breast cancer frequently forming metastatic lesions, and its resistance to conventional treatments markedly exacerbates patients' prognosis. Therefore, novel therapeutic measures are required. Differentiation-inducing factor-1 (DIF-1) was identified in *Dictyostelium discoideum* (Figure 1a) (Morris, Taylor, Masento, Jermyn, & Kay, 1987). Here, we investigated whether DIF-1 shows anti-proliferative and anti-metastatic effects on TNBC by in vivo and in vitro experiments.

Experimental Approach: In vivo, we used cancer xenograft model mice. Murine TNBC 4T1/Luc cells were trypsinized and resuspended in 50% Matrigel in PBS at a concentration of $\times 10^7$ cells·ml⁻¹. The suspension (0.1 ml) was injected into the left #4 mammary fat pads to evaluate the effects of intragastric administration of DIF-1 suspended in soybean oil (300 mg·kg⁻¹·day⁻¹, every 12 hr 5 days a week) on the primary tumour growth and lung metastasis. In vitro, we used 4T1/Luc and siSTAT3- and siSnail-transfected 4T1/Luc cells. We carried out assays for cell proliferation, migration, and invasion to evaluate the anti-proliferative and anti-metastatic effects of DIF-1. We also conducted Western blotting and real-time RT-PCR to identify the mechanisms for DIF-1's anti-cancer effects. Differences between means were analysed by Student's *t* test, one-way ANOVA with the Bonferroni post hoc test.

Key Results: In vivo, administration of DIF-1 suppressed the primary tumour growth (Figure 1b) and lung metastasis (Figure 1c) without adverse effects (Figure 1d). In vitro, DIF-1 reduced cyclin D1 ($n = 3$; $P < .05$ vs. control) by inhibiting transcription and promoting degradation of the

protein via reduction of STAT3 expression. We examined the correlation between STAT3 and cyclin D1 using siSTAT3-transfected 4T1/Luc cells. Knockdown of STAT3 suppressed cyclin D1 expression ($n = 3$; $P < .01$ vs. control). DIF-1 also suppressed cell migration ($n = 3$; $P < .001$ vs. control) and invasion ($n = 3$; $P < .001$ vs. control) via reduction of snail ($n = 3$; $P < .05$ vs. control), crucial factors in epithelial-mesenchymal transition (EMT), vimentin ($n = 3$; $P < .05$ vs. control), and MMP-2 ($n = 3$; $P < .05$ vs. control) mesenchymal markers. We also performed cell migration and invasion assay using siSnail-transfected 4T1/Luc cells. Knockdown of Snail suppressed cell migration ($n = 3$; $P < .01$ vs. control) and invasion ($n = 3$; $P < .05$ vs. control) in 4T1/Luc cells.

Conclusion and Implications: DIF-1 exerts anti-cancer effects in TNBC by reducing cyclin D1 and reversing EMT. Our findings suggest that using DIF-1 as a lead compound could develop a novel anti-cancer agent for TNBC.

REFERENCE

- Morris, H. R., Taylor, G. W., Masento, M. S., Jermyn, K. A., & Kay, R. R. (1987). Chemical structure of the morphogen differentiation inducing factor from *Dictyostelium discoideum*. *Nature*, 328(6133), 811–814.

OC063 | P2X7 receptor signalling in normal and cancer urothelial cells

Karen McCloskey; James Boncan; Conor Breen; Niamh McKerr

Queen's University Belfast

Background and Purpose: Urothelial cancer is the ninth most common cancer worldwide and represents an area of unmet clinical need. Urothelial cells express a number of purinergic receptors (P2), and these have been implicated in urothelial cancer (Shabbir et al., 2007). P2X7 is an ionotropic ATP-gated receptor which acts as a non-selective cation channel and may also form large pores. P2X7 activation has been implicated in pro-tumourigenic processes across several cancer types. The aim of this study was to investigate the expression and function of P2X7 in urothelial cancer cells.

Experimental Approach: Immortalised normal urothelial cells, SVHUC, and urothelial cancer cells, HT1376 and T24, were used. Western blot and immunofluorescence protocols were used to assess P2X7 protein expression. Functional expression of purinergic receptors was tested in live-cell Ca²⁺-imaging experiments and cell viability assays. YO-PRO-1 dye uptake assays were performed to test for pore formation. Scratch wound assays were performed to evaluate changes in cell migration. At least three independent experiments were performed in each series. Data were analysed using Excel and Graphpad Prism for descriptive statistics and statistical tests including ANOVA and *t* tests where $P < .05$ was considered as significant.

Key Results: Immunofluorescence showed protein expression of P2X7R in the three cell lines. Western blotting indicated that P2X7R expression was higher in HT1376. SVHUC, HT1376, and T24 responded to ATP (1 mM) with Ca²⁺ transients that were reduced in the absence of extracellular Ca²⁺ ($N = 3$, each cell line). ATP-evoked

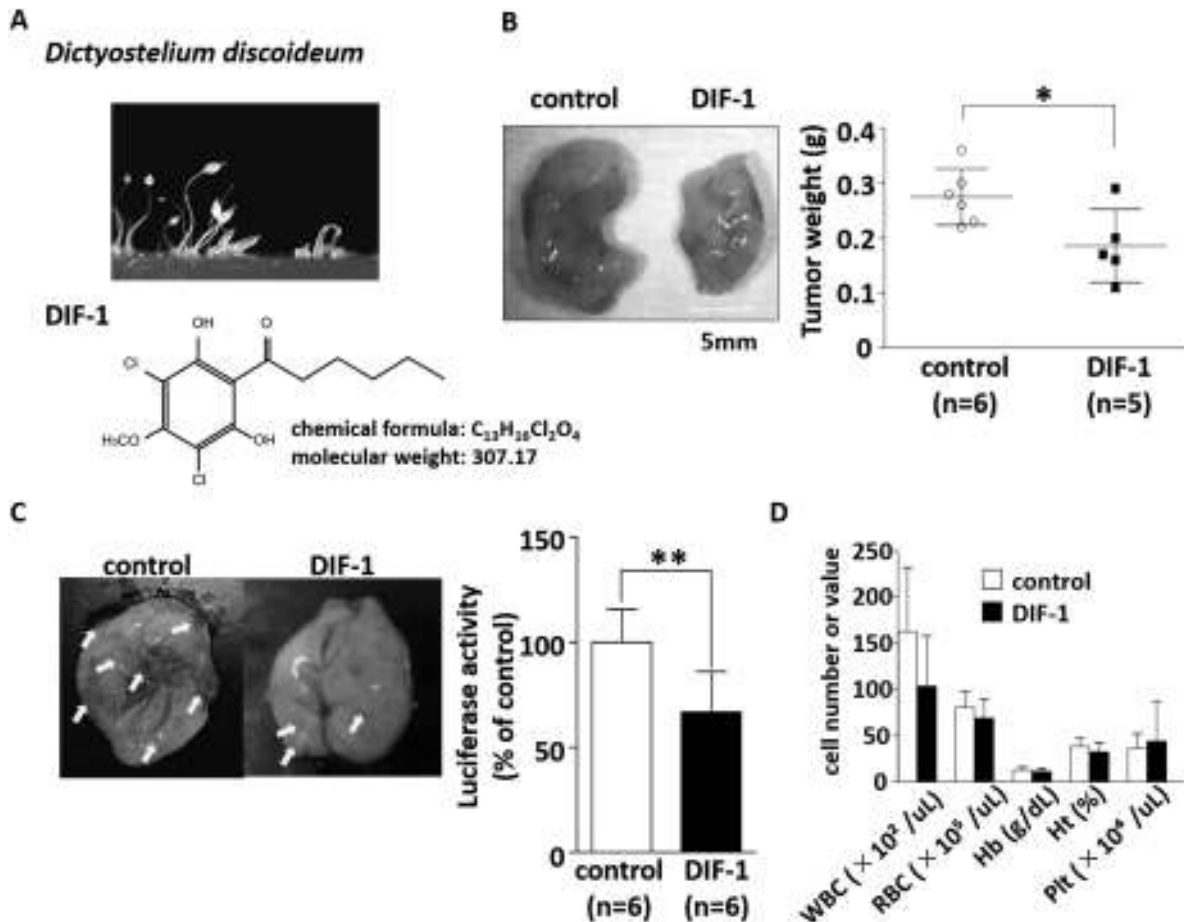


FIGURE 1. DIF-1 inhibited cell proliferation and metastasis without side effects in 4T1/Luc cells. * $P < .05$; ** $P < .01$ versus control

Ca²⁺ transients were reduced by the P2X7R antagonist A740003 (10 μM, N = 3). The P2X7R agonist 3'-O-(4-benzoyl)benzoyl-ATP (BzATP; 0.5 mM) evoked Ca²⁺ transients in HT1376. In pore formation assays, ATP did not evoke development of pores in any of the cell lines; however, BzATP induced pore formation in a sub-population of HT1376 and in positive control bone marrow-derived macrophages. In SVHUC and T24, ATP (1 mM) inhibited cell migration (fold wound closure 52% and 62%, respectively, both $P < .05$). These effects were not impacted by A438079 (10 μM, N = 3) nor A740003 (10 μM, N = 3). ATP (1 μM–10 mM) reduced cell viability in the three cell lines in a concentration-dependent fashion. The concentration–response curves were unaffected by A740003 (10 μM, N = 3).

Conclusion and Implications: These experiments indicate functional expression of P2X7 in normal urothelial cells and urothelial cancer cells. The data suggest that P2X7 activation enabled Ca²⁺ influx; however, pore formation was uncommon. ATP signalling reduced urothelial cell migration and negatively impacted viability; these effects were apparently independent of P2X7 signalling, indicating involvement of other purinergic receptors.

REFERENCE

Shabbir, M., Ryten, M., Thompson, C., Mikhailidis, D., & Burnstock, G. (2008). Purinergic receptor-mediated effects of ATP in high-grade bladder cancer. *BJU International*, 101(1), 106–112.

OC064 | Development of long-acting β2-selective antagonists as a potential treatment to reduce tumour growth and metastasis

Jillian Baker; Christophe Fromont; Richard Proudman; Barrie Kellam; Peter Fischer

University of Nottingham

Background and Purpose: β-Antagonists, acting via β2-adrenoceptors (AR), may reduce cancer growth and metastasis; however, most clinical β-antagonists are relatively short-acting, non-selective ligands. To minimise cancer growth and metastasis and minimise side effects of long-term cardiac β1-blockade, long-acting β2-selective antagonists may be optimal. Salmeterol is a highly β2-selective agonist. The head group (salbutamol) binds within the transmembrane (TM) domains. The alkyloxyphenyl side chain binds to a unique β2-exosite in extracellular loop (EL) 2 and 3 and the extracellular ends of TM6 and TM7. This additional alkyloxyphenyl chain gives salmeterol higher β2 affinity and β2 selectivity and longer duration of action than salbutamol (Baker et al., 2015; Masureel et al., 2018). This study aimed to produce long-acting β2-selective antagonists.

Experimental Approach: Salmeterol's alkyloxyphenyl chain (C6-O-C4-phenol) and chains with the O atom in different positions were added to three antagonists: S-propranolol, ICI118551, and bupranolol. Compounds were studied using ^3H -CGP12177 whole cell binding (affinity, selectivity, and duration of binding) and ^3H -cAMP production in CHO cells stably expressing the human β_1 , β_2 , or $\beta_2\text{K305D}$ (a single point mutation in EL3 important for salmeterol binding) as previously described (Baker et al., 2015).

Key Results: Alkyloxyphenyl chain additions increased β_2 selectivity of three different β -antagonists, but unlike salmeterol, more by reducing β_1 affinity rather than increasing β_2 affinity (Table 1). The O atom position was crucial: C5-O-C4 chains had maximal β_2 selectivity although C7-O-C3 chains were most sensitive to the K305D mutation. Duration of ligand binding was examined with washout assays (Baker et al., 2015). Washout of propranolol, ICI118551, and bupranolol gave right-shifted binding inhibition curves compared with control (β_2 -AR, log shift S-propranolol 1.66 ± 0.27 , $n = 4$; ICI118551 0.86 ± 0.10 , $n = 8$; bupranolol 1.41 ± 0.6 , $n = 3$). No rightward shift was seen following washout of any novel alkyloxyphenyl chain ligand ($n = 4$), suggesting longer duration of binding. Although ^3H -cAMP agonist responses occurred with salbutamol and salmeterol, no agonist responses were seen to any of the novel ligands tested ($n = 3-4$).

Conclusion and Implications: Adding alkyloxyphenyl side chains to β -antagonists does result in compounds with higher β_2 selectivity and longer duration of action without inducing any agonism. These pharmacological characteristics may be more useful for examining reduction of cancer growth than current clinically available β -blockers.

REFERENCES

- Baker, J. G., et al. (2015). *Molecular Pharmacology*, 87, 103–120.
Masureel, M., et al. (2018). *Nature Chemical Biology*, 14, 1059–1066.

Neuropharmacology Oral Communications 2

OC065 | Antiepileptic potentials of lupeol from *Sterculia setigera*

Maryam Adenike Salaudeen; Mohammed Garba Magaji;
Muben Danjuma

Ahmadu Bello University, Zaria, Nigeria

Background and Purpose: The prevalence of epilepsy still remains at its peak in low- and middle-income countries like Nigeria. This together with serious untoward effects of conventional anti-epileptic agents and refractoriness of some epilepsy necessitates the search for novel anticonvulsants with better efficacy and safety profiles. *Sterculia setigera* has been reportedly used in traditional medicine in the management of epilepsy. Steroids have been used in the treatment of intractable and

infantile epilepsy for ages (Prasad, Stafstrom, Holmes, 1996). This study therefore aims at investigating the anticonvulsant activity of lupeol, a steroidal compound derived from the leaves of *S. setigera*.

Experimental Approach: The anticonvulsant activity of lupeol ($6.25-50 \text{ mg}\cdot\text{kg}^{-1}$) was evaluated using the maximum electroshock test (MEST) in day-old chicks and pentylenetetrazol (PTZ) model in mice. In the MEST model, six groups of six chicks each were used and treated with normal saline, phenytoin ($20 \text{ mg}\cdot\text{kg}^{-1}$, i.p.), and the graded dose of lupeol. Animals were allowed 30 min post-treatment period before the application of electroshock via corneal electrodes using the following electrical parameters: current of 80 mA, frequency of $100 \text{ Hz}\cdot\text{s}^{-1}$, pulse rate of $0.6 \text{ m}\cdot\text{s}^{-1}$, and shock duration of 0.6 s. The quantal protection and the recovery time from tonic hind limb extension (THLE) were recorded. In the PTZ model, adult male Swiss Albino mice were used and were divided into six groups of six mice each treated with normal saline, graded lupeol doses, and sodium valproate ($200 \text{ mg}\cdot\text{kg}^{-1}$, i.p.). After 30 min post-treatment, each mouse was administered with $85 \text{ mg}\cdot\text{kg}^{-1}$ pentylenetetrazole, i.p. The ability of the compound to protect the mice from clonic spasm of at least 5-s duration was considered as index of anticonvulsant activity. The onset of seizure in unprotected animals was also recorded.

Key Results: For the MEST, lupeol at all doses tested did not protect the chick from tonic hind limb extension (THLE). It also did not significantly reduce the recovery time after THLE at doses used. In the PTZ model, lupeol significantly ($P < .001$) reduce the onset of seizure/increase seizure threshold at 25 and $50 \text{ mg}\cdot\text{kg}^{-1}$.

Conclusion and Implications: Lupeol possesses moderate anticonvulsant activity and can therefore be a potential lead compound in the development of novel anticonvulsants.

REFERENCE

- Prasad, A. N., Stafstrom, C. F., & Holmes, G. L. (1996). Alternative epilepsy therapies: The ketogenic diet, immunoglobulins, and steroids. *Epilepsia*, 37, S81–S95.

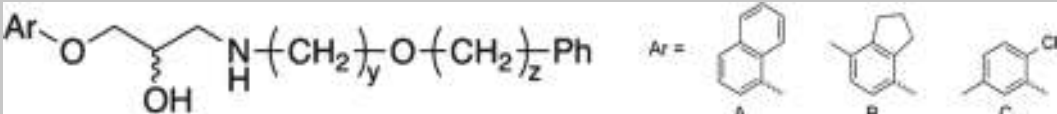
OC066 | Investigating the cold induced vascular response in ageing

Dibesh Thapa; Joao Valente; Fulye Argunhan; Sheng Lee;
Brentton Barrett; Susan Brain

King's College London

Background and Purpose: It is well known that older subjects are not able to maintain their core body temperature compared to younger subjects, which makes them susceptible to various secondary complications as we have witnessed with NHS winter crisis. Cold induces a biphasic vascular response of brief vasoconstriction followed by a prolonged vasodilation. It is a crucial physiological response that prevents drop in core body temperature, which otherwise could cause cellular dysfunctions and can lead to serious cardiovascular complications. We have shown that cold induced signalling is highly dependent on transient receptor potential (TRP)

TABLE 1 Affinity (pK_D values, mean \pm SEM of n values) and selectivity of ligands for the β_2 -AR versus β_1 -AR as determined from ^3H -CGP 12177 whole cell binding



Ar	y	z	CHO- β_1	CHO- β_2	β_2/β_1 selectivity	CHO- $\beta_2\text{K305D}$	$\beta_2/\beta_2\text{K305D}$ selectivity	
Salbutamol			4.80 \pm 0.04 (6)	5.89 \pm 0.03 (6)	12	-5.78 \pm 0.06 (6)	1.3	
Salmeterol	6	4	5.71 \pm 0.07 (7)	8.87 \pm 0.07 (7)	1,445	-7.41 \pm 0.06 (6)	28.8	
S-propranolol			8.50 \pm 0.03 (4)	9.44 \pm 0.05 (4)	9	9.49 \pm 0.11 (4)	0.9	
1	A	2	8	5.99 \pm 0.03 (4)	7.36 \pm 0.11 (4)	23	6.94 \pm 0.08 (4)	2.6
2	A	3	7	5.98 \pm 0.06 (4)	7.52 \pm 0.08 (4)	35	7.04 \pm 0.04 (4)	3.0
3	A	4	6	6.64 \pm 0.04 (6)	8.19 \pm 0.09 (6)	35	7.49 \pm 0.04 (6)	5.0
4	A	5	5	6.89 \pm 0.03 (6)	9.15 \pm 0.11 (5)	182	8.22 \pm 0.05 (6)	8.5
5	A	5	4	7.03 \pm 0.03 (4)	9.60 \pm 0.11 (4)	372	9.15 \pm 0.05 (4)	2.8
6	A	6	4	6.89 \pm 0.04 (6)	9.11 \pm 0.07 (6)	166	8.13 \pm 0.07 (6)	9.5
7	A	6	3	7.01 \pm 0.05 (4)	9.30 \pm 0.09 (4)	195	8.42 \pm 0.10 (4)	7.6
8	A	7	3	6.69 \pm 0.03 (6)	9.06 \pm 0.08 (6)	234	7.75 \pm 0.02 (5)	20.4
9	A	7	2	6.90 \pm 0.06 (4)	9.27 \pm 0.11 (4)	234	8.68 \pm 0.11 (4)	3.9
10	A	8	2	6.71 \pm 0.04 (6)	8.50 \pm 0.05 (6)	62	7.65 \pm 0.06 (6)	7.1
11	A	9	1	6.23 \pm 0.05 (4)	7.52 \pm 0.09 (4)	19	7.16 \pm 0.06 (4)	2.3
12	A	10	0	6.09 \pm 0.06 (4)	7.23 \pm 0.05 (4)	14	6.90 \pm 0.06 (4)	2.1
\pm ICI118551			6.73 \pm 0.02 (9)	9.09 \pm 0.04 (9)	245	9.05 \pm 0.03 (9)	1.1	
13	B	2	8	5.80 \pm 0.03 (4)	6.91 \pm 0.04 (4)	13	6.78 \pm 0.01 (4)	1.3
14	B	3	7	6.19 \pm 0.06 (4)	7.72 \pm 0.09 (4)	34	7.02 \pm 0.02 (4)	5.0
15	B	4	6	6.34 \pm 0.03 (4)	8.07 \pm 0.01 (4)	54	7.42 \pm 0.10 (4)	4.5
16	B	5	5	6.35 \pm 0.04 (6)	8.85 \pm 0.02 (6)	316	7.95 \pm 0.03 (6)	7.9
17	B	5	4	6.53 \pm 0.03 (4)	9.43 \pm 0.11 (3)	794	8.92 \pm 0.08 (4)	3.2
18	B	6	4	6.74 \pm 0.02 (4)	9.17 \pm 0.16 (4)	269	8.08 \pm 0.05 (4)	12.3
19	B	6	5	6.35 \pm 0.03 (6)	8.76 \pm 0.05 (6)	257	7.79 \pm 0.09 (6)	9.3
20	B	7	3	6.37 \pm 0.04 (6)	8.79 \pm 0.05 (6)	263	7.54 \pm 0.04 (6)	17.8
21	B	7	2	6.57 \pm 0.03 (4)	9.04 \pm 0.09 (4)	295	8.28 \pm 0.06 (4)	5.8
22	B	8	2	6.05 \pm 0.05 (4)	7.86 \pm 0.08 (4)	65	7.15 \pm 0.05 (4)	5.1
23	B	9	1	5.99 \pm 0.04 (4)	7.58 \pm 0.11 (4)	39	7.13 \pm 0.04 (4)	2.8
24	B	10	0	5.92 \pm 0.04 (4)	7.10 \pm 0.05 (4)	15	6.90 \pm 0.06 (4)	1.6
\pm Bupranolol			8.77 \pm 0.03 (3)	9.76 \pm 0.04 (4)	10	9.65 \pm 0.03 (4)	1.3	
25	C	5	5	6.79 \pm 0.01 (4)	9.27 \pm 0.11 (4)	302	8.24 \pm 0.05 (4)	10.7
26	C	5	4	6.54 \pm 0.02 (4)	9.27 \pm 0.06 (4)	537	8.64 \pm 0.12 (4)	4.3
27	C	6	4	6.58 \pm 0.02 (4)	9.11 \pm 0.10 (3)	339	8.22 \pm 0.06 (4)	7.8
28	C	6	3	6.64 \pm 0.03 (4)	8.99 \pm 0.07 (4)	224	7.83 \pm 0.04 (4)	14.5
29	C	7	3	6.36 \pm 0.04 (4)	8.91 \pm 0.06 (4)	354	7.47 \pm 0.05 (4)	27.5
30	C	7	2	6.65 \pm 0.03 (4)	9.14 \pm 0.04 (4)	309	7.95 \pm 0.08 (4)	15.5

Note. Affinity for compounds for the $\beta_2\text{K305D}$ receptor and the β_2 versus $\beta_2\text{K305D}$ are also given.

TABLE 1 Effect of lupeol on onset and duration of seizure in animals

Treatment (intraperitoneal administration)	MEST	PTZ model
	N = 5–6; animals = day-old chicks	N = 5; animals = adult male Swiss Albino mice
	Recovery time from seizure (s)	Onset of seizure (s)
Normal saline (10 ml·kg ⁻¹)	430.00 ± 28.6	373.00 ± 29.3
Lupeol (6.125 mg·kg ⁻¹)	375.33 ± 26.31	420.00 ± 62.9
Lupeol (12.5 mg·kg ⁻¹)	415.50 ± 29.5	648.0 ± 89.8
Lupeol (25 mg·kg ⁻¹)	292.33 ± 37.8	912.00 ± 181.4 [*]
Lupeol (50 mg·kg ⁻¹)	359.67 ± 36.0	1,176.00 ± 119.4 [*]

Note. Data are presented as mean ± SEM.

**P* < .05 versus normal saline.

channels: TRP ankyrin 1 (TRPA1) and TRP melastatin (TRPM8) (Aubdool et al., 2014). So we aim to investigate whether the cold induced vascular response becomes dysfunctional with ageing, and how much does TRPA1/TRPM8 and sympathetic signalling contribute to this impairment.

Experimental Approach: In vivo procedures were carried out according to the UK Home Office Animals (Scientific Procedures) Act, 1986. Female CD1 mice (young: 2–3 months; aged: 13–16 months) were anaesthetised (i.p.) by ketamine (75 mg·kg⁻¹) and medetomidine (1 mg·kg⁻¹), and blood flow was recorded by Moor Full-Field Laser Perfusion Imager (FLPI). The TRPA1 antagonist A967079 (100 mg·kg⁻¹) and TRPM8 antagonist AMTB (30 mg·kg⁻¹) were dissolved in 10% DMSO–10% Tween saline and administered (i.p.) 30 min before the cold exposure. RT-qPCR was performed in dorsal root ganglion and western blotting in hind paw skin.

Key Results: Cold induced vascular response was significantly impaired in aged mice compared to the young mice (Figure 1a–c). The TRPA1/TRPM8 antagonist treatment significantly blunted the vascular response induced by cold in both young and aged mice. The RT-qPCR analysis showed that the TRPM8 expression was significantly down-regulated in the aged mice compared to the young mice; no change was observed with TRPA1 expression. There was a blunted sympathetic signalling in the aged mice with a significant reduction in the α2 adrenoceptor expression. The aged mice also produced significantly blunted vasoconstriction in response to intraplantar noradrenaline/medetomidine injection (Figure 1d,e). The cold plate (10°C and 20°C) assay revealed significant delayed reaction to cold in aged mice. (For all experiments, *P* < .05 was considered significant, *n* > 8.)

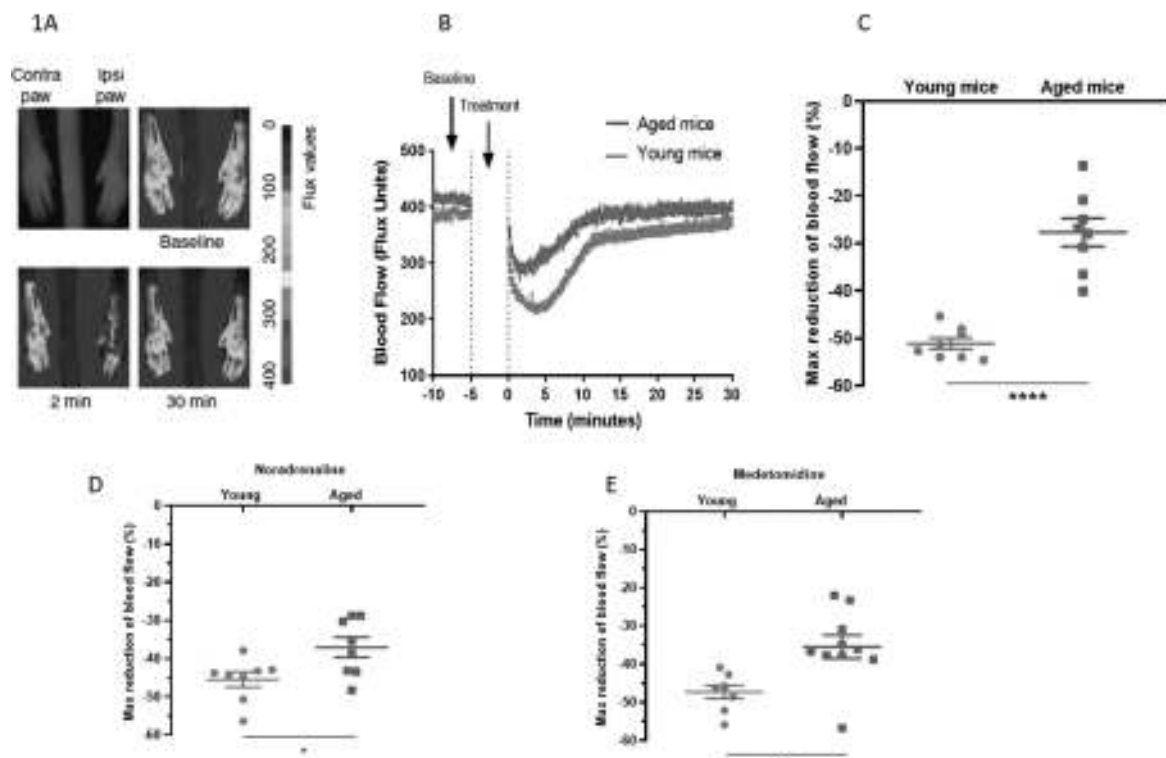


FIGURE 1: Cold induced vascular response. The mouse was placed on a heating mat at 37°C, and the baseline blood flow of the hind paw was recorded for 5 min, after which the ipsilateral paw was immersed in cold ice water (4°C, 5 min) for cold treatment. The blood flow was recorded for another 30 min to measure recovery. (a) Representative FLPI images showing blood flow at baseline, 2, and 30 min after cold water treatment. (b) The blood flow trace of cold induced vasoconstriction and vasodilation in young and aged mice. (c) Maximum % reduction in blood flow from baseline after cold water treatment (maximum vasoconstriction). (d, e) Maximum % reduction in blood flow caused by intraplantar injection of noradrenaline (20 ng) and medetomidine (20 ng). Data are presented as mean with SEM. **P* < .05, ***P* < .01, *****P* < .001, two-tailed *t* test, *n* = 8–10

Conclusion and Implications: The results in our study showed that the cold induced vascular response deteriorates with ageing, and impairment in both sensory signalling (TRPA1/TRPM8) and motor signalling (sympathetic) contributes to this decline.

Acknowledgement

We thank the BBSRC for support (BB/P005616/1).

REFERENCE

Aubdool, A. A., *et al.* (2014). *Nature Communications*, 5, 5723–5736.

OC068 | Worsening cardiac autonomic neuropathy on progression to type 2 diabetes: Localized versus systemic inflammation

Nour Mounira Bakkar; Nahed Mougharbil; Ali Mroueh; Souha Fares; Fouad Zouein; Ahmed Fawzi El-Yazbi

American University of Beirut

Background and Purpose: Cardiac autonomic neuropathy (CAN) occurs early in the course of diabetes with significant cardiovascular risks. While linked to hyperglycaemia, current understanding extends CAN development to pre-diabetes. The instigating cause of CAN, its temporal progression, and responsiveness to treatment remain ill-defined. Here, we used a rat model of mild metabolic challenge with delayed development of hyperglycaemia to trace these parameters in different disease stages.

Experimental Approach: Male Sprague Dawley rats (5–6 weeks old, $n = 8$ per group) were fed a mild hypercaloric diet (4.035 vs. 3 kcal·g⁻¹) leading to hyperinsulinaemia after 12 weeks representing the prediabetic stage. Type 2 diabetes was induced by two consecutive injections of low-dose streptozotocin (40 mg·kg⁻¹) at Weeks 8 and 9. Drug treatment (metformin of 100 mg·kg⁻¹·day⁻¹, pioglitazone of 2.5 mg·kg⁻¹·day⁻¹, insulin titrated to control glucose levels, or their combination) was started at Week 10. CAN was assessed by estimating baroreceptor sensitivity using the vasoactive method. ELISA, immunohistochemistry, and western blotting were used to examine markers of structural deterioration and inflammation in serum, heart, and brainstem.

Key Results: CAN was detected in the prediabetic state as blunted parasympathetic reflex (slope of the Δ MAP vs. Δ HR line for phenylephrine stimulation was -0.73 ± 0.07 in prediabetic vs. -0.34 ± 0.04 bpm·mmHg⁻¹ in control rats). It progressed with the transition to diabetes with further blunting of parasympathetic function (slope reduction to -0.09 ± 0.03) and de novo sympathetic dysfunction (slope reduction from -0.35 ± 0.01 to -0.08 ± 0.02). While prediabetic parasympathetic dysfunction responded to treatment with non-hypoglycaemic, anti-inflammatory doses of metformin (slope = -0.67 ± 0.11) or pioglitazone (-0.75 ± 0.06), this was not the case in diabetic rats. Interestingly, diabetic sympathetic dysfunction was readily reversed by insulin treatment (slope = -0.34 ± 0.04).

However, parasympathetic dysfunction in diabetic rats only responded to combination treatments, with insulin and Met/Pio (slope = -0.4 ± 0.03 for Ins + Met and -0.4 ± 0.05 for Ins + Pio). Notably, whereas prediabetic dysfunction was associated with localized perivascular adipose inflammation, the exaggerated CAN observed in diabetes was accompanied by significant systemic inflammation manifesting as elevated serum IL-1 β levels. Significantly, only combination treatment produced a considerable decrease in serum IL-1 β , consistent with their corrective effect on CAN in the diabetic stage. Hyperglycaemic rats showed signs of focal cardiac ischaemia, left ventricular dysfunction, in addition to elevated brainstem oxidative stress, inflammation, and microglial activation. These manifestations were ameliorated in rats receiving combination treatment.

Conclusion and Implications: Our results highlight a temporal framework whereby deteriorating metabolic state leads to exaggerated CAN possibly related to the progression of localized adipose inflammation to a systemic inflammatory state affecting cardiac and brainstem function.

OC069 | An overview of the relation between blood glucose level and bladder enlargement in various diabetes models

Zeynep Elif Yesilyurt¹; Jan Matthes²; Tamara R. Castañeda³; Urs Christen⁴; Ebru Arioglu-Inan⁵; Martin Christian Michel⁶

¹Ankara University Faculty of Pharmacy; ²Centre of Pharmacology, University of Cologne; ³Sanofi Research and Development;

⁴Pharmazentrum, Goethe University; ⁵Department of Pharmacology, Faculty of Pharmacy, Ankara University; ⁶Department of Pharmacology, Johannes Gutenberg University

Background and Purpose: Urinary bladder enlargement is a consistent feature of animal models of type 1 diabetes (T1DM) across many studies but inconsistent based on few studies in those of type 2 diabetes (T2DM) (Ellenbroek, Arioglu Inan, & Michel, 2018). While bladder enlargement has been proposed to result from glucose-induced diuresis, the correlation between mean bladder weight and mean glucose levels across models is moderate at best. Therefore, we have tested bladder enlargement across a wider range of animal models and explored its relationship to glucose levels based on individual animal data.

Experimental Approach: Data were obtained from ongoing studies in rodent models of T1DM (rat insulin promotor lymphocyticchoriomeningitis virus [RIP-LCMV] mice) and T2DM (ob/ob and insulin receptor substrate 2 [IRS2] knockout mice and 20- and 28-week-old ZSF rats) and their euglycaemic controls. Blood glucose concentration and bladder weight were determined at the end of each study, and correlation analysis was carried out between those values. Since the analysis of bladder weight across models was explorative, hypothesis-testing statistical analysis was not applied. Group means are shown \pm SD, effect sizes with 95% confidence intervals,

TABLE 1 Blood glucose and bladder weight across animal models

Model	n		Blood glucose (mg·dl ⁻¹)			Bladder weight (mg)		
	Con	Dia	Con	Dia	Difference	Con	Dia	Difference
T1DM								
RIP-LCMV	12	9	155 ± 19	489 ± 172	334 (230, 438)	25.9 ± 4.1	41.9 ± 15.5	16.0 (6.3, 25.7)
T2DM								
ob/ob	9	14	169 ± 40	166 ± 52	-4 (-47, 39)	25.9 ± 5.6	36.6 ± 13.1	10.7 (1.6, 19.8)
IRS2 knockout	12	12	162 ± 29	289 ± 169	127 (25, 228)	30.3 ± 6.1	26.0 ± 7.3	-4.3 (-10.0, 1.4)
ZSF (20 weeks)	6	6	82 ± 15	234 ± 48	152 (106, 198)	95 ± 16	193 ± 23	98 (68, 129)
ZSF (28 weeks)	6	6	96 ± 6	300 ± 23	203 (182, 225)	114 ± 10	232 ± 40	118 (81, 155)

Note. Difference between control (Con) and diabetic (Dia) is shown with 95% confidence interval.

TABLE 2 Correlation between blood glucose and bladder weight based on individual animals in various models

Model	n	r ²	P
T1DM			
RIP-LCMV	21	.7257	<.0001
T2DM			
ob/ob	23	.062	.2519
IRS2 knockout	24	.126	.0893
ZSF (20 weeks)	30	.363	.0004
ZSF (28 weeks)	34	.437	<.0001

Note. Data on ZSF rats include additional groups receiving various specific diets not included in Table 1.

and correlations as squared Spearman correlation coefficient with descriptive *P* value.

Key Results: Compared to controls, blood glucose was increased strongly in RIP-LCMV mice, moderately in ZSF rats and IRS2 knockout mice, but not in ob/ob mice. In contrast, bladder weight was increased in all models except for IRS2 knockout mice (Table 1). Among ob/ob mice, differences between control and diabetic animals were similar in male and female animals. This indicates a lack of correlation between blood glucose and bladder weight at the group level.

Strength of correlations between blood glucose and bladder weight based on individual animals within a model ranged from strong in RIP-LCMV mice over moderate in ZSF rats to weak or non-existent in ob/ob and IRS2 knockout mice (Table 2).

Conclusion and Implications: We conclude that bladder enlargement can occur in the absence of blood glucose elevation (ob/ob mice) and may be absent despite blood glucose elevation (IRS2 knockout mice). Accordingly, strength of correlation between glucose levels and bladder weight varied widely across models. These data do not support the hypothesis that increased glucose excretion is the main driver of bladder enlargement in experimental diabetes.

REFERENCE

Ellenbroek, J. H., Arioglu Inan, E., & Michel, M. C. (2018). A systematic review of urinary bladder hypertrophy in experimental diabetes: Part 2. Comparison of animal models and functional consequences. *Neurourology and Urodynamics*, 37, 2346–2360.

Toxicology Oral Communications 1

OC052 | Transfer of hepatocellular microRNA regulates cytochrome P450 2E1 in renal tubules

Olivia Matthews¹; Emma E. Morrison¹; John D. Tranter¹; Neil C. Henderson¹; Dominic Williams²; James W. Dear¹

¹The University of Edinburgh; ²AstraZeneca

Background and Purpose: Extracellular microRNAs are taken up by recipient cells to induce a change in cellular phenotype. In this study, we tracked microRNA transfer using the hepatocyte-enriched microRNA-122 (miR-122). Our hypothesis was that miR-122 will be transferred from liver to kidney as it is known that the kidney tubular cells internalise microRNA containing extracellular vesicles.

Experimental Approach: Dicer^{flox/flox} mice were treated with a hepatotropic Cre recombinase-expressing adenovirus (AAV8-Cre) to inhibit mature microRNA production selectively in hepatocytes (conditional KO [CKO]). MicroRNA expression was analysed by PCR ± FACS sorting and by in situ hybridisation, with and without acute liver injury induced by paracetamol (150 and 300 mg·kg⁻¹). A murine model of myocardial infarction was used as a non-hepatic model of microRNA release secondary to tissue injury. To determine the functional consequences of miR-122 transfer, we measured the RNA and protein expression and drug metabolising activity of cytochrome P450 2E1 (established miR-122 target and key enzyme responsible for paracetamol toxicity). In humans, we measured microRNA expression in urinary extracellular vesicles.

Key Results: Dicer CKO mice had a time-dependent decrease in liver miR-122 (4 weeks after AAV8-Cre treatment, % of baseline miR-122: median 3% [IQR 2–6], *N* = 20, *P* < .0001). This was accompanied by a substantial decrease in kidney miR-122 (5% of baseline [IQR 2–7], *N* = 20, *P* = .007) without a change in kidney Dicer expression or other kidney microRNA species. There was no change in Dicer or microRNA in heart, lung, or brain. Liver injury increased kidney miR-122 (9.5-fold increase, *N* = 5, *P* = .008); this increase was abolished in the Dicer

CKO mouse (14-fold difference when AAV8-Cre compared to AAV8-null control after 300 mg·kg⁻¹ paracetamol, $N = 5$, $P = .008$). FACS sorting demonstrated miR-122 uptake selectively into kidney tubular epithelial cells. Cardiac injury released circulating miR-499, which was also increased in the kidney. Depletion of hepatocyte miR-122 increased CYP2E1 expression and activity in the liver and kidney (twofold increase in kidney mRNA expression, $N = 5$, $P = .008$). In human acute liver injury, miR-122 was increased in urinary extracellular vesicles.

Conclusion and Implications: In summary, in normal physiology, miR-122 is transferred from liver to kidney, and this signalling pathway is increased by liver injury. Kidney enzyme regulation by liver microRNA represents a new paradigm in drug metabolism.

OC053 | Mechanisms of NADPH-cytochrome P450 oxidoreductase induction by dexamethasone in the H4IIE rat hepatoma cell line

David S. Riddick; Anne K. Mullen Grey

University of Toronto

Background and Purpose: Expression of NADPH-cytochrome P450 oxidoreductase (POR), electron donor for microsomal P450s, is induced in rat liver by dexamethasone (DEX), a glucocorticoid that activates the glucocorticoid receptor (GR) and the pregnane X receptor (PXR). We showed that POR regulation in rat liver is primarily PXR mediated, although GR may contribute to POR mRNA induction (Hunter et al., 2017). The present study aimed to determine the role of GR and PXR in the DEX induction of POR mRNA and protein in the H4IIE rat hepatoma cell line.

Experimental Approach: Cultured H4IIE cells were treated with a range of DEX concentrations (1 nM to 100 μ M); lower concentrations activate GR selectively. Target transcript levels provided indicators of activated GR (tyrosine aminotransferase [TAT] and PXR) and PXR (CYP3A23). Triamcinolone acetonide (TA, 100 nM) and pregnenolone-16 α -carbonitrile (PCN, 10 μ M) served as selective agonists for GR and PXR, respectively. We combined a GR-activating DEX concentration (100 nM) with the GR antagonist, RU486 (1 μ M), and a DEX concentration activating GR and PXR (10 μ M) with the PXR antagonist, FLB-12 (25 μ M). After 24 hr of drug treatment, transcript levels were determined by real-time PCR, with normalization to β -actin ($n = 3-4$), and POR protein levels were assessed by immunoblot, with normalization to total microsomal protein ($n = 3$). Statistical significance was determined by one-way ANOVA followed by Newman-Keuls test.

Key Results: The DEX EC₅₀ for a PXR target, CYP3A23 ($3.3 \pm 0.6 \mu$ M), was higher than that for the GR targets, TAT (5.2 ± 1.1 nM) and PXR (2.5 ± 1.4 nM), as well as POR (59.7 ± 52.3 nM) ($P < .001$). POR protein levels were induced threefold and fourfold, respectively, by low (100 nM) and high (10 μ M) DEX ($P < .001$). POR mRNA and protein were induced by TA ($P < .001$), but not PCN. At the mRNA and

protein levels, POR induction by low DEX (100 nM) was blocked by RU486 ($P < .05$), but POR induction by high DEX (10 μ M) was minimally influenced by FLB-12 ($P < .05$). The basal half-life for POR mRNA (8.6 ± 0.8 hr), but not β -actin mRNA, was extended by DEX at both 100 nM (12.8 ± 2.9 hr) and 10 μ M (14.3 ± 1.6 hr) ($P < .05$).

Conclusion and Implications: GR plays a more important role in DEX-induced POR expression in H4IIE cells compared to rat liver in vivo, raising questions about the suitability of this hepatoma cell line as a model for mechanistic studies of POR induction.

ACKNOWLEDGEMENT

This study was supported by CIHR.

REFERENCE

Hunter, et al. (2017). *Drug Metabolism and Disposition*, 45, 118–129.

OC055 | AChE activity difference between capillary and venous blood, and its relevance to the assessment of nerve agent exposure

Sarah Judge; Adam Potts; Lydia Alcock; Peter Blain

Newcastle University

Background and Purpose: Following a nerve agent incident, rapid screening of a large number of people would allow early treatment of exposed individuals and release of non-exposed individuals. However, screening a large number of people with current assessments would be slow. Organophosphates, including nerve agents, inhibit AChE. Exposure is assessed by measuring red blood cell AChE activity. Currently, AChE activity assessments are normally conducted on venous blood and frequently normalised against blood volume, despite evidence indicating that normalisation against Hb reduces variability (Worek, Mast, Kiderlen, Diepold, & Eyer, 1999). Rapid point of care testing (POCT) for a large number of people is likely to use capillary blood from a finger prick. The aim of this study was to determine if AChE activity measured in capillary blood is consistent with venous blood activity.

Experimental Approach: Venous and capillary blood samples were collected from 15 healthy volunteers (18–41 years old). Whole blood samples were diluted in saponin and rapidly assayed in triplicate for AChE activity in a 96-well plate using a modified Ellmans method; the substrate acetylthiocholine, the butyrylcholinesterase inhibitor iso-OMPA, and 5,5'-dithiobis(2-nitrobenzoic acid) were added, and a kinetic reading was taken (412 nm). Hb in the samples was assessed using a colorimetric commercial assay kit. Average AChE was calculated from the triplicates for each sample and then normalised against blood volume or Hb content. Statistical significance between AChE activity and Hb content in capillary and venous blood was calculated using paired t tests.

Key Results: AChE activity per ml of capillary blood was $12 \pm 4\%$ lower than venous blood ($n = 15$; $3,442 \pm 146$ vs. $3,999 \pm 199$ nmol·min⁻¹·ml⁻¹; $P < .01$). Hb levels in capillary blood were

also significantly lower than in venous blood (107 ± 4 vs. 123 ± 4 mg·ml⁻¹; $P < .01$). When AChE activity was normalised against Hb, there was no significant difference in activity between capillary and venous blood (32 ± 1 vs. 32 ± 1 nmol·min⁻¹·mg⁻¹ Hb; $P = .8$).

Conclusion and Implications: These data indicate that normalising AChE activity against blood volume does not take into account red blood cell differences between venous and capillary blood. Normalising AChE activity against Hb levels should be considered when developing rapid POCT for a large number of people. Data are expressed as mean \pm SEM.

ACKNOWLEDGEMENT

This study was funded by the NIHR.

REFERENCE

Worek, F., Mast, U., Kiderlen, D., Diepold, C., & Eyer, P. (1999). Improved determination of acetylcholinesterase activity in human whole blood. *Clinica Chimica Acta*, 288, 73–90.

Toxicology Oral Communications 2

OC056 | Modelling the global challenge of drug-induced liver injury in zebrafish

Sarah Stedman; Bastiaan Vliegenthart; Chunmin Wei;
Jorge del Pozo; James Dear

University of Edinburgh

Background and Purpose: Drug-induced liver injury (DILI) is a global challenge. In China, herbal medicines are a major cause of DILI. In Africa, anti-tuberculosis drugs are the major cause. Conducting toxicology studies in zebrafish larvae enables relatively cheap and high-throughput assessment of toxicity in the context of a whole organism. In this study, we develop triptolide (Chinese herbal medicine) and anti-tuberculosis DILI models. In addition, we develop a novel method of extracting hepatocytes and immune cells from transgenic zebrafish larvae using FACS and quantify the microRNA response to DILI using small RNA sequencing.

Experimental Approach: Wild-type (WIK) or transgenic (hepatocyte-GFP, immune cell-mCherry) zebrafish larvae were used for experiments ($N = 30$ per experiment). Zebrafish larvae were exposed to triptolide, pyrazinamide, or isoniazid from 3 to 5 days post fertilisation at different concentrations and for different periods of time. Liver injury was assessed by mortality, morphology, histology, liver size, liver fluorescence intensity, and the quantification of miR-122 (liver-specific microRNA). Following the development of the triptolide model, wild-type (WIK) zebrafish larvae underwent small RNA sequencing. Transgenic zebrafish larvae were digested to generate a single-cell solution. GFP-positive and mCherry-positive cells were collected using FACS, and miRNAs were quantified using qPCR.

Key Results: There was a dose–mortality relationship for all three drugs, along with morphological and histological changes. Histology demonstrated that exposure to all three drugs resulted in hepatic vacuolation and necrosis. There was a significant relationship between concentration/length of exposure and liver size, liver fluorescence intensity, and concentration of miR-122. miRNA sequencing of triptolide-exposed zebrafish larvae demonstrated down-regulation of 198 miRNAs and up-regulation of 105 miRNAs. qPCR quantification of miR-122 (hepatocytes specific) and miR-155 (immune specific) demonstrated that the GFP- and mCherry-positive cells collected via FACS were hepatocytes and immune cells. Further quantification of four miRNAs (miR-122, miR-155, miR-124, and let-7c) demonstrated that the changes identified in the miRNA sequencing correlate with the changes seen in hepatocytes but not immune cells.

Conclusion and Implications: The Chinese herbal medicine triptolide and anti-tuberculosis drugs pyrazinamide and isoniazid cause dose-dependent hepatotoxicity in zebrafish larvae as determined by mortality, morphology, imaging, histology, and quantification of miR-122. Specific cell populations can be collected via FACS from transgenic zebrafish lines, and small RNA sequencing can be used to explore the toxicity mechanisms. Zebrafish larvae represent a high-throughput toxicity model that allows mechanistic investigation in a whole organism.

OC057 | Drug-induced liver injury cannot be accurately assessed by standard assays for circulating microRNA-122 due to the presence of isomiRs

James Dear¹; John Tranter¹; Lianne Chahman-Vos²; Neeraj Dhaun¹;
Matthew Bailey¹

¹The University of Edinburgh; ²Utrecht University

Background and Purpose: Circulating microRNAs (miRs) are promising biomarkers, regularly measured by quantitative RT-PCR (RT-qPCR). Small RNA sequencing has revealed the existence of isoforms of miRs termed “isomiRs,” which vary in length compared with the canonical species. 3′-Dumbbell-PCR (3′-Db-PCR) is a novel assay for selective quantification of miRs and their respective 3′-isomiRs through the ligation of a sequence-specific stem-loop adapter prior to RT-qPCR (Honda & Kirino, 2015). microRNA-122 (miR-122) is an hepatocyte-specific miR which is a biomarker of drug-induced liver injury (DILI). Our objective was to determine if isomiRs of miR-122 affect its accurate quantification by “industry standard” RT-qPCR, and to utilise 3′-Db-PCR to selectively quantify the miR-122 canonical form and its isomiRs.

Experimental Approach: The presence of miR-122 isomiRs in both healthy and DILI human serum ($n = 3$) was determined by small RNA sequencing. Synthetic canonical miR-122 (22 nucleotides [nt]) and the clinically relevant isomiRs underwent RT-qPCR (concentration range:

5×10^{-2} – 10^6 fM) using both Qiagen miScript (SYBR green) and TaqMan microRNA systems that are widely used in research and drug development. The 3'-Db-PCR assay was adapted and optimised for the detection of miR-122 isomiRs.

Key Results: Small RNA sequencing of serum from healthy subjects and patients with DILI ($n = 3$) demonstrated the presence of multiple miR-122 isomiRs, with 3' variants being in high concentration. Canonical miR-122 and its 21, 20, 19, and 18 nt 3'-isomiRs were detectable by both miScript and TaqMan systems with amplification efficiency substantially decreasing as 3' nucleotides were removed. Using SYBR green PCR, canonical miR-122 and its 21 and 20 nt 3'-isomiRs were detectable at all concentrations tested, whereas 19 and 18 nt 3'-isomiRs were only detectable at concentrations $\geq 5 \times 10^2$ and 5×10^3 fM, respectively. Comparatively, TaqMan exhibited a similar relationship but with reduced efficiency. By contrast, 3'-Db-PCR was able to clearly discriminate equimolar 19 nt 3'-isomiR from canonical miR-122 with a large difference of around 10 cycle threshold (C_T) values.

Conclusion and Implications: The isomiR profile of miR-122 is different between healthy and DILI patient serum samples. The quantification of miR-122 by gold standard RT-qPCR is inaccurate as both SYBR green and TaqMan systems detect miR-122 and its isomiRs with varying amplification efficiencies. 3'-Db-PCR is an alternative qPCR-based assay that may be used to selectively quantify miR-122 isomiRs and should be taken forward to full validation.

REFERENCE

Honda, S., & Kirino, Y. (2015). *Nucleic Acids Research*, 43(12), e77.

OC058 | From stratified to individualised precision dosing: Development of a liquid biopsy technique for measuring hepatic drug-metabolising enzymes

Brahim Achour¹; Zubida Al-Majdoub¹; Kristi Lea²; Jill Barber¹; Jeoffrey Schageman²; Amin Rostami-Hodjegan¹

¹University of Manchester; ²Life Technologies (Thermo Fisher)

Background and Purpose: Precision dosing aims to deliver the right drug dose for a specific patient based on individual characteristics in order to improve efficacy and reduce toxicity. "Liquid biopsy" is expected to define the metabolic capacity of an individual patient beyond the typical genotyping and hence facilitate precision dosing by linking the administered dose to expected clearance.

Experimental Approach: Liver tissue (20–250 mg) and plasma (1–3 ml) samples from the same cancer patients ($n = 9$) were analysed using proteomic (targeted and global) and transcriptomic (next generation sequencing [NGS]) methods. Healthy controls ($n = 5$) were used as baseline. In-house QconCAT (Achour, Russell, Barber, Rostami-Hodjegan, 2014) methodology was used for protein quantification on nanoHPLC-Orbitrap Elite system (Thermo Fisher) with an inclusion list

focusing on drug-metabolising enzymes (CYP1A2, CYP2A6, CYP2C9, and CYP3A4). NGS followed Ampliseq workflow (Millat, Chanavat, Rousson, 2014) performed at Life Technologies (Thermo Fisher Scientific, Texas) at a depth of 8 million reads-ml⁻¹. Expression levels of drug-metabolising enzymes were normalised using a novel liver-specific shedding correction factor (LSCF), computed based on a combination of 13 liver-specific marker genes measured in plasma to account for variability in the level of liver exosomal shedding.

Key Results: Proteins (~2,500) were measured, including key drug-metabolising enzymes, in non-cancerous liver samples from cancer patients, alongside RNA transcripts (~21,000) in matched plasma. Coverage of targets and markers was 80–100% in the protein data and 64–100% in RNA data. Exosome shedding was higher and more variable in cancer patients than healthy controls; $LSCF_{(cancer)} = 26.08 \pm 19.63$ reads per million (rpm), $n = 9$; $LSCF_{(healthy)} = 0.83 \pm 0.26$ rpm, $n = 5$; t test, $P < .01$. Tissue protein and LSCF-corrected plasma RNA levels were assessed for correlation; major drug-metabolising enzymes were significantly correlated between plasma (RNA) and liver (protein); CYP3A4 (Pearson $r = .98$, $P < .01$, $R^2 = .95$); CYP2C9 ($r = .76$, $P = .03$, $R^2 = .57$); CYP1A2 ($r = .93$, $P = .02$, $R^2 = .86$); and CYP2A6 ($r = .98$, $P < .01$, $R^2 = .96$).

Conclusion and Implications: A liquid biopsy test based only on plasma samples to determine liver content of key enzymes was established; this was relevant to (a) enzymes exclusively/predominantly expressed in liver and (b) predominantly shed into the blood. This technology should facilitate efforts towards precision dosing, as an essential element of precision medicine.

REFERENCES

- Achour, B., Russell, M. R., Barber, J., & Rostami-Hodjegan, A. (2014). Simultaneous quantification of the abundance of several cytochrome P450 and uridine 50-diphospho-glucuronosyltransferase enzymes in human liver microsomes using multiplexed targeted proteomics. *Drug Metabolism and Disposition*, 42, 500–510.
- Millat, G., Chanavat, V., & Rousson, R. (2014). Evaluation of a new NGS method based on a custom AmpliSeq library and Ion Torrent PGM sequencing for the fast detection of genetic variations in cardiomyopathies. *Clinica Chimica Acta*, 433, 266–271.

OC059 | Estimated prevalence of exposure to potential drug–drug interactions in France: A retrospective study from 2006 to 2016

Cécile Souty¹; Titouan Launay²; Olivier Steichen³; Cécile Conte⁴; Maryse Lapeyre-Mestre⁴; Thomas Hanslik⁵

¹INSERM Sorbonne Université; ²Sorbonne Université, INSERM, Institut Pierre Louis d'épidémiologie et de Santé publique (IPLESP UMRS 1136), Paris, France; ³Sorbonne Université, Inserm, Université Paris 13, Laboratoire d'informatique médicale et d'ingénierie des connaissances en e-santé, LIMICS, Paris, France; ⁴INSERM, Université de Toulouse, Centre Hospitalo-Universitaire de Toulouse (CHU Toulouse), UMR 1027, Toulouse, France; ⁵Assistance Publique - Hôpitaux de Paris (APHP), Hôpital Ambroise Paré, Service de Médecine Interne, Boulogne Billancourt, France

Background and Purpose: Drug–drug interactions (DDIs) are a major risk factor in drug safety that requires monitoring in an ageing population with increasing polypharmacy exposure. We aimed to estimate prevalence of exposure to drug–drug interactions in France between 2006 and 2016, for six DDIs with various clinical relevance: angiotensin II receptor antagonists or angiotensin-converting enzyme inhibitors and nonsteroidal anti-inflammatory drugs (ARBs-ACEIs + NSAIDs), antiplatelet agents and NSAIDs (AAP + NSAIDs), serotonergic drugs and tramadol (SD + T), statins and macrolides (S + M), oral anticoagulant and NSAIDs (OAC + NSAIDs), and colchicine and macrolides (C + M).

Experimental Approach: We used exhaustive claims data concerning a random sample of 1/97th of the French population covered by the

French health care insurance system (EGB, *Echantillon généraliste de bénéficiaires*) between 2006 and 2016 (694,488 individuals in 2016). Exposure to a DDI was defined as exposure to two interacting drugs with overlapping coverage, estimated using the World Health Organization's Defined Daily Dose. We also computed the proportions of co-prescription of two interacting drugs prescribed by the same health professional and dispensed by the same pharmacy on the same day. The prevalence of exposure to DDI was estimated by year, considering the study population as denominator.

Key Results: Prevalence of exposure to DDIs in 2016 was estimated at 3.67% for ARBs-ACEIs + NSAIDs (40.1% of co-prescription), 1.52% for AAP + NSAIDs (42.6% of co-prescription), 0.76% for SD + T (58.2% of co-prescription), 0.36% for S + M (26.2% of co-prescription), 0.24% for OAC + NSAIDs (31.8% of co-prescription), and 0.02% for C + M (30.3% of co-prescription).

The elderly (≥ 85 years) were the most affected age group for two DDIs: C + M (0.06%) and SD + T (1.87%) in 2016; whereas people aged between 65 and 84 years were more affected for the four others DDIs: 11.73% for ARBs-ACEIs + NSAIDs, 5.83% for AAP + NSAIDs, 1.53% for S + M, and 0.75% for OAC + NSAIDs in 2016.

Prevalence of three DDIs increased between 2006 and 2016: +38.8% for OAC + NSAIDs, +34.8% for SD + T, +14.7% for ARBs-ACEIs + NSAIDs, and +13.2% for AAP + NSAIDs; while the two other DDIs decreased: –21.0% for S + M and –4.1% for C + M.

Conclusion and Implications: Exposure to these selected DDIs in France is not uncommon with a high proportion resulting from a co-prescription. Monitoring prevalence of exposure to DDIs in population is needed to implement prevention measures. Claims data allow this surveillance among large cohort representative of the population.